Tier 2 Water Budget, Climate Change, and Ecologically Significant Groundwater Recharge Area Assessment for the Ramara Creeks, Whites Creek and Talbot River Subwatersheds

Prepared for:

Lake Simcoe Region Conservation Authority

120 Bayview Parkway, Box 282
Newmarket, Ontario L3Y 4X1

Prepared by:

Earthfx Incorporated

3363 Yonge Street
Toronto, Ontario M4N 2M6

October 2014

October 21st, 2014

Shelly Cuddy, P.Geo.
Hydrogeologist
Lake Simcoe Region Conservation Authority
120 Bayview Parkway, Box 282
Newmarket, Ontario, L3Y 4X1

RE: Tier 2 Water Budget, Climate Change, and Ecologically Significant Groundwater Recharge Area Assessment for the Ramara Creeks, Whites Creek and Talbot River Subwatersheds.

Dear Ms. Cuddy:

We are pleased to provide a copy of our final report for the Tier 2 Water Budget, Climate Change, and Ecologically Significant Groundwater Recharge Area Assessment for the Ramara Creeks, Whites Creek and Talbot River Subwatersheds. The report describes the physical setting, conceptual hydrogeologic model, and the development of an integrated surface water and groundwater flow model for the Ramara Creeks, Whites Creek and Talbot River Subwatersheds. The model was applied to conduct the Tier 2 water budget analysis and stress assessment for the subwatersheds and to analyze the impacts of long-term climate change. An analysis of high volume and ecologically significant groundwater recharge areas (HVRAs and ESGRAs) and the effect of climate change on the hydrology of the study area were completed with the calibrated model.

We trust this report meets with your satisfaction. Should you have any questions, please contact us. We thank you again for the opportunity to work with you on this important study for LSRCA.

Yours truly,

Earth*fx* Incorporated

Dirk Kassenaar, M.Sc., P.Eng.
President, Earth*fx* Inc.

E.J. Wexler, M.S.E., M.Sc., P.Eng.
Vice-President, Earth*fx* Inc.

3363 Yonge St., Toronto, Ontario, Canada M4N 2M6
Tele: 416.410.4260 e-mail: info@earthfx.com
www.earthfx.com

Executive Summary

A Tier 2 water budget and stress assessment was conducted for the Ramara Creeks, Whites Creek and Talbot River subwatersheds as required under the Lake Simcoe Protection Act (2008). A Tier 2 water budget is defined as: "a water budget developed using computer-based three-dimensional groundwater flow models and computer based continuous surface water flow models to assess groundwater flows and levels, surface water flows and levels, and the interactions between them". An integrated surface water/groundwater (SW/GW) flow model was developed using the U.S. Geological Survey GSFLOW code, calibrated, and applied to quantify the components of the groundwater and surface water budgets for the subwatersheds and to assess the potential stress levels within each subwatershed. The GSFLOW model represents an integration of the surface water and groundwater sub-models in which each system can provide feedback to the other. The integrated SW/GW model provides a better representation of the complex flow processes that occur in natural systems particularly those with a highly responsive shallow water table.

A second objective of this study was to apply the integrated SW/GW model to identify and analyze ecologically significant groundwater recharge areas (ESGRAs) within the subwatersheds. The third objective of this study was to apply the integrated SW/GW model conduct long-term transient simulations to assess how the subwatersheds might respond to potential stresses, including long-term drought and future climate change.

An assessment of the hydrologic setting was presented including an analysis of climate and streamflow data. Climate data, primarily, precipitation, air temperature, and solar radiation, were compiled from a number of sources and used to construct a complete climate dataset for 1951 through 2012. Streamflow data are extremely limited in the study area, both in the number of gauged locations and the period of record. Special consideration was given to the operations of the Trent-Severn Waterway which affects both the surface water flow and groundwater flow in the Talbot River subwatershed.

A review of the geologic setting of the subwatersheds and the surrounding area was undertaken. The study area was extended beyond the subwatershed boundaries to allow accurate representation of cross-watershed flows. A key feature of the study area is the low relief topographic plain referred to as the Carden Plain alvar, which is characterized by very thin drift on weathered bedrock. The exposed bedrock exhibits both open fractures and low permeability blocks. Quantifying the recharge in these areas was important for understanding the water budget in the subwatersheds. The remainder of the area is dominated by glacial till plains.

A conceptual stratigraphic model was developed for the study area. A three-dimensional representation of the conceptual stratigraphic model was created by mapping the tops of each geologic unit and then overlaying them. A three-dimensional hydrostratigraphic model was then created by mapping the aquifers and aquitards in the study area. The 14 hydrostratigraphic model layers represented five overburden and nine bedrock units. Groundwater level data were analyzed to provide information on regional groundwater flow patterns as well as to assess seasonal and multi-year variability.

A steady-state groundwater flow sub-model was constructed for the study area. The hydrostratigraphic surfaces, with some simplifications and modifications to preserve minimum thicknesses, were transformed into the layer tops and bottoms needed for the seven-layer groundwater flow sub-model extending down from the surficial sediments and alvar weathered bedrock to the Precambrian basement. Hydraulic parameters were assigned to models layers after assessing field measurements from previous studies. These were refined through model calibration. The model represented all streams, lakes, and wetlands in the study area along with all permitted groundwater takings from commercial and domestic wells, and operational dewatering for the 11

active quarries. Calibration targets included static water level measurements from the MOE Water Well Information System, quarry monitoring reports and consultant studies, as well as streamflow measurements for Whites Creek and quarry discharges. Model calibration statistics indicated an excellent fit with the available groundwater dataset, providing validation the subsequent application of the model for updated Tier 2 water budget and ESGRA analyses.

The updated Tier 2 stress assessments conducted under steady-state conditions showed that none of the study subwatersheds are currently in a stressed condition. To simulate future conditions, pumping rates at the municipal wells were increased to reflect anticipated population growth and quarry depth and extents were modified to represent future quarry build-out (based on 20-year projections). Results of the future conditions simulations showed that the study subwatersheds will not be stressed over the 20-year horizon.

Two-year (extreme) and 10-year (historic) drought conditions were analyzed with the integrated SW/GW model. The largest impacts due to drought were seen in the headwater tributaries across the study area, which are the most sensitive to small changes in the position of the water table. The alvar plain was found to provide high recharge to portions of the study area subwatersheds but the feature has low storage capacity. As such, the watersheds fed directly by the alvar are less buffered from the effects of long-term drought due to the relatively small storage capacity. No municipal pumping wells were found to go dry during either the 2-year or 10-year drought simulations.

An ESGRA assessment was completed for the subwatersheds using the integrated SW/GW model. Reverse particle tracking techniques were used to establish linkages between ecologically significant surface water features and the areas that provided recharge. For this study, all streams and all wetlands in the three study area subwatersheds were considered to be ecologically significant. The particle tracking analysis indicated that the subwatersheds are dominated by local-scale hydrologic systems, for example, the tops of incised bedrock valleys in the Talbot River and Whites Creek subwatersheds act as local recharge zones for the surface water features in the valleys below.

Cluster analysis techniques were used to evaluate the distribution of particle endpoints and produce the ESGRA maps. The final ESGRA delineation comprised 33% of the combined area of the three subwatersheds. Comparisons with previously defined significant groundwater recharge areas (SGRAs) showed that only parts of the SGRAs (about half the area) contributed to ecologically significant features.

The effects of global climate change on surface water and groundwater in the subwatersheds was conducted with the integrated SW/GW model using climate information derived from Global Circulation Models (GCMs). A total of 9 GCM datasets were identified using the percentile method, a statistically-based method for ensuring that selected climate scenarios represent both the central tendencies of the GCMs, as wells as the more extreme projections. Because the GCMs cannot directly predict local-scale behavior, the “change-field” method was selected to generate a series of climate change datasets for the local area from baseline (historic) climate data. Temperature data were generated by shifting the data on a monthly basis and precipitation data were scaled by monthly change factors.

Analysis of the climate change scenarios showed that monthly precipitation will increase in the majority of scenarios except during the months of June and July, resulting in a generally wetter fall, winter and spring, with a drier warm season. All the scenarios showed an increase in temperature of at least 1 C in all months . The median temperature shift ranged from 1.8 to 3.2 C with winter (January and February) and late summer/fall (August and September) having the highest increase. The average of annual average precipitation for all climate runs was 1,129 mm/year representing a 9.1% increase over baseline conditions (1,029 mm/year).

Groundwater recharge is predicted to increase with climate change. Warmer and wetter fall and winter seasons allow more water to enter the groundwater system. Furthermore, the timing of the spring recharge is predicted to shift, with more recharge occurring earlier in the spring. The warmer winters predicted by the climate change models result in less accumulated snow, and with less water stored in the snowpack into mid-spring, groundwater recharge in April and May is expected to decrease.

Groundwater heads under the climate change scenarios experienced an earlier and more prolonged response to the spring freshet, combined with less dramatic decreases in water levels over the winter months of January to March. This was attributed to the wetter, warmer winters predicted by the GCMs, with a larger portion of the winter precipitation expected to fall as rain rather than snow. The seasonal pattern of groundwater discharge to surface water features echoes the water level response to climate change, with discharge into surface water features experiencing an increase during the winter months due to the larger hydraulic gradient towards the surface water features.

There was a predicted increase in the median monthly streamflow December through March, with decreases predicted in all other months. This pattern of change is predicted in streams across the watershed, with median winter streamflow increasing by as much as 50%. While the decrease in average summer flows does not approach this magnitude, the severity of drought and extreme low flow periods is predicted to increase. These predicted changes to the hydrologic regime will undoubtedly have impacts on stream ecology and geomorphology. Further study into the specific impacts of these predicted changes should be incorporated into future watershed assessments.

Earthfx recommends that LSRCA continue to maintain and expand the environmental monitoring network in the three study subwatersheds. Meteorological data are sparse in the study area, and this area is hydro-climatically distinct from the southern and western portions of the Lake Simcoe watershed. Of particular importance is further monitoring and study of the alvar areas which are sensitive to drought conditions and future shifts in climate.

Table of Contents

List of Tables

List of Figures

Tier 2 Water Budget, Climate Change and Ecologically Significant Groundwater Recharge Area Assessment for the Ramara Creeks, Whites Creek and Talbot River Subwatersheds

1 Introduction

The Province of Ontario established the Lake Simcoe Protection Act (2008) and the Lake Simcoe Protection Plan (LSPP) in 2009 (Ontario Ministry of the Environment) to "protect, improve or restore the ecological health of the Lake Simcoe Watershed including water quality, key natural heritage features and their functions, and key hydrologic features and their functions". The LSPP outlines a number of policies to support the maintenance of adequate flows required to maintain healthy aquatic ecosystems in the Lake Simcoe watershed. Specifically, Policy 5.2.SA requires that LSRCA complete a "Tier 2" water budget and stress assessment for all subwatersheds in the Lake Simcoe and Couchiching/Black River area that have not been assessed at that level under the Source Water Protection program established by the Clean Water Act (2006). Other policies require LSRCA to consider the potential impacts of climate change on water quantity including streamflow and groundwater resources.

A Tier 2 water budget is defined as: "a water budget developed using computer-based three-dimensional groundwater flow models and computer based continuous surface water flow models to assess groundwater flows and levels, surface water flows and levels, and the interactions between them" (Director's Technical Rules for the Clean Water Act, 2006). The development and calibration of an integrated groundwater/surface water flow model for the Ramara Creeks, Whites Creek and Talbot River subwatersheds is the main subject of this report. The model was applied to evaluate water quantity stress levels in the subwatersheds, assess the potential impacts of future long-term climate change, and delineate ecologically significant groundwater recharge areas.

1.1 Scope of Work

The Scope of Work for this project includes three main parts: (1) the development, calibration, and use of an integrated groundwater and surface water flow model to conduct a Tier 2 water budget analysis and stress assessment for the Ramara Creeks, Whites Creek and Talbot River subwatersheds; (2) a modelling analysis of how climate change may affect the water budget in the study area subwatersheds; and (3) the identification and analysis of ecologically significant groundwater recharge areas (ESGRAs).

The Tier 2 water budget and stress assessment includes the following tasks:

- compile and assess available background information and data on the hydrologic and hydrogeologic setting;
- analyze information and data gaps and define additional data requirements needed to refine previously developed rainfall/runoff models for use as a hydrologic submodel in this study;
- create a conceptual geological/hydrogeological model for the study area;
- develop and calibrate the hydrologic submodel (PRMS);
    - enable the model to use hourly climate information as input;
    - calibrate the model to daily observed streamflow records concurrently with monthly and annual volumes to achieve the best overall fit;
    - simulate channel routing; and

    - simulate open-water (i.e., lake/wetland) evaporation and recharge;
- develop and calibrate the three-dimensional groundwater flow submodel (MODFLOW);
- link the submodels in GSFLOW and calibrate the integrated surface water/groundwater model;
- estimate surface water/groundwater consumptive use and represent in model;
- assess water budget elements for each subwatershed with the GSFLOW model;
- use the GSFLOW model for scenario analysis (existing and future land use and water use conditions and drought conditions);
- delineate ESGRAs using the integrated model to identify the portions of the landscape that contribute discharge to stream reaches and wetlands identified by LSRCA;
- assess the water budget and groundwater and streamflow response under a changed climate; and
- identify data and knowledge gaps for future improvements.

Additional tasks include:

- prepare interim memoranda, meeting minutes, and draft and final reports;
- present various aspects of the project to LSRCA staff and Provincial staff;
- undertake all required project management;
- transfer all digital information (including modelling files, GIS files, data files, etc.) to LSRCA staff -- this includes model set up on LSRCA staff computers and basic instructions of how to run the model; and
- populate the Provincial Water Quantity Geodatabase (in ESRI Geodatabase format) using the subwatershed results from the Tier 2 Water Budget and Stress Assessment.

This report describes the background data analysis, creation of the conceptual hydrologic and hydrogeologic models, the development and calibration of the hydrologic and groundwater submodels, development and calibration of the integrated groundwater/surface water model; the Tier 2 water budget assessment tasks including drought analysis, ESGRA delineation, and future climate assessments.

2 Background and Data Compilation

2.1 Study Area Extents

The Ramara Creeks, Whites Creek and Talbot River Subwatersheds are located in the northeast portion of the Lake Simcoe watershed (Figure 2.1). The subwatersheds are contained mainly within the Township of Ramara (a part of Simcoe County) and the City of Kawartha Lakes (formerly Victoria County). A small portion of the Whites Creek subwatershed is within the Regional Municipality of Durham. Some general properties of the subwatersheds are provided in Table 2.1.

The LSPP emphasizes a subwatershed assessment approach and, accordingly, the primary focus of this study is on the hydrology and hydrogeology of the three subwatersheds. It is important, however, to recognize that groundwater flow can cross subwatershed boundaries and that these subwatershed inflows and outflows must be quantified as part of a Tier 2 study. Accordingly, a larger area, labelled as "Model Boundary", was defined as shown in Figure 2.1, to incorporate portions of neighbouring watersheds that could potentially contribute to the study area subwatersheds. The model boundary defines the extent of the integrated groundwater and surface water flow model developed for the purpose of this Tier 2 study. The model area includes portions of catchments contributing to Balsam Lake, Dalrymple Lake, the Head River, and Lake Couchiching.

Table 2.1: Tier 2 subwatershed areas.

Subwatershed	Minimum Elevation (masl)	Maximum Elevation (masl)	Mean Elevation (masl)	Area (km^2)
Ramara Creeks	217.5	254.1	228.1	144
Whites Creek	219.3	302.3	257.4	105
Talbot River	218.6	278.6	237.3	71
Upper Talbot River	239.2	302.6	265.6	297
Total				617

The study area includes a number of lakes and canals which form part of the Trent-Severn Waterway. The lakes are tightly regulated by Parks Canada. Requests for information on operations, flows, and water levels were made but no data were provided other than what were available on the Parks Canada website (http://www.pc.gc.ca/lhn-nhs/on/trentsevern/visit/ne-wl/trent_e.asp). Other significant local features, discussed later in this report, include the Carden Plain, numerous wetland complexes, and a number of active limestone quarries.

2.2 Previous Work and Models

The LSPP was developed to build on existing work such as the Source Water Protection Program (SWPP) studies completed under the Clean Water Act (2006). A SWPP Tier 1 water budget study was conducted by LSRCA for the Lake Simcoe watershed including the Ramara Creeks, Whites Creek and the lower part of the Talbot River subwatersheds (LSRCA, 2004). The Tier 1 level assessment found that the Ramara Creeks subwatershed had a surface water stress in September. However, a Tier 2 study was not triggered as a result of Technical Rule 4. The Upper Talbot subwatershed was assessed as part of the Black-Severn Tier 1 Water Budget.

2.2.1 Groundwater Studies

As noted, several quarry operations are located in the study area. Most have had various levels of hydrologic and hydrogeologic studies done as part of their Permit to Take Water applications. Some of these site investigations have included groundwater models. In particular, Waterloo Hydrologic Incorporated (WHI, 2002) developed a local numerical groundwater model for the proposed McCarthy quarry site and Golder Associates Limited (GAL, 2007) developed a larger-scale model for the proposed Tomlinson Quarry. GAL (2004) used a simple one-layer model to analyze drawdowns near the LaFarge Brechin Quarry while others (e.g., Harden Environmental Incorporated, 2004 and Jagger Hims Limited, 1991) used analytical models.

Earth*fx* (2008) conducted a cumulative impact assessment of quarries in the study area as part of a permit application for the proposed McCarthy Quarry. Golder Associates Limited conducted another cumulative impact study of the same area in 2012 (Golder, 2012). In addition, Golder (2005) evaluated the municipal water supplies in Ramara Township as part of the North Simcoe County municipal groundwater study.

The current study integrated the principal findings of the previous hydrogeologic and modelling investigations with additional hydrogeologic data collected by Earth*fx* to develop the conceptual and numerical models used in this study. As part of this effort, available reports and maps, which included wellfield investigations, permit applications, annual monitoring reports from quarries, and numerous spreadsheets and data files (supplied by LSRCA or the quarry operators), were compiled and reviewed by Earth*fx* staff. Electronic copies of reports were added to the database created for this study. Paper copies of reports and maps were scanned and also added to the database. The reports were “mined” for additional information including new (i.e., not previously added to the project database), test pits, geotechnical boreholes, wells, aquifer tests, observed water levels and flows, and geologic logs. Quality assurance was done on the locations and the observation data before the information was added. Data were also extracted from Water Well Information System (WWIS) database maintained by the Ontario Ministry of Environment. A map of borehole locations, identified by type, is shown in Figure 2.2.

2.2.2 Surface Water Studies

Earth*fx* Incorporated conducted a regional-scale assessment of the water balance in the Lake Simcoe basin (Earth*fx*, 2010). The study used an earlier version of the U.S. Geological Survey’s Precipitation-Runoff Modelling System (PRMS) (Leavesley *et al.*, 1986) to estimate rainfall, runoff, evapotranspiration, and groundwater recharge.

Other hydrology studies, completed for the purpose of flood plain mapping, cover parts of the Tier 2 study area. For example, Cole Engineering (Cole, 2013) prepared a hydrologic model for the Orillia Creeks and Talbot River watersheds using the Visual OTTHYMO code. Results were used to establish peak flows within the watersheds and generate the flood line mapping. Design storms with 2, 5, 10, 25, 50, and 100 year return periods and the Regional storm (Hurricane Hazel) were analyzed. The model was not calibrated directly to observed streamflow data from the Trent-Severn Waterway at Gamesbridge, but favourable comparisons were obtained to these flows and flows from other streams draining to Lake Simcoe. The study found that routing through the system of canals and dams within the Talbot River watershed, along with natural storage in the form of lakes and wetlands, helps attenuate peak flows compared to other watersheds. Little change was noted in peak flows between the existing and future conditions due to the limited development forecast to take place in the Talbot River watershed.

MMM Group (2008) conducted a hydrologic investigation of the Pefferlaw River, Uxbridge Brook, Beaver River, Whites Creek, and Beaverton Creek watersheds also using the Visual OTTHYMO

code. The study updated previous (1980) modelling results. The model was calibrated primarily to event data for the Beaver River. There was no streamflow gauge for Whites Creek at the time of the MMM study (a gauge was established by LSRCA in 2005).

Streamflow models were constructed by LSRCA for some streams in the study area using model codes developed by the U.S. Army Corps of Engineers Hydrologic Engineering Center (HEC). A HEC-RAS hydraulics model was developed in 2012 for the Talbot River. Canal data were provided by the Trent-Severn Waterway and Talbot River data were supplied by Cole Engineering. The model data sets were provided to Earth*fx* by LSRCA. A HEC-2 water surface profile model was developed for flood line mapping along Whites Creek. The model files were also provided to Earth*fx* by LSRCA.

2.1 Key Technical Issues

Some key technical issues were identified at the outset of this study. These include:

Tunnel Channel Geologic Control on Wetland Features: A key objective of this study is to relate recharge and the groundwater flow system to the ecological features. A dominant characteristic of the sub-watersheds is that they are dissected by a series of northeast–southwest trending tunnel valleys. These valleys were formed by sub-glacial processes that in many cases eroded deep into the bedrock. The tunnel valleys were subsequently partly in-filled with sediments and today many of the lowland portions of the valleys are now wetlands and lakes (e.g., Canal Lake). The hydrogeologic model will represent these valleys and the bedrock aquifers, such as the green marker bed zone, that subcrop and discharge into the tunnel valley aquifers.

Alvar Plain Recharge: Much of the Talbot River watershed is a low relief topographic plain referred to as the Carden Plain alvar and characterized by very thin drift on weathered bedrock. The exposed bedrock exhibits a high contrast, with both open fractures and low permeability blocks (shown in Figure 2.3). Quantifying the recharge in these areas is important for the understanding the water budget in the Upper Talbot River subwatershed.

Cumulative Impact of Quarry Operations: As noted, earlier efforts by Earth*fx* and others attempted to address the cumulative impact of multiple quarry operations in the Talbot watershed. Our approach then was to develop a single model that encompassed all the quarry areas. This will be expanded on with the integrated groundwater/surface water model and will consider current conditions as well as future expansion of the quarries. The ability to model future conditions will depend strongly on the amount of information supplied by the quarry operators.

Limited Stream Gauging and Trent-Severn Waterway Operations: The limited stream gauging in the study area is a significant issue that will limit the degree of model calibration that can possibly be achieved. Efforts will be made to collect all short term flow records from temporary gauges at quarries, from LSRCA gauges, and from the Trent-Severn Waterway to make up for the lack of permanent Environment Canada gauges. Water level management in the lakes that feed the TSW and the scheduling of releases to the Talbot River can be represented in the model but requires data from Parks Canada. As was noted earlier, no data were provided by Parks Canada other than what were available on their website.

Wetlands: Storage of water in wetlands can be significant on both a seasonal and longer-term basis. The integrated model represents the transient behaviour of the streams and wetlands under a variety of climate and drought conditions and considers the stage-dependent interaction with the groundwater system. Full representation of wetlands and reservoirs was necessary to simulate where and when the streams and wetlands gain and lose flow to the aquifers and how those losses help sustain groundwater takings and streamflow under drought conditions.

2.2 Figures

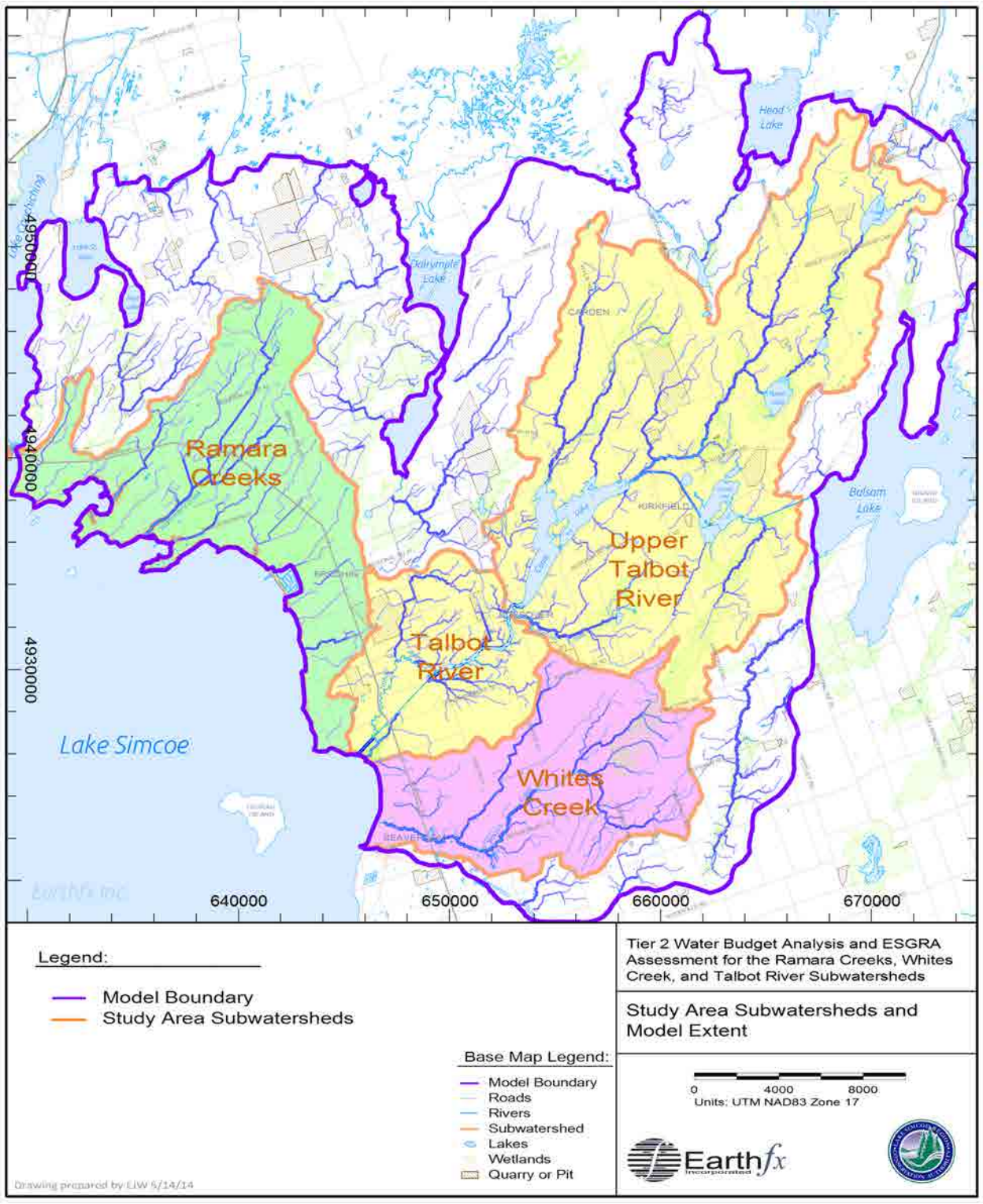

Figure 2.1: Location of the Ramara Creeks, Whites Creek, and Talbot River subwatersheds and the model extent.

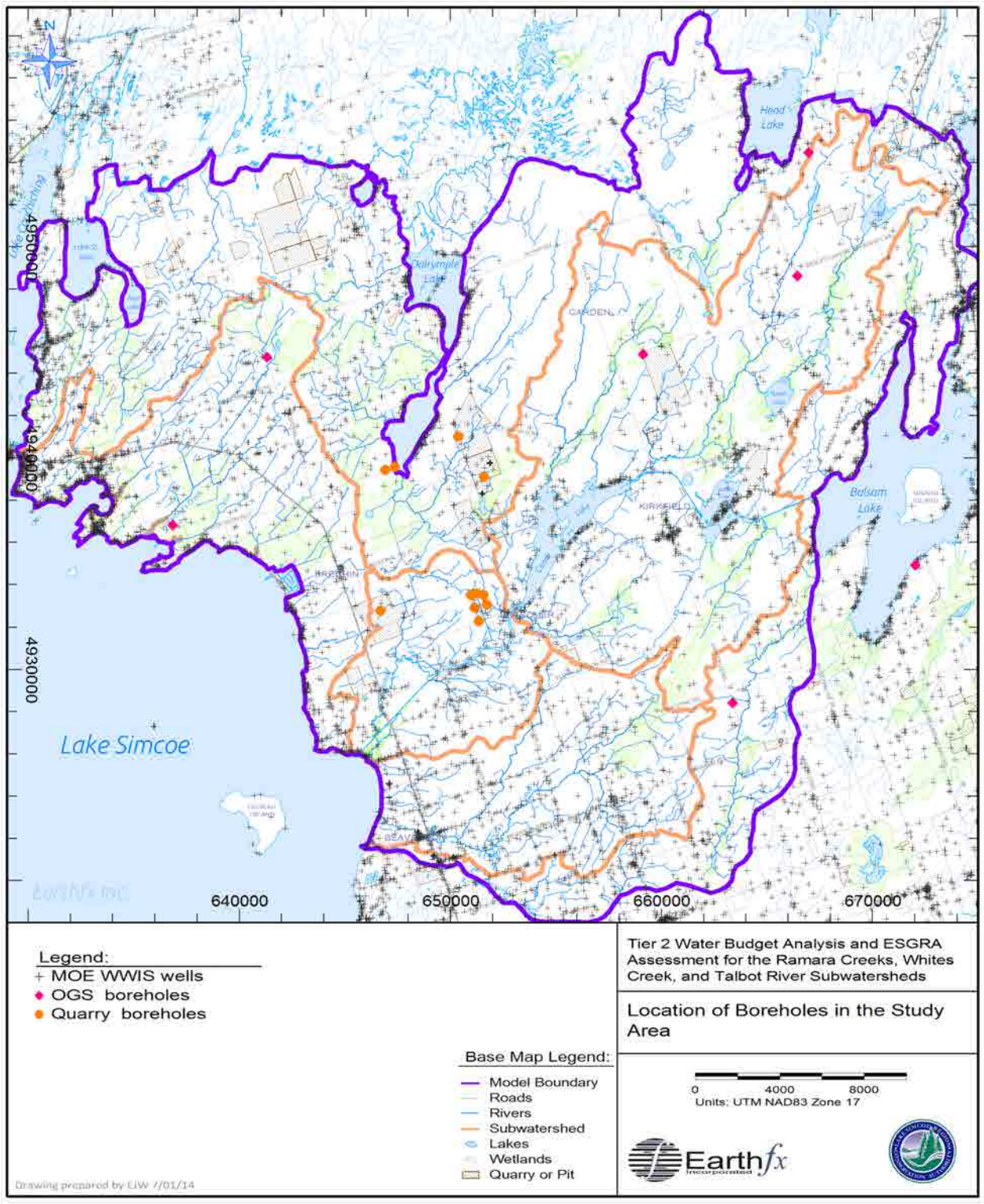

Figure 2.2: Boreholes in the study area.

Figure 2.3: Karst topography formed by solutional weathering of limestone pavement, typical of Carden Plain physiographic region.

3 Geologic Setting

3.1 Introduction

The physical setting, including the topography, physiography, and geologic setting of the study area, is presented here to provide a context for discussions and development of the conceptual and numerical models.

3.2 Topography and Physiography

Land surface topography based on a 5-metre digital elevation model (DEM) is shown in Figure 3.6. In general, the study area has low topographic relief with maximum elevations of 304 masl just north of the Talbot River subwatershed and elevations of 217 masl at Lake Simcoe. As noted, much of the relief within the subwatersheds is due to the parallel sets of northeast–southwest trending tunnel valleys which strongly influence drainage patterns.

The study area watersheds lie mainly within the Carden Plain and Simcoe Lowlands physiographic regions of Chapman and Putnam (1984, 2007) with a small section of the southeastern part of the area in the Peterborough Drumlin Field (Figure 3.7). The extended model area takes in more of the Carden Plain and the Peterborough Drumlin Field. The Georgian Bay Fringe lies north of the Precambrian-Paleozoic contact, and is characterized by shallow soils and exposed Precambrian bedrock, with numerous swamps and wetlands occupying the bedrock basins (illustrated in Figure 3.1). Relief is quite subdued in the area with the lowest elevation at 219 metres above sea level (masl) along the Lake Simcoe shoreline and maximum elevation of about 300 masl east of the hamlet of Argyle, near Kirkfield, and east of Head Lake. The land rises gently from west to east.

Figure 3.1: Shallow soils and exposed Precambrian bedrock, characteristic of Georgian Bay Fringe region to the north of the study area.

The Simcoe Lowlands part of the study area is characterized by clay plain punctuated with numerous drumlins and tract of organic deposits in poorly-drained areas. Lacustrine sand plains are common in low lying areas. A small moraine ridge known as the Simcoe Moraine strikes southeasterly across the western part of the study area. The extensive Carden Plain area has flat to gently undulating topography and is characterized by bare to very thinly soil-covered limestone. This type of landscape is known as alvar. The Peterborough Drumlin field is an extensive till plain with numerous northeast-southwest oriented drumlins. There are several shallow, south- to southwest-trending valleys in the eastern part of the study area that are not shown on Chapman and Putnam's map (2007; *see* discussion of tunnel channels below).

3.3 Conceptual Stratigraphic Model

The geology of the Ramara-Whites-Talbot area and the surrounding region consists of Quaternary sediments of variable thickness overlying a gently southward dipping sequence of Middle Ordovician carbonate and clastic sedimentary rocks. The Ordovician sedimentary rocks lie unconformably on a basement of Precambrian igneous and metamorphic rocks which are part of the Central Gneiss Belt (CGB) and Central Metasedimentary Belt (CMB) of the Proterozoic Grenville Structural Province (Easton, 1992). Bedrock geology for the study area is shown in Figure 3.8.

3.3.1 Bedrock Geology

Precambrian Geology: Precambrian igneous and metamorphic rocks outcrop extensively north of the study area and form a basement to younger, relatively undeformed Paleozoic sedimentary rocks in the model area. The Precambrian rocks are part of the Grenville Structural Province of the Canadian Shield and are Middle Proterozoic – about 1.6 to 1.0 billion years before present - in age (Easton, 1992). The Grenville Province in this region is divided into two major subdivisions: the Central Gneiss Belt in the western and central parts of the area and the Central Metasedimentary Belt in the east. This part of the CGB is known as the Fishog Domain and is characterized by metaplutonic rocks and metasedimentary gneisses and migmatites of medium to high metamorphic rank. CMB rocks outcrop east of Head Lake and include marble, clastic metasedimentary rocks, and felsic plutonic rocks. The Central Metasedimentary Belt Boundary Zone (CMBBZ) is a south to southwesterly striking zone which separates the rocks of the CGB and CMB and consists mainly of tectonites, rocks that have been tectonically and cataclastically disrupted and deformed (Easton, 1992). The Precambrian geology of the region appears on the map compiled for the Geology of Ontario volume (OGS, 1992, 2011).

Within the study there are several inliers of Precambrian rock, high points on the Precambrian bedrock surface that pierce through the younger Paleozoic cover rocks. Notable inliers include a Precambrian outcrop west of Sebright, an outcrop northeast of Dalrymple Lake and the Rohallion inlier, a knoll of outcropping granitic gneiss near the north end of Canal Lake. In the subsurface, "granite" has been reported in numerous water well records but only the logs from boreholes drilled by the OGS in 1993 have adequate descriptions of the Precambrian basement rocks encountered during drilling (see Armstrong, 1999). Generally, the OGS reported felsic to intermediate gneiss in the western and central parts of the area (CGB) with pegmatite noted in the central part of the area. Amphibolite, brecciated gneiss, pegmatite and felsic gneiss appear in the logs for holes drilled in the eastern part of the study area and further east (CMB).

The OGS logs also note varying degrees of weathering in the Precambrian rocks, weathering that must have taken place before the deposition of the Ordovician sedimentary rocks. Di Prisco and Springer (1991) observed that paleoweathering at the Precambrian-Paleozoic unconformity in

southern Ontario can exhibit a variety of features, such as red hematite mineralization, textured surfaces, endokarstic dissolution features, and residual soils. In their study area, which ranged along the Precambrian-Paleozoic contact in the Central Metasedimentary Belt from Bobcaygeon to the Tweed area and included Paleozoic outliers, Di Prisco and Springer (1991) found well developed paleosols (ancient soil profiles) on Precambrian rocks overlain by Paleozoic rocks at two sites - their locality 1, with Precambrian slate, and 12, with Precambrian amphibolite. They also found paleosols on CMB rocks at several sites without Paleozoic cover. The weathering noted in the OGS borehole logs in the present study area ranges from visible hematite staining to the presence of 35 centimetres of regolith (unconsolidated rock fragments and mineral grains). Signs of weathering were absent in a few of the OGS boreholes. The reported zones of paleoweathering are up to about 2.5 metres thick.

Paleozoic Geology: The Precambrian rocks are overlain unconformably by a sequence of Middle Ordovician marine sedimentary rocks. East-west trending subcrop belts of progressively younger Ordovician units occur as one moves southward through the area, as depicted on the OGS compilation map of southern Ontario Paleozoic geology (Armstrong and Dodge, 2007) and in Figure 3.8. The regional Paleozoic geology is well described by Armstrong (2000), from which the following descriptions have largely been adapted. It should be noted that the transitions between the Ordovician units are considered gradational.

At the base of the Ordovician sequence is a predominantly clastic unit, the Shadow Lake Formation, made up of sandstone, siltstone, and shale with minor dolostone, and which can be up to about 9 m thick. It is thought to be the product of sedimentation in a supratidal environment (Johnson *et al*., 1992). This unit weathers readily and has only limited outcrop in the study area. Thickness of this unit in the OGS boreholes ranges from 1.63 to 9.15 m.

The Shadow Lake Formation is conformably overlain by the micritic to fine-grained limestones of Gull River Formation, which Armstrong (2000) has informally divided into two members. The lower member is up to 14 m thick and the upper member has a maximum thickness of about 10 m. One feature at the top of the lower member of the Gull River Formation is the ‘green marker bed’ – a distinctive 1.5 m thick bed of uniform, light green argillaceous dolomitic limestone – at the top of the lower member (Armstrong, 2000) that has been considered an aquifer in earlier hydrogeologic studies. All three members can be seen along the Monck Road cut, near Head Lake (shown in Figure 3.2). The depositional environment was probably tidal flat to shallow subtidal lagoon. The unit has a fairly extensive subcrop belt across the northern part of the study area (Figure 3.8).

Figure 3.2: Exposed upper and lower members of the Gull River separated by interpreted green marker beds (top of tape), Monck Rd cut near Head Lake.

The next unit in the sequence is the Bobcaygeon Formation, which is composed of coarser-grained and more fossiliferous limestones than the underlying Gull River Formation. The depositional environment ranged from shoal to shallow marine shelf. This unit is subdivided into three members. The lower member has very fine- to fine-grained limestones in its lower part (known as the Moore Hill beds) and fine- to coarse-grained fossiliferous limestone in the upper part. The middle member is generally more argillaceous than the other two members and is characterized by fine- to medium-grained limestone interbedded with shale. The upper member is fossiliferous, fine- to coarse-grained limestone with shaly partings and a few thin shale beds. Locally, in the Moore Hill beds and in the upper member, there are thin clayey shale beds that appear to be K-bentonites and are correlative with two widespread volcanic ash beds that were products of activity during the Taconic Orogeny (mountain-building episode) in the Appalachian tectonic belt (Armstrong, 2000). Low, mainly northerly- or easterly-facing questas are common in areas where the Bobcaygeon and Gull River formations outcrop.

Overlying the Bobcaygeon Formation is the Verulam Formation, which ranges from 45 to 60 m thick and is divided into two informal members. The lower member is mainly calcareous shale interbedded with limestones that range from micritic mudstones to coarse-grained packstones and grainstones. The upper member is generally less than 10 m thick and consists of coarse-grained limestones, which are commonly cross bedded. The Verulam Formation has a broad subcrop belt across the southern part of the study area, but, because of the high shale content, it weathers easily and only the upper member forms good outcrops. An exception is along road cuts, such as along the Kirkfield Road cut south of Kirkfield (Figure 3.3), where the interbedded shale and limestones are exposed.

Figure 3.3: Interbedded shale and limestone of the Verulam Formation, Kirkfield Road cut.

The Lindsay Formation is the youngest bedrock unit in the study area and subcrops in the southern part of the Whites Creek watershed. The unnamed lower member consists of argillaceous, micritic to coarse-grained, fossiliferous limestone with a distinctly nodular appearance (Johnson *et al*., 1992), although locally it can be interbedded limestone and shale. The upper member is not present in the study area.

Karst: Karst features are formed through the dissolution of rock by aqueous solutions (i.e., rainwater with dissolved CO_2) and typically develop on carbonate rocks (e.g., limestone, dolostone, and marble) but can also include dissolution of gypsum and rock salt. Mature karst landscapes have features such as sink holes, blind valleys, well-developed underground drainage systems, and few or no surface streams (Brunton and Dodge, 2008). Even areas of 'juvenile karst' have solutionally-enlarged joints that are pathways for water movement. Brunton and Dodge (2008) consider the Carden Plain to be one of the key karst regions of southern Ontario and discuss the importance of the stratigraphic interval containing the Lower Bobcaygeon-Upper Gull River contact, but do not discuss any caves or other significant karst features in the present study area. Brunton (Frank Brunton, OGS geologist, personal communication, 2013) has said that the Gull River and Bobcaygeon formations are susceptible to karst processes because of the relative lack of shale in these units. The Verulam and Lindsay formations contain too much shale for significant karst development, however. Of the known karst features in the present study area, joints enlarged by solution (also known as grikes) are probably the most important and extensive and have been observed in both the Gull River and Bobcaygeon formations and at one outcrop of the fairly shale-free upper member of the Verulam Formation. Solutionally–enlarged bedding planes are possibly also significant. In a regional study of joint orientation and the relationship of joints in Paleozoic and Precambrian terrains, Andjelkovic *et al.* (1996) found that the Carden Plain area had a major joint set with a mean trajectory of 25^{o} (range of 0^{o} to 69^{o}), with a secondary set at 80^{o} and a minor set at 128^{o}. However, they did not publish any information about joint spacing, depth, or evidence of solutional enlargement.

3.3.2 Quaternary Geology

Like all of southern Ontario, the Ramara-Whites-Talbot area was repeatedly glaciated during the Pleistocene Epoch, although locally there is only clear evidence for glacial activity during the Wisconsinan glacial episode, the final major glacial episode. Regionally, sediments of Quaternary age form a blanket of unlithified deposits on the bedrock surface. Most of these sediments were deposited either directly from glacier ice, in meltwater streams, or in ice-marginal or ice-dammed lakes. Quaternary sediments in much of the area, as mentioned above, are thin to absent; the surficial geological mapping (OGS, 2010) shows extensive areas of either bare rock or thin soil over bedrock. Quaternary sediments are thicker in the western and southern parts of the area. Glacial ice movement in the area was out of the northeast, as indicated by drumlin orientation and glacial striations on the bedrock. The study area was probably occupied by ice for most of the Late Wisconsinan (also called the Michigan Subepisode). Quaternary mapping for the area includes the work of Barnett and Mate (1998) and Finamore and Bajc (1983 and 1984), all of which is included on the digital compilation map of southern Ontario Quaternary geology (OGS, 2010). Quaternary geology mapping for the study area is shown in Figure 3.9.

The regional surface till is a sandy silt to stony, gritty silty sand diamicton (Finamore and Bajc, 1983, 1984) that the OGS (2010) correlates with the Newmarket Till. This till is typically compact and fissile and clast content is about 10 percent. It outcrops and subcrops extensively in the southern and western parts of the study area. There are a number of narrow, elongated, southwest-trending drumlins developed on this till unit, which are clearly visible on the digital elevation model (Figure 3.6) and, as mentioned above, are depicted on the map of physiography (Figure 3.7).

Another till or till-like sediment is present in the eastern part of the study area and referred to as the Dummer moraine of Chapman and Putnam (1984). This till is described by Finamore and Bajc (1983) as extremely stony with angular clasts ranging from pebbles to large boulders in a sandy matrix. The clasts are overwhelmingly of Paleozoic origin; there are typically less than two percent Precambrian clasts. The exact stratigraphic relationship between this 'Dummer Till' and the Newmarket Till is unclear. Finamore (1982) has observed the bouldery Dummer Till overlain by the typical lodgement till (Newmarket Till?) at several exposures within the Dummer moraine and has suggested that they are facies of the same till sheet. The mapped relationship of the two tills,

particularly with respect to interpreted tunnel channels (see below), suggests that, in the present study area, the Dummer till is generally younger than the Newmarket Till.

Late in the Wisconsinan, possibly during the Mackinaw Phase, there were widespread, vigorous subglacial drainage events in south-central Ontario that produced a network of erosional channels known as tunnel channels (or tunnel valleys; Barnett, 1992). In areas with thick unlithified surficial deposits, such as the Oro Moraine area (west of Lake Simcoe), these channels were deeply incised and then partly filled by fluvial sediments deposited as flow in the channels waned. However, in the present study area, the drift is rather thin and the tunnel channels are cut into bedrock. These channels are relatively shallow – from 5 to 20 m deep, trend south-southwest, and range from less than 500 m to more than 2.5 km wide. They were interpreted initially using the 10-m DEM but this interpretation was later refined using the interpolated bedrock surface. Tunnel channels cannot be traced very far onto the Precambrian terrain north of the study area. This reflects the contrast between the relatively soft Ordovician limestones and shales and the tougher, crystalline metamorphic rocks of the Shield. The abrasive material – mainly quartz sand – which the fast-flowing water used to cut the channels was derived from the Shield. Fluvial channel fill sediments are very limited in the study area but within many of the tunnel channels there are local till deposits – both Newmarket Till and Dummer till - as well as glaciofluvial sediments, glaciolacustrine deposits, and modern organic deposits. These sediments were deposited after the erosion of the channels.

Ice-contact stratified deposits developed in the waning stages of glaciation, when meltwater streams either on or within the glacier deposited bodies of sand and gravel. There are a number of southwest-trending eskers and kame terraces in the area. Many of the kame terraces are associated with tunnel channels which probably contained local residual ice during deglaciation. The tunnel channel deposits, ice-contact stratified, and esker deposits were all included within the “Mackinaw Interstadial (MIS) deposits” for this study.

As the Late Wisconsinan ice receded, much of the area was inundated by the waters of Early Glacial Lake Algonquin, the first in a series of major postglacial lakes in the region. Part of the study area may have been affected earlier during the Mackinaw Phase by a major ice-dammed lake (*see* Barnett, 1992, Figure 21.56d). Glacial sedimentation in postglacial lakes produced fine-grained deposits of silt and clay and coarser shallow water deposits of sand. Beach deposits of gravel and sand developed where wave action reworked older sediments. At one stage, Lake Algonquin was controlled by an outlet at Kirkfield (*see* Chapman and Putnam, 1984; Barnett, 1992) with drainage through what is now the Trent River system to the Lake Ontario basin.

Sediments of Recent age are mainly in the form of organic deposits, which are common, particularly in the western part of the area, where they overlie glaciolacustrine silt and clay deposits and in tunnel channel valleys in the east. The glaciolacustrine silts and clays are less conductive than the overlying organics, as evidenced by seepage observed at the contact between these two materials (illustrated in Figure 3.4). An extensive area of silt and fine sand in the Bolsover area is considered Recent in age and was probably deposited in a non-glacial lake that was a precursor to modern Lake Simcoe (Barnett, 1997).

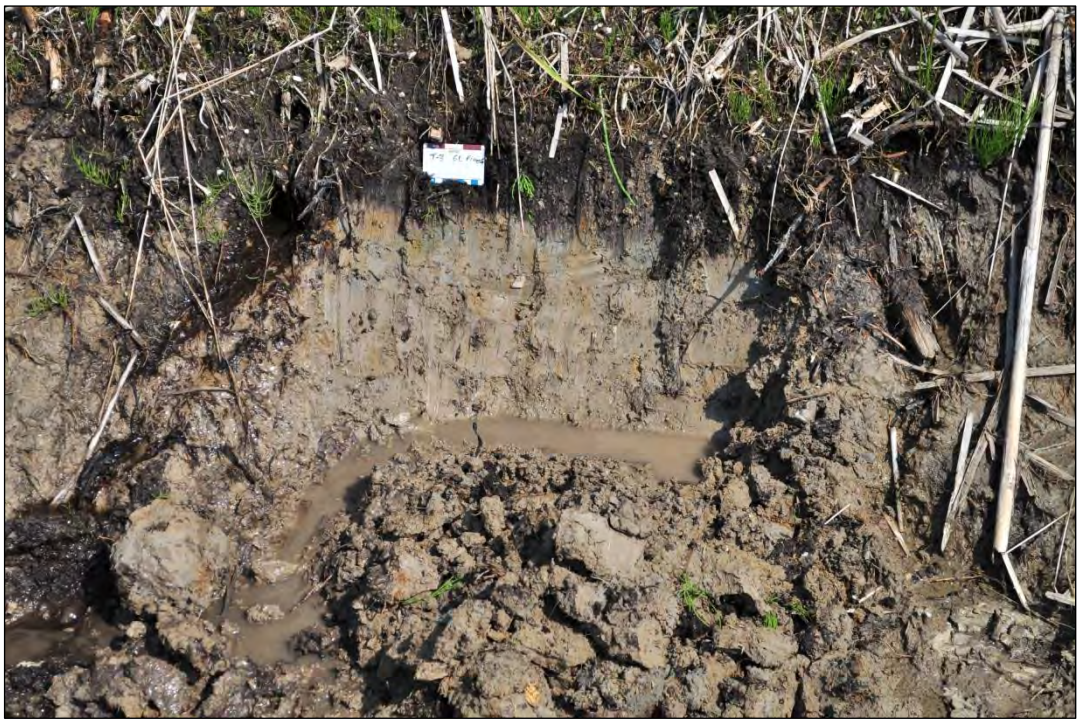

Figure 3.4: Glaciolacustrine silt and clay deposits overlain by organic materials, roadside ditch on Highway 12.

3.4 Stratigraphic Model Layers

A conceptual model of the Quaternary geology was developed based on the information discussed above supplemented with borehole data. The model consists of five units. Unit 1 is the uppermost and includes Recent organic deposits and lacustrine sediments and late postglacial glaciolacustrine sands and fine-grained deposits. Unit 2 takes in ice-contact stratified deposits of glaciofluvial sand and gravel. Unit 3 is the very stony Dummer Till, which is present mainly in the extreme eastern part of the study area. Unit 4 is the regionally-extensive Newmarket Till. Unit 5 is the lowest unit in the Quaternary sequence and consists mainly of lacustrine (or glaciolacustrine) sand, silt and clay.

The conceptual model for the bedrock consists of 9 additional units. Only the Gull River Formation is subdivided. Unit 6 is the Lindsay Formation and represents the uppermost bedrock unit. Unit 7 is the Verulam Formation and Unit 8 is the Bobcaygeon Formation. Units 9, 10 and 11 represent the upper Gull River Formation, the 'green marker bed', and the remainder of the lower Gull River Formation, respectively. Unit 12 is the Shadow Lake Formation and forms the base of the Paleozoic sequence. Unit 13 is the thin, discontinuous weathered horizon at the top of the unsubdivided Precambrian rocks. Unit 14 consists of unweathered Precambrian rocks.

A schematic of the proposed conceptual model in presented in the following sketch (Figure 3.5). A three-dimensional representation of the conceptual stratigraphic model was created by mapping the tops of each geologic unit and then overlaying them. This process is described in the next section.

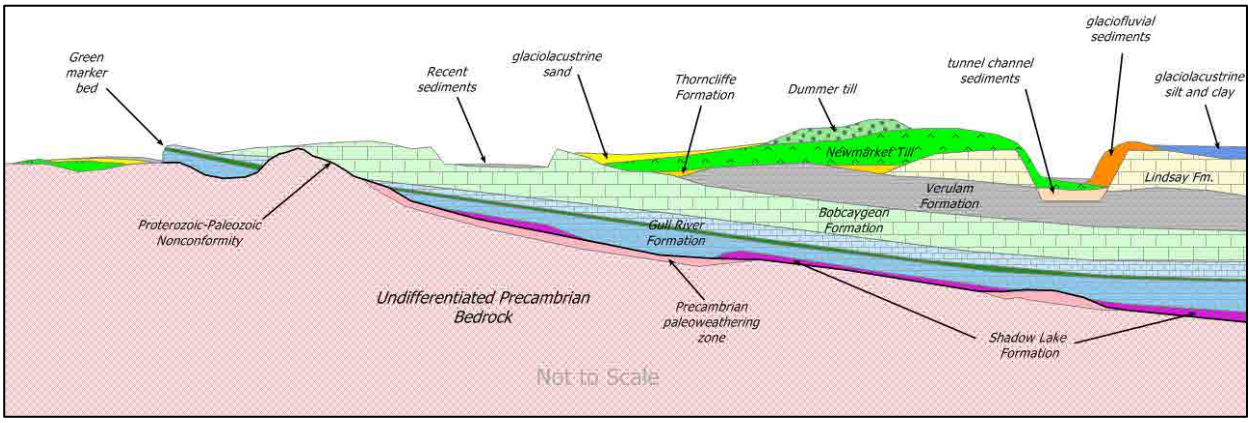

Figure 3.5: Conceptual sketch of proposed geologic model.

3.4.1 Three-dimensional Stratigraphic Model Construction

Tops of the overburden units were determined by inspecting lithologic logs from the MOE WWIS database, quarry monitoring wells, and high-quality boreholes drilled by the Ontario Geological Survey. The tops of bedrock units are also described in the oil and gas well database compiled by the Ontario Ministry of Natural Resources. The geologic "picks" were then interpolated using a geostatistical technique known as “kriging” to form provisional surfaces. For some units, such as the Shadow Lake Formation, the thickness of the unit was interpolated (rather than the top elevations) and grid algebra was then used to either add it to the top of the next unit down or subtract it from the overlying unit to calculate a ‘top surface’. The mapped extents of outcrop/subcrop areas were used to constrain many of the units.

Geologic picks also included wells where the formation was absent (assigning an elevation based on the top of the underlying unit) and wells where the base of the unit was known to be below the base of the well (push-down points). Post-processing of the layers was conducted to identify areas where the surfaces crossed (a common occurrence where data are sparse) or the interpolation did not appear correct. The surfaces were corrected where needed. The interpolation was also corrected where the units exceeded land surface elevations. The bedrock surface was adjusted to reflect the depth of excavations at the time the DEM was compiled.

Figure 3.10 through Figure 3.18 show the final interpolated tops and isopachs for the overburden units. The total overburden thickness, in metres, is shown in Figure 3.19. Figure 3.20 shows the top of the Lindsay formation, where present, and the top of the uppermost bedrock unit elsewhere. In addition to naturally occurring valleys and scour features in the bedrock, the pits and quarries represent additional, anthropogenic, topographic low points in the bedrock surface. Figure 3.21 shows the thickness of the Lindsay Formation which is present only in the southern part of the study area. Figure 3.22 through Figure 3.34 show the final interpolated tops and isopachs for the other bedrock units. As can be seen, many of the units are not continuous throughout the study area. The top elevations shown for the unit outside of the area where it is present represents the elevation of the next underlying unit. Locations of the wells used in defining the top surfaces are shown in the figures.

The three-dimensional nature of the conceptual stratigraphic model is most easily viewed in cross sections through the study area. The locations of two cross-section lines are shown in Figure 3.34, while the sections are shown in Figure 3.35 and Figure 3.36.

The conceptual geologic model provided the framework for identifying the major aquifers and aquitards underlying the study area. Construction of the hydrostratigraphic model for the study area is described further on in Section 5.

3.5 Figures

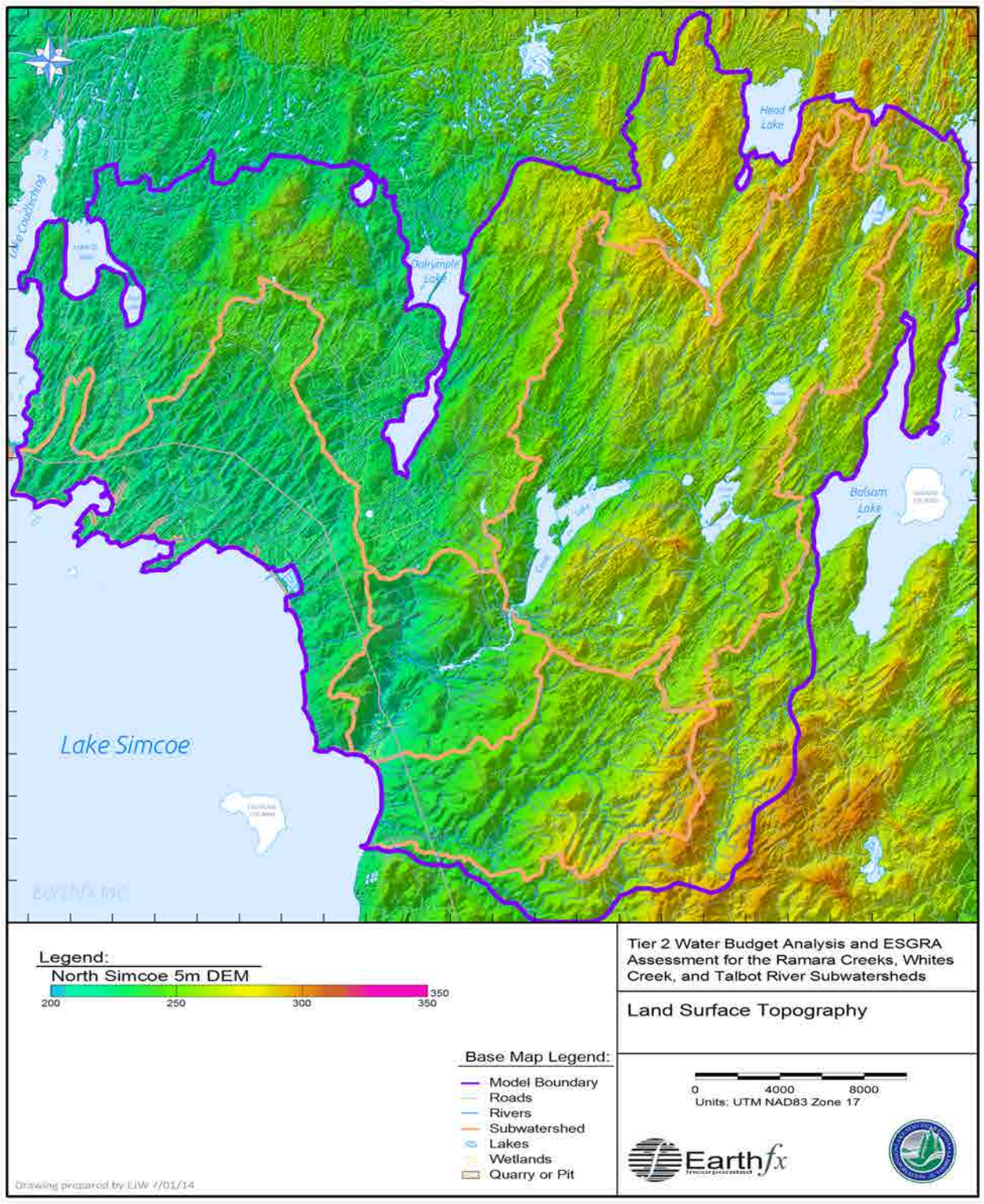

Figure 3.6: Land surface topography from the 5-m digital elevation model.

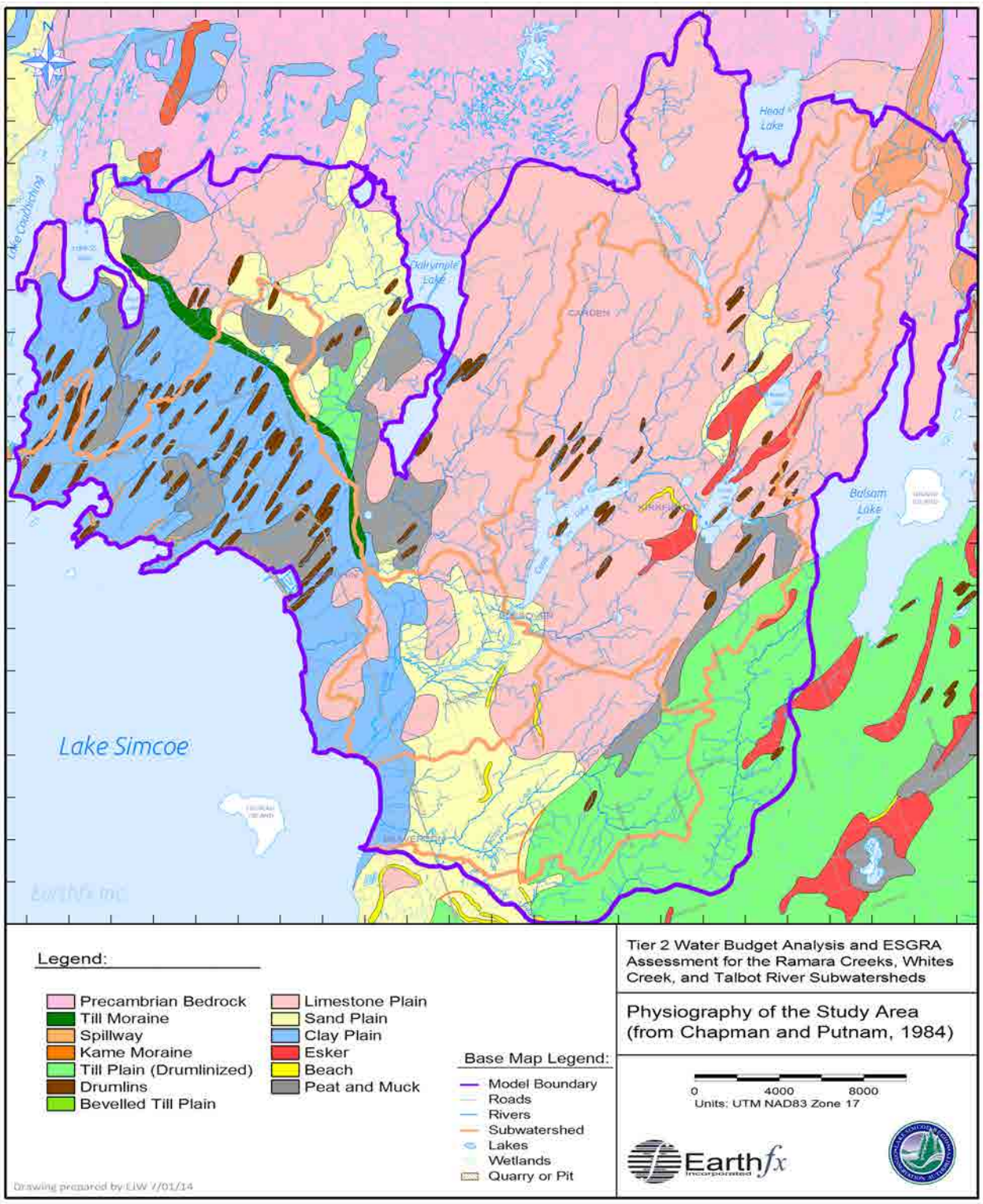

Figure 3.7: Physiographic units in the study area (from Chapman and Putnam, 1984, 2007).

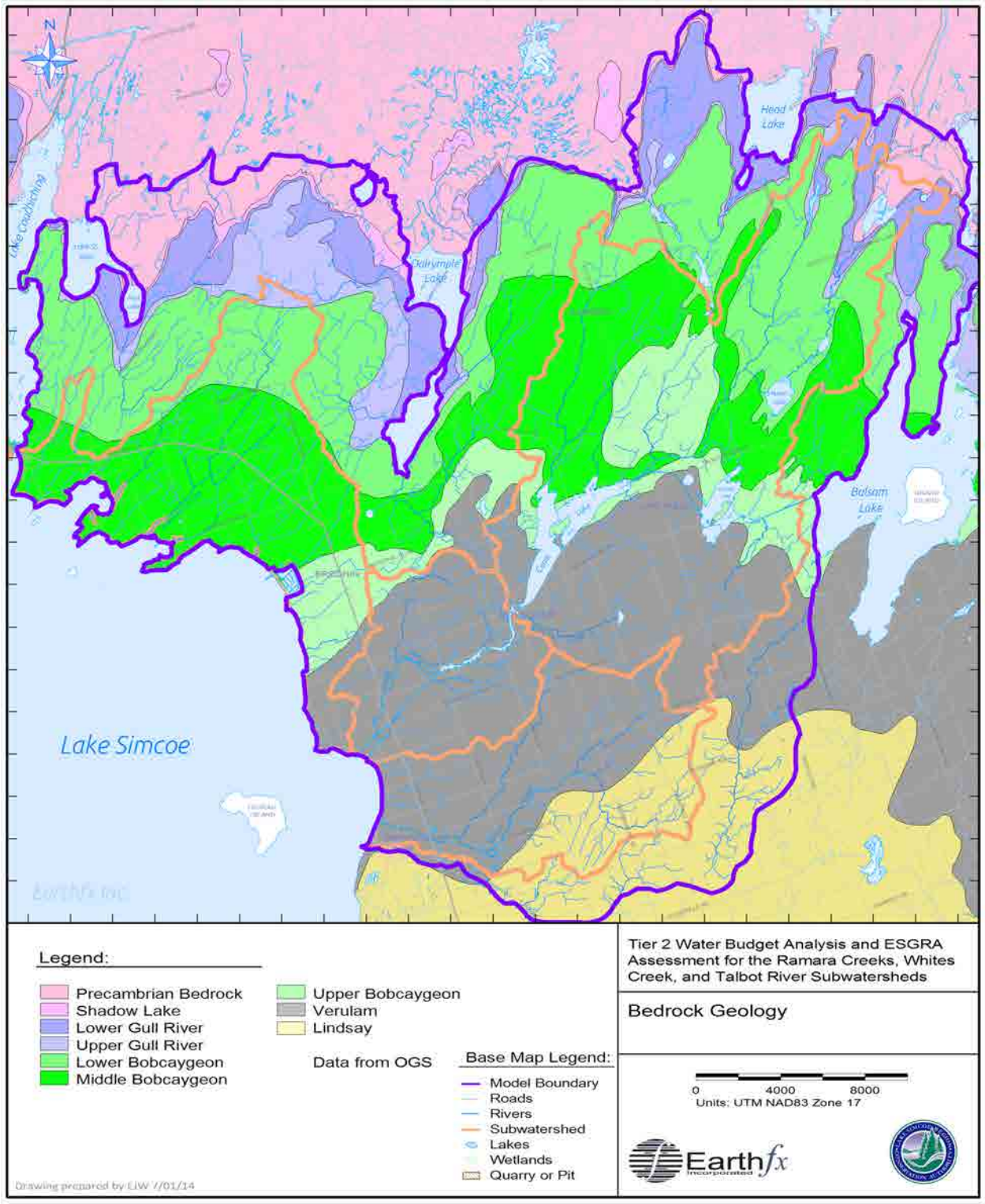

Figure 3.8: Bedrock geology for the study area (data from OGS, 2007, 2011).

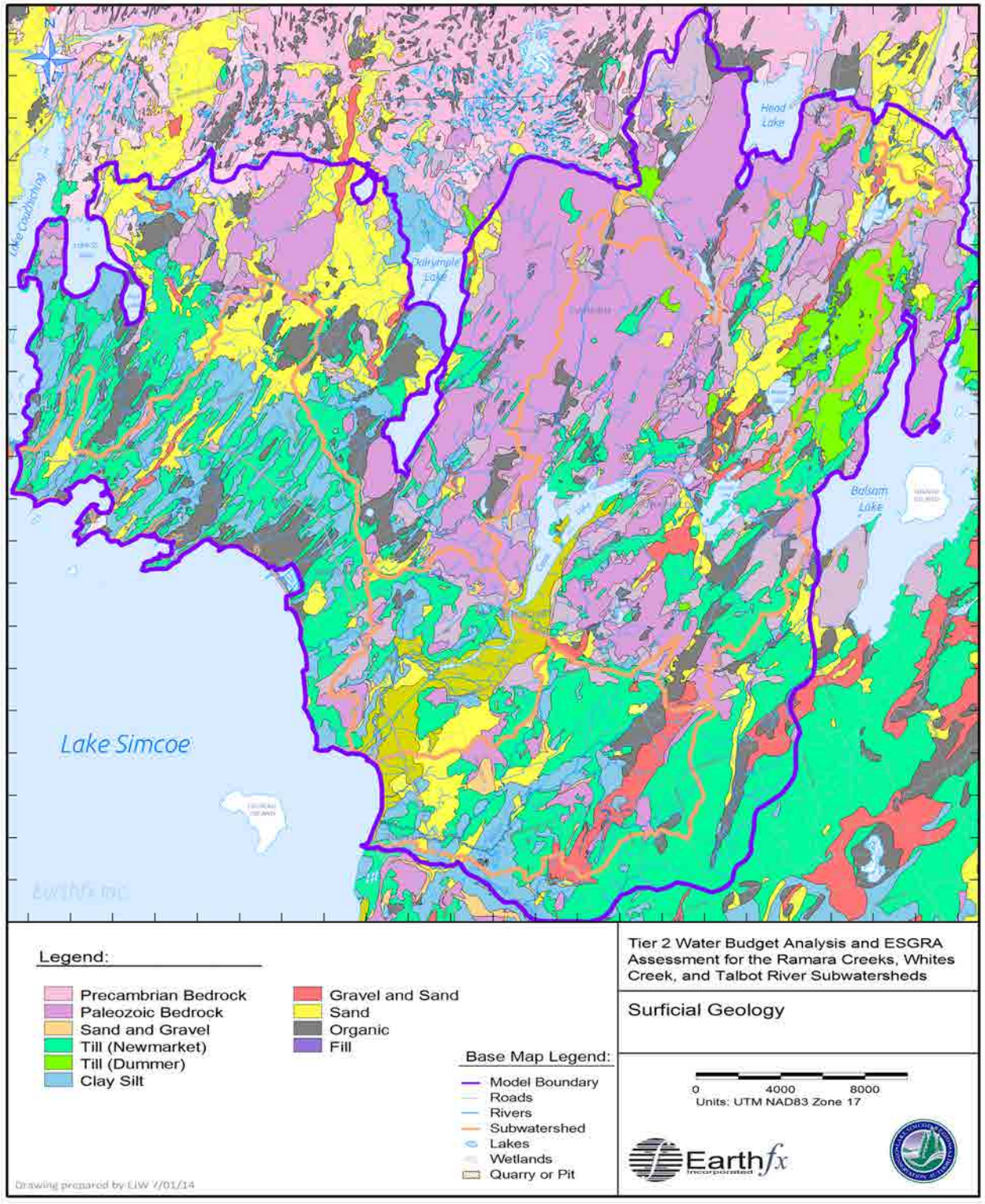

Figure 3.9: Surficial geology for the study area (data from OGS, 2010).

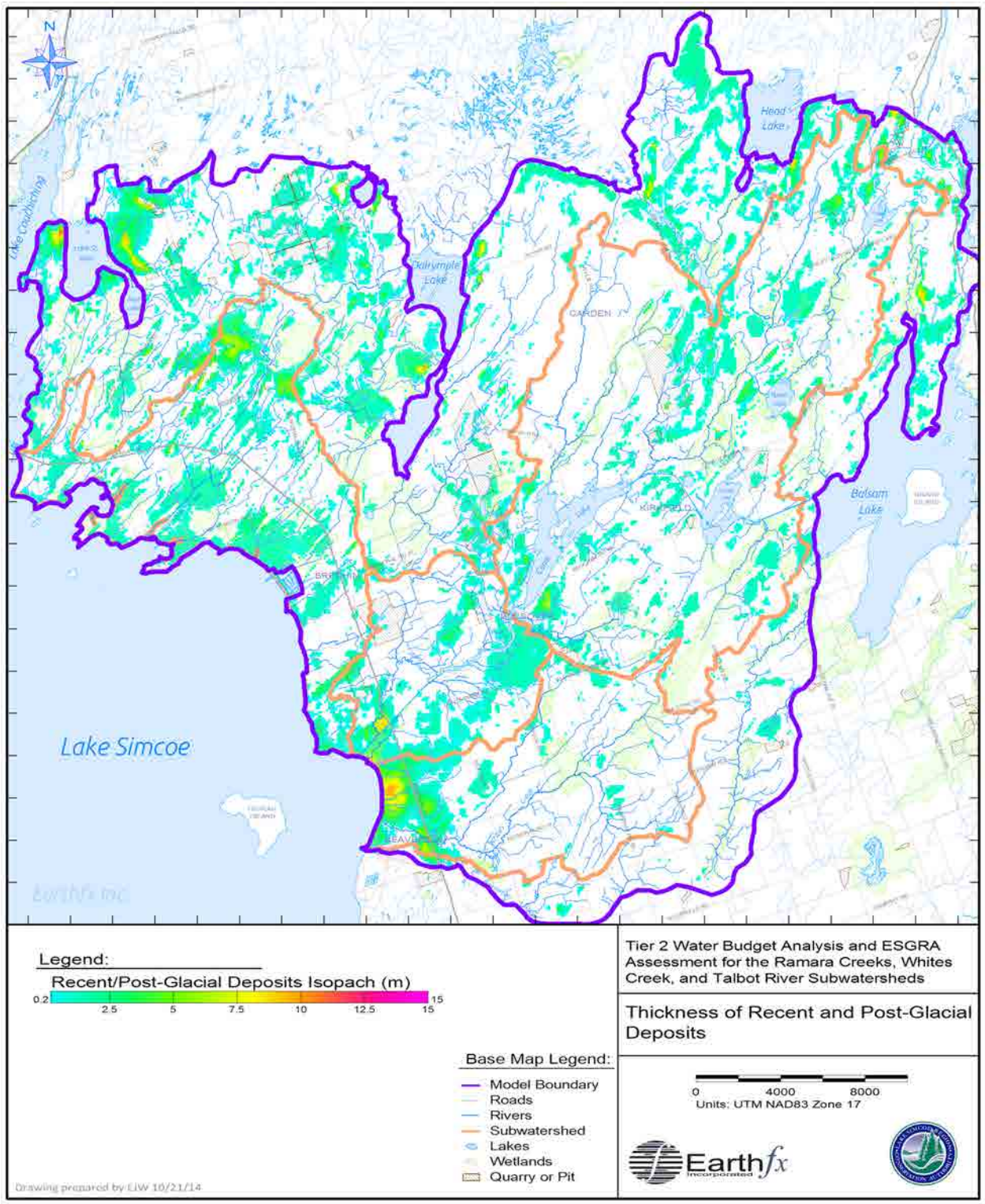

Figure 3.10: Thickness of Recent and post-glacial deposits, in metres.

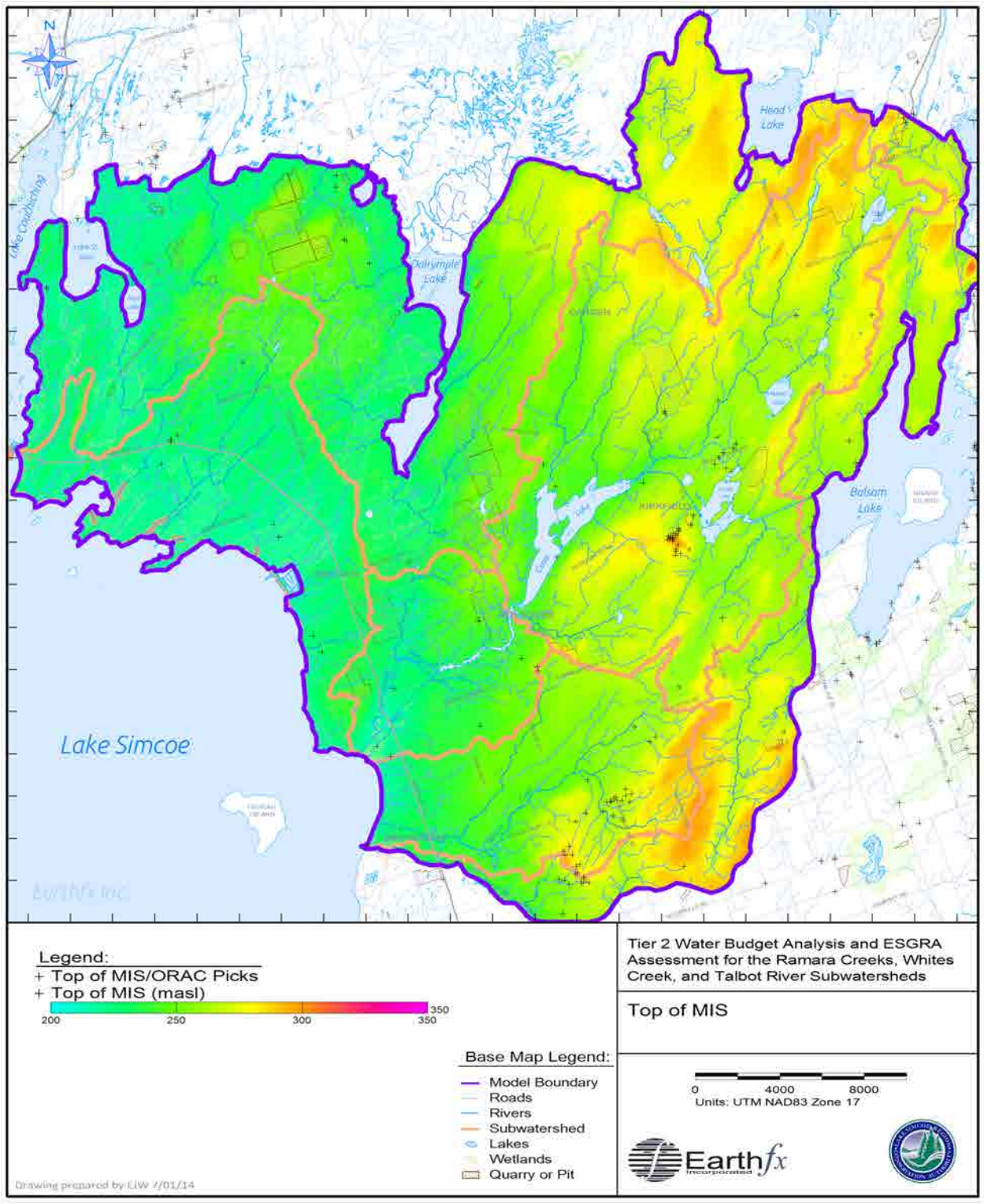

Figure 3.11: Top of the Mackinaw Interstadial Sediments, in metres above sea level (masl).

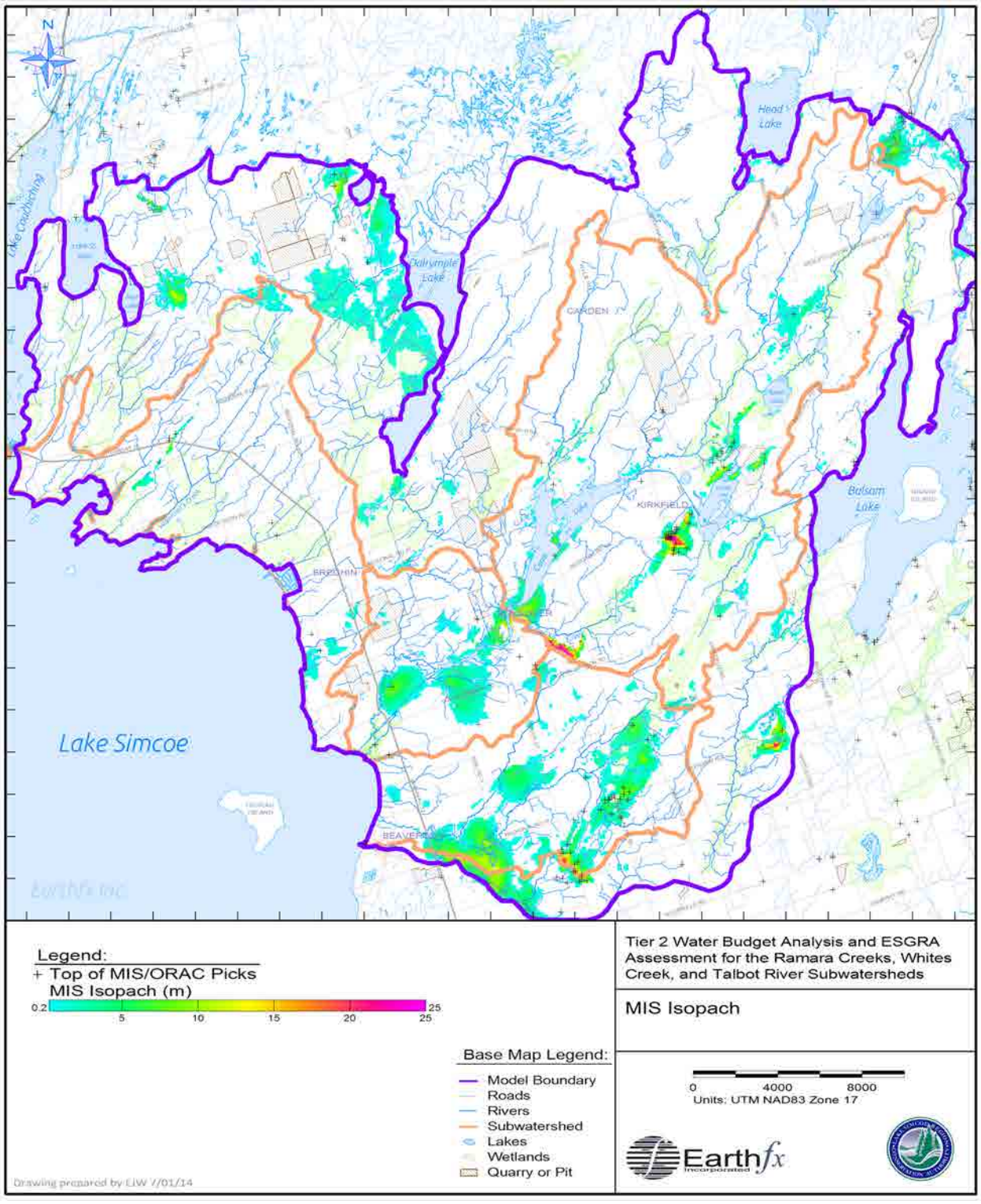

Figure 3.12: Thickness of the Mackinaw Interstadial Sediments, in metres.

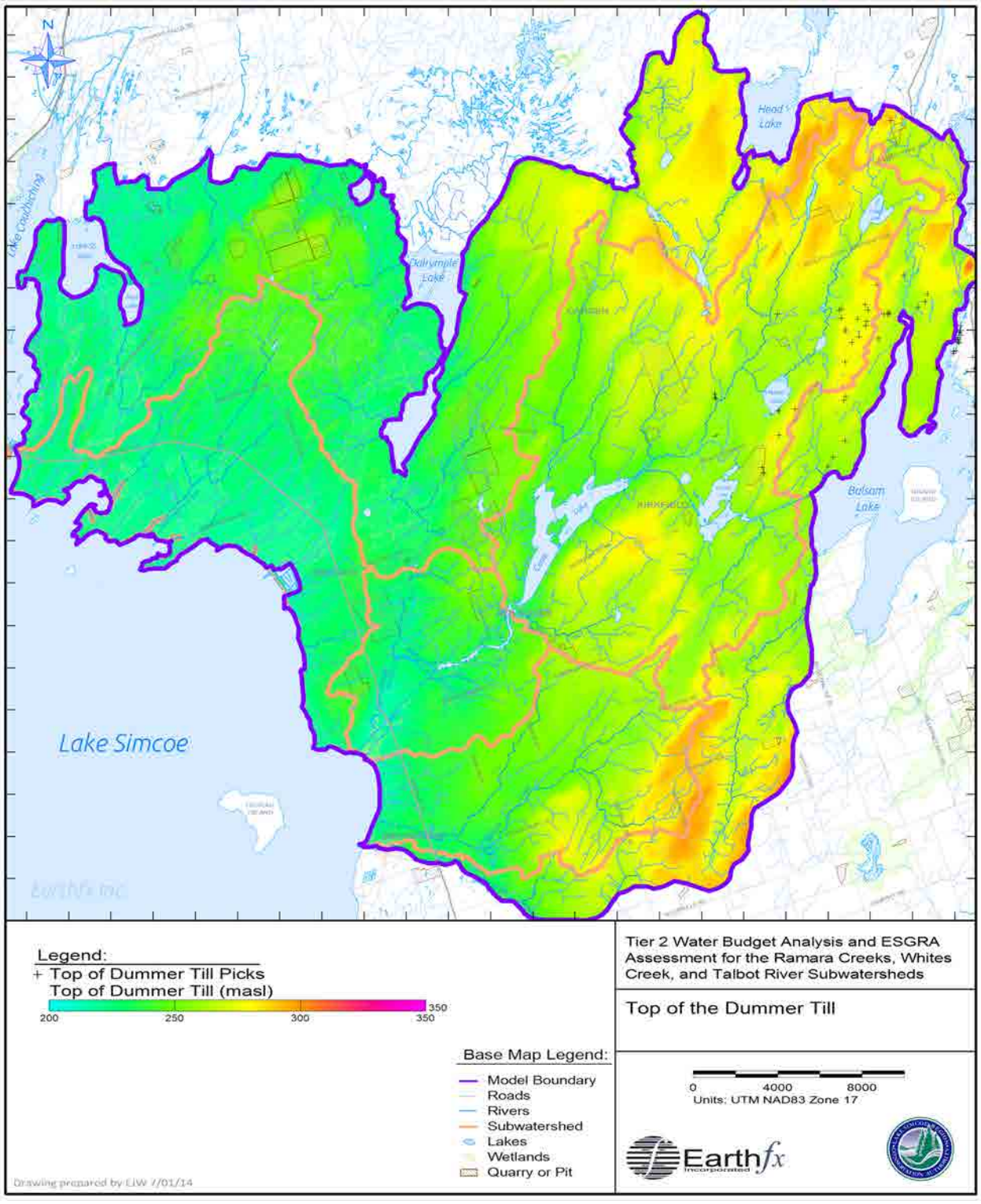

Figure 3.13: Top of the Dummer Till, in masl.

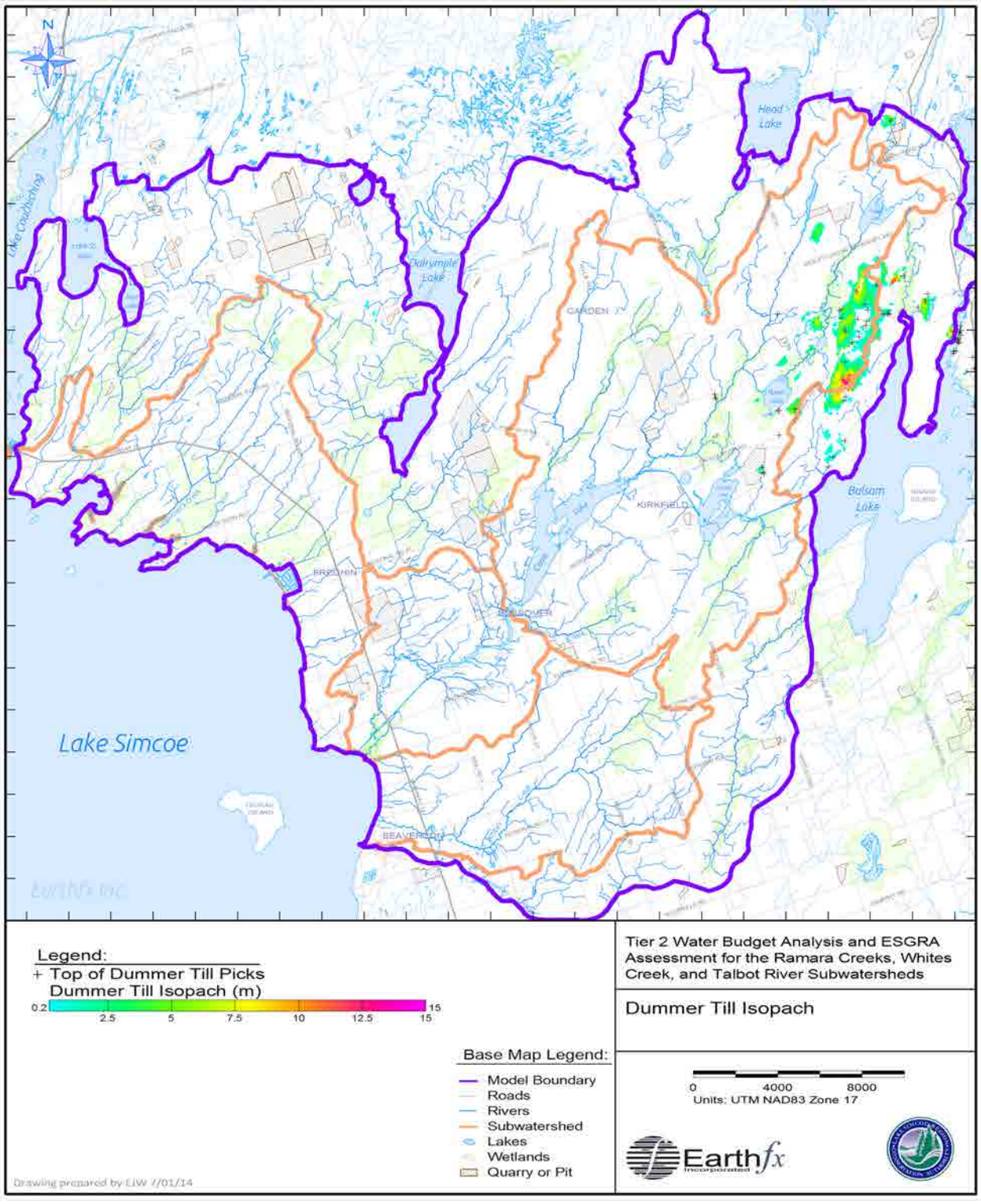

Figure 3.14: Thickness of the Dummer Till, in metres.

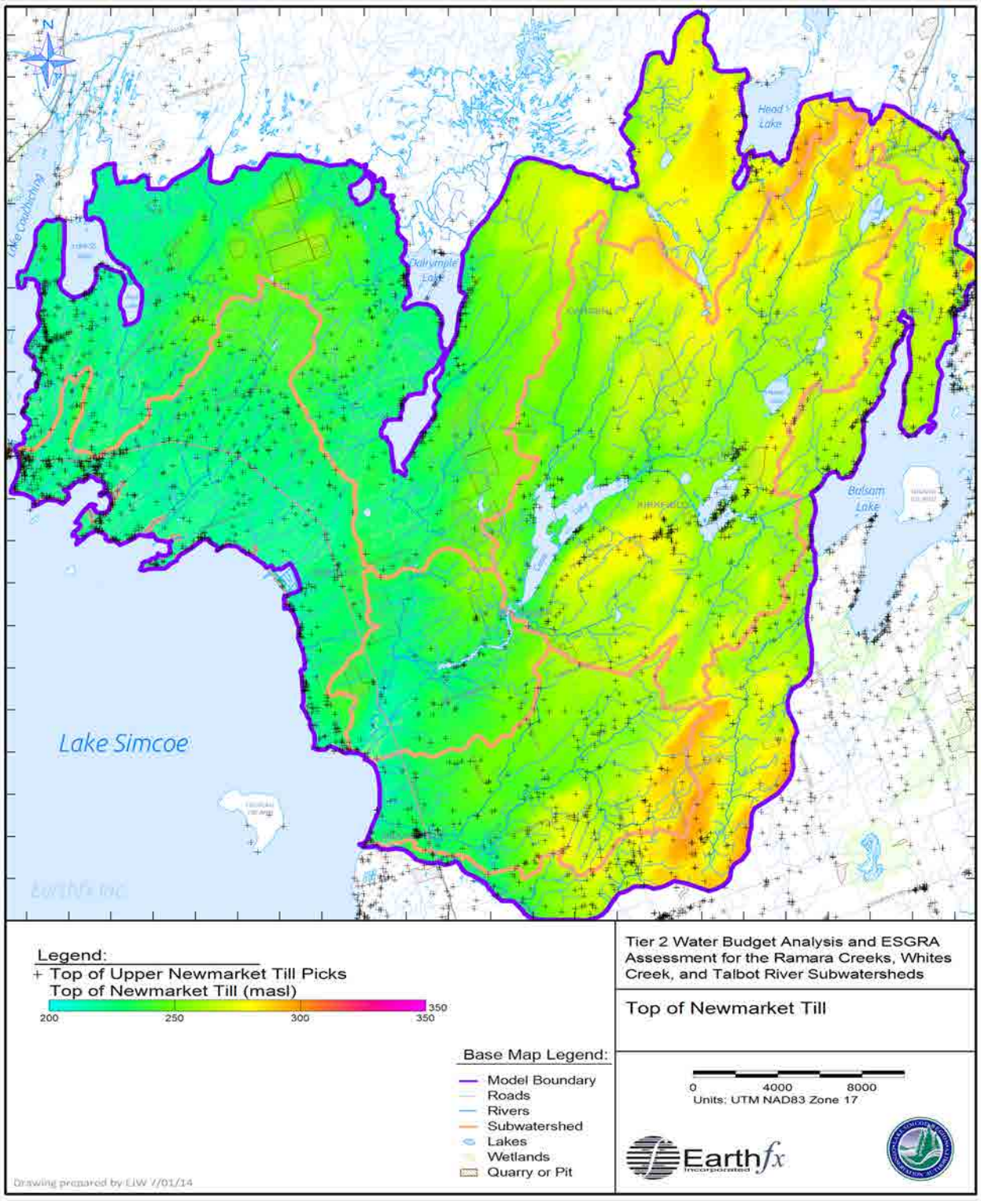

Figure 3.15: Top of the Newmarket Till, in masl.

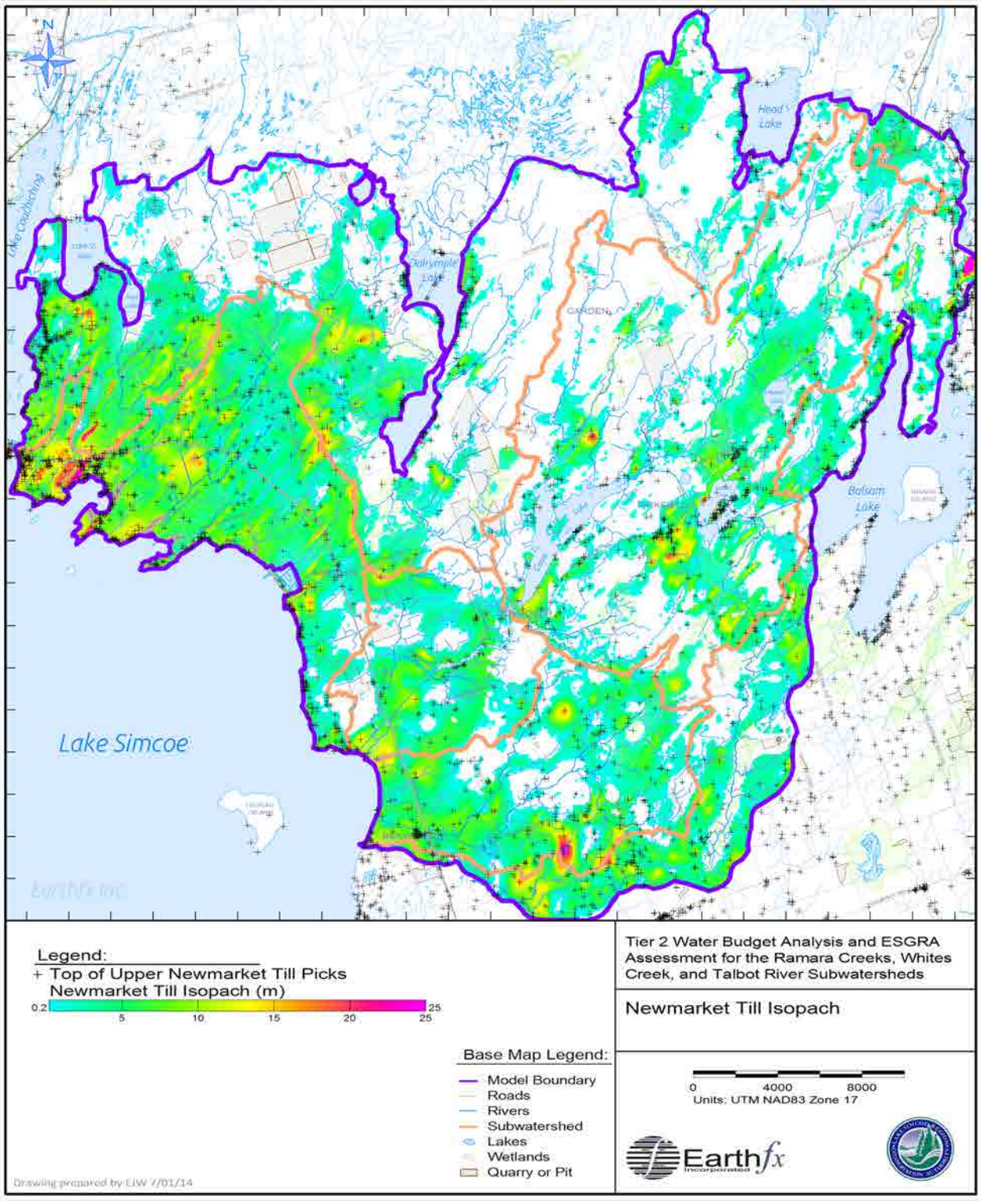

Figure 3.16: Thickness of the Newmarket Till, in metres.

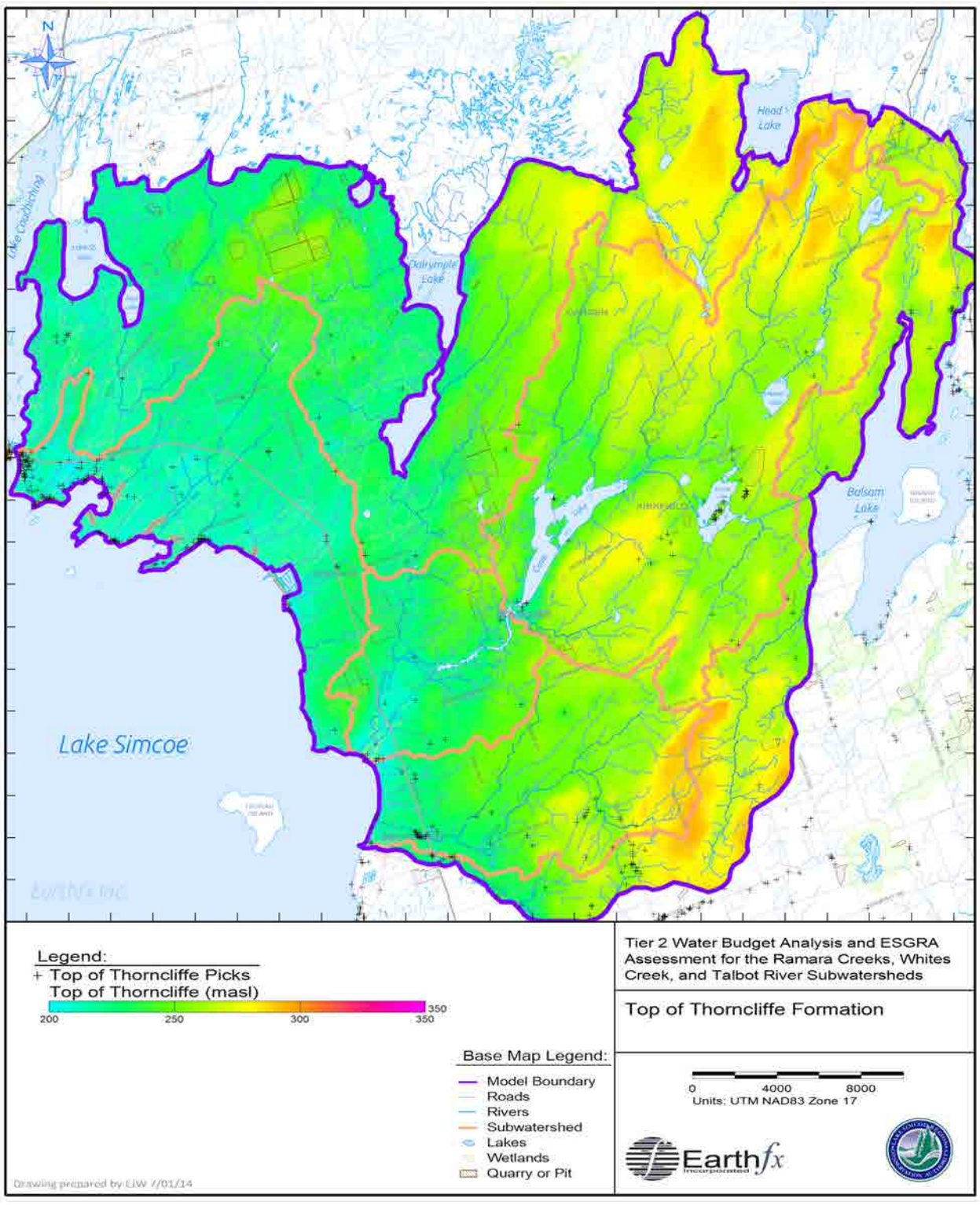

Figure 3.17: Top of the Thorncliffe Formation, in masl.

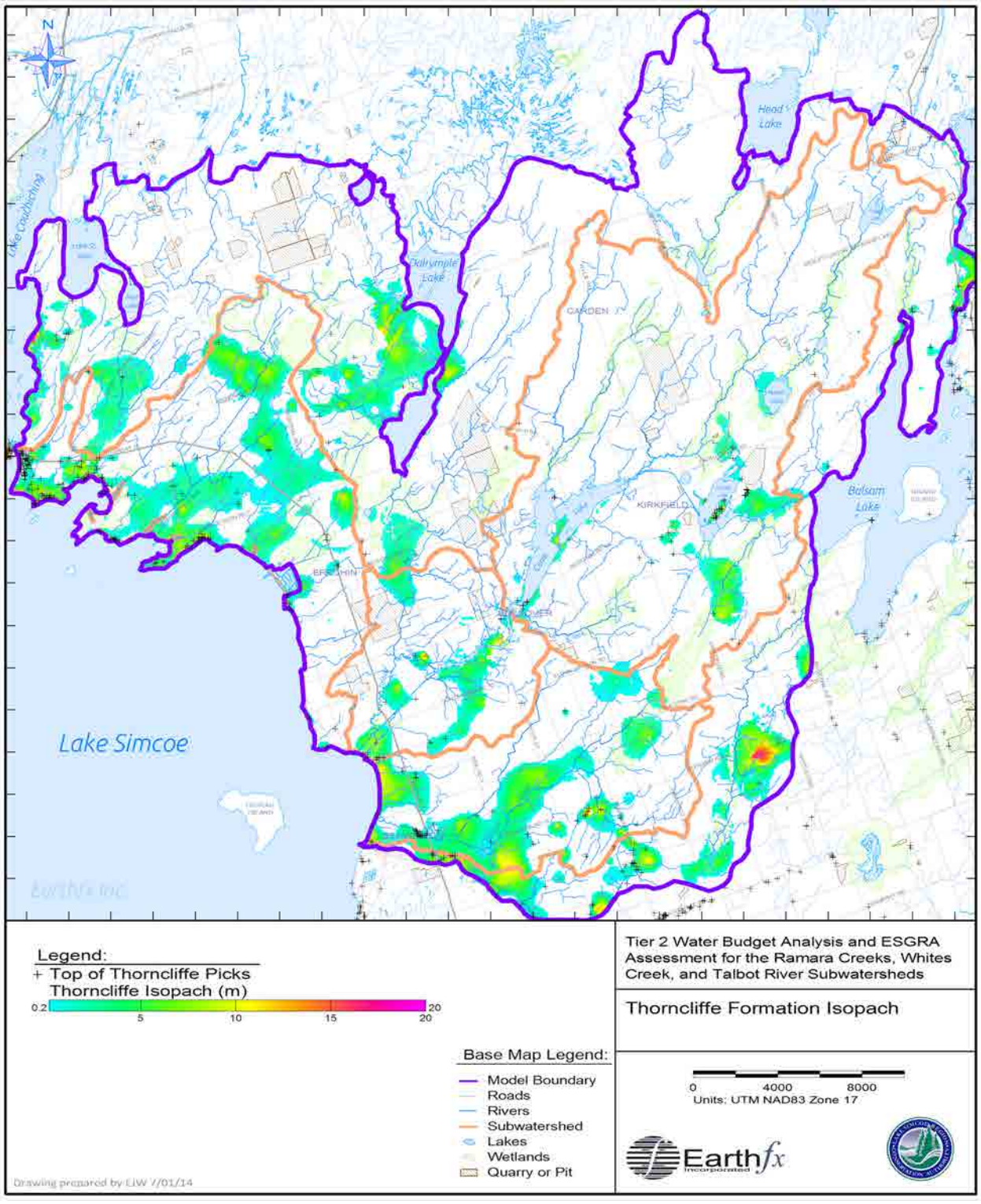

Figure 3.18: Thickness of the Thorncliffe Formation, in metres.

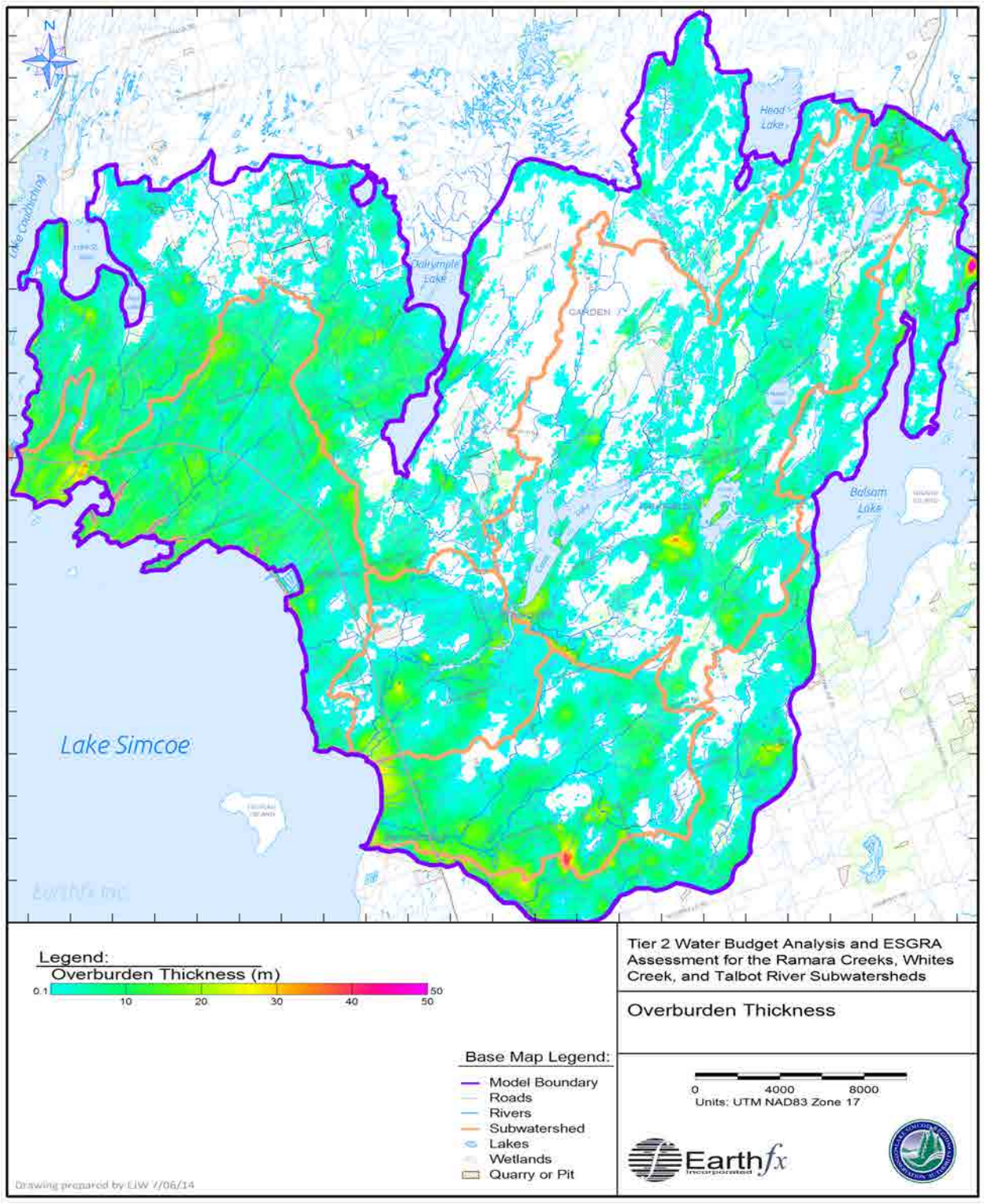

Figure 3.19: Overburden thickness, in metres.

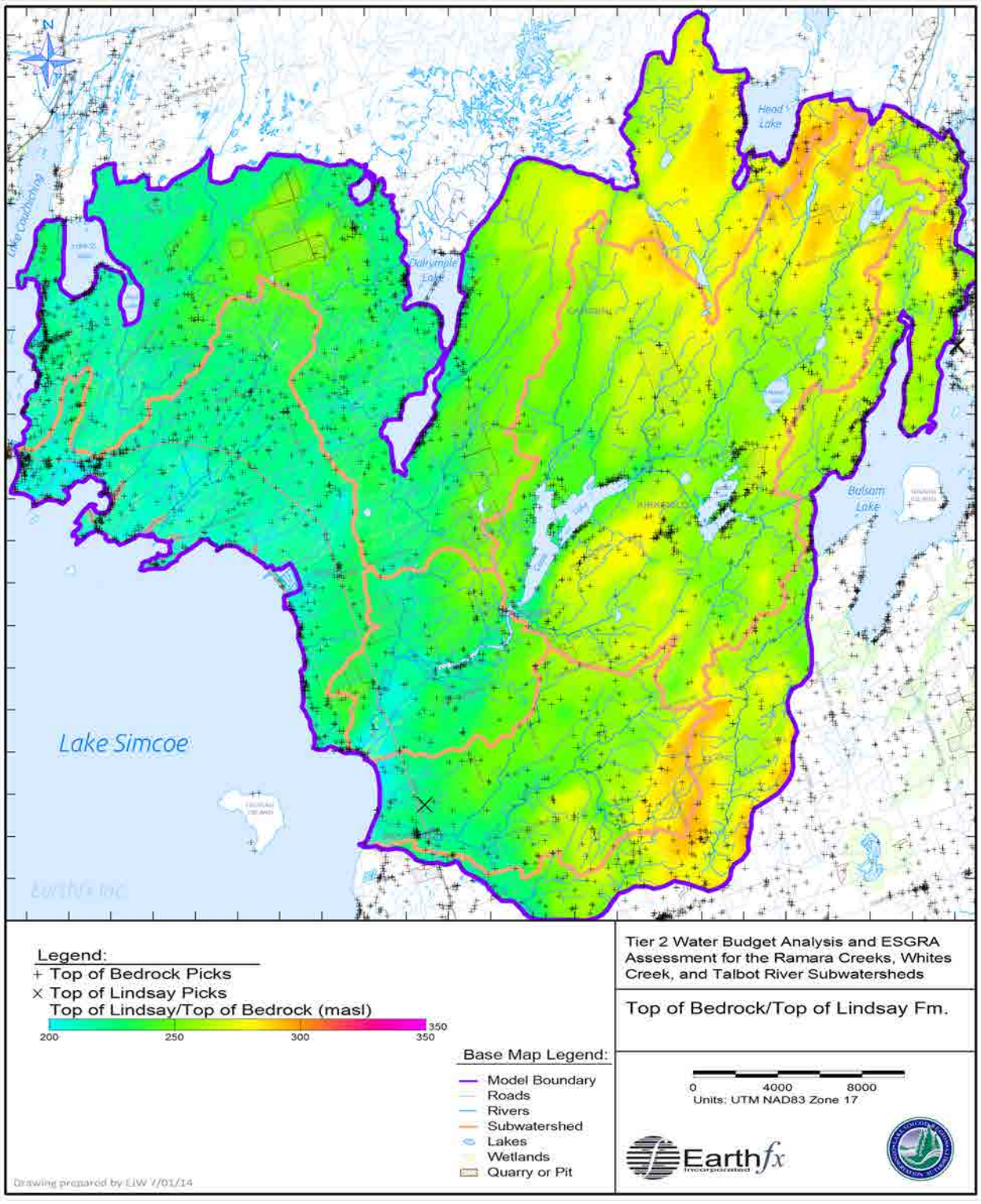

Figure 3.20: Top of Bedrock and Top of Lindsay Formation, in masl.

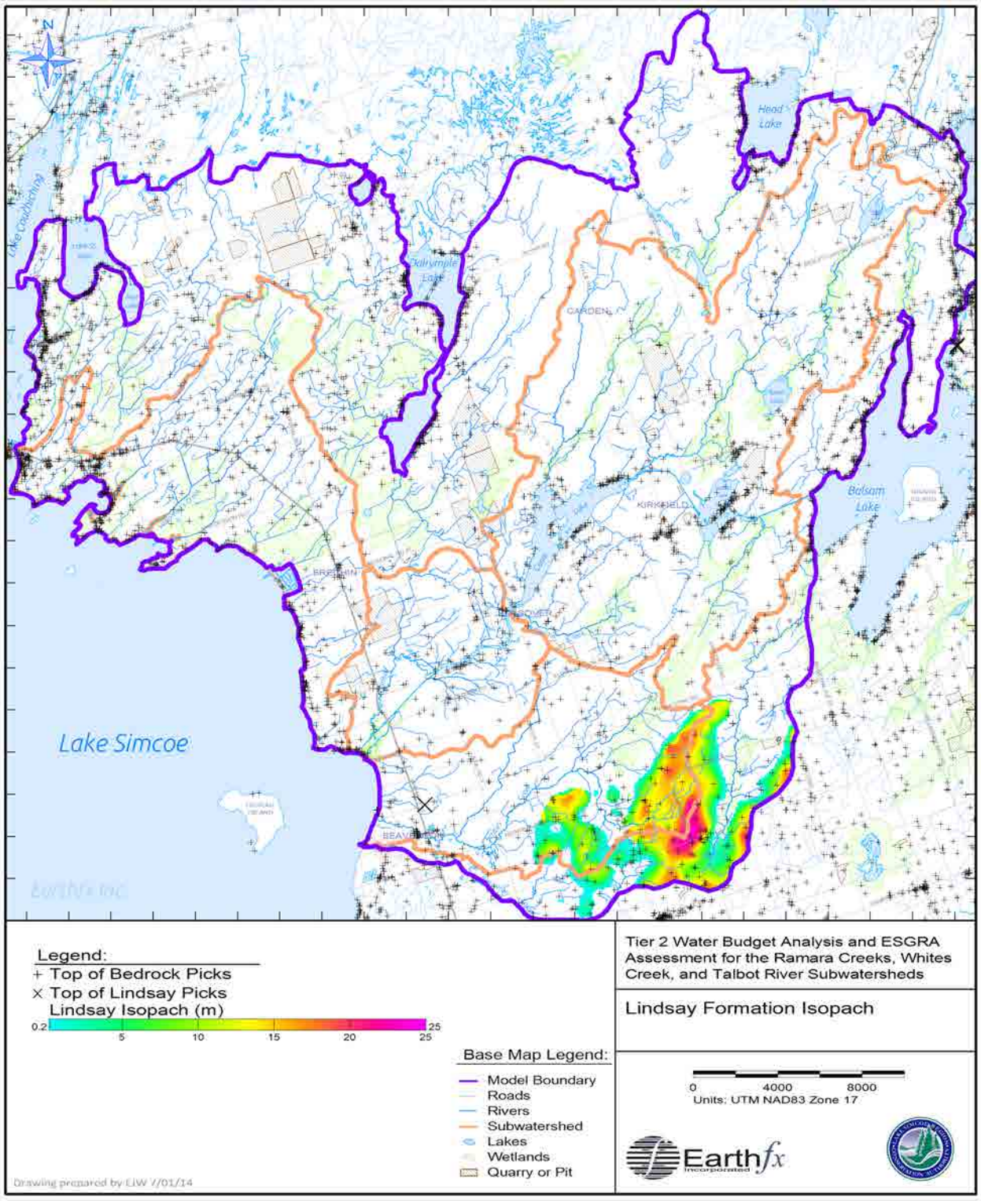

Figure 3.21: Thickness of the Lindsay Formation, in metres.

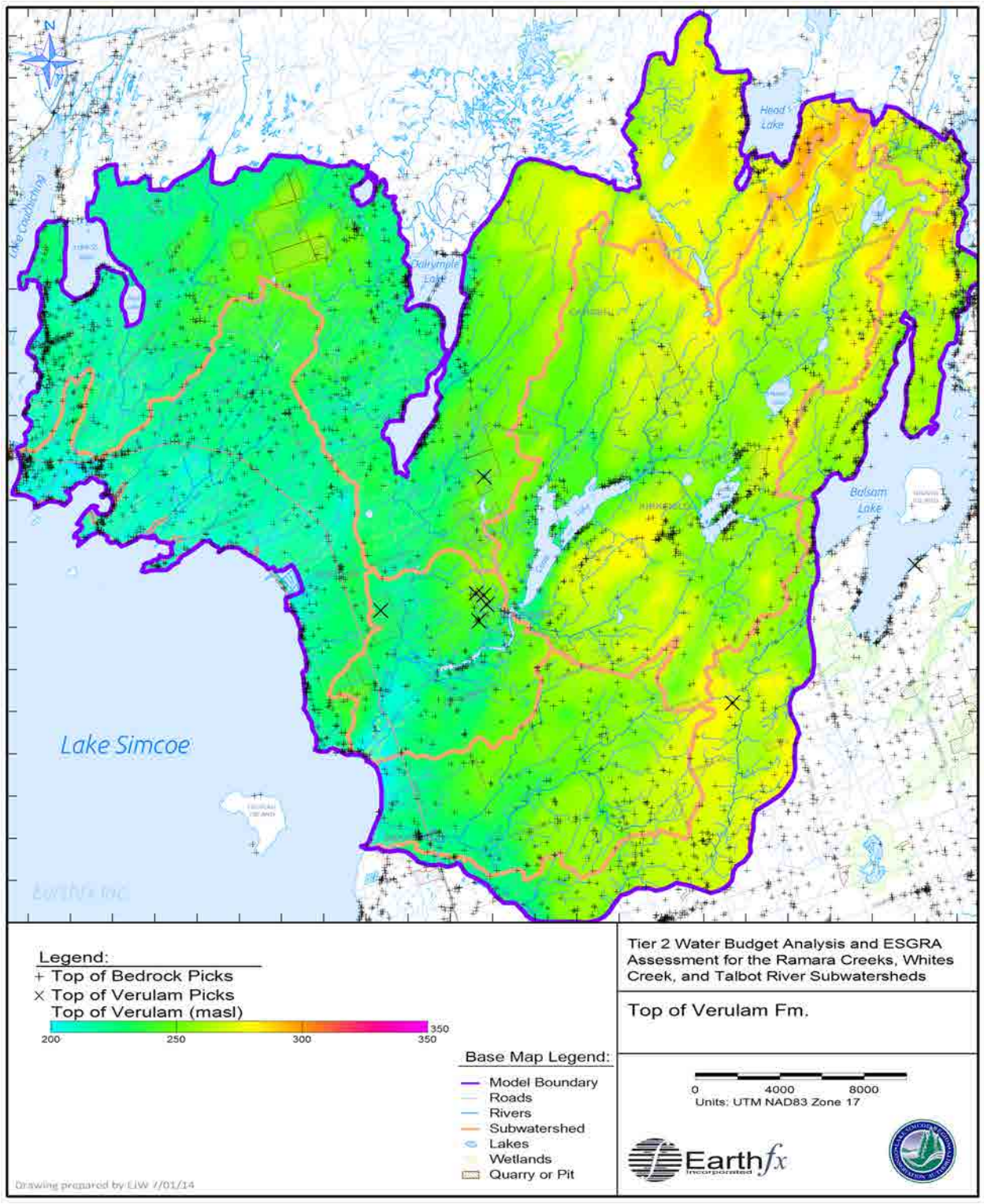

Figure 3.22: Top of the Verulam Formation, in masl.

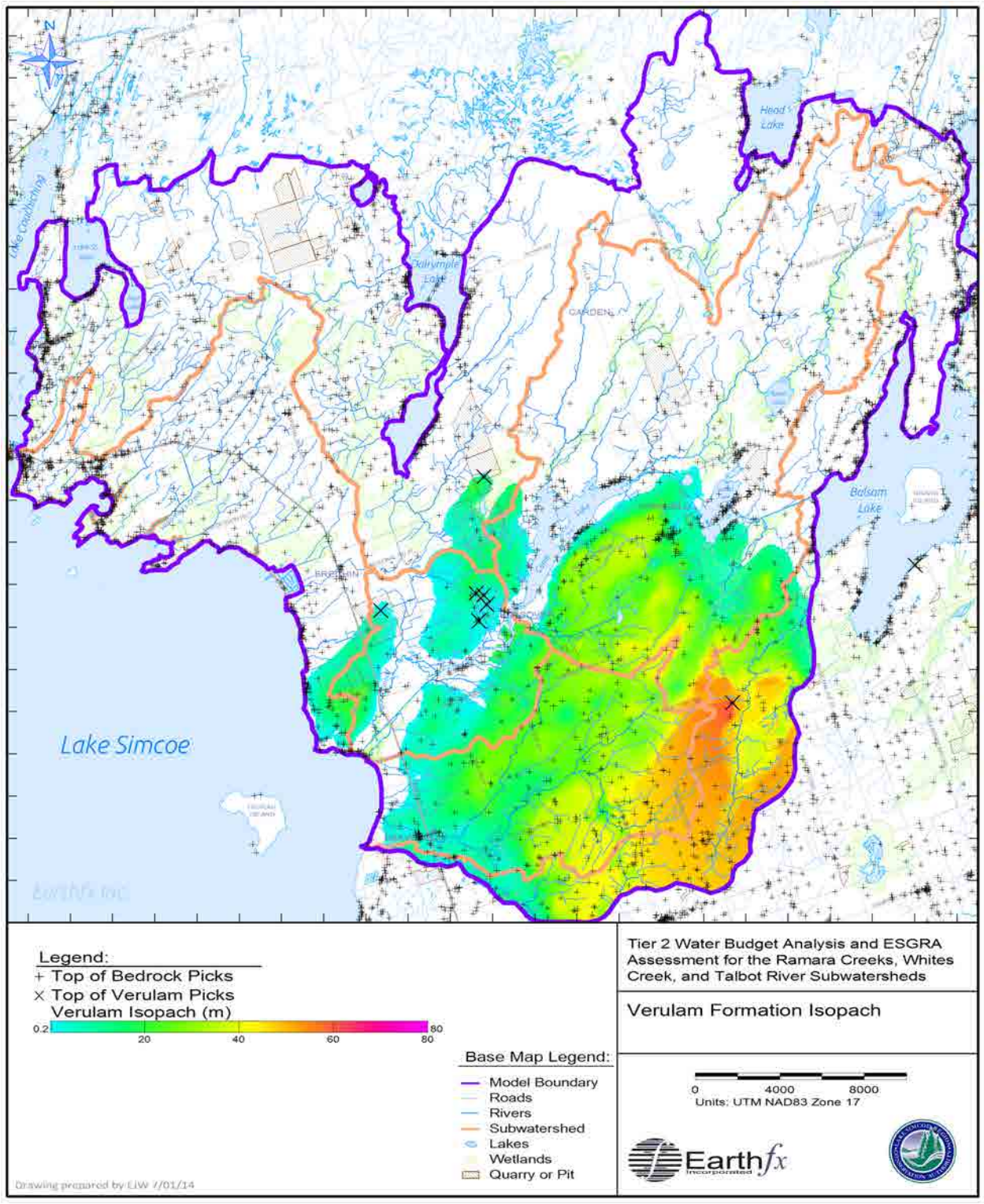

Figure 3.23: Thickness of the Verulam Formation (Upper and Lower Members), in metres.

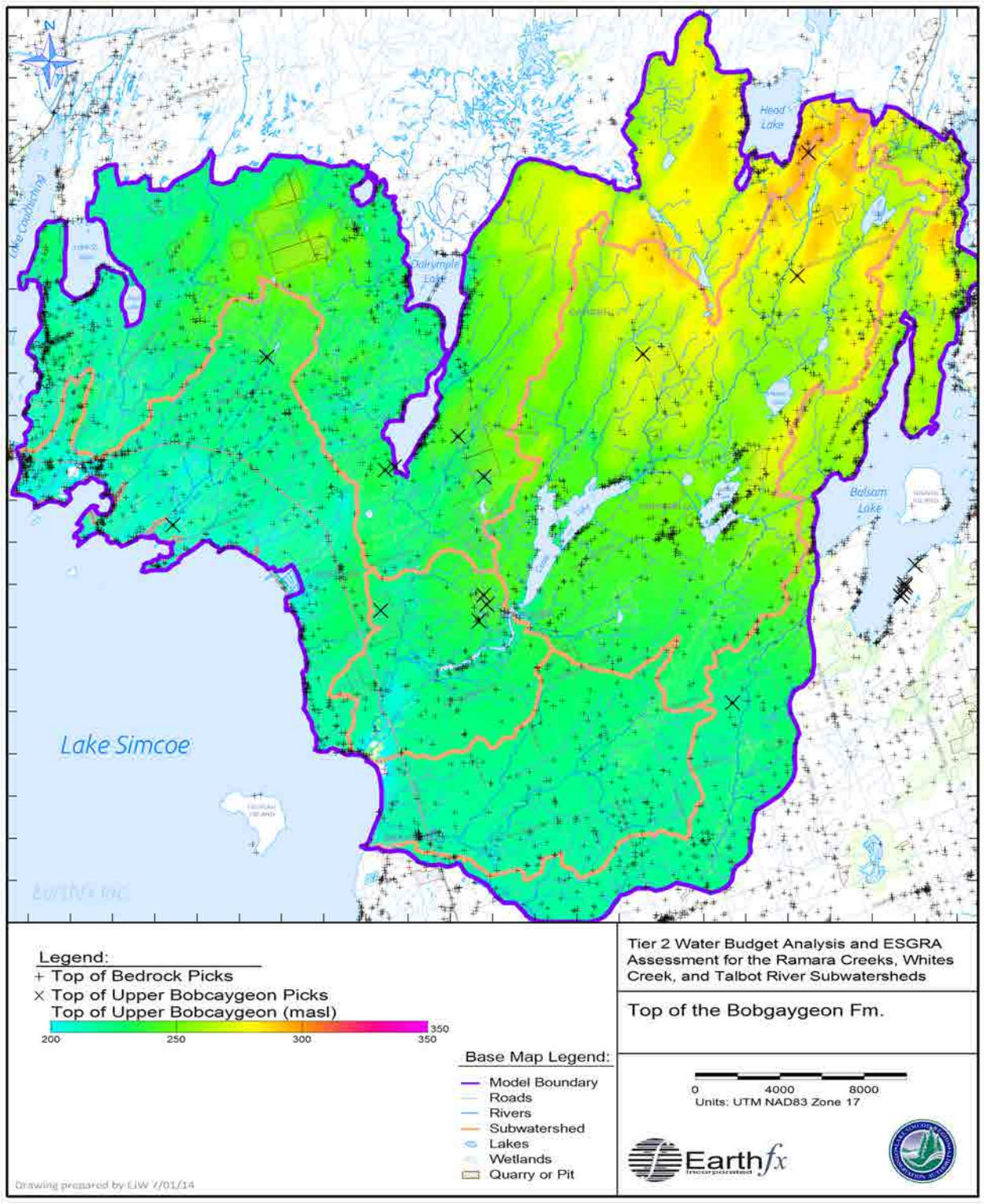

Figure 3.24: Top of the Bobcaygeon Formation, in masl.

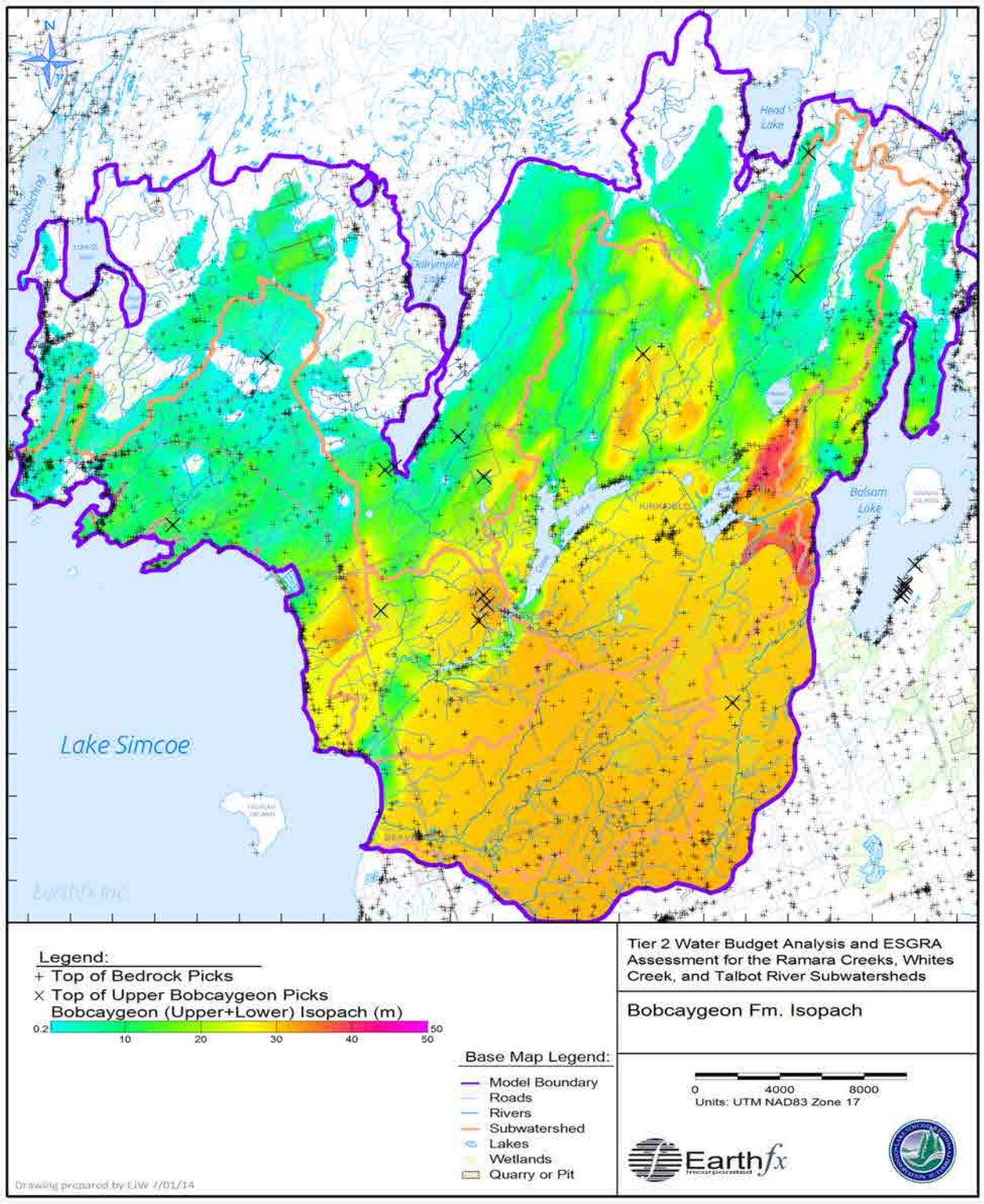

Figure 3.25: Thickness of the Bobcaygeon Formation (Upper, Middle, and Lower Members), in metres.

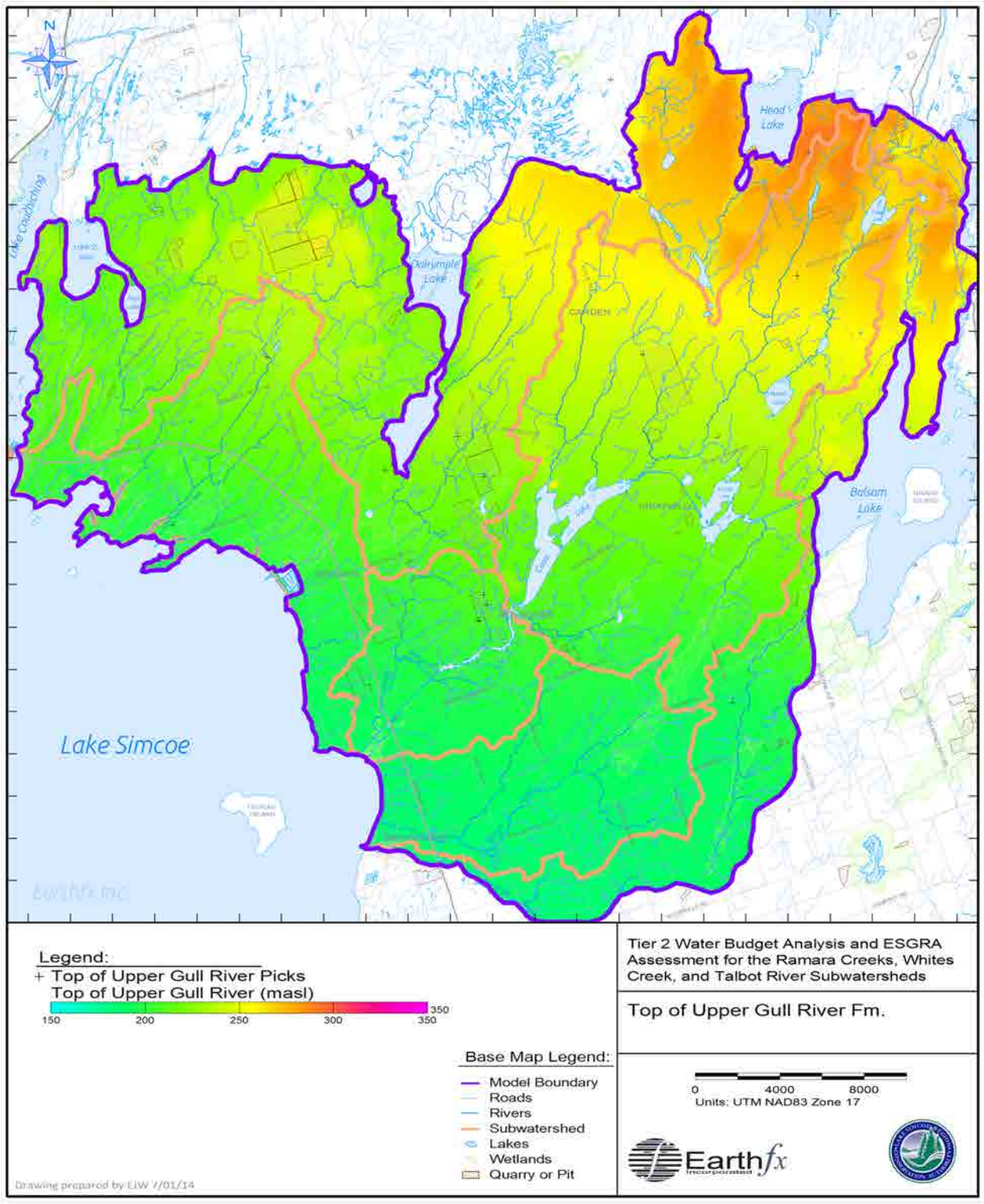

Figure 3.26: Top of the Upper Gull River Formation, in masl.

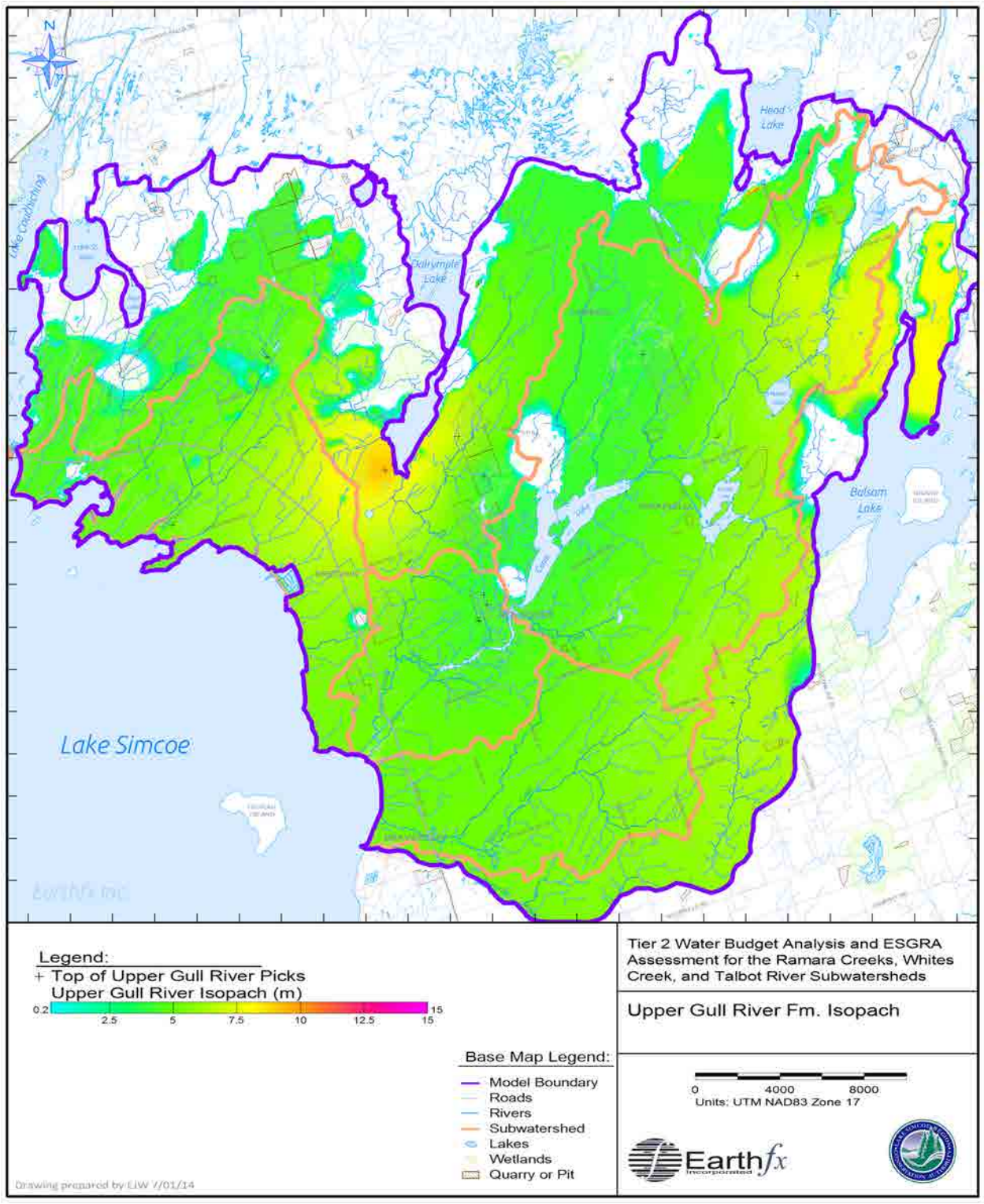

Figure 3.27: Thickness of the Upper Gull River Formation, in metres.

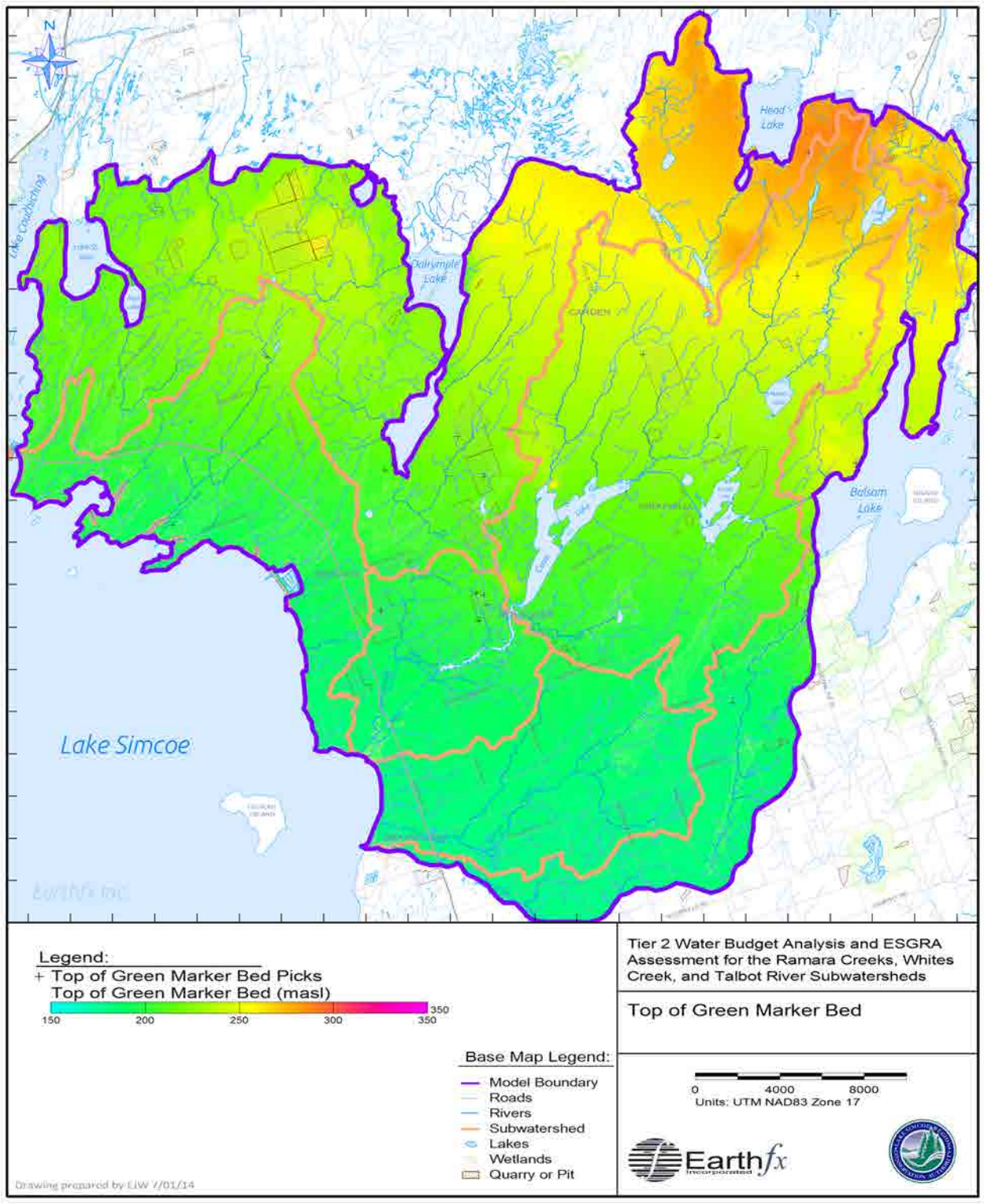

Figure 3.28: Top of the Green Marker Bed, in masl.

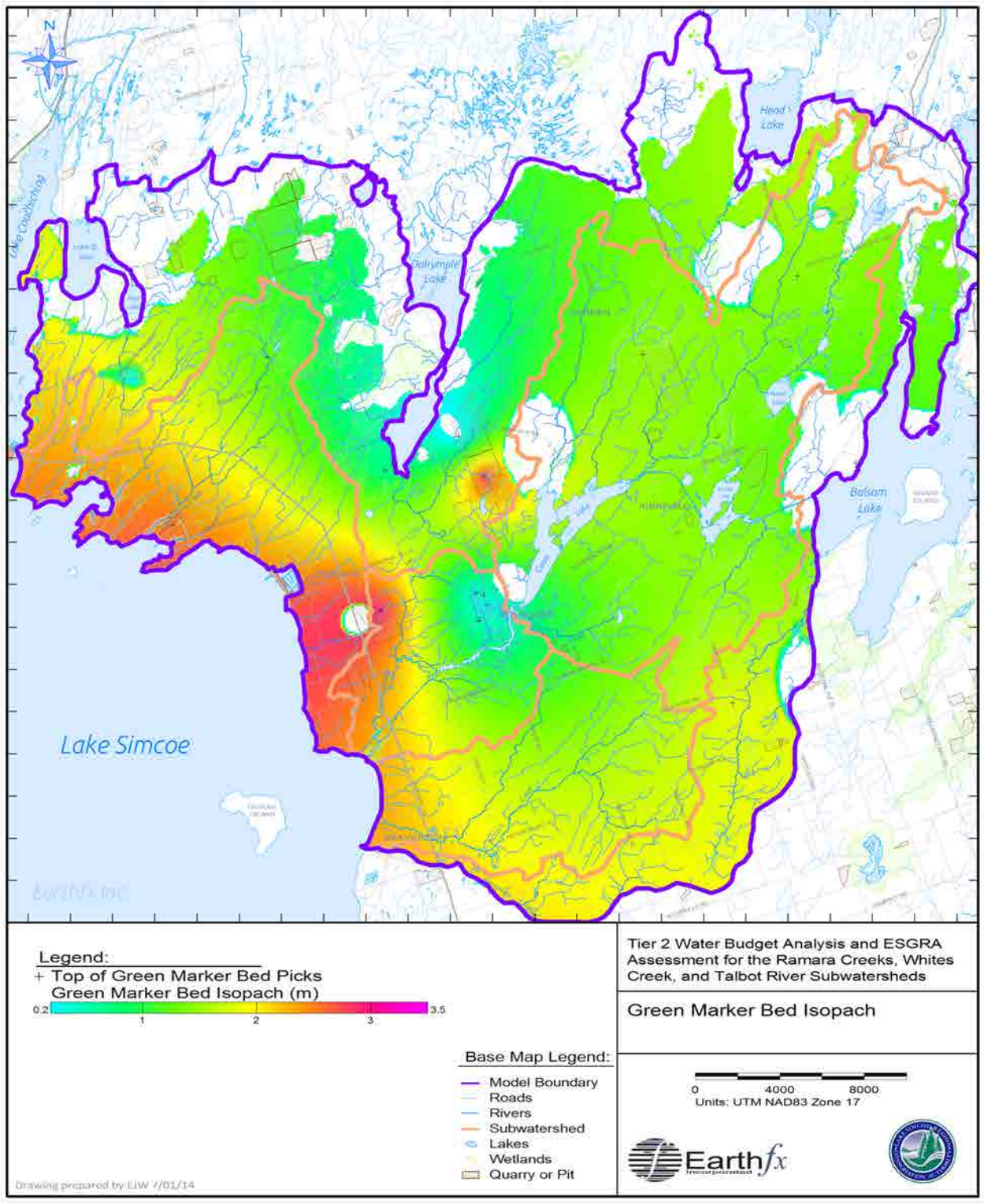

Figure 3.29: Thickness of the Green Marker Bed, in metres.

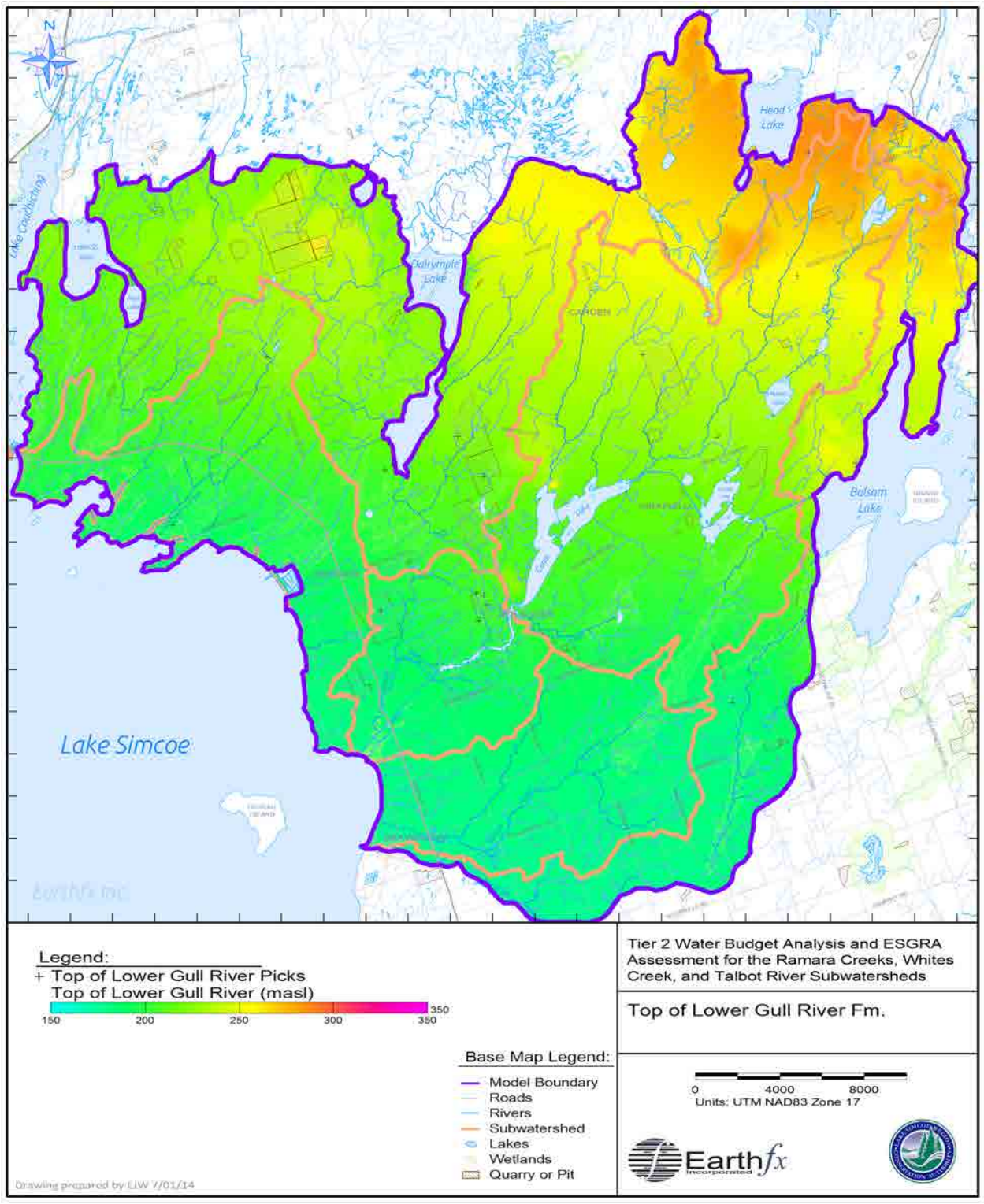

Figure 3.30: Top of the Lower Gull River Formation, in masl.

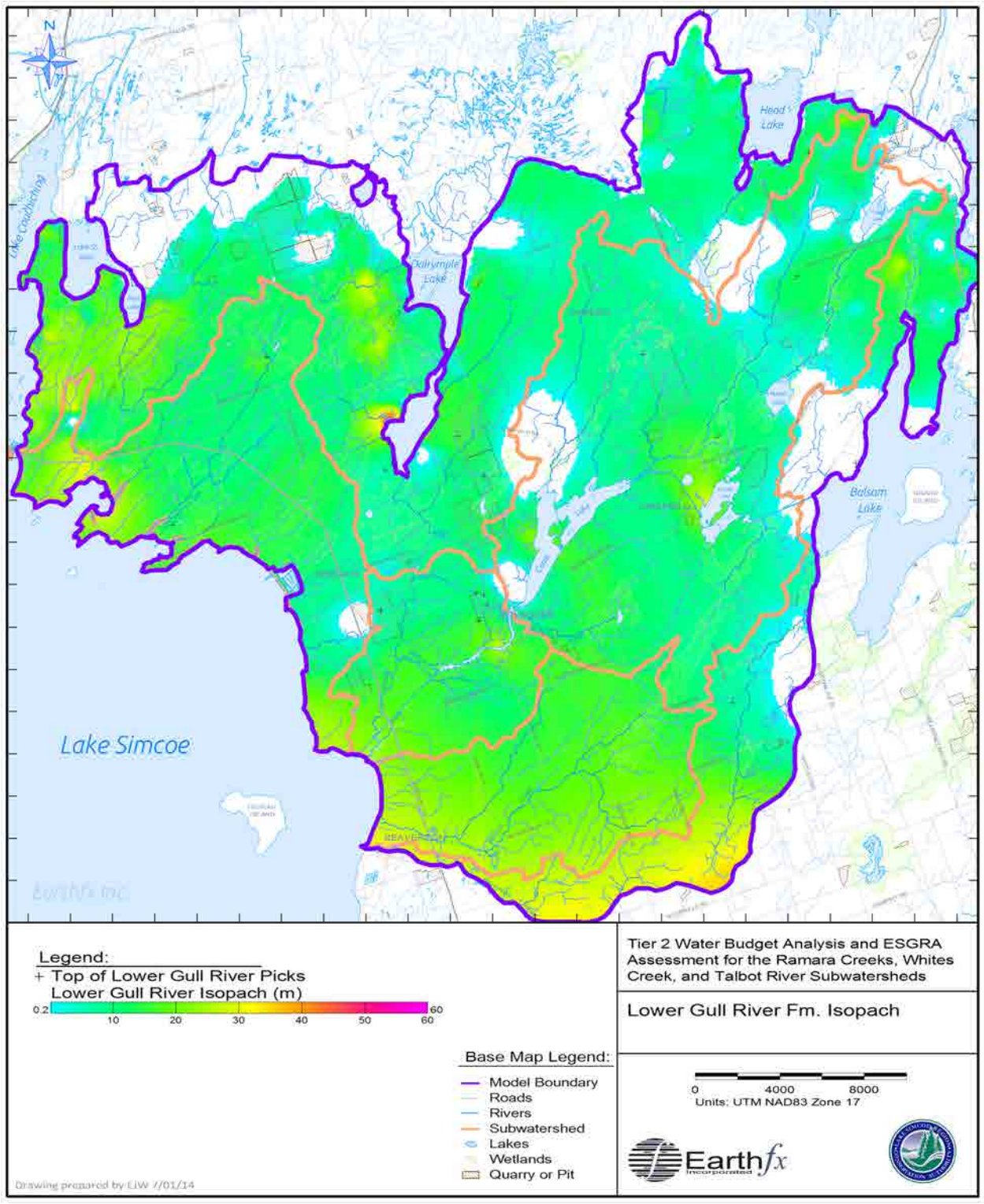

Figure 3.31: Thickness of the Lower Gull River Formation, in metres.

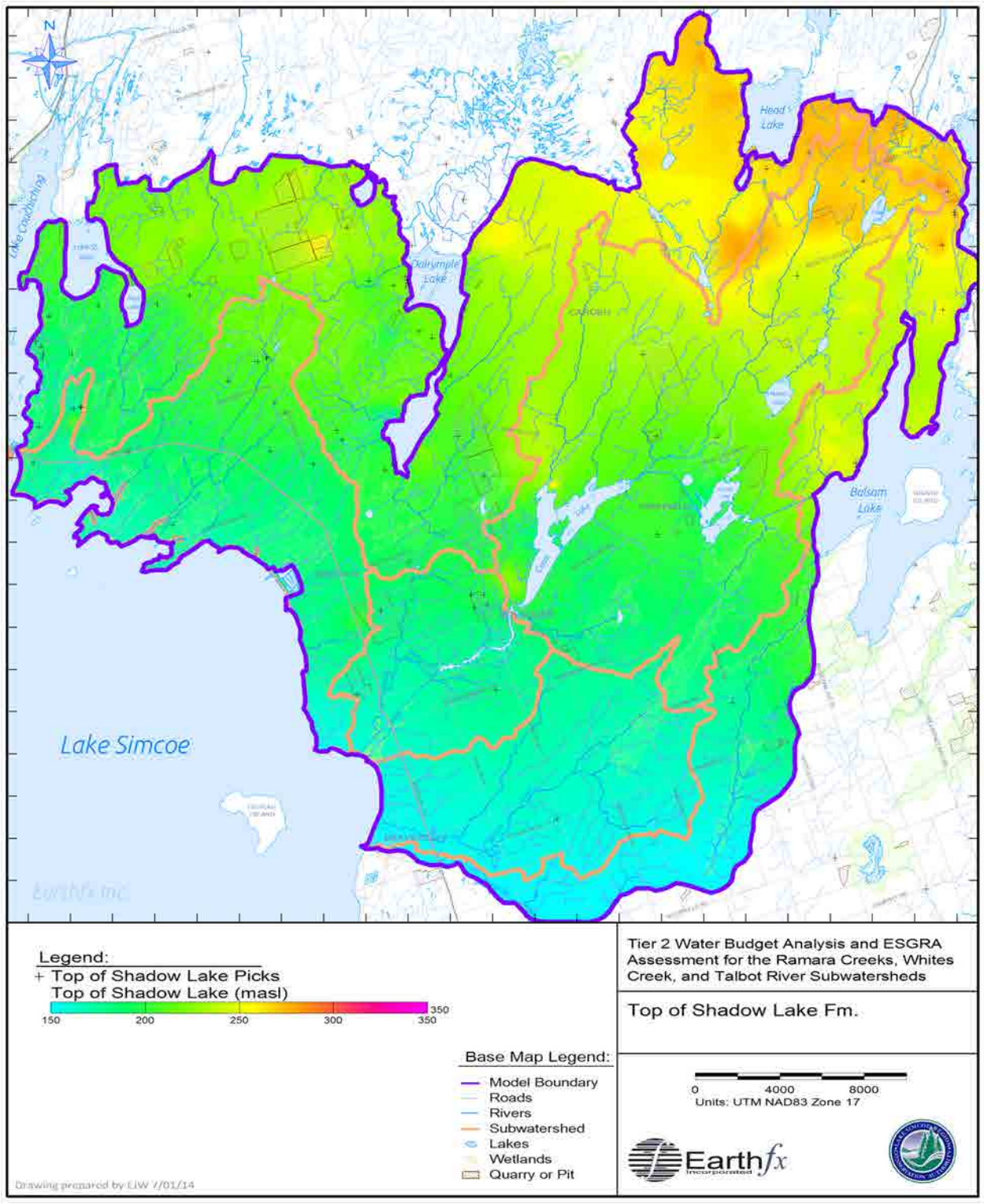

Figure 3.32: Top of the Shadow Lake Formation, in masl.

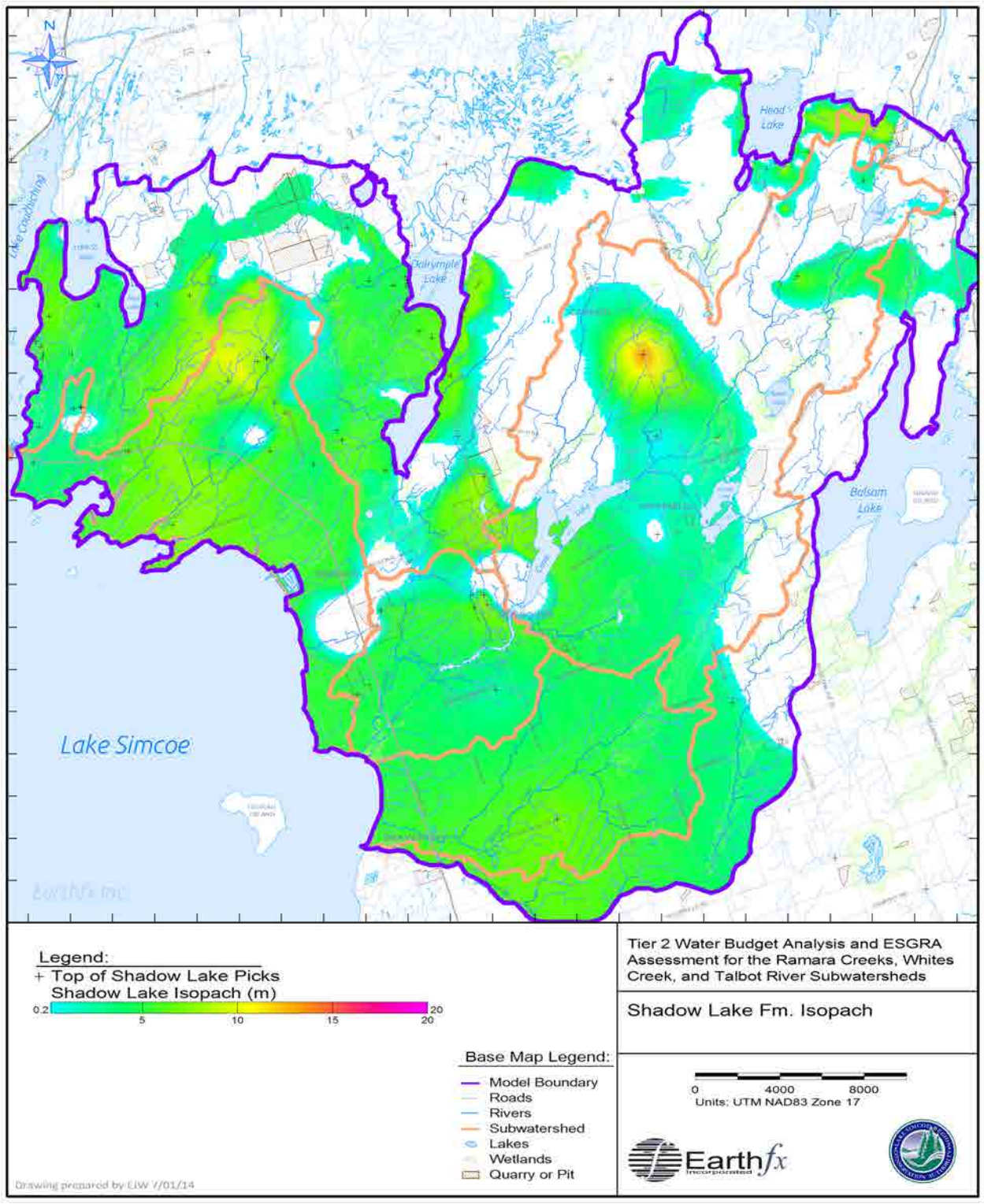

Figure 3.33: Thickness of the Shadow Lake Formation, in metres.

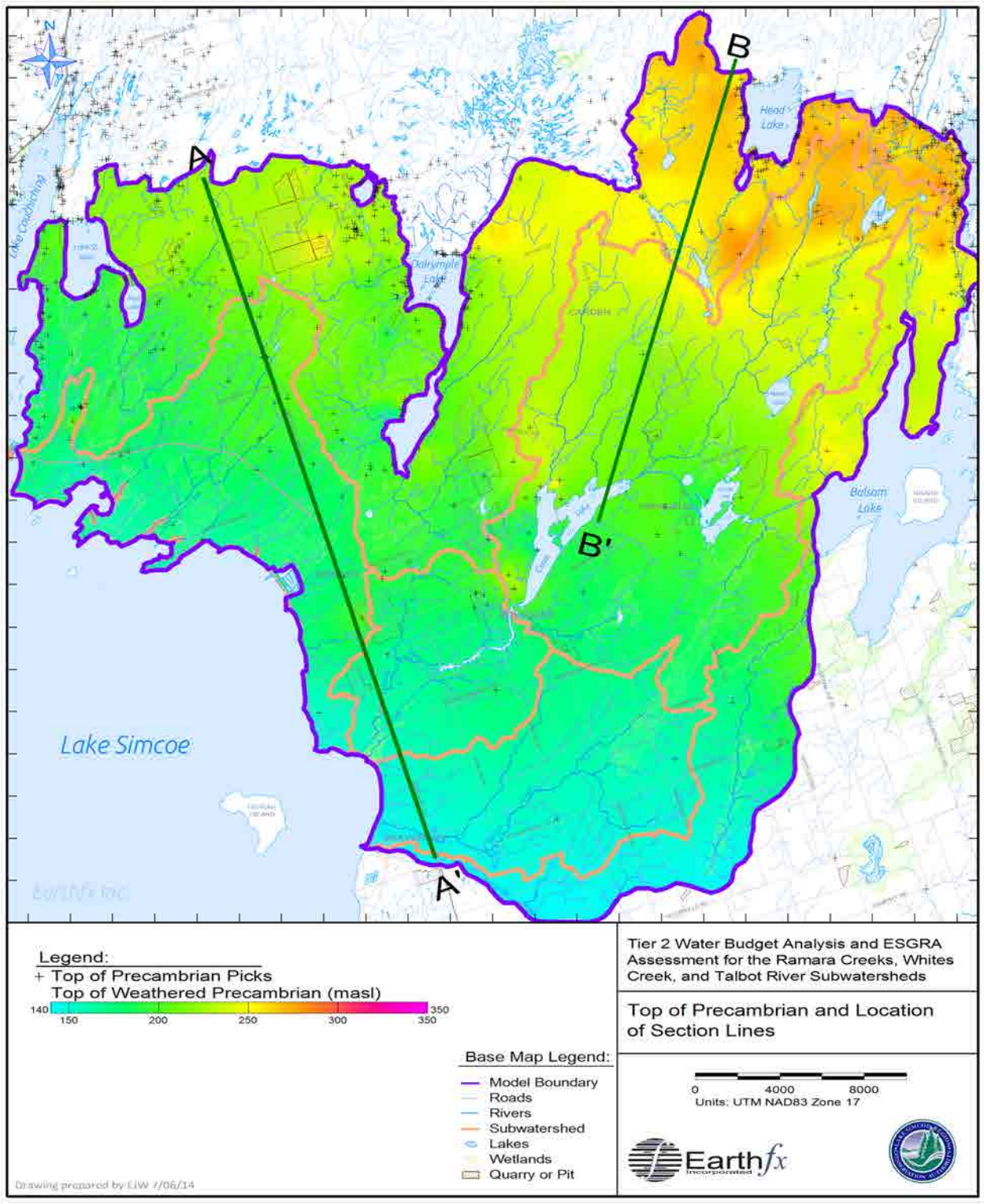

Figure 3.34: Top of the weathered Precambrian, in masl, and location of section lines.

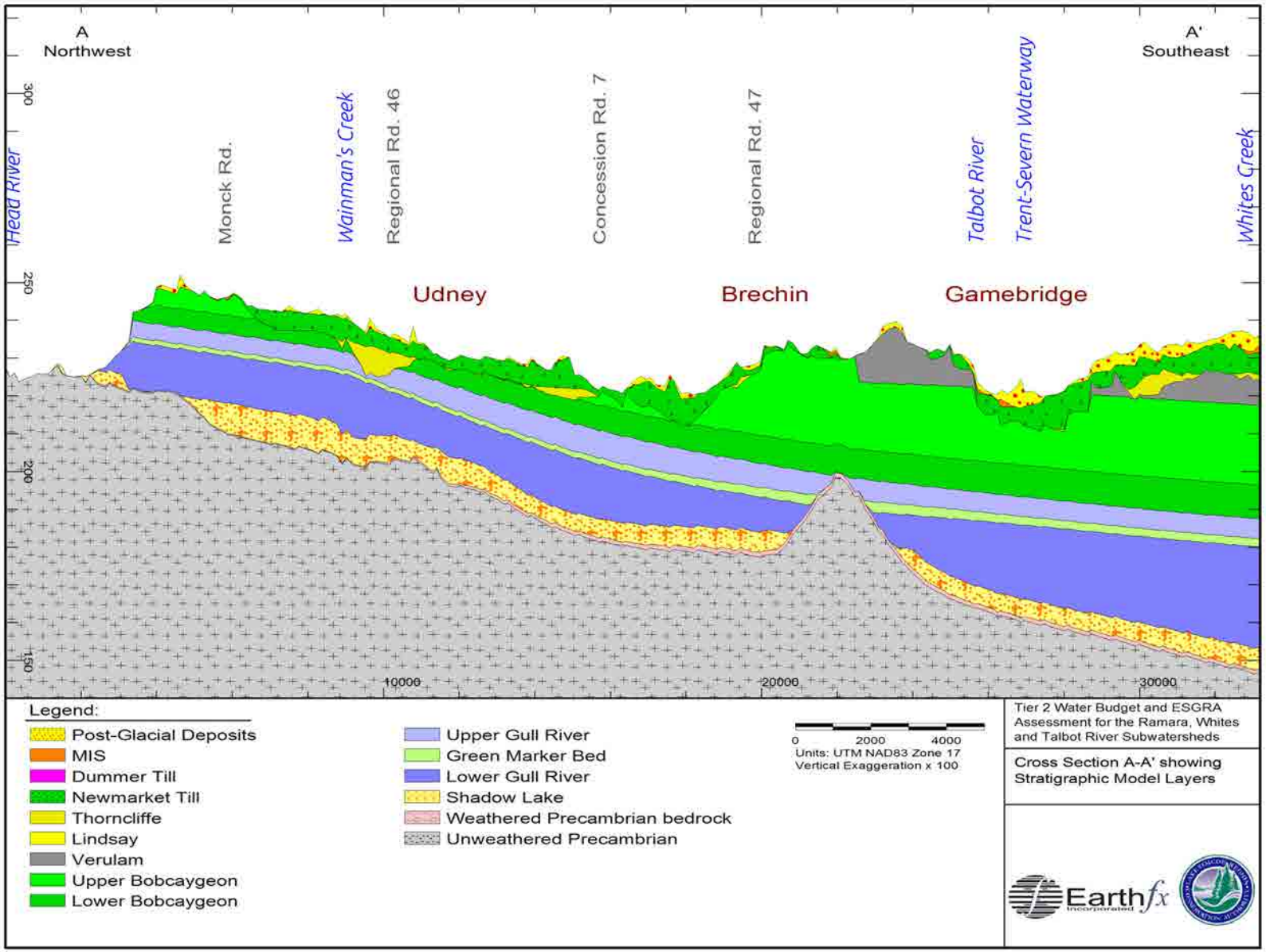

Figure 3.35: Northwest-southeast stratigraphic cross section A-A'.

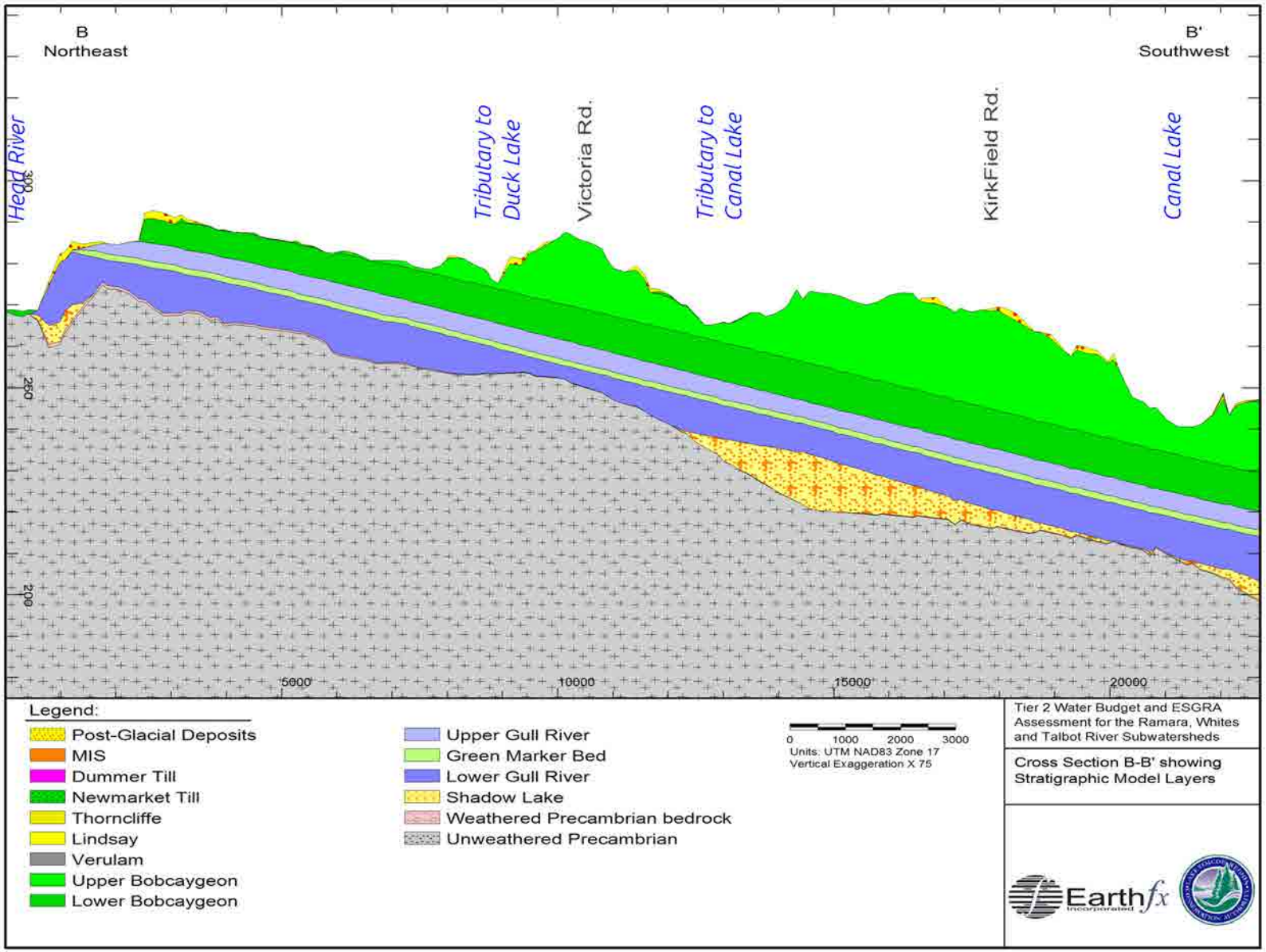

Figure 3.36: Northeast-southwest stratigraphic cross section B-B'.

4 Hydrologic Setting

4.1 Climate Data

Climate data used for this study has been compiled from four main sources: Environment Canada's Atmospheric Environment Service (AES), the LSRCA, NEXRAD-derived rainfall data, and the hourly infilled climate data provided by the Ontario Ministry of Natural Resources (MNR). The Ramara, Whites, and Talbot (RWT) creek subwatershed study area has few climate stations, as can be seen in Figure 4.2. While there are three stations with recent data, there are no climate stations in the central or northern portion of the study area with data after 2000. There are four main climate time-series required for the GSFLOW model:

1. **Precipitation**: (as separate rainfall and snowfall data)
2. **Daily minimum and maximum temperature**: required for calculation of evaporation/ET and snowmelt)
3. **Daily net solar irradiation**: also required for calculation of evaporation/ET and snowmelt
4. **Hourly rainfall intensity distribution**: required for calculation of intensity-based runoff

Periods of records vary among the many available data source. These data were used to construct a complete climate dataset for WY1951 through WY2012 (note: a water year (WY) begins on October 1st of the preceding calendar year). In all, 28 AES stations were available within this period (including the 6 MNR infilled stations for which hourly data were interpolated to existing AES station locations). Station information is presented in Table 4.2 and Figure 4.3. Only 2 of the 22 AES stations had hourly measurements of temperature and humidity; these stations did not have hourly precipitation. An additional station, Whites Creek at Regional Rd 23, is operated by LSRCA and includes a solar radiometer. The greatest distance from the study area to a station was about 28 km, the average distance was 10 km, and there were seven stations within the study area.

4.1.1 Precipitation and Temperature

4.1.1.1 Environment Canada Atmospheric Environment Service Climate Stations

Characterization of the climate of the study area began with an assessment of data the 22 AES climate stations. Annual precipitation totals are shown in Figure 4.4 for the period spanning 1955 to 2011. Over the 55 year period, median annual rainfall varied from 580 mm to 1130 mm. Interstation variability is quite high with the inter-quartile range (i.e., the difference between the 75th and 25th percentile) averaging 180 mm. Agreement between stations appears to improve during the mid-1990s (as the number of stations with data decreased).

Monthly precipitation totals are illustrated in Figure 4.5 for the period spanning 2000 to 2010. Over this 11 year period, median monthly precipitation ranged from 20 to 175 mm. Interstation variability remains high, with the inter-quartile range reaching nearly 100 mm for some periods. Figure 4.6 shows average monthly precipitation quartiles at AES stations over the 11-year period. The winter months have slightly lower average median precipitation (as either rain or snow). Average monthly median precipitation ranges from a late-winter low of 60 mm to a summer/fall plateau of about 80 mm. Average monthly median precipitation does not appear to vary much between June and November, however, interstation variability is still as high as 25 mm (or 35%) for some months.

Figure 4.7 presents the daily precipitation exceedance probability function (EPF) for the 55-year period between 1955 and 2010. Only about 5% of daily precipitation events (i.e. days with

measured precipitation) exceed 25 mm/d. Additionally, daily precipitation totals exceed 1 mm for 80% of days with measured precipitation.

The relative distributions of precipitation events exceeding 0, 1, 5, 10, 25 mm/d are presented in absolute and normalized form on Figure 4.8. These figures compare both seasonal frequency and relative distribution, respectively, of precipitation events greater than a given exceedance. The absolute distribution (Figure 4.8a) allows comparison of frequencies of rainfall events of a given intensity. Figure 4.8b illustrates the seasonal frequency of events of given intensities and shows that intensities less that 25 mm/day are distributed fairly evenly during the month of April to November. Higher-volume (>25 mm/day) events tend to occur mainly in the summer months (June through September), likely in the form of high-intensity convective storms.

Precipitation form (as snow, rain, or mixed event) is illustrated in Figure 4.9, for the full range of observed temperatures. For the selected AES stations, 68% of precipitation events are rain only, 27% are snow only, and 5% are mixed. The precipitation form is an important input to the snowmelt and snow accumulation model. Other snowpack model parameters will be discussed in detail in Section 9.

A critical temperature, T_c, is defined where snow-only events occur when the maximum daily temperature T_{max} is less than T_c, rain-only events occur when the minimum daily temperature, T_{min}, is above T_c, and mixed events occur when T_c falls between T_{min} and T_{max}. A default value of 0 °C is suggested. As precipitation form data is available for a number of AES stations, a range of temperature values were tested to determine a local optimal value for T_c. A critical temperature value of 0 °C produced predictions of event form that best matched the AES data.

4.1.1.2 NEXRAD

As noted, the study area has a small number of climate stations, and data quality and the period of record for each station varies. There is no hourly data available for any stations adjacent to the study area past 2010. Additionally, on some days; points in the study area can be more than 10 km from the nearest station with usable data. With distributed models such as PRMS and GSFLOW, the rain gauge data must be interpolated to create a continuous coverage of spatially-distributed rainfall. While the limitations of spatial interpolation methods for rainfall data have long been recognised (see Coulibaly and Evora, 2007, for example), all interpolation methods are dependent on the accuracy of the gauge data used.

One alternative is to make use of a dataset which captures the distributed nature of precipitation patterns. The Next-Generation Radar (NEXRAD) is a climate dataset distributed by the National Weather Service (NWS), an agency of the National Oceanic and Atmospheric Administration (NOAA). This study utilized the NEXRAD Digital Precipitation Array (DPA) which consists of spatially-distributed one-hour precipitation accumulations reported every 6-10 minutes. The NEXRAD network consists of 159 high-resolution Doppler weather stations such as the one pictured in Figure 4.12. The KBUF station in Buffalo, NY was closest to the study area. The KBUF dataset is provided in 9087 distributed 18.5 km² cells which span a radius of 232 km around the station (Figure 4.13). The study site and the stations used for NEXRAD bias correction are located roughly 170 km from the KBUF radar station.

To create the continuous coverages, a virtual climate station (VCS) was assigned to the centroid of every NEXRAD cell (VCSs are shown on Figure 4.2). An inverse-distance squared technique was used to interpolate the precipitation data between the VCSs. The interpolation was done to a regular grid with a uniform cell size of 500 m using the 329 closest VCSs. The period of record for NEXRAD data was from February 23, 1996 to April 20, 2013.

There are a number of data quality issues related to the NEXRAD dataset. For example, the radar detects rainfall at higher altitudes with distance from the station. As a consequence, rainfall detected at higher altitudes may be subject to evaporation and wind drift before it hits the ground. Some correction is therefore needed. Extensive NEXRAD error and availability analysis, ground-truthing, and bias correction were completed for this study and are discussed in Appendix A. In brief, a data correlation analysis indicated that the NEXRAD data accurately represented rainfall measured at locations in the study area. Bias in the NEXRAD data was assumed to be systematic and could be remedied using correction factors. Previous studies have indicated that the NEXRAD DPA data, as provided, does not detect precipitation in the form of snow (Earth*fx*, 2013). Therefore, that NEXRAD data was used to represent rainfall only, with snowfall data supplemented from other sources.

4.1.2 Solar radiation

Incoming solar radiation is controlled primarily by the number of possible hours of sunshine per day and the percent cloud cover. Solar radiation data are collected at very few stations in Ontario; therefore, data had to be compiled from a variety of sources. Through linear regression analysis, it was shown (Earth*fx*, 2010c) that the widely-separated Ontario solar radiation stations exhibited good inter-station correlation. Accordingly, a continuous dataset for 1956 through 2012 was created by averaging and infilling of daily solar radiation information from 11 southern Ontario stations. Data provided in sub-daily increments were summed to daily energy gains and converted to langleys per day (ly/d = cal/cm²/day or 41.84 kilojoules/m²), the input units required by the hydrologic model.

The incoming solar radiation dataset was based primarily on the average of measurements from four climate stations maintained by EC after 1985. These stations include: 611KBE0 (Egbert CARE); 6142285 (Elora Research Station); 6158350 (Toronto); and 6158740 (Toronto MET Research Station). Unfortunately, the period of record of these four sites does not extend beyond August 31, 2003; therefore the remaining data up to the end of the study period (2011) had to be infilled using measurements from the University of Waterloo, the University of Toronto Mississauga campus, and recent observations from MESONET (Kelso Wellfield, HRCA Main Office, and the McMaster Campus stations). The properties of climate stations used to create the composite solar radiation dataset are summarized in Table 4.3.

4.1.3 Final Climate Dataset Selection

Four input climate datasets were necessary to complete the modelling analyses for this study:

1. A dataset for model calibration (WY2005-WY2011);
2. A 25-year dataset for the quantification of long-term average conditions;
3. A 10-year (historic) time series for the drought scenario; and,
4. A series of long-term climate change scenarios.

All four input datasets require daily precipitation, daily minimum and maximum temperature, daily net solar irradiation, and hourly rainfall intensity distribution. Input datasets were assembled for each water year.

NEXRAD precipitation data were used for the model calibration period. The data cover a time period during which the publically available EC climate data become more limited and EC data were not verified or calibrated after 2006. The NEXRAD dataset provided the best continuous, spatially distributed and temporally complete estimate of hourly rainfall for this period.

Daily rainfall volumes were adjusted using the monthly correction factors determined in Appendix A. In winter months, the NEXRAD data was assumed to be in the form of rain (unless the maximum

temperature for that day was below the critical temperature (0°C)). These data were supplemented with median snowfall determined at the EC stations shown in Figure 4.2. Daily totals were summed on a synoptic basis (8am-8am) to be consistent with the EC AES dataset.

Long-term daily data for WY1986 to WY2010 were taken from the MNR Infilled Climate Database (Figure 4.11) and were used for the assessment of long-term average conditions and the drought scenario, which will be simulated using historic climate data from the 1960s. The historic drought scenario is discussed in Section 13. The climate change scenario selection and data processing are discussed in Section 15.

4.2 Land Cover and Land Use

Land use and land cover are important structural inputs to the GSFLOW and PRMS models because they strongly influence hydrologic response. A large number of land use categories are found in the study area. For illustrative purposes, only the five primary types (forests, agriculture, urban, water bodies, and wetlands) are shown in Figure 4.14. Natural areas, including forests and wetlands, cover 50% of this relatively rural area. Agricultural land use covers 44% of the model area, while developed/settled areas (i.e., rural residential, transportation, parks, industrial, commercial, etc.) cover another 3.1% of the model area. Quarry and pit operations affect 1.2% of the study area. Discussions of how hydrological properties were assigned to different land use categories are presented in Section 9.

The primary sources for land use/land cover data was (listed in order of applied priority) were:

- Ecological Land Classification (ELC) provided by the LSRCA (2014);
- Southern Ontario Land Resource Information System (SOLRIS v1.2) compiled by MNR (2008); and
- Southern Ontario Interim Land Cover (SIL) product also provided by MNR (2006).

Using these three sources, a contiguous land cover map was produced as shown on Figure 4.15.

4.3 Surface Water

The streams, lakes, and wetlands that drain the study area are shown in Figure 4.16. The study area contains three major subwatersheds: the Talbot River, Whites Creek, and Ramara Creeks catchments. These watersheds are bounded by the Beaver River to the south, the Head River to the immediate north and the 12,500 km^2 Trent River watershed to the east which drains south-east through the Trent-Severn Waterway to Lake Ontario at Trenton.

Surface water data from several sources, including streamflow measurements, previous modelling efforts, canal operations, and surface feature mapping were complied. Stream networks were mapped and classified using the Ontario Ministry of Natural Resources (MNR) OHN Watercourses (OHNWCRS) coverage (from September 2010). The collected stream, lake, and wetland coverage has been processed and is illustrated on Figure 4.16.

The Trent-Severn Waterway bisects the study area through the Talbot River, Canal and Mitchell Lakes, to Balsam Lake as illustrated on Figure 4.17. The Waterway is managed and maintained by Parks Canada. Six control structures maintain a navigable channel from Lake Simcoe at 219 masl to Balsam Lake at 256 masl; the highest point in the Trent-Severn Waterway. The Waterway structures and operating rules are discussed in detailed in Section 4.3.3.

4.3.1 Streamflow Monitoring

Streamflow monitoring locations are shown on Figure 4.18. LSRCA operates two active stream gauges within the study area; one on the Talbot River near Gamebridge (LS0109), the other on Whites Creek at Regional Rd. 23 (LS0402). Seasonal streamflow monitoring was undertaken by Dr. P.J. Dillon of Trent University during 2010 and 2011 at five locations in the Whites Creek watershed. This monitoring was to support a 2011 project to estimate nutrient loading to Lake Simcoe from Whites Creek. Lake stage records for Canal and Mitchell Lakes were requested from Parks Canada; however, data were not made available for this project. There are no Water Survey of Canada (WSC) stream gauges within the study area. Table 4.5 provides a summary of the gauge properties and streamflow characteristics for the available stations.

Streamflow on the Talbot River at the LSRCA gauge (Figure 4.19) appears to be strongly influenced by canal operations. The large events recorded during January 2008 and December 2009 were the result of control operations by Park Canada staff to divert water from the upper Trent watershed to Lake Simcoe (Lance Aspden, LSRCA, oral communication, 2014). These operations are routinely undertaken to create additional winter storage in the central Trent-Severn to accommodate predicted spring freshet flow. The influence of TSW control structures can also be observed during the summer and fall months as gradual or sudden changes in discharge. The TSW structures and operating rules will be discussed further in the subsequent section. Because flows at this gauge are influenced by canal operations, and because the timing and volume of releases were not provided, these data were unsuitable for model calibration.

While there are six monitoring locations within the Whites Creek watershed, only the LSRCA gauge at Regional Rd. 23 provides a multi-year record (Figure 4.20). The LSRCA gauge also provides a relatively continuous record with few gaps due to ice or vegetation. While having short periods of record, the TrentU-Dillon stations provided valuable insight into the response of the watershed (Figure 4.21 though Figure 4.24). A large portion of the annual flow is released from the Whites Creek catchment as freshet, and the peak annual flows generally correspond to the spring freshet. This agrees with observation that the bulk of the annual flood peaks in rural Ontario watersheds are a result of rain-on-snow events (Dickinson *et al.*, 1992). However, there are also large runoff events observed during the summer and fall months. This may be due to the till soils and to the influence of agricultural land use (i.e., tile drains) that cause rapid response to convective storm events.

Given the small contributing area for the headwater TrentU-Dillon gauge stations (see Table 4.5 or Figure 4.18), only WR06 and WR12A (with catchment areas over 10 km^2) were expected prove useful as model calibration targets. WR06 also has a very short period of record. Therefore, LS0402 and TrentU-Dillon site WR12A were used as the primary calibration targets for calibration of the hydrologic model.

The uncertainly with the individual measurements in the provided streamflow data was difficult to quantify precisely. While the TrentU-Dillon stream discharge measurements are extremely useful, it should be noted that the inherit uncertainty in these data is likely higher given the short period of record because it can be difficult to build a complete rating curve without repeated discharge measurements over the range of expected stage. With regards to individual discharge measurements, several authors report a measurement uncertainty of 5% at the 95% confidence interval (Terzi, 1981 and Herschy, 2002). As a comparison, open water discharge measurements obtained by the WSC are typically fitted to within a 5% window, and under ice measurements to within a 10% window (Hamilton, 2012). Hamilton (2008) observes that this uncertainty cannot be assumed to be uniform across the entire range of possible discharge values. He further goes on to reason that the uncertainly in small discharge and velocity measurements (i.e., at low flow) may be high due to unavoidable limits on measurement equipment scale and dimension. Awareness of the

inherent uncertainty within the stream gauge data is critical when producing model calibration targets and evaluating the quality of the model calibration.

4.3.2 Baseflow

Hydrograph separation techniques were applied to the continuous flow data to split the two components of streamflow: (1) overland runoff and (2) baseflow. Baseflow is generally assumed to be primarily composed of groundwater discharge. It should be noted that the separation methods cannot, by themselves, distinguish between groundwater discharge and other relatively steady flows such as discharge from reservoirs or large wetlands. Numerous techniques are available to estimate baseflow including curve processing and statistical techniques.

Baseflow was estimated using the modified United Kingdom Institute of Hydrology (UKIH) smoothed minima method devised by National Water Research Institute and Meteorological Service of Canada (Piggott *et al.,* 2005). The average annual discharge and the Q_{50} are provided in Table 4.5 for each stream gauge in the study area. Given the short period of record of the at the TrentU-Dillon measurement locations and the influence of the canal system on the LSRCA gauge on the Talbot River, meaningful baseflow estimates could only be obtained for the LSRCA Whites Creek gauge. A baseflow value of 0.36 m^3/s was estimated for this gauge.

While the average yearly baseflow discharge is treated as a secondary MODFLOW steady-state calibration target, the relative uncertainty in this single value remains high. Fortunately, when the two models are integrated in GSFLOW simulations, the need for separated baseflow targets is removed because the GSFLOW model is calibrated to total flows at the gauge rather than to estimated baseflow.

4.3.3 Trent-Severn Waterway

The Trent-Severn Waterway (TSW) provides a 386 km navigable chain of interconnected rivers and lakes from Lake Ontario at Trenton to Port Severn in Georgian Bay. The TSW was constructed piecemeal between 1833 and 1920 primarily to serve commercial traffic; however, the completion of the Welland Canal in 1932 rendered it obsolete for this purpose. The canal system now serves thousands of recreational boaters during its May to October operating season.

Prior to the construction of the TSW between Lake Simcoe and Balsam Lake between 1895 and 1907, the lower Talbot was difficult to navigate, and was typically bypassed by native Hurons and fur traders (Angus, 1988). The portage, called “Ouskebawkning” or “the green leafy place where we leave the river” was an artery of the fur trade network in the 17th and 18th centuries (Fleming, 1991; Allen, 2004). Old Portage Road approximately follows the route of the former 17km carry. The Bolsover Dam at Lock 37 backs up water 12km to the Kirkfield Lift lock, submerging numerous serpentine bends in the Talbot River to create Canal Lake and a navigable link across the formerly swampy valley.

Water levels are maintained by a series of dams, and navigation is accomplished through locks which raise and lower boats between adjacent sections of the waterway. There are six such structures between Lake Simcoe and Balsam Lake (Figure 4.17), the first five of which are pound locks (typical: Figure 4.1a) with a hydraulic lift lock at Kirkfield providing the final 14.9 m rise into Mitchell Lake (Figure 4.1b). Mitchell Lake and Balsam Lake are interconnected though a short section of canal, and operate at the same water level during the navigation season.

a)  b) 

Figure 4.1: TSW Lock (a) #37 - Bolsover and (b) #36 – Kirkfield.

To ensure safe navigation, consistent water levels are maintained during the operating season (Table 4.1). The canal system is drawn down in the late fall to provide storage capacity to capture mid-winter and spring melt. The representation of the TSW within the hydraulic sub-model will be discussed in Section 8.5.

Table 4.1: Navigable TSW water level elevations towards Trenton from Lake Simcoe.

Lock Name	Lock Number	Rise (m)	Navigation Level* (masl)	
			Minimum	***Maximum***
Gamebridge	41	3.0	221.82	--
Thorah	40	4.3	226.04	--
Portage	39	4.0	230.34	--
Talbot	38	4.3	234.58	--
Bolsover	37	6.6	241.15	241.25
Kirkfield Liftlock	36	14.9	256.16	256.19

* Values provided by Parks Canada (n.d.)

4.3.4 Cross-boundary flow from the Trent Watershed to the Talbot Watershed

Given that Balsam Lake drains both southeast into Cameron Lake and west into Mitchell Lake, it is very likely that a considerable amount of flow crosses the topographic boundary between the Lake Simcoe and Trent River watersheds. The Gull River, which feeds Balsam Lake, drains an area of 1,300 km^2 at Norland alone. To determine if, on average, there is flow from the Trent watershed into the Talbot River subwatershed, an analysis was undertaken to compare observed streamflow at the two LSRCA gauge stations; Talbot River near Gamebridge (LS0109) and Whites Creek at Regional Rd. 23 (LS0402). The streamflow at these two gauges is shown on Figure 4.25 for the overlapping period, 2009 through 2011. Streamflow can be converted to total runoff by normalizing the data to the contributing area of each gauge, 88.0 km^2 and 328 km^2 for Whites and Talbot, respectively, as shown in Figure 4.26. It can be observed that the Talbot River watershed appears to contribute a significantly larger amount of runoff than the Whites Creek watershed. Assuming that runoff volumes between these two adjacent catchments are similar, it is likely this extra runoff represents flow from the Trent watershed (i.e., Balsam Lake) into the Talbot subwatershed through the connection to Mitchell Lake. The low flow portion of the hydrograph is also dramatically affected,

both by this excess inflow and by the additional storage provided by the canal system (Figure 4.27 and Figure 4.28).

Discharge and runoff can also be presented as flow duration curves for the overlapping period at the two LSRCA stream gauges (Figure 4.29 and Figure 4.30, respectively). When considering the runoff duration curve, the median runoff in the Talbot Watershed is 1 mm/day while only 0.4 mm/day in the White Creek catchment (indicating that Talbot River has anomalously high runoff volumes). The effect of the considerable storage in Canal and Mitchell Lake can also be noted at the extreme end of the runoff duration curve where above the Q_5 (5% exceedance), the daily runoff in Whites Creek surpasses that of the Talbot River.

The estimated excess runoff, or the estimated additional runoff diverted from the Trent watershed westward, can be estimated by subtracting the average monthly runoff (Figure 4.32) between the Talbot and Whites Creek gauge stations. This estimated additional runoff is presented on Figure 4.33 and suggests an additional monthly runoff between 11 mm and 25 mm for the months of April through January. On average, 14 mm per month, or 168 mm per year, of additional runoff is diverted into the Talbot River subwatershed. The estimate of excess total monthly runoff can be converted to discharge by multiplying by the gauged area at the Talbot station. Figure 4.34 presents the estimated monthly discharge diverted into the Talbot subwatershed. The average discharge observed at the LSRCA Talbot gauge between 2009 and 2010 was 5.0 m^3/s, the estimated diverted flow is 1.74 m^3/s, or approximately 35% of the observed flow. This represents 5.5 million cubic meters of diverted water a year, or the equivalent of an extra 170 km2 of contributing area to the Talbot River subwatershed (an additional 5% to the overall Lake Simcoe Watershed (3,400 km2)).

As was noted, the above analysis is based on based on only 3 years of streamflow data and on the assumption that the annual runoff volumes are similar (i.e., that precipitation volumes and watershed characteristics are also similar). The presence of alvar in the Upper Talbot watershed should decrease runoff volumes as compared to Whites Creek, suggesting that the analysis may be underestimating the net inflows from Balsam Lake.

Given the scope of the current project, it is not possible to incorporate Balsam Lake and its contributing area into the GSFLOW model. To account for the additional discharge from the Trent watershed, the estimated monthly excess discharge was added as a diversion into Mitchell Lake, as discussed further on in Section 8.

4.4 Tables and Figures

Table 4.2: List of climate stations available from 1955 to present.

Station ID	Station Name	Easting	Northing	Distance from Model Area (km)	Period of Record
6110480	BALDWIN	634081	4903234	21.7	2004 - 2011
6117700	BARRIE-ORO	615311	4926210	21.8	2003 - 2011
611095R	BRECHIN BEACH	643023	4932317	0.0	1985 - 1994
6161682	COBOCONK	676977	4940936	5.8	1970 - 1978
6111769	COLDWATER WARMINSTER	615809	4942886	19.9	1971 - 2011
6111965	DALRYMPLE LAKE	648407	4940218	0.0	1970 - 1975
6162375	FENELON FALLS	680368	4933248	9.4	1915 - 1970
6162376	FENELON FALLS	678626	4938758	7.2	1981 - 2000
611K661	GAMEBRIDGE	650995	4931386	0.0	1989 - 1993
6163360	HARTLEY	667146	4921779	3.2	2001 - 2008
6164207	KIRKFIELD	660394	4937169	0.0	1978 - 1980
6114295	LAGOON CITY	641385	4934504	0.0	1994 - 2011
6164430	LINDSAY	679329	4913210	17.8	1880 - 1971
6164432	LINDSAY FILTRATION PLANT	680923	4913254	18.9	1964 - 1990
6164433	LINDSAY FROST	680157	4912121	19.2	1974 - 2007
6164615	LORNEVILLE	663027	4927232	0.0	1965 - 1987
6115811	ORILLIA BRAIN	623805	4939701	11.6	1992 - 2010
6115820	ORILLIA STP	625349	4941953	10.3	1965 - 1993
6115856	ORO WAM	623180	4930799	13.0	1974 - 1977
6116309	PEFFERLAW	641917	4910067	12.1	1971 - 1972
616PA87	ROSEDALE	676274	4937582	4.9	1975 - 1994
6117682	SEVERN BRIDGE	632147	4958757	11.8	1975 - 1995
6118142	STROUD LEONARDS BEACH	617201	4909577	28.0	1971 - 1974
6119055	UDORA	646875	4902397	18.1	1989 - 2011
6119129	VALLENTYNE	646052	4903490	17.2	1983 - 1989
6119325	WASHAGO	632193	4956536	10.2	1927 - 1970
6169648	WOODVILLE	667231	4918446	5.9	1981 - 1982
6169647	WOODVILLE	660860	4918286	3.0	1987 - 2000
LS0402	Whites Creek at Regional Rd 23	647493	4922512	0.0	2010 - present

Table 4.3: List of solar radiation stations used to compile study-area solar radiation estimates

Station	Location	Coordinates	Sensor type(s)	Data interval	Units	Period of record
McMaster (on-campus) weather station	McMaster University campus, 1280 Main Street West, Hamilton, Ontario, L8S 4K1, Canada	43°15'42.93" N, 79°55'11.86" W, elevation: 90 masl	Kipp and Zonen, model CNR1 net radiometer and a CM3 Pyranometer	15 minute	W/m²	2009-2011
McMaster (MESONET) weather station: HRCA weather station	HRCA Main Administration Office	E: 588654 N: 4808841	unknown	30 minute	W/m²	2006-2011
McMaster (MESONET) weather station: Kelso weather station	Kelso wellfield	E: 586316 N: 4818708	unknown	30 minute	W/m²	2006-2011
University of Waterloo weather station	North campus	43°28'25.6" N, 80°33'27.5" W, elevation is 334.4 masl	Kipp & Zonen Model: CM11	15 minute	W/m²	1998-2010
University of Toronto weather station*	University of Toronto at Mississauga Meteorological Station (UTMMS)	43° 33’ N, 79° 40’ W	Kipp & Zonen model CM-5 and Kipp & Zonen CM-11 (from July 2007)	hourly	mv and W/m²	1999-2012
Environment Canada**	611KBE0 Egbert Care	E: 597434 N: 4898143	unknown	daily	MJ/m²	1988-2003
Environment Canada**	6142285 Elora Research Station	E: 546774 N: 4833164	unknown	daily	MJ/m²	1970-2003
Environment Canada**	6143083 Guelph OAC	E: 562230 N: 4818850	unknown	daily	MJ/m²	1962-1970
Environment Canada**	6158350 Toronto	E: 628988 N: 4836465	unknown	daily	MJ/m²	1956-2000
Environment Canada**	6158740 Toronto Met Res Station	E: 616643 N: 4850681	unknown	daily	MJ/m²	1967-1988
Environment Canada**	6158776 Toronto Scarborough	E: 642575 N: 4842297	unknown	daily	MJ/m²	1959-1973

*mv to W/m² conversion factor was 93.63 W/m²/mv for the CM-5 and 77.276 W/m²/mv for the CM-11 (Ken Turner, Department of Geography, University of Toronto, Mississauga, pers. comm. 2010).

**All EC stations correlate quite well (LSRCA, 2010), having correlation coefficients greater that $R^2>0.9$ amongst all parings with very little systematic error.

Table 4.4: Study area land use classification (simplified).

Classification	**Area (km^2)**	**Percentage**
Forest and Wetlands	540	50%
Agricultural	490	44%
Urbanized/Transportation/Rural Residential	35	3.1%
Open Water	20	1.8%
Quarries and Pits	14	1.2%

Table 4.5: Streamflow and baseflow statistics at study area stream gauges.

ID	Name	UTM Northing (m)	UTM Easting (m)	Available Period of Record	Days of Available Data	Watershed Area* (km^2)	Average Discharge (m^3/s)	Q_{50} (m^3/s)	Estimated Baseflow (m^3/s)
LS0109	Talbot River at Gamebridge	4,929,960	649,498	2005-2011	2,389	328	5.45	3.79	--
LS0402	Whites Creek at Regional Rd 23	4,922,512	647,493	2009-2013	1,679	88.0	0.863	0.394	0.36
WR06	--	4,924,713	652,365	2010-2011	535	20.7	0.104	0.040	--
WR12A	--	4,921,733	652,210	2010-2011	275	61.6	0.348	0.193	--
WR23	--	4,923,459	657,862	2010-2011	543	2.23	0.019	0.002	--
WR29	--	4,926,417	656,860	2010-2011	520	10.8	0.103	0.071	--
WR30	--	4,927,133	656,590	2010-2011	534	2.56	0.016	0.006	--

* Watershed areas were derived from the 50m DEM developed for the PRMS submodel. These areas may not agree exactly with other delineations undertaken with different topographic interpretations.

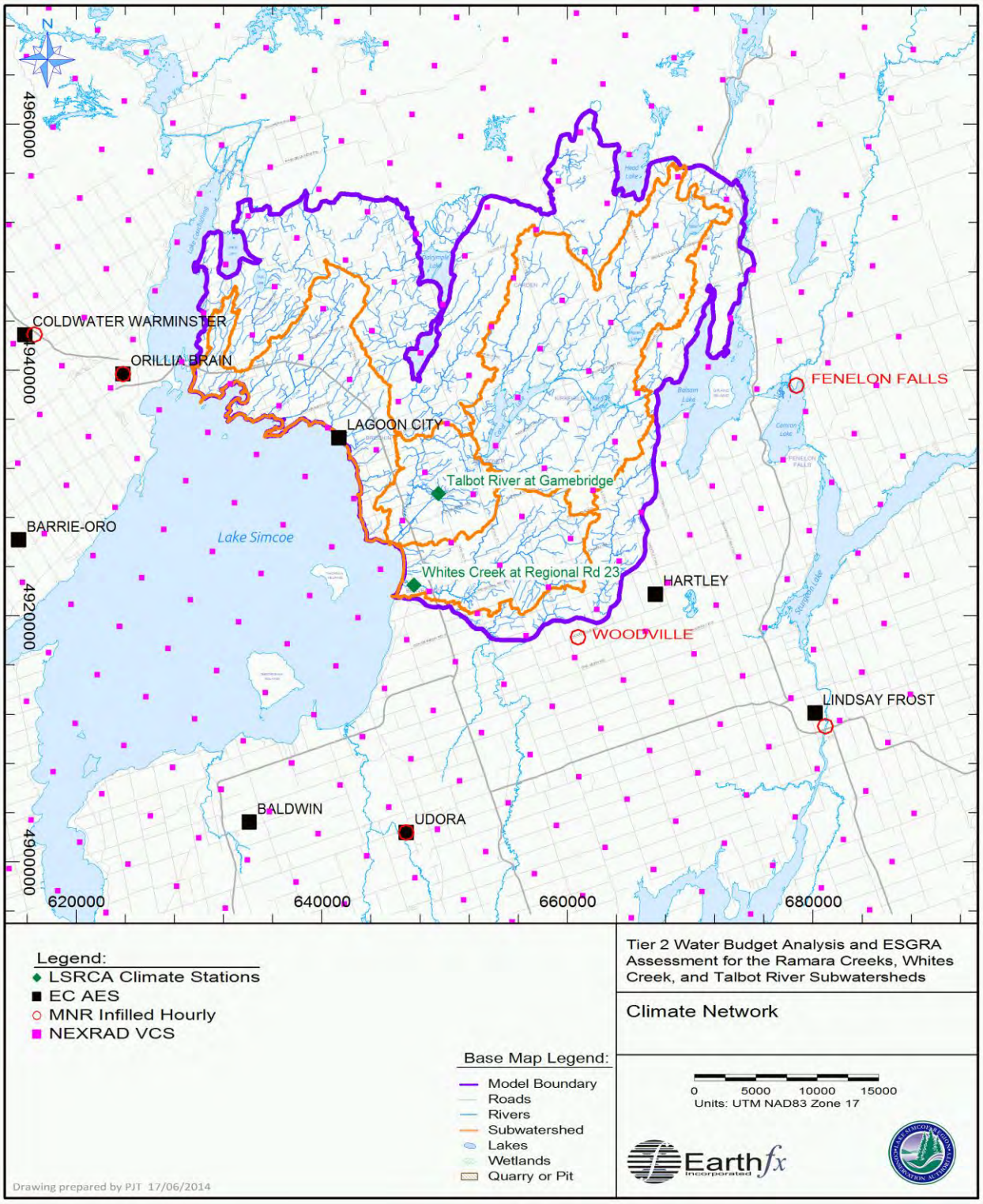

Figure 4.2: Distribution of available climate stations with data after 2000.

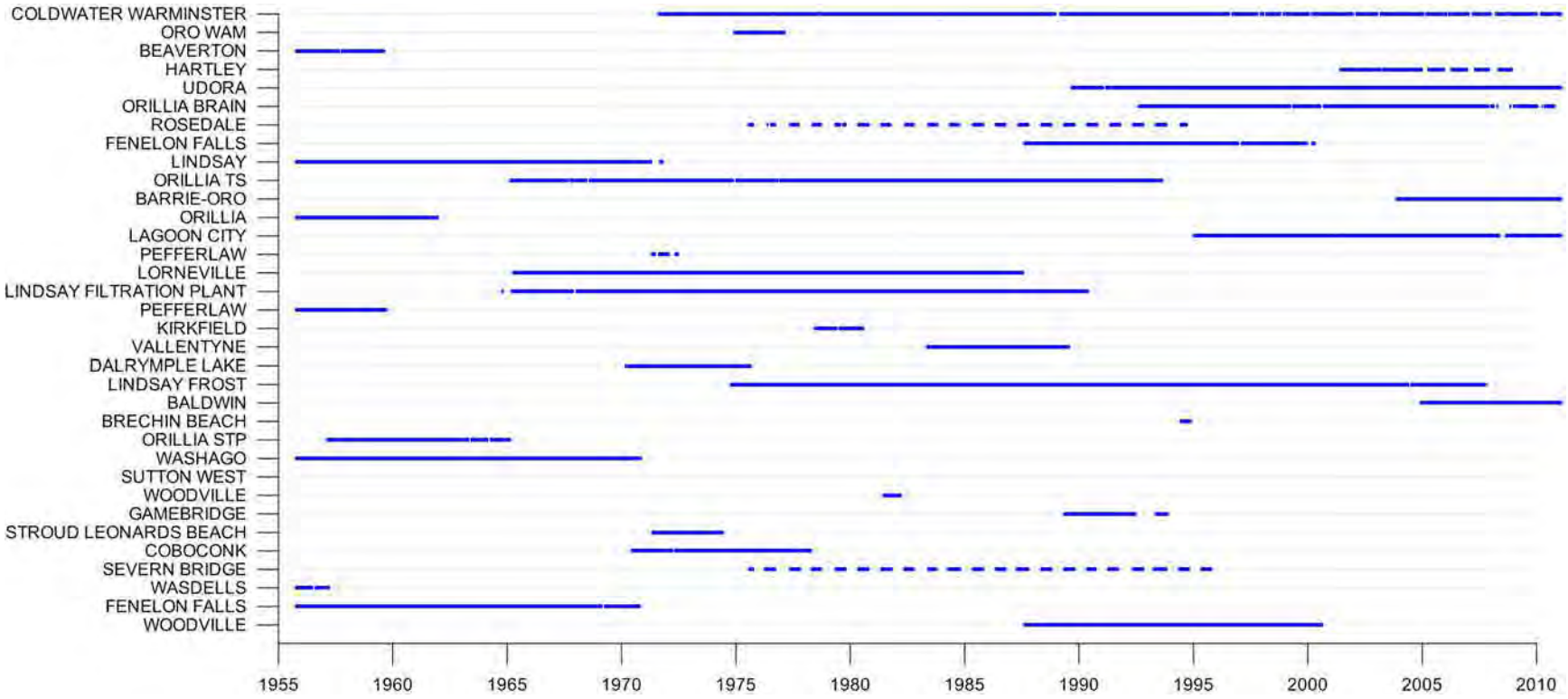

Figure 4.3: Available period of record at Environment Canada AES climate stations proximal to the study area.

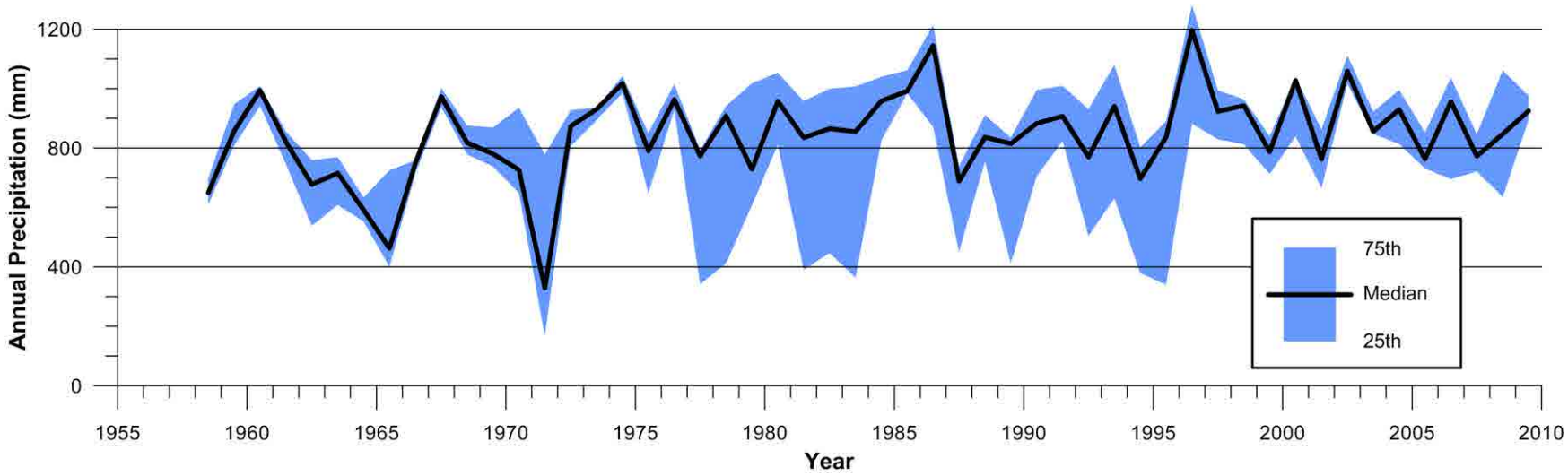

Figure 4.4: Annual precipitation quartiles at AES climate stations.

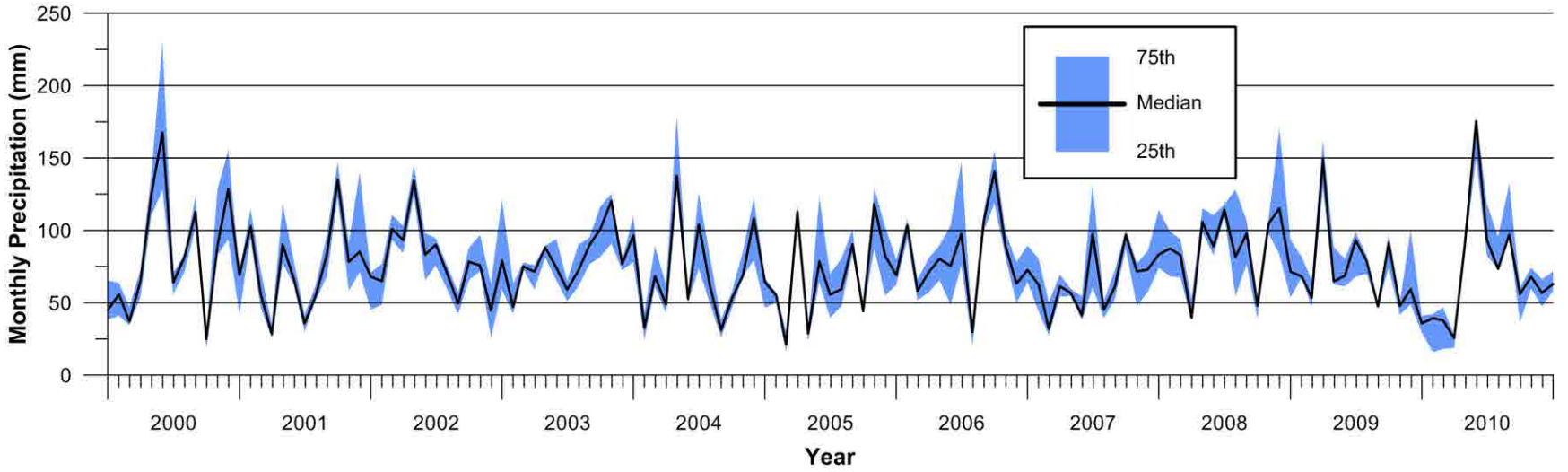

Figure 4.5: Monthly precipitation quartiles at AES climate stations (2000 through 2010).

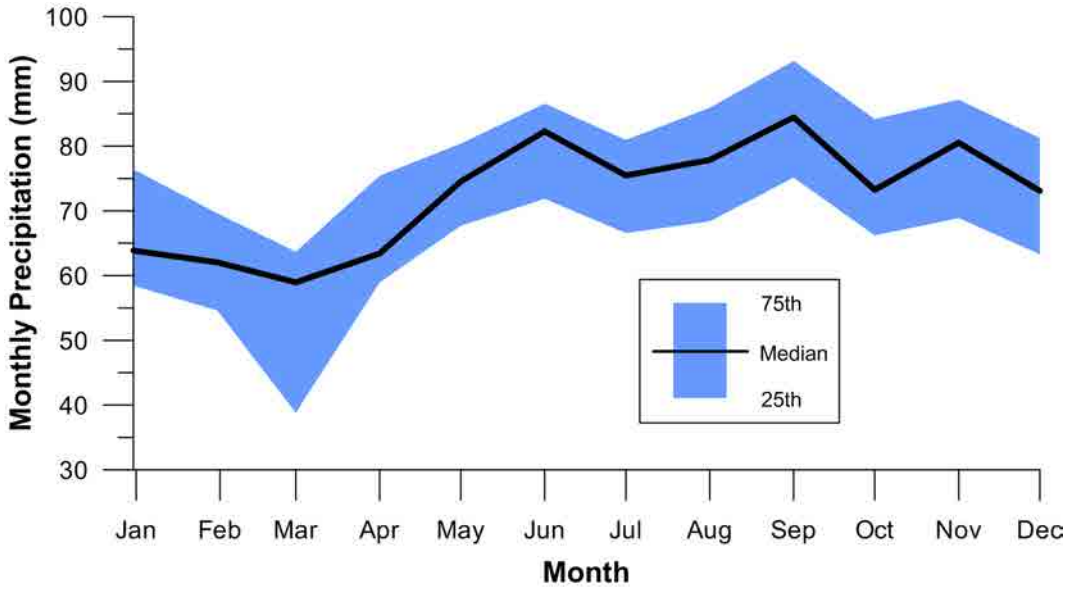

Figure 4.6: Average monthly precipitation quartiles for AES climate stations (2000-2010).

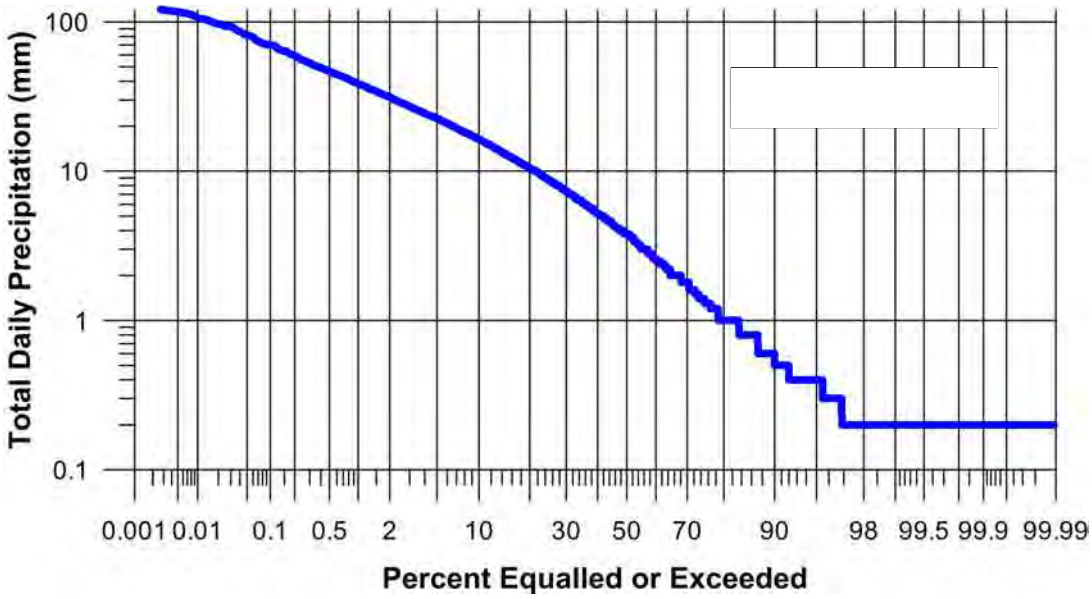

Figure 4.7: Precipitation exceedance plot for AES climate stations (1955-2010).

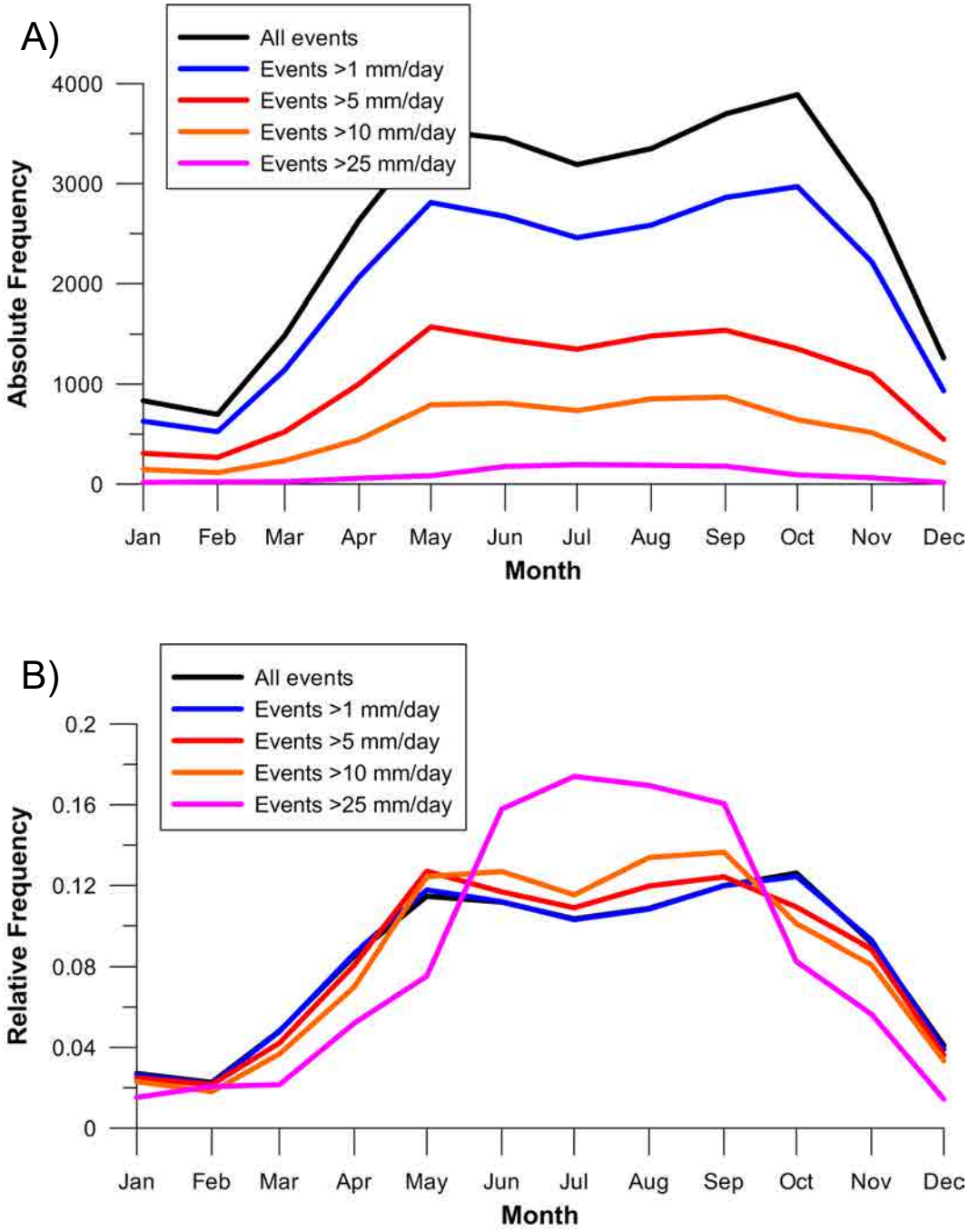

Figure 4.8: (A) Absolute (total number of occurrences) and (B) Normalized (area under each curve = 1) distribution of daily rainfall totals at AES Climate Stations (1955-2010).

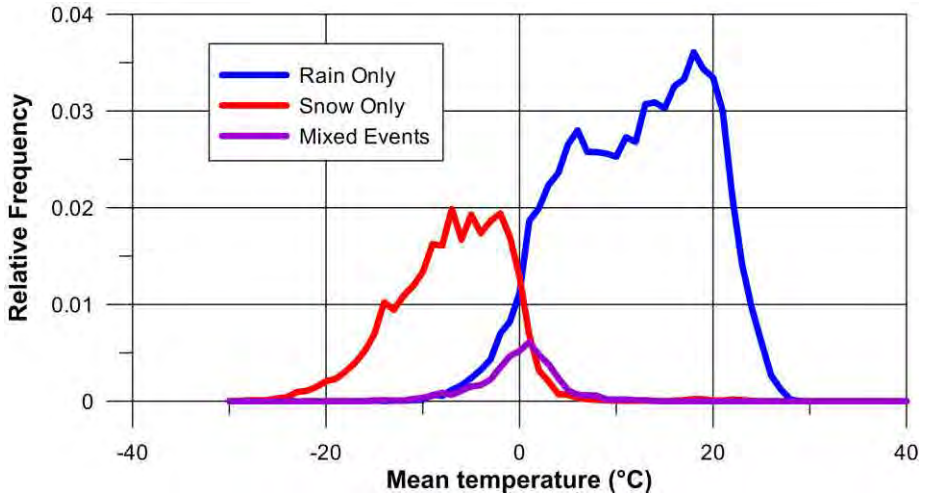

Figure 4.9: Relative frequency and daily mean temperature of observed precipitation types at AES Climate Stations (1955-2010).

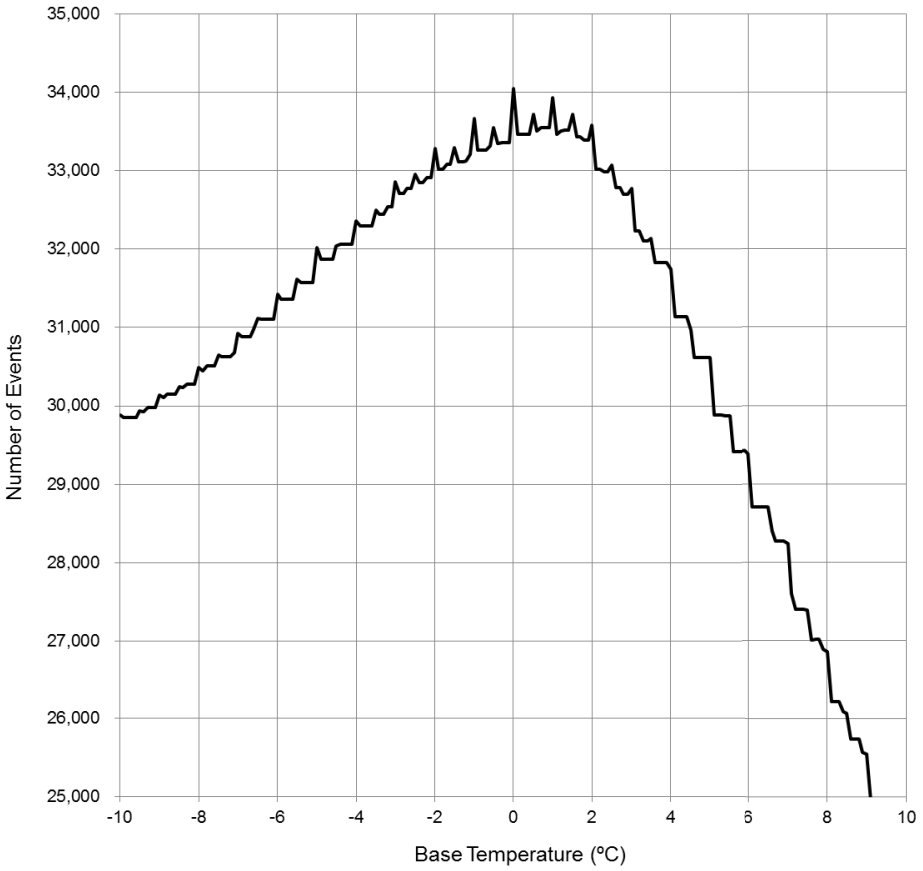

Figure 4.10: Correct predictions of precipitation form at AES stations versus the value for critical (base) temperature (1955-2010).

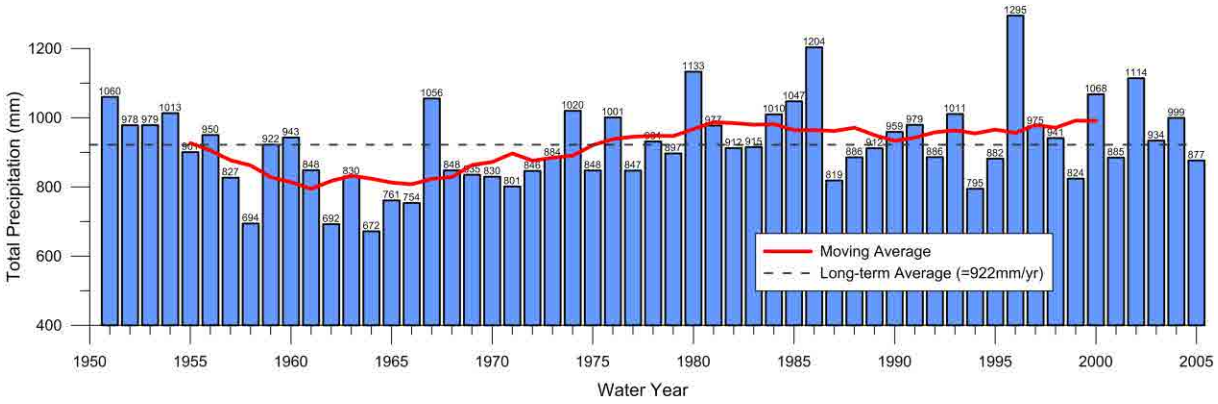

Figure 4.11: Annual average precipitation in the study area (MNR Infilled Climate Dataset, 1950-2005)

Figure 4.12: NEXRAD WSR-88D Radar Installation (Norman, Oklahoma).

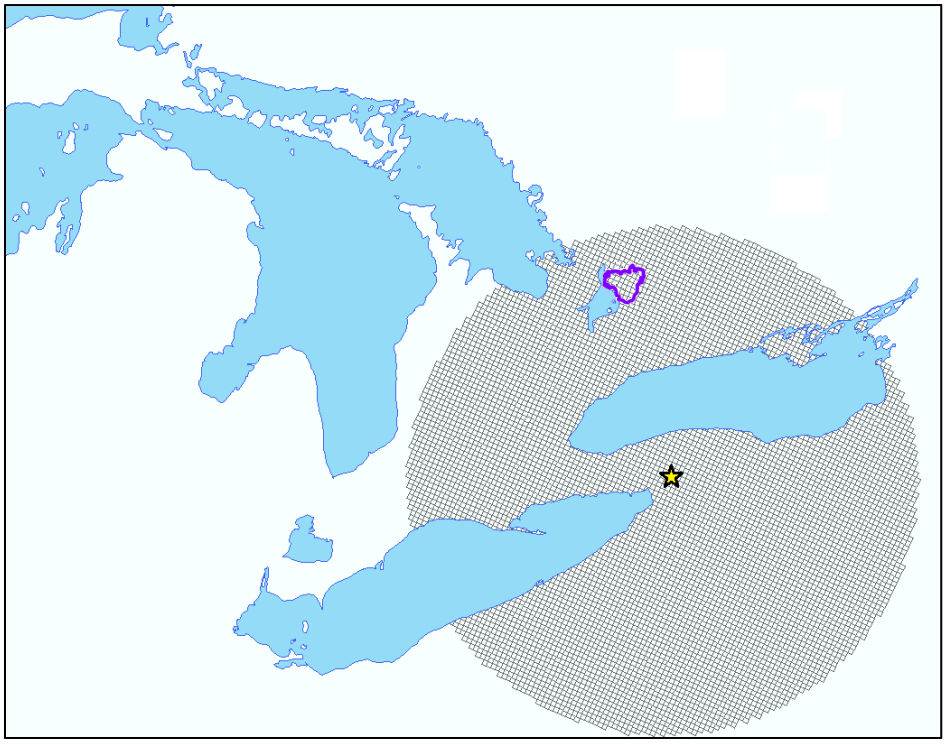

Figure 4.13: Extent of the KBUF NEXRAD VCS network with study area. Yellow star highlights the approximate location of the NEXRAD radar station.

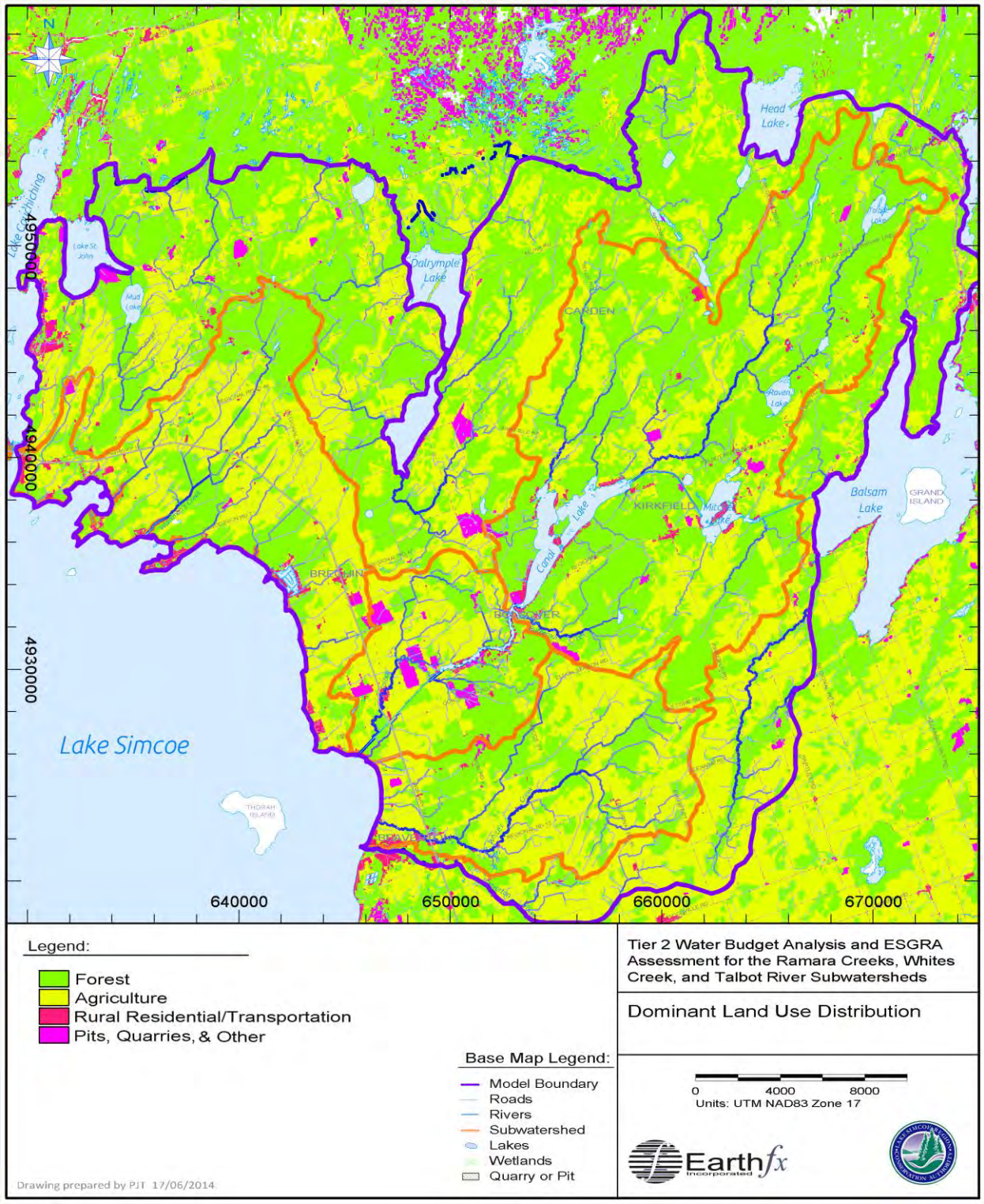

Figure 4.14: Distribution of dominant land use types.

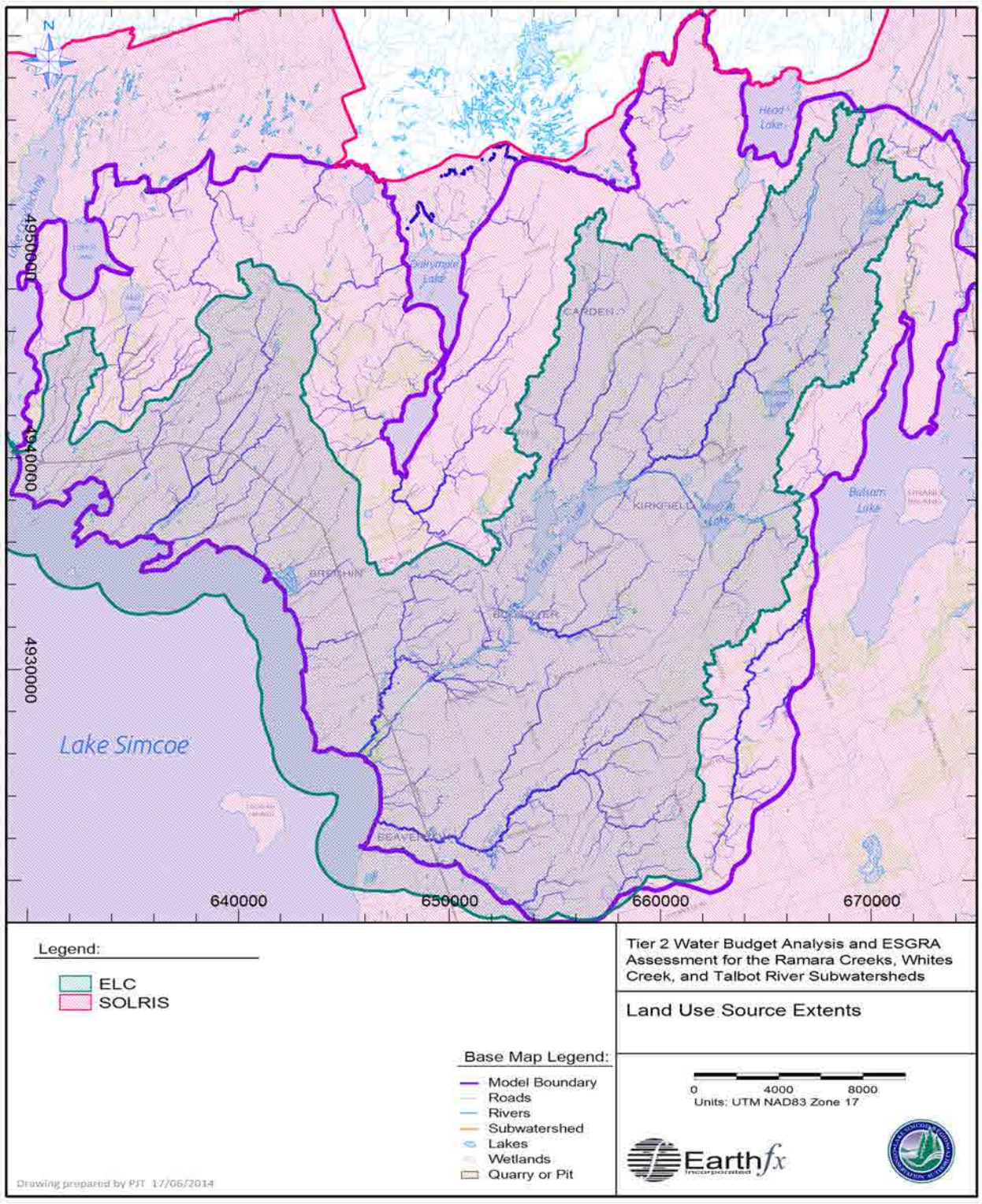

Figure 4.15: Extents of land use sources.

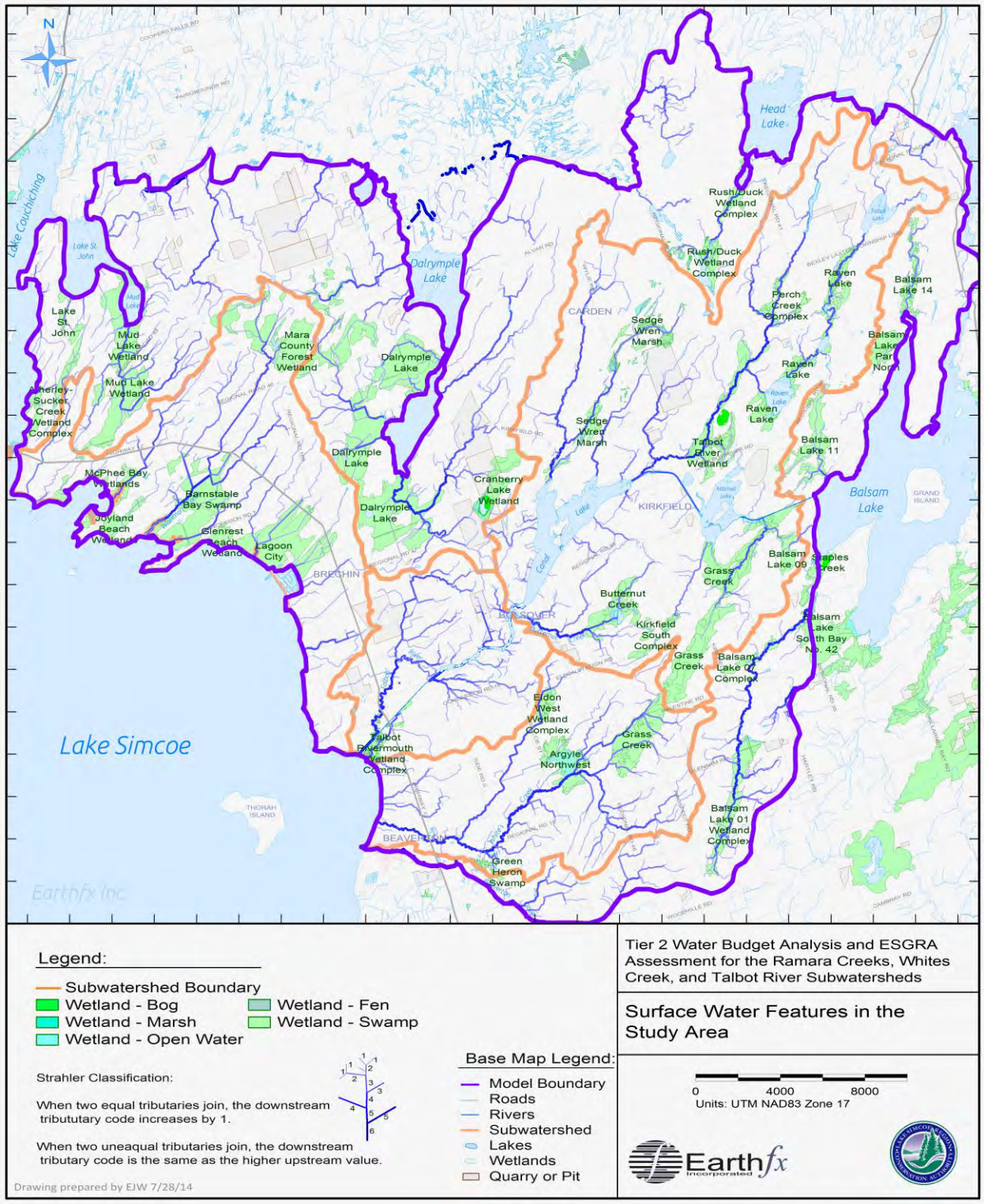

Figure 4.16: Study area surface water features.

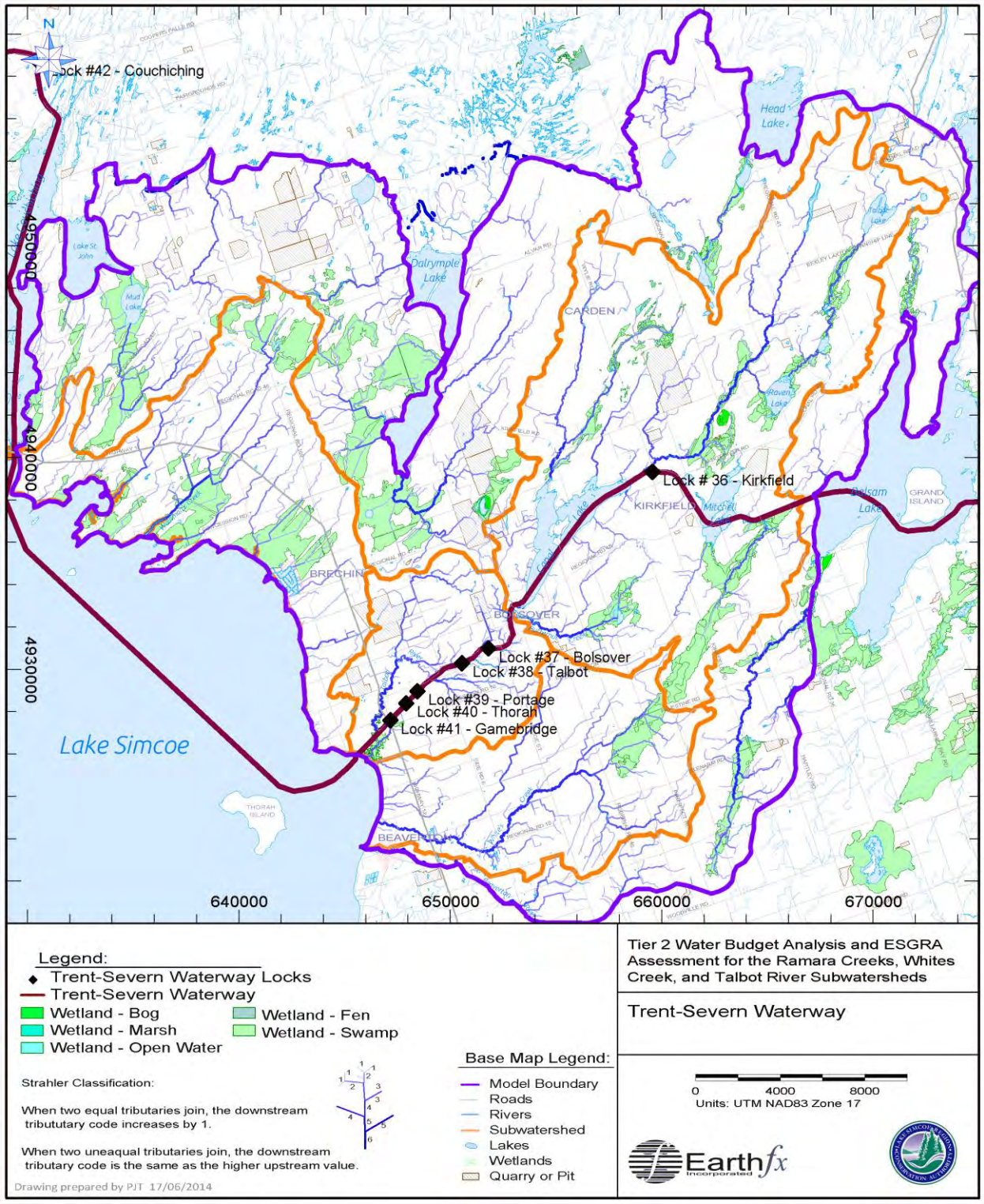

Figure 4.17: Trent-Severn Waterway with lock locations.

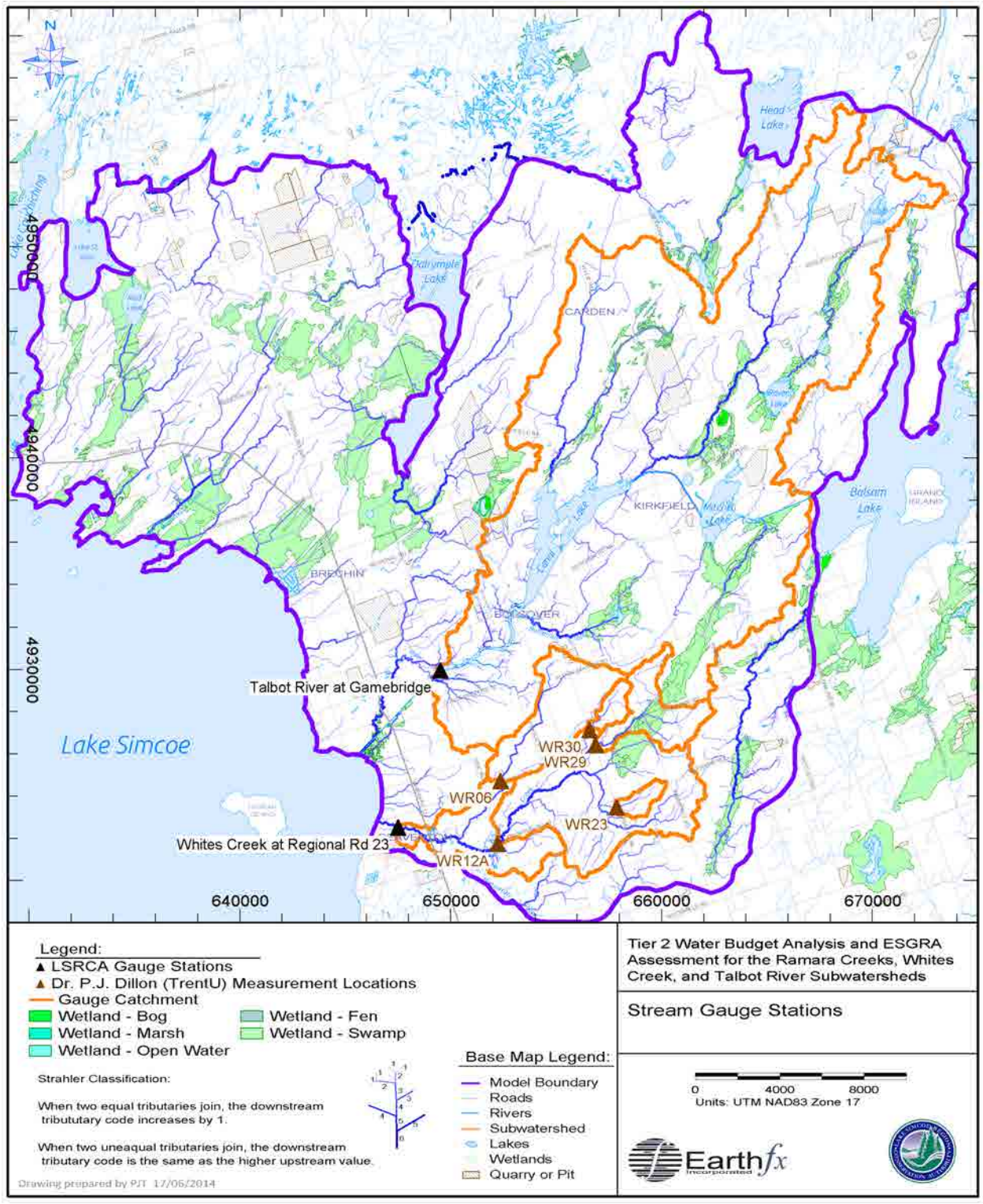

Figure 4.18: Stream discharge measurement locations within the study area.

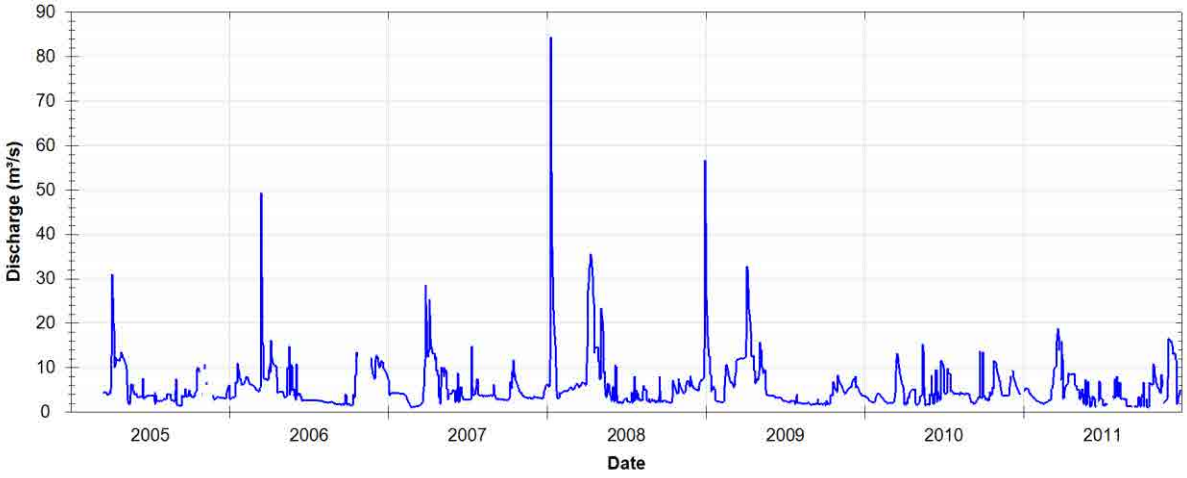

Figure 4.19: Mean daily discharge observed at Talbot River near Gamebridge (LS0109).

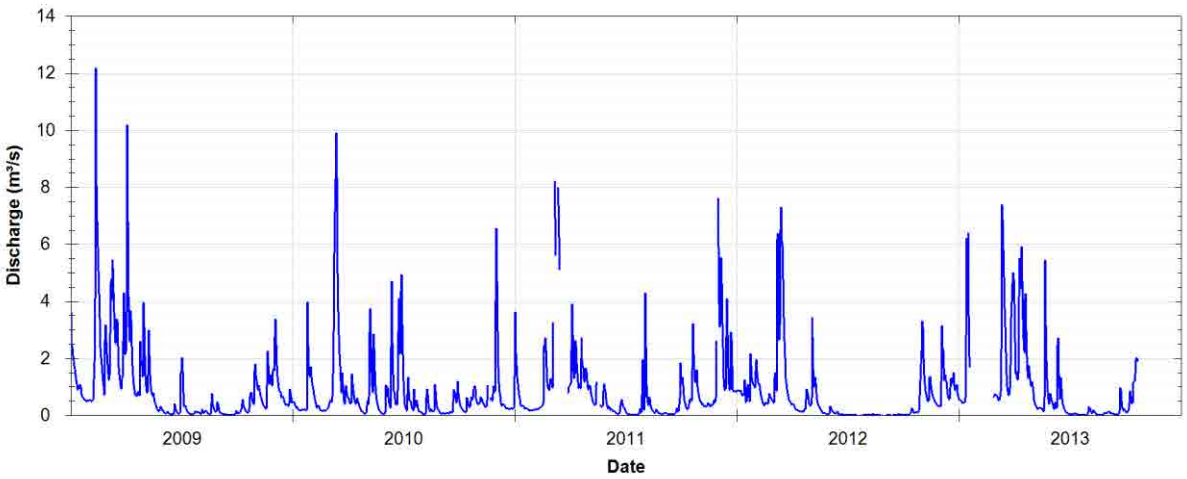

Figure 4.20: Mean daily discharge observed at Whites Creek at Regional Rd. 23 (LS0402).

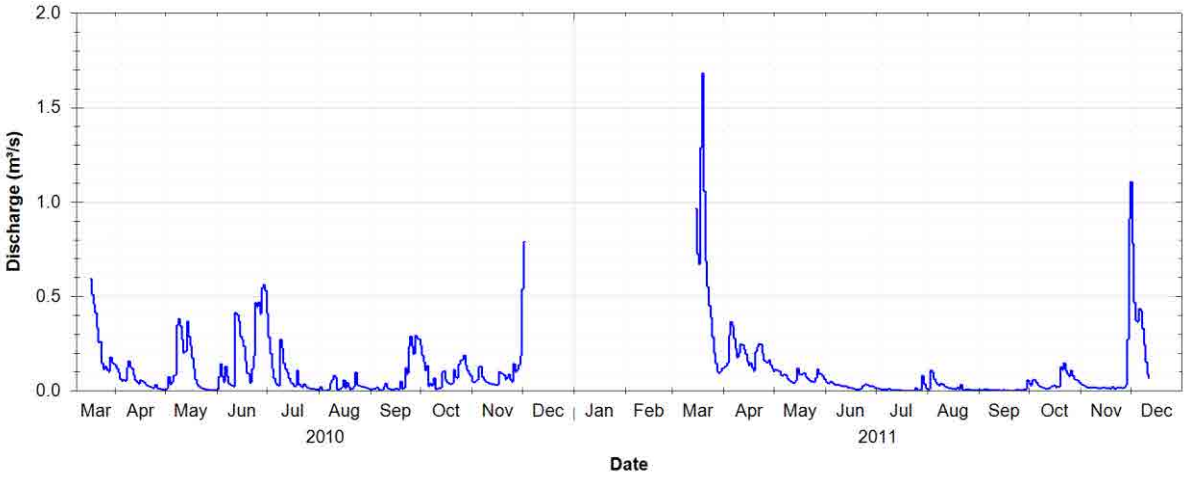

Figure 4.21: Mean daily discharge observed at TrentU-Dillon gauging location WR06.

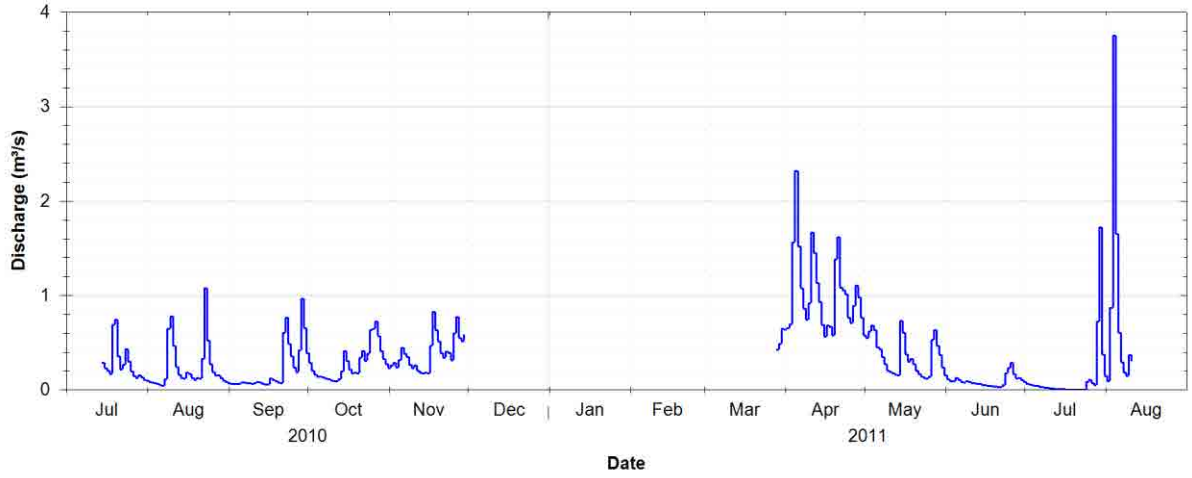

Figure 4.22: Mean daily discharge observed at TrentU-Dillon gauging location WR12A.

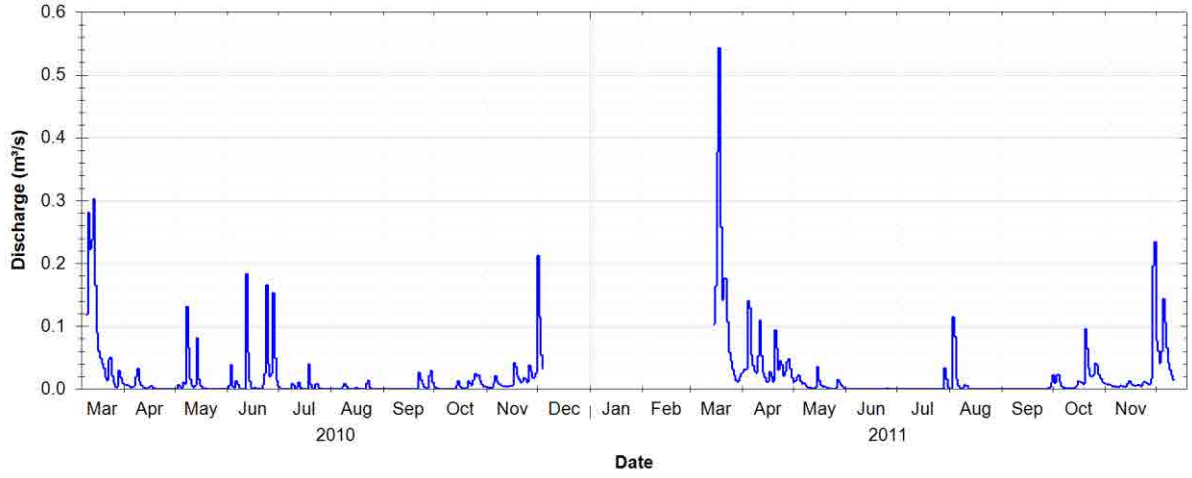

Figure 4.23: Mean daily discharge observed at TrentU-Dillon gauging location WR23.

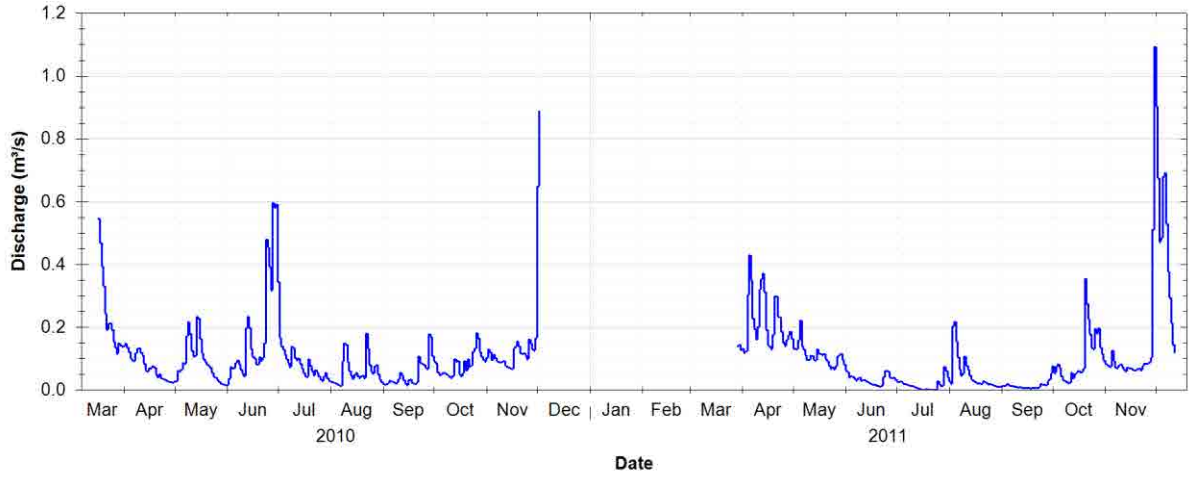

Figure 4.24: Mean daily discharge observed at TrentU-Dillon gauging location WR29.

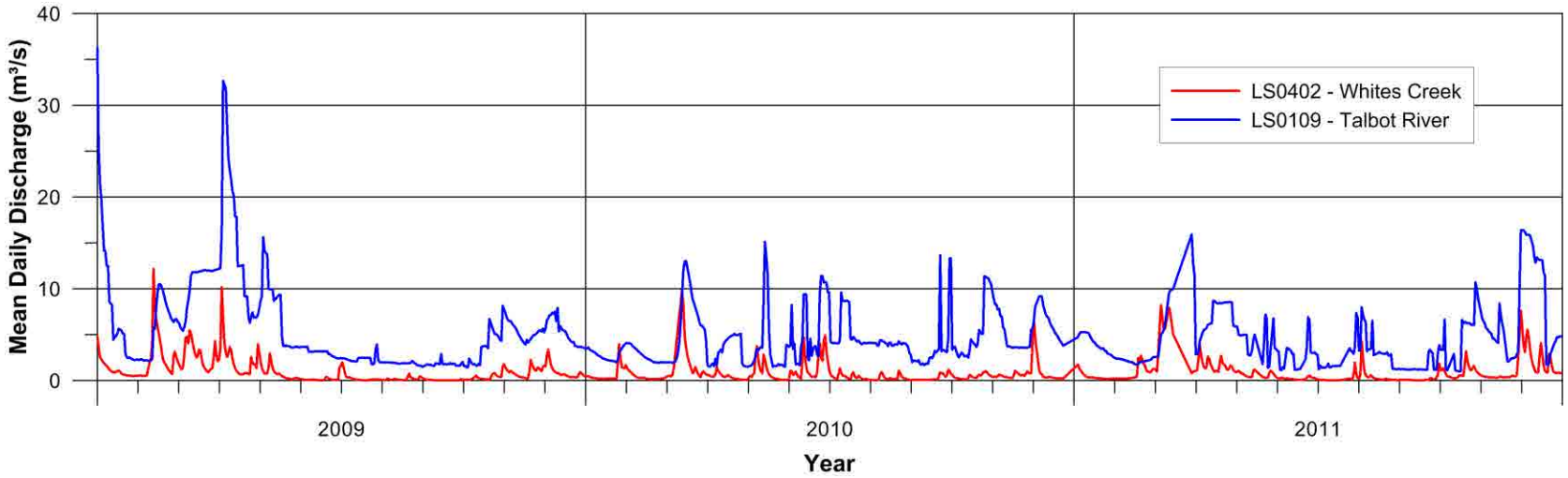

Figure 4.25: Mean daily discharge observed at LSRCA gauge stations Talbot River near Gamebridge (LS0109) and Whites Creek at Regional Rd. 23 (LS0402).

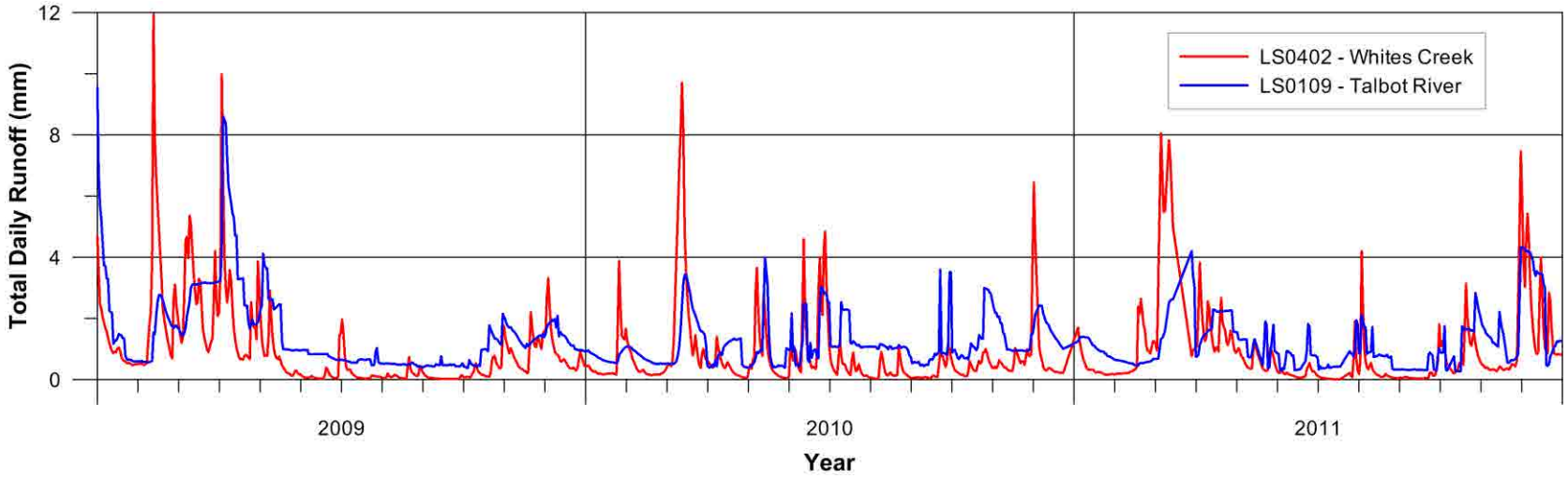

Figure 4.26: Normalized daily watershed runoff observed at LSRCA gauge stations Talbot River near Gamebridge (LS0109) and Whites Creek at Regional Rd. 23 (LS0402).

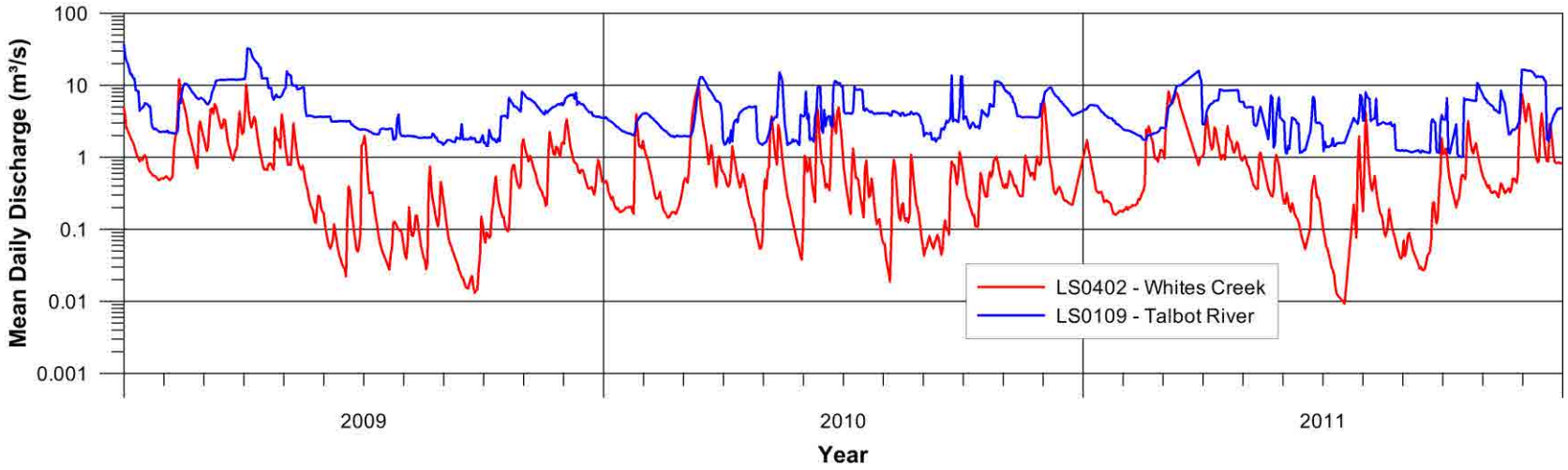

Figure 4.27: Log mean daily discharge observed at LSRCA gauge stations Talbot River near Gamebridge (LS0109) and Whites Creek at Regional Rd. 23 (LS0402).

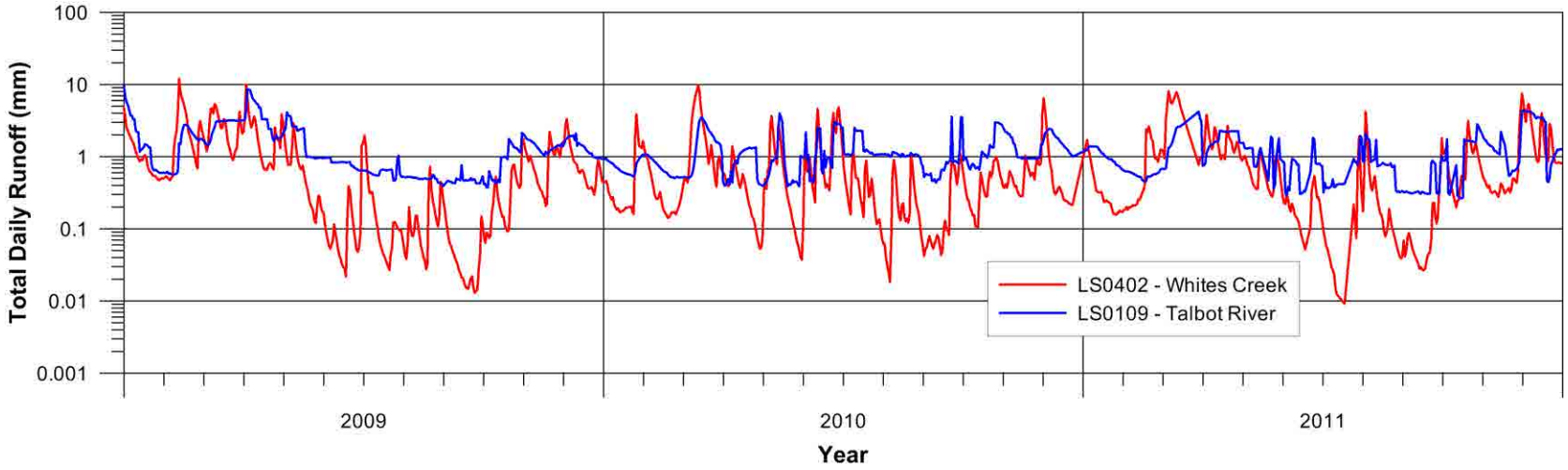

Figure 4.28: Normalized log daily watershed runoff observed at LSRCA gauge stations Talbot River near Gamebridge (LS0109) and Whites Creek at Regional Rd. 23 (LS0402).

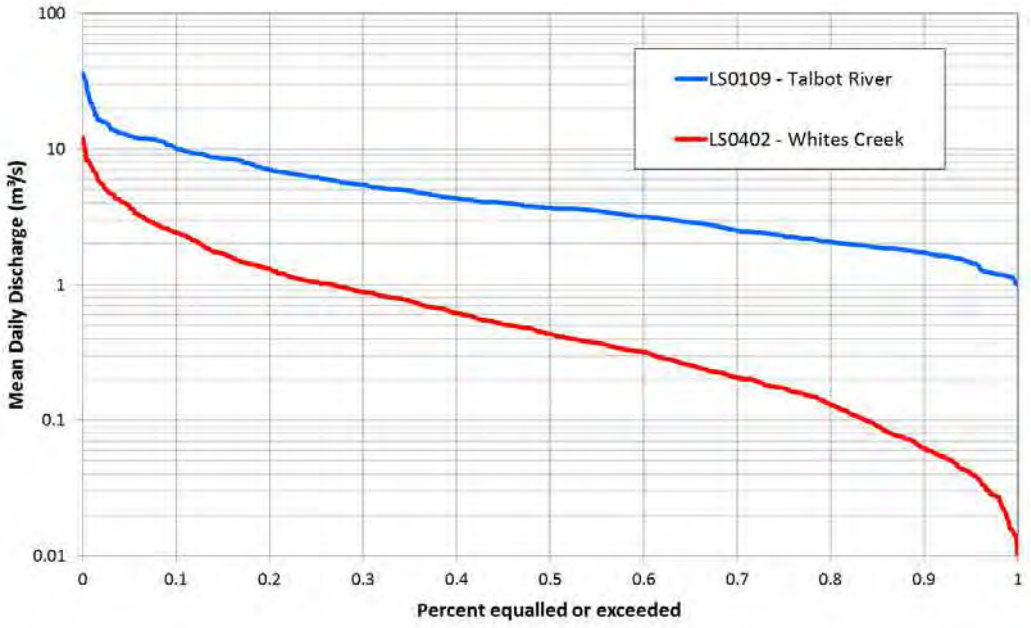

Figure 4.29: Mean daily flow duration curves for the overlapping period of record (2009-2011) at LSRCA gauge stations Talbot River near Gamebridge (LS0109) and Whites Creek at Regional Rd. 23 (LS0402).

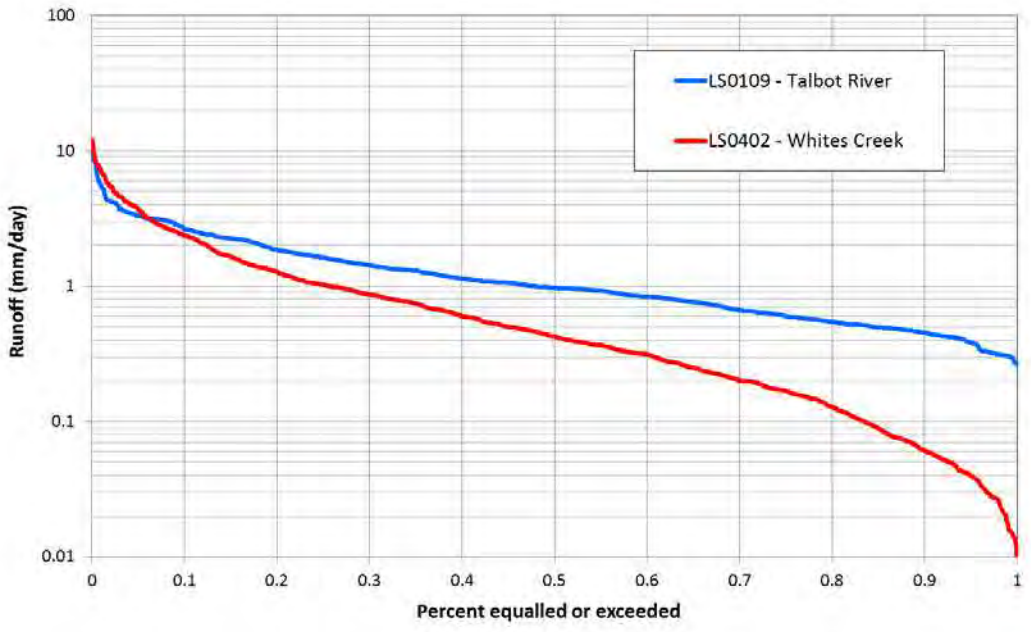

Figure 4.30: Mean daily runoff duration curves for the overlapping period of record (2009-2011) at LSRCA gauge stations Talbot River near Gamebridge (LS0109) and Whites Creek at Regional Rd. 23 (LS0402).

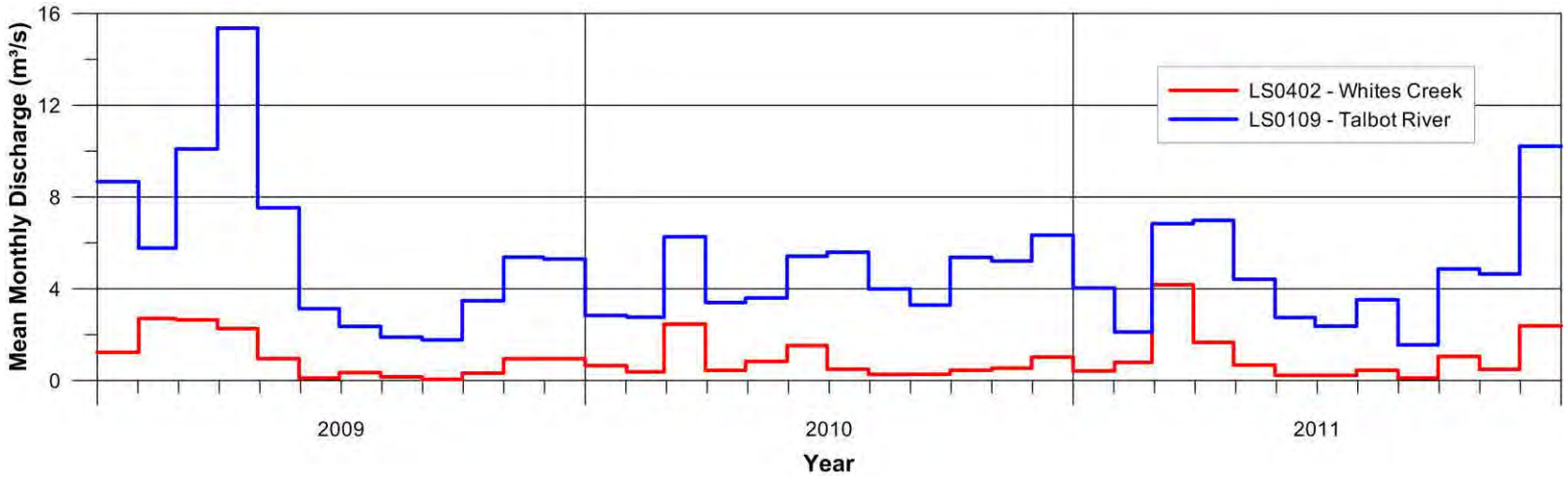

Figure 4.31: Monthly averaged daily discharge observed at LSRCA gauge stations Talbot River near Gamebridge (LS0109) and Whites Creek at Regional Rd. 23 (LS0402).

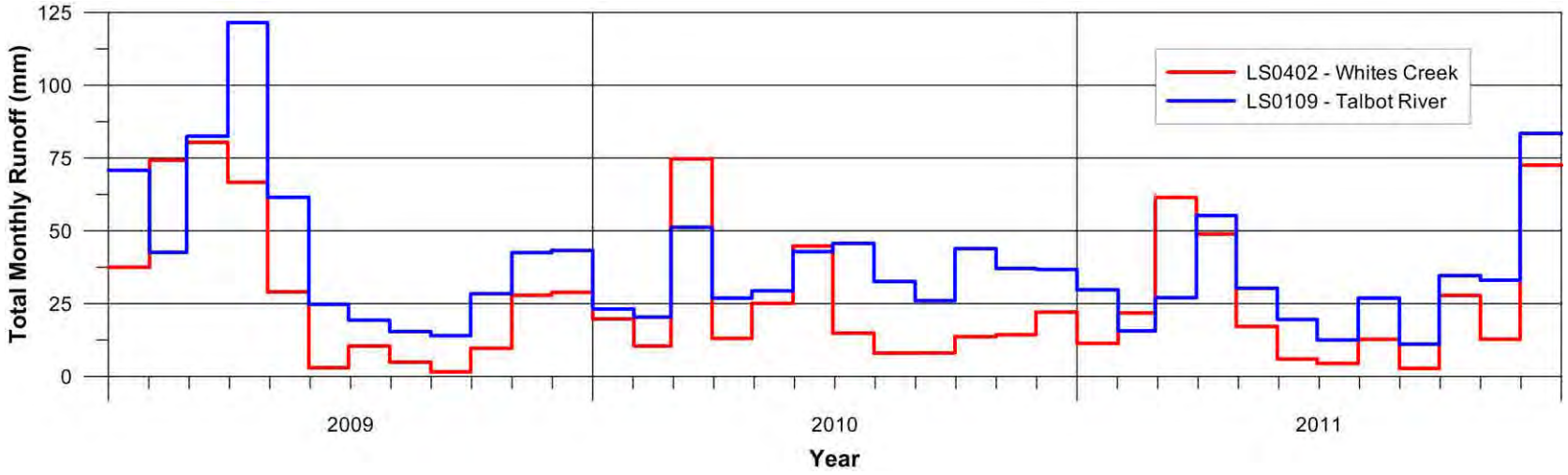

Figure 4.32: Monthly averaged normalized daily watershed runoff observed at LSRCA gauge stations Talbot River near Gamebridge (LS0109) and Whites Creek at Regional Rd. 23 (LS0402).

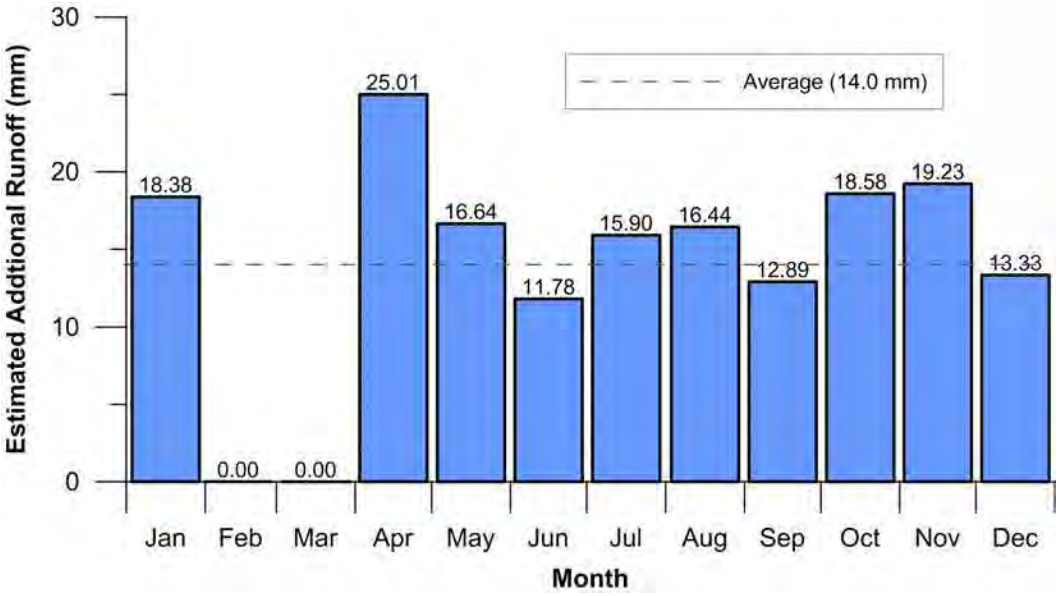

Figure 4.33: Estimated additional monthly runoff into the Talbot River watershed due to canal operations.

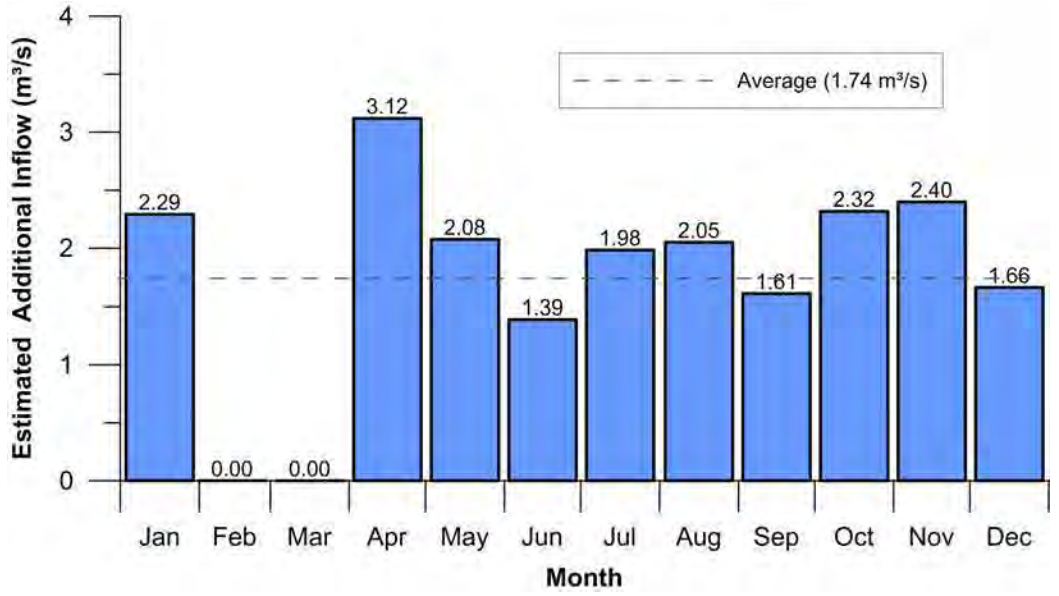

Figure 4.34: Estimated monthly inflow into Mitchell Lake due to canal operations.

5 Hydrogeologic Setting

5.1 Introduction

The stratigraphic model layers, presented in Section 3.4, provided a framework for delineating the aquifer and aquitard layers in the study area. The conceptual hydrostratigraphic model incorporates information related to the primary properties of the geologic units. It also takes into account the degree of weathering and fracturing within the individual bedrock units as well as the similarity of properties in adjacent units so that units can be combined. The hydrostratigraphic model layers, described later on in this section, also served as a framework for compiling and interpreting static and transient water level data to characterize regional groundwater patterns. Field determinations and reported values for hydraulic parameters are also discussed in this section.

5.2 Conceptual Hydrostratigraphic Model

The stratigraphic and hydrostratigraphic surfaces are closely related simply because the stratigraphic units can generally be characterized as either aquifers or aquitards. In some cases, stratigraphic units with similar hydraulic properties and with similar roles in the groundwater system have been combined into a single hydrostratigraphic unit.

An important conceptual change from the stratigraphic model is the incorporation of a zone of increased permeability at the bedrock surface as a separate “weathered bedrock” aquifer. Weathered bedrock or “contact zone” aquifers are widely observed in the upper portion of the limestone and dolostone units across southern Ontario. This enhanced permeability is frequently attributed to a combination of weathering, glacial modification, and stress-relief fracturing.

The Carden Plain physiographic region (Figure 5.1) is a unique hydrogeologic feature in the study area. The pattern of weathering and degree of bedrock exposure in this region differs from that seen elsewhere in the study area. Solutional weathering of the limestone bedrock has produced an open fracture network with a very high permeability, allowing water infiltrating the thin soil cover to rapidly move vertically through the shallow bedrock. Overland runoff from the flat bedrock surface is also quickly captured by the open network of fractures (grikes) at ground surface. The result is an unconfined shallow bedrock aquifer that is extremely responsive to recharge events producing large amounts of vertical and lateral groundwater flow.

The shallow “contact zone” aquifer (including both the regional weathered bedrock and the Carden Plain alvar region) was assumed to be present across the entire study area, except where the relatively un-weathered Precambrian plutonic and metamorphic rocks occur at surface, mainly along the northern edge of the study area.

In addition to the upper bedrock “contact zone” aquifer described above, two other major bedrock zones are targeted by private and municipal water supply wells: 1) a middle aquifer unit associated with the “Green Marker Beds” of the Gull River Formation, where increased permeability is attributed to a higher frequency of water bearing fractures; and 2) a lower aquifer system corresponding to the regional nonconformity between the Shadow Lake Formation and the Precambrian basement.

Competent bedrock aquitard units separate the three regional aquifers across most of the study area, except in the north (close to the Paleozoic-Precambrian contact), where the subcropping middle and lower aquifer units intersect the regionally extensive upper bedrock contact zone aquifer.

Further south of the Paleozoic-Precambrian contact, the upper bedrock contact aquifer is separated from the Green Marker Beds aquifer by the interbedded limestone and shale of the Lindsay and Verulam Formations as well as the thickly bedded limestone of the Bobcaygeon and upper Gull River. The lower member of the Gull River Formation functions as a hydraulic barrier between the overlying Green Marker Bed aquifer and the lower Shadow Lake-Precambrian contact aquifer.

The overburden materials are not considered to be productive aquifer units, with the exception of kame deposits and glaciofluvial sand and gravel deposits contacting the bedrock in tunnel channels. The discontinuous sand and gravel units were assumed to be in good contact with the underlying weathered bedrock aquifer. Where overburden till sequences are present, the shallow bedrock aquifer may function as a confined or semi-confined aquifer, depending largely upon the local thickness of the till.

5.3 Hydrostratigraphic Units

A seven-layer model consisting of 14 hydrostratigraphic units was created by modifying the stratigraphic layers according to the hydrogeologic conceptualization presented above. The five overburden and nine bedrock units of the hydrostratigraphic model are described below:

Mackinaw Interstadial Sediments: The material associated with this unit is variable in composition; however, it generally consists of glaciolacustrine deposits in the subsurface, and glaciofluvial sand and gravel at surface. The unit represents a higher permeability sand overburden material that functions as a regionally discontinuous aquifer.

Newmarket Till: The Newmarket Till covers more than half of the study area and represents a regional aquitard that confines the underlying bedrock aquifers. It is continuous over most of the Ramara Creeks watershed but patchy in the Talbot and Whites Creek watersheds. The high density sandy silt to silty sand composition of the Newmarket Till tends to be regionally consistent and gives the unit a relatively low hydraulic conductivity.

Weathered till: In areas where till (Newmarket Till or Dummer Till) was identified as being exposed at ground surface, a ‘weathered till’ zone of increased permeability was assumed to occupy the top 2 m of till thickness. Enhanced hydraulic conductivity (particularly vertical hydraulic conductivity) in the till due to weathering was recognized by Sharpe et al. (2002).

Glaciolacustrine and Post-Glacial Deposits: These fine-grained silts and clays, interpreted to have originated from post-glacial lakes, represent a discontinuous and locally-variable hydrostratigraphic unit. Where present, these materials are the shallowest of the overburden units and typically unsaturated. The unit is not considered a productive water bearing unit for domestic water wells and is considered to be a poor aquitard.

Dummer Till: The materials that comprise the Dummer Moraine ridges are herein referred to as a ‘till’ by virtue of their depositional origin (i.e., glacial wasting); however, the composition is dominated by angular sand, coarse gravel and boulders (Gravenor, 1957). The Dummer Till unit was expected to have a higher hydraulic conductivity than the Newmarket Till. Nevertheless, this unit acts as a local aquitard with respect to the underlying overburden/bedrock interface aquifer.

Weathered Lindsay/Verulam and Bedrock Interface Sand and Gravel: The weathered bedrock layer combined with permeable overburden material serves as a regional shallow aquifer and is exploited by a number of private wells in the study area. This weathered zone was assumed to extend 7 m below the top of the bedrock surface. The overlying glaciofluvial sand and gravel is generally associated with tunnel channel features. The prevalent shale beds of the Lindsay and

Verulam Formations make these bedrock units less susceptible to extensive karstification than the underlying limestone of the Bobcaygeon and Gull River Formations. The difference in bedrock weathering patterns was incorporated into the hydrostratigraphic model. The weathered Lindsay/Verulam aquifer is only present in the southern half of the study area.

Weathered Bobcaygeon/Gull River and Bedrock Interface Sand and Gravel: This hydrostratigraphic unit was defined based on the same assumptions as above, with the exception that the degree of weathering is greater due to their susceptibility to karstification. The base of the unit was assumed to extend 7 m below the top of the bedrock surface in the northern half of the study area where the Bobcaygeon or Gull River Formations form the bedrock surface.

Alvar (High Erosion) and Alvar (Medium Erosion): In the Carden Plain Alvar region (see Figure 5.1), two unique units were incorporated into the hydrostratigraphic model to represent the solutionally weathered grikes and fractures in the near-surface bedrock. The High Erosion Alvar and underlying Medium Erosion Alvar units are each assumed to be 1 m in thickness. Where these units occur, the underlying "weathered Bobcaygeon/Gull River bedrock" unit is reduced by 2 m (with a remaining thickness of 5 m). The role of these two units in the shallow flow system is to allow for rapid fluctuations in the water table in response to recharge events, as well as the rapid lateral conveyance of groundwater through extensive fracture networks. The degree of karstification was assumed to decrease with depth such that the Medium Erosion Alvar layer is slightly less conductive than the overlying High Erosion Alvar.

Upper Bedrock Aquitard: This hydrostratigraphic unit consists of the upper member of the Gull River Formation overlying the Green Marker Bed, as well as the overlying Bobcaygeon, Verulam and Lindsay Formations. These units were all considered to represent regional aquitards where they are intact and unweathered. Although the argillaceous limestones and interbedded shales of the Verulam and Lindsay Formations are geologically quite distinct from the more thickly bedded limestones of the underlying Bobcaygeon and upper Gull River Formations, these units all have similarly low hydraulic conductivity and are generally not exploited by water wells in the area. In the northern half of the study area, where the Lindsay and Verulam Formations have pinched out, the upper bedrock aquifer is typically between 5 to 25 m thick, confining the underlying Green Marker Bed aquifer from the weathered bedrock. In the southern half of the model, the Upper Bedrock Aquitard thickness increases to a maximum of 100 m, where the Lindsay, Verulam and Bobcaygeon and upper Gull River are all present.

Green Marker Bed: The Green Marker bed represents a zone of argillaceous limestone with increased fracture occurrences between the lower and upper members of the Gull River Formation. Though the thickness of this unit is typically less than 1.5 m, it can be a productive aquifer for domestic water supply.

Lower Bedrock Aquitard: This hydrostratigraphic unit consists of the lower member of the Gull River Formation, underlying the Green Marker Bed aquifer. The composition of this unit varies from fine-grained dolostone to argillaceous limestone with typically low hydraulic conductivity values. The lower member of the Gull River Formation is considered to be a regional aquitard.

Shadow Lake and Weathered Precambrian: The composition of the Shadow Lake Formation is highly variable; however, it is generally associated with basal coarse-grained arkosic sandstone and argillaceous sandstone that exhibits an upward transition to more fine-grained argillaceous and sandy dolostone into the lower member of the overlying Gull River Formation (Armstrong and Carter, 2009). Varying degrees of weathering of the Precambrian basement (prior to deposition of the Ordovician units) have been documented in OGS logs, which further support the interpreted presence of a zone of increased permeability at the Paleozoic-Precambrian contact. The Shadow Lake and Weathered Precambrian contact were therefore considered to represent a regional water-

bearing zone, particularly toward the northern part of the study area where recharge is expected to be higher where the overlying confining Paleozoic bedrock is thin to absent.

Unweathered Precambrian: The unweathered Precambrian age bedrock is regional extensive and represents the low permeability basement of the model. The unweathered Precambrian basement was not explicitly represented in the model except in a few areas where Paleozoic and overburden units are absent (e.g., the exposed Precambrian inlier at the south end of Head Lake). In these cases, properties of the unweathered Precambrian unit were assigned to the model layers.

5.4 Groundwater Levels

5.4.1 Water Level Data Sources

Compilation of water-level data was necessary to establish calibration targets for the steady-state and transient groundwater flow models. Water level data are available from three primary sources:

5.4.1.1 MOE WWIS Static Water Levels

Static water level data from wells in the MOE WWIS database (2012) provide general insight into the water level patterns in the study area. Well locations are shown in Figure 5.2. The water levels recorded in the database represent a one-time measurement taken when the well was constructed. Numerous biases and errors are known to exist in the water well record data. These are discussed further in the next section. Assessment of the intrinsic error and variation in this data set is discussed in Kassenaar and Wexler (2006). Despite these limitations, the WWIS data set has good regional coverage. A total of 4,518 MOE static water levels were used in the characterization of groundwater patterns and for model development.

There are some regions of relative data scarcity, most notably in the largely unsettled alvar terrain of the Carden Plain (to the east of Dalrymple Lake) and within the areas of outcropping Canadian Shield along the northern limit of the study area beyond the Precambrian-Paleozoic contact. The Ramara Creeks, Talbot River and Whites Creek sub-watersheds are generally well represented in the MOE WWIS data coverage.

5.4.1.2 Provincial Groundwater Monitoring Network

There is only one Provincial Groundwater Monitoring Network (PGMN) well within the entire study area. Well W0000408 is located near the outfall of the Trent-Severn Waterway into Lake Simcoe (Figure 5.3). Water level data for the PGMN well were obtained from Lake Simcoe Region Conservation Authority and included datalogger measurements from January 2005 to December 2010. A review of construction details for the PGMN well indicated that it was completed to a depth of 13.7 metres below ground surface with a monitoring interval of 7.0 m (ranging from 212.9 masl to 219.9 masl). The monitoring interval corresponds to the overburden/weathered bedrock interface aquifer unit.

PGMN wells typically provide extremely useful information on natural seasonal and climactic variation in water levels because of the long period of record and continuous monitoring. Because Well W0000408 is situated within 400 m of Lake Simcoe, the measured water levels are likely influenced by near-shore conditions and may not reflect more regional trends.

5.4.1.3 Quarry Monitoring Data

A number of quarries in the study area are required to conduct regular monitoring of groundwater levels. Monitoring data were provided for 7 of the 11 quarries. The data associated with these monitors range in quality and completeness. Of the 168 monitoring wells provided for this project, 9 wells had less than 10 water level measurements and only 35 of the wells had more than 50. Although individual measurements are still useful for interpreting the static water level patterns, seasonal fluctuations and transient trends are difficult to infer without frequent long-term monitoring.

The locations of the quarry monitoring wells are shown in Figure 5.3. The completion details for the 168 wells are summarized in Table 5.1. Water level data include manual and datalogger measurements. The data provide limited information on natural groundwater fluctuations as many of the wells are affected by quarry excavation and dewatering activities. A subset of these wells, those with continuous measurements, long-term record, and locations distant from the excavation face were used in the transient model calibration.

5.4.2 Regional Water Level Patterns

Regional water level patterns were evaluated using the MOE WWIS static water level data and static water levels from other geotechnical and consultant wells in the area.

5.4.2.1 Data Screening

There are a number of problems that have been identified in the static water level data in drillers' logs submitted to the MOE. Sources of error include positional and depth measurement errors and questions as to whether static conditions were achieved prior to measurement. Seasonal and year-to-year water level variations also introduce noise in the data which is noticeable when analyzing clusters of water level data. Although the data were filtered to reduce the number of erroneous data points, some degree of uncertainty as to the accuracy of individual measurements will always remain. The accuracy of the maps produced from these data is similarly affected. However, the MOE WWIS data are the only data set with sufficient spatial coverage to allow mapping of potentiometric surfaces over the entire study area. Furthermore, the water levels and spatial trends observed in the mapped water level surfaces appear consistent and reasonable when obvious outliers are removed from the data.

The filtered static water level data were analyzed and measurements were assigned to one of the 14 hydrogeologic units identified within the study area based on their reported screened interval. It should be noted that for the purposes of this discussion, the term "screened interval" is used interchangeably in reference to wells with both a slotted screen installed below the casing and wells with simply a length of open hole in the bedrock, as is common across the study area. Data points were assigned to the hydrologic units following a hierarchical assignment process that considered the length of each hydrogeologic unit intercepted by the screened interval, with higher weighting given to aquifers over aquitards. For example, a well with a screened interval that intersects 2 m of Green Marker Bed (a regional aquifer) along with 2 m and 4 m of the upper and lower confining bedrock aquitard units, respectively, would be assigned to the Green Marker Bed because it represents the largest screened *aquifer* unit for this well. In cases where the screened interval was contained with a single unit, that data point was assigned to the unit, regardless of whether it was classified as an aquifer or aquitard.

A total of 2,533 static water level measurements were assigned to the 14 hydrostratigraphic units. The vast majority of these data points (2,198 wells) were screened in the shallow overburden/weathered bedrock interface aquifer. This finding reflects the importance of this

productive zone for domestic water supply across the study area. The remaining 313 wells belong to the deeper bedrock units, the Green Marker Bed and the Shadow Lake/weathered Precambrian.

The relatively high number of data points combined with their wide spatial distribution made it possible to reliably interpolate the shallow system water levels. The water-level data were interpolated using a geostatistical technique known as “kriging”. Kriging is a weighted-averaging interpolation method that attempts to minimize variance and bias in the results while honouring the local values at the data points. The kriged water level data for the shallow groundwater system is shown in Figure 5.4. Flow is perpendicular to the contours shown and the map can be used to infer general patterns of groundwater flow.

Data for the deeper system were too sparse to interpolate. Individual measurements were still used in the model calibration. The comparatively fewer static water level measurements for the deeper system should be taken into consideration when interpreting the interpolated deeper system levels. Nevertheless, the approach taken here helped to maximize the spatial coverage of the MOE WWIS dataset and allowed for the development of a reasonable representation of regional flow patterns and vertical gradients across the study area.

5.4.2.2 Regional Trends

The interpolated water levels presented in Figure 5.4 show that the potentiometric surface tends to be a subdued replica of the land surface topography. Groundwater flow patterns (based on the interpolated water levels) show that radial flow occurs from four large groundwater mounds; two associated with higher elevations in the upper Talbot watershed separated by Canal Lake, one at the southeast end of the Whites Creek subwatershed, and a mound west of Dalrymple Lake at the top of the Ramara Creeks subwatershed. The contours also show that the major surface water bodies (Dalrymple Lake, Balsam Lake, Canal Lake, Mitchell Lake, the Head River, and Lake Simcoe) represent areas of groundwater discharge. Along the lower reaches of the Talbot River below Canal Lake, “v-shaped” groundwater contours can be seen pointing upstream suggesting significant groundwater discharge to the river.

MOE well records from across the study area indicate that water levels are at their lowest elevation of 220 masl along the eastern shores of Lake Simcoe. Regional high points in water level elevation are found within the northeast and southeast portions of the study area at approximately 290 masl. The northeastern water level high is found in the vicinity of Head Lake, where overburden thickness is minimal and confining sequences of Paleozoic bedrock provide topographic control on groundwater levels by limiting downward drainage. The water level high toward the southeast (also at an elevation of approximately 290 masl) is found in an area with thicker sequences of Newmarket Till overlying the argillaceous limestone of the Lindsay Formation. In both cases, interpolated water levels are located within the upper few metres of the sub-cropping or outcropping bedrock.

Groundwater is generally found less than 10 metres below ground surface, extending as deep as 28 m (Figure 5.5). The few areas where interpolated groundwater water levels extend above ground surface (as high as 8 metres) correspond to riparian wetlands and marshes along topographic depressions in the bedrock surface.

A comparison between interpolated groundwater levels and the bedrock surface elevation (Figure 5.6) shows that water levels across much of the study area are within 10 m of the bedrock surface. This would seem to support the regional interpretation of groundwater levels being strongly controlled by bedrock topography, and the existence of a productive overburden interface/weathered zone within the top few metres of bedrock. Within the Carden Plain alvar region, water levels are found more consistently below the bedrock surface. This is to be expected because the bedrock in this area generally occurs at or near ground surface and the highly weathered surface is dissected

by grikes and solutionally enhanced fractures. The water table likely rises only to the base of this highly transmissive zone most of the year.

5.4.2.3 Water Level Fluctuations

A review of the available long-term water level data was conducted to quantify seasonal fluctuations in groundwater levels. As noted earlier, a limited amount of transient groundwater level data is available from the single PGMN monitoring well and subset of quarry monitoring wells. The spatial distribution of these monitors is also limited to a relatively small area to the west of Canal Lake and south of Dalrymple Lake (Figure 5.3).

Water levels in the PGMN well are presented in Figure 5.7, and show a seasonal fluctuation of approximately 2 m (between 219 masl and 221 masl). Water levels generally increase in late winter/spring until they peak between April and May, after which they experience gradual declines into late fall/early winter. These fluctuations are slightly offset from the seasonal patterns at Lake Simcoe, where stage fluctuates approximately 0.5 m seasonally, with an increase from mid-March to April, a plateau until July, followed by a water level decline into the winter months.

Water level hydrographs for data collected from five of the quarry and aggregate operations provide a valuable source of long-term transient groundwater data. Hydrographs for these wells are presented as follows:

- Holcim Quarry (Figure 5.8 to Figure 5.11)
- McCarthy Quarry (Figure 5.12 to Figure 5.14)
- Ramara Quarry (Figure 5.15 to Figure 5.17)
- Tomlinson Quarry (Figure 5.18 to Figure 5.21)
- Kirkfield Quarry (Figure 5.22 to Figure 5.24)

Several of the quarry monitors appear to provide a good record of long-term groundwater levels that have not been impacted by quarry operations. The pattern of seasonal fluctuations described for the PGMN well can be seen in the majority of the non-impacted quarry monitoring wells, although the range in water levels varies from quarry to quarry. In general, water levels in the quarry monitoring wells fluctuate by 1 to 3 m, with larger fluctuations occurring in the shallower of the nested wells (e.g., Figure 5.18 and Figure 5.20). The McCarthy Quarry monitoring wells are considered to be fairly representative of natural conditions because, the quarry is in the early stages of land clearing and aggregate extraction has yet to commence. Shallow water levels in the McCarthy Quarry monitors (Figure 5.12 and Figure 5.13) fluctuate by approximately 1.5 to 2 m seasonally. Water level measurements from the deeper Green Marker Beds and Shadow Lake aquifers at the McCarthy Quarry are difficult to interpret because of the relatively infrequent measurements and apparent anomalous data points; however, the data show a downward hydraulic gradient from the Green Marker Bed aquifer to the Shadow Lake aquifer suggesting a fairly competent confining unit separates the two units. Seasonal fluctuations in water levels for the Green Marker Bed range from 2 to 4 m. Season fluctuations in the Shadow Lake aquifer could not reliably be interpreted from the McCarthy Quarry data.

The impacts of quarrying and aggregate extraction can be seen in several of the long-term monitoring datasets, indicated by a gradual decline in water levels. Shallow monitors screened in the upper contact aquifer are typically more susceptible to quarry influences, because the excavated area acts as a local depression in the water table. Ramara Quarry monitors OW1 (Figure 5.15) and TH3 (Figure 5.17) are screened in the contact aquifer where it is comprised of the weathered Verulam Formation. These wells show a water level decline of between 1 and 2 m compared to 2005 levels. The Kirkfield monitoring nest OW10-I and OW10-II (Figure 5.24), shows that quarry-

related dewatering resulted in a decline in groundwater heads in the upper contact aquifer to the point that gradients between the shallow and deeper units was reversed by early 2000. The deeper groundwater system also shows impacts of quarry operations where competency of confining units may be compromised by excavation and blasting. Holcim Quarry deep monitor CQ6, completed in the lower bedrock aquitard (Lower Gull River), showed a 15 m decline in water levels since 1990.

Apart from the single PGMN well in the study area, the few groundwater monitors with transient water level data are related to the quarry operations in the region. The frequency at which quarries are required to collect groundwater levels varies between the different operations and over time. Although some of the quarries have installed dataloggers in their wells for more frequent monitoring of water levels, these data were not made available for this project. Water levels data for most of the quarry monitors reflect monthly monitoring.

5.5 Hydraulic Properties

The reported estimates of the hydraulic properties of the geologic units present were compiled as part of the report review process. Sources of hydraulic conductivity values included estimates from aquifer testing as well as calibration values from previous modelling studies of the area, including:

1) Cumulative Impacts Assessment for Groundwater Takings in the Carden Plain Area (Golder Associates, 2012).
2) Additional 72-hour pumping test results McCarthy Quarry (Azimuth Environmental Consulting Inc., 2009).
3) Hydrogeological and Hydrological Assessments in Support of a Category 2 Class A Quarry Below Water – R.W. Tomlinson Ltd. (Golder Associates, 2006).
4) Hydrogeologic Review in Support of an Application to Renew Permit to Take Water 74-P-3069 Lafarge Brechin Quarry (Golder Associates, 2004).
5) Level 2 Hydrogeology Study Lot 1 Concession 1 Geographic Township of Mara (Dixon Hydrogeology Ltd., 2001).
6) Hydrogeological Study for Permit to Take Water Carden Quarry - Miller Paving Ltd. (Gartner Lee Ltd., 1995).
7) Gormley Aggregates Division, Essroc Canada Inc. Permit to Take Water Application (Long Associates consulting Ltd., 1993).
8) Summary of Hydrogeological and Hydrological Report - Carden Quarry (Monenco Consultants Ltd., 1991).
9) Detailed Geological and Hydrogeological Evaluation Marden Quarry Property, Township of Mara (Jagger Hims Ltd., 1991)

Table 5.2 presents the typical values and reported ranges for hydraulic conductivity of the geologic units based on the review. The variability in reported hydraulic conductivity values for similar materials was often found to be two or more orders of magnitude. Part of this variability can be attributed to the different methods used to determine hydraulic conductivities. For example, estimates of hydraulic conductivity from single well response tests are known to provide lower estimates than multi-well pumping tests of the same material (Fetter, 2001).

As expected, most of the reported values were for the bedrock aquifers and aquitards, since the majority of the referenced reports pertain to quarry development and approvals. Sources for the

hydraulic properties of the overburden materials were less numerous in the historical reports, and are generally not differentiated according to the specific formation (or corresponding material type) being tested. A limited number of reported hydraulic conductivity measurements were found for the 'till' overburden (presumed Newmarket Till based on location) in the study area. The values are summarized in Table 5.2 and generally fall within the expected range for clay- and silt-dominated glacial till as reported by Freeze and Cherry (1979))

The hydraulic conductivity for the sandier Dummer till material would be expected to fall within the range of 10^{-7} to 10^{-5} m/s (Fetter, 2001; Batu, 1998). The Mackinaw Interstadial deposits have characteristically more sand and less fine-grained materials than either of the tills; reported hydraulic conductivity values fall within the range of 10^{-3} to 10^{-7} m/s, according to reported values in literature (Freeze and Cherry, 1979; Fetter, 2001).

As outlined above, the weathered bedrock/overburden interface represents a regional aquifer within the study area. Numerous groundwater takings in the area draw from this aquifer. The hydraulic properties of this aquifer were assumed to be related to the original stratigraphic unit that subcrops at the bedrock surface. To this end, regions where the more argillaceous limestones of the Verulam and Lindsay Formations subcrop were given a different set of hydraulic properties than those assigned to the cleaner, more karst-prone limestones of the Gull River and Bobcaygeon Formations. The properties assigned to the weathered bedrock were adjusted through model calibration, as discussed later on in this report.

The specific yield and specific storage parameters are important for transient groundwater flow calibration; however, field measurements of these values (especially specific yield) are limited and localized considering the high degree heterogeneity both between and within the individual units. To provide initial estimates for model development, published values for similar materials were assigned to the hydrostratigraphic units, as presented in Table 5.3. A few field measurements of specific storage, calculated from multiple-well drawdown tests (Azimuth Environmental, 2009; Golder Associates, 2006), were available for the Verulam, Bobcaygeon and Gull River Formations. The average field measurements of specific storage were $4x10^{-5}$ m^{-1} for the Verulam Formation, $9x10^{-6}$ m^{-1} for the Bobcaygeon Formation, and $1x10^{-5}$ m^{-1} for the Gull River Formation. These values fall within the published range for fissured/jointed rock matrices, presented in Table 5.3. As with hydraulic conductivity, the specific yield and specific storage estimates were revised and refined through the calibration process. Final calibration values are presented in the following chapters.

5.6 Tables and Figures

Table 5.1: Summary of Quarry Monitoring Well Completion Details.

Well Name	Easting	Northing	Ground Elevation (masl)	Depth (m)	Top of Screen (masl)	Bottom of Screen (masl)	Data Period Start	Data Period End
Bot Quarry Monitors (6 monitors)								
OW1A	642918	4950122	257.4	7.6	251.3	249.8	2010-05-01	2012-09-27
OW1B	642918	4950122	257.4	32.5	237.4	224.9	2010-05-01	2012-09-27
OW2A	642203	4949860	254.7	7.6	252.9	247.1	2010-05-01	2012-09-27
OW2B	642203	4949860	254.7	32.5	23.7	222.2	2010-05-01	2012-09-27
OW11-D	642202	4949437	254.4	26.8	239.6	227.6	2010-05-01	2012-09-27
OW11-S	642202	4949437	254.4	8.5	253.0	245.9	2010-05-01	2012-09-27
Holcim Quarry Monitors (37 monitors)								
CQ1A	650174	4937770	238.8	46.8	191.0	192.0	1989-07-03	2011-12-08
CQ1B	650174	4937770	238.8	31.8	206.0	207.0	1989-07-03	2011-12-08
CQ1C	650174	4937770	238.8	26.8	211.0	212.0	1989-07-03	2011-12-08
CQ1D	650174	4937770	238.8	16.8	221.0	222.0	1989-07-03	2011-12-08
CQ3A	651808	4936122	249.0	60.0	192.0	189.0	1989-07-03	2003-01-16
CQ3B	651808	4936122	249.0	44.0	208.0	205.0	1989-07-03	2010-05-20
CQ3C	651808	4936122	249.0	37.0	215.0	212.0	1989-07-03	2008-12-05
CQ3D	651808	4936122	249.0	28.0	224.0	221.0	1989-07-03	2010-04-21
CQ3E	651808	4936122	249.0	14.0	238.0	235.0	1989-07-03	2003-01-16
CQ4A	651455	4937082	247.0	60.0	188.0	187.0	1989-07-03	2011-12-08
CQ4B	651455	4937082	247.0	45.0	203.0	202.0	1989-07-03	2011-12-08
CQ4C	651455	4937082	247.0	36.0	212.0	211.0	1989-07-03	2011-12-08
CQ4D	651455	4937082	247.0	29.0	219.0	218.0	1989-07-03	2011-12-08
CQ4E	651455	4937082	247.0	15.0	233.0	232.0	1989-07-03	2011-12-08
CQ6	650604	4937377	243.0	39.0	206.0	204.0	1989-07-03	2012-12-04
CQ7	651358	4936580	244.0	31.0	216.0	213.0	1989-07-03	2012-12-04
CQ8	651121	4936453	245.0	39.0	245.0	206.0	1989-07-03	1999-04-23
CQ8R	651121	4936453	245.0				2004-12-09	2012-12-04
CQ9	650714	4936234	248.0	13.5	237.5	234.5	1989-07-03	2012-12-04
CQ10-1	650671	4936517					2005-09-29	2005-09-29
CQ10-2	650671	4936517					2004-10-01	2012-12-04
CQ10-3	650671	4936517					2004-10-01	2012-12-04
CQ11-1	650917	4936875	227.0	39.0	192.0	188.0	2005-09-29	2012-12-04
CQ11-2	650917	4936875	227.0	29.5	200.5	197.5	2004-10-01	2012-12-04
CQ11-3	650917	4936875	227.0	14.5	216.5	212.5	2004-10-01	2012-12-04
CQ12-D	651251	4937313					2008-12-08	2012-12-04
CQ12-M	651251	4937313					2008-12-08	2012-12-04
CQ12-S	651251	4937313					2010-07-19	2012-12-04
CQ13-D	651087	4937437					2008-12-08	2012-12-04
CQ13-M	651087	4937437					2008-12-08	2012-12-04
CQ13-S	651087	4937437					2008-12-08	2012-12-04
CQ3R-50	651808	4936122	249.0				2010-07-19	2012-12-04
CQ3R-96	651808	4936122	249.0				2010-07-19	2012-12-04
CQ3R-121	651808	4936122	249.0				2010-07-19	2012-12-04

Well Name	Easting	Northing	Ground Elevation (masl)	Depth (m)	Top of Screen (masl)	Bottom of Screen (masl)	Data Period Start	Data Period End
CQ3R-150	651808	4936122	249.0				2010-07-19	2012-12-04
CQ3R-205	651808	4936122	249.0				2010-07-19	2012-12-04
SG1	651175	4937459					2008-07-23	2012-11-08
Kirkfield Quarry Monitors (8 monitors)								
OW4	659401	4941400	257.5	16.3	0.0	241.2	1991-11-11	2002-04-01
OW7-I	659603	4940663	252.4	31.8	225.1	220.6	1991-11-11	2010-10-01
OW7-II	659604	4940663	252.6	18.8	252.6	233.8	1991-11-11	2010-10-01
OW8-I	659322	4941159	257.9	31.2	230.6	226.7	1991-11-11	2010-10-01
OW8-II	659322	4941159	258.0	19.0	258.0	239.0	2010-05-01	2010-10-01
OW9	659586	4941265	256.6	18.9	0.0	237.8	1991-11-11	2002-11-26
OW10-I	659788	4941338	261.6	30.4	235.3	231.2	1991-11-11	2010-10-01
OW10-II	659792	4941340	261.7	18.8	261.7	242.9	1991-11-11	2010-10-01
McCarthy Quarry Monitors (26 monitors)								
AM1a	651297	4932408	248.4	8.3	241.1	240.1	2000-10-16	2007-12-04
AM1b	651297	4932408	248.4	5.7	243.7	242.7	2000-10-16	2007-12-04
AM2	651473	4932764	248.0	3.7	245.3	244.3	2000-10-16	2007-12-04
AM3	651669	4932672	248.0	7.0	242.0	241.0	2000-10-16	2006-02-03
AM4	651003	4933489	253.6	1.3	252.6	252.3		
AM5	651405	4933528	252.5	2.2	251.5	250.3		
AM6	651197	4933612	254.1	1.5	253.1	252.6		
AM7	651133	4932904	248.2	4.6	244.6	243.6	2000-10-16	2007-12-04
AMX	651112	4933274	252.4	31.2	222.2	221.2	2000-10-16	2007-12-04
OW4-I	651298	4932403	248.4	11.0	238.4	237.4	2006-04-29	2007-12-04
OW4-II	651298	4932403	248.4	15.2	236.3	233.2	2006-03-02	2007-12-04
OW-5I	651669	4932675	248.0	10.1	238.9	237.9	2006-04-29	2007-12-04
OW-5II	651669	4932675	248.0	15.9	233.7	232.1	2006-04-29	2007-11-08
SP1	651382	4933710	255.5	1.4	255.5	254.1		
SP2	651321	4933658	254.0	1.2	254.0	252.8		
SP3	651088	4933613	254.5	1.2	254.5	253.3		
TW1-1	651207	4933590	253.8	30.2	224.6	223.6	2000-10-27	2007-12-04
TW1-2	651207	4933590	253.8	59.4	203.5	194.4	2000-10-16	2007-12-04
TW2-1	650967	4933510	253.7	26.0	228.7	227.7	2000-10-27	2007-12-04
TW2-2	650967	4933510	253.7	43.9	212.8	209.8	2006-04-29	2007-12-04
TW3	651131	4932909	248.2	63.8	243.0	184.4	2000-10-16	2007-12-04
Amy	651264	4933473	253.0	29.7	224.3	223.3	2000-10-16	2007-12-04
Barn	651718	4932476	248.1				2000-10-16	2007-12-04
Degroot	651864	4932503	248.9				2006-03-02	2007-06-06
Lamare	651211	4932280	246.5	17.4	229.7	229.1	2006-03-02	2007-04-19
Southwell	652017	4932324	248.4				2006-03-02	2007-06-06
Miller Paving Monitors (6 monitors)								
GL1-I	650772	4940063	237.7	27.6	213.7	210.1	2008-07-31	2010-10-01
GL1-II	650772	4940063	237.7	19.0	222.2	218.7	2008-07-31	2010-10-01
GL1-III	650772	4940063	237.8	10.0	234.0	227.8	2008-07-31	2010-10-01
GL2-I	650141	4941613	246.2	30.6	219.2	215.6	2008-07-31	2010-10-01
GL2-II	650141	4941613	246.3	23.0	227.3	223.3	2008-07-31	2010-10-01
GL2-III	650141	4941613	246.2	10.0	242.9	236.2	2008-07-31	2010-10-01

Well Name	Easting	Northing	Ground Elevation (masl)	Depth (m)	Top of Screen (masl)	Bottom of Screen (masl)	Data Period Start	Data Period End
Ramara Quarry Monitors (9 monitors)								
OW1	645848	4928788	247.9	37.9	245.0	210.0	2004-05-28	2012-03-21
OW2	645408	4928681	244.1	37.6	242.6	206.5	2004-05-28	2012-03-21
OW3	646261	4928953	237.9	27.1	235.0	210.8	2004-05-28	2012-03-21
TH1	645443	4928663	245.4	83.7	244.2	161.7	2001-10-01	2012-03-21
TH2	646378	4929333	235.5	37.0	233.9	198.5	2001-10-01	2012-03-21
TH3	644348	4928274	241.6	22.4	224.9	219.2	1990-11-14	2012-03-21
TH4	643880	4929529	232.3	19.9	215.5	212.4	1990-11-14	2012-03-21
TH5	645014	4929937	242.0	22.7	223.8	219.3	1990-11-14	2012-03-21
TH6	645612	4930156	237.1	30.6	235.6	206.5	2001-10-01	2012-03-21
Tomlinson Quarry Monitors (76 monitors)								
MW2-A	651898	4939750	247.1	29.0	221.2	218.1	2004-10-14	2006-10-26
MW2-B	651898	4939750	247.1	8.8	241.4	238.3	2004-10-14	2006-09-28
MW3-A	651523	4938298	246.3	45.7	203.6	200.6	2004-10-13	2006-10-26
MW3-B	651523	4938298	246.3	3.1	244.7	243.2	2004-10-13	2006-05-16
MW4-A	650785	4939831	236.7	35.5	236.7	201.1	2005-01-13	2006-05-16
MW4-B	650785	4939831	236.7	35.5	233.8	201.1	2004-10-15	2006-10-26
OW-10A	651732	4938687	248.4	32.0	219.5	216.4	2004-10-13	2006-10-26
OW1-B	651193	4938696	254.2	15.5	241.8	238.7	2004-10-13	2006-10-26
OW1-C	651193	4938696	254.2	3.0	252.7	251.2	2004-10-13	2006-10-26
OW-20A	651521	4938314	246.4	32.2	217.3	214.2	2004-09-07	2006-10-26
OW-2B	651463	4938897	250.5	14.8	238.7	235.7	2004-08-27	2006-10-26
OW-2C	651463	4938897	250.5	2.7	249.3	247.8	2004-10-13	2006-10-26
OW-3A	651039	4939203	242.7	31.8	213.9	210.9	2004-10-14	2006-10-26
OW-3B	651039	4939203	242.7	15.6	230.1	227.1	2004-08-27	2006-10-26
OW-3C	651039	4939203	242.7	2.7	241.5	240.0	2004-10-14	2006-10-26
OW-4A	652030	4939457	246.1	30.8	218.3	215.3	2004-10-14	2006-10-26
OW-4B	652030	4939457	246.1	15.8	233.3	230.3	2004-10-14	2006-10-26
OW-4C	652030	4939457	246.1	2.5	245.1	243.6	2004-10-14	2006-10-26
OW-5A	651257	4939683	241.1	26.8	214.3	214.3	2005-03-23	2006-10-05
OW-5B	651257	4939683	241.1	14.4	228.2	226.7	2004-08-27	2006-10-26
OW-6A	651482	4939956	242.7	31.9	213.8	210.8	2004-08-27	2006-10-26
OW-6B	651482	4939956	242.7	15.9	229.9	226.8	2004-10-15	2006-10-26
OW-6C	651482	4939956	242.7	2.9	241.3	239.8	2004-10-15	2006-10-16
OW-7A	651917	4940358	247.4	27.1	247.2	220.3	2004-08-27	2006-10-26
OW-7B	651917	4940358	247.4	15.5	235.0	231.9	2004-10-14	2006-10-26
OW-7C	651917	4940358	247.4	3.2	245.8	244.2	2004-10-14	2006-10-26
OW-8A	651789	4940058	246.0	31.9	217.1	214.1	2004-10-14	2006-10-26
OW-8B	651789	4940058	246.0	15.5	233.6	230.5	2004-08-27	2006-10-26
OW-8C	651789	4940058	246.0	2.5	245.1	243.5	2004-10-14	2006-10-26
OW-9A	651614	4939534	246.4	31.6	217.8	214.8	2004-10-14	2006-10-26
OW-9B	651614	4939534	246.4	15.9	233.6	230.5	2004-08-27	2006-10-26
OW-9C	651614	4939534	246.4	2.9	245.0	243.5	2004-10-14	2006-10-26
MW1	651592	4939121	249.5	32.8	219.7	216.7	2004-10-13	2006-10-26
OW-10B	651732	4938687	248.4	15.1	236.4	233.3	2004-08-27	2006-10-26
OW-10C	651732	4938687	248.4	2.9	247.0	245.5	2004-10-13	2006-10-26

Well Name	Easting	Northing	Ground Elevation (masl)	Depth (m)	Top of Screen (masl)	Bottom of Screen (masl)	Data Period Start	Data Period End
OW-11A	651844	4939731	246.9	31.4	218.5	215.5	2004-08-27	2006-10-26
OW-11B	651844	4939731	246.9	15.6	234.4	231.3	2004-08-27	2006-10-26
OW-11C	651844	4939731	246.9	3.0	245.4	243.9	2004-10-07	2006-10-26
OW-12A	651869	4939748	247.0	31.6	218.5	215.4	2004-10-07	2006-10-26
OW-12B	651869	4939748	247.0	15.6	234.4	231.4	2004-08-27	2006-10-26
OW-12C	651869	4939748	247.0	3.0	245.5	244.0	2004-10-07	2006-10-26
OW-13A	651877	4939754	247.0	31.7	216.4	215.3	2004-10-06	2006-10-26
OW-13B	651877	4939754	247.0	15.8	234.3	231.2	2004-08-27	2006-10-26
OW-13C	651877	4939754	247.0	3.3	245.3	243.7	2004-07-20	2006-10-26
OW-14A	651882	4939769	247.1	32.0	218.2	215.1	2004-08-27	2006-10-26
OW-14B	651882	4939769	247.1	15.4	234.7	231.7	2004-08-27	2006-10-26
OW-14C	651882	4939769	247.1	3.0	245.6	244.1	2004-10-06	2006-10-26
OW-15A	651878	4939778	247.1	31.8	218.3	215.3	2004-08-27	2006-10-26
OW-15B	651878	4939778	247.1	15.8	234.4	231.3	2004-10-06	2006-10-26
OW-15C	651878	4939778	247.1	2.7	245.9	244.4	2004-10-06	2006-10-26
OW-16A	651868	4939806	247.1	31.7	218.5	215.4	2004-04-11	2006-10-26
OW-16B	651868	4939806	247.1	15.8	234.4	231.3	2004-10-06	2006-10-26
OW-16C	651868	4939806	247.1	3.1	245.5	244.0	2004-10-06	2006-10-26
OW-17A	651468	4938304	246.5	31.3	218.0	215.2	2004-08-27	2006-10-26
OW-17B	651468	4938304	246.5	15.7	233.9	230.8	2004-08-27	2006-10-26
OW-17C	651468	4938304	246.5	2.9	245.1	243.6	2004-10-13	2006-10-26
OW-18A	651498	4938305	246.4	31.9	217.5	214.5	2004-08-27	2006-10-26
OW-18B	651498	4938305	246.4	15.6	233.8	230.8	2004-08-27	2006-10-26
OW-18C	651498	4938305	246.4	3.1	244.9	243.3	2004-10-13	2006-10-26
OW-19A	651508	4938305	246.4	32.1	217.4	214.3	2004-09-07	2006-10-26
OW-19B	651508	4938305	246.4	15.7	233.7	230.7	2004-10-12	2006-10-26
OW-19C	651508	4938305	246.4	3.1	244.8	243.3	2004-10-12	2006-10-26
OW1-A	651193	4938696	254.2	31.4	225.8	222.8	2004-08-27	2006-10-26
OW-20B	651521	4938314	246.4	15.6	233.8	230.8	2004-09-07	2006-10-26
OW-20C	651521	4938314	246.4	3.0	245.0	243.4	2004-10-08	2006-10-26
OW-21A	651524	4938324	246.4	31.9	217.5	214.5	2004-09-07	2006-10-26
OW-21B	651524	4938324	246.4	15.5	234.0	230.9	2004-10-12	2006-10-26
OW-21C	651524	4938324	246.4	1.7	246.3	244.7	2004-10-12	2006-10-26
OW-22A	651532	4938352	246.6	32.7	218.0	213.9	2004-09-07	2006-10-26
OW-22B	651532	4938352	246.6	15.6	234.1	231.0	2004-09-07	2006-10-26
OW-22C	651532	4938352	246.6	3.1	245.1	243.5	2004-10-12	2006-10-26
OW-23	651566	4939109	249.9	32.0	220.9	217.9	2004-08-27	2006-10-26
OW-2A	651463	4938897	250.5	31.8	220.9	218.7	2004-08-17	2006-10-26
PW-1	651885	4939759	247.0	32.8	247.0	214.2	2004-08-27	2006-10-26
PW-2	651517	4938307	246.4	32.7	246.4	213.6	2004-08-27	2006-10-26
PW-3	651583	4939117	249.7	31.7	249.7	218.0	2004-08-27	2006-10-26

Table 5.2: Reported hydraulic conductivity values from previous studies.

Material	Geometric Mean Hydraulic Conductivity (m/s)	Range in Values (m/s)	Sources*
Overburden (undifferentiated)	$2x10^{-5}$	$4x10^{-7}$ - $3x10^{-3}$	1,3,5
Newmarket Till	$1x10^{-7}$	$2x10^{-8}$ - $6x10^{-7}$	1
Weathered Lindsay/Verulam	$5x10^{-6}$	$4x10^{-7}$ - $5x10^{-5}$	1,3,4
Weathered Bobcaygeon/Gull River	$6x10^{-6}$	$6x10^{-8}$ - $4x10^{-4}$	1,4
Verulam	$4x10^{-7}$	$1x10^{-10}$ - $6x10^{-4}$	1,2,3
Bobcaygeon (undifferentiated)	$4x10^{-7}$	$1x10^{-9}$ - $2x10^{-4}$	1
Upper Bobcaygeon	$1x10^{-7}$	$5x10^{-10}$ - $6x10^{-3}$	1,2,3,7,8,9
Lower Bobcaygeon	$1x10^{-8}$	$1x10^{-11}$ - $1x10^{-5}$	1,3,6,7,8,9
Gull River (undifferentiated)	$1x10^{-8}$	$2x10^{-11}$ - $2x10^{-5}$	1,8,9
Upper Gull River	$6x10^{-7}$	$5x10^{-11}$ - $2x10^{-3}$	1,3,6,7,8
Green Marker Bed	$7x10^{-6}$	$4x10^{-9}$ - $2x10^{-3}$	1,3
Lower Gull River	$6x10^{-7}$	$2x10^{-11}$ - $1x10^{-4}$	1,3,6,7,8
Shadow Lake / Precambrian Contact	$5x10^{-8}$	$1x10^{-11}$ - $6x10^{-4}$	1,3,6,7,8,9
Precambrian	$1x10^{-9}$	$1x10^{-10}$ - $6x10^{-8}$	7

* Number refers to source listed in the Section 5.5.

Table 5.3: Representative values of specific yield (S_y) and specific storage (S_s).

Geologic Unit	Specific Yield [1]	Specific Storage (m^{-1}) [2]
Newmarket Till	0.06 - Silt-dominated till	$1.3x10^{-3}$ – $1.3x10^{-4}$ - Medium-hard clay - Dense sand
Mackinaw Interstadial	0.23 - Fine sand 0.08 - Silt	$1.0x10^{-3}$ – $1.3x10^{-4}$ - Loose sand - Dense sand
Dummer till	0.16 - Sand-dominated till	$1.3x10^{-3}$ – $1.3x10^{-4}$ - Medium-hard clay - Dense sand
Bedrock Units	0.14 - Limestone	$6.9x10^{-5}$ - $3.3x10^{-6}$ - Rock, fissured, jointed Less than $3.3x10^{-6}$ - Rock, sound

Notes:
[1] Representative values of Specific Yield from Morris and Johnson, 1967.
[2] Range of values adapted from Domenico, 1972.

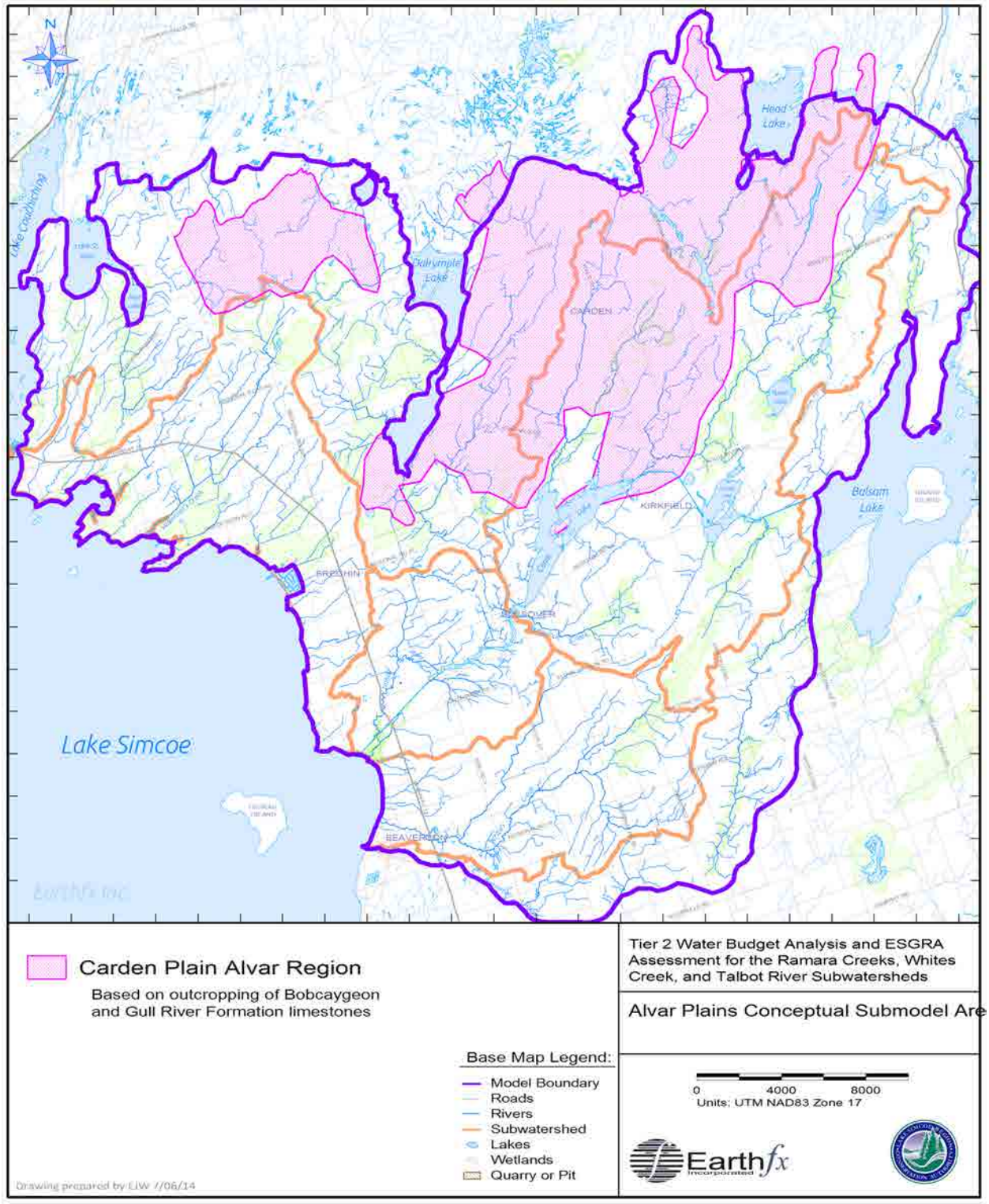

Figure 5.1: Carden Plains alvar region conceptual submodel area.

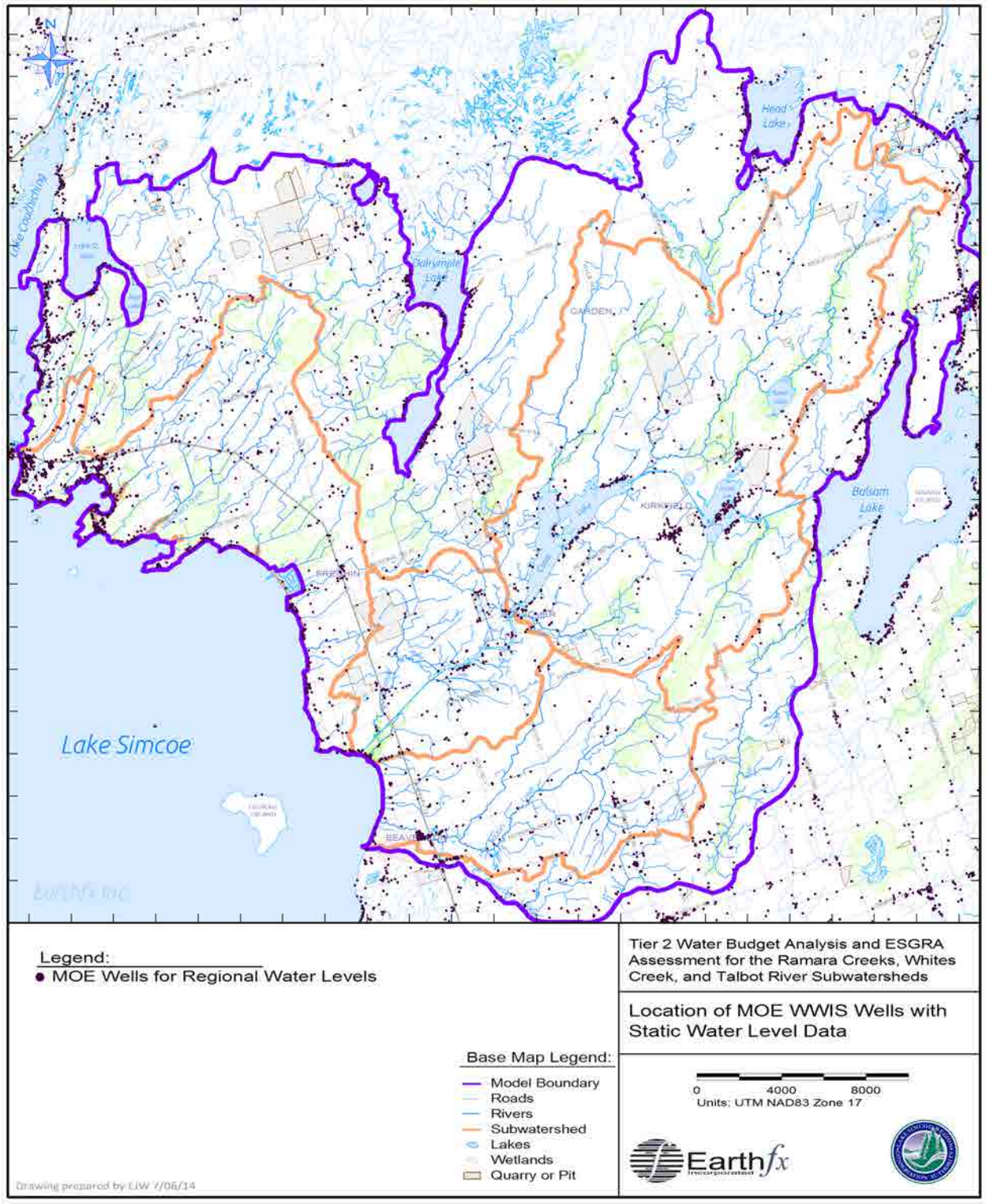

Figure 5.2: Location of MOE wells with static water level data.

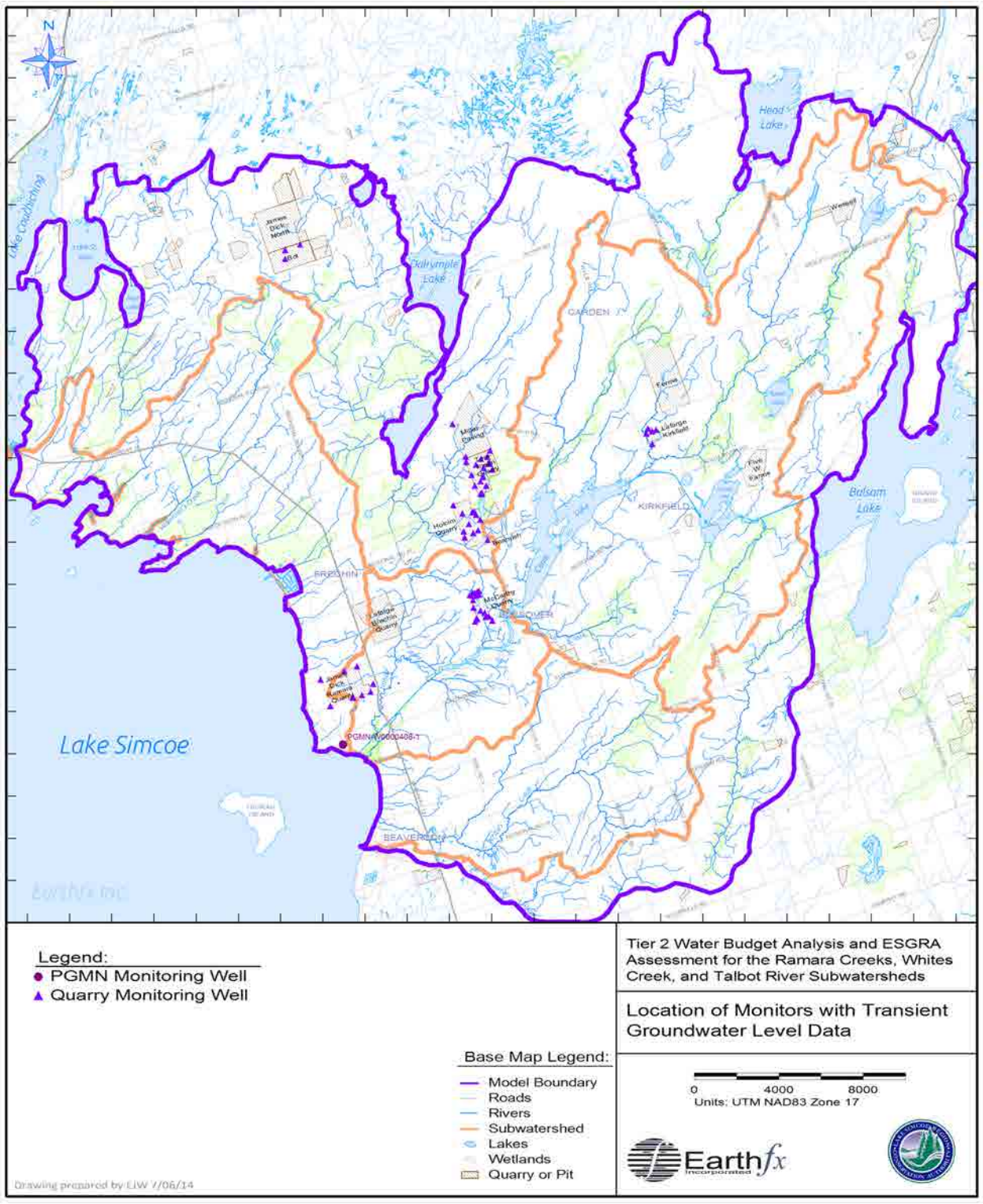

Figure 5.3: Location of transient groundwater monitoring wells.

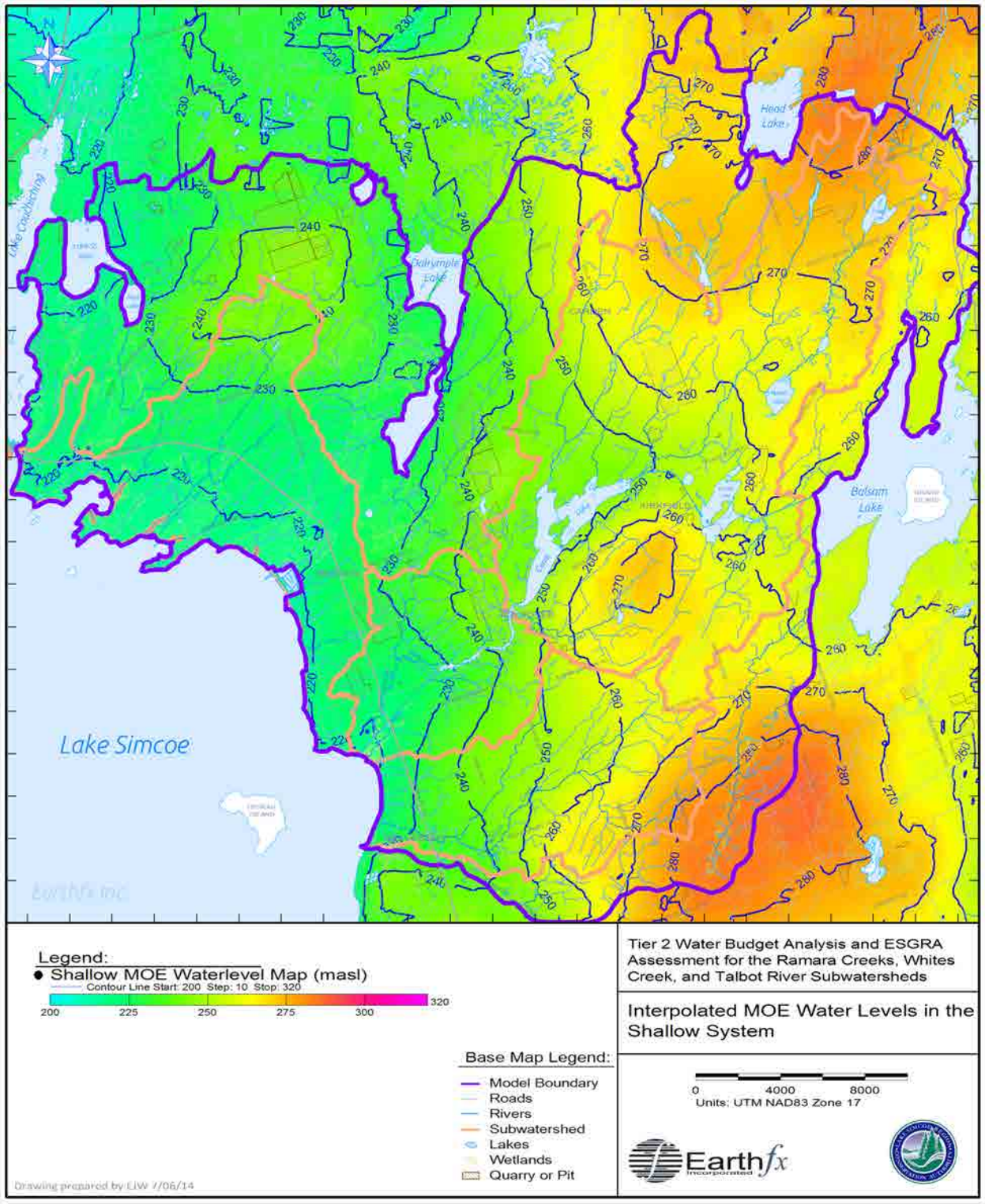

Figure 5.4: Interpolated MOE water levels in the shallow system.

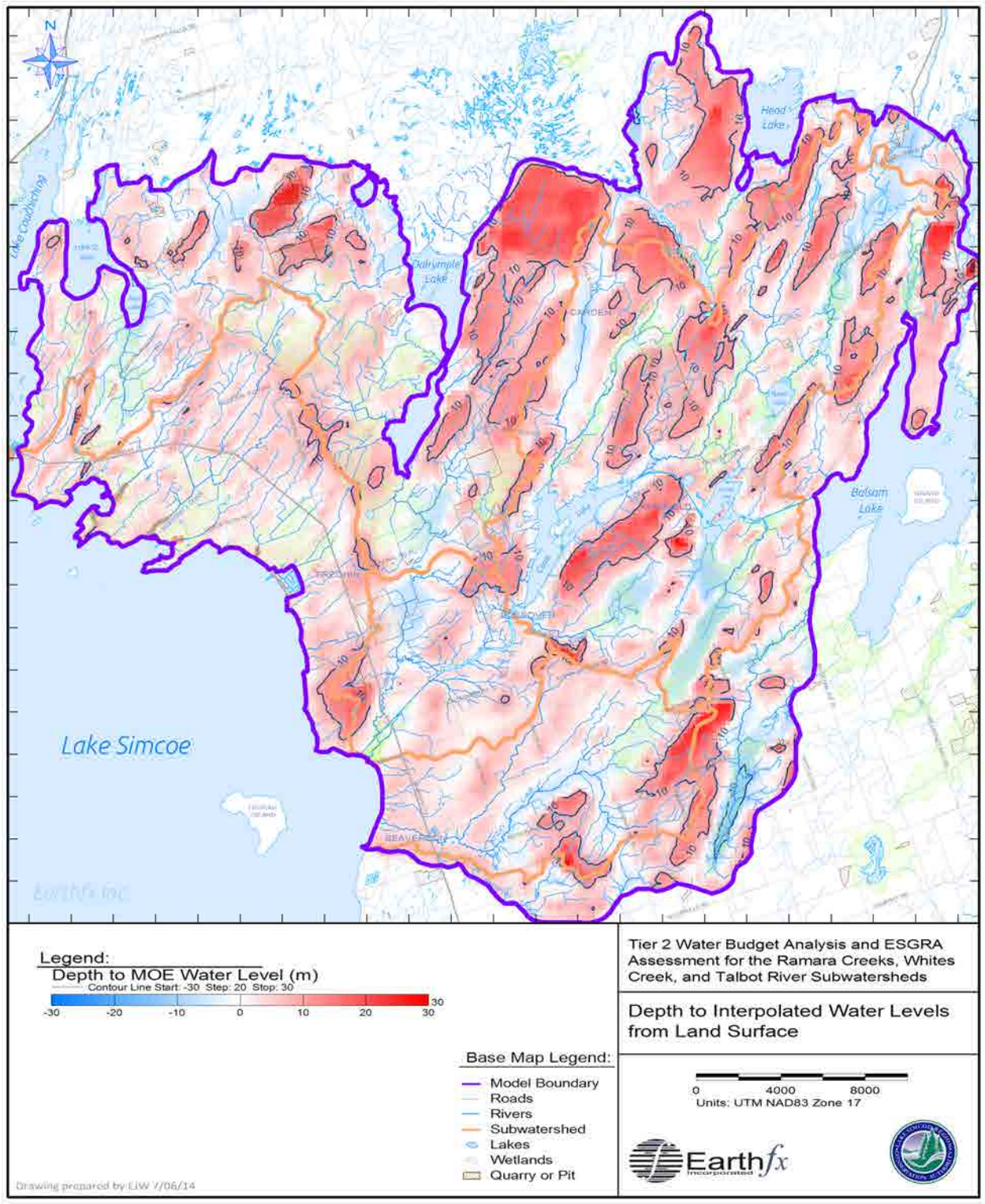

Figure 5.5: Depth to interpolated water level from ground surface.

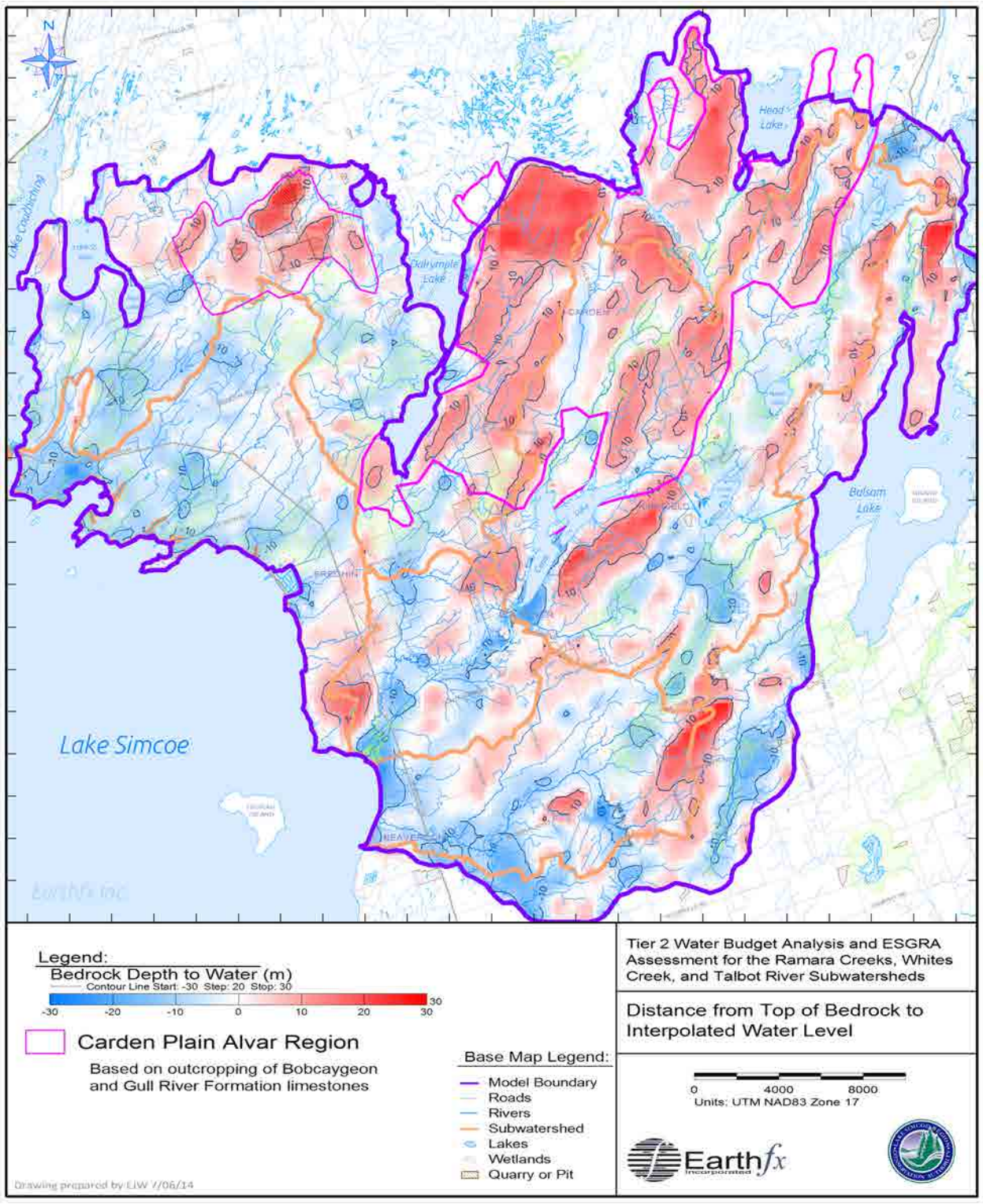

Figure 5.6: Distance from top of bedrock to interpolated water level.

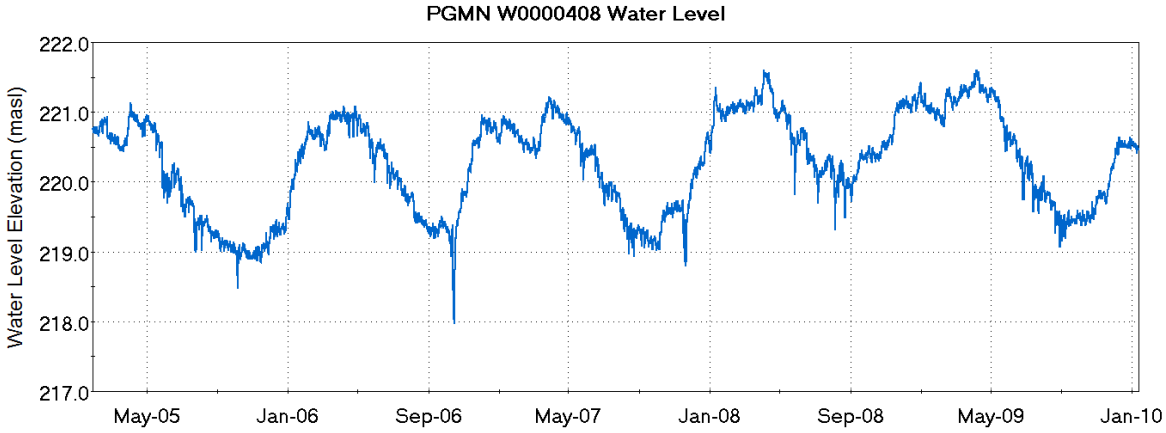

Figure 5.7: Water levels at PGMN well W0000408 (Contact Aquifer).

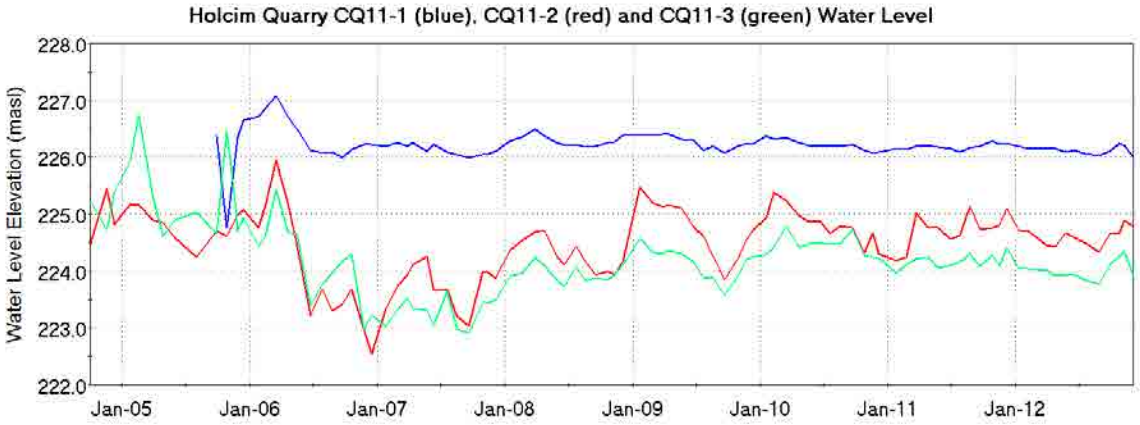

Figure 5.8: Water levels at Holcim Quarry nested wells CQ11-1 (Shadow Lake), -2 (Lower Gull) and -3 (Bobcaygeon/Upper Gull).

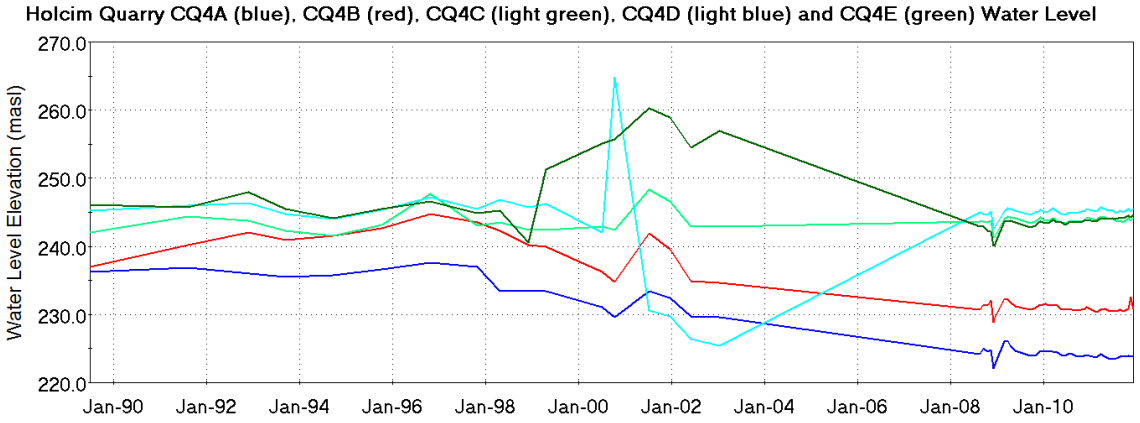

Figure 5.9: Water levels at Holcim Quarry nested wells CQ4A (Shadow Lake), 4B (Gull River), 4C (Green Beds), 4D (Bobcaygeon) and 4E (Contact Aquifer).

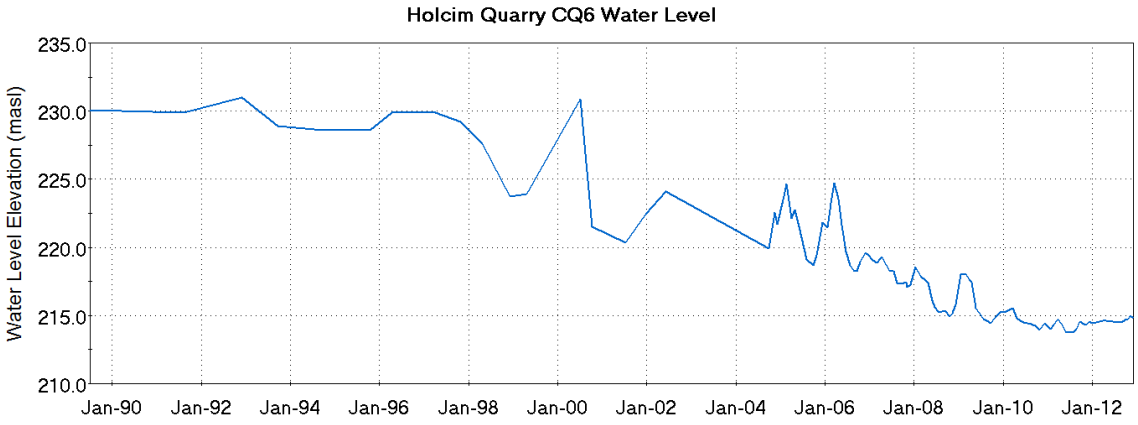

Figure 5.10: Water levels at Holcim Quarry well CQ6 (Lower Gull).

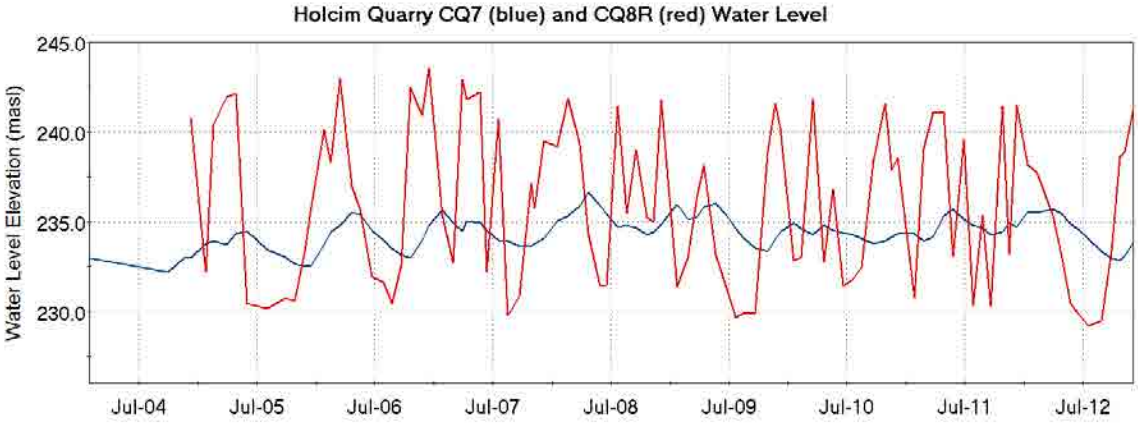

Figure 5.11: Water levels at Holcim Quarry wells CQ7 (Upper Gull) and CQ8R (open hole to Lower Gull).

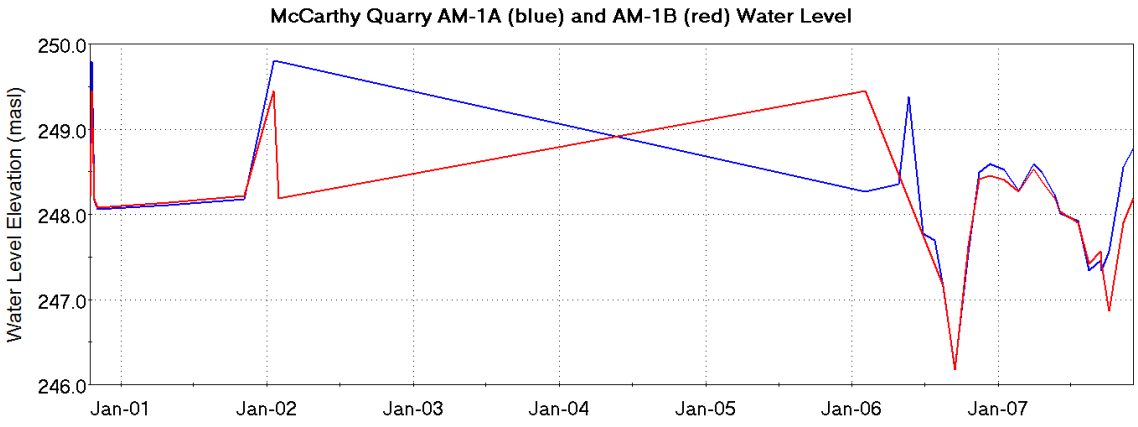

Figure 5.12: Water levels at McCarthy Quarry nested wells AM-1A and 1B (Newmarket Till).

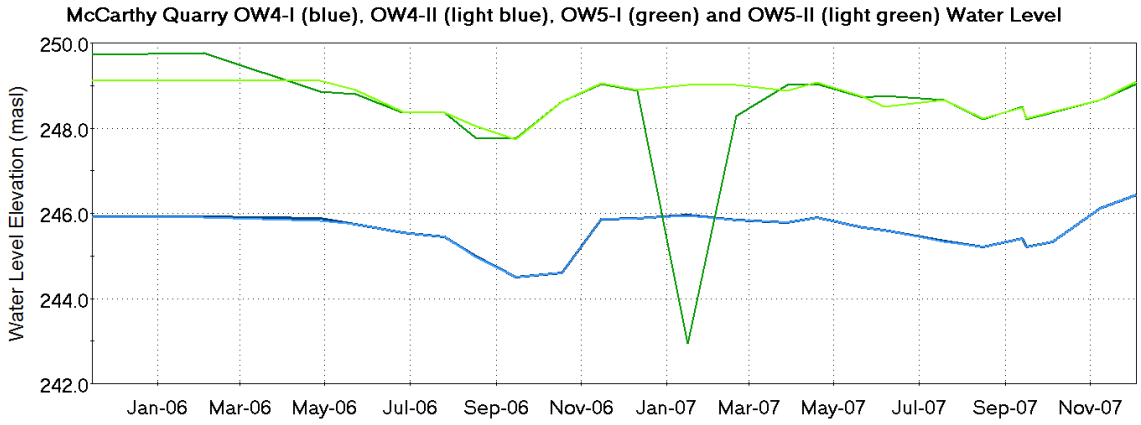

Figure 5.13: Water levels at McCarthy Quarry nested wells OW4-I (Contact Aquifer), OW4-II (Verulam), OW5-I (Contact Aquifer), and OW5-II (Verulam).

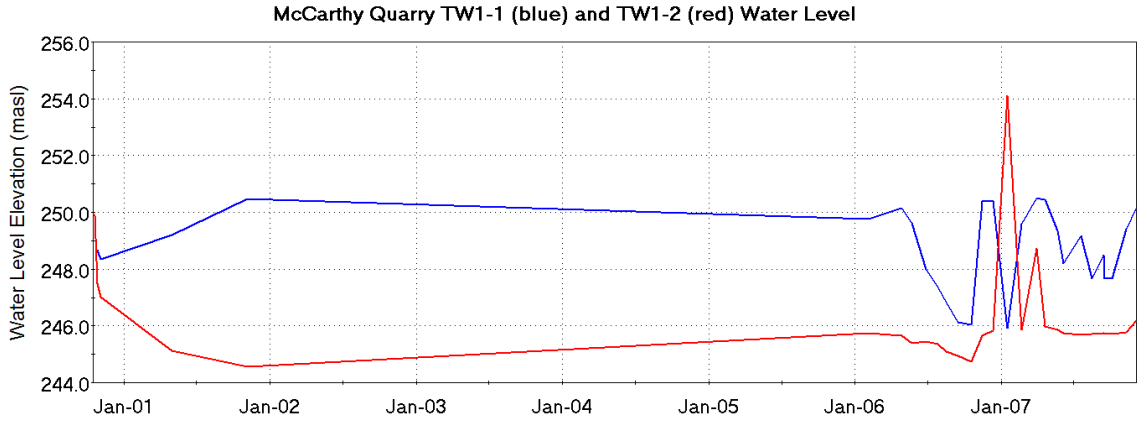

Figure 5.14: Water levels at McCarthy Quarry nested wells TW1-1(Green Bed) and -2 (Shadow Lake).

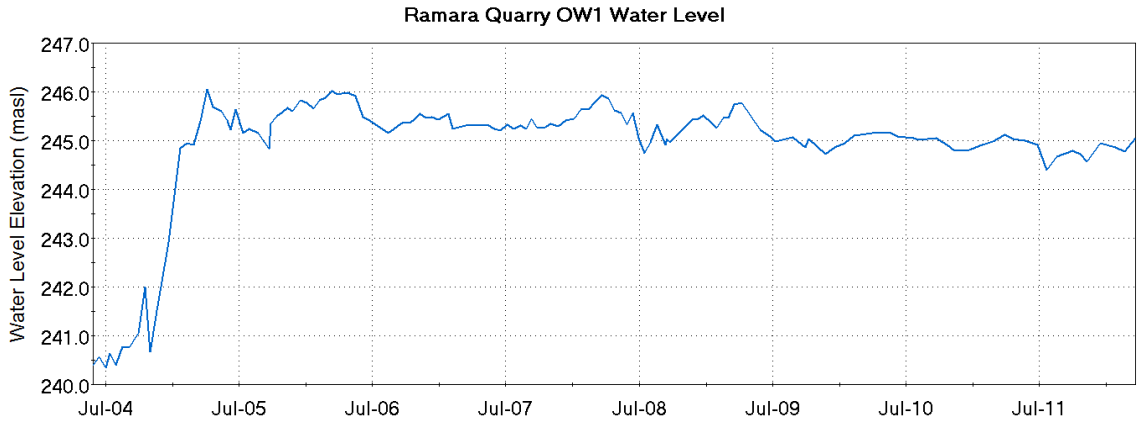

Figure 5.15: Water levels at Ramara Quarry well OW1 (Verulam).

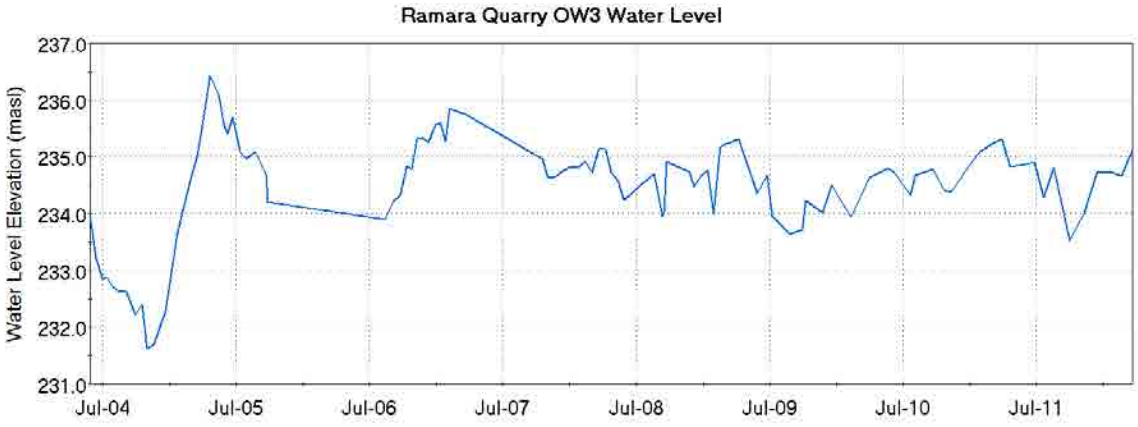

Figure 5.16: Water levels at Ramara Quarry well OW3 (Verulam).

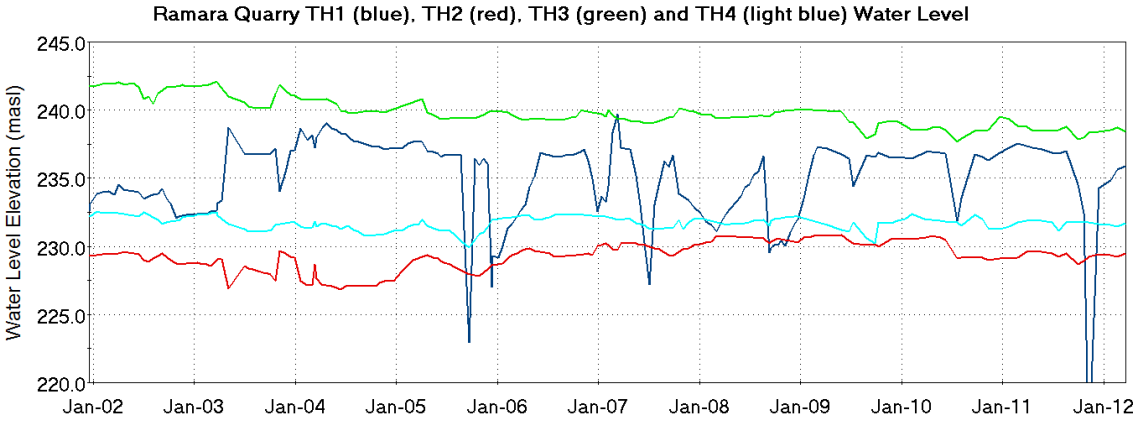

Figure 5.17: Water levels at Ramara Quarry well TH1 (open hole to Precambrian), TH2 (Verulam/Bobcaygeon), TH3 (Verulam), and TH4 (Verulam).

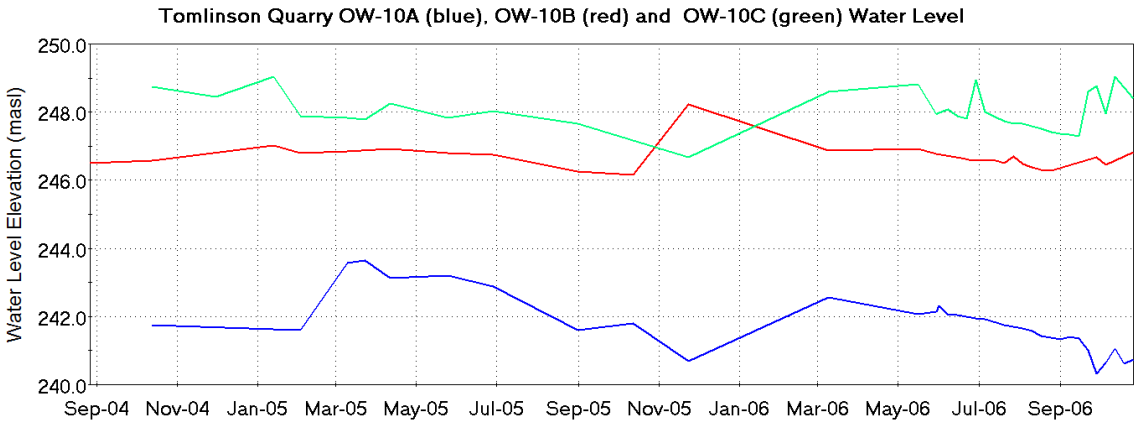

Figure 5.18: Water levels at Tomlinson Quarry nested wells OW-10A (Gull River), -10B (Verulam) and -10C (Contact Aquifer).

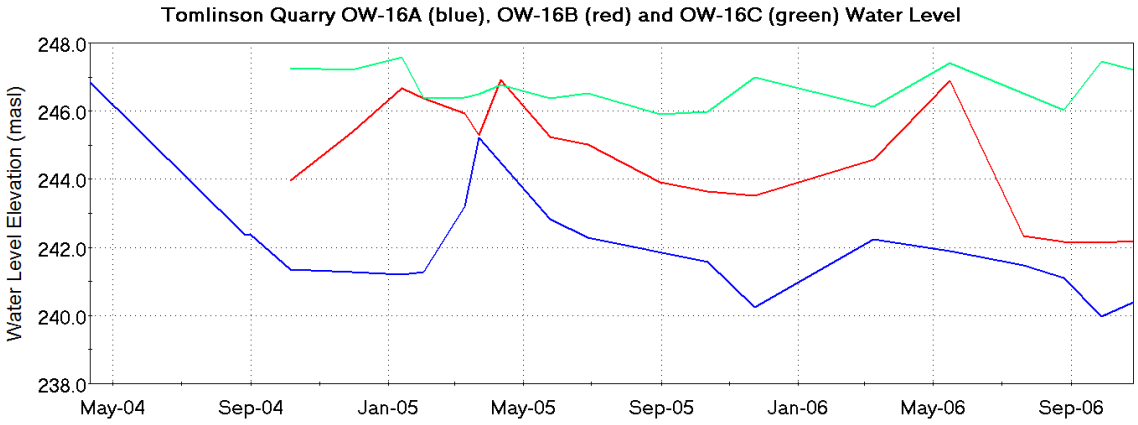

Figure 5.19: Water levels at Tomlinson Quarry nested wells OW-16A (Gull River), -16B (Bobcaygeon) and -16C (Verulam).

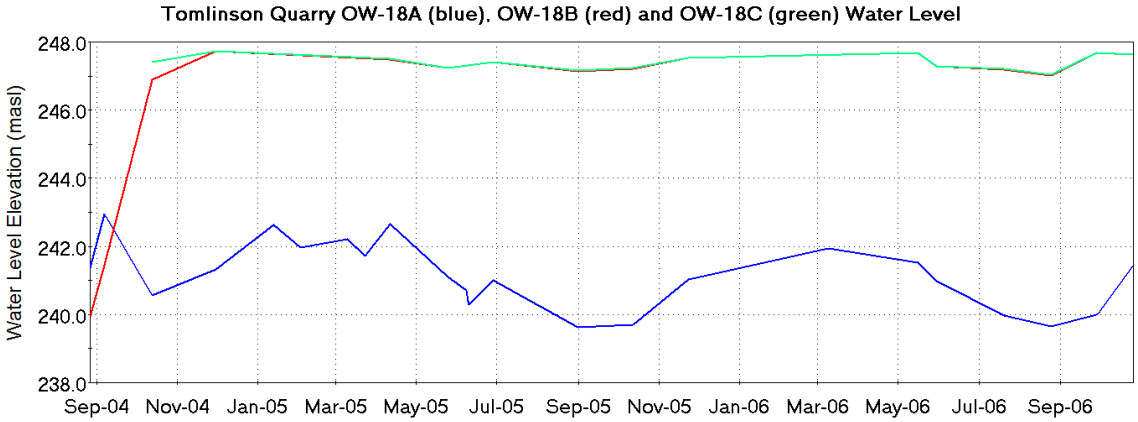

Figure 5.20: Water levels at Tomlinson Quarry nested wells OW-18A (Bobcaygeon/Gull River), -18B (Lower Verulam) and -18C (Upper Verulam).

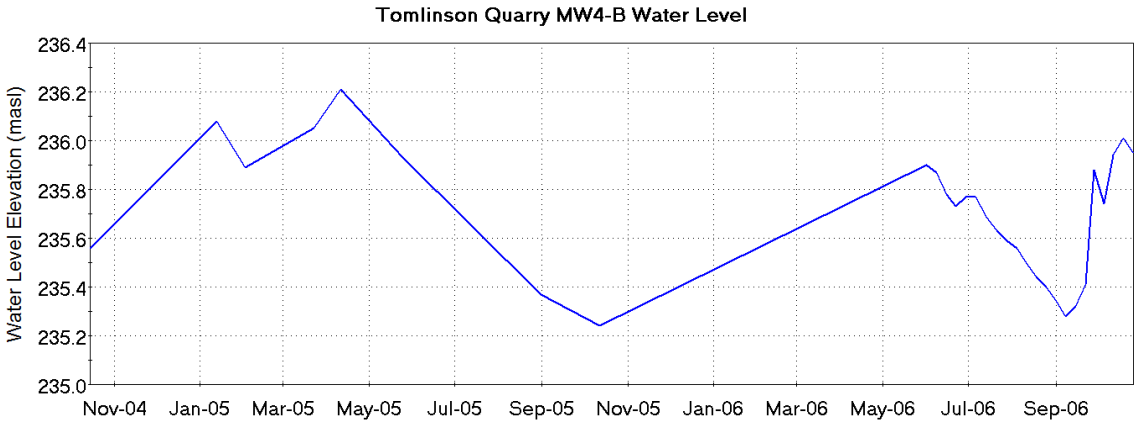

Figure 5.21: Water levels at Tomlinson Quarry well MW4-B (Contact Aquifer).

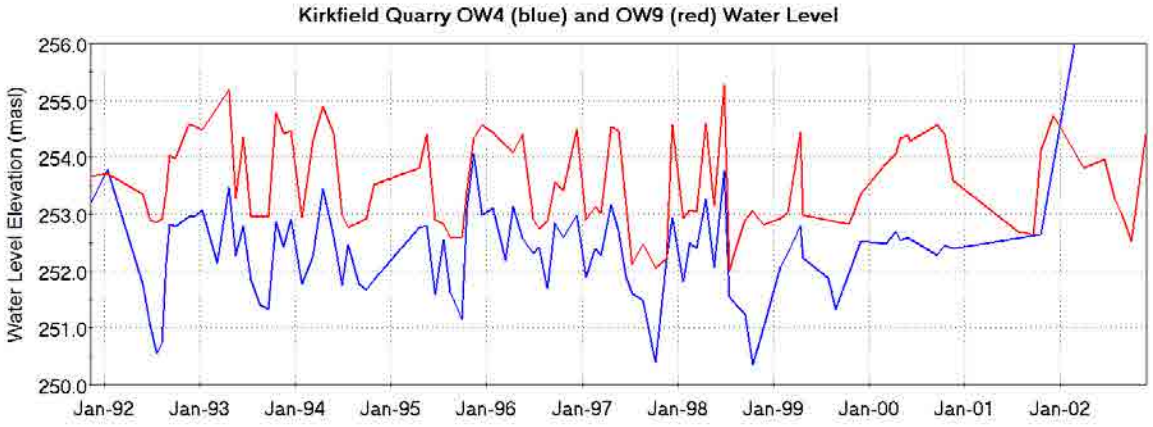

Figure 5.22: Water levels at Kirkfield Quarry wells OW4 (Bobcaygeon/Gull River) and OW9 (Lower Bobcaygeon).

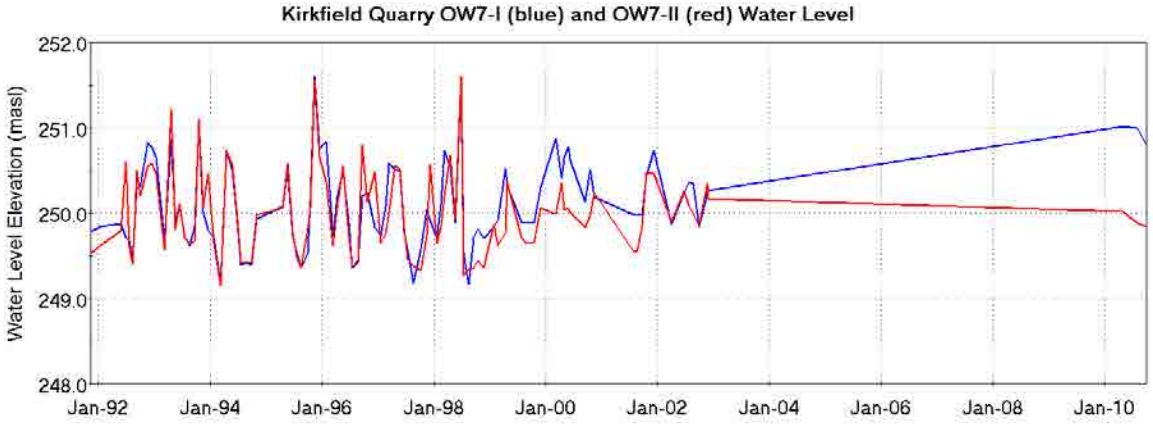

Figure 5.23: Water levels at Kirkfield Quarry wells OW7-I (Contact Aquifer/Bobcaygeon) and OW7-II (Green Marker Bed).

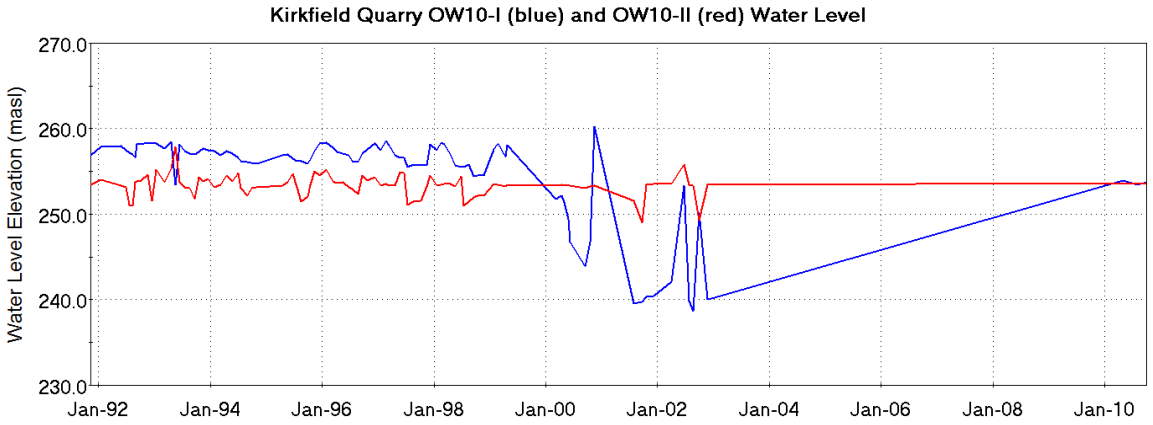

Figure 5.24: Water levels at Kirkfield Quarry wells OW10-I (Contact Aquifer/Upper Bobcaygeon) and OW10-II (Upper Gull River).

6 Water Demand Estimation

6.1 Overview

Compiling and assessing surface and groundwater use is a central objective in this water quantity risk assessment. Groundwater and surface water are extracted from the aquifers, streams and lakes in the study area for communal water supply, agricultural use, commercial and industrial use, golf course irrigation, and private (domestic) water supply. Extraction of over 50,000 litres of water per day (L/d) from a surface or groundwater source requires a Permit to Take Water (PTTW) from the Ministry of Environment. Permits are designated as surface water, groundwater, or both.

Assessing water use is a complex task. The reporting of water use is somewhat sporadic and frequently inaccurate. The MOE Permitting and Water Taking Reporting Systems have undergone significant changes in recent years, in some cases making assessment of historic use more difficult because of changes in the permitting system. Actual use is frequently lower than the maximum permitted taking, and can vary on a seasonal basis. Finally, estimating the consumptive portion of the taking can be difficult, however general guidelines are provided for consumptive use by type of taking (MNR, 2011).

The locations of 16 wells associated with groundwater permits (not including quarry takings) and 19 surface water intakes associated surface water permits from the 2012 PTTW database are presented in Figure 6.1. In addition, 15 takings related to quarry and aggregate extraction operations were identified in the study area; locations are presented in Figure 6.1.

The MOE Water Taking Reporting System (WTRS) database contains self-reported information on actual takings (as opposed to permitted takings). Data for municipal wells are generally complete. Some known problems exist with the database for non-municipal pumping due to changing permit numbers, incomplete records, backlogs in the transcription of paper records, and non-compliance with reporting requirements. A subset of the WTRS data for 2005 to 2011 was used in this study, although data gaps and inconsistencies are considered to be more frequent in the records prior to 2007. For takings where no historical reported rates could be found, it was assumed that pumping rates were at their maximum permitted daily value (as was the case for PTTW 0664-9BTKX4).

Permits for pumping tests are not included in this analysis because they were likely issued on a temporary basis. In the case of expired permits, an effort was made to identify whether the permit was renewed under a different PTTW number. This included a search of the Environmental Registry, maintained by the MOE, and a review of WTRS database for on-going reporting beyond the stated permit expiration date. Expired permits found to be discontinued were not included in the water budget analyses.

6.2 Consumptive Use Corrections

A Tier 2 Water Budget Assessment requires an estimation of consumptive demand from all permitted and non-permitted water takings in each subwatershed. Consumptive demand refers to the amount of extracted water that is not returned locally to the same source in a reasonable amount of time. To correct the observed or estimated pumping rates, a *consumptive use factor* was applied. For example, a permit to pump groundwater for golf course irrigation could have a consumptive use factor of 80%, reflecting that 20% of the pumped water is returned to the source aquifer while 80% is lost to other processes such as evapotranspiration. Table 3-1 of the Water Budget and Water

Quantity Risk Assessment Guide (MNR, 2011) provides consumptive use factors for different usage classes and sub-classes that were applied to the permitted takings.

A consumptive use factor for the unserviced population was estimated at 20% (i.e., 80% of the water use in areas with private sewage treatment systems was assumed to be returned to the shallow aquifer). This value is consistent with water supply consumption values listed in MNR (2011). The consumption factor for non-permitted agricultural use (primarily livestock, including dairy operations) was estimated as 80%, close to the recommended factor of 78% suggested by de Loe (2001).

To be conservative, all takings by municipal wells were assumed to be 100% consumptive. This is a reasonable assumption because the municipal wells are considered to access confined aquifer units to which return flow of extracted water is unlikely to occur within a short period of time.

6.3 Seasonal Water Use Correction

Many water permit holders do not extract water at a constant rate throughout the year. For example, there are several golf course irrigation permits and campgrounds water supply permits in the study area subwatersheds. Additionally, many of the permits in the study area have specified periods in which water takings are allowed. For permits without WTRS data, monthly allocation of takings was done based on the restrictions listed in the individual permit. If the permit did not have any restrictions, the monthly allocation was assigned based on the suggested monthly values for the usage classes and sub-classes listed in Table 3-2 in MNR (2011). Overall, permitted water demand in the study subwatersheds is higher in the summer due to these seasonal activities.

The agricultural demand estimates given by de Loe (2001) were reported on an annual basis. Although it is quite likely that agricultural demand for the summer season exceeds winter demands, there was no information available to allocate seasonal water taking using the data provided by de Loe (2001). Therefore, the annual agricultural water demand estimates were assumed to be constant year-round.

6.4 Municipal Water Supply

Six permits to take water for municipal water supply were identified within the study area: four permits for groundwater withdrawal from 11 supply wells, and two permits for surface water takings, both from Lake Simcoe. Average pumping was calculated from data provided by LSRCA and the WTRS database. Municipal takings are summarized in Table 6.1 and discussed further below.

6.4.1 Val Harbour

The Val Harbour subdivision is supplied by a municipal wellfield with three wells (Well 1, Well 2, and Well 3R), operated under PTTW 7653-87TS7U (replacing 94-P-3026). Under the PTTW, Well 1 is permitted to pump at a maximum rate of 67.7 m^3/d, Well 2 is permitted to pump at a maximum rate of 139.7 m^3/d, and Well 3R is permitted to pump at a maximum rate of 207.4 m^3/d. The Val Harbour wellfield services approximately 56 residential lots (approximately 148 residents) as of 2007.

Well 1, Well 2 and Well 3 were drilled in 1972 to depths of 18.9 m, approximately 15.6 m and 16.6 m, accessing the fractured limestone bedrock contact aquifer. The exact reported completion depth of Well 2 is unknown because of damage to the original well record. Well 3R was completed in 2009 to replace the old Well 3 according to the Township of Ramara Drinking Water Systems annual report for the Val Harbour Water Works. According to reported takings in the WTRS

database, average daily pumping rates for Well 1, Well 2 and Well 3R are 11 m^3/d, 24 m^3/d and 0 m^3/d, respectively. Estimates of average monthly consumptive demand based on the available WTRS data for the Val Harbour well field are presented in Figure 6.2.

The Val Harbour municipal wellfield has not been classified as groundwater under the direct influence of surface water (GUDI). The system is connected to a water treatment system that employs chlorination of the raw water. Two 45 m^3 underground reservoirs are used in series to extend chlorine contact time.

6.4.2 Western Trent/Palmina

The Western Trent/Palmina drinking water system draws water from two wells: Well #1 (Palmina) and Well #1 (Western Trent). Well #1 (Palmina) operates under PTTW 6784-7JDRFS, which allows a maximum daily pumping rate of 294 m^3/d. Well #1 (Western Trent) operates under PTTW 7211-7JCMRV and is allowed a maximum daily pumping rate of 392 m^3/d.

Well #1 (Palmina) was constructed in 1972 to a depth of 28.3 m. Well #1 (Western Trent) was also constructed in 1972 to a depth of 32 m. Both of the municipal wells are completed in the Paleozoic-Precambrian nonconformity, which is regionally recognized as a productive aquifer unit due to enhanced fracturing in the weathered Precambrian. Locally, the Shadow Lake-Precambrian aquifer is confined by the overlying limestone of the Bobcaygeon Formation and the argillaceous limestone and interbedded shale of the Verulam Formation.

Based on reported takings in the WTRS database for Well #1 (Palmina) and Well #1 (Western Trent), the average daily pumping rates are 36.5 m^3/d and 36.0 m^3/d, respectively. The estimated average monthly consumptive demand using the available WTRS data for the Western Trent/Palmina wells are presented in Figure 6.3.

The Western Trent/Palmina municipal wells are considered to be GUDI. A water treatment system has been installed which includes membrane cartridge filtration and chlorination. A 170 m^3 storage reservoir for treated drinking water is also part of the municipal drinking water system.

No planned system or increase in future demand is anticipated for this system based on consultations with the City of Kawartha Lakes and the LSRCA.

6.4.3 Bayshore Village

The Bayshore Village wellfield consists of three water supply wells (Well 3, Well 4 and Well 5) in the Bayshore Village subdivision. Under PTTW 4512-66JSJZ, Well 3 has a maximum permitted pumping rate of 196.4 m^3/d, Well 4 has a maximum permitted pumping rate of 807.4 m^3/d, and Well 5 has a maximum permitted pumping rate of 240 m^3/d. The total daily pumping rate allowed for the Bayshore Village municipal wellfield is 1243.8 m^3/d. As of 2007, the Bayshore Village wellfield was estimated to service 288 lots (about 749 residents).

All three of the municipal wells were completed in the fractured bedrock contact aquifer of the upper Bobcaygeon Formation. Well 3 was completed to a depth of 17 m, while Well 4 and Well 5 were completed to a depth of 13 m. Overburden material in the area of the wellfield is comprised of 6 to 8 metres of Newmarket Till, underlain by 2 to 5 metres of glaciofluvial sand.

The average daily pumping rates for Well 3, Well 4 and Well 5 are 44.6 m^3/d, 163.8 m^3/d and 59.5 m^3/d, respectively, based WTRS data. Figure 6.4 presents the estimated average monthly consumptive demands for the Bayshore Village municipal wells. The Bayshore Village municipal

wells are not considered to be GUDI. Raw groundwater from each of the three wells undergoes chlorination before flowing into a 114 m^3 underground storage tank.

6.4.4 Lagoon City

The Lagoon City Water Treatment Plant is located in the community of Lagoon City on the east shore of Lake Simcoe. The facility operates under PTTW 8118-79KPLD, which allows for a maximum daily intake of 3,993.3 m^3/d from Lake Simcoe. In 2007, it was estimated that the Lagoon City Water Treatment Plant services the equivalent of 1211 single family dwellings (about 3,028 people) in Lagoon City and Brechin. Because the Lagoon City/Brechin Water Treatment Plant intakes directly from Lake Simcoe, this municipal water supply permit was not simulated in this study.

6.4.5 South Ramara

The South Ramara Water Treatment Plant is a municipal surface water taking located on the shore of Lake Simcoe, south of Brechin. The facility operates under PTTW 2683-5YWNWN, which allows for the withdrawal of 542.9 m^3/d from Lake Simcoe. The water treatment facility has provided water to the community of Heritage Farm since 1982 and the Mara Shores Estates subdivision since 2001, servicing a total of 87 lots (approximately 226 residents) as of 2007. Because the South Ramara Treatment Plant intakes directly from Lake Simcoe, this municipal water supply permit was not simulated in this study.

6.5 Non-Municipal Groundwater Takings

Six non-municipal groundwater permits (governing 8 wells) in the PTTW database were identified within the model area. Although two of these permits (1871-8HSSMB and 3827-8ADMLG) are located outside of the study subwatersheds, these takings were represented as they are located within the model boundaries and could affect cross-boundary groundwater flows. Table 6.3 summarizes the permitted non-municipal groundwater takings. Average monthly pumping from the non-municipal groundwater takings (not including the quarries) are presented in Figure 6.5, along with the monthly municipal pumping for comparison.

Estimation of actual water use was possible for five of the eight groundwater permits using WTRS data. In the case of PTTW 0664-9BTKX4 and 3827-8ADMLG (TW#1 clubhouse well), the maximum permitted rate was assumed because no reported takings were available. The groundwater taking for PTTW 92-P-3079 was included in the Tier 1 study but was not identified in the WTRS database. This permit was assumed to be active and included in the Tier 2 model as it represents a golf course taking in close proximity to the Bayshore Village municipal supply wells.

6.6 Non-Municipal Surface Water Takings

Eight non-municipal permitted surface water takings (governing 17 intakes) were identified in the study area. Of these, four of the permits (governing six intakes) were excluded from the model: two of these excluded permits have intakes in Lake Simcoe and the other two permits are for wetland and wildlife conservation, which are considered to have no net consumptive water demand. For the remaining permitted surface water takings, at least one year of reported daily takings were available in the WTRS database, which were used to establish existing demand for each of these permits. Table 6.5 summarizes the permitted non-municipal surface water takings.

6.7 Unserviced Domestic and Non-Permitted Agricultural Consumption

The number of persons in each watershed living outside of the areas with municipal supply is referred to as the “unserviced” population. This population is assumed to be consuming groundwater water from individual wells or small communal supplies.

Estimates of non-serviced domestic water use were taken from the Tier 1 Water Budget and Water Quantity Stress Assessment (LSRCA, 2009) and were based on 2006 population census data. The estimates were corrected for actual consumption (20%) because a significant portion of this water would be returned to the groundwater system. Table 6.6 presents the unserviced demand for the three study subwatersheds.

Under the Ontario Water Resources Act (Revised Statutes of Ontario 1990, Chapter O.40), farmers using less than 50,000 L/d and farmers who are taking water for livestock watering but not storing the water do not require a PTTW and are therefore "non-permitted" agricultural consumers. To estimate agricultural consumption, MNR (2011) suggested using water use coefficients developed by de Loe (2001 and 2005). The 2001 data compiled by de Loe have been allocated to subwatersheds using area weighting to estimate subwatershed water use as described below.

Agricultural demand was estimated for each study subwatershed in LSRCA (2009) using de Loe’s methodology. Although this method provides an estimate of total water consumption, there is no differentiation between groundwater and surface water takings. For the purpose of this study, the non-permitted agricultural demand was treated as a groundwater taking. Table 6.6 presents the agricultural demand.

6.8 Quarry Takings

There are 11 quarry-related permits to take water in the study area were identified; locations are shown in Figure 6.1. The permits represent combined surface water and groundwater takings because surface water runoff and groundwater leakage are both collected and stored in sumps in the quarry floors. These sump ponds are dewatered to control local groundwater levels and water is use in processing (e.g., aggregate washing and dust control). The quarry permits are summarized in Table 6.7.

Of the 11 quarries identified, eight are located in (or partially in) the Talbot River subwatershed boundary; this includes Holcim quarry, although the majority of the quarry area is outside of the subwatershed. Maximum permitted takings for quarry operations within the Talbot subwatershed range from 1,569.6 m^3/d to 12,528 m^3/d. The Lafarge Brechin quarry, located along the Talbot River subwatershed boundary, is the only quarry operation within the Ramara Creeks subwatershed, with a maximum taking of 3,600 m^3/d. There are no quarries located within the Whites Creek subwatershed. The Bot, Tomlinson and Miller quarries are located outside of the study subwatersheds, but have been included to account for possible impacts of quarrying operations that might extend into the nearby study subwatersheds.

Three of the quarries – McCarthy Quarry, Lafarge Kirkfield Quarry and Beamish Quarry - are not currently dewatering their sites, as indicated by an average demand of 0 m^3/d in Table 6.7. The Lafarge Kirkfield Quarry operated under PTTW 1346-7ELPP2 which allowed a maximum taking of 4,320 m^3/d; however, this quarry is currently flooded and no active extraction operations. The McCarthy Quarry is in the early stages of site development and aggregate extraction below the water table had not yet started at the time of this study. The quarry operated by K.J. Beamish Construction Ltd. is also in the early stages of site clearing and does not extend below the water

table at this time. The quarry is permitted to extract material below the water table, at which point it will be allowed to dewater at a maximum rate of 5,011 m^3/d under PTTW 6758-883KVV. The anticipated takings related to quarrying operations will be represented in the future demand/build out scenarios discussed in Section 6.9. Further discussions on how the quarry water use was represented in the numerical model are provided in Section 8.6.

6.9 Future Demand Estimates

Based on discussions with LSRCA staff, the Ramara Creeks subwatershed is anticipated to experience a population increase of 3,300 by 2031 from a 2011 population of 5,330. It is further anticipated that 90% of this population growth will be centred in the three designated settlement areas of Brechin, Lagoon City and Atherley-Uptergrove. As stated previously, Brechin and Lagoon City are serviced by surface water takings from Lake Simcoe and are not represented in the model. The Atherley-Uptergrove settlement area is serviced by private domestic wells, which are not explicitly represented in the model. The 10% of the estimated growth not associated with these three designated settlement areas (an estimated 330 residents) are assumed to be serviced by the Val Harbour and Bayshore Village wellfields. The projections of future populations for the Val Harbour and Bayshore Village communities were used to estimate future demand on their respective wellfields, as summarized in Table 6.8.

In the Talbot River subwatershed, 2031 population estimates provided by LSRCA and the City of Kawartha Lakes are similar to the current population, and as such no future demand increases are anticipated at the Western Trent/Palmina wellfield. An additional increase of 10% was added to the Western Trent/Palmina municipal wells to represent possible future increases in demand. Estimating future demand as the maximum permitted pumping rate at these well was considered too conservative for this study given that no major municipal expansion is expected in the study area. Estimated future pumping rates are summarized in Table 6.9 for the municipal wells within the study area.

For the Tier 2 assessment, only the future demand of the municipal water supply wells and surface water intakes are considered in the future scenarios; future demands of other permitted and non-permitted takings are not considered. This does not apply to the various quarry and aggregate extraction operations within the study area, as discussed below.

Future changes in land use and their effect on groundwater recharge is part of a Tier 2 assessment. In this study, quarries are treated as land use change. The quarries are required to report their build-out strategy as part of the approval process. Through consultation with LSRCA staff, it was decided that the 20-year build-out plans for the 12 quarries would be used to estimate the future depth and areal extents of the excavation. This was consistent with the time frame for the future demand estimates for the municipal water supply systems, which are based on 2031 Growth Plan. The 20-year development strategy was also used in a previous Cumulative [Quarry] Impact Assessment in the area (Golder Associates Ltd., 2012).

Consistent with the Golder Associates Ltd. (2012) study, the quarry depths and build out were estimated by calculating the total material volume removed in a 20-year period assuming the maximum permitted extraction rate (tonnage per year) and applying it uniformly over the full licensed extraction area for each of the quarries. The projected future extraction was always assumed to start in the undisturbed areas of the licenced extraction areas and extended down toward the existing quarry floor. Quarry depths and excavated areas at the end of the 20-year build-out are summarized in Table 6.10. Groundwater and surface water inflows into the quarries were calculated by the models used in the Tier 2 assessment and were assumed to be equal to the future discharge from the quarries, as explained further in Section 8.6.

6.10 Tables and Figures

Table 6.1: Summary of operational limits and historical average pumping rates for municipal takings.

Permit Holder	MOE Permit Number	Source Name	Subwatershed	Maximum Permitted Taking (m^3/d)	Average Demand (m^3/d)
Val Harbour Subdivision Municipal Well	7653-87TS7U (94-P-3026)	Well 1	Ramara Creeks	67.7	11.0
		Well 2	Ramara Creeks	139.7	24.0
		Well 3R	Ramara Creeks	207.4	0.0
Western Trent Municipal Well	6784-7JDRFS	Well #1 (Palmina)	Talbot River	294.0	36.5
	7211-7JCMRV	Well #1 (Western Trent)	Talbot River	392.0	36.0
Bayshore Village Municipal Well	4512-66JSJZ	Well No. 3	Ramara Creeks	196.4	43.8
		Well No. 4	Ramara Creeks	807.4	162.2
		Well No. 5	Ramara Creeks	240.0	59.5
South Ramara Municipal Supply	2683-5YWNWN	Lake Simcoe	Ramara Creeks	542.9	61.5
Lagoon City Municipal Supply	8118-79KPLD	Lake Simcoe	Ramara Creeks	3,993.3	975.9

Notes:

1) *South Ramara and Lagoon City municipal surface water takings (grey) are not included in the subwatershed water budgets because both systems take water directly from Lake Simcoe.*
2) *Takings from Lake Simcoe and Wildlife/Conservation permits were not included.*

Table 6.2: Average monthly pumping for municipal wells.

Well	Jan	Feb	Mar	Apr	May	Jun	Jul	Aug	Sep	Oct	Nov	Dec
Val Harbour Well 1	332	305	316	327	363	465	567	343	299	293	278	303
Val Harbour Well 2	694	610	632	660	756	939	1,153	800	694	680	633	673
Val Harbour Well 3	0	0	0	0	0	0	0	0	0	0	0	0
Well #1 (Palmina)	986	799	1,030	1,079	1,214	1,245	1,597	1,295	1,133	1,027	1,002	1,024
Well #1 (Western Trent)	971	811	1,055	1,059	1,218	1,311	1,343	1,253	1,174	1,018	1,014	1,020
Bayshore Well No. 3	1,191	996	1,004	1,023	1,282	1,501	1,913	2,006	1,442	1,369	1,029	1,086
Bayshore Well No. 4	4,226	3,670	3,872	4,153	5,221	5,898	7,112	7,230	5,318	3,921	3,955	4,289
Bayshore Well No. 5	1,538	1,335	1,416	1,502	1,881	2,157	2,327	2,554	1,961	1,964	1,426	1,520
Monthly Total (m^3/mo)	*9,938*	*8,526*	*9,325*	*9,804*	*11,934*	*13,515*	*16,011*	*15,480*	*12,021*	*10,271*	*9,335*	*9,914*

Notes:

1) *All values provided in m^3/month.*
2) *Monthly totals subject to round-off error.*

Table 6.3: Summary of operational limits and historical average pumping rates for permitted groundwater takings.

Permit Holder	MOE Permit Number	Sub-watershed	Well Name	Purpose	Maximum Permitted Taking (m^3/d)	Average Demand (m^3/d)
Bayshore Village Golf Course	92-P-3079	Ramara Creeks	Well #1	Agricultural - Golf Course	81.8	14.0
Western Trent Golf Club Ltd.	0664-9BTKX4 (8422-5ZKNND)	Talbot River	Well #1	Water Supply	64.8	64.8 [2]
Green Line Properties Ltd.	1871-8HSSMB	---	Artisan Spring Well	Campgrounds - Water Supply	45.5	26.2
		---	Campground Well	Campgrounds - Water Supply	45.5	0.0
City of Kawartha Lakes Campgrounds Well	2424-6SKJ9R	Talbot River	Well 1	Campgrounds - Water Supply	200.0	19.0
Mara Provincial Park	5227-79UJ6E	Ramara Creeks	Campground Well	Campgrounds - Water Supply	56.4	7.3
Monck's Landing Golf Club	3827-8ADMLG (5377-6UML3K)	---	Source Pond	Agricultural - Golf Course	402.5	5.6
		---	TW-1 Clubhouse Well	Water Supply	10.0	10.0 [2]

Notes:

1) *Average demand is estimated for 2005 to 2011.*
2) *Average demand for Western Trent Golf Ltd. and Monck's Landing Golf Club well based on maximum permitted taking.*

Table 6.4: Average monthly non-municipal permitted groundwater takings.

Permit No.	Jan	Feb	Mar	Apr	May	Jun	Jul	Aug	Sep	Oct	Nov	Dec
92-P-3079	0	0	0	0	1,035	1,002	1,035	1,035	1,002	0	0	0
0664-9BTKX4	2,009	1,831	1,944	2,009	1,944	2,009	1,944	2,009	1,944	2,009	1,944	2,009
1871-8HSSMB	0	0	0	0	1,386	1,341	1,386	1,386	1,341	1,386	1,341	0
1871-8HSSMB	0	0	0	0	0	0	0	0	0	0	0	0
2424-6SKJ9R	0	0	0	89	858	1,333	1,724	1,487	1,127	494	0	0
5227-79UJ6E	1	0	0	116	380	348	843	846	145	0	0	0
3827-8ADMLG	0	0	0	0	0	667	689	689	0	0	0	0
3827-8ADMLG	310	280	310	300	310	300	310	310	300	310	300	310
Monthly Total (m^3/mo)	*2,319*	*2,111*	*2,254*	*2,513*	*5,913*	*6,999*	*7,931*	*7,762*	*5,858*	*4,199*	*3,585*	*2,319*

Notes:

1) *All values provided in units of m^3/month.*
2) *Consumptive use factors have not been applied to the monthly pumped volumes in the table.*
3) *Monthly totals subject to round-off error.*

Table 6.5: Summary of operational limits and historical average pumping rates for permitted surface water takings.

Permit Holder	MOE Permit Number	Watershed	Source Name	Purpose	Maximum Permitted Taking (m^3/d)	Average Demand (m^3/d)
Woodville Farms Limited	6742-64PJDT	---	Pond No. 1	Field Crops and Pasture	3,028.8	0.0
			Pond No. 2	Field Crops and Pasture	1,008.0	5.0
			Runoff - Pond 1	Field Crops and Pasture	4,909.8	0.0
			Spring - Pond 2	Field Crops and Pasture	2,182.1	0.0
Beverley Turf Farms Ltd.	0256-8EDKHX	Talbot	Talbot River Property 1	Sod Farm	3,926.9	0.0
			Talbot River Property 2	Sod Farm	3,926.9	60.6
			Talbot River Property 3	Sod Farm	3,926.9	0.0
			Talbot River Property 4	Sod Farm	3,926.9	0.0
			Talbot River Property 5	Sod Farm	3,926.9	0.0
Associated Gospel Churches	6625-8KUPAU	Talbot	Talbot River	Other Water Supply	250.0	41.1
Western Trent Golf Club Ltd	8422-5ZKNND	Talbot	Canal Lake	Golf Course Irrigation	655.2	43.4

Notes:

1) *Average demand is estimated for 2005 to 2011.*
2) *Takings from Lake Simcoe and Wildlife/Conservation permits were not included.*

Table 6.6: Summary of unserviced domestic and non-permitted agricultural consumption.

Subwatershed	Unserviced Domestic Demand (m^3/yr)	Unserviced Domestic Consumption (m^3/yr)	Non-permitted Agricultural Demand (m^3/yr)	Non-permitted Agricultural Consumption (m^3/yr)
Ramara Creeks	410,477	82,095	17,948	14,358
Whites Creek	146,119	29,224	39,950	31,960
Talbot River	33,626	6,725	23,259	18,607
Total	**590,222**	**118,044**	**81,157**	**64,926**

Notes:

1) *Unserviced Domestic Consumption per year based on consumptive use factor of 0.2 for domestic use.*
2) *Non-permitted agricultural consumption per year based on consumptive use factor of 0.8 for agricultural use.*

Table 6.7: Summary of operational limits and historical average pumping rates for permitted quarry takings.

Permit Holder	MOE Permit Number	Well Name	Purpose	Maximum Permitted Taking (m^3/d)	Average Demand (m^3/d)
Five W Farms Inc.	3274-62UJCV	Quarry Sump	Quarry Dewatering	12,528.0	537.2
James Dick South	6536-7QJH9L	Sump Pond	Quarry Dewatering	2,880.0	500.3
Lafarge Kirkfield Quarry [1]	1346-7ELPP2	Quarry Sump (Kirkfield Quarry)	Quarry Dewatering	4,320.0	0.0
Lafarge Brechin Quarry	2446-98JKGW (4100-8T2R5R)	Quarry Sump (Brechin Quarry)	Quarry Dewatering	3,600.0	982.1
Bot Aggregates Ltd.	7614-8C6N8N	Quarry Sump	Quarry Dewatering	1,226.9	18.0
Ferma Aggregates Inc.	3745-648QTH	Quarry Sump A	Quarry Dewatering	1,569.6	7.7
Holcim (Canada) Inc.	1573-7RYPR7	Carden Quarry Sump	Quarry Dewatering	5,237.3	1,877.1
		Carden Quarry Clear Pond 2	Industrial	1,310.4	163.2
McCarthy Quarry	5716-7L6KBF	Quarry Sump (McCarthy Quarry)	Quarry Dewatering	6,544.8	0.0
R.W. Tomlinson Ltd.	4340-86NRP9 (7251-7ZGPEF)	North Quarry Sump	Quarry Dewatering	18,230.4*	25.5
		South Quarry Sump	Quarry Dewatering	10,281.6*	0.0
K.J. Beamish Construction Ltd. [2]	6758-883KVV	Sump Pond	Quarry Dewatering	5,011.0	0.0
		West Pond	Industrial	50.0	0.0
Miller Paving Ltd.	2426-86HQ55	Sump Pond	Quarry Dewatering	6,500.0	2,783.1
			Industrial	2,400.0	1,099.3

Notes:

1) *Sump discharge is historically re-infiltrated in on-site settling ponds. No net discharge off-site is reported (Gartner Lee Ltd., 2003).*
2) *No extraction or dewatering pumping currently underway at K.J. Beamish Construction Ltd.*
3) *Average demand is estimated for 2005 to 2011.*

Table 6.8: Estimated future demand for Val Harbour and Bayshore Village.

Settlement	Current Serviced Population	Future Growth	Future Serviced Population	Current Demand (m^3/d)	Future Demand (m^3/d)
Val Harbour	148	54 (36.5%)	202	35.0	47.8
Bayshore Village	749	276 (36.8%)	1,025	265.5	363.2
Total	**897**	**330 (36.8%)**	**1,227**	**302.9**	**414.3**

Notes:

1) *Total future growth estimate based on 10% of 2031 predicted growth estimate (3,300 people) assumed to be serviced entirely by Val Harbour and Bayshore Village.*
2) *Growth distributed between Bayshore Village and Val Harbour proportional to current populations.*
3) *Future demand assumed to increase proportionately to growth in serviced population (i.e., a population increase of 36.5% results in an estimated increase in demand of 36.5%).*

Table 6.9: Current and future demand for municipal wellfields.

Settlement	Well	Current Demand (m^3/d)		Future Demand (m^3/d)	
Val Harbour (Ramara Creeks)	Well 1	35.0	11.0	47.8	15.0
	Well 2		24.0		32.8
	Well 3R		0.0		0.0
Bayshore Village (Ramara Creeks)	Well No. 3	265.5	43.8	363.2	59.9
	Well No. 4		162.2		221.9
	Well No. 5		59.5		81.4
Western Trent/Palmina (Talbot River)	Well #1 (Palmina)	72.5	36.5	79.8	40.2
	Well #1 (Western Trent)		36.0		39.6

Notes:

1) *Future demand for Western Trent/Palmina well field conservatively assumed to reflect a 10% increase from current demand.*

Table 6.10: Estimated quarry extraction areas and floor elevations after 20-year build-out.

Quarry	Current Extraction Area (ha)	Licensed Annual Tonnage (tonnes/yr)	Current Floor Elevation (masl)	Final Extraction Area (ha)	Lowest Final Floor Elevation (masl)	Un-disturbed Area (ha)	Average Un-disturbed Ground Elevation (masl)[3]	Annual Lowering over Un-disturbed Areas (m)	20-Year Floor Elevation (masl)
Bot Aggregates Ltd.	2.5	1,500,000	249	194.0	248	190.0	257	0.32	249 - 251
Beamish Construction Ltd.	<1	1,500,000	244	75.0	206	75.0	250	0.80	234
Holcim (Canada) Inc.	40	1,814,000	211	197.0	187	156.6	247	0.46	211 - 238
James Dick South	11	870,000	212	82.0	210	71.0	237	0.49	212 - 227
Lafarge Brechin Quarry	43	2,800,000	198	251.0	181	208.0	231	0.54	198 - 220
McCarthy Quarry	0	500,000	250	29.5	234	29.5	249	0.68	235
Miller Paving Ltd.	47	2,721,000	224	226.0	215	179.0	245	0.61	224 - 233
Tomlinson Brechin Quarry	<1	2,700,000	238	131.0	222	131.0	249	0.82	233
Ferma Aggregates Inc.	6	1,000,000	260	186.0	230	180.0	270	0.22	260 - 266
Lafarge Kirkfield Quarry	21	453,000	234	22.1	211	1.1	259	0.82	218
Five W Farms Inc.	16	500,000	262	134.0	240	118.0	275	0.17	262 - 272

Notes:

1) *Table of reproduced from Golder Associates Ltd. (2012).*
2) *Assumed rock density of 2,500 kg/m^3.*
3) *Approximate average ground surface elevation outside of current extraction area based on DEM.*

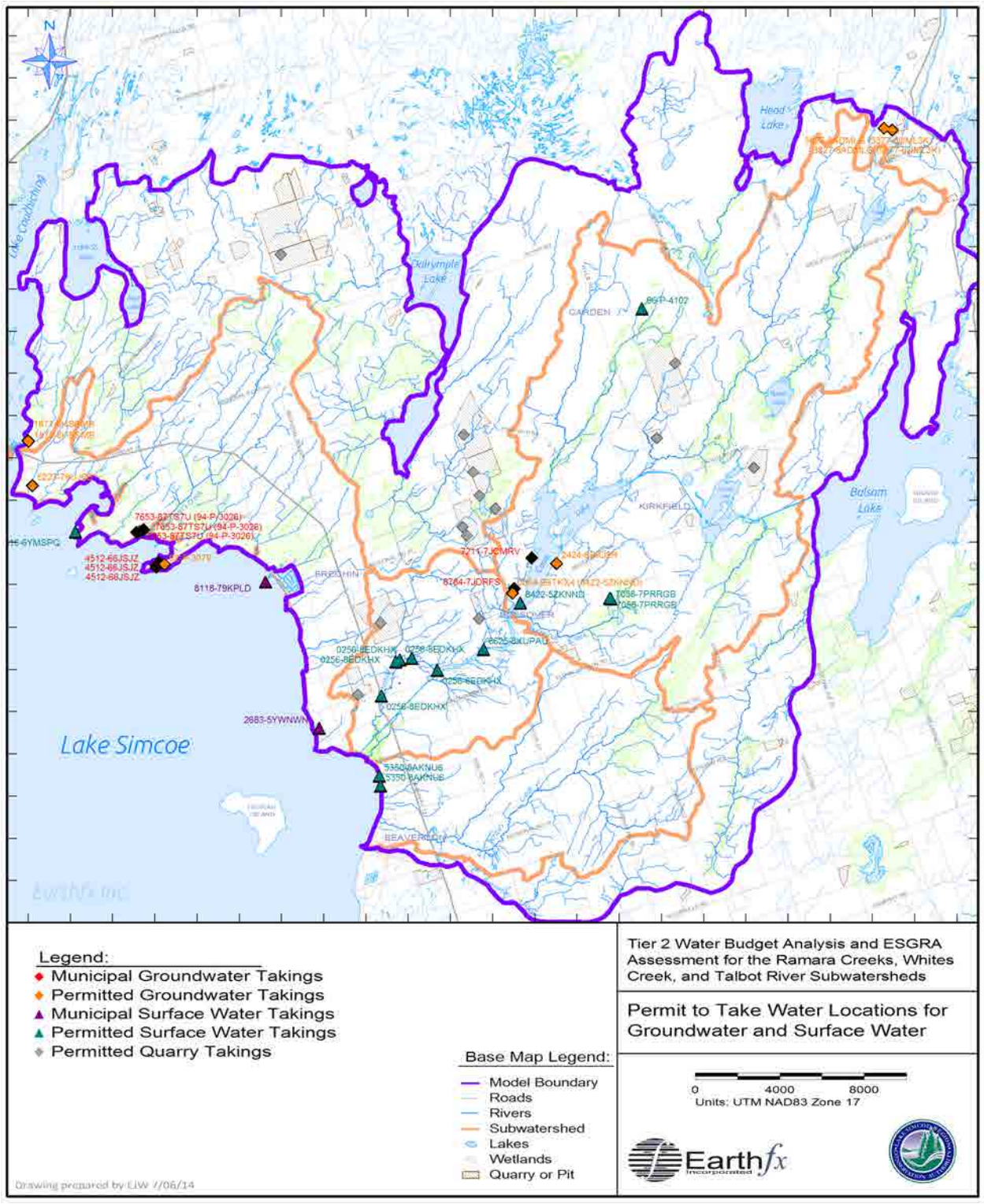

Figure 6.1: Permit to Take Water locations for groundwater and surface water takings.

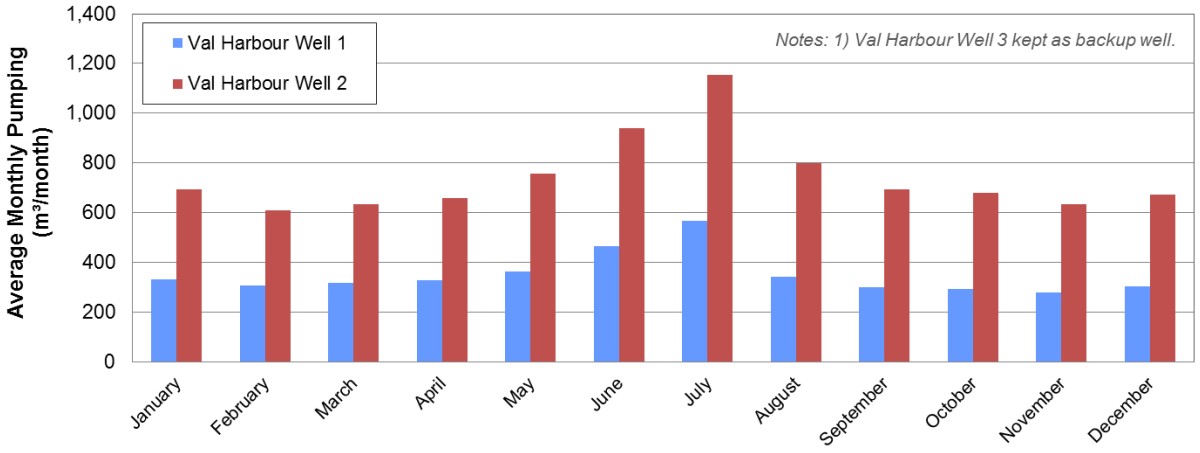

Figure 6.2: Average total monthly pumping for Val Harbour Wells.

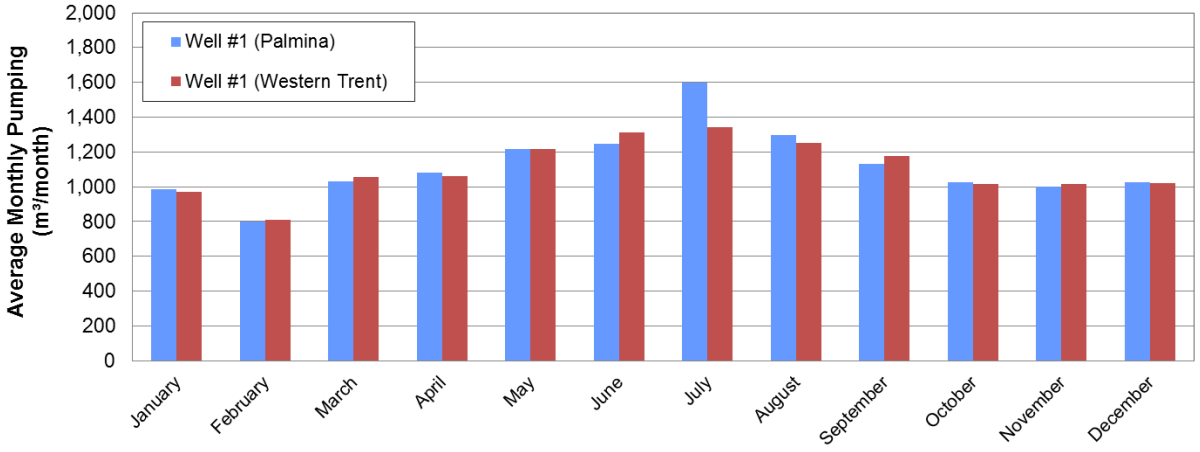

Figure 6.3: Average total monthly pumping for Western Trent/Palmina Wells.

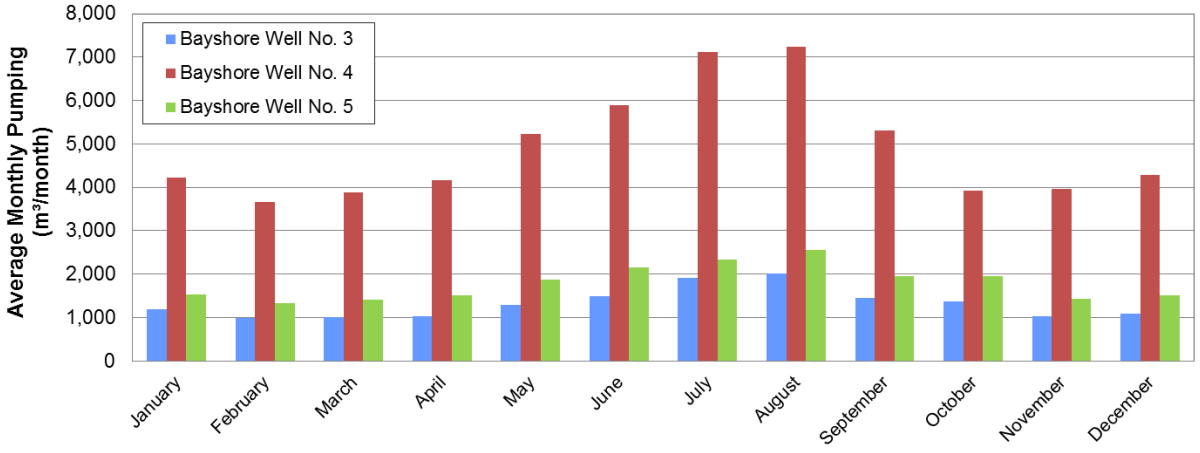

Figure 6.4: Average total monthly pumping for Bayshore Wells.

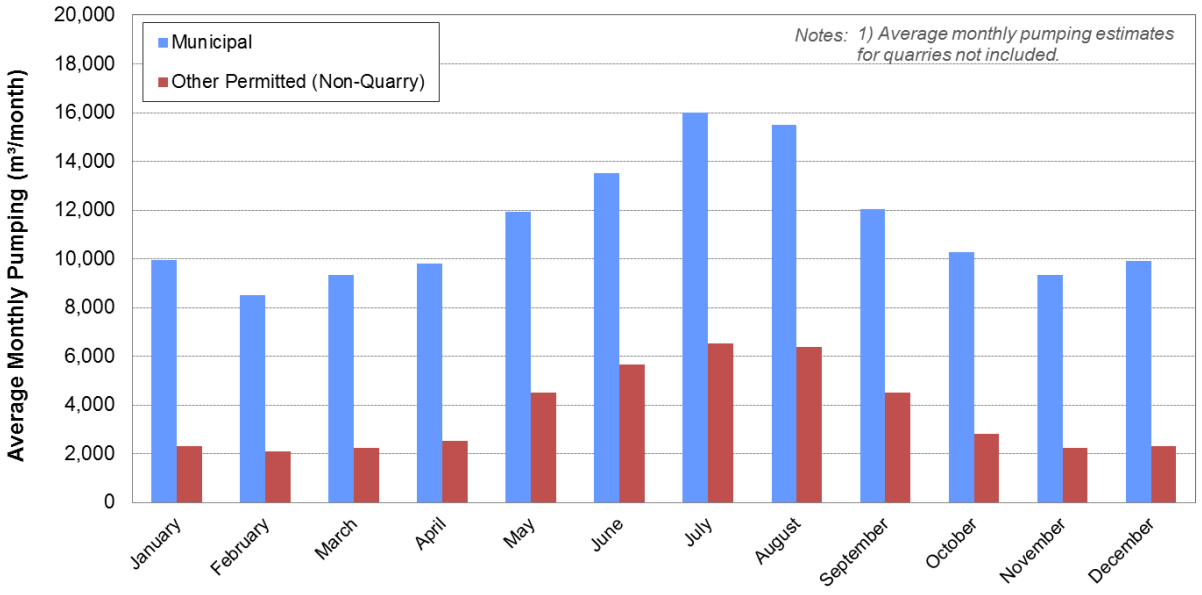

Figure 6.5: Average total monthly municipal and other permitted (non-quarry) pumping.

7 GSFLOW Model Development Overview

7.1 Introduction

A key objective of this Tier 2 Water Budget Assessment was to construct an integrated surface water and groundwater model of the study area, and then apply that model to assess future water use, land use change, drought scenarios, climate change, and ecologically significant recharge areas. An integrated, fully distributed, model (schematically shown in Figure 7.1) was also applied to address the surface water and groundwater issues identified in Section 2.1.

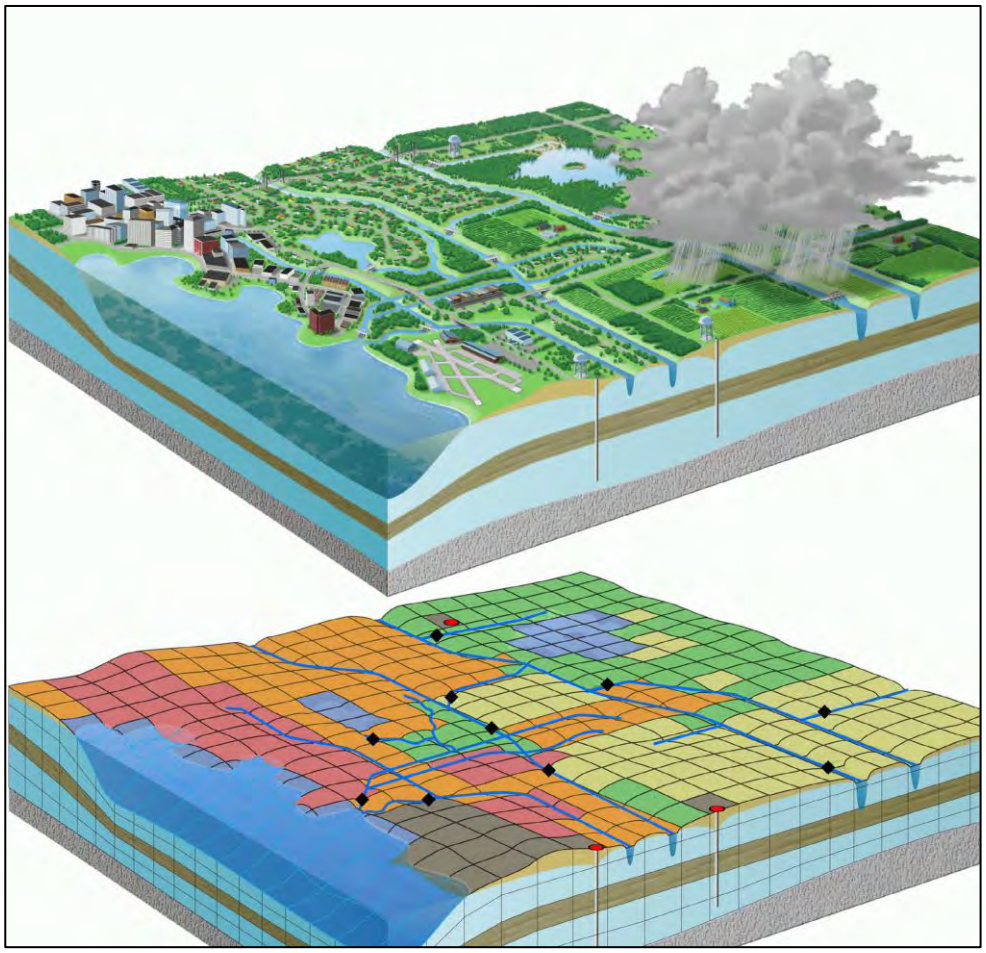

Figure 7.1: The physical system (upper image), and a numerical model representation in a fully distributed, cell-based, integrated model (lower image).

7.2 USGS GSFLOW

The model selected for this study is the U.S. Geological Survey (USGS) GSFLOW code (Markstrom *et al.*, 2008). GSFLOW is a mature, well-tested model code and has been utilized to investigate surface water-groundwater interactions in a number of recent peer-reviewed studies (Huntington and Niswonger, 2012; Hunt et al., 2013; Woolfenden and Nishikawa, 2014; Tanvir Hassan et al., 2014; Niswonger et al., 2014). GSFLOW is a fully integrated model developed from three widely-

recognized USGS sub-models: the Precipitation Runoff Modelling System (Leavesly *et al.*, 1986), the modular groundwater flow model MODFLOW-NWT (Niswonger *et al.*, 2011) and the USGS SFR2 and LAK Surface Water modules (Niswonger and Prudic, 2005 and Merritt and Konikow, 2000). The process regions and sub-models are listed below:

Table 7.1: GSFLOW regions and sub-models.

Region	Process Component	GSFLOW Sub-model
1	Hydrology	PRMS sub-model
2	Streamflow, lakes and wetlands	SFR2 and LAK modules for MODFLOW
3	Groundwater flow	MODFLOW-NWT groundwater sub-model

The USGS refers to the sub-model domains as process "regions". The regions include hydrology, hydraulics and groundwater, and are shown schematically in Figure 7.2. A flowchart showing the interaction between the regions is provided in Figure 7.3. The sub-models for each region include numerical representations of the physical system and the processes that occur in each region.

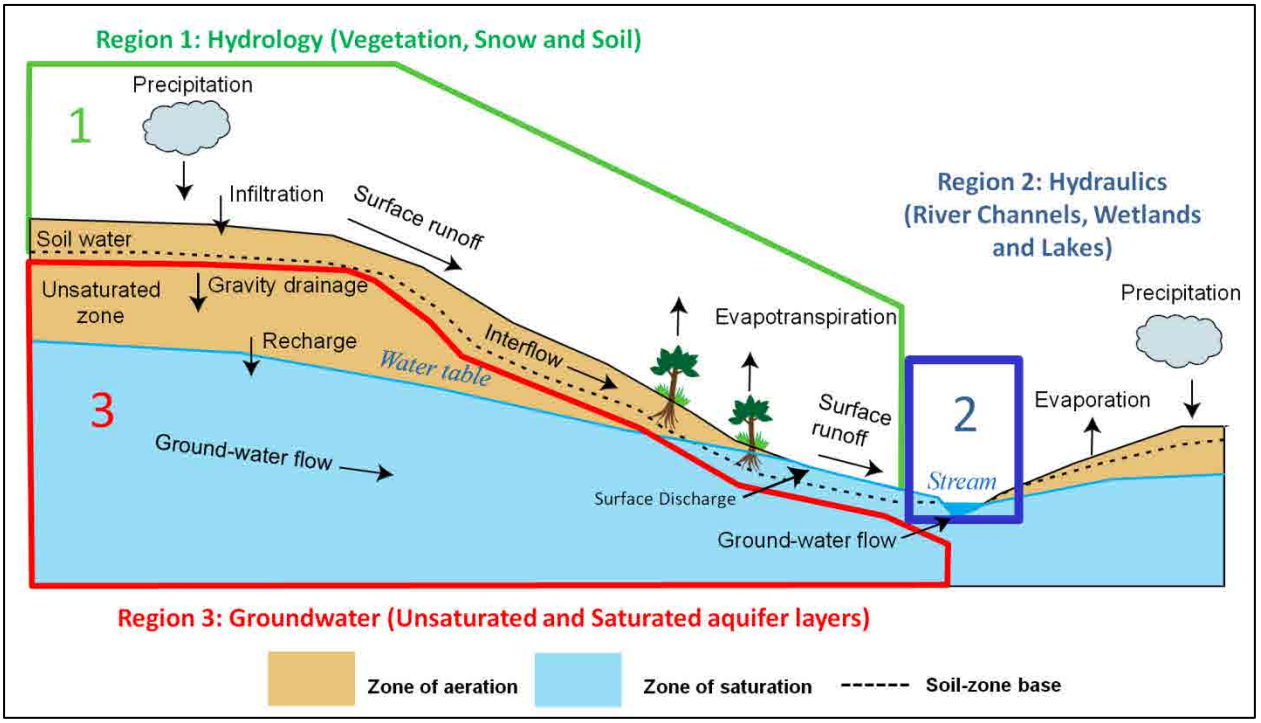

Figure 7.2: Schematic diagram of the GSFLOW process regions.

The first objective of this chapter is to provide a "big picture" overview of the integrated GSFLOW model. This perspective can be difficult to see when discussing the details of each sub-model. The second objective is to introduce the individual sub-models and briefly describe their main processes and interconnections. In the three following chapters, the sub-models are further described, along with a detailed description of how the sub-model was specifically configured for this study. Finally, the integrated GSFLOW model calibration results are presented in Section 11.

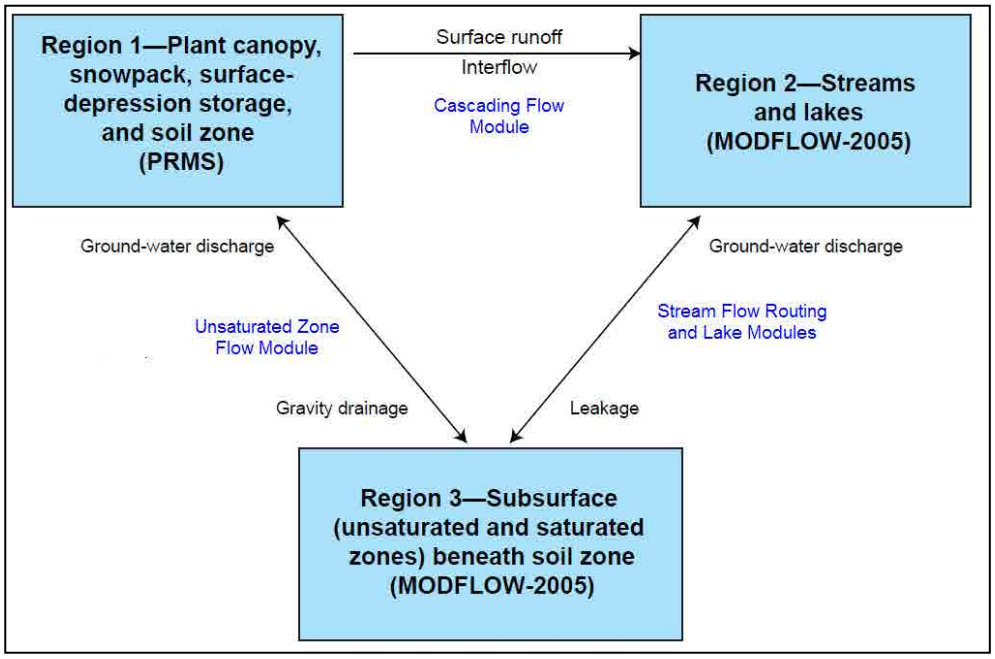

Figure 7.3: GSFLOW process region flowchart.

7.3 GSFLOW Process Integration Overview

Integrated modelling is complex. The following is a simplified description of GSFLOW and the key aspects of its representation of the physical system.

7.3.1 Spatial Discretization

GSFLOW uses a fully-distributed model representation of the physical system (upper image in Figure 7.1). The term “fully distributed” refers to the fact that the study area is subdivided into small cells, each with unique physical and hydrologic properties (lower image in Figure 7.1). During a simulation, each cell receives unique, spatially variable, inputs values (e.g., rainfall, snowmelt and solar radiation), and the model calculates a cell-specific response to those inputs.

The spatial representation in GSFLOW is unique in two ways. First, different grid cell resolutions can be used for the climate, surface hydrology and subsurface groundwater processes (Figure 7.4). This allows the model to be refined in each of the three regions to meet the specific issues associated with those processes and input data. For example, the shallow hydrology region is frequently rich in data, so a fine resolution (10 to 50-m cell size, for example) can be important to represent processes such as focussed recharge in swales, ditches and other anthropogenic modifications to the ground surface. On the other hand, climate inputs, such as NEXRAD radar data, are available on a much coarser resolution (2-km cell size), and therefore a grid resolution optimised for climate inputs is beneficial. Finally, groundwater sources and sinks (e.g., wells) are frequently unevenly distributed, so a variable cell sized grid is often used to represent areas of high stress, for example in the vicinity of wellfields and quarry excavations.

A second useful aspect of GSFLOW is that the hydrology processes represented in Region 1 can be further refined within a single cell (often referred to as a hydrologic response unit or HRU). Each HRU can be partitioned into pervious and impervious areas, with different processes simulated in

each (Figure 7.4, right side). Runoff from the impervious to the pervious areas within an HRU can also occur.

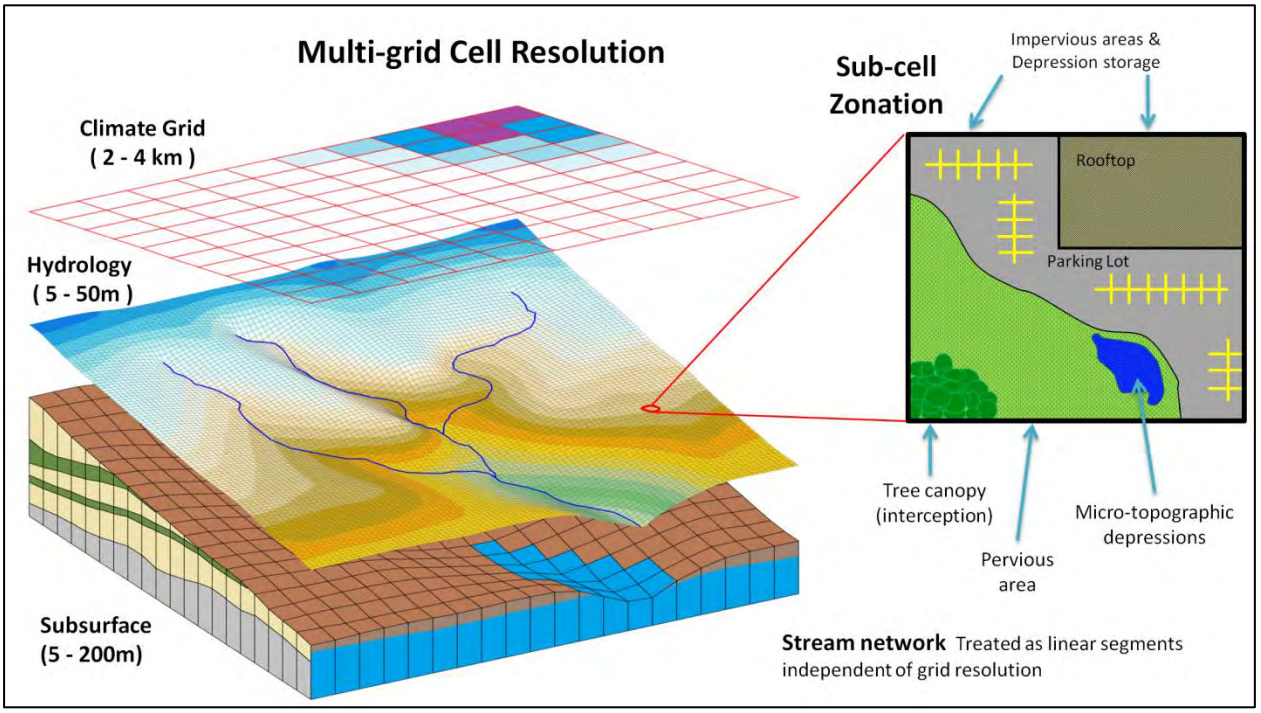

Figure 7.4: GSFLOW grid resolution and sub-cell pervious and impervious zones.

7.3.2 Inter-Region Movement of Water: Overview

A key aspect of an integrated model is the representation of the movement of water between the regions. In very general terms, there are three main processes (shown as arrows between the Regions in Figure 7.3) that control the movement of water between the GSFLOW Regions:

1. **Gravity drainage:** Gravity drainage is the principle process driving groundwater recharge. Gravity drainage occurs when moisture in the soil zone is above field capacity. Feedback can occur if the hydraulic conductivity of the unsaturated zone is low enough that the total volume of soil moisture cannot pass through. In this case, the moisture content of the soil zone will increase to saturation and no further infiltration can occur. Additional rain falling on the area will run off as saturation-excess Dunnian flow. No feedback occurs when the unsaturated zone is permeable and the soil zone is located far enough above the water table.

2. **Groundwater discharge to the soil zone:** Groundwater discharge to the soil zone occurs when the water table rises to intersect the base of the soil zone. Excess soil moisture and rainfall can then discharge as another form of Dunnian runoff. Surface discharge can move through the soil zone as interflow or become surface runoff. Once in Region 1 this water moves downslope via the cascade flow network where it can subsequently discharge to a stream (or re-infiltrate into the groundwater system).

3. **Topography-driven cascading flow:** Cascading overland flow and interflow are a simplified representation of the numerous processes that together enhance the movement of water downslope (e.g., micro-channelization, surface rill formation, sheet flow, preferential pathways) or inhibit flow (e.g., depression storage). Overland runoff is generated by both Hortonian processes (excess infiltration) and Dunnian processes (excess saturation, discussed further below).

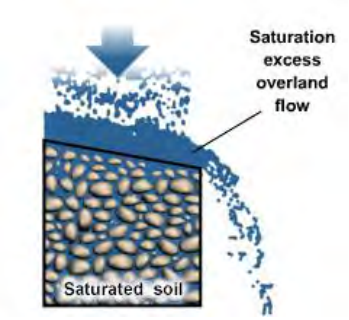

Figure 7.5: Saturation excess or Dunnian rejected recharge process.

4. **Head-dependent discharge or leakage:** Head-dependent leakage or discharge assumes that the rate of water movement between the aquifer system and the stream or lake is proportional to the difference in head (water level elevation) between the two systems, and the permeability of the intervening streambed or lakebed. The exchange of water can occur in either direction as shown in Figure 7.6.

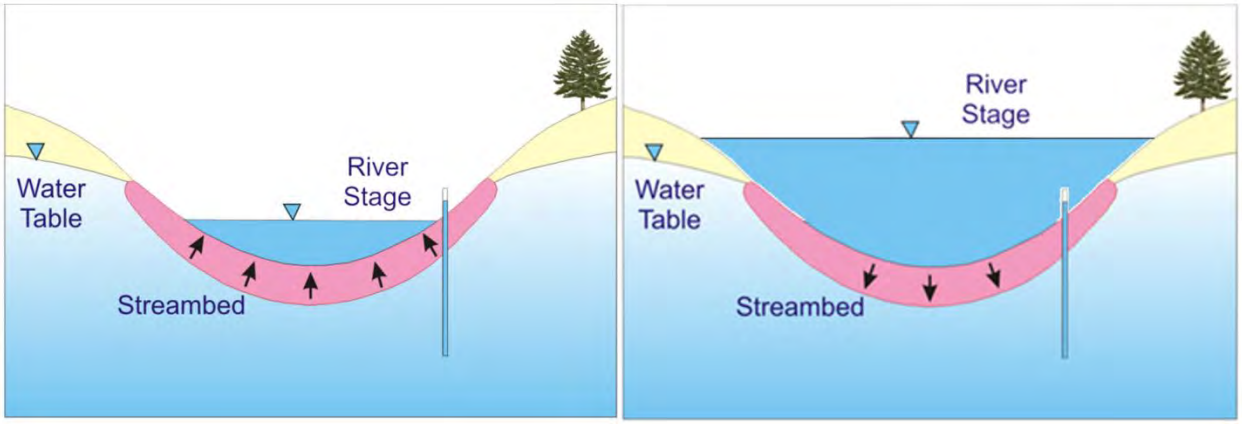

Figure 7.6: Head dependant groundwater discharge (right), leakage (left) to streams.

The portion of the model area where feedback from the groundwater system occurs can change with seasonal or other fluctuations in the water table. The portion of the watershed where this occurs has been referred to as the “contributing area” (Dickinson and Whiteley, 1970), and it can change significantly on a seasonal basis. A schematic showing the change in the contributing area between spring and summer is shown in Figure 7.7.

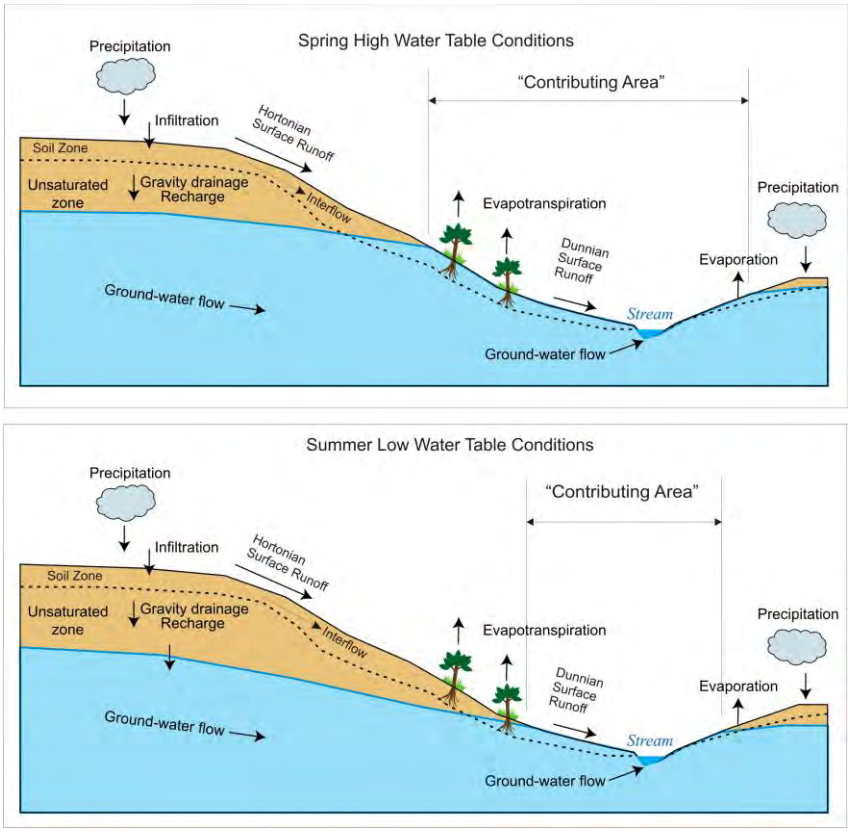

Figure 7.7: Changes in the spring and summer "Contributing Area".

Rainfall and snowmelt events generate more runoff during the spring because the “contributing area” is larger and saturation excess (Dunnian runoff) is more prevalent. Frozen soils can also contribute to saturation excess runoff. Larger event volumes are generated during this period.

7.3.3 Temporal Discretization and Sub-model Coupling

During an integrated GSFLOW simulation, each sub-model receives a set of input stresses (rainfall, change in pumping, etc.) and then computes a system response to those stresses in each cell. The result of those computations (i.e., a new groundwater recharge rate, increased seepage to a stream reach, or an updated water table position) is then passed as input to the other sub-models. Overall, the sub-models are “synchronized” on a daily time step. In addition, the flux of water between Region 2 (streams and lakes) and Region 3 (groundwater) is determined in an iterative manner within a single time step.

7.4 Approach to GSFLOW Model Development

A multi-stage model development and calibration approach was followed in which:

- a preliminary “PRMS-only" surface water model was developed and “pre-calibrated” to observed streamflow. The pre-calibration recognized that, without groundwater feedback, soil zone drainage properties may be selected with a bias towards generating Hortonian runoff rather than Dunnian processes.

- an interim "MODFLOW-only" steady state groundwater model was developed as a means of testing aquifer property estimates and matching regional groundwater flow patterns; and
- a stream routing and reservoir model was developed to represent streamflow routing, quarry discharge, surface water takings, and TSW operations; and,
- finally, an integrated calibration was done with two sub-models coupled in GSFLOW in which parameter values for both MODFLOW and the PRMS sub-models were adjusted.

This stepwise process was needed because of the complexity of the surface water and groundwater systems. The sub-model approach simples the testing and calibration of the overall GSFLOW model. Specific model parameters can be isolated and independently calibrated. Ideally, this reduces the effort required to recalibrate the model after the sub-models are integrated together in GSFLOW.

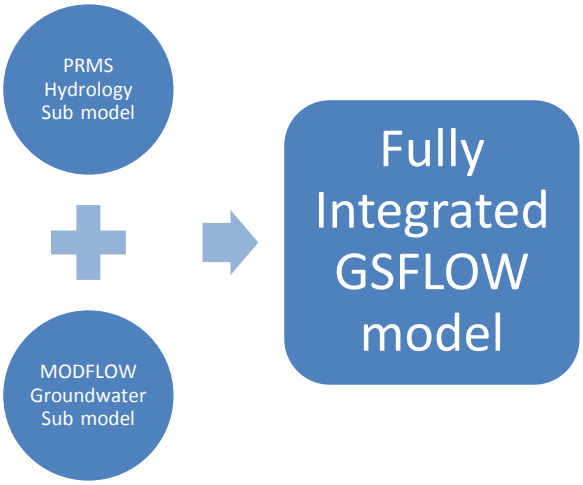

Best practices for groundwater modelling and professional judgment were followed when applying and calibrating the numerical models as outlined in the ASTM (2000) standards for groundwater flow modelling.

8 Hydraulic Sub-model Development and Calibration

8.1 Introduction

This section describes the methods employed to represent the surface water features (i.e., streams and lakes) in the GSFLOW model. A brief description is presented of each process simulated along with a discussion of related Input datasets and model parameters.

8.2 Surface Water Network Routing

The GSFLOW model uses the SFR2 streamflow routing module (Niswonger and Prudic, 2005) to route streamflow. Water bodies (e.g., lakes and ponds) are simulated with a separate module, LAK3 (Merritt and Konikow, 2000). The two modules communicate to route flows into and out of lakes.

It should be noted that in a MODFLOW-only uncoupled simulation, the stream routing module routes only groundwater discharge (baseflow) through the stream network, although an option is available to route rejected recharge and groundwater discharge to the soil zone. This option was selected for the RWT simulations. In a GSFLOW simulation, both groundwater discharge and overland runoff (Hortonian and Dunnian) are routed through the stream network, significantly improving the representation of changing stream stage and head-dependent discharge between the stream network and groundwater system during and after precipitation events.

8.2.1.1 Channel Network

Rivers are represented as network of linear channel reaches that are intersected with the model grid and connected to groundwater cells through a streambed layer that exists under each reach. The full length of the stream within the cell is represented and the interaction between the stream and aquifer is based on the reach length, width and groundwater elevation in the cell. Lakes are represented as special cells within one or more model layers, and are similarly connected to the groundwater system through a lakebed layer.

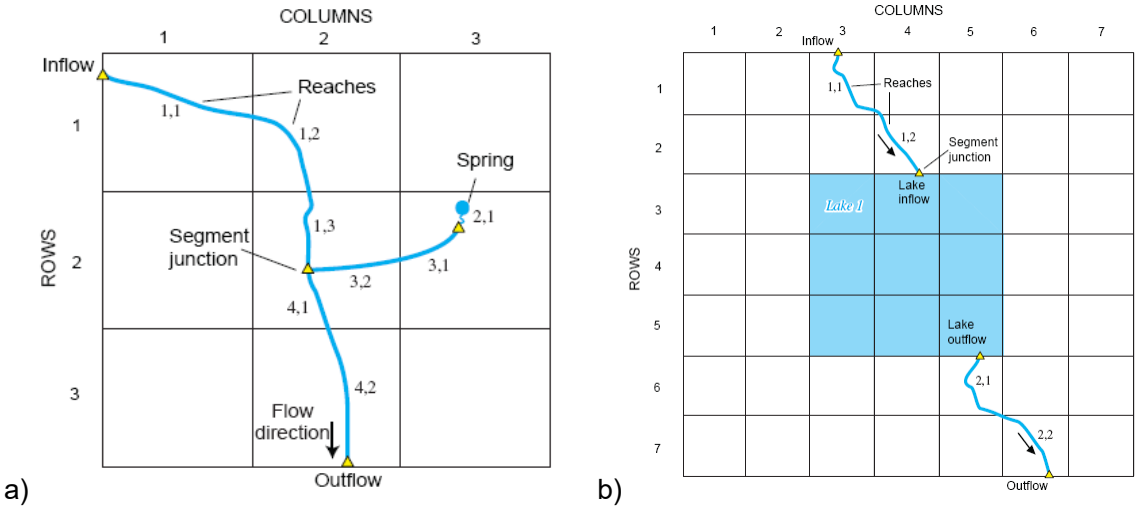

Figure 8.1: (a) Stream network representation in the SFR2 module, and (b) lake representation in LAK3 module.

8.2.1.2 Stream Reach Inflows and Outflows

Inputs into the streams include inflow from upstream reaches, discharge from lakes, direct precipitation, overland runoff (as computed by the PRMS sub-model), and leakage into the stream segment from the underlying aquifer (Figure 8.2). Outputs include evaporation, losses to groundwater, and net outflow. Leakage between the stream and aquifer is calculated using a head dependent Darcy's Law representation that is proportional to the difference between the stream stage and aquifer head (see Figure 7.6 and Section 10.6.2).

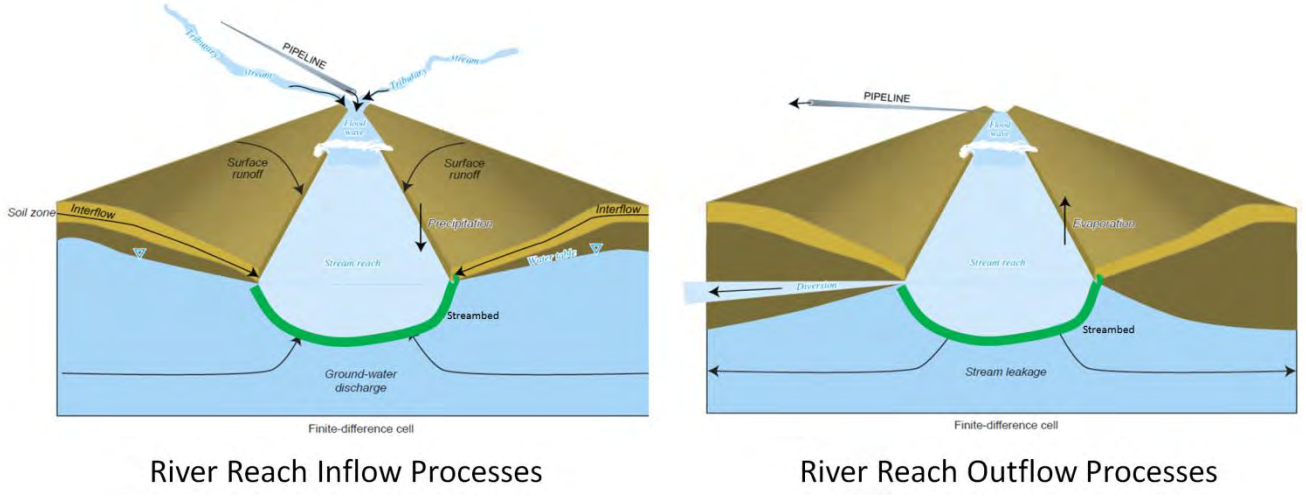

Figure 8.2: Streambed layer (shown in green), and river inflows and outflow processes in a full GSFLOW simulation.

8.2.1.3 Depth of Flow (Stream Stage) Calculations

The SFR2 module uses conservation of mass and stage/discharge relationships to determine daily average flows, depth-of-flow, and stage in each stream reach.

The depth-of-flow calculation is a key aspect of the GSFLOW simulation because it is critical to the calculation of head-dependent stream leakage to and from the aquifer system (Figure 7.6). There are four options available in GSFLOW to represent the channel cross section (rectangular or non-prismatic) and compute depth-of-flow in each reach. Each stream reach can use any one of the four different depth-of-flow options.

Depth-of-flow Options 1 and 2 use the general form of Manning's equation to relate streamflow as a function of depth for all reaches in a stream segment. For Option 1, a wide rectangular channel is assumed resulting in a simplified Manning's equation. Wetted perimeter is equal to the stream width plus twice the depth-of-flow.

For Option 2, the channel reach cross section is divided into three parts using eight paired horizontal and vertical locations (Figure 8.3). The eight point section is used to compute stream depth, top width, and wetted perimeter. Stream depth, width, and wetted perimeter also are dependent on the slope of the streambed, and the two roughness coefficients—one for the center part of the cross section and another for the two outer parts that represent the overbank. Option 2 was used for the majority of streams in the RWT Tier 2 model, as described below.

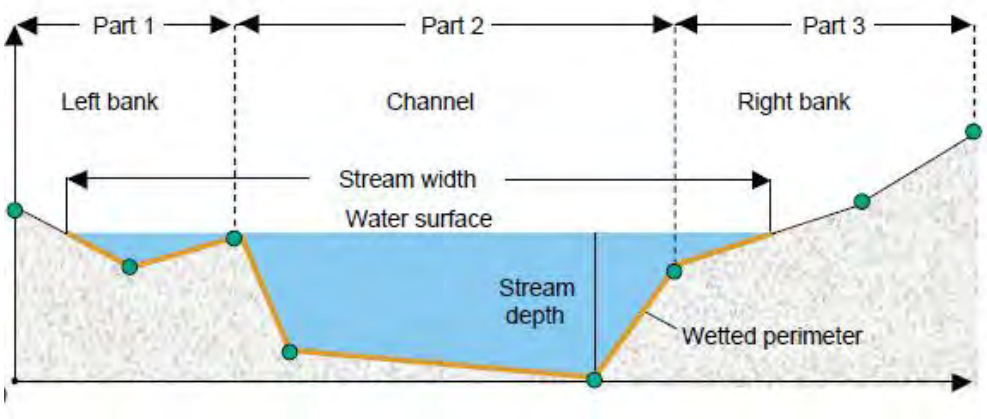

Figure 8.3: Stream channel cross section for DOF Option 2.

Option 3 uses a power-law equation that relates stream depth and width to streamflow. This option assumes that the wetted perimeter is equal to the stream width. Earth*fx* added a modified version of Option 3 (Options 5, 6, and 7) to calculate stream depth and width for simple structures including a rectangular orifice, simple weir, and compound weir.

Finally, Option 4 allows the user to enter a look-up table of stream depth, width, and corresponding streamflow for a stream segment. These values typically are determined from rating curves at streamflow-gaging stations or reservoir or dam outflows locations.

Using any one of these depth-of-flow calculation methods, the computed depth is added to the top of streambed elevation to determine the stream stage in each reach. The stage is used to compute leakage across the streambed (Figure 7.6).

8.2.1.4 Stream Routing Calculations

As noted, SFR2 uses the conservation of mass principle to route streamflow down the dendritic channel network to determine daily average flows in each stream reach. As described in Markstrom *et al.* (2008), outflow from the end of a stream reach is set equal to the sum of all inflows to the reach minus any upstream outflows (in that reach). The depth-of-flow is then calculated and leakage is added (or subtracted from the outflow) and also passed to the groundwater model so that aquifer heads can be updated across the model. The leakage terms, aquifer heads, and routing calculations are all nonlinear because flow in the reach is dependent on upstream inflows and leakage rates, which are in turn dependent on aquifer heads. Therefore, the flow routing and groundwater flow equation are solved iteratively until the calculated stream stage and heads in all aquifers converge to a specified tolerance. This computationally intensive calculation is a key element of the design of GSFLOW as it involves multiple groundwater and surface water system iterations within each time step. This iterative solution is performed to determine the average groundwater and surface water flows and levels for each time step.

8.2.1.5 Lake and Wetland Representation

The LAK3 module is used to represent ponds, lakes and open water portions of the wetlands in GSFLOW (Figure 8.4). The wetland margins, where water can pond on an occasional basis, are represented in the PRMS model.

Lakes are represented as occupying cells in one or more layers of the groundwater model as shown in Figure 8.1b. Lakes can penetrate one or more aquifer layers (Figure 8.4) and interaction (i.e., head-dependent leakage into or out of the aquifer) can occur between the lake cells and adjacent and/or underlying cells. The lake can grow in size or shrink (i.e., inundate more cells) based on lake stage and pre-defined stage-storage and stage-area relationships.

Inputs into the lakes include inflow from one or more upstream reaches, direct precipitation, overland runoff, interflow, and leakage into the lake from one or more aquifer layers (Figure 8.4). Outputs include evaporation, losses to groundwater, water takings, and outflow to one or more downstream reaches. The LAK3 module computes a separate continuous water balance for each lake or pond based on computed inflows and outflows. Stage-storage and stage-area relationships are used to update the lake depth, stage, and wetted area. The stage is passed back to SFR2 to update the stage-dependent outflows and to the groundwater model to update the heads. The interactions are strongly non-linear and the lake water balance and groundwater flow equation are solved iteratively until the calculated lake stage and heads in all aquifers converge to a specified tolerance.

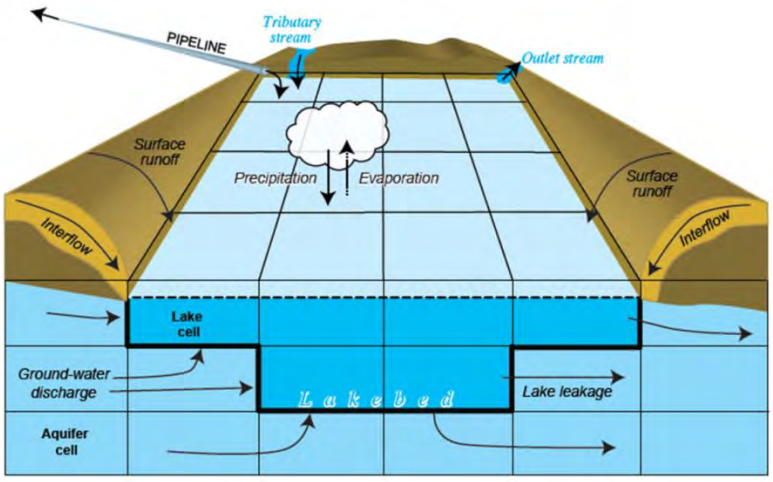

Figure 8.4: GSFLOW representation groundwater interaction with lakes, reservoirs and wetlands.

8.2.2 Surface Water Routing: Summary

A number of advantages of the GSFLOW representation of groundwater/surface water interaction include:

- both groundwater and surface water volumes are routed through the network on a continuous basis;
- the spatial distribution of gains and losses in streamflow due to the interaction with the groundwater system is well represented (specifically, the non-linear effects of stage and head change on groundwater inflows and outflows to the stream);
- the full drying and rewetting of headwater channels as the water-table rises or falls is represented (seasonal springs and seepage are represented);
- stage and storage in surface water bodies (lakes, wetlands, and reservoirs) and their connectivity to the aquifer system is fully simulated.

GSFLOW provides full three-dimensional routing of water through both the groundwater and surface water systems within a watershed. Storage in lakes, wetlands, reservoirs and the aquifer system is well represented. Non-linear head-dependent interactions between the groundwater and surface

water system are fully simulated. Detailed stream network, channel geometry and control structure operations are represented. Overall, these capabilities make the model ideal for assessing baseflow, drought, seasonal storage, climate change impacts, and other water budget issues.

8.3 SFR2 Stream Representation

To apply SFR2 to the RWT study area, a dendritic stream network was first created by defining stream "segments" and junctions at the confluence of two or more tributary segments as in the sketch below. Segments are numbered from upstream to lowest downstream and in such a way that all upstream flows are calculated when two sub-networks join at a junction (for example, Segment 1 in the sketch on the left joins Segment 3 at a junction and the confluent flow moves downstream to Segment 4). Stream reaches are defined as the portion of a stream segment within a model cell. These are also numbered in downstream order.

VIEWLOG (Kassenaar, 2013) was used to construct the stream network topology (i.e., assigning reach and segment numbers, defining junctions, and assigning segment-based properties) and overlay the stream network on the groundwater model grid to determine the reach length and slope. Maps of the existing streams were obtained from the MNR stream coverage (MNR, 2010). The version of the MNR OHNWCRS geospatial database employed for this study dates to September 2010. All the streams represented in this dataset were represented in the model (i.e., all first-order and higher streams). The actual coverage itself is an amalgamation of data from dozens of sources spanning over 100 years. Detailed documentation of the MNR OHNWCRS database is available from Land Information Ontario (LIO).

The study area contained 1,734 stream segments broken into 10,126 stream reaches. Depth of flow in each reach was determined by SRF2 using Manning's equation assuming uniform flow in a non-prismatic section. The method computes stream depth, top width, and wetted perimeter based on the channel geometry provided. A typical eight-point section, which included a main channel and an overbank (Figure 8.3), was assigned to each reach based on the Strahler Class (Class 1 to Class 4) or canal characteristics. The total modelled length of each Strahler Class and the properties assigned are presented in Table 8.1. The hydraulic conductivity of the streambed material was set to $5x10^{-7}$ m/s for all streams, which is in the range of silt to silty-fine alluvial sand. The bed thickness for all of the streams was set to 0.2 m. Stream slope was defined for each reach as interpolated from the study area DEM.

As noted earlier, leakage to or from the aquifer is calculated based on the difference between stream stage and the head in the underlying aquifer. Total flow in each reach is then calculated as the sum of all upstream inflows, precipitation, evaporation, groundwater inflow (or outflow), and overland runoff cascading to the reach. Stage in the reach, which is calculated based on total flow and stream channel properties, is then updated using the latest estimate of total flow. The outflow from the reach is routed to the next downstream segment. Stream segments can terminate in a lake or exit the model area (as shown in the sketch to the right).

Because the rates of leakage in one reach of a stream can affect stage and aquifer heads at other points along the stream, the response to groundwater/surface water interaction can be highly non-linear. Therefore, streamflow routing and the groundwater flow equations are solved in an iterative manner for each time step until convergence is achieved (i.e., changes in simulated flows and heads between successive iterations fall below threshold levels).

8.4 Modelled Lakes and Structures

The lake simulation (LAK3) module was used to represent the major lakes and ponds in the study area. Two channel segments of the Trent-Severn Waterway between Lock 37 and Lock 39 were also represented at lakes. All lakes were contained in the uppermost model layer. The locations of model lakes are shown in Figure 8.10. Lake bed conductance (i.e., hydraulic conductivity divided by lakebed thickness) was assigned to each lake as indicated in Table 8.2.

Discharge from the lake is calculated by the SFR2 package with rates determined by a specified lake stage/discharge relationship. Four lakes in the model are represented with man-made outlet structures (i.e., locks) and the properties of these structures were used to determine the outflow from the lake. The ability to calculate stage-discharge relationships for two additional types of lake outlet structures were added to the SFR2 package for an earlier study (Earth*fx*, 2010). The outlet types included a simple rectangular weir and an orifice (which behaves as a weir when the stage is below the top of the orifice) which can also be used to simulate gates and values. Where control structures exist, such as at the dams along the Trent-Severn waterway, weirs and gates were simulated with these relationships. Governing equations are provided below:

$$Q_{\text{rect.weir}} = 3.2\ W\ H^{3/2} \qquad \text{(Eq. 7)}$$

$$Q_{\text{orifice}} = 0.6\sqrt{2g}\ W\ h\sqrt{(H - h/2)} \qquad \text{(Eq. 8)}$$

where:
- Q = volumetric flow rate in (cfs);
- H = height above the base of the weir or orifice;
- W = width of the weir or orifice;
- G = gravitational acceleration;
- H = height of the orifice;

8.5 Trent Severn Waterway Representation

The TSW is represented in the model as a series of connected lakes, stream segments, and control structures. All canal segments were assumed to have a stream slope of 0.0001 m/m. The structure location and streamflow patterns in the TSW are described below followed by a description of the operating rules as incorporated into the model. Given the integrated nature of this model, and the focus on accurately representing interactions with the groundwater system, preference was given to accurately representing stream stage as opposed to matching the generally unknown discharge in the Talbot River.

8.5.1 Mitchell to Canal Lake

Figure 8.5 provides a schematic representation of the TSW between Mitchell and Canal Lake as simulated in the RWT model. Inflows from Balsam Lake are specified on a monthly basis as derived in Section 4.3.4. For the steady-state model, the annual average diverted inflow was assumed to be 1.74 m^3/s (Figure 4.34). Mitchell Lake and Canal Lake were represented as MODFLOW lakes and were connected by the Upper Talbot River and a segment of the TSW canal. The water level in Mitchell Lake is controlled by the Victoria Rd. Dam (represented as a movable weir; Table 8.3), which drains north into the Talbot River. During the navigable season, a specified flow of 3,000 m^3/d is diverted from Mitchell Lake to fill the canal. It is assuimed that 3,000 m^3/d would be suffient to operate the lock on a daily basis. Flow through the waste weir structure upstream of the Kirkfield Lift Lock to the Upper Talbot River was ignored for this study.

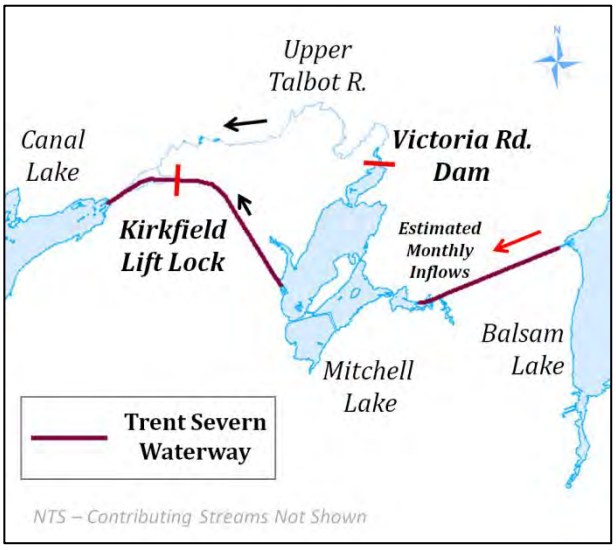

Figure 8.5: Model representation of the TSW between Balsam and Mitchell Lake.

8.5.2 Canal Lake to Lake Simcoe

Figure 8.6 provides a schematic representation of the TSW between Canal Lake and Lake Simcoe as simulated in the RWT model. Given the width of the Talbot River below Canal Lake, the two river segments between Lock #37, Lock #38, and Lock #39 were represented as MODFLOW lakes. Lock #37, Lock #38, and the Talbot River dam were represented as movable weirs within the model and control the stage in Canal Lake and the two Talbot River segments respectively. Model parameters are provided in Table 8.3.

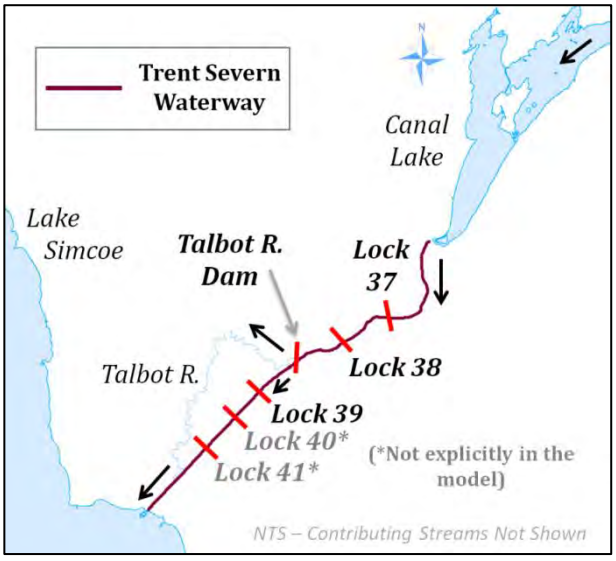

Figure 8.6: Model representation of the TSW between Canal Lake and Lake Simcoe.

A more detailed schematic of the lower reaches of the Talbot River is provided in Figure 8.7. The water level in the lower segment of the Talbot River below Lock #38 is controlled by the Talbot River Dam. A specified flow of 3,000 m^3/d is diverted southwest into the TSW during the operating season to maintain the water levels in the canal. The majority of streamflow moving downstream discharges

over the Talbot River Dam into the remaining natural portion of the Talbot River and, eventually, into Lake Simcoe.

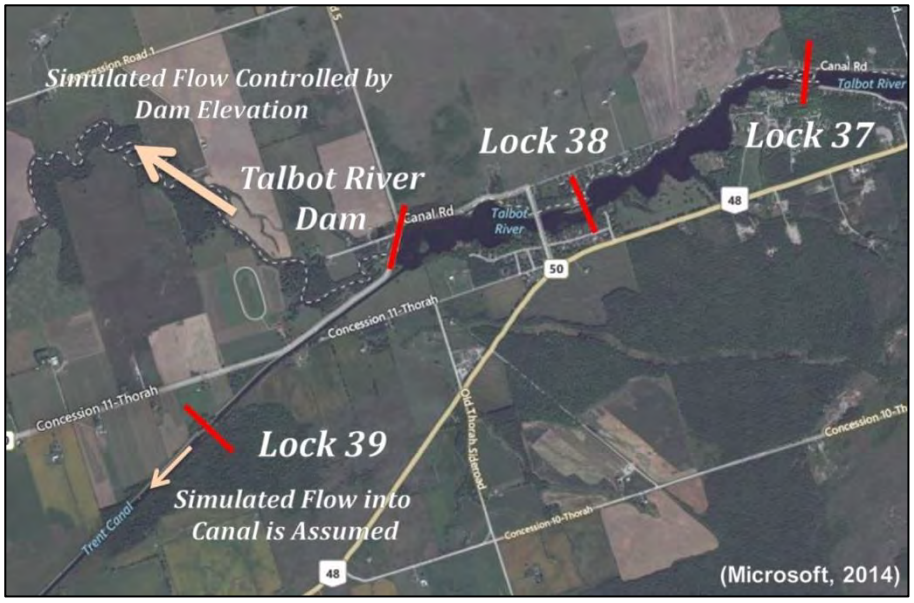

Figure 8.7: Detail of TSW model representation in the Lower Talbot River.

8.5.3 TSW Operating Rules

Given that the operations along the TSW are complex and that no electronic records exist for the daily control settings of the gates, valves, and weirs, a simplified approach was taken. For each day of the simulation, the invert of each simulated dam or weir structure was set to the elevation from the control curve for that day. This allowed the lake stage, which directly influences the groundwater system, to be accurately simulated. Additionally, during the drought and long-term simulations where no historical control information is available, the reservoir follows the general control curve. In the simulation, freshet is captured in the system in spring as the available storage capacity of the lakes is filled. During the summer months, the stage-storage relationship and the weir elevation control the flow out of the lakes. Given that the dam elevations do not change during the summer months, most flow will pass through the lakes on a daily basis; however, some detention will occur during larger events. Downstream flows will increase from mid-September to mid-November as the TSW is drawn down to winter holding levels.

Information on operating procedures and historical lake stage was requested from Parks Canada but was not received before completion of this project. Instead, operating rules for the four control structures (Table 8.3) were inferred from the safe navigation ranges (Table 4.1) and 25-year average Canal and Balsam Lake stage plots provided on the Parks Canada website (http://www.pc.gc.ca/lhn-nhs/on/trentsevern/visit/ne-wl/trent_e.asp). A typical operating curve is shown in Figure 8.8.

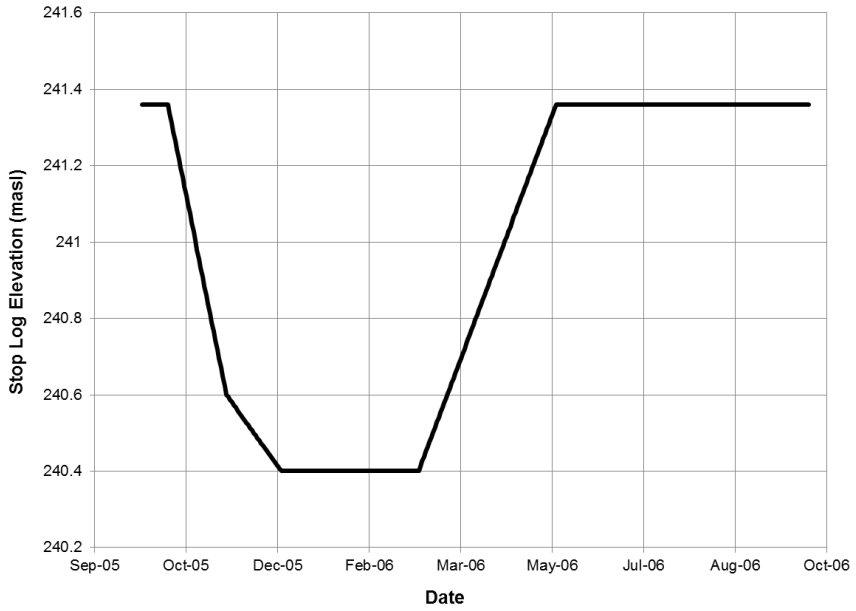

Figure 8.8: Typical annual operating curve (Lock #37) as inferred from published average water levels.

8.6 Quarry Representation

The 11 quarries and aggregate extraction operations, discussed in Section 6.8, were represented in the numerical model. The permits related to quarry water management represent combined surface water and groundwater takings because surface water runoff and groundwater leakage are both collected and stored in sumps in the quarry floors.

The management of water in the quarries is complex and varies in response to the operational needs of the quarries and on-site hydrologic conditions. The intention of the model representation is for discharge out of the quarries to be passively simulated. The outflows respond to precipitation, runoff into the quarries, and groundwater seepage. The operation of the quarries varies from year-to-year based on environmental conditions. The model approach is intended to capture change in onsite stage and discharge based on these conditions.

To simulate the active area of excavation for each of the quarries, a combination of MNR air photos and (where available) site schematics from annual quarry reports were reviewed. Using this information, a quarry cut area was projected onto the model grid, along with associated bench elevations for each model cell representing an area of active quarry excavation to create a “quarry bench mask” (Figure 8.9). A “quarry bench mask” was created for both the current conditions and the 20-year build-out. The “quarry bench masks” were then cut into the regional geologic model during the construction of the GSFLOW model layers.

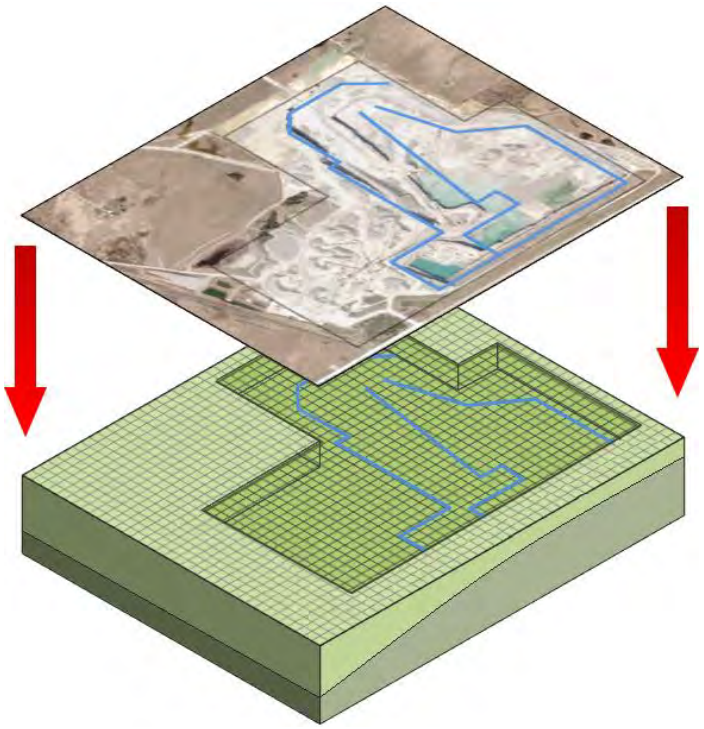

Figure 8.9: Schematic of quarry representation in the numerical model.

A network of ditches was added to the stream network to drain the quarry floors and route groundwater seepage and runoff to the offsite discharge point, as specified by the Sewage Works Certificate of Approval for each site. Unlike the natural streams which were situated in the top layer of the model, quarry ditches were assigned to model Layer 2. By adjusting the bottom elevation of the ditches (thalweg elevations), hydraulic gradients between groundwater in the quarry sides and the ditches could be increased, improving the ability to dewater the surrounding bedrock.

Three quarries were identified as having no reported offsite discharges under current conditions (McCarthy Quarry, Beamish Quarry, and Lafarge Kirkfield Quarry). The McCarthy Quarry and Beamish Quarry are in the early stages of site development and aggregate extraction below the water table has not yet started. Because overburden clearing and, in the case of Beamish quarry, some drainage infrastructure has been completed; these quarries are represented by minimal ditching in the MODFLOW model and little to no revision of the DEM used to represent the top of model Layer 1. The Kirkfield Quarry has been allowed to flood with water since dewatering was discontinued, and no quarry drains were added for this quarry under current conditions. For the simulation of future conditions, MODFLOW ditches and adjustment of the model geometry using quarry bench masks was carried out based on the projected 20-year build-out of the quarries (introduced in Section 6.9). Reported takings and sump discharge rates were used as calibration targets for fine-tuning the quarry representation in the model. .

8.7 Tables and Figures

Table 8.1: SFR Section Properties.

Type	Class 1	Class 2	Class 3	Class 4	Canal	Quarry Ditch
Model Length (km)	716.2	308.4	184.8	68.3	13.5	15.9
n, Bank[3]	0.045	0.045	0.045	0.045	0.020	0.020
n, Channel[3]	0.035	0.035	0.035	0.035	0.020	0.020
Incision (m)[4]	0.7	0.8	1.0	1.2	1.3	3
Eight-Point Channel Cross-Section: Horizontal Points (m from left bank[2])						
X1	0.0	0.0	0.0	0.0	0.0	0.0
X2	20.0	30.0	40.0	50.0	30.0	20.0
X3	27.0	37.0	46.0	55.0	64.0	28.0
X4	27.5	38.0	48.0	59.0	69.0	28.0
X5	28.1	39.5	51.0	61.0	84.0	32.0
X6	28.5	40.0	53.0	65.0	89.0	33.0
X7	41.0	52.0	64.0	76.0	120.0	41.0
X8	61.0	82.0	104.0	126.0	150.0	61.0
Eight-Point Channel Cross-Section: Vertical Points (m above thalweg)						
Z1	2.0	2.5	2.5	3.0	3.5	4.0
Z2	0.8	1.0	1.3	1.5	2.0	3.1
Z3	0.7	0.8	1.2	1.3	1.5	3.0
Z4	0.0	0.0	0.0	0.0	0.0	0.1
Z5	0.3	0.3	0.3	0.3	0.3	0.3
Z6	0.7	0.8	1.2	1.3	1.5	3.0
Z7	0.9	1.0	1.3	1.5	2.0	3.4
Z8	2.0	2.5	2.5	3.0	3.5	4.0

Notes:

[1] Horizontal cross-section distances relative to the left bank (when looking downstream).

[2] n = Manning's coefficient of roughness (unitless).

[3] Incision is the assigned depth of the thalweg (of the 8 point cross-section) below the top of the model cell.

Table 8.2: Properties used to represent study area lakes and ponds.

Feature	Lake Number	Lake Bed Hydraulic Conductivity (m/s)	Lake Depth (m)	Lake Bed Thickness (m)
Brush Lake	1	$1x10^{-7}$	2	1
Perch Lake	2	$1x10^{-7}$	2	1
Talbot Lake	3	$1x10^{-7}$	2	1
Johnston Lake	4	$1x10^{-7}$	2	1
Unnamed Lake (Alvar & Victoria Rd)	5	$1x10^{-7}$	2	1
Duck Lake	6	$1x10^{-7}$	2	1
Raven Lake	7	$1x10^{-7}$	2	1
Mitchell Lake	8	$1x10^{-7}$	(bathymetry)	1
Canal Lake	9	$1x10^{-7}$	(bathymetry)	1
Kirkfield Lake	10	$1x10^{-7}$	11	1
Cranberry Lake	11	$1x10^{-7}$	2	1
Kelly Lake	12	$1x10^{-7}$	2	1
Canal Segment	13	$1x10^{-7}$	(bathymetry)	1
Canal Segment	14	$1x10^{-7}$	(bathymetry)	1

Table 8.3: Properties of hydraulic controls at along Trent-Severn Waterway.

Structure	Type	Width (m)	Height (m)	Sill Elevation (masl)
Lock 37	Simple Weir	47.2	Variable	241.36
Lock 38	Simple Weir	33.5	Variable	234.93
Talbot River Dam	Simple Weir	27.4	Variable	230.3
Victoria Rd (Mitchell Lake) Dam	Simple Weir	9.75	Variable	256.2

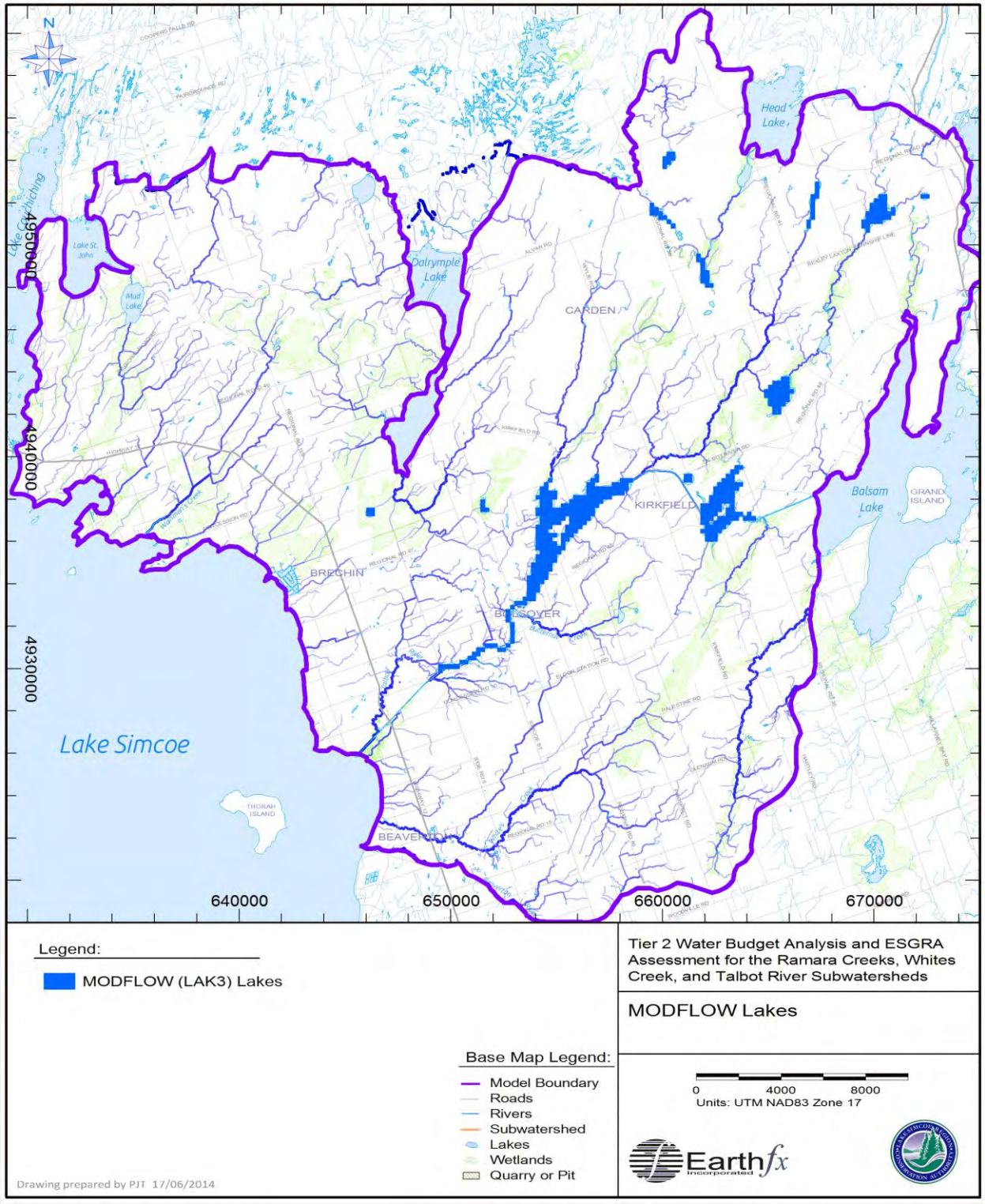

Figure 8.10: MODFLOW lakes.

9 Hydrology Sub-model Development and Pre-Calibration

9.1 Introduction

Surface water and hydrological processes were simulated using the U.S. Geological Survey (USGS) Precipitation-Runoff Modeling System (PRMS) code. The original version of the code is documented in Leavesley *et al.* (1983); a modified version of the code was implemented as a sub-model in GSFLOW (Markstrom *et al.*, 2008). The PRMS sub-model in GSFLOW can run separately or in a fully-integrated manner, which combines the PRMS model with the MODFLOW-NWT groundwater model. The following section describes the construction and initial calibration of the PRMS portion of the GSFLOW model. It should be recognized that during this PRMS sub-model calibration development stage, feedback from the groundwater flow system is assumed to be negligible.

9.2 Model Description

PRMS is an open-source code for calculating all components of the hydrologic cycle at a watershed, subwatershed, or cell-based scale. PRMS is a modular, deterministic, physically-based, fully-distributed model developed to evaluate the impacts of various combinations of precipitation, climate, topography, soil type, and land use on streamflow and groundwater recharge. The modular design provides a flexible framework for model enhancement. The PRMS code is extremely well documented in Leavesley *et al.* (1983) and has been used recently in many applications across the US, in Europe (Barth, 2005; Ely, 2006; Yeung, 2005), and in nearby watersheds (e.g., TRCA (2008), Earth*fx* (2008a), CLOCA (2008), Earth*fx* (2010c), Earth*fx* (2010d), and Earth*fx* (2013)). The integration of the PRMS sub-model with MODFLOW to form GSFLOW is documented in Markstrom *et al.* (2008). As noted, GSFLOW can be run in its fully-integrated manner, or the PRMS portion of GSFLOW can be run independently (i.e., in PRMS-only mode), using a simple cell-based linear groundwater reservoir in place of MODFLOW. The version of GSLOW employed in this study was 1.1.6 which itegrates PRMS version 3.0.5 and MODFLOW-NWT version 1.0.7.

9.2.1 Spatial Discretization

To use PRMS as a fully-distributed model, the study area was first discretized into a grid of cells. Each cell was then assigned a unique set of hydrologic properties. Property values and methods for assigning properties are discussed further on. The PRMS cell size does not need to correspond to the MODFLOW cells, allowing for finer representation of the shallow soil zone processes including overland runoff and interflow.

For this study, square cells, 50 m on a side, were found to adequately represent the distribution of land use, topography, and soil properties within the model boundary while minimizing the number of model cells. The PRMS grid contained 964 rows and 956 columns (921,584 cells) covering an area of 2,304 km². Cells that covered areas outside of the MODFLOW sub-model boundaries were designated as inactive and were not included in the water balance computations.

9.2.2 Temporal Discretization

The PRMS sub-model in GSFLOW and the groundwater sub-model are integrated on a daily time step basis. Select rainfall-related processes within the PRMS sub-model can be run on a finer (and even variable) time step. As previously discussed in Section 4.1, distributed hourly rainfall rates were derived from NEXRAD radar data to better capture the spatial and temporal distribution of

small-scale storm events. Climate data (i.e., rainfall, snowfall, and minimum and maximum temperature) from multiple stations were interpolated to each grid cell using an inverse-squared-distance weighting scheme and solar radiation was adjusted for slope and slope aspect for each cell. Individual water and energy balances were computed for every cell and for every daily time step.

9.2.3 Inter-Cell Runoff, Interflow and Imperviousness

The routing of overland runoff and interflow between cells is defined by a cascade flow network created based on basin topography. The cascade directs outflows (i.e., overland runoff and interflow) of one (or many) upslope cells to downslope cells. Overland runoff onto a cell from upstream (also referred to as run-on) is factored into the water budget for the downstream cell, thereby allowing the run-on to re-infiltrate and/or contribute to the runoff to the next cell. Interflow from upstream cells is directly added to the soil water budget for the downstream cell where it can contribute to groundwater recharge and/or Dunnian runoff. Runoff and interflow is eventually directed to the catchment outlet or to streams and lakes.

Each cell can contain both pervious and impervious sub-areas and separate water balance computations are done for each sub-area at every time step. For both subareas, the model first computes interception by vegetation. The amount intercepted depends on vegetation type, precipitation type (rain, snow, or mixed) and winter/summer vegetation cover density. When interception storage capacity is exceeded, the surplus is allowed to fall through onto the snowpack, if present, or directly onto the ground surface (a process termed throughfall or net rainfall). In impervious areas, the model computes the capture of precipitation by depression storage. When depression storage capacity is exceeded, the surplus is discharged as overland runoff. Water is removed from the depression storage reservoir in each cell by evaporation.

9.2.4 Hydrologic Processes

A flow chart describing the physical processes simulated by the PRMS code is shown in Figure 9.1. A more complete description of the program code and underlying theory can be found in Leavesley *et al.* (1983) and Markstrom *et al.* (2008). The PRMS model tracks volumes of water for each HRU cell in a number of storage reservoirs. These include interception storage, depression storage (discussed above), snowpack storage, capillary soil moisture zone storage, gravity soil moisture zone storage (i.e., water in excess of field capacity), preferential flow storage, and groundwater storage (if GSFLOW is run in the PRMS-only mode).

A two-layer, energy-balance model for the snowpack, shown schematically in Figure 9.2, computes snowpack depth, density, albedo, temperature, sublimation, and snowmelt on a daily basis using maximum and minimum air temperature, solar radiation, and precipitation data. The linear, energy-balance snowpack model is combined with an areal snow depletion curve to simulate the sub-cell spatial distribution of snow melt at shallow snowpack depths (DeWalle and Rango, 2008).

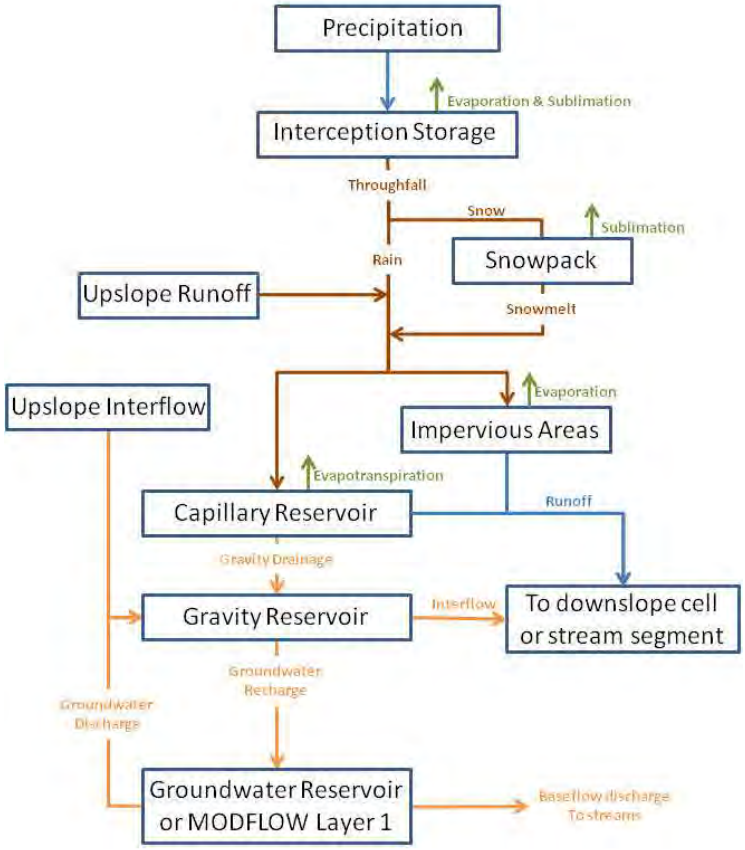

Figure 9.1: Flow chart of PRMS hydrological processes.

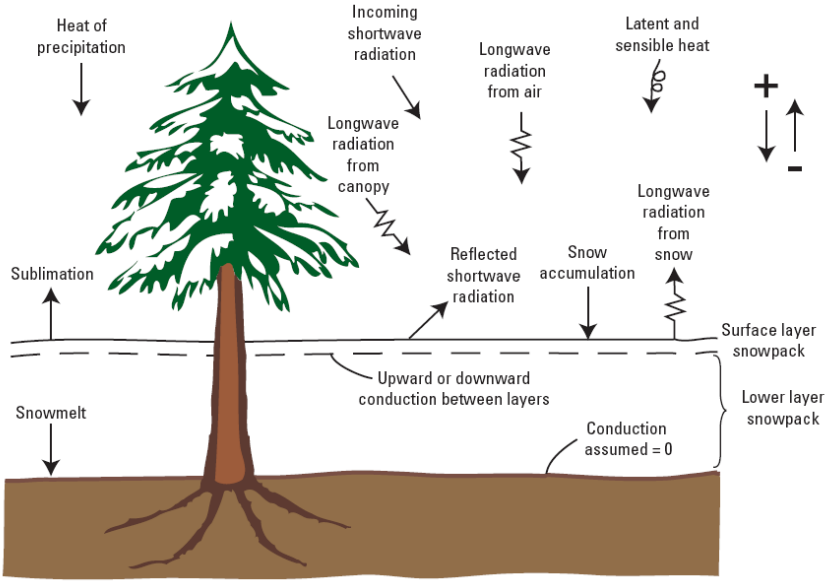

Figure 9.2: PRMS two-layer snowpack conceptualization and the processes accounted for in the energy balance snowmelt algorithm.

The snowpack energy balance model is used to determine the amount of snowmelt on pervious and impervious areas on a sub-daily basis to account for differences in the night and day energy flux. Detailed descriptions of the energy balance model can be found in Anderson (1968), Obled and Rosse (1977), and Leavesley *et al*. (1983). The snowpack is treated as a porous media, where liquid water can be stored and potentially re-freeze.

During precipitation events, the model first checks whether a snowpack exists. If the temperature is below a user-defined base (or critical) temperature (T_c), all throughfall (i.e., precipitation in excess of interception storage) is added to the snowpack as new snow. If the temperature is higher, the throughfall is added as rain to the snowpack and is used to raise the temperature of the snowpack through sensible and latent heat exchange. If the energy input is high enough and the snowpack has become isothermal, all or part of the snowpack can melt.

Snowmelt is assumed to infiltrate the soil up to a maximum daily amount and any excess is allowed to runoff. For this study, a maximum rate of frozen soil infiltration was assigned to be 5% of the saturated hydraulic conductivity of the soil. Water remaining in the snowpack can refreeze based on air temperature change. The albedo (reflectivity) of the snow decreases over time allowing the snowpack to absorb more energy as it ages. The albedo is reset every time there is a new snowfall event. The snowpack is also subject to sublimation.

Throughfall in the absence of a snowpack is partitioned between infiltration and runoff. The standard PRMS code uses a “contributing area” method (Dickinson and Whiteley, 1970) to partition throughfall on a daily basis. Earth*fx* added the Green and Ampt method used in the original PRMS code (see Leavesly *et al.,* 1983) back into the PRMS sub-model to calculate infiltration using hourly precipitation data. In this code, infiltration is computed with the Green and Ampt (1911) equation using information on the saturated hydraulic conductivity of the soil, the volume of water in the soil (i.e., antecedent conditions), the capillary drive (capillary drive is equal to the product of the initial capillary potential (at the start of infiltration), and the initial moisture deficit (field capacity minus the initial moisture content)). Runoff is calculated as the excess over the infiltration capacity and referred to as “Hortonian” runoff.

Percolation to groundwater is assumed to have a maximum daily limit. The maximum daily limit was assigned based on the saturated vertical hydraulic conductivity of the surficial soils (assuming a unit gradient). Excess infiltration is diverted back to overland runoff when the gravity and capillary (i.e., soil zone) storage reservoirs reach capacity. This form of saturation-excess runoff is termed “Dunnian” runoff (Markstrom *et al.,* 2008) and is the predominant form of runoff in humid climates such as southern Ontario. The volume of water held in the gravity reservoir is updated every day and can be depleted by evapotranspiration, discharge to downslope HRUs as interflow, or percolate to the groundwater reservoir as gravity drainage.

During PRMS-only simulations (i.e., without the use of MODFLOW), percolation is fed to a linear groundwater reservoir associated with every HRU cell. Lateral groundwater movement can be approximated using a separate groundwater reservoir cascade algorithm or it can be sent to a single groundwater reservoir for the entire catchment. The latter option was used in this phase of the calibration. Discharge from the groundwater reservoirs to streams occurs at a rate dependent on the volume of water stored in the groundwater reservoir and a linear decay coefficient that can be determined using gauge discharge records (Linsley *et al.*, 1975). When combined with MODFLOW (i.e., GSFLOW mode), MODFLOW simulates the groundwater processes and the cascading linear groundwater reservoirs are not used. In addition, MODFLOW calculates the volume of water transferred back to the soil reservoirs when the water-table intersects the soil zone. This water can fill the soil reservoirs zone and contribute to Dunnian runoff. This feedback mechanism is very important in low-lying areas such as stream valleys and wetlands.

9.3 Parameter Assignment for the Tier 2 PRMS Model

Initial estimates of model parameters were defined prior to starting PRMS model runs and the calibration process. For parsimony, consistent assumptions and parameter values were, where possible, applied across all subwatersheds within the study area. Discussion of model parameters is grouped into four sub-sections, including:

1. topography-related properties (e.g., slope, slope aspect, and the cascade network);
2. soil-type properties (e.g., field capacity and wilting point);
3. vegetation and land-cover related properties (e.g., cover density and percent imperviousness);
4. other parameters related to hydrological processes such as snowmelt.

The software package VIEWLOG (Kassenaar, 2013) was used to create or interpolate gridded data (such as slopes and elevations) and to assign parameters using lookups for tabulated values and cell-based indices.

9.3.1 Topography-related Properties

Topography for the model area is based on a 5 m hydrologically- corrected digital elevation model (DEM) provided by MNR (WRIP, 2005) (Figure 3.6). Documentation of the MNR WRIP DEM version 2 dataset is available from Land Information Ontario (LIO). The 5 m DEM was up-scaled to the 50 m grid by averaging the 100 DEM elevation values for each 50 m cell.

Slope and slope aspect affect the amount of shortwave solar radiation arriving at land surface. For example, a north-facing valley slope will get less solar radiation than the south-facing slope and will therefore have lower potential ET rates and a longer persisting snowpack. Recorded daily solar irradiation data were corrected for each cell based on its slope and slope aspect as well as for time of year before being used in snowmelt and ET calculations. Slope and slope aspect values were calculated from the DEM using a nine-point planar regression technique that fits a plane to every cell and its eight surrounding cells (see Moore *et al.,* (1991)).

As noted earlier, the PRMS code incorporates a cascading flow algorithm that routes overland flow and interflow from one cell to adjacent cells (Markstrom *et al.*, 2008). In many catchment models, runoff generated at a point in the model is routed directly to stream channels, without having the possibility of infiltrating somewhere along the pathway. The cascading algorithm transfers runoff from one cell and adds it (as run-on) to the total volume of water available for infiltration and/or runoff to the downslope cell. Accumulation of runoff from upstream cells and the convergence of the generally dendritic flow network results in more physically realistic patterns of ET, runoff to streams, and enhanced recharge in the downslope areas.

Topographic data and terrain analysis techniques were used to define the cascade overland flow routing network. An 8-direction steepest-descent method was selected because it generates an efficient many-to-one cascade network (i.e., only one outflow path per cell is defined) and it avoids undesirable upslope numerical dispersion (see Seibert and McGlynn, 2007). A small portion of the cascade flow network around Mitchell Lake is shown in detail on Figure 9.3 along with the up-sampled land surface topography. A cascade pathline goes from cell to cell until a stream reach, lake, or “swale” (i.e., a closed depression) is encountered.

The amount of runoff allowed to cascade on a particular day can be specified. For this study, it was set to be dependent on the cell slope. Two threshold slope values were used to define this amount. On mild slopes (i.e., slopes below a lower threshold), all runoff is retained in the cell. On steep slopes (i.e., slopes exceeding an upper threshold), all runoff is released to the cascade. On moderate slopes; the amount of runoff released is determined by a linearly-interpolated value

between the lower and upper thresholds. The retained water remains available for infiltration or runoff on the following day.

9.3.2 Soil Properties

Soil properties have a significant influence on hydrological processes because they control the amount of water that can infiltrate and be transmitted to the water table as well as the amount of water lost to evaporation and transpiration by plants (i.e., actual ET). In PRMS, the soil zone is divided into two main reservoirs: the capillary reservoir represents the tension storage between field capacity and wilting point. This reservoir can be depleted by ET losses. The gravity reservoir represents the remaining available storage within the soils column above field capacity where water can drain freely to recharge the groundwater system. Soil water movement is controlled by two main factors: (i) the ability of the soil to transmit water (hydraulic conductivity); and (ii) the gravity and suction forces acting on the soil water. The PRMS model simplifies the simulation of unsaturated flow in the soil zone by assuming that inflow to this reservoir occurs at a rate limited by the Green and Ampt model. For PRMS-only simulations, all water above field capacity (remaining after ET) is available to percolate to the water table or to discharge to adjacent cells as interflow. If the soil permeability is low, water will be retained in the gravity reservoir and gradually percolate or discharge over a period of days. Soil water-holding capacity in the capillary and gravity reservoirs (see Markstrom et al., 2008) were input as model parameters that were assumed to be functions of soil zone thickness, porosity, field capacity, and wilting point. Parameters that control the partitioning of flow between interflow and percolation were also specified as soil-type properties.

To simplify parameter assignment and for the sake of parsimony, soil properties were assigned to cells using tabulated look-up values for each surficial geology type. An example of a parameter based on surficial geology, in this case the hydraulic conductivity of the soil zone, is shown in Figure 9.4. An underlying assumption was that soil properties for Newmarket Till, for example, were the same in one part of the model area as another. Where this was not true, subclasses of the same surficial geologic unit were created.

OGS (2003) surficial geology maps were used to assign soil types found in the study area (Figure 3.9). The surficial geology classes and associated parameter values used by the PRMS sub-model are listed in Table 9.1. Hydraulic conductivities and other soil properties were estimated initially from previous PRMS models (e.g., Earth*fx*, 2008) or the available literature (e.g., Chow, 1964; Linsley et al., 1975; Fetter, 1980; Todd, 1980; DeWalle and Rango, 2008) and refined (where necessary) during model calibration to improve the match between observed and simulated flows. The PRMS code expects inputs in a mix of imperial and metric units. Conversions were applied to the tabulated values in the data pre-processors.

Some soil properties were estimated from land use data (rather than surficial geology) for agriculture, natural (i.e., forests and wetlands), and urban areas. It was assumed that soil characteristics that relate to wilting point, field capacity, and porosity would be relatively consistent for these three land-use types across the region. For example, all agricultural soils were assumed to be a sandy loam with a large Plant Available Water (PAW) store (Ward and Trimble, 2003) having a wilting point, field capacity, and porosity of 0.1, 0.2, and 0.4, respectively. Natural areas, which exist mainly in riparian areas, were assumed to be rather peaty having a wilting point, field capacity, and porosity of 0.05, 0.1, and 0.9, respectively (Fetter, 1980; Todd, 1980). Urban areas were assumed to be mostly grass lawns and parks with 150 mm deep root zones and were given a wilting point, field capacity, and porosity of 0.1, 0.2, and 0.4, respectively. Making this assumption reduced the amount of parameterization and allowed the calibration effort to focus on adjusting effective soil depth values through model calibration. The proportion of the model area consisting of agricultural, natural, and urban areas is 44%, 50%, and 3%, respectively; the remaining 3% consists of other land use type such as pits and quarries or open water.

9.3.3 Representation of the Alvar

Much of the area in the upper Talbot is described as alvar. These limestone plains are characterized as having a thin, sparsely-vegetated, drift overlying heavily karstified bedrock. This type of setting is unique in the region and special attention was paid to representing this feature correctly in the PRMS model.

The alvar can be covered with very thin drift or exposed at surface. Where covered, the model represented the limited amount of available storage in the capillary zone. The thickness of the gravity reservoir was set to zero. This forced all water above field capacity to percolate directly to the groundwater reservoir (or MODFLOW Layer 1 in the integrated model) allowing no partitioning to interflow. Two low-storage, highly conductive MODFLOW layers were added to the groundwater model in the alvar area (see Section 10.4) to represent the fracture network.

9.3.4 Land Use-related Properties

A number of other hydrologic properties used in the PRMS model could be reasonably correlated with land use type. For the sake of parsimony and to simplify property assignment, these were assigned to model cells using a look-up table with parameter values for each land-use category. An underlying assumption was that properties for a particular land-use class (e.g., “built-up area - pervious”) were the same in one part of the model area as another. The hydrological properties included:

- percent imperviousness - the proportion of the cell area assumed to be impervious;
- depression storage - the amount of water that can be retained over the impervious area;
- vegetation index – dominant vegetation type (bare, grass, shrub, or trees) in the cell;
- vegetative cover density - the fraction of pervious area covered by vegetation and/or tree canopy. Two values are provided: one for the growing season and one for winter;
- interception storage - the amount of precipitation retained on vegetative surfaces and/or tree canopy. Three values are provided: interception storage for summer rain, winter rain, and winter snow. Effective interception capacity is the product of vegetative cover density and interception storage;
- specific soil zone properties (porosity, field capacity, wilting point, and soil depth) for certain land use types. Soil depths are typically represented as vegetation rooting depths;
- soil moisture capacity - the product of soil depth and the difference between field capacity and wilting point;
- saturation threshold - the volume of drainable storage in the soil column (soil depth times the difference between porosity and field capacity);
- evaporation extinction depth - the depth below the soil surface where evaporative loss becomes negligible. Note that transpiration losses may still occur below this depth.

As discussed in Section 4.2, the primary source for land use data in the model area is the LSRCA ELC dataset (2014) with additional data obtained from MNR SOLRIS (v1.2). The land use lookup table for the study area is provided in Table 9.2. The assumption of consistent property values across the study area was felt to be reasonable for most land use classes. While the breakdown of urban areas into “built-up area pervious” and “built-up area impervious” may be overly simplified, the portion of the study area with these classifications is small.

9.3.5 Hydrological Processes Parameters

The PRMS model contains a number of sub-models, such as the Green and Ampt infiltration sub-model, the energy balance snowmelt model, and the ET sub-models. These sub-models have numerous parameters, of which many can be assigned on a cell-by-cell basis. For simplicity and

consistency, global values were used where appropriate. Where possible, independent testing of the sub-models was done to determine optimal values for these parameters.

9.3.5.1 Areal Snow Depletion Curve Parameters

A localized snowpack area depletion curve was developed to simulate the variability in snowpack coverage during late snowmelt events (i.e., when bare areas begin to appear). The linear energy-balance snowmelt model employed in PRMS is dependent on areal snow depletion curves that relate snow pack volume (in water equivalents) to the areal distribution of snow coverage. Documented snow curves are rare and the default snow curve in PRMS is based a curve developed for a site in the primarily alpine state of Colorado (Anderson, 1968).

The refinement of snowmelt estimation was considered necessary based on previous modeling exercises (see Earth*fx*, 2010). These studies demonstrated that snowmelt was a significant component of the water balance and was the hydrological process that required the greatest calibration effort. Roughly one-third of annual precipitation in the study area is in the form of snow and the majority of runoff to streams and groundwater recharge occurs during the snowmelt season. Remote-sensing techniques and applied snow hydrology methods, such as those described in DeWalle and Rango (2008), Reese (2006), and Seidel and Martinec (2004), were used to develop a representative areal snow depletion curve for Southern Ontario. This snow curve, (Figure 9.5) was employed in this study.

9.3.5.2 Evapotranspiration

Water entering the soil in pervious areas is subject to evapotranspiration (ET). The PRMS code has three methods for calculating potential evapotranspiration (PET). The Jensen and Haise method, which requires only two climate parameters, temperature and incident radiation, was used in this study to estimate daily PET.

Actual evapotranspiration (AET) processes are assumed to follow a hierarchy whereby ET is first extracted from interception storage and then depression storage. If there is insufficient water to meet the total PET demand, the deficit is extracted from the capillary zone (i.e. the upper soil zone) at a rate based on soil type and the ratio of the current volume of water stored in the capillary zone to its maximum storage capacity. If PET demand is still not met, moisture is extracted indirectly from the gravity soil zone reservoir which is used to replenish the capillary deficit (Markstrom *et al.*, 2008). Once below a specified evaporation extinction depth, transpiration can continue at a rate dependent on canopy coverage, vegetation type, soil type, and the ratio of the current volume of water stored in the capillary soil zone to its maximum storage capacity. Soil zone depth is defined by the average rooting depth of the predominant vegetation and adjusted during model calibration. Initial storage in the upper soil zone was set to 50% of soil zone capacity.

9.4 PRMS Pre-Calibration Modelling Results

As noted, a PRMS submodel was calibrated independently to test the models ability to represent the hydrological processes in the study area and to derive reasonable values for model parameters. Although the groundwater processes simulated were simplified and no feedback was allowed, it was expected that model results and parameter values would be were generally transferable to GSFLOW running as a fully-integrated groundwater/surface water model. The large difference in model run times between PRMS-only runs and GSFLOW runs precluded calibrating the fully-integrated model at the outset. The intent of the PRMS-only calibration was not to achieve a final calibration but rather to derive a set of reasonable parameter values that could be used in the GSFLOW model with a minimum of recalibration effort. Some adjustments of PRMS parameters were needed in the final

calibration to account for transfer of flows through feedback mechanisms not fully represented in PRMS-only simulations such as discharge from the shallow water table to the soil zone.

The following section presents results from the 7-year PRMS-only calibration and from the 25-year long-term PRMS run used to derive a long-term average groundwater recharge distribution. The latter was used in the preliminary calibration of the steady-state MODFLOW sub-model. Because these do not represent the results of the final GSFLOW calibration, the discussions presented here are brief. Final GSFLOW calibration and results are discussed in Section 11.

9.4.1 PRMS Calibration Results and Discussion

The PRMS sub-model was calibrated between WY2005 and WY2012 (inclusive). Precipitation inputs for the calibration period were derived from NEXRAD data, as described in Section 4.1. The calibration effort focused on Whites Creek and on matching observed flows primarily at LS0402 (Whites Creek at Regional Rd. 23) shown in Figure 4.18 and discussed in Section 4.3.1.

Figure 9.6 shows the observed mean daily discharge hydrograph for the LSRCA gauge on Whites Creek (LS0402) compared with the simulated PRMS flows. A satisfactory agreement between simulated and observed daily flow was achieved overall, with the exception of the systematic overestimation of summer storm event peaks. A comparison of log simulated and observed daily flows are provided on Figure 9.7. The low flow response is not consistent, with the sub-model generally over predicting streamflow during dry periods. Coupling PRMS to the groundwater sub-model in GSFLOW to better represent groundwater discharge to streams will improve the representation of low flow conditions. As shown on Figure 9.8, the simulated volumes match closely, with the simulated volume over predicted by 6%. The model achieves a Nash-Sutcliffe (1970) Efficiency (NSE) of 0.28 and a Log- Nash-Sutcliffe Efficiency of 0.55 at the Whites Creek gauge at the daily time step. The model achieves a Nash-Sutcliffe (1970) Efficiency (NSE) of 0.67 and a Log-Nash-Sutcliffe Efficiency of 0.66 at the Whites Creek gauge at a monthly time step. There is much better agreement between simulated and observed discharge at the longer temporal scale, which suggest that the long-term water balance of the model is valid.

Despite the short period of record and the relatively small magnitudes of discharge at the TrentU-Dillon streamflow monitoring locations, several gauges demonstrate a good agreement with simulated flows. Simulated versus observed discharge at WR06 and WR23 are presented on Figure 9.9 and Figure 9.10 respectively.

9.4.2 Long-term Results and Discussion

After calibration, the PRMS-only sub-model was run from WY1986 to WY2010 (inclusive) using MNR infilled hourly precipitation to assess the water budget and, specifically, provide an estimate of average groundwater recharge on a long-term basis. Four distributed sub-model outputs are discussed below.

Average annual generated overland runoff is shown in Figure 9.11. Figure 9.12 shows average annual cascading flow. Generated runoff is defined as the runoff generated at specific locations and does not include cascading run-on from upslope cells. Cascading flow defines the average volume of water that is likely to pass a given location. Visually, the difference between the two maps is that the cascading flow paths are not apparent on the generated runoff map, which is useful when highlighting the impacts of the soil properties on runoff. For example, areas of high runoff in Figure 9.11 are mainly associated with lower values of hydraulic conductivity. Low runoff is associated with surficial sands in rural settings, and the alvar located in the northern part of the model area. The cascading runoff map highlights the role topography and run-on have on the distribution of runoff. For example, it can be seen that runoff in the study area follows a dendritic pattern.

Figure 9.13 shows average annual actual evapotranspiration (AET). AET patterns are sensitive to land use/land cover. The model indicates low ET rates over the drought prone alvar and in the quarries. For urban areas, there is a reduction in pervious area, resulting in increased runoff and decreased infiltration and, therefore, a reduction in the soil moisture available for ET. In the quarries, there is no vegetation for transpiration and much of the runoff on the quarry floor is routed directly to the stream network. The AET distribution shows some evidence of the dendritic patterns seen in Figure 9.12. As might be expected, areas at the downstream end of the cascade will have more run-on and infiltration, and therefore, more soil water available for ET.

Lastly, Figure 9.14 shows average annual groundwater recharge which is affected by all the factors noted previously as well as by surficial geology. Greater recharge tends to occur on the alvar as compared to the quarries and or Newmarket and Dummer Till regions. Higher recharge occurs in the sandier areas. Recharge is likely overestimated in the wetland areas but this is corrected in the integrated GSFLOW model. Based on the long-term estimates from the calibrated PRMS sub-model, the average annual groundwater recharge for the study area was found to be 151 mm/year. About 39% of the study area receives between 0 and 50 mm/yr while 31% receives between 50 and 200 mm/yr and about 28% receives between 200 and 500 mm/yr (Figure 9.15).

9.4.3 Constraints of PRMS Groundwater Recharge Estimates

Groundwater recharge is defined as the amount of water percolating from the PRMS gravity soil zone to the linear groundwater reservoir (or to the underlying MODFLOW finite-difference cell in GSFLOW simulations). It should be noted that recharge cannot easily be measured directly over large areas. Instead, surface water models are used to estimate the primary components of the water balance (interception, overland runoff, ET, and recharge for example) and are calibrated to stream discharge measurements. The assumption is that if the model matches the observed streamflow, than the components of the water budget have been estimated in a reasonable manner.

There are a number of practical limits that help to constrain the models. For example, assuming that the total volumes of precipitation and streamflow can be measured accurately, the total losses due to ET and interception cannot exceed the difference between precipitation and streamflow. Similarly, if (1) groundwater discharge to streams is a significant component of estimated baseflow at the gauge and (2) there is little net cross-watershed groundwater flow, then the total recharge cannot exceed the estimated baseflow.

The preceding constraints are applicable on a catchment-wide basis and over the longer term; where change in storage is assumed to be negligible. While these same constraints cannot be readily applied to individual cells in a transient distributed model, the model results can be aggregated over space and time and subjected to the same watershed-scale checks for reasonableness.

One of the advantages of using an integrated model over the hydrologic model alone is that if unreasonable values of recharge are provided to the groundwater model, the calculated groundwater levels will also appear unreasonable. This feedback provides a separate check on the estimated spatial distribution of recharge. The PRMS-only groundwater recharge map was used as an initial input during independent calibration of the groundwater sub-model. Groundwater recharge estimates were refined during calibration of the GSFLOW model which considered feedback mechanism in an integrated manner.

As with all models, it must be recognized that there are inherent simplifications in the model conceptualisation of distributed hydrologic processes and in the simplified assignment of parameters. There are also limitations and uncertainty in the input and calibration target data. Accordingly, it is unlikely to achieve a perfect or unique calibration. However, the results obtained with the PRMS-only model appear reasonable and were improved after integration in GSFLOW.

9.5 Tables and Figures

Table 9.1: List of surficial geology types and properties used in the PRMS sub-model.

Material	Percent coverage of model area	Hydraulic Conductivity of Soil Zone (m/s)	Hydraulic Conductivity of Frozen Soil (m/s)	Green-Ampt Infiltration Rate (m/s)
Bedrock, Precambrian, Exposed	0.8%	$8.0x10^{-11}$	$4.0x10^{-12}$	$5.0x10^{-05}$
Bedrock, Discontinuous drift cover (>1m thick)	0.9%	$1.0x10^{-06}$	$5.0x10^{-08}$	$5.0x10^{-05}$
Bedrock, Paleozoic	23.6%	$8.0x10^{-07}$	$4.0x10^{-08}$	$5.0x10^{-05}$
Bedrock, drift complex, pleistocene	10.1%	$1.0x10^{-05}$	$5.0x10^{-07}$	$5.0x10^{-05}$
Bedrock, areas overlain by shallow stoney till	2.8%	$1.0x10^{-05}$	$5.0x10^{-07}$	$1.4x10^{-08}$
Till (Newmarket), Moderately stoney to stoney sandy silt to silt till	22.8%	$1.2x10^{-07}$	$6.0x10^{-09}$	$1.4x10^{-08}$
Till (Dummer), very stoney silty sand, numerous large boulders	2.7%	$1.7x10^{-07}$	$8.5x10^{-09}$	$1.4x10^{-08}$
Pleistocene ice-contact deposits, Pleistocene ice-contact deposits (sand and gravel)	2.8%	$7.0x10^{-04}$	$3.5x10^{-05}$	$1.2x10^{-07}$
Glacialfluvial outwash, sand and gravel; proglacial deposits (outwash)	0.1%	$1.0x10^{-05}$	$5.0x10^{-07}$	$1.5x10^{-07}$
Glacialfluvial outwash, fine to coarse sand, minor gravel	0.0%	$1.0x10^{-04}$	$5.0x10^{-06}$	$1.5x10^{-07}$
Fine-textured glaciolacustrine deposits, Silt and clay, massive to laminated	9.7%	$1.0x10^{-07}$	$5.0x10^{-09}$	$1.2x10^{-07}$
Glaciolacustrine deposits, sand and gravel	0.5%	$7.0x10^{-04}$	$3.5x10^{-05}$	$1.5x10^{-07}$
Glaciofluvial/lacustrine deposits, Sand	10.8%	$1.0x10^{-04}$	$5.0x10^{-06}$	$1.5x10^{-07}$
Fluvial, alluvial, deltaic, Pleistocene	0.0%	$5.0x10^{-06}$	$2.5x10^{-07}$	$1.2x10^{-07}$
Lacustrine, coarse-grained, sand	3.0%	$5.0x10^{-04}$	$2.5x10^{-05}$	$1.5x10^{-07}$
Aeolian deposits, Fine to very fine sand	0.0%	$1.0x10^{-04}$	$5.0x10^{-06}$	$1.5x10^{-07}$
Modern Alluvium, sand/silt and organic deposits (floodplain)	0.2%	$1.0x10^{-06}$	$5.0x10^{-08}$	$1.2x10^{-07}$
Peat and Muck, Wetlands (organic deposits)	9.1%	$1.0x10^{-08}$	$5.0x10^{-10}$	$1.4x10^{-08}$
Fill, Anthropogenic	0.1%	$1.0x10^{-07}$	$5.0x10^{-09}$	$1.2x10^{-07}$

Table 9.2: Land-use based parameters lookup table.

Description	Percent Impervious	Depression Storage (mm)	Summer Cover Density	Winter Cover Density	Summer Inter-ception Storage (mm)	Winter Inter-ception Storage (mm)	Winter Rain Inter-ception Storage (mm)	Soil Depth (mm)	Porosity	Field Capacity	Wilting Point	ET Extinction Depth (mm)
Open Cliff and Talus	0.00	1.0	0.00	0.00	0.0	0.0	0.0	300.0	0.35	0.10	0.05	300.0
Shoreline	0.00	1.0	0.00	0.00	0.0	0.0	0.0	300.0	0.35	0.10	0.05	300.0
Open Shoreline	0.00	1.0	0.00	0.00	0.0	0.0	0.0	300.0	0.35	0.10	0.05	300.0
Open Bluff	0.00	1.0	0.00	0.00	0.0	0.0	0.0	300.0	0.35	0.10	0.05	300.0
Open Sand Barren and Dune	0.00	1.0	0.00	0.00	0.0	0.0	0.0	300.0	0.35	0.10	0.05	300.0
Open Tallgrass Prairie	0.00	1.0	1.00	1.00	1.0	1.0	1.0	300.0	0.35	0.10	0.05	300.0
Tallgrass Savannah	0.00	1.0	1.00	1.00	1.0	1.0	1.0	300.0	0.35	0.10	0.05	300.0
Tallgrass Woodland	0.00	1.0	1.00	1.00	1.0	1.0	1.0	300.0	0.35	0.10	0.05	300.0
Forest	0.00	1.0	1.00	0.25	1.0	1.0	1.0	500.0	0.40	0.10	0.05	300.0
Coniferous Forest	0.00	1.0	1.00	1.00	1.0	1.0	1.0	500.0	0.40	0.10	0.05	300.0
Mixed Forest	0.00	1.0	1.00	0.25	1.0	1.0	1.0	500.0	0.40	0.10	0.05	300.0
Deciduous Forest	0.00	1.0	1.00	0.10	1.0	1.0	1.0	500.0	0.40	0.10	0.05	300.0
Plantations – Treed	0.00	1.0	0.85	0.10	1.0	1.0	1.0	300.0	0.35	0.25	0.08	300.0
Hedge Rows	0.00	1.0	0.25	0.25	1.0	1.0	1.0	300.0	0.35	0.25	0.08	300.0
Transportation	0.65	1.0	0.35	0.35	1.0	1.0	1.0	200.0	0.35	0.20	0.10	200.0
Extraction	1.00	0.0	0.00	0.00	0.0	0.0	0.0	0.0	0.00	0.00	0.00	0.0
Built-Up Area Pervious	0.00	1.0	1.00	1.00	1.0	1.0	1.0	200.0	0.35	0.20	0.10	200.0
Built-Up Area Impervious	0.85	1.0	0.15	0.15	1.0	1.0	1.0	200.0	0.35	0.20	0.10	200.0
Swamp	0.00	1.0	1.00	0.50	1.0	1.0	1.0	300.0	0.90	0.10	0.05	300.0
Fen	0.00	1.0	1.00	1.00	1.0	1.0	1.0	300.0	0.90	0.10	0.05	300.0
Bog	0.00	1.0	1.00	1.00	1.0	1.0	1.0	300.0	0.90	0.10	0.05	300.0
Marsh	0.00	1.0	1.00	1.00	1.0	1.0	1.0	300.0	0.90	0.10	0.05	300.0
Open Water	0.00	1.0	0.00	0.00	0.0	0.0	0.0	300.0	0.90	0.10	0.05	0.0

Description	Percent Impervious	Depression Storage (mm)	Summer Cover Density	Winter Cover Density	Summer Inter-ception Storage (mm)	Winter Inter-ception Storage (mm)	Winter Rain Inter-ception Storage (mm)	Soil Depth (mm)	Porosity	Field Capacity	Wilting Point	ET Extinction Depth (mm)
Undifferentiated	0.00	1.0	1.00	0.10	1.0	1.0	1.0	300.0	0.35	0.25	0.08	300.0
Agricultural	0.00	1.0	1.00	0.10	1.0	1.0	1.0	300.0	0.35	0.25	0.08	300.0
Bare Soil	0.00	1.0	0.00	0.00	0.0	0.0	0.0	300.0	0.40	0.30	0.10	300.0
Barn	1.00	1.0	0.00	0.00	1.0	1.0	1.0	200.0	0.35	0.20	0.10	200.0
Bedrock	1.00	1.0	0.00	0.00	0.0	0.0	0.0	100.0	0.05	0.00	0.00	100.0
Cemeteries	0.00	1.0	1.00	1.00	1.0	1.0	1.0	200.0	0.35	0.20	0.10	200.0
Commercial	1.00	1.0	0.15	0.15	1.0	1.0	1.0	200.0	0.35	0.20	0.10	200.0
Commercial / Industrial	1.00	1.0	0.15	0.15	1.0	1.0	1.0	200.0	0.35	0.20	0.10	200.0
Confinement Yard	0.00	1.0	1.00	1.00	1.0	1.0	1.0	300.0	0.35	0.25	0.08	300.0
Extraction	0.00	0.0	0.00	0.00	0.0	0.0	0.0	0.0	0.00	0.00	0.00	0.0
Field	0.00	1.0	1.00	1.00	1.0	1.0	1.0	200.0	0.35	0.20	0.10	200.0
Forest - Coniferous	0.00	1.0	1.00	1.00	1.0	1.0	1.0	500.0	0.40	0.10	0.05	300.0
Forest - Deciduous	0.00	1.0	1.00	0.10	1.0	1.0	1.0	500.0	0.40	0.10	0.05	300.0
Forest - Mixed	0.00	1.0	1.00	0.25	1.0	1.0	1.0	500.0	0.40	0.10	0.05	300.0
Golf Course	0.00	1.0	1.00	1.00	1.0	1.0	1.0	200.0	0.35	0.20	0.10	200.0
Grass	0.00	1.0	1.00	1.00	1.0	1.0	1.0	200.0	0.35	0.20	0.10	200.0
Greenhouse	1.00	1.0	0.15	0.15	1.0	1.0	1.0	200.0	0.35	0.20	0.10	200.0
Hedge Row - Coniferous	0.00	1.0	1.00	1.00	1.0	1.0	1.0	300.0	0.35	0.25	0.08	300.0
Hedge Row - Deciduous	0.00	1.0	1.00	0.10	1.0	1.0	1.0	300.0	0.35	0.25	0.08	300.0
Hedge Row - Mixed	0.00	1.0	1.00	0.25	1.0	1.0	1.0	300.0	0.35	0.25	0.08	300.0
High Density Residential	1.00	1.0	0.15	0.15	1.0	1.0	1.0	200.0	0.35	0.20	0.10	200.0
Impervious	1.00	1.0	0.15	0.15	1.0	1.0	1.0	200.0	0.35	0.20	0.10	200.0
Industrial	1.00	1.0	0.15	0.15	1.0	1.0	1.0	200.0	0.35	0.20	0.10	200.0
Institutional	1.00	1.0	0.15	0.15	1.0	1.0	1.0	200.0	0.35	0.20	0.10	200.0
Marsh	0.00	1.0	1.00	1.00	1.0	1.0	1.0	300.0	0.90	0.10	0.05	300.0
Nursery	0.00	1.0	0.85	0.10	1.0	1.0	1.0	300.0	0.35	0.25	0.08	300.0

Description	Percent Impervious	Depression Storage (mm)	Summer Cover Density	Winter Cover Density	Summer Inter-ception Storage (mm)	Winter Inter-ception Storage (mm)	Winter Rain Inter-ception Storage (mm)	Soil Depth (mm)	Porosity	Field Capacity	Wilting Point	ET Extinction Depth (mm)
Orchard	0.00	1.0	0.85	0.10	1.0	1.0	1.0	300.0	0.35	0.25	0.08	300.0
Parking Lot	1.00	1.0	0.15	0.15	1.0	1.0	1.0	200.0	0.35	0.20	0.10	200.0
Pasture	0.00	1.0	1.00	1.00	1.0	1.0	1.0	300.0	0.35	0.25	0.08	300.0
Plantation - Coniferous	0.00	1.0	0.85	0.85	1.0	1.0	1.0	300.0	0.35	0.25	0.08	300.0
Plantation - Deciduous	0.00	1.0	0.85	0.10	1.0	1.0	1.0	300.0	0.35	0.25	0.08	300.0
Private Road	1.00	1.0	0.10	0.10	1.0	1.0	1.0	200.0	0.35	0.20	0.10	200.0
Railway	0.35	1.0	0.35	0.35	1.0	1.0	1.0	200.0	0.35	0.20	0.10	200.0
Recreational	1.00	1.0	0.15	0.15	1.0	1.0	1.0	200.0	0.35	0.20	0.10	200.0
Rural Residential	0.30	1.0	0.15	0.15	1.0	1.0	1.0	200.0	0.35	0.20	0.10	200.0
Trailer Park	0.30	1.0	0.15	0.15	1.0	1.0	1.0	200.0	0.35	0.20	0.10	200.0
Transportation	1.00	1.0	0.35	0.35	1.0	1.0	1.0	200.0	0.35	0.20	0.10	200.0
Urban Residential	0.50	1.0	0.15	0.15	1.0	1.0	1.0	200.0	0.35	0.20	0.10	200.0
Water	0.00	1.0	0.00	0.00	0.0	0.0	0.0	300.0	0.90	0.10	0.05	0.0
Wetland - Coniferous	0.00	1.0	1.00	1.00	1.0	1.0	1.0	300.0	0.90	0.10	0.05	300.0
Wetland - Deciduous	0.00	1.0	1.00	0.50	1.0	1.0	1.0	300.0	0.90	0.10	0.05	300.0
Wetland - Mixed	0.00	1.0	1.00	0.50	1.0	1.0	1.0	300.0	0.90	0.10	0.05	300.0

Note: Cells shaded blue are values that have been set equal to other tabled values for rows of similar land use types

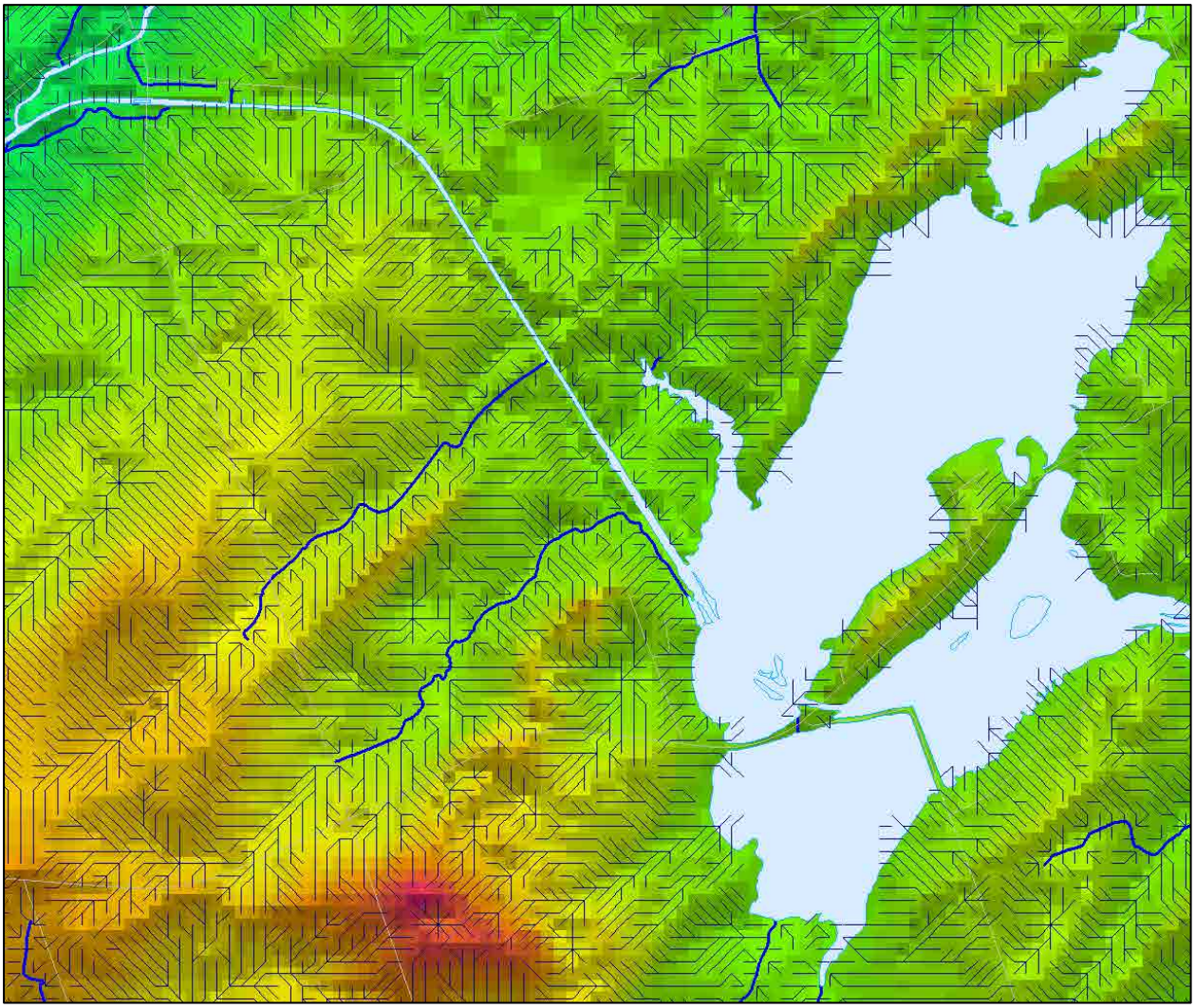

Figure 9.3: Close-up of the topography surrounding Mitchell Lake and the resulting cascade flow network.

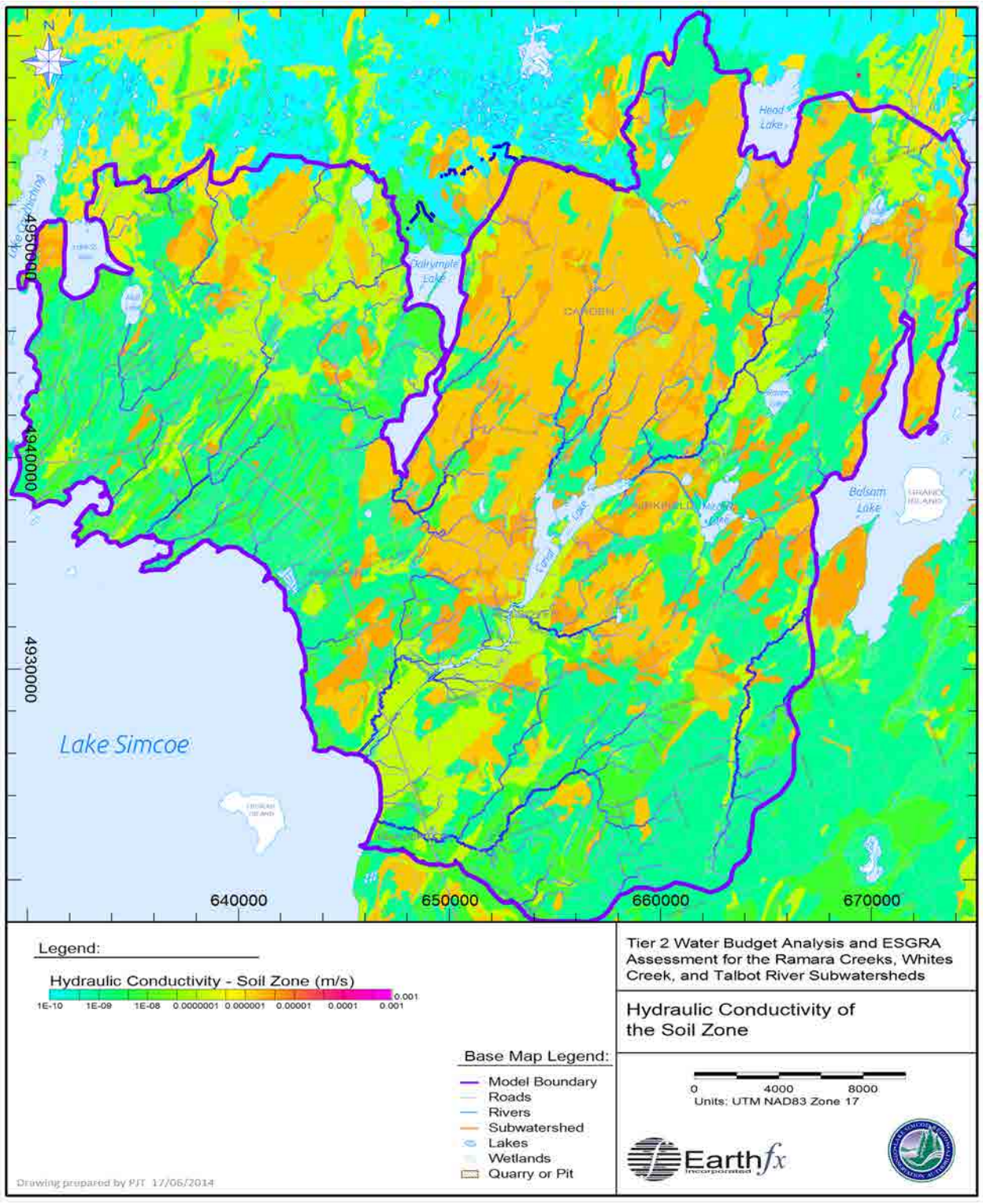

Figure 9.4: Distribution of soil zone hydraulic conductivity.

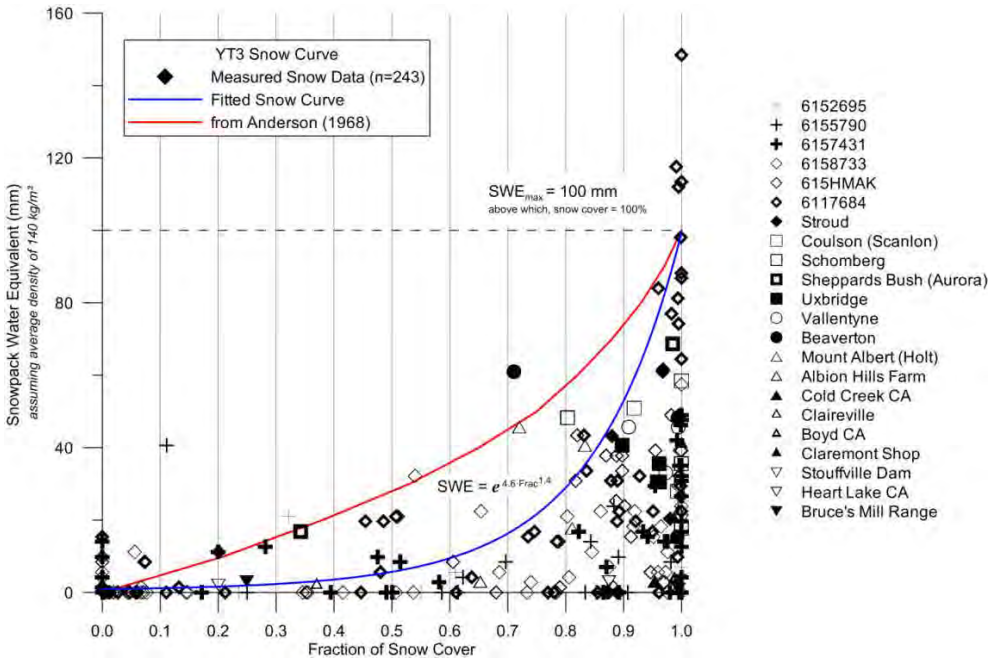

Figure 9.5: Southern Ontario areal snowpack depletion curve (Earth*fx*, 2012).

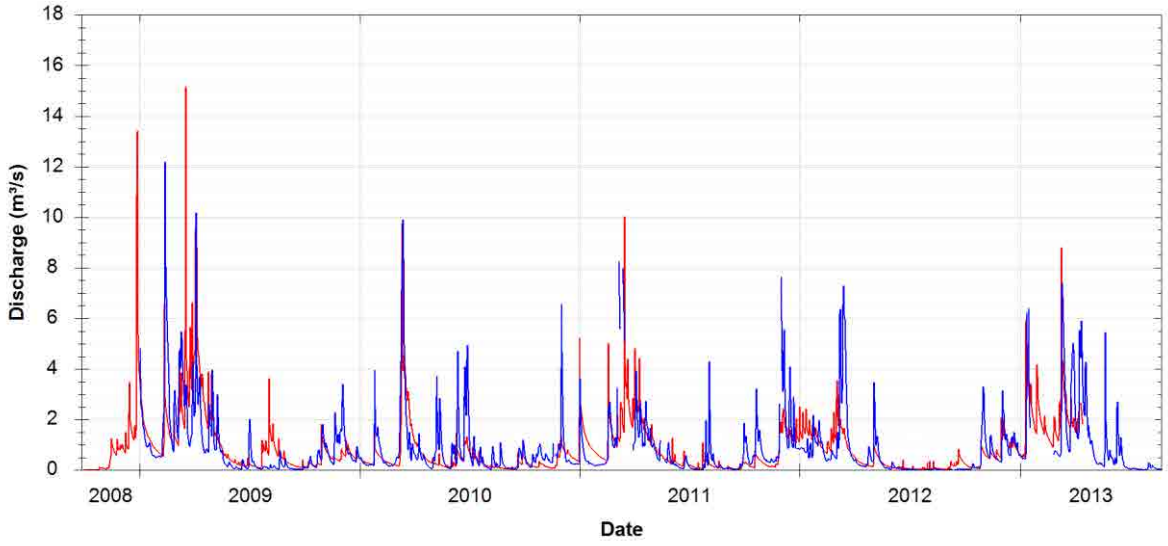

Figure 9.6: Simulated PRMS flow (red) versus observed mean daily streamflow (blue) at Whites Creek at Regional Rd. 23 (LSRCA ID: LS0402).

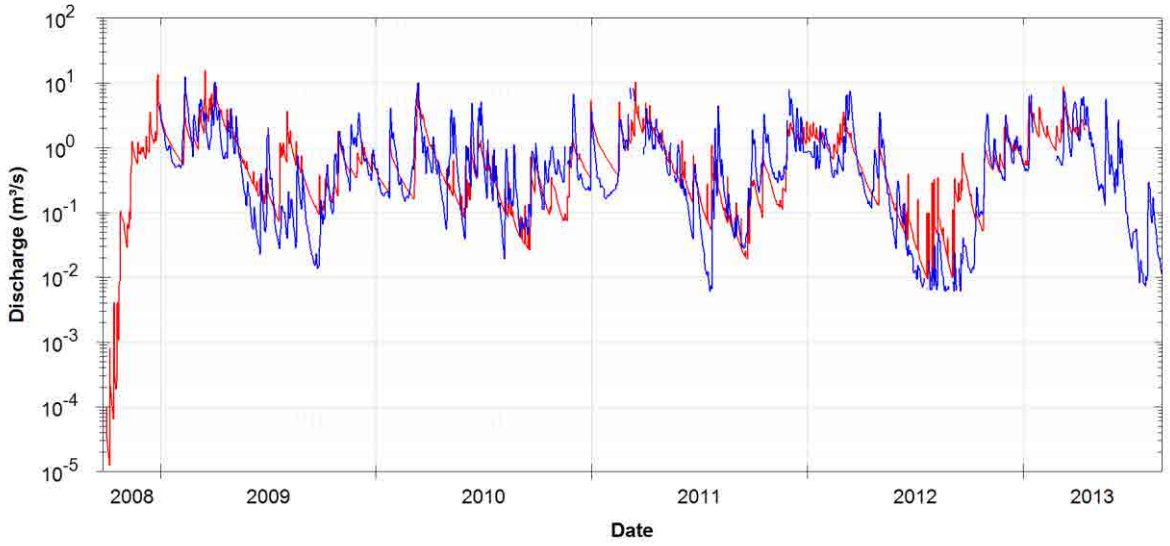

Figure 9.7: Log Simulated PRMS flow (red) versus observed mean daily streamflow (blue) at Whites Creek at Regional Rd. 23 (LSRCA ID: LS0402).

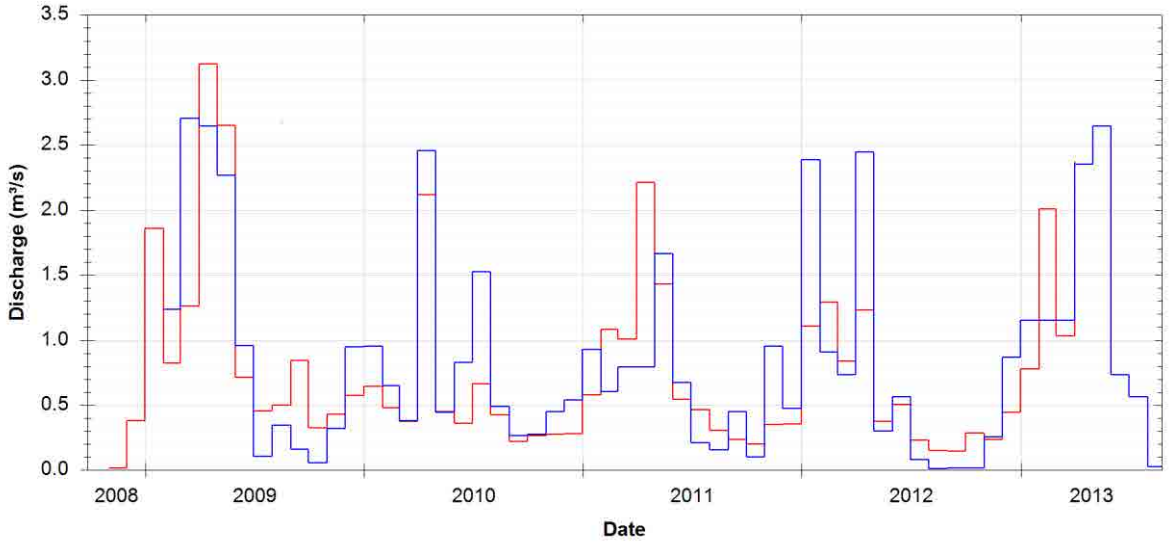

Figure 9.8: Monthly simulated PRMS flow (red) versus observed streamflow (red) at Whites Creek at Regional Rd. 23 (LSRCA ID: LS0402).

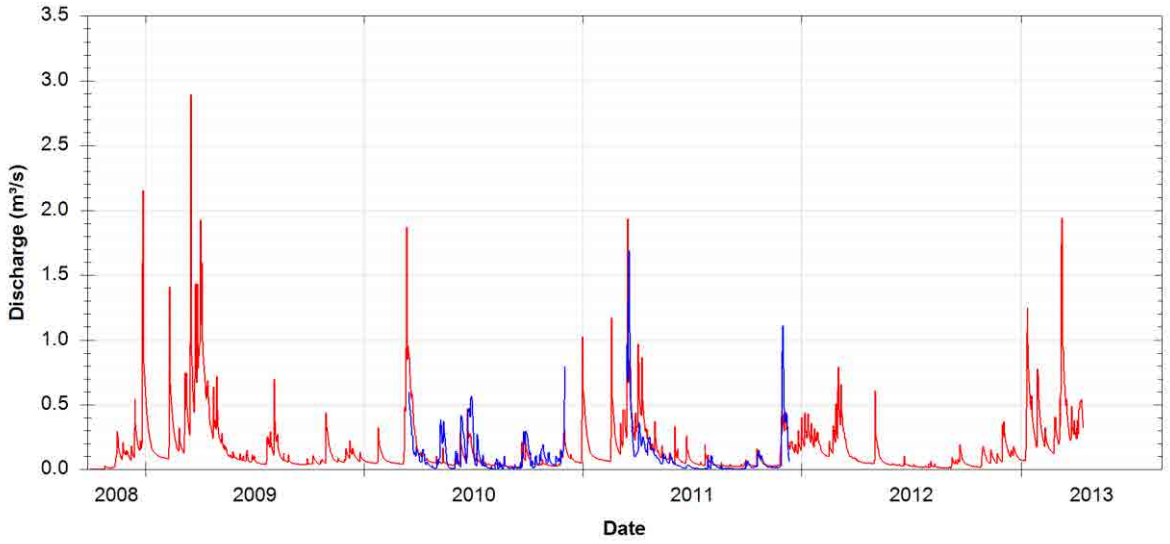

Figure 9.9: Simulated PRMS flow (red) versus observed daily streamflow (blue) at Whites Creek (TrentU-Dillon ID: WR06).

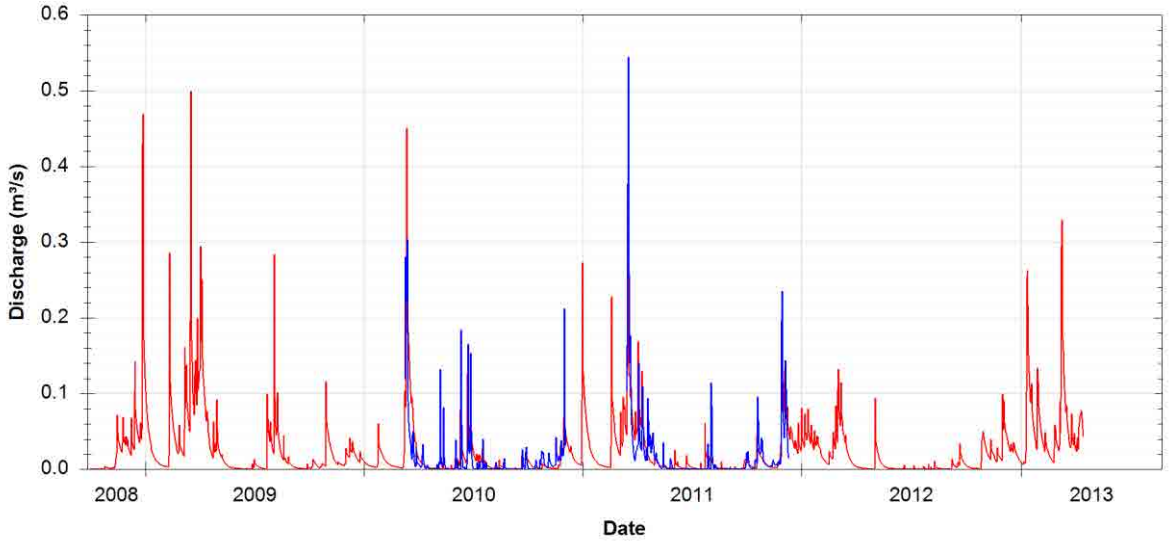

Figure 9.10: Simulated PRMS flow (red) versus observed daily streamflow (blue) at Whites Creek (TrentU-Dillon ID: WR23).

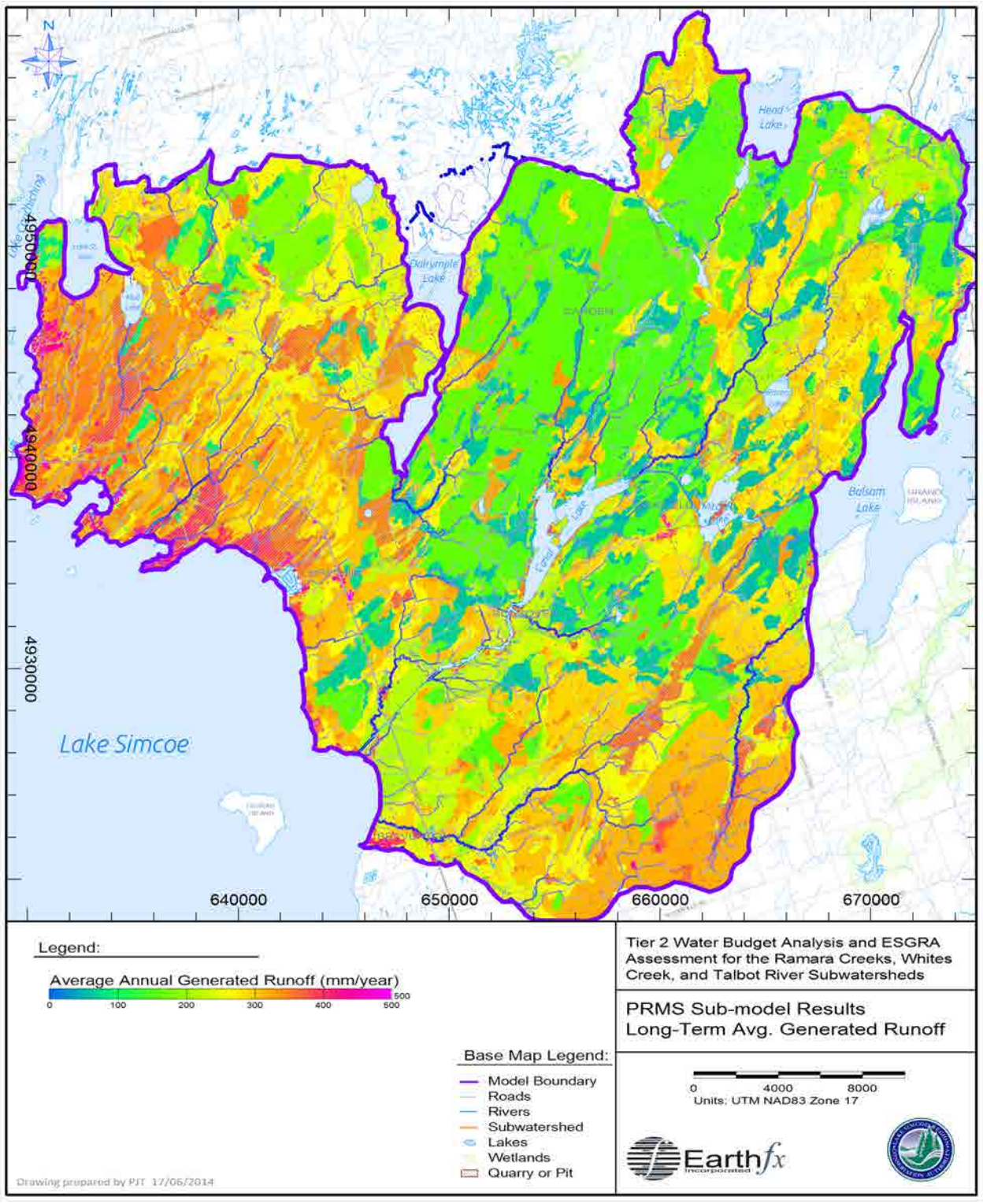

Figure 9.11: Simulated long-term average distribution of generated overland runoff.

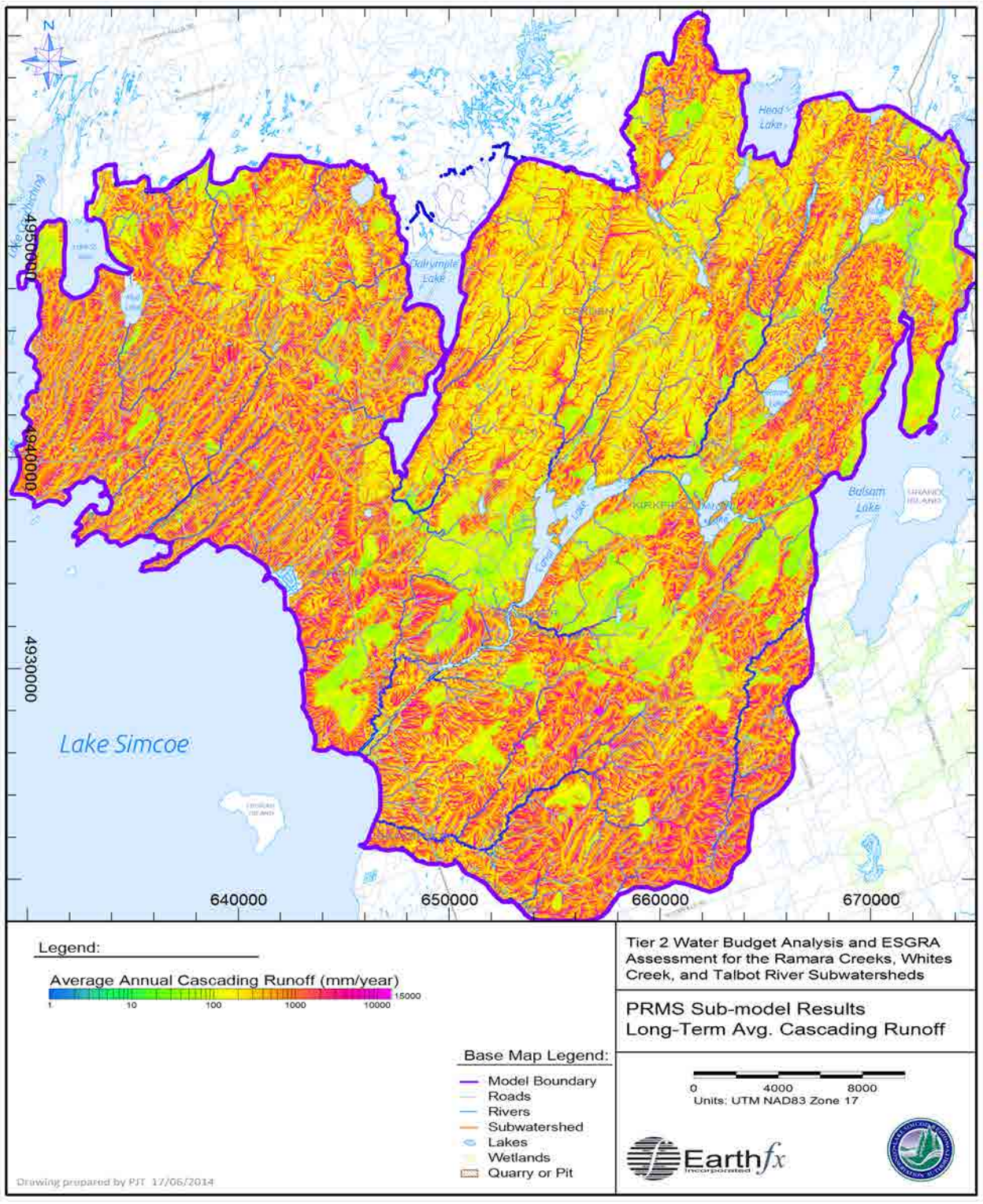

Figure 9.12: Simulated long-term average distribution of accumulated cascading runoff.

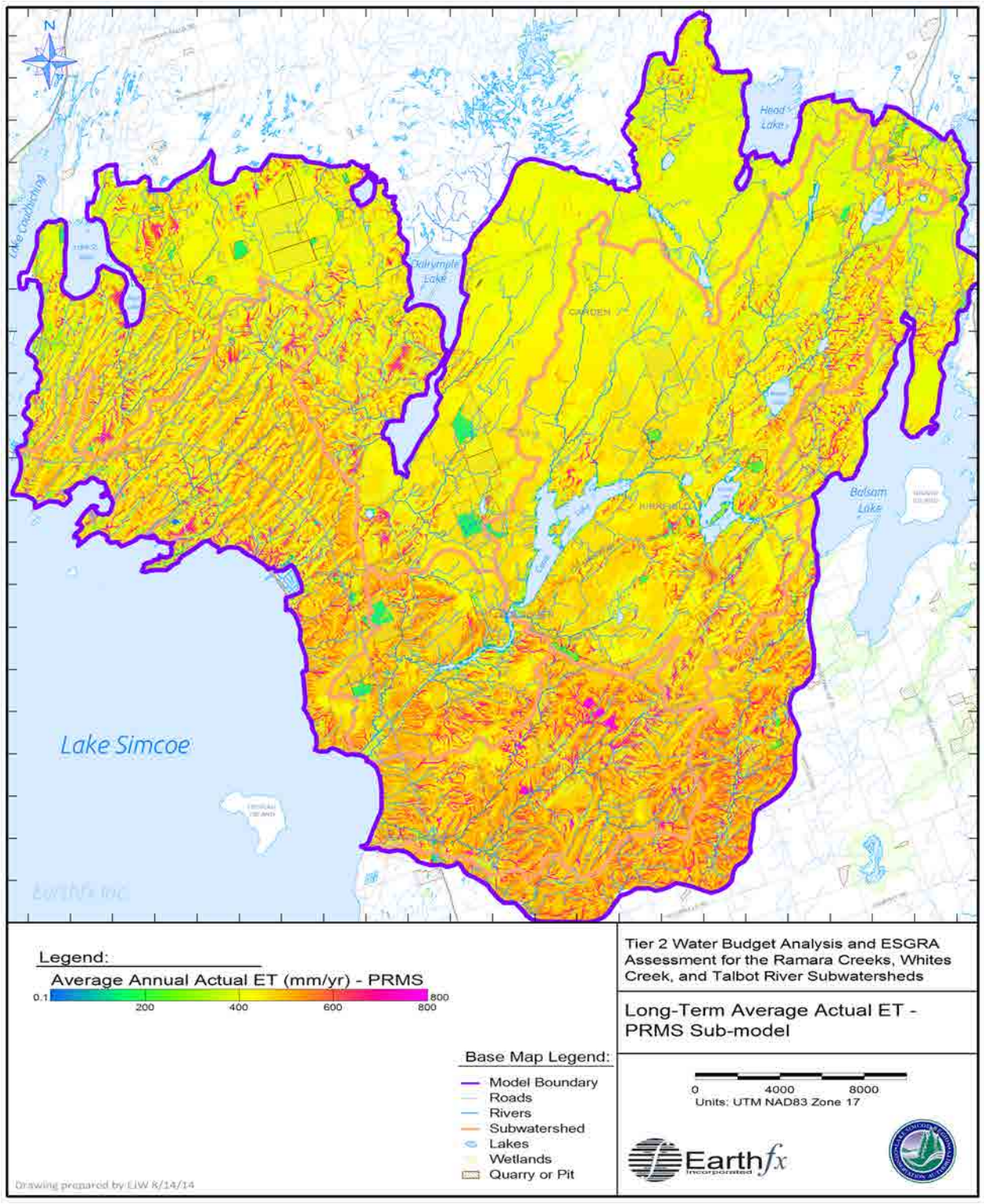

Figure 9.13: Simulated long-term average distribution of actual evapotranspiration.

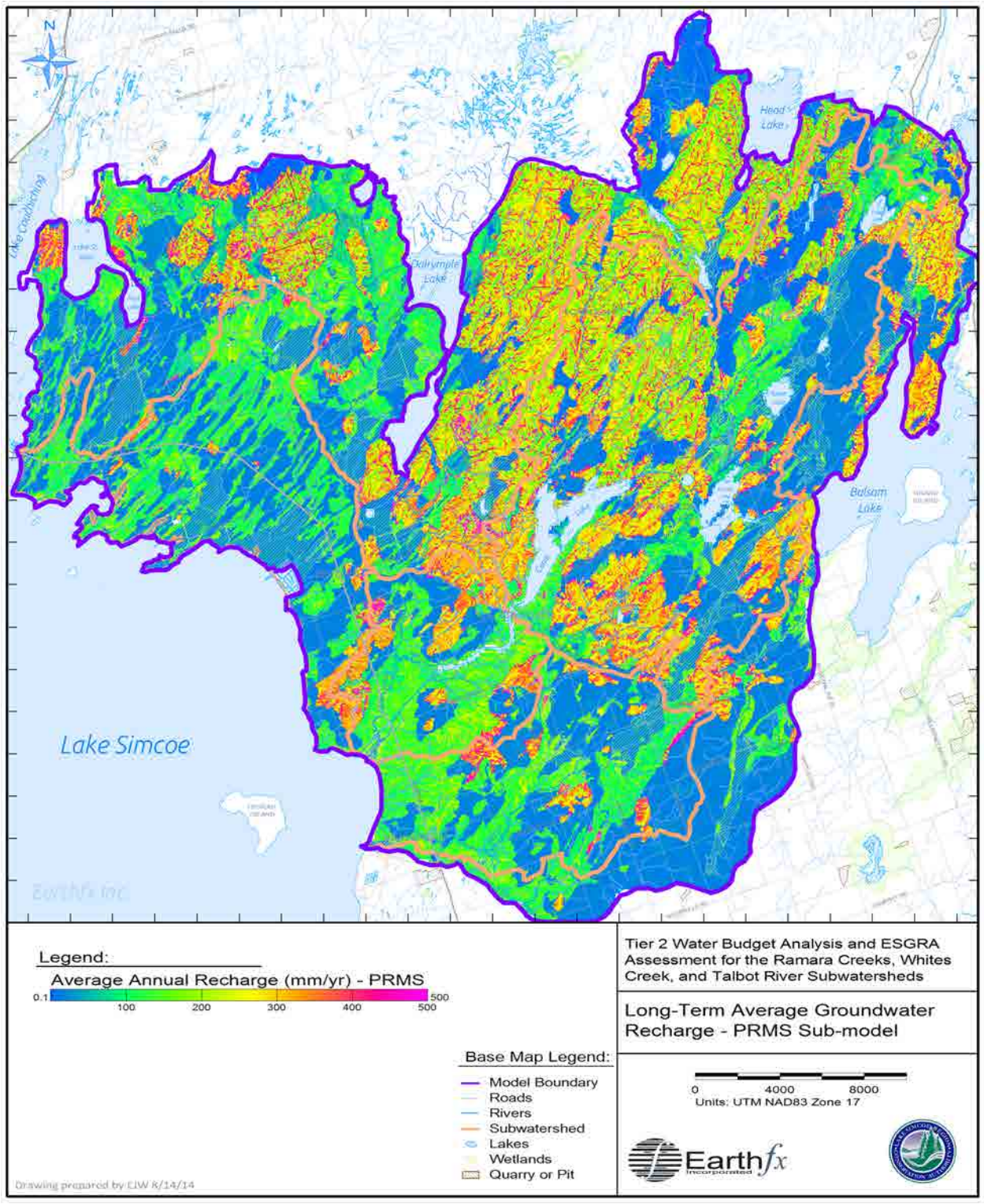

Figure 9.14: Simulated long-term average distribution of groundwater recharge.

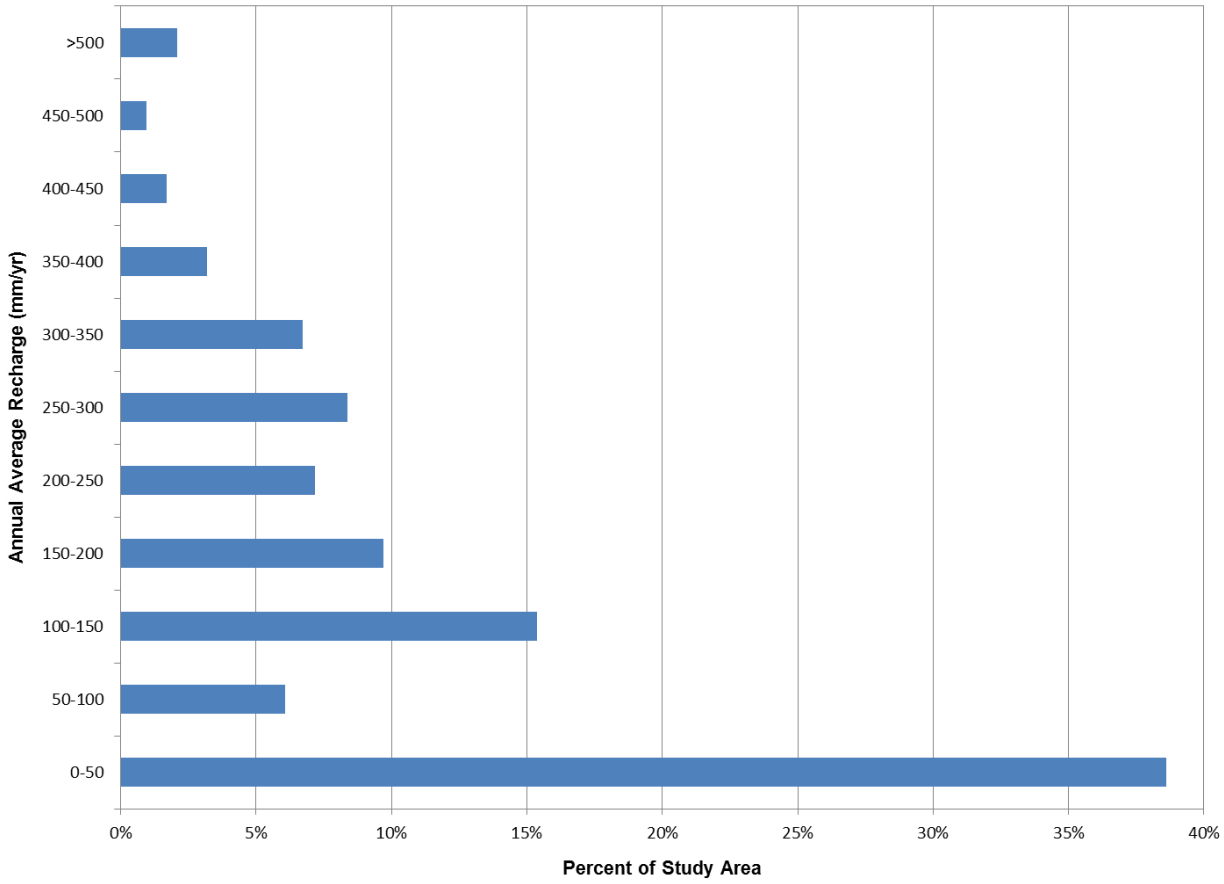

Figure 9.15: Percent of study area for each recharge class.

10 Groundwater Sub-model Development and Calibration

10.1 Overview

The following section describes the construction and steady-state calibration of the groundwater sub-model which is an important component of the integrated GSFLOW model. The independent calibration of the groundwater sub-model was done to test the conceptual hydrostratigraphic model as well as to obtain reasonable values for parameters such as hydraulic conductivity of the aquifers and aquitards that would not change significantly once the sub-model was integrated into GSFLOW.

10.2 Groundwater Flow Model

A groundwater flow model is a simplified representation of the complex physical, hydrologic and hydrogeological processes that affect the rates and direction of groundwater flow. These processes relate to physical characteristics of the study area and include:

- stratigraphy (i.e., the bedrock and overburden stratigraphic layers, unit top and bottom elevations, lateral extent of the formations, and unit thickness);
- hydrostratigraphy (i.e., descriptions of the aquifers and aquitards in the study area, their top and bottom surface elevations, and their lateral extent, thickness, and degree of continuity;
- aquifer and aquitard properties (i.e., estimated hydraulic conductivity, anisotropy, saturated thickness, transmissivity, and storage properties);
- inputs to the hydrologic system (i.e., rates of groundwater recharge and discharge and the underlying processes that affect these rates (e.g., precipitation, evapotranspiration, overland runoff, infiltration, and baseflow));
- properties of the surface-water system and factors controlling groundwater/surface water interaction; and
- anthropogenic inputs and outputs from the groundwater system (e.g., pumping rates and return flows).

The groundwater flow sub-model was developed based on a synthesis of information presented earlier in this report. The conceptual model was refined over the course of this study as our understanding of the study area and the behaviour of the groundwater system and its response to changes in stress improved. Key features of the conceptual model have been presented in the previous report sections. This section primarily describes features of the conceptual model directly related to the construction of the numerical groundwater flow sub-model.

10.2.1 Groundwater Flow Equation

Groundwater flow is governed by Darcy's Law, which states that flow is proportional to the hydraulic gradient and to the hydraulic conductivity of the aquifer material. Darcy's Law can be written as:

— (Eq. 1)

where q is the specific discharge or rate of flow per unit area, K is the hydraulic conductivity, and dh/dx is the hydraulic gradient (change in hydraulic head per unit length). Groundwater flow is also

governed by the Law of Conservation of Mass which states that all inflows to an area must be balanced by outflows and/or by a change in aquifer storage. When the mass balance equation is combined with Darcy's Law, it yields the governing equation for three-dimensional groundwater flow.

$$\frac{\partial}{\partial x}\left(K_{xx}\frac{\partial h}{\partial x}\right)+\frac{\partial}{\partial y}\left(K_{yy}\frac{\partial h}{\partial y}\right)+\frac{\partial}{\partial z}\left(K_{zz}\frac{\partial h}{\partial y}\right)=S_0\frac{\partial h}{\partial t} \qquad \text{(Eq. 2)}$$

where: K_{xx} = Hydraulic conductivity in the x direction;
K_{yy} = Hydraulic conductivity in the y direction;
K_{zz} = Hydraulic conductivity in the z direction;
h = hydraulic head;
S_0 = Specific storage

Hydraulic conductivity is a measure of how easily water can pass through the pores in the geologic unit. Specific storage is a measure of how much water is released from aquifer storage per unit decline in aquifer head per unit volume of aquifer. Water is released from storage when the head decreases due to expansion of the water and due to compression of the pore structure by the increase in intergranular stress. The intergranular stress increases as the water pressure decreases because total stress due to the weight of the overburden remains constant.

In the hydraulic approach to aquifer flow (see Bear, 1979), Equation 2 can be simplified by integrating over the thickness of the aquifer. The resulting equation for two-dimensional flow in a confined aquifer of thickness B with recharge, discharge, and leakage from above and below can be written mathematically (Bear, 1979) as:

$$\frac{\partial}{\partial x}\left(T_{xx}\frac{\partial h}{\partial x}\right)+\frac{\partial}{\partial y}\left(T_{yy}\frac{\partial h}{\partial y}\right)+\left|\frac{K'_U}{B'_U}\left(H_U-h\right)\right|+\left|\frac{K'_O}{B'_O}\left(H_O-h\right)\right|+N-\sum_{k=1}^{Nwell}Q'_k=S\frac{\partial h}{\partial t} \qquad \text{(Eq. 3)}$$

where: T_{xx} = Transmissivity in the x direction (where $T_{XX} = K_{XX}B$);
T_{yy} = Transmissivity in the y direction;
h = hydraulic head;
K' = vertical hydraulic conductivity of an overlying (or underlying) confining unit
B' = thickness of the overlying (or underlying) confining unit;
H_O/H_U = head in the aquifer layer overlying/underlying the confining unit;
N = rate of groundwater recharge;
Q'_K = Pumping rate (per unit area) at well k
S = Storativity or storage coefficient (where $S = S_0B$)

A similar equation can be written for each aquifer in a layered sequence of aquifers and confining units. When an aquifer layer is unconfined, the transmissivity terms T_{XX} and T_{YY} are replaced by the effective transmissivity, equal to $K_{XX}(h-b)$ and $K_{YY}(h-b)$, where b is the elevation of the base of the aquifer. The storage coefficient for an unconfined aquifer is usually replaced with the specific yield, S_Y, which is used to represent water "released from storage" due to the draining of the pore space above the water table as the water table drops. S_Y is generally several orders of magnitude larger that compressive storage.

Equation 3 is a differential equation which formed the basis of the mathematical model developed for the study area. The equation is "solved" to determine aquifer heads at all points in the model area.

Information in the form of aquifer properties, recharge and discharge rates, and conditions along the study area boundaries, are provided as input to the model to make the solution unique to the study area. Numerical methods are needed to solve Equation 3 because study area boundaries are irregular and aquifer/aquitard properties, aquifer geometry (stratigraphy), and rates of recharge and discharge can vary spatially.

If the variation of head over time is considered to be small, for example, when considering equilibrium or long-term average conditions, the term on the right hand side of Equation 5 can be set to zero. This yields the steady-state form of the groundwater flow equation. The steady-state equation is often solved first because it provides information on aquifer hydraulic conductivity properties independent of the aquifer storage properties. Once the hydraulic properties are adjusted sufficiently through calibration to average flows and water levels, then the transient form can be solved to refine estimates of hydraulic properties and determine the storage properties of the aquifer.

10.3 MODFLOW Code

The U.S. Geological Survey (USGS) MODFLOW code was developed to solve Equation 3 using the finite-difference method. The basic MODFLOW-2005 code is documented in Harbaugh (2005). The MODFLOW code is extremely suitable for modelling transient groundwater flow in multi-layered aquifer systems and can easily account for irregular boundaries, complex stratigraphy, and variations in hydrogeologic properties.

A recent version of the MODFLOW code, MODFLOW-NWT (Niswonger *et al.*, 2011), is especially well suited for representing thin aquifers and sharp changes in model layer stratigraphy, such as that occurring along the Niagara Escarpment. MODFLOW-NWT is incorporated in Version 1.1.6 of GSFLOW, which was employed in this study.

10.4 Model Layers

MODFLOW uses the finite-difference method and requires that the study area be subdivided vertically into several layers, where each layer can represent a hydrogeologic unit or subunit (such as the Green Marker Beds of the Gull River Formation or the weathered bedrock layers). There are a several possible approaches that can be used to represent hydrostratigraphy with the MODFLOW code. In the Ramara-Whites-Talbot Tier 2 model, the study area was subdivided vertically into seven numerical model layers, where each layer was occupied by one or more of the fourteen hydrostratigraphic units discussed in Section 5.3.

The Carden Plain physiographic region, with it's thin to absent overburden and high degree of karstification of the exposed limestone bedrock, was represented in the model using a separate and distinct conceptualization from the regional model. Where the top two layers in the model are generally assigned properties of overburden materials, the top two layers in the Carden Plains region were used to represent the solutionally enhanced bedrock. The underlying Layers 3 through 7 were kept conceptually consistent with those of the regional model. The seven layer model is presented below in Figure 10.1.

<table>
<tr><th colspan="2">GEOLOGIC LAYERS
(Earthfx, 2013)</th><th colspan="2">HYDROSTRATIGRAPHIC LAYERS
Regional Conceptual Model | Carden Plains (Alvar Conceptual Model)</th></tr>
<tr><td rowspan="5">OVERBURDEN</td><td>Post-Glacial Deposits</td><td rowspan="4">Layer 1 and Layer 2 - Surficial Deposits</td><td rowspan="4">(PRMS Soil Zone Representation)</td></tr>
<tr><td>Glaciofluvial Sediments</td></tr>
<tr><td>Dummer till</td></tr>
<tr><td>Newmarket Till</td></tr>
<tr><td>Thorncliffe / Channel Sediments</td><td>Layer 3 (aquifer) - Thorncliffe/Channel Sediments/Weathered Bedrock</td></tr>
<tr><td rowspan="6">PALEOZOIC BEDROCK</td><td>Lindsay Formation</td><td rowspan="4">Layer 4 (aquitard) - Interbedded Limestone and Shale of Verulam and Lindsay Formations/ Unweathered limestone of Bobcaygeon Formation and Upper Gull River</td><td rowspan="2">(Formations Not Present)</td></tr>
<tr><td>Verulam Formation</td></tr>
<tr><td rowspan="2">Bobcaygeon Formation</td><td>Layer 1 and Layer 2 - Alvar Fracture Network</td></tr>
<tr><td>Layer 3 (aquifer) - Weathered Bedrock</td></tr>
<tr><td>Upper Gull River</td><td rowspan="2">Layer 4 (aquitard)</td></tr>
<tr><td>Green Marker Bed</td><td>Layer 5 (aquifer) - Green Marker Bed</td><td>Layer 5 (aquifer) - Green Marker Bed</td></tr>
<tr><td>Lower Gull River</td><td>Layer 6 (aquitard)</td><td>Layer 6 (aquitard)</td></tr>
<tr><td>Shadow Lake Formation</td><td rowspan="2">Layer 7 (aquifer) - Shadow Lake/Fractured Precambrian</td><td rowspan="2">Layer 7 (aquifer) - Shadow Lake/Fractured Precambrian</td></tr>
<tr><td>PRECAM BEDROCK</td><td>Precambrian</td></tr>
<tr><td colspan="2"></td><td>(model base)</td><td>(model base)</td></tr>
</table>

Figure 10.1: MODFLOW model layers (regional and alvar conceptual models).

An important consideration in translating the conceptual model layers to numerical model layers is that MODFLOW requires continuity of aquifer layers whereas the hydrostratigraphic model can have layers of zero thickness. The hydrostratigraphy of the study area presented a unique challenge because all of the Paleozoic bedrock units gradually pinch out towards the northern end of the study area and the regional overburden distribution is both discontinuous and highly variable.

To observe layer continuity requirements for the numerical model, a minimum layer thickness of 1.0 m was set when generating of MODFLOW model layers. Where fewer than seven geologic layers were present to assign to the seven numerical model layers, the minimum model layer thickness was applied and hydraulic properties were “inherited” from the next underlying layer. For example, in areas where no appreciable thickness of overburden was present, the top two layers (which typically represented the tills and post-glacial sediments) would each be assigned a thickness of 1.0 m and take on the hydraulic properties of the underlying weathered bedrock hydrostratigraphic unit.

Figure 10.2 and Figure 10.3 present the hydrostratigraphic layers used in the numerical model for section A-A’ which crosses through the regional conceptual model and section B-B’ which crosses through the alvar conceptual model. Section locations are shown in Figure 3.34.

10.5 Model Grid

The finite-difference method also requires that the study area be subdivided into a grid of small square or rectangular cells. One particular feature of the GSFLOW formulation is that the grid used for the soil water balance can be different from the one used for the groundwater model (Figure 7.4). As discussed in the previous chapter, the PRMS sub-model grid was composed of uniform square cells, 50 m on a side.

A uniform grid was designed for the MODFLOW sub-model with square cells, 200 m on a side. The model grid consists of 217 rows and 233 columns and contains 50,561 grid cells for each of the seven model layers. The cell size of 200 m was selected to reduce model run times, while still providing sufficient resolution to capture hydrogeologic features for the water budget analysis.

MODFLOW works in a local, grid coordinate system based on row and column numbers. The software package VIEWLOG (Kassenaar, 2013) was used to help translate geo-referenced map data into MODFLOW coordinates. The local origin for the model grid is at UTM coordinates 628400 E and 4918000 N. The grid shared the same origin as the PRMS sub-model grid. All digital maps and well data for the study area were referenced using NAD83 (UTM Zone 17) coordinates.

10.6 Model Boundary Conditions

Boundary conditions were specified for cells that lie along lines corresponding to the physical boundaries of the groundwater flow system. MODFLOW can represent three general types of boundary conditions: constant-head; no-flow; and head-dependent discharge boundaries. All three types were employed in the Ramara-Whites-Talbot Tier 2 model.

10.6.1 Constant-Head and No-Flow Boundary Conditions

Constant head (Type 1) boundary conditions were applied along the model boundary in areas corresponding to lakes and water courses. It was assumed that the groundwater heads in the model layers are in hydrostatic equilibrium with water levels in the hydrologic features. As presented in Figure 10.5, constant head boundary cells along the top of the model represent Lake St. John, Dalrymple Lake, and Head Lake, loosely following the path of the Black River and Head River. From Head Lake, the constant head cells follow the Gull River east to Shadow Lake and then to Balsam Lake to the south. Representative lake stages were assigned based on local Ontario Base Maps (National Topographic System, 1999a; 1999b, 1999c, 1999d), and are presented in Table 10.1.

Groundwater heads assigned to constant head cells associated with rivers, streams, and wetland complexes were assumed to be at ground surface and were therefore assigned values based on elevations in model Layer 1.

Constant head cells were placed at the southern end of the model boundary, extending inland from the eastern shore of Lake Simcoe along the Beaver River. Constant heads along this boundary ranged from 221.3 masl to 241.2 masl. The model boundary transects a 2.5 km span of gently west-sloping terrain across which flow is interpreted to be normal to the model boundary, before intercepting a tributary of the Beaver River where heads are assumed to once again be at land surface, ranging from 259.8 masl to 263.6 masl.

A topographic high in the southeast corner of the model was identified as an area of groundwater recharge from which groundwater is expected to flow radially outward, parallel to the model

boundary. The model boundary in this area was therefore assumed to be a no-flow boundary. The analysis of MOE static water levels in the area supported this interpretation. To the south of Balsam Lake, the model boundary follows a wetland complex, through which groundwater heads are assumed to be at ground surface, between 256.6 masl and 260.0 masl.

Along the shorelines of Lake Simcoe and Balsam Lake (Figure 10.5), constant head boundary conditions were varied seasonally to capture the impacts of fluctuating lake levels on the nearby groundwater systems. The Lake Simcoe water levels were adjusted according to a rule curve while water levels in Balsam Lake were varied according to the average historical water levels reported by Parks Canada (Figure 10.6).

A no-flow boundary condition was applied along the remaining lateral boundaries of the model, indicating that flow across the external boundaries was expected to be negligible. A no-flow boundary condition was also applied at the base of the lowest model layer. This assumes that little flow is exchanged between the model layers and the unweathered Precambrian basement.

10.6.2 Head-Dependent Discharge

A third type of boundary condition, head-dependent discharge, was used extensively to represent groundwater/surface water interaction processes. Flow between the groundwater and surface water systems was assumed to be exchanged as "leakage" across a lake bed or streambed assumed to be of lower hydraulic conductivity than the underlying aquifer. The rate of leakage is determined based on Darcy's Law where:

$$Q_{Leak} = \frac{K'}{B'} A_L (H_L - h) \qquad \text{(Eq. 6)}$$

where:
- Q_{LEAK} = volumetric flow rate between aquifer and stream or lake;
- K' = vertical hydraulic conductivity of the stream or lake bed;
- B' = thickness of the streambed or lake bed;
- A_L = wetted area of the streambed or lake bed and sides;
- H_L = stream or lake stage (in masl); and
- H = head in the aquifer

Leakage between the stream and the aquifer is calculated on a cell-by-cell basis using the SFR2 module in MODFLOW (Niswonger and Prudic, 2005). In SFR2, a stream "reach" is defined as the portion of a stream within a model cell (see sketch below). The area A_L in Equation 6 is equal to the wetted area of the reach. Head in the aquifer, h, is the head in the cell and H_L is the stage in the centre of the reach. Stream stage in the reach is calculated based on stream channel properties and the sum of upstream inflows, precipitation, evaporation, and overland flow to the reach (as calculated by the PRMS sub-model). Multiple reaches can occur within a single cell although, ideally, the cells should be small so that the head in the cell accurately represents the head in the aquifer beneath the streambed. The representation of the stream network and the calculation of stream stage and flow within the GSFLOW model are discussed in greater detail in Section 8.2.

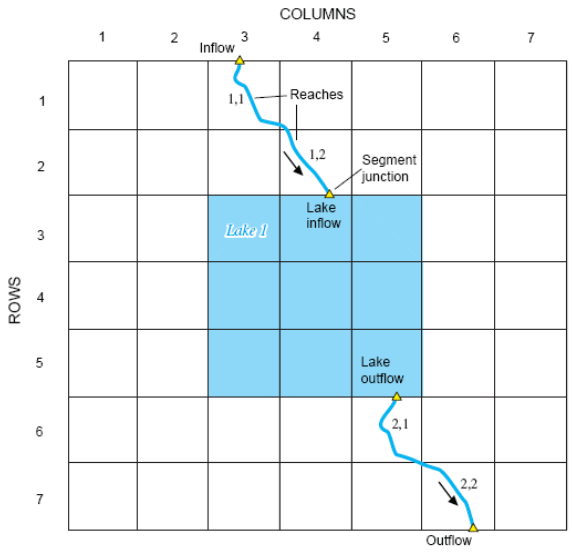

Leakage between lakes or other standing bodies of water and the aquifer is also governed by Equation 6 and is calculated on a cell-by-cell basis using the LAK3 module in MODFLOW (Merritt and Konikow, 2000). In LAK3, a cell can represent all or a portion of a lake (see sketch above). The area A_L in Equation 6 is equal to the cell area. Head in the aquifer, h, is the head in the cell underlying the lake and H_L is the lake stage. Lake volumes are calculated in a separate water budget analysis based on the sum of upstream inflows (as computed by the SFR2 module), precipitation, evaporation, overland flow to the lake (as calculated by PRMS), and outflow from the lake (also calculated by SFR2 based on lake stage). Lake stage is calculated from stage-volume relationships. Lakes can penetrate multiple model layers and leakage to cells adjacent as well as underlying the lake. Further discussion on the representation of the lakes and quarry ponds in the model can be found in Section 8.6.

10.7 Groundwater Recharge

When MODFLOW-only simulations are run, recharge to the upper model surface must be specified as an input value. The rate of groundwater recharge is often not known precisely, however, and must be estimated. For the steady-state calibration described in this section, groundwater recharge rates were estimated based on the long-term average of annual recharge rates from the PRMS-only simulations described in Section 9.4.2 and shown in Figure 9.14. PRMS sub-model results were resampled to the model grid (Figure 10.7) and ranged from near zero to 500 mm/yr, reflecting the combined effects of spatial variation in climate, topography, land cover, and soil properties. It should be noted that the MODFLOW-only simulations do not provide feedback to the PRMS sub-model.

Recharge is simulated in the MODFLOW sub-model with the UZF unsaturated flow module (Niswonger *et al.*, 2005). The module simulates percolation of moisture from the soil zone to the water table, groundwater ET processes, and the return of excess infiltration to the surface. The UZF module also handles the particularly complex problem of the water table rising into the soil zone or highly weathered exposed alvar bedrock units in the Carden Plain.

For transient GSFLOW simulations, net recharge to the unsaturated zone is calculated by the PRMS sub-model on a daily basis. Because the position of the water table can affect the amount of net recharge, the PRMS sub-model is run iteratively with the MODFLOW sub-model until convergence is achieved between the two models and a mass balance is obtained for the time step (Markstrom & Niswonger, 2008).

10.8 Groundwater Takings

Groundwater use in the study area was discussed in Section 6. Non-quarry related takings are represented in the MODFLOW sub-model using the WEL module. Withdrawals for permitted municipal and non-municipal groundwater takings were represented in the model. The water takings were assigned to the appropriate model layer based on the placement of the well screen (where known or reasonably estimated).

For the steady-state MODFLOW-only simulations, average pumping rates were applied. Averages of the reported actual takings from the WTRS database (2005 to 2011) were used where available. Where no WTRS data were available, average daily withdrawals were estimated based on the maximum permitted takings.

The three municipal well fields (consisting of 8 wells) were assigned average takings based on the reported WTRS data for the calibration period and to simulate existing conditions. As discussed in Section 6.9, future demand for the municipal wells was estimated based on projected population increases for the Ramara Creeks and Talbot River subwatersheds. Future demands are presented in Table 10.2. Non-municipal groundwater takings were not increased for future scenarios, consistent with the MNR (2011).

MNR (2011) provides consumptive use factors for different usage classes and sub-classes. Consumptive use was determined by multiplying the estimated takings by consumptive use factors that account for the return flow of water back to the aquifer from which they were extracted. The simulated demands for the permitted groundwater takings, corrected for consumptive use, are presented also in Table 10.2. To be conservative, all municipal wells were simulated as being 100% consumptive, although it is likely that some return flow to the aquifer occurs through septic systems and lawn watering.

Discharge from the quarries was not represented directly as a groundwater taking. Instead, quarry floor drains that conveyed seepage to the sump were represented in SFR2, as described in the next section. Water pumped out of the sumps is discharged offsite, usually to a stream or wetland.

10.9 Groundwater Model Parameters

Aquifer properties, such as top and bottom elevations for each layer, hydraulic conductivity, and storage coefficients are assigned to each cell. Layer tops and bottoms were assigned using information from the hydrostratigraphic model (Section 10.4). Initial estimates for hydraulic properties were made based on the data presented in Section 5.5.

A considerable amount of effort was spent to refine the estimates of hydraulic properties through model calibration. Property values were adjusted to best match observed static and time-dependent groundwater levels and the limited streamflow data. Calibration was mostly done through a trial-and-error procedure with simulated values checked visually against observed data (see Section 5.4).

Where possible, automated parameter estimation techniques were employed to refine the calibration of some hydraulic conductivity values. Monte Carlo analyses were employed for selected parameters to assist with understanding parameter sensitivity and optimal ranges. Calibration of the upper and lower bedrock aquitards and the Green Marker Bed aquifer was undertaken using this approach. The results of nearly 5,000 realizations are presented in Figure 10.8, which shows an

optimal regional for the Upper and Lower Bedrock aquitards at $1x10^{-8}$ to $5x10^{-8}$ m/s with slightly higher permeability expected in the Upper Bedrock aquitard. The results of the Monte Carlo analysis yielded a lower than anticipated hydraulic conductivity for the Green Marker Bed aquifer (approximately $1x10^{-7}$ m/s). It should be noted that this value is still within the range of field measurements for this unit (as presented in Table 5.2). The lower calibration value suggests that the observed fracturing may be localized and not regionally extensive as initially thought.

For the sake of parsimony, the spatial variation of hydraulic properties was represented in a manner that was simple yet did not compromise the reliability of the model. To this end, uniform properties were assigned to the hydrostratigraphic units. Table 10.3 lists the final calibrated properties for each material and hydrostratigraphic unit. Maps showing the spatial distribution of the final calibrated hydraulic conductivity values for Layers 1 through 7 are presented in Figure 10.9 through Figure 10.15, respectively.

Figure 10.16 and Figure 10.17 show the assigned hydraulic conductivity values for each model layer along sections A-A' and B-B', respectively. Examples of the application of property inheritance can be seen in the sections.

10.10 Steady-State Groundwater Model Calibration

10.10.1 Calibration Targets

As discussed earlier, the model was first calibrated for steady-state conditions to provide information on aquifer hydraulic conductivity properties independent of the aquifer storage properties. Insights gained through testing of the steady-state model served to inform the calibration of the transient, integrated GSFLOW model.

The steady-state analysis also provided an opportunity to match general flow patterns across the model area based on an analysis of static water levels obtained from multiple sources including the MOE WWIS database, static water levels from other geotechnical and consultant wells (mainly quarry related), and average water levels from long-term water-level monitoring sites (i.e., the PGMN well and quarry monitors).

Processing and filtering of the data were discussed previously in Section 5.4.2.1. The locations of available static water levels from well records were shown in Figure 5.2. Gaps in the spatial coverage were noted in the largely unsettled portions of the Carden Plain toward the northern end of the study area, while the study subwatersheds were generally well represented.

The interpolated groundwater levels (Figure 5.4) showed a number of significant features that needed to be matched by the numerical model, including:

- a westward to southwestward trend in regional groundwater flow toward the eastern shores of Lake Simcoe, where water levels approach average lake elevation of approximately 220 masl.
- radial groundwater flow patterns from a groundwater mound located to the north of the Ramara Creeks subwatershed, to the west of Dalrymple Lake;
- a second regional mounding of groundwater located directly southeast of Canal Lake, likely associated with the top of one or more incised bedrock valley features;
- the influence of major water courses on the groundwater system, as evidenced by characteristic "v-shaped" contours along the Talbot River, downstream of Canal Lake;

- a regional groundwater high along the southeastern study boundary and another along the northeastern study boundary; and
- groundwater patterns with characteristically gentler gradients approaching the shores of Lake Simcoe, compared to steeper gradient (evidenced by closely spaced equipotential contours) within the upper portions of the study subwatersheds.

In addition to average groundwater potentials, the steady-state model provides information on stream discharge. It should be recognized that the simulated average discharges do not reflect total streamflow. Critical surface/subsurface processes are not represented (e.g., interflow, through-flow, Hortonian runoff). Instead, stream discharges in the groundwater model represent long-term averages of the groundwater contribution (baseflow) to the stream reaches, routed down the dendritic stream network. This important distinction highlights both the limitations of the groundwater-only steady-state model, as well as a clear advantage of the fully integrated surface water/groundwater modelling approach.

Estimated baseflow at the WSC streamflow gauges served as a useful secondary calibration target for other steady-state models built for other watersheds in southern Ontario (e.g., Earth*fx*, 2013). As discussed in Section 4.3.2, the period of record for the gauges in the study area is quite limited and the Talbot River gauge is affected by canal operations. Other limitations of baseflow separation methods were noted including the inability to distinguish between groundwater discharge and other relatively steady flows such as discharge from reservoirs, highly regulated navigational waterways, or large wetlands. As such, only Whites Creek gauge LS0402 was considered to be a reasonable candidate location for a baseflow separation analysis.

As noted earlier, the reported on-site and off-site quarry discharges served as another calibration target for the steady-state model. Quarry discharges were particularly sensitive to the aquifer and aquitard properties because groundwater seepage into the excavations represents a major portion of the flows recorded at the quarry sump ponds and off-site diversions. By calibrating to the average quarry discharge, the steady-state model was further constrained.

10.10.2 Calibration Results – Groundwater

Model calibration was conducted by adjusting aquifer properties and refining estimates of recharge provided by the PRMS model until a good match was achieved between the simulated and observed heads. Figure 10.18 provides a comparison between the simulated steady-state water levels and interpolated static water levels for the weathered bedrock interface aquifer. A visual check indicates that good matches were achieved to the interpolated WWIS data. Areas where the match was not as good tended to be areas where observation data were sparse and the interpolated values were less certain.

Statistical analyses can also be applied to test the quality of the calibration. A scatterplot comparing all WWIS water levels to the simulated steady-state heads is shown in Figure 10.19. Ideally, all data points should fall on the 1:1 line shown on the plot. For the most part, the data point fall within the ±10 m error interval, defined by the dashed red lines.

Three calibration statistics were used to assess and demonstrate model accuracy: the mean error (ME), mean absolute error (MAE), and root mean squared error (RMSE). These are given by Anderson and Woessner (1992) as:

$$\text{Mean Error} \quad -\Sigma \qquad \text{(Eq. 10)}$$

Mean Abolute Error -∑ |Eq.11)

Root Mean Squared Error $\sqrt{\sum}$- (Eq. 12)

where;

= observed head;
= simulated head; and
= number of observations.

Individual calibration statistics for the three major aquifer units (consisting of the weathered bedrock interface, the Green Marker Beds, and the Shadow Lake/Precambrian nonconformity) are presented along with the overall calibration statistics for the 2,533 observed water levels in Table 10.4. A scatterplot comparing the observed water levels within these aquifers to the simulated steady-state heads is shown in Figure 10.20.

The negative sign on the Mean Error (ME) indicates that model predicted values are generally higher than the observed values by 0.5 m (specifically, 0.67 m higher in the weathered bedrock aquifer, 1.24 m higher in the Green Marker beds aquifer, yet 0.13 below observed water levels in the Shadow Lake aquifer). The Mean Absolute Error (MAE) and the Root Mean Squared Error (RMSE) provide a good estimate of the average magnitude of the difference and variance between observed and simulated values. Overall, the calibrated groundwater sub-model had a MAE of 2.40 m and a RMSE of 3.25 m.

Generally accepted guidelines indicate that the model is well calibrated when the RMSE is less than 10% of the range of water levels (Spitz and Moreno, 1996). The overall RMSE expressed as a percentage of the range in MOE observation data was 3.8%, which is less than this calibration guideline. Using the same criterion to independently evaluate the calibrations of the weathered bedrock, Green Marker Bed, and Shadow Lake aquifers yields values of 3.7%, 6.2%, and 4.9%, respectively. The MODFLOW mass balance error for the steady state model was 0.00 percent.

10.10.3 Calibration Results – Baseflow

Figure 10.21 shows the simulated average groundwater discharge to streams (in m^3/d) on a cell by cell basis as determined using the calibrated steady-state model. Areas in blue are reaches where groundwater is discharging to the streams (gaining reaches) which dominate the study area. Areas in red, such as downstream of the Talbot Lock #38 are reaches that lose water to the aquifer (losing reaches). Losing streams can also be seen around the simulated quarries where lowered groundwater heads from quarry dewatering and increased discharges to streams imparts a downward gradient into the groundwater system.

Figure 10.22 shows the accumulated flow as it is routed downstream in m^3/s. The flows were assigned to the model cells containing the stream reach for visualization purposes. Rates range from near zero in some of the headwater reaches to 3.36 m^3/s and 0.24 m^3/s where the Talbot River and Whites Creek discharge to Lake Simcoe, respectively.

Simulated baseflow at the Whites Creek gauge and the estimated baseflow values for the LSRCA streamflow gauge LS0402 (Whites Creek at Regional Road 23) were compared as one of the secondary calibration targets. The simulated average groundwater discharge was 0.24 m^3/s, which

is approximately 33% lower than the estimated baseflow of 0.36 m³/s. Discharge from the large wetland complex located approximately 12 km upstream of the gauge may account for a significant component of the estimated baseflows and the actual groundwater discharge component is smaller than the estimated baseflow value. Summertime low flows at this gauge historically drop to within the range of 0.007 m³/s to 0.10 m³/s, suggesting that the simulated value is not unreasonable for this location.

The second LSRCA operated streamflow gauge in the study area – LS0109 – is located on the Talbot River near Gamebridge. This monitoring location is considered to be highly influenced by the operations of the upstream diversions within the Trent-Severn waterway. Despite the high degree of uncertainty in the estimates of observed baseflow, the simulated baseflow value of 3.11 m³/s is close to the average observed discharge of 5.45 m³/s, which includes both baseflow and contributing runoff volumes.

Average recorded discharges for eleven quarry operations are compared to the simulated (baseflow) discharges for the off-site diversions in Table 10.5Table 10.5: Simulated and reported off-site quarry discharges. It should be recognized when comparing the observed (average discharge) and predicted (simulated) discharges, that the simulated values do not account for the storage of collected seeped groundwater or surface runoff in quarry sumps or settling ponds, which would be subject to evaporative losses and reduce off-site discharges. This resulted in a tendency to overestimate the quarry discharge rates. Furthermore, average reported discharges date back as far as 2005, while simulated quarry footprints and bench elevations are based on more recent records (2012); as excavations extend outward and into deeper units, increased dewatering requirements (and offsite discharge volumes) are expected to increase. Average reported off-site discharge volumes may therefore be biased lower as a result.

10.11 Figures and Tables

Table 10.1: Lake Elevations Applied to Constant Head Boundary Cells.

Lake Name	Elevation (masl)
Lake St. John / Mud Lake	219.4
Young Lake	227.2
Dalrymple Lake	226.0
Head Lake	268.0
Oak Lake	276.0
Beechnut Lake	278.0
Shadow Lake	259.0
Balsam Lake*	255.6 – 256.2
Lake Simcoe / Lake Couchiching*	218.5 – 219.5

Note:
** Constant head boundary condition varied seasonally to reflect changes in lake levels.*

Table 10.2: Simulated groundwater takings used for the steady-state model calibration.

Permit Holder	Well Name	Sub-watershed	Layer	Row	Column	Consumptive Use Factor	Current Rate [m³/d]	Future Rate [m³/d]
Val Harbour	Well 1	Ramara	3	125	34	1.0	11.0	15.0
	Well 2		3	125	35	1.0	24.0	32.8
	Well 3R		3	124	36	1.0	0.0	0.0
Bayshore Village	Well No. 3	Ramara	3	133	39	1.0	43.8	59.9
	Well No. 4		3	133	39	1.0	162.2	221.9
	Well No. 5		3	132	39	1.0	59.5	81.4
Western Trent/Palmina	Well #1 (Palmina)	Talbot	7	138	124	1.0	36.5	40.2
	Well #1 (Western Trent)		7	131	128	1.0	36.0	39.6
Bayshore Village Golf Course	Well #1	Ramara	3	133	41	0.7	9.8	9.8
Western Trent Golf Club Ltd.	Well #1	Talbot	6	140	123	0.2	13.0	13.0
Green Line Properties Ltd	Artisan Spring Well	--	5	103	8	0.2	5.2	5.2
	Campground Well		3	104	9	0.2	0.0	0.0
City of Kawartha Lakes	Campgrounds Well 1	Talbot	7	132	134	0.2	3.8	3.8
Mara Provincial Park	Campground Well	Ramara	3	114	9	0.2	1.5	1.5
Monck's Landing Golf Club	Source Pond	--	3	30	213	0.7	4.0	4.0
	TW-1 Clubhouse Well		6	29	211	0.2	2.0	2.0

Table 10.3: Calibrated aquifer and aquitard properties.

Hydrostratigraphic unit	Hydraulic Conductivity (m/s)	Aniso-tropy (K_H/K_V)	Specific Yield	Specific Storage
Post-glacial Deposits	7.1×10^{-6}	5	0.20	3.0×10^{-4}
Mackinaw Interstadial Sands	5.0×10^{-5}	3	0.20	3.0×10^{-4}
Newmarket Till	1.3×10^{-7}	4	0.07	3.0×10^{-4}
Weathered Till	1.8×10^{-6}	4	0.07	3.0×10^{-4}
Dummer Till	1.8×10^{-6}	6	0.07	3.0×10^{-4}
Weathered Lindsay/Verulam Aquifer	3.9×10^{-5}	3	0.20	1.0×10^{-5}
Weathered Bobcaygeon./Gull River Aquifer	8.0×10^{-5}	3	0.20	1.0×10^{-5}
Alvar (Highly Weathered)	1.0×10^{-4}	3	0.07	1.0×10^{-6}
Alvar (Less Weathered)	7.0×10^{-5}	3	0.07	1.0×10^{-6}
Upper Bedrock Aquitard	3.3×10^{-8}	50	0.07	1.0×10^{-6}
Green Marker Bed	1.0×10^{-7}	10	0.07	5.0×10^{-6}
Lower Bedrock Aquitard	1.1×10^{-8}	50	0.07	1.0×10^{-6}
Shadow Lake-Precambrian Aquifer	1.5×10^{-4}	8	0.07	5.0×10^{-6}
Unweathered Precambrian	2.6×10^{-9}	50	0.07	1.0×10^{-6}

Table 10.4: Calibration statistics for the shallow and deep groundwater systems.

	Weathered Bedrock	*Green Marker Bed*	*Shadow Lake*	*Other*	**Overall**
No. of Observations, n	1,787	79	213	454	**2,533**
ME (m)	-0.67	-1.24	0.13	0.00	**-0.50**
MAE (m)	2.36	2.77	2.94	2.26	**2.40**
RMSE (m)	3.14	3.95	3.91	3.18	**3.25**
Range in Observations (m)	85.73	63.56	80.04	76.37	**85.73**
RMSE as % of Range (%)	3.7%	6.2%	4.9%	4.2%	**3.8%**

Table 10.5: Simulated and reported off-site quarry discharges.

Permit Holder	Well Name	Maximum Permitted Taking (m^3/d)	Average Demand (m^3/d)	Simulated Average Discharge (m^3/d)
Five W Farms Inc.	Quarry Sump	12,528.0	537.2	388.5
James Dick South	Sump Pond	2,880.0	500.3	675.6
Lafarge Kirkfield Quarry [1]	Quarry Sump (Kirkfield Quarry)	4,320.0	0.0	0.0
Lafarge Brechin Quarry	Quarry Sump (Brechin Quarry)	3,600.0	982.1	1,606.7
Bot Aggregates Ltd.	Quarry Sump	1,226.9	18.0	213.5
Ferma Aggregates Inc.	Quarry Sump A	1,569.6	7.7	117.1
Holcim (Canada) Inc.	Carden Quarry Sump	5,237.3	1,877.1	2,174.4
McCarthy Quarry	Quarry Sump (McCarthy Quarry)	6,544.8	0.0	0.0
R.W. Tomlinson Ltd.	North Quarry Sump	18,230.4*	25.5	613.8
	South Quarry Sump	10,281.6*	0.0	0.0
Beamish Quarry	Sump Pond	5,011.0	0.0	0.0
Miller Paving Ltd.	Sump Pond	6,500.0	2,783.1	5,587.1

Note:

[1] Average quarry discharges are based on reported values from 2005 to 2011.

[2] Simulated discharge represents accumulated baseflow (groundwater discharge) only; predicted discharge rates do not account for considerable contributions from runoff, direct precipitation, snowmelt etc.

[3] Only dewatering related permitted discharges are included in this table; permitted water use for industrial purposes (i.e., aggregate washing or dust suppression) are not included.

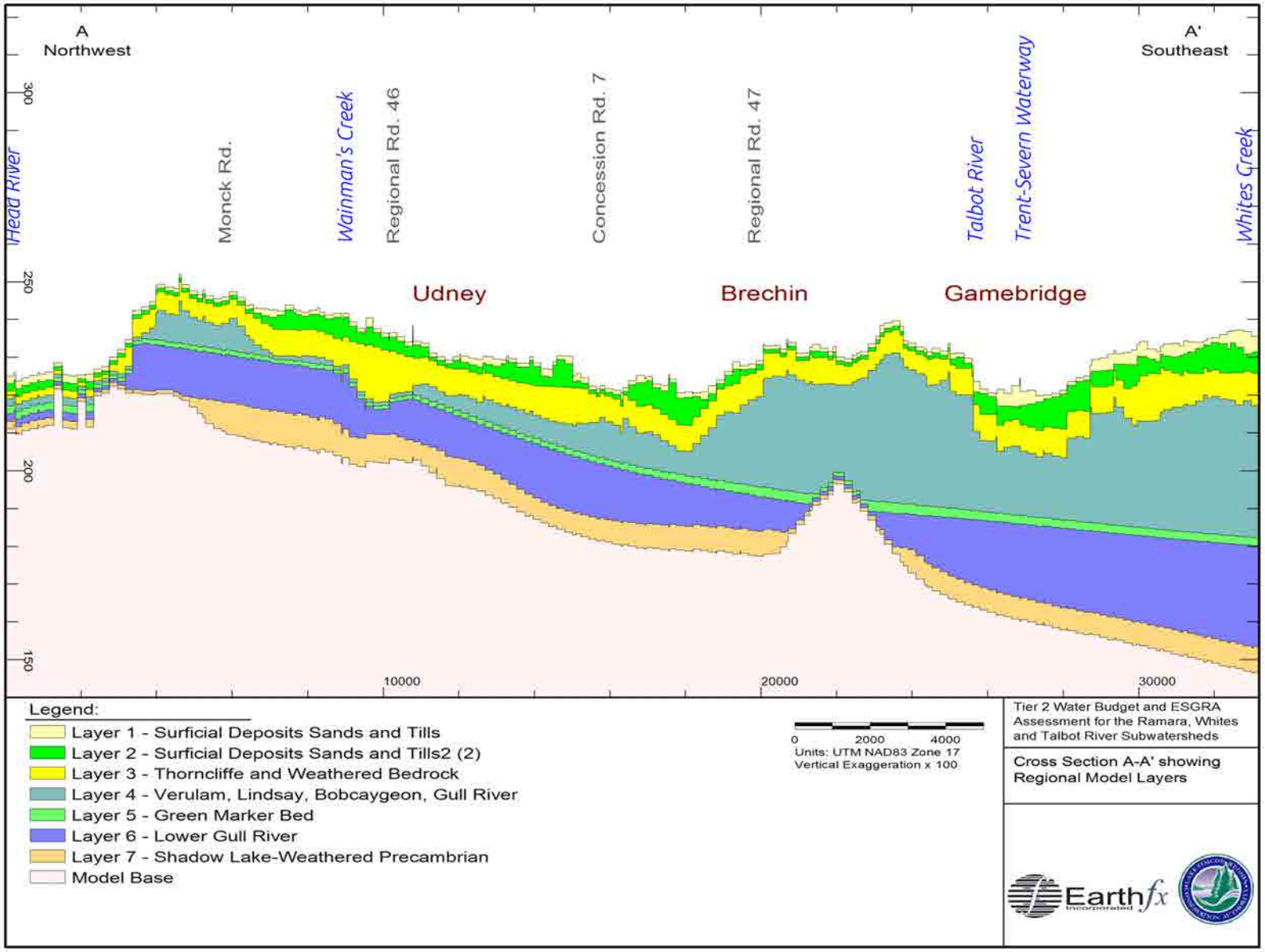

Figure 10.2: Northwest-southeast section A-A’ showing numerical model layers for the regional conceptual model.

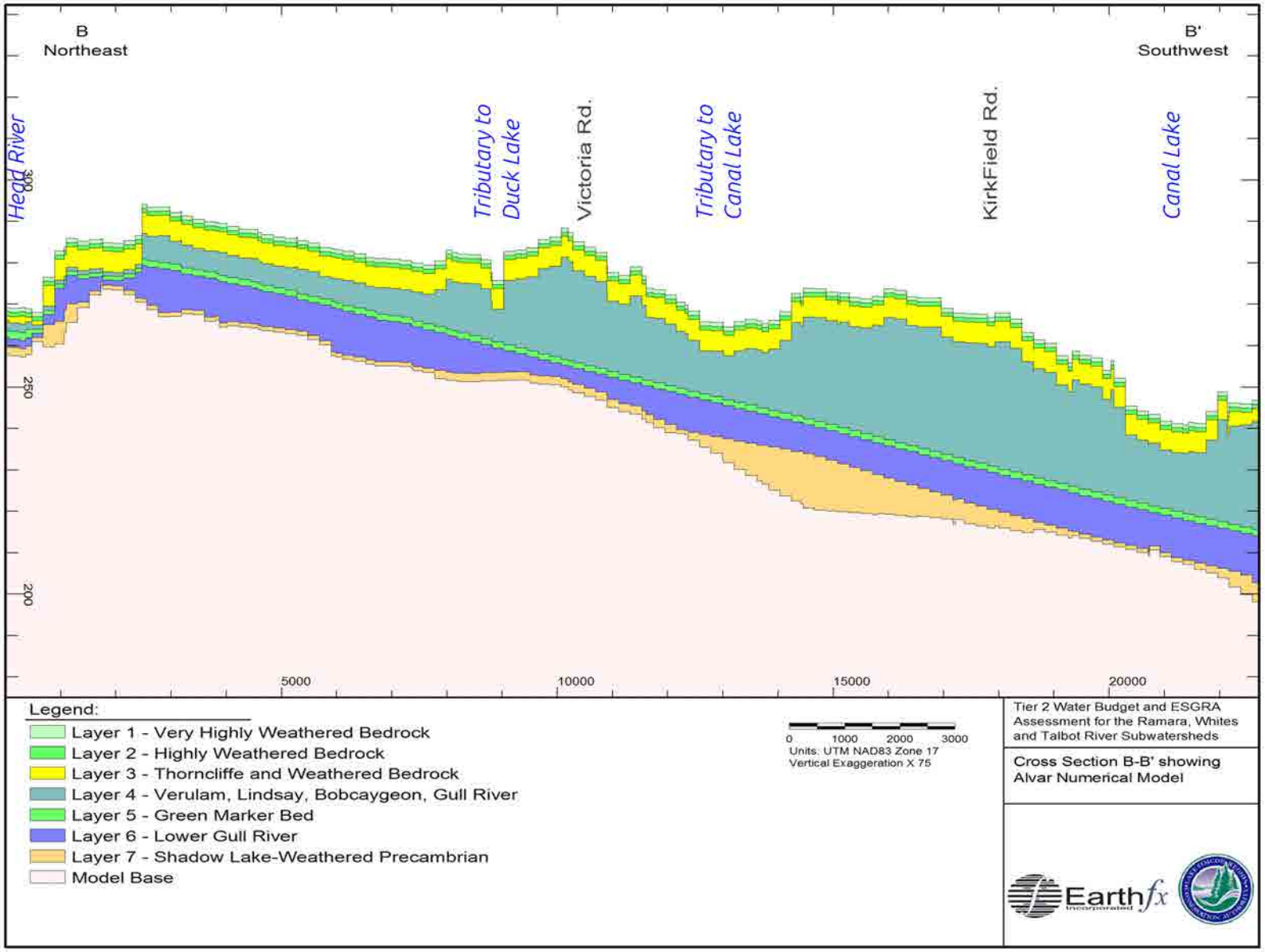

Figure 10.3: Northeast-southwest section B-B’ showing numerical model layers for the alvar conceptual model.

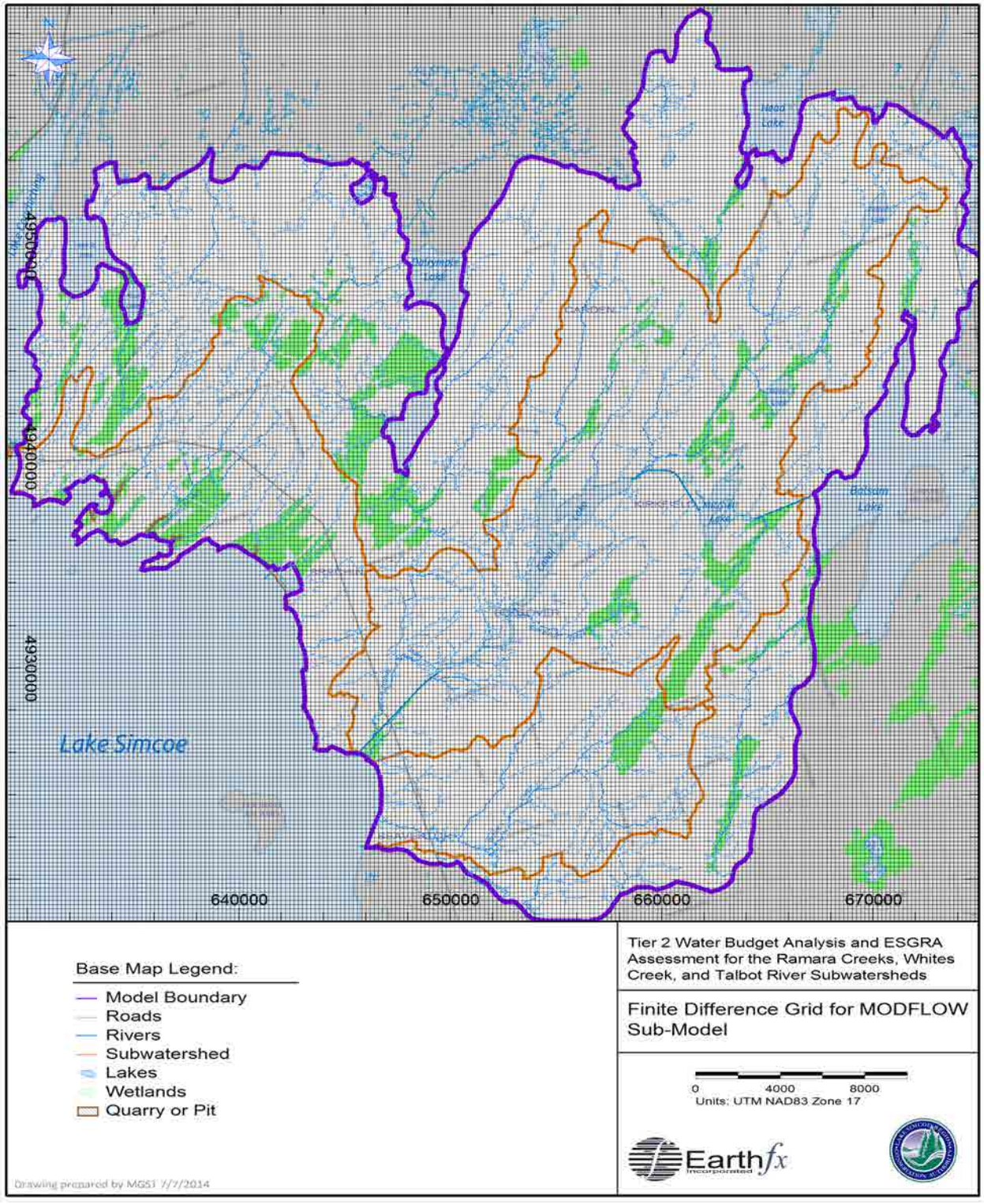

Figure 10.4: Finite-difference grid for the MODFLOW sub-model.

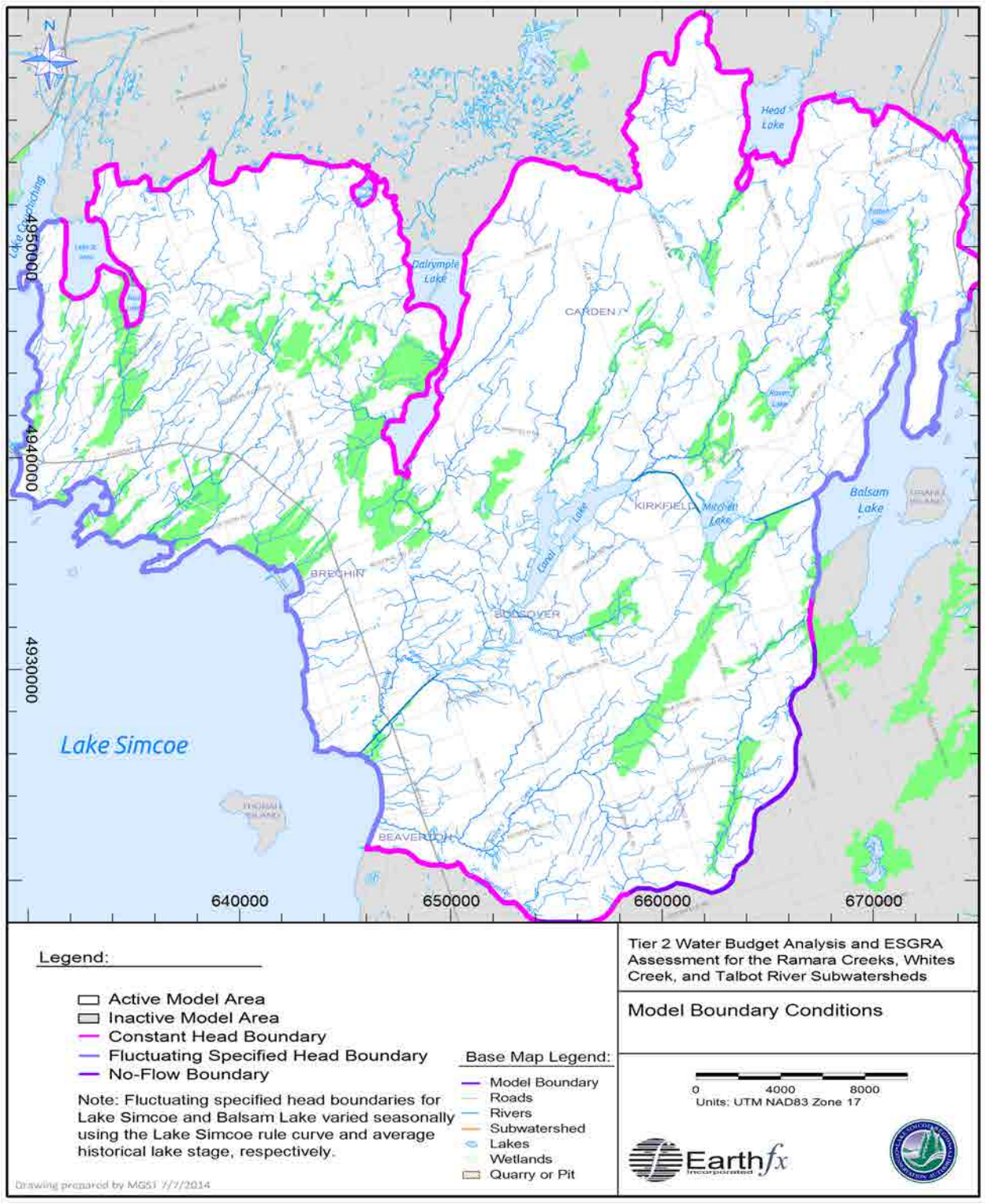

Figure 10.5: Model boundary conditions.

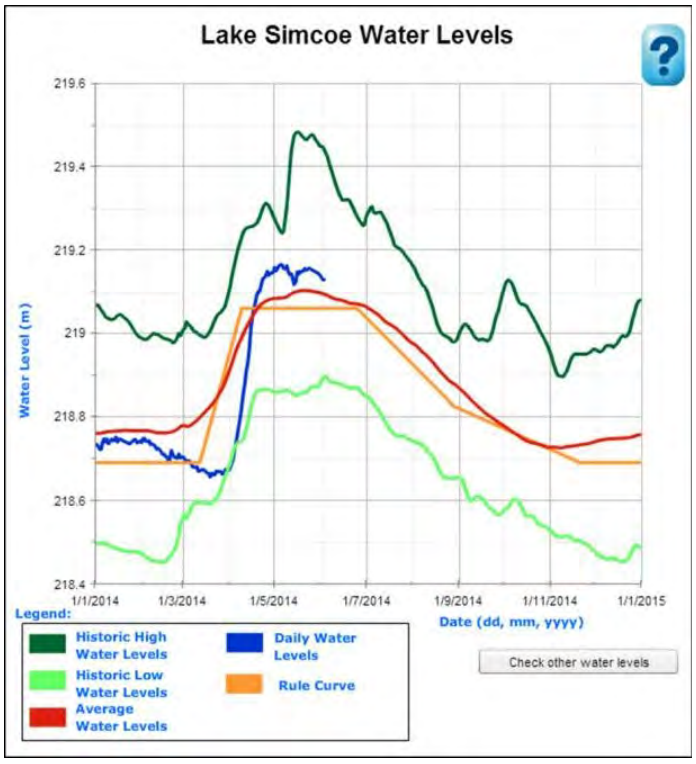

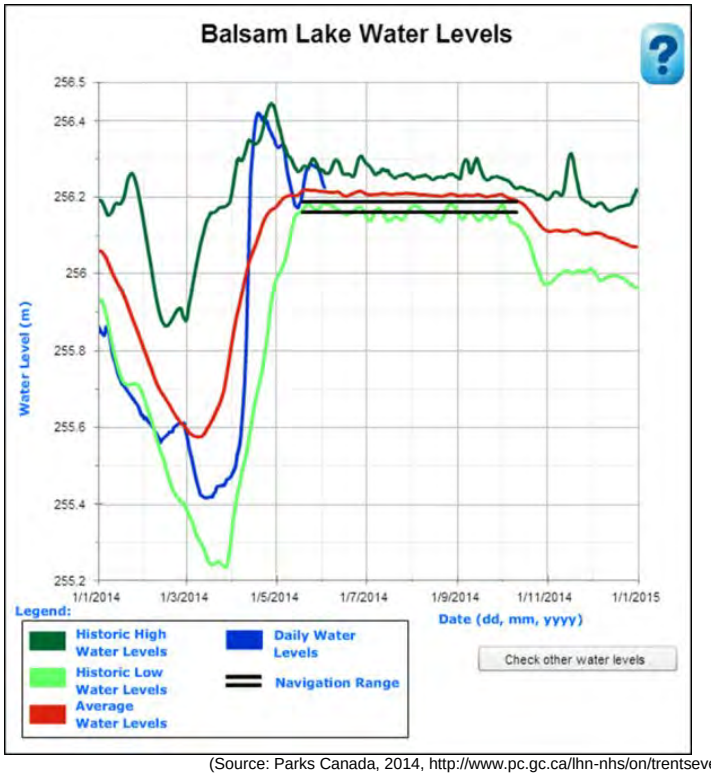

(Source: Parks Canada, 2014, http://www.pc.gc.ca/lhn-nhs/on/trentsevern/visit/ne-wl/trent_e.asp)

Figure 10.6: Water levels for Lake Simcoe (top) and Balsam Lake (bottom).

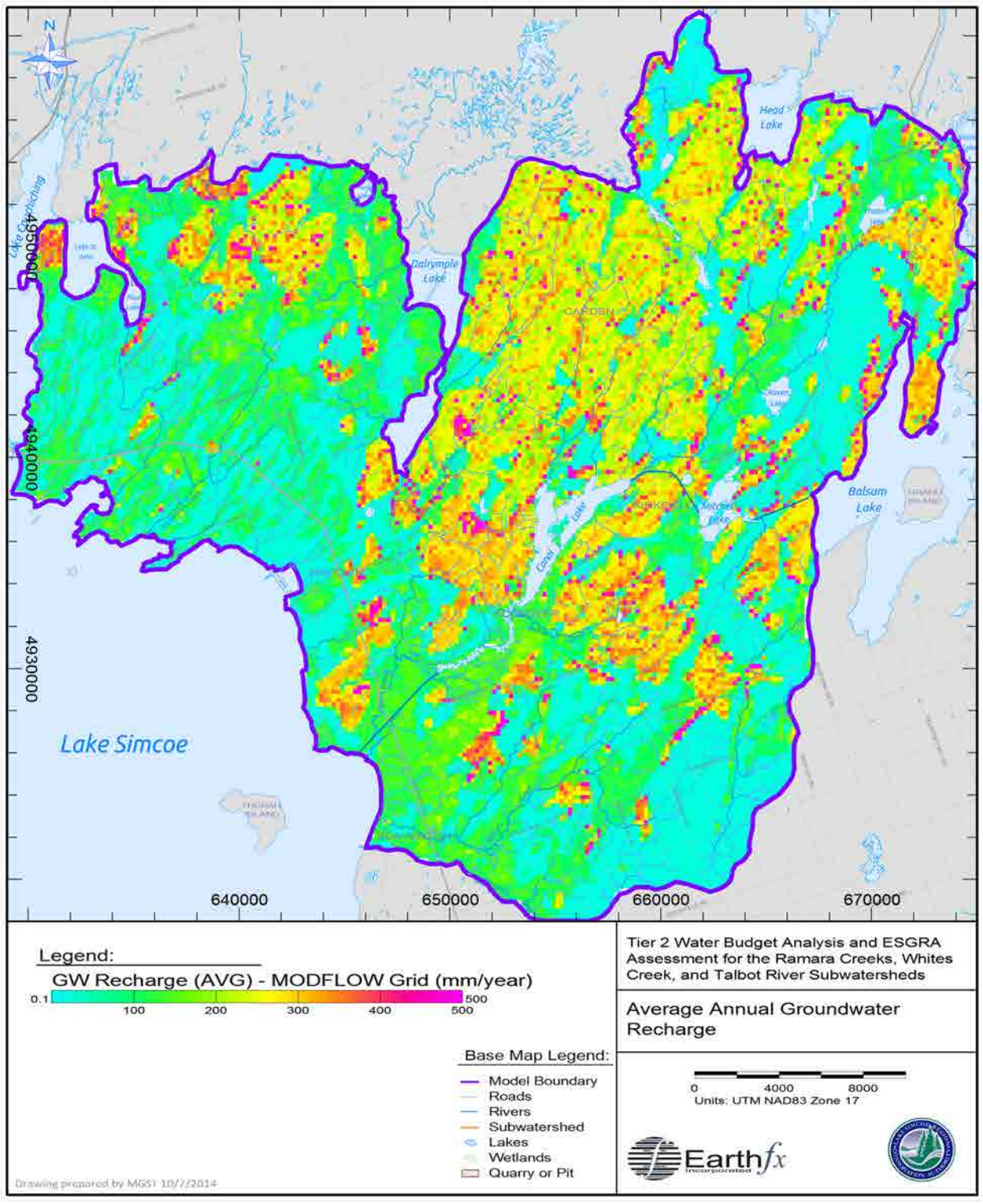

Figure 10.7: Annual average recharge, in mm/yr, used in the steady-state simulations.

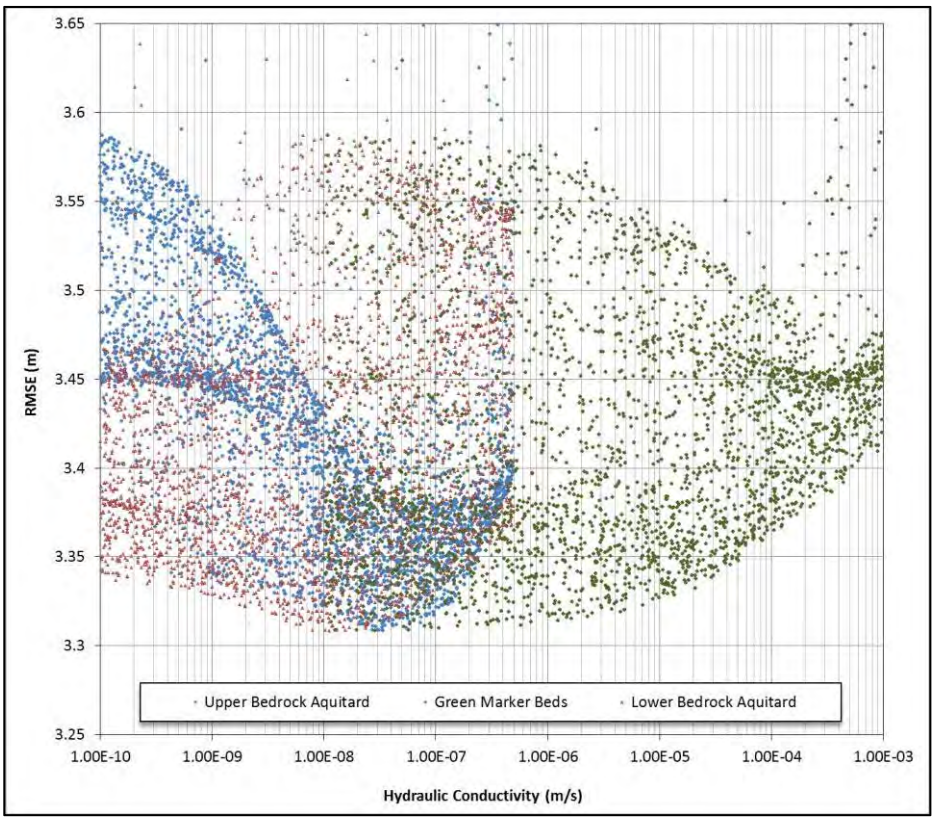

Figure 10.8: Monte Carlo analysis results for hydraulic conductivity of Upper and Lower Bedrock aquitards and Green Marker Bed aquifer.

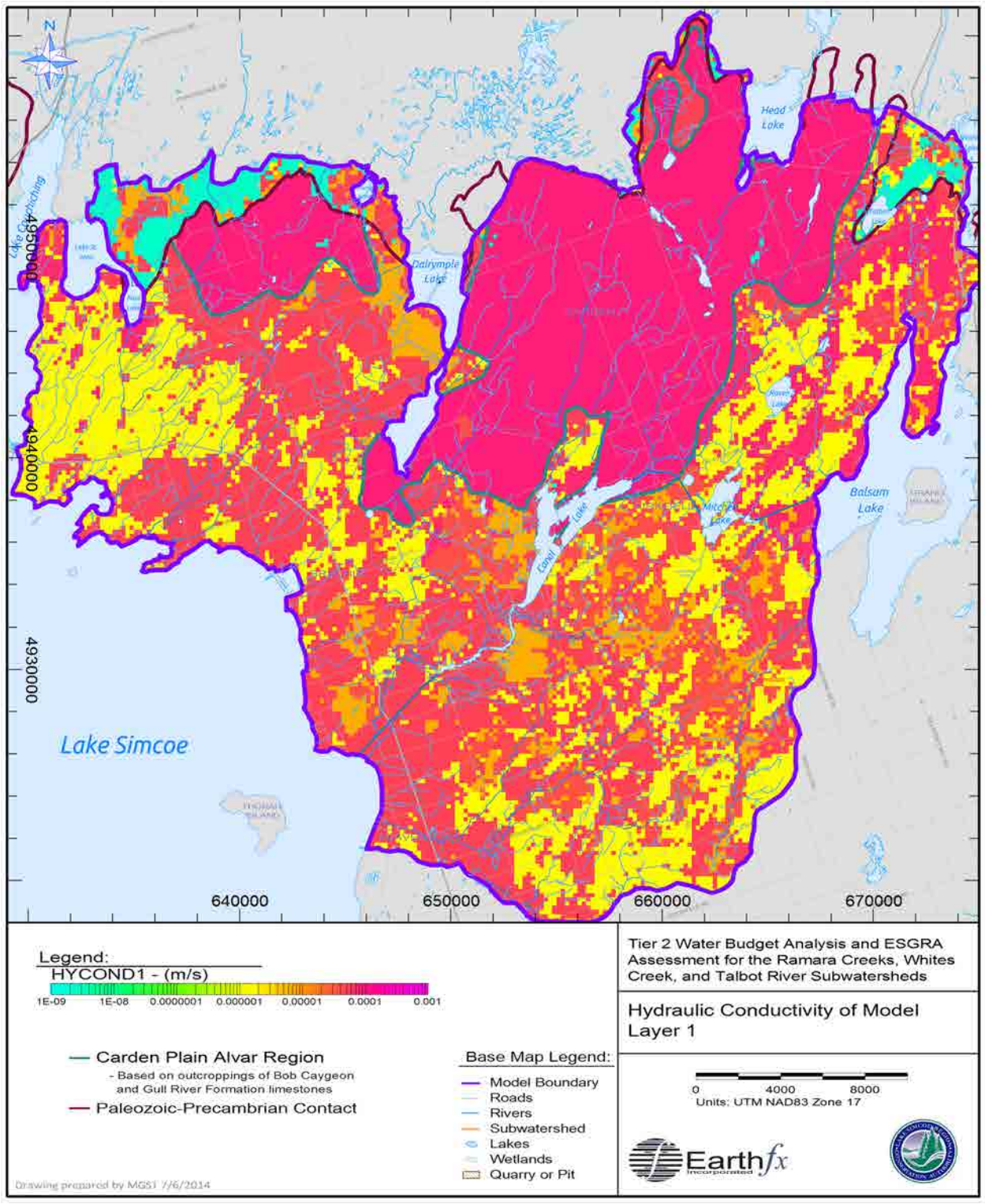

Figure 10.9: Hydraulic conductivity of Layer 1 (surficial deposits/highly weathered alvar).

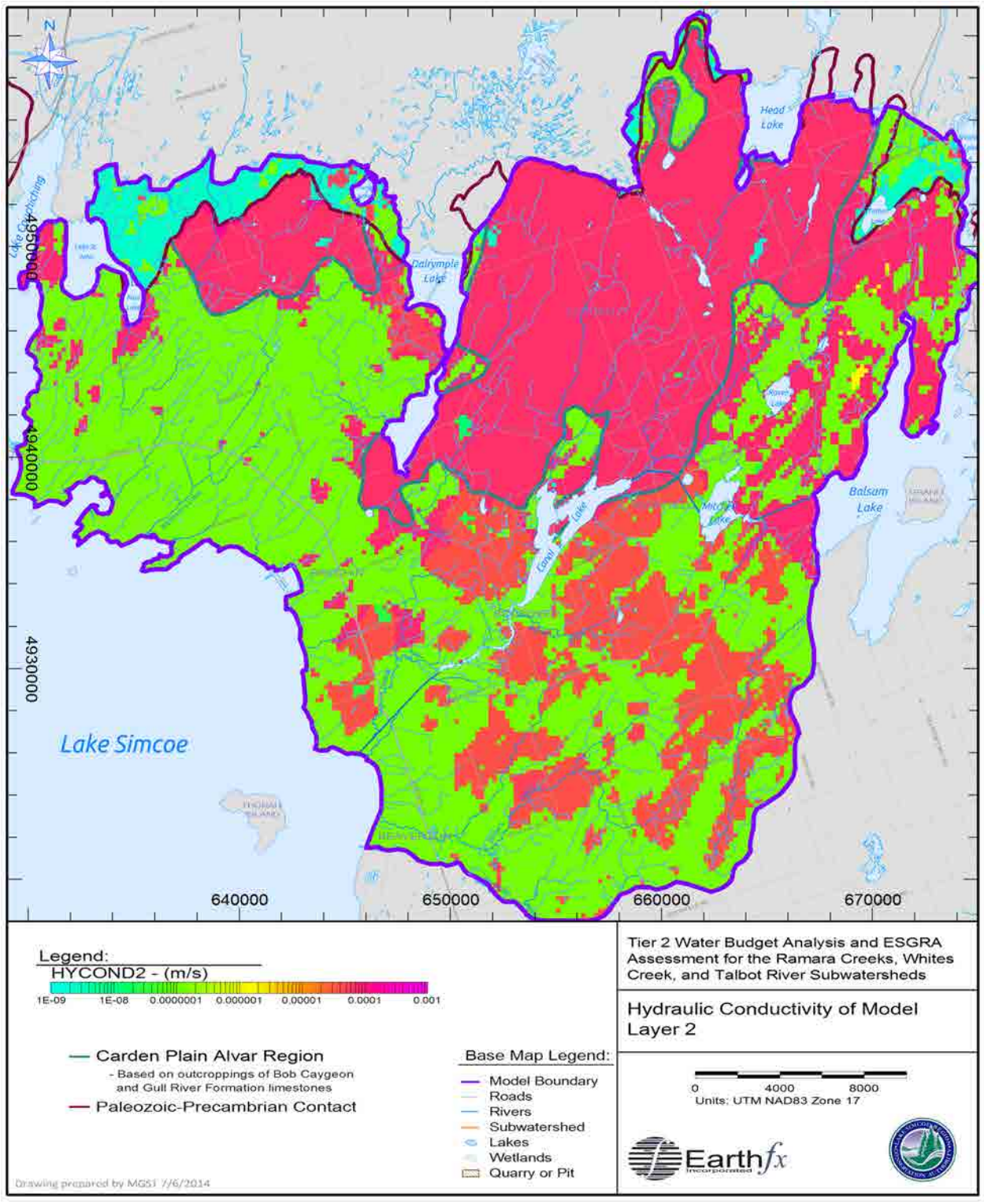

Figure 10.10: Hydraulic conductivity of Layer 2 (till units/medium weathered alvar).

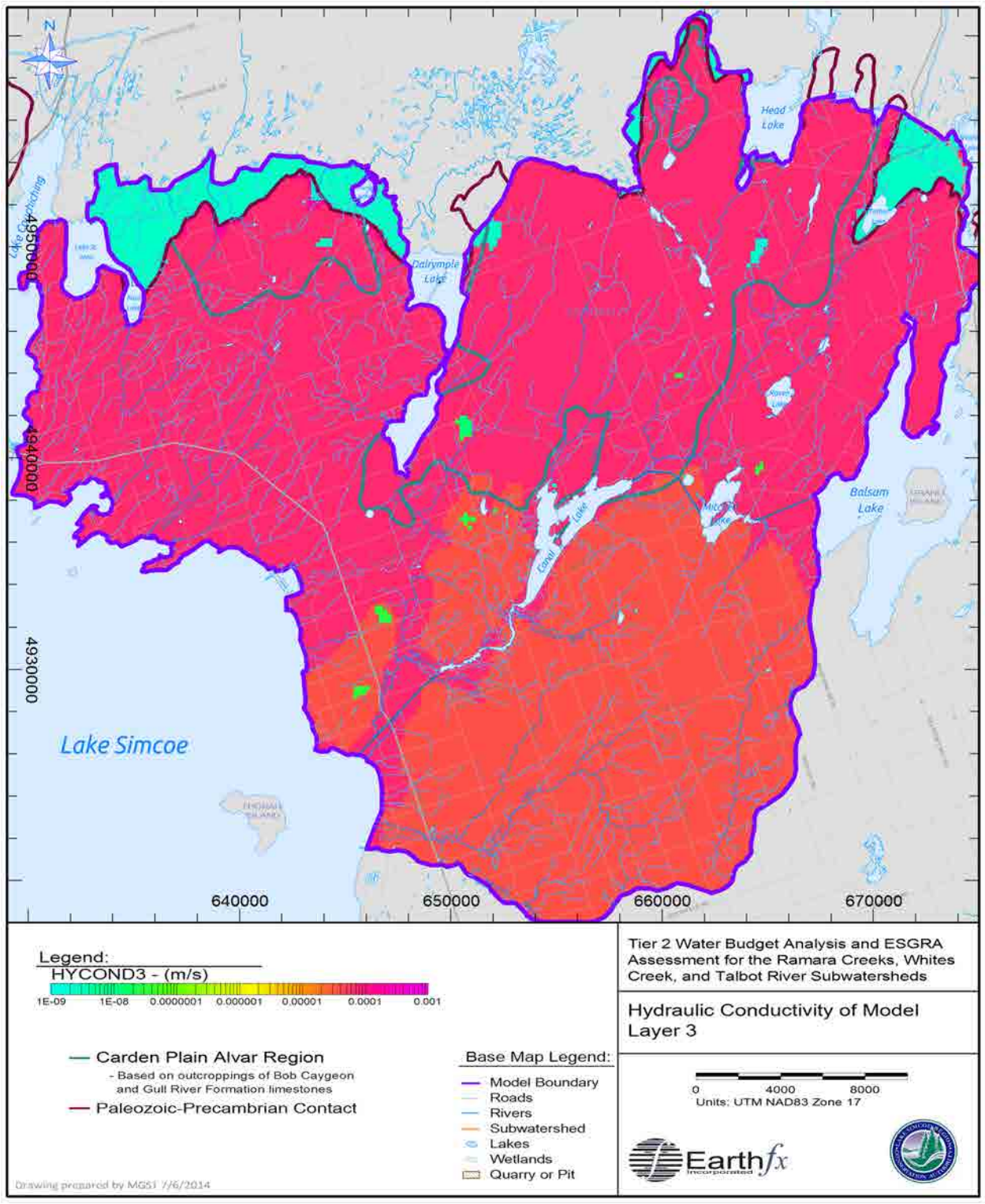

Figure 10.11: Hydraulic conductivity of Layer 3 (weathered bedrock interface aquifer).

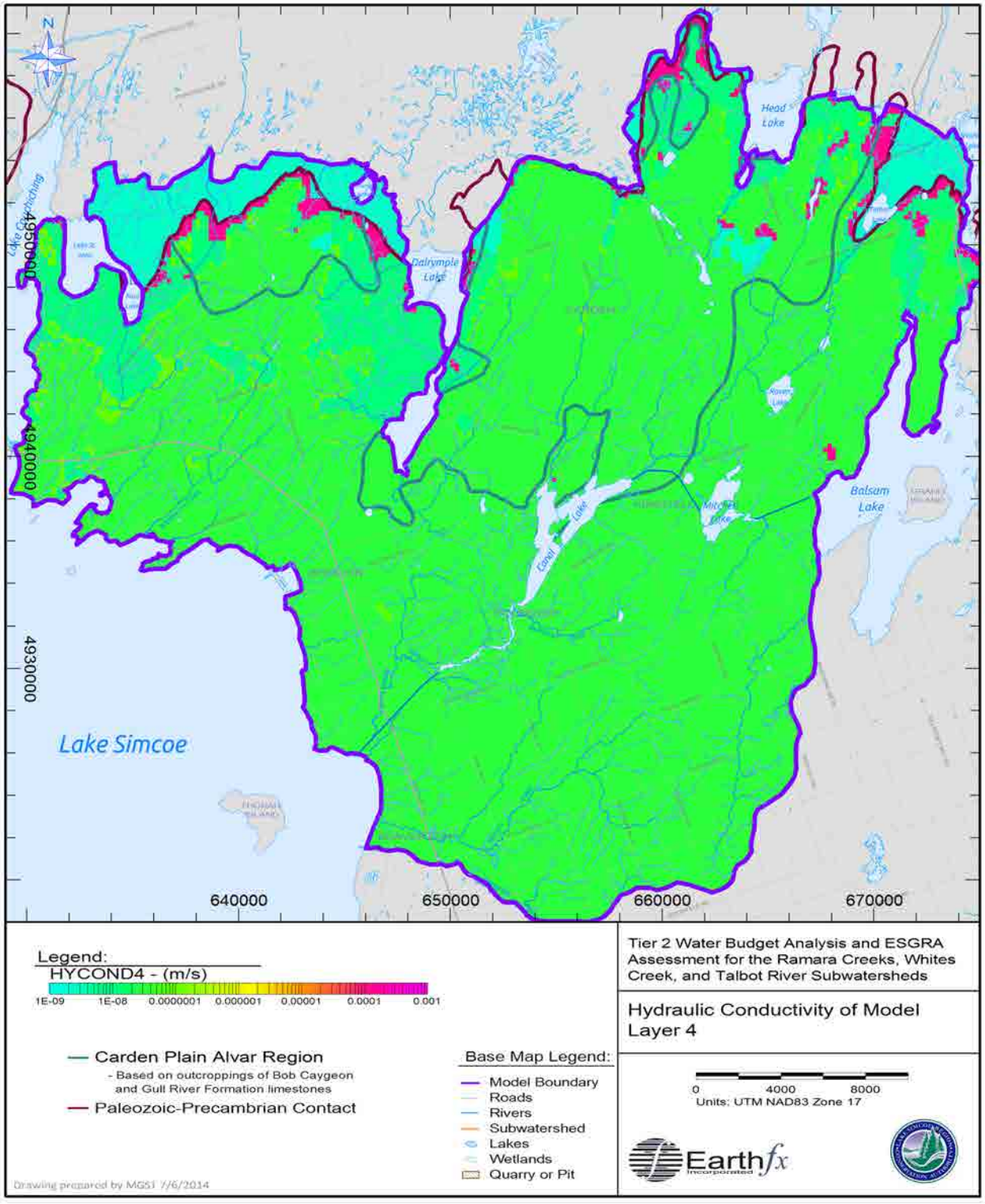

Figure 10.12: Hydraulic conductivity of Layer 4 (upper bedrock aquitard).

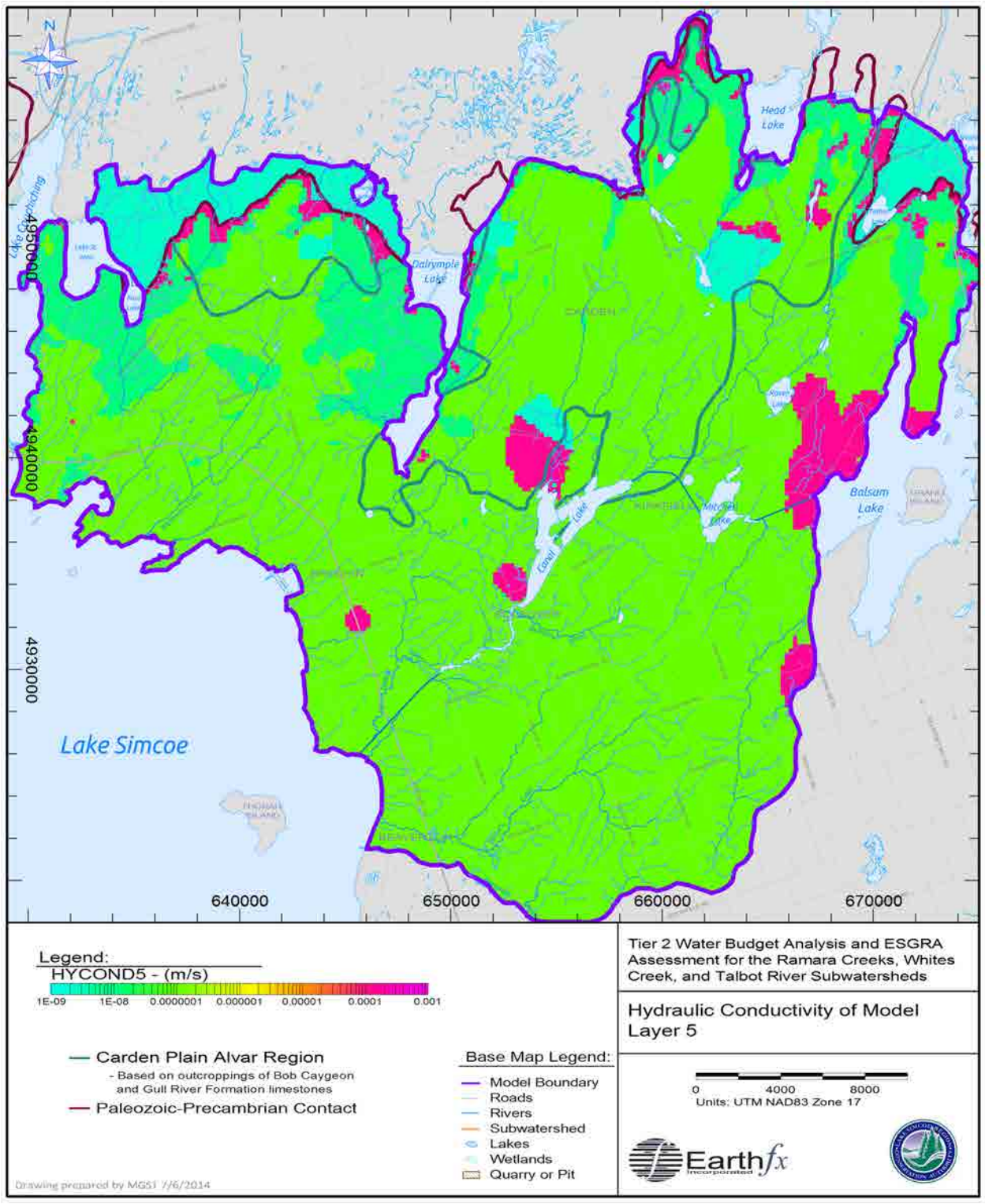

Figure 10.13: Hydraulic conductivity of Layer 5 (Green Marker Beds aquifer).

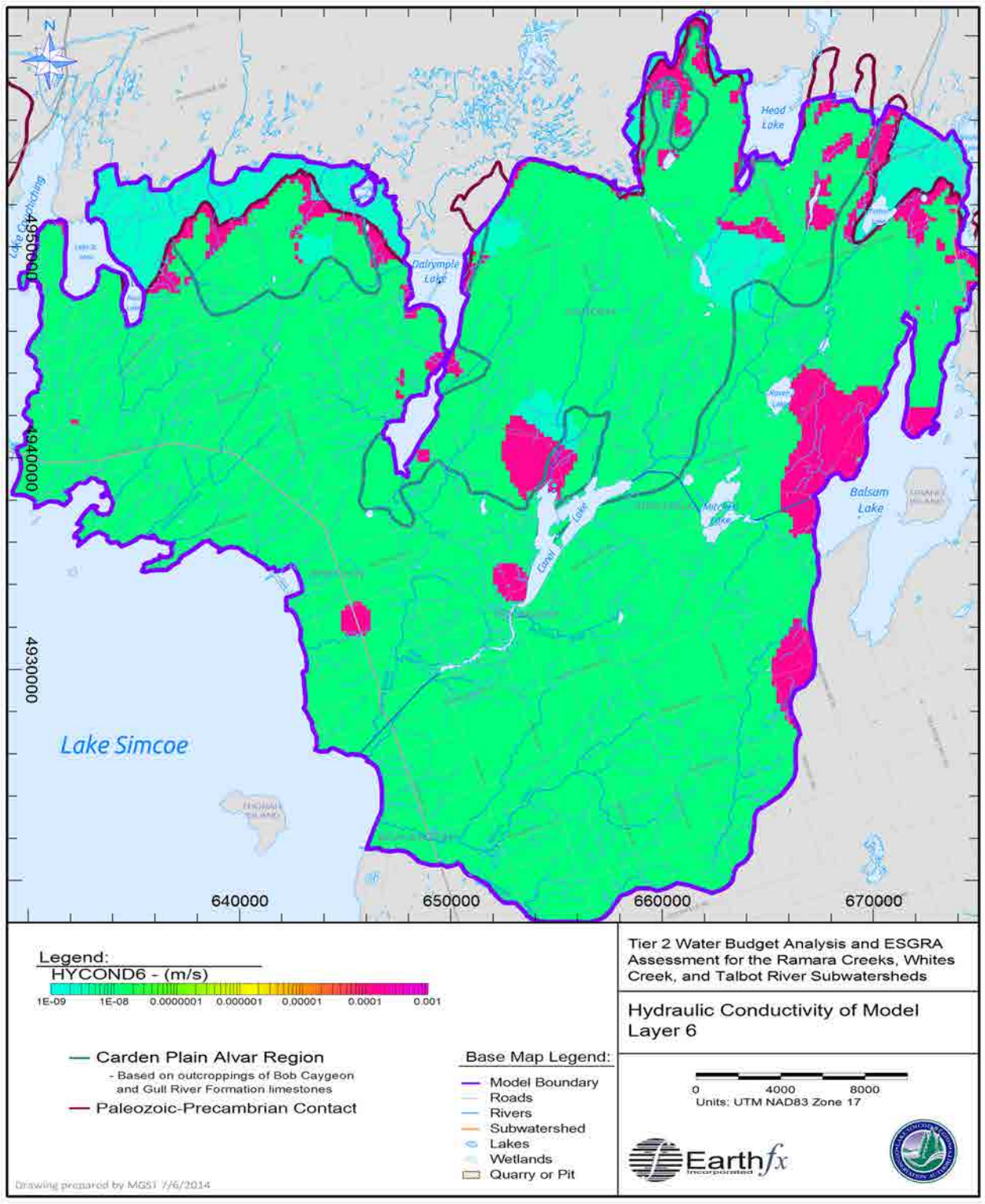

Figure 10.14: Hydraulic conductivity of Layer 6 (lower bedrock aquitard).

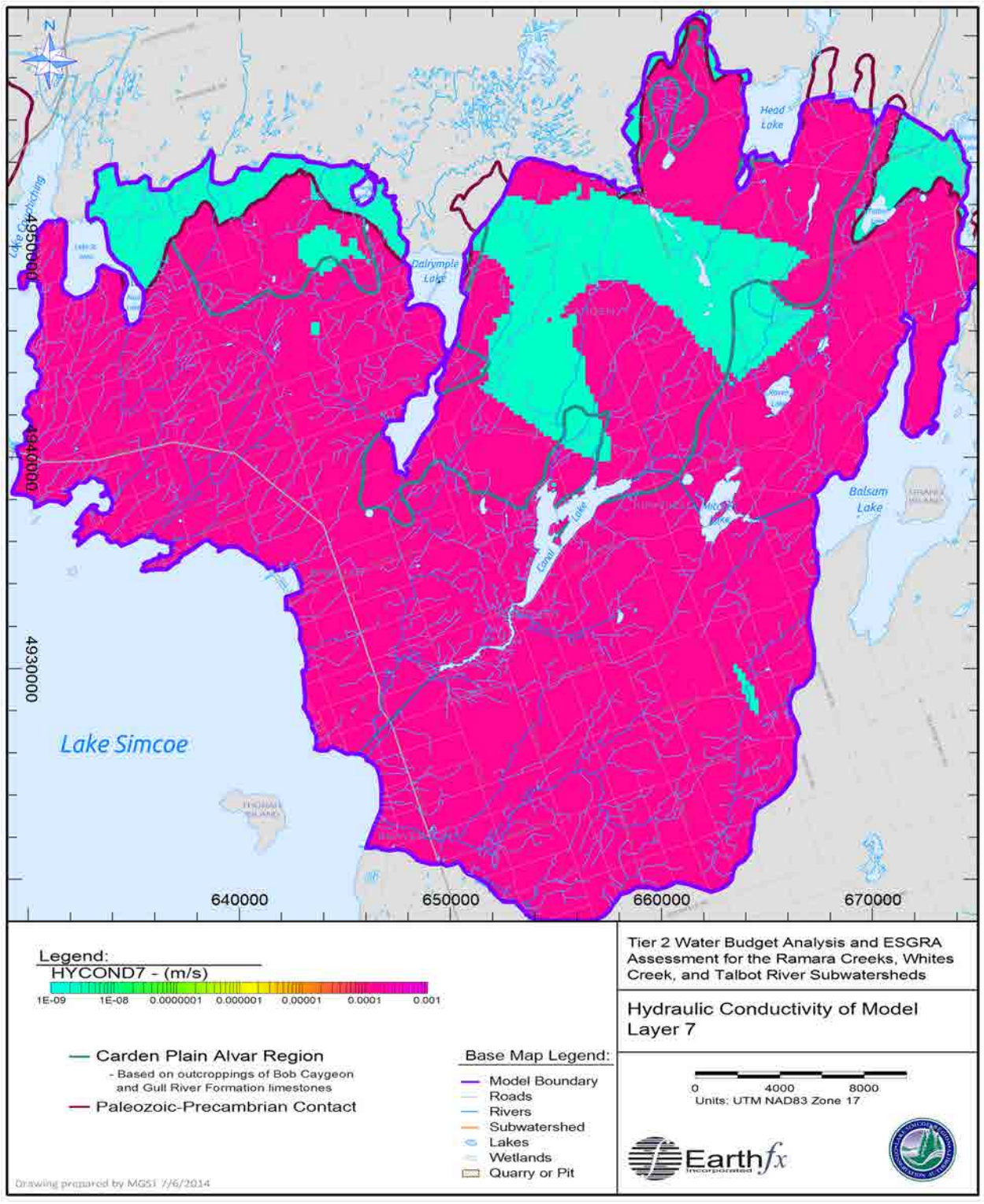

Figure 10.15: Hydraulic conductivity of Layer 7 (Shadow Lake-Precambrian contact aquifer).

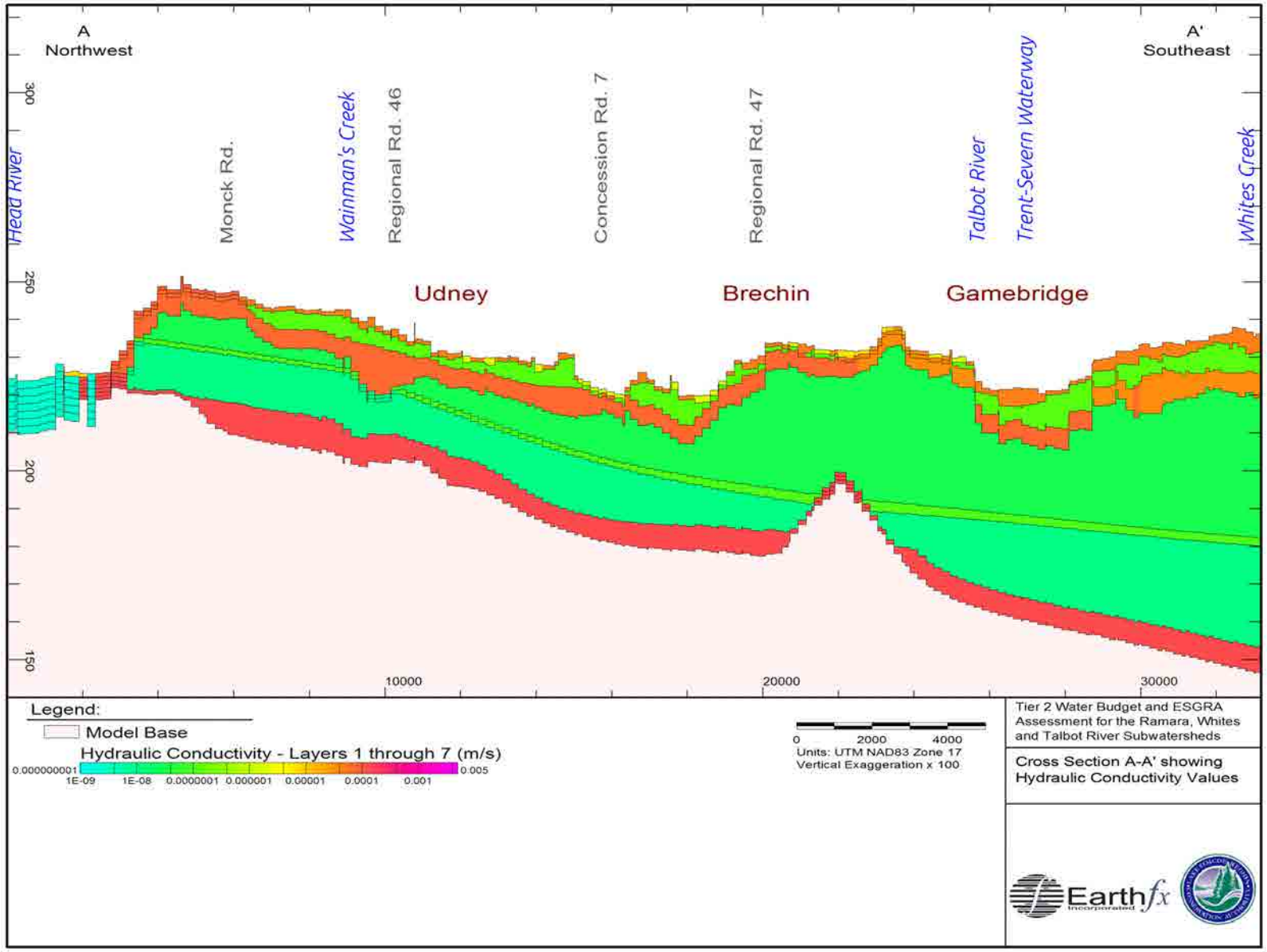

Figure 10.16: Regional north-south section A-A’ showing hydraulic conductivity distribution in numerical model layers.

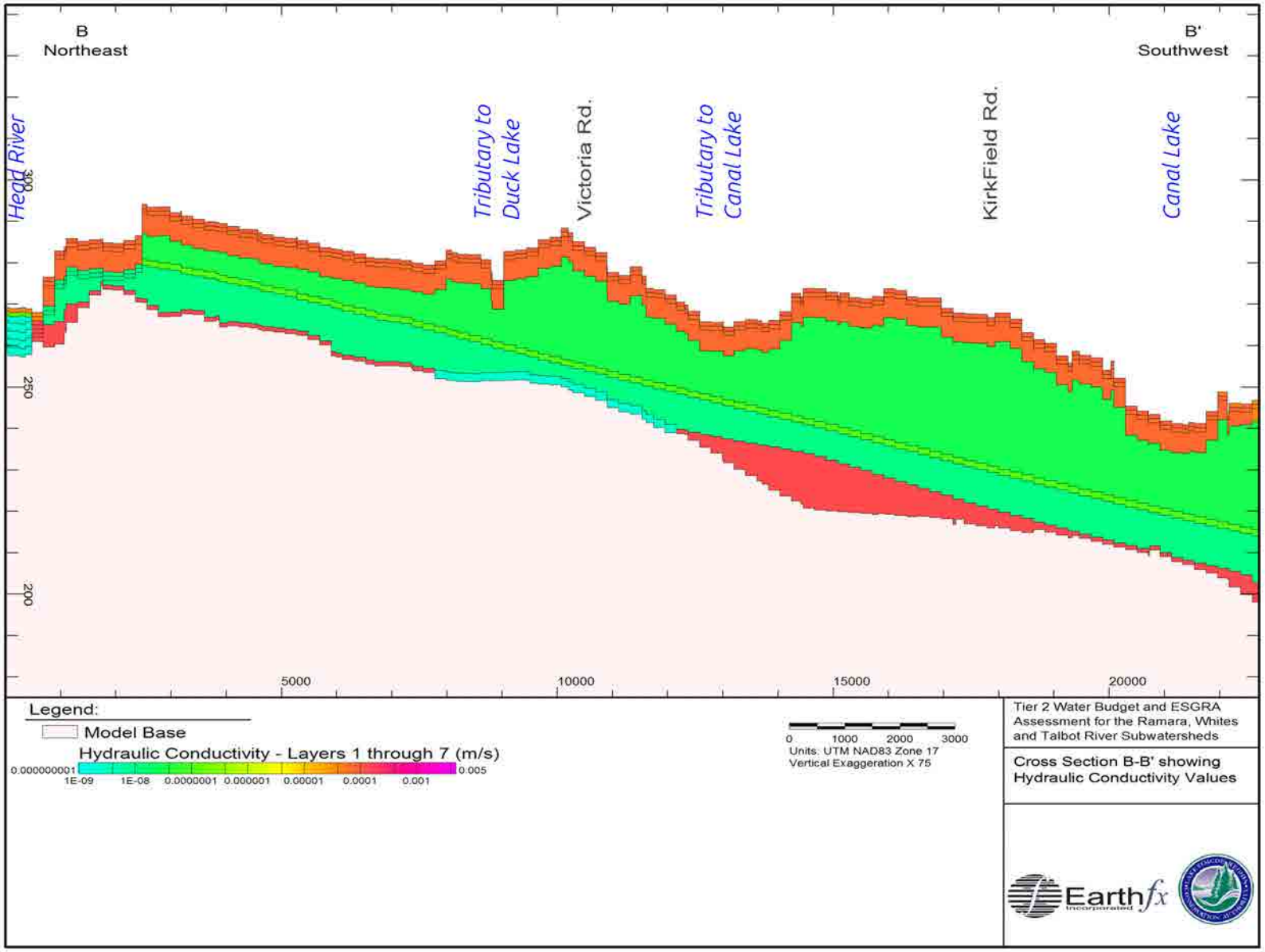

Figure 10.17: Regional north-south section B-B' showing hydraulic conductivity distribution in numerical model layers.

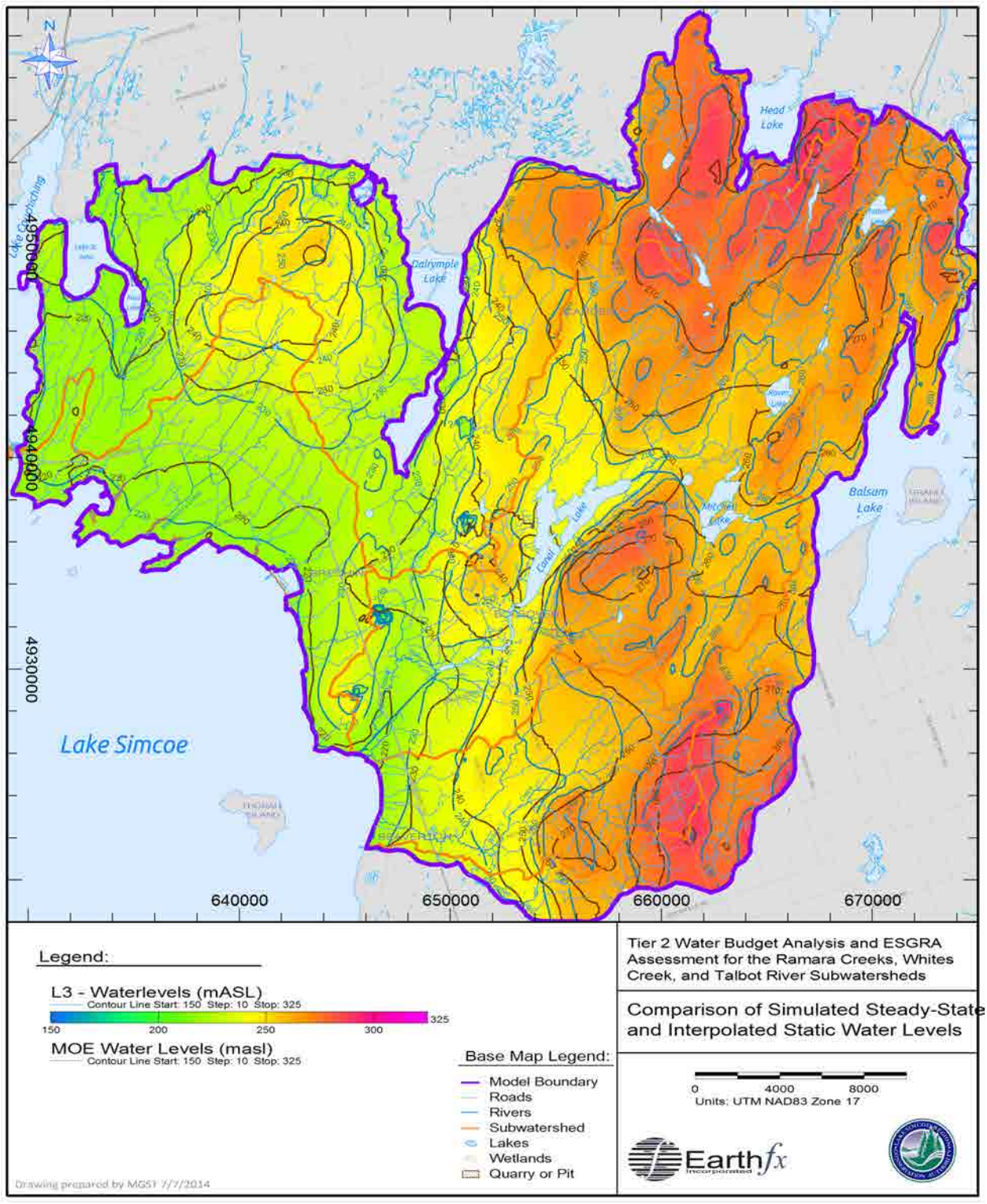

Figure 10.18: Comparison of simulated (blue) and interpolated static water levels (brown) in the weathered bedrock interface aquifer.

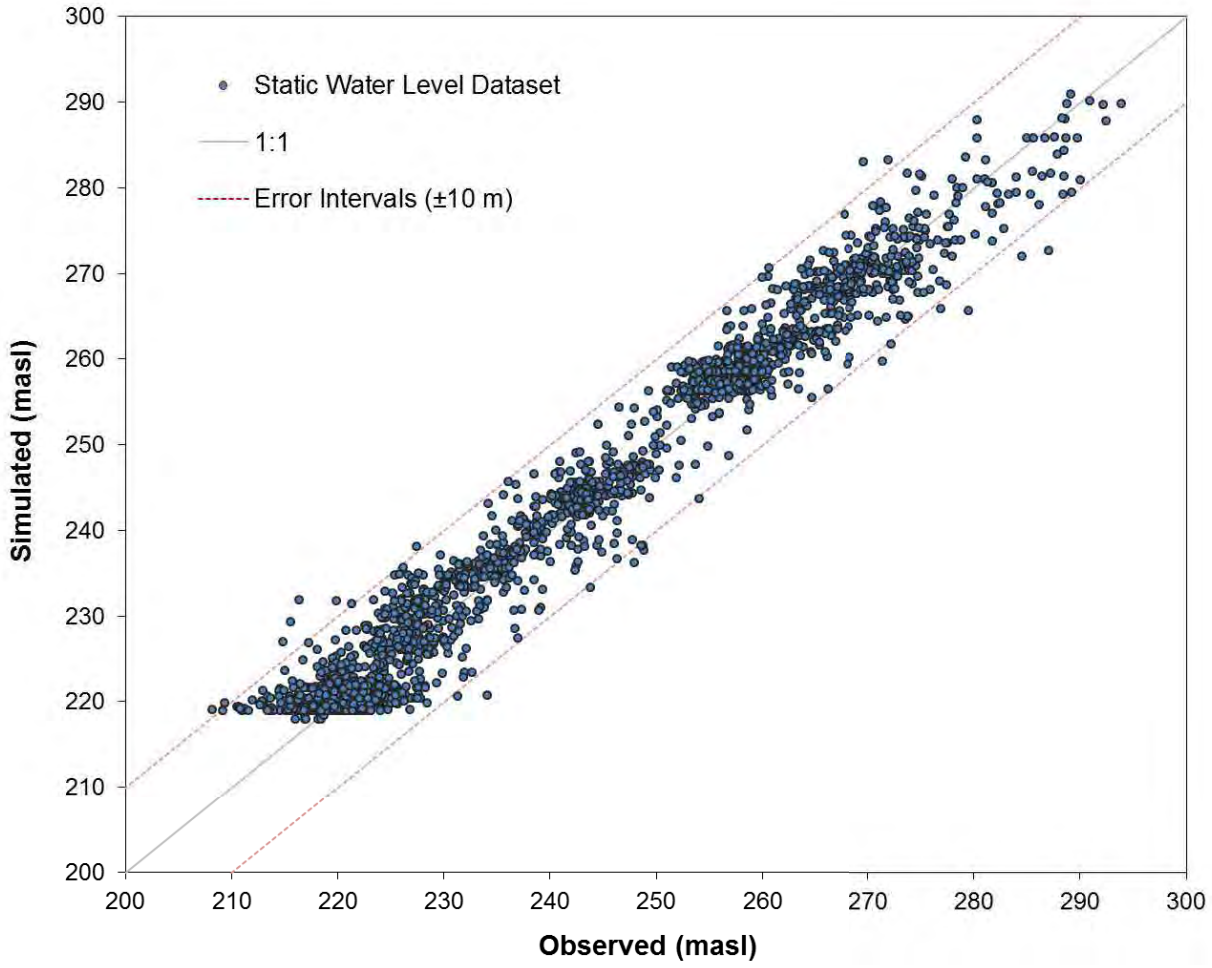

Figure 10.19: Scatter plot of observed versus simulated heads for the weathered bedrock contact aquifer (model Layer 3).

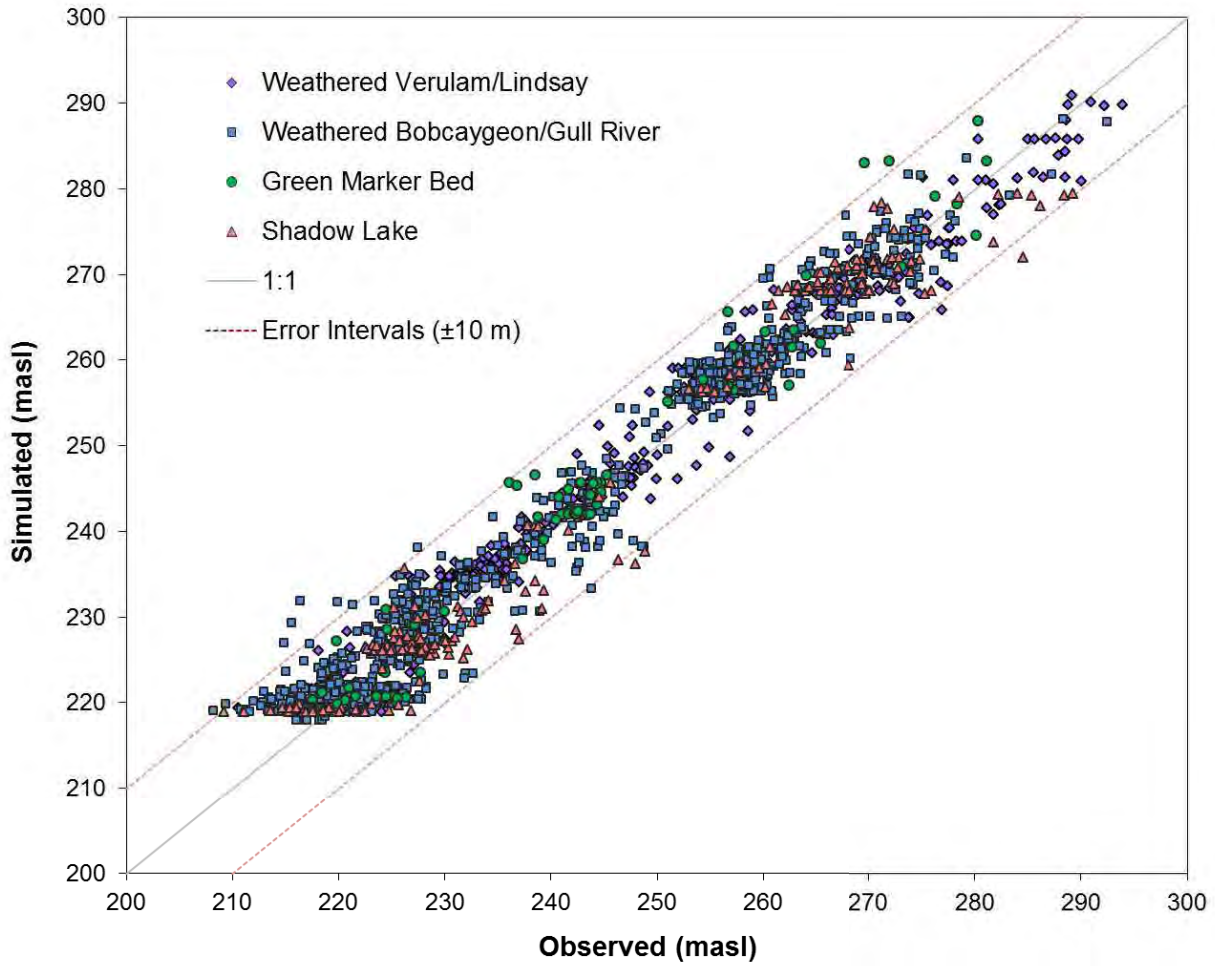

Figure 10.20: Scatter plot of observed versus simulated heads for the three major aquifer units. (Note: Weathered bedrock units have been represented separately.)

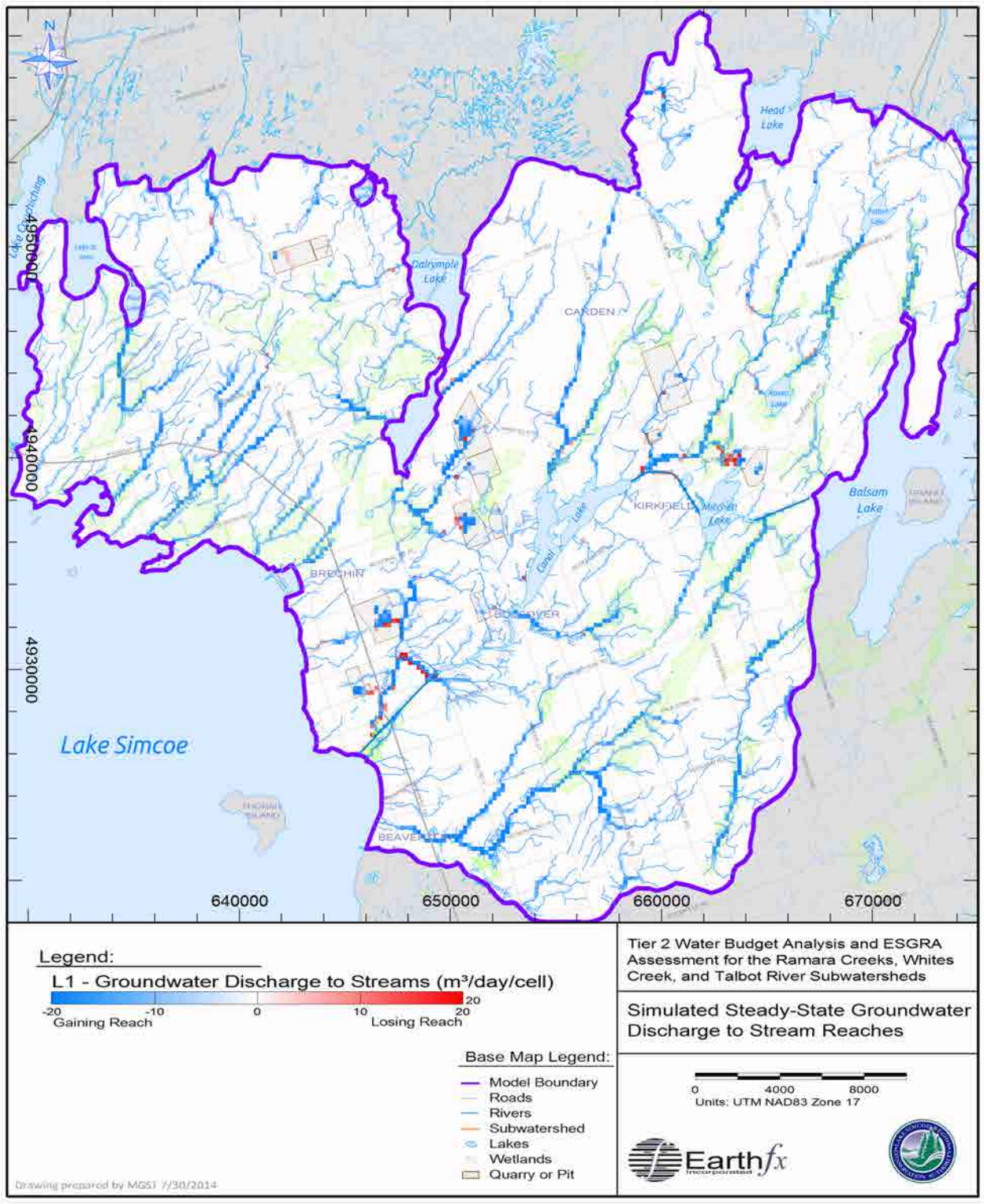

Figure 10.21: Simulated cell-by-cell groundwater discharge to streams (in m^3/d, red colour indicates reach is losing water to the aquifer).

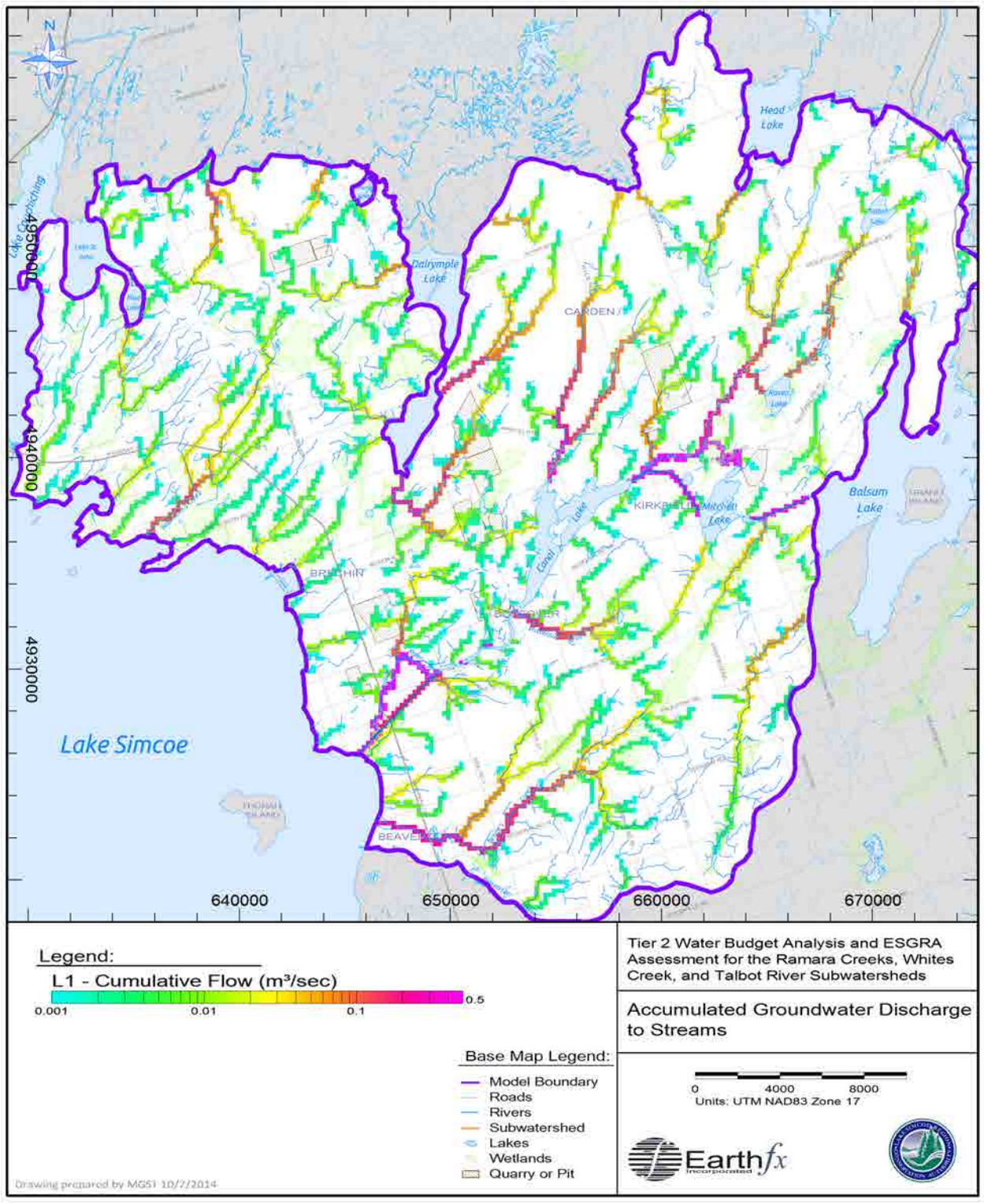

Figure 10.22: Accumulated groundwater discharge to streams (in m^3/s).

11 GSFLOW Model Calibration Results

11.1 GSFLOW Inputs and Calibration Targets

Once the PRMS and MODFLOW sub-models were reasonably well calibrated, the additional data sets and required changes to the model input to set up GSFLOW model runs were made. The GSFLOW model was calibrated to the nearly seven-year period from October 2005 to April 2013. The calibration period covers an extreme dry year (WY2007) and a number of relatively wet years. This period also contains the largest amount of higher quality data for input and calibration purposes including PGMN and other continuous water level data, WTRS data for actual water takings, LSRCA and TrentU-Dillon streamflow observations, and NEXRAD hourly climate data.

Data on daily water use from permitted takings, quarries, and municipal wells were assembled for the transient analyses (Section 6). Climate data were already assembled for the PRMS-only analyses. The continuous groundwater level data, discussed in Section 5.4, and the WSC stream flow data, discussed in Section 4.3, served as the primary calibration targets.

11.2 GSFLOW Outputs

GSFLOW model outputs are similar to those generated for the PRMS and MODFLOW sub-models but with a number of significant enhancements. For example, over 86 different groundwater and surface water flow components can be output on a cell-by-cell basis each simulation day. Earth*fx* has added and aggregated a number of flow components so that local (cell-based) and subcatchment-based water balances can be easily obtained. These include PRMS sub-model flow volumes such as observed (interpolated) precipitation, canopy interception, potential ET, actual ET, lake evaporation, Dunnian (saturation excess) overland runoff, Hortonian (infiltration excess) overland runoff, infiltration, and groundwater recharge. System state variables are also generated on a cell-by-cell basis and include the volumes of water in canopy interception storage, detention storage, and in the various soil zone reservoirs every day. Streamflow, depth of flow, lake stage and depth, as well as simulated heads, groundwater discharge to streams and to the soil zone, as well as other numerous state variables for the groundwater system are also saved on a daily basis. These data were interrogated interactively through VIEWLOG-GIS to generate the hydrographs and maps presented in the following sections of this report. VIEWLOG-GIS was directly linked to the project database to facilitate model comparisons with the transient data from gauges and monitoring wells.

11.3 Calibration Results

Model calibration was performed using an iterative process in which results of successive model runs were used to improve the initial estimates of model parameters. As noted earlier, much of the calibration was done using the stand-alone models. Model parameters were subject to additional refinement during the transient calibration. Storage properties for the groundwater system were a particular area of emphasis.

Checks on the calibration were done by visual comparison of hydrographs of simulated and observed flows and groundwater levels. The groundwater results are presented here as comparisons between relative potentials, as differences in the absolute elevations were found despite the close match obtained with the steady-state model. Some of the differences are attributed to positional or elevation error in the observation data set. Model parameter adjustments were made to improve the match to both relative and absolute values.

Hydrographs for the water levels in W0000408, the single PGMN well in the study area, and simulated potentials in model Layer 3 (weathered bedrock aquifer) are shown in Figure 11.1. As can be seen, the transient model shows considerably less variation in water level than the observed data. The large fluctuations observed at this well (larger than average 0.5–1.0 m seasonal fluctuations of the nearby Lake Simcoe) could be caused by the drying of discrete fractures near the top of the 7-m long open interval during the summer months, followed by a gradual decline in water levels as water seeps into the less permeable material toward the bottom of the well. Because the transient model does not capture this complex in-well process, the simulated values are muted by comparison. The cell containing the PGMN well is also very close to the model boundary which can be muting the model response.

Figure 11.2 through Figure 11.12 compare simulated and observed biweekly response at quarry monitors. The matches are generally good in terms of seasonal and year-to-year response. It should be noted that the quarry operations are simulated using simplified operating rules as explained in Section 8.6; specific dewatering-related responses (such as increased pumping out of sump ponds and pit areas at the start of the season) may not be captured.

A commonly-used statistic for testing the quality of transient simulations is the Nash-Sutcliffe (1970) efficiency (NSE), given by:

$$\text{Nash Sutcliffe Efficiency} = 1 - \frac{\sum_{n=1}^{nobs} (Q_o - Q_s)^2}{\sum_{n=1}^{nobs} (Q_o - \overline{Q_o})^2} \quad \text{(Eq. 14)}$$

where Q_o is the observed flow and Q_s is the simulated flow. The NSE can range from 1 to minus infinity, with 1 being a perfect fit. The NSE statistic for log-transformed flows is a good measure of the fit to low flows rather than the peak flows. NSE values are presented in Table 11.1.

Table 11.1: Nash Sutcliffe efficiency for the GSFLOW simulation.

ID	Station Name	Nash-Sutcliffe Efficiency		Log-Nash Sutcliffe Efficiency	
		Daily	*Monthly*	*Daily*	*Monthly*
LS0402	Whites Creek at Regional Rd. 23	0.31	0.53	0.49	0.59

A Nash-Sutcliffe efficiency of 0.6 is considered a reasonable value (Chiew and McMahon, 1993). It must be recognized that the model simulates flow on a daily basis and would not be expected to achieve perfect matches with observed mean daily flows. Because of the emphasis on baseflow and low flows, the Log Nash-Sutcliffe which is considered a better measure of the model calibration to low flows (Krause *et al.*, 2005).

Figure 11.13 through Figure 11.17 compare simulated streamflow to the active LSRCA stream gauge (LS0402) and two TrentU-Dillon gauges located within the model area. The gauge on the lower part of the Talbot River was not used for model calibration because flows at this gauge are influenced by canal operations and because the timing and volume of releases were not provided. The calibration to the Whites Creek at Regional Road 23 gauge is generally satisfactory (Figure 11.13), with the peaks and recessions of many of the larger events being well matched. Some of the observed peaks are not captured by the model; because the model simulates flow on a daily basis, it was not expected that it would match peaks exactly. The low flows, emphasised using a semi-log plot of stream discharge in Figure 11.14, tended to be overpredicted by the model for streamflow at

the LS0402 gauge during dryer periods. The monthly average discharges for the simulated and observed values at the LS0402 gauge are presented in Figure 11.15 and show that monthly volumes are generally well matched by the model. Similar results can be seen in the other Whites Creek gauges WR06 and WR23, presented in Figure 11.16 and Figure 11.17, respectively.

11.4 Figures

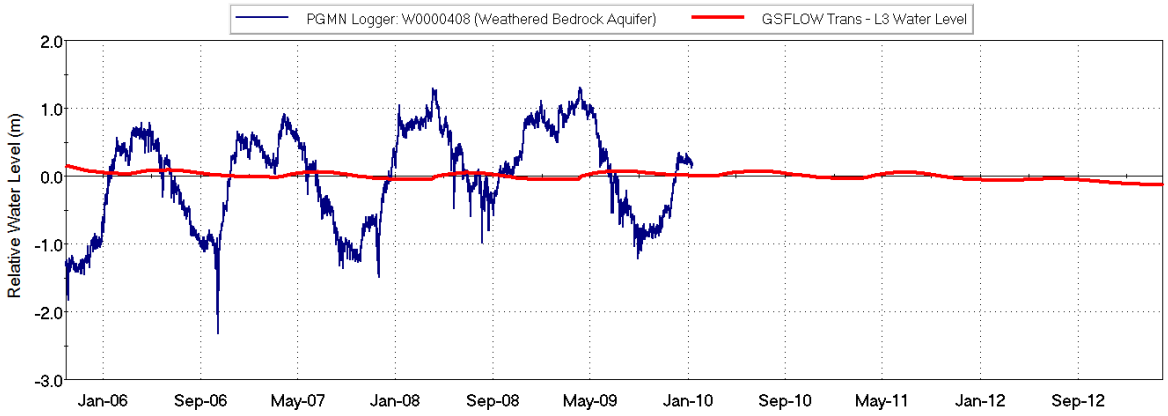

Figure 11.1: Simulated heads in Layer 3 and observed heads at PGMN Well W0000408.

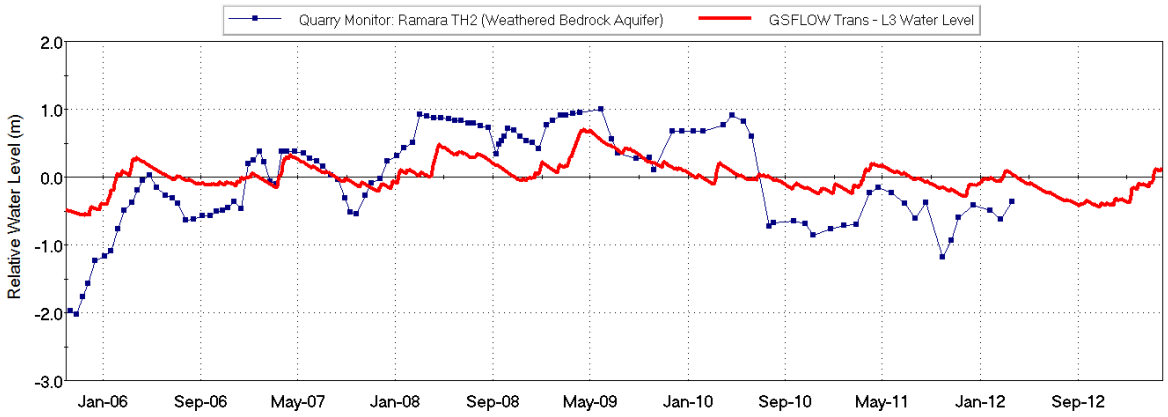

Figure 11.2: Simulated heads in Layer 3 and observed heads at James Dick Construction's Ramara Quarry Well TH2.

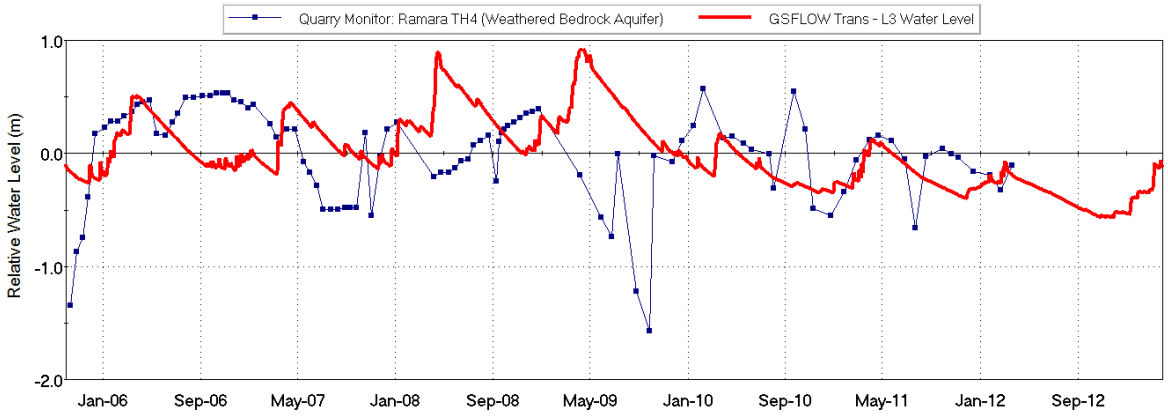

Figure 11.3: Simulated heads in Layer 3 and observed heads at Dick Construction's Ramara Quarry Well TH4.

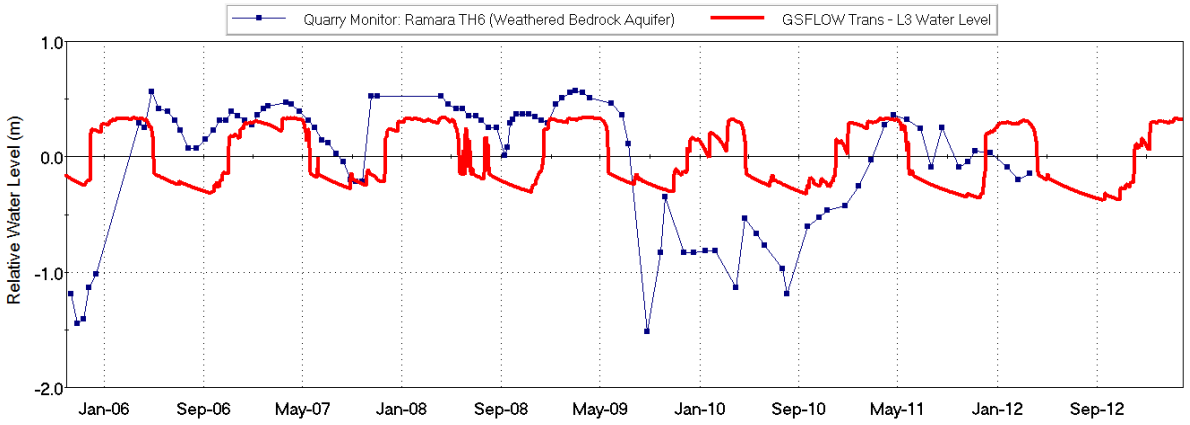

Figure 11.4: Simulated heads in Layer 3 and observed heads at Ramara Quarry Well TH6.

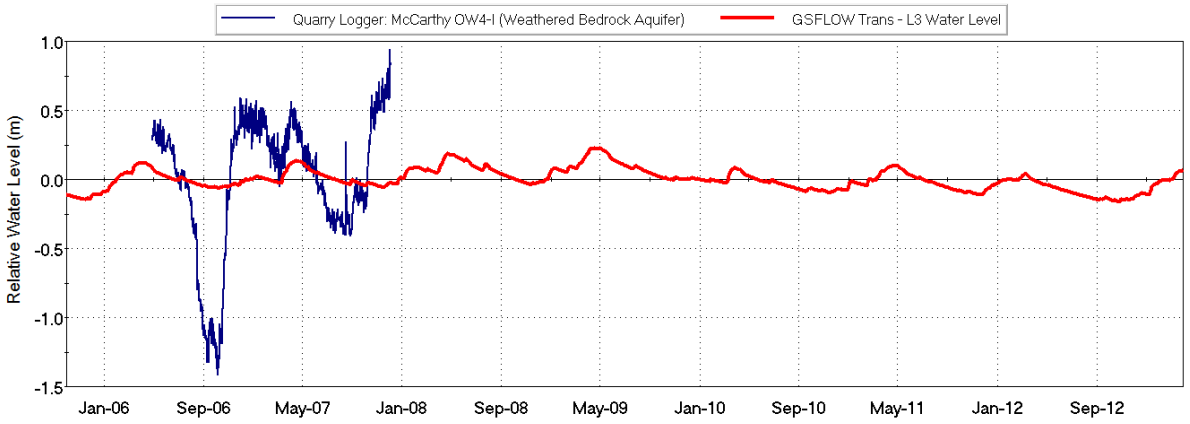

Figure 11.5: Simulated and observed heads in Layer 3 at McCarthy Quarry Well OW4-I.

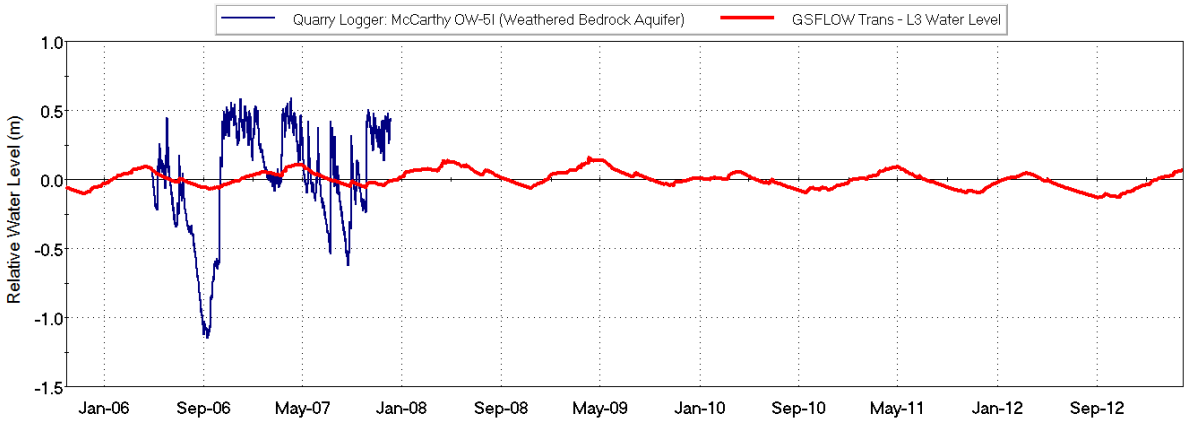

Figure 11.6: Simulated and observed heads in Layer 3 at McCarthy Quarry Well OW5-I.

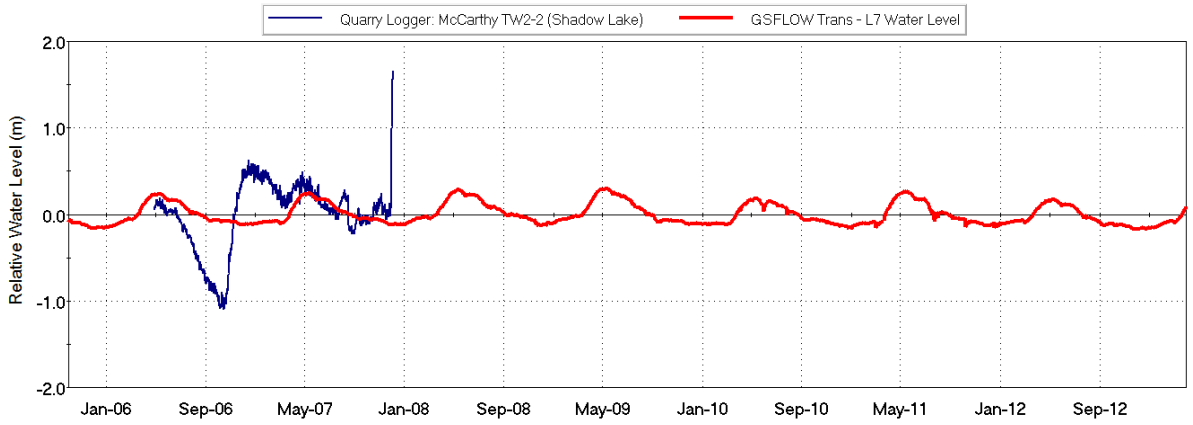

Figure 11.7: Simulated and observed heads in Layer 7 at McCarthy Quarry Well TW2-2.

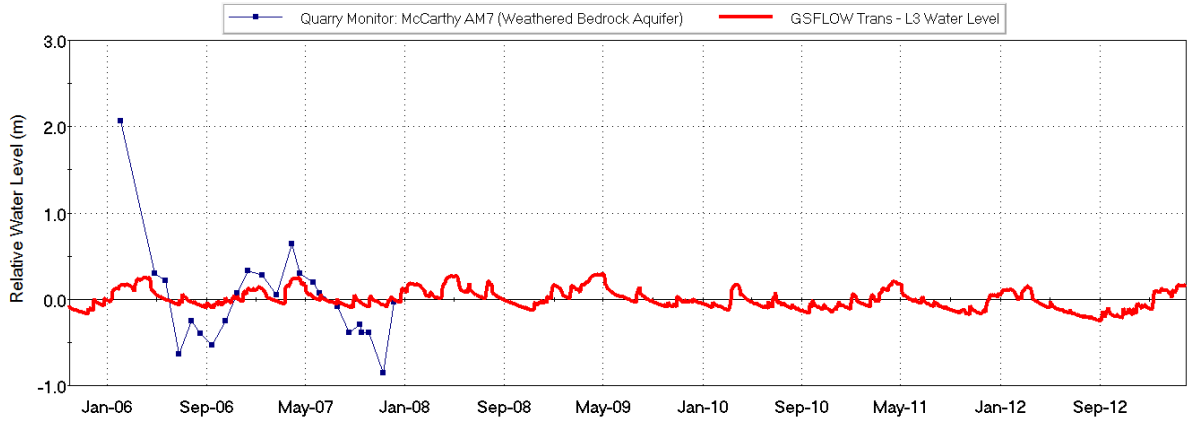

Figure 11.8: Simulated and observed heads in Layer 3 at McCarthy Quarry Well AM7.

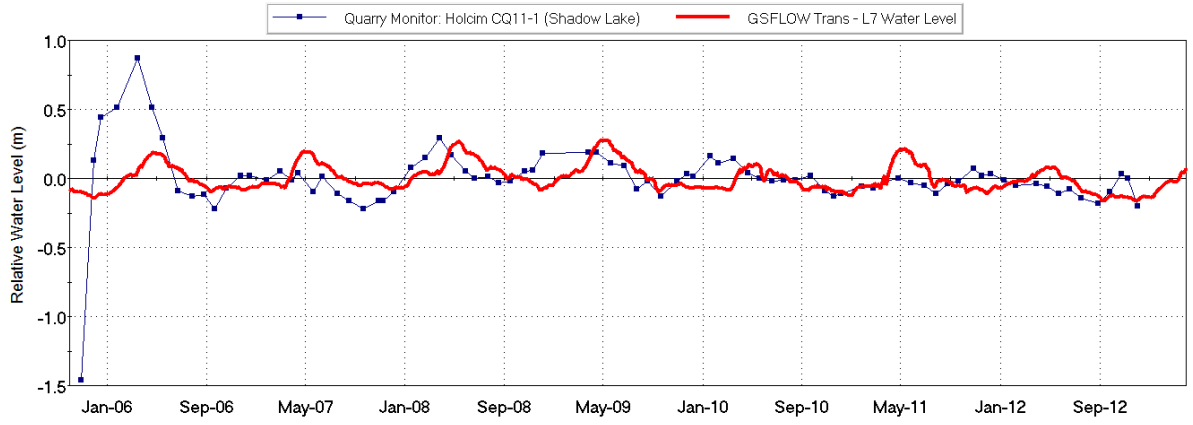

Figure 11.9: Simulated and observed heads in Layer 7 at Holcim Quarry Well CQ11-1.

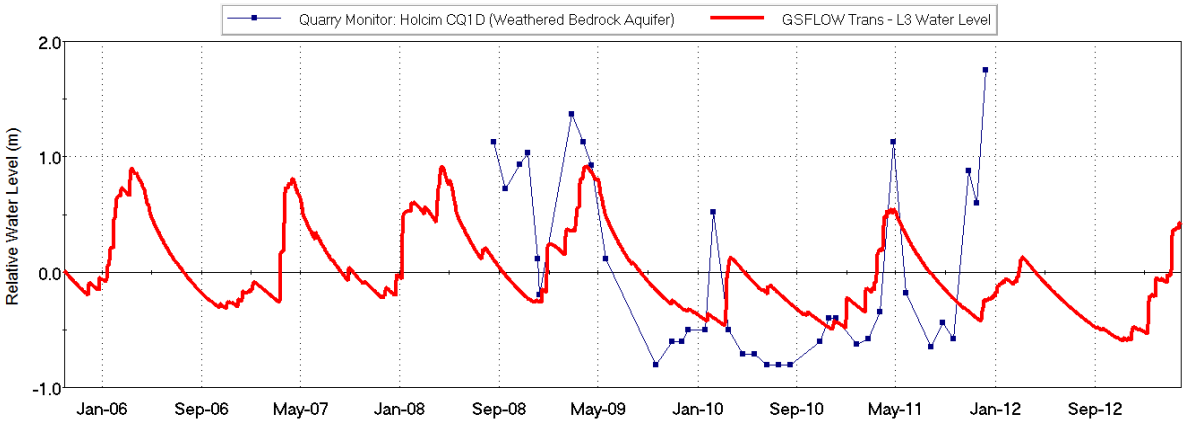

Figure 11.10: Simulated and observed heads in Layer 3 at Holcim Quarry Well CQ1D.

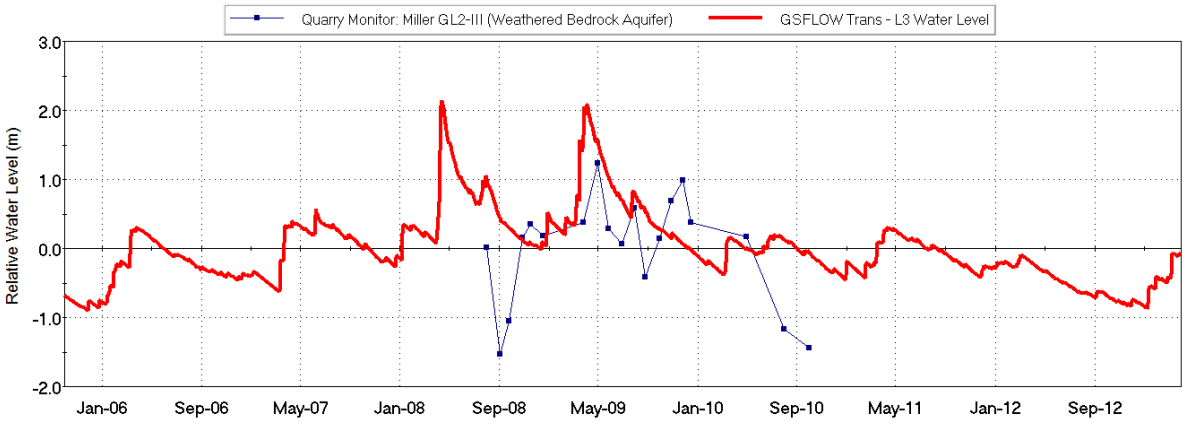

Figure 11.11: Simulated and observed heads in Layer 3 at Miller Quarry Well GL1-III.

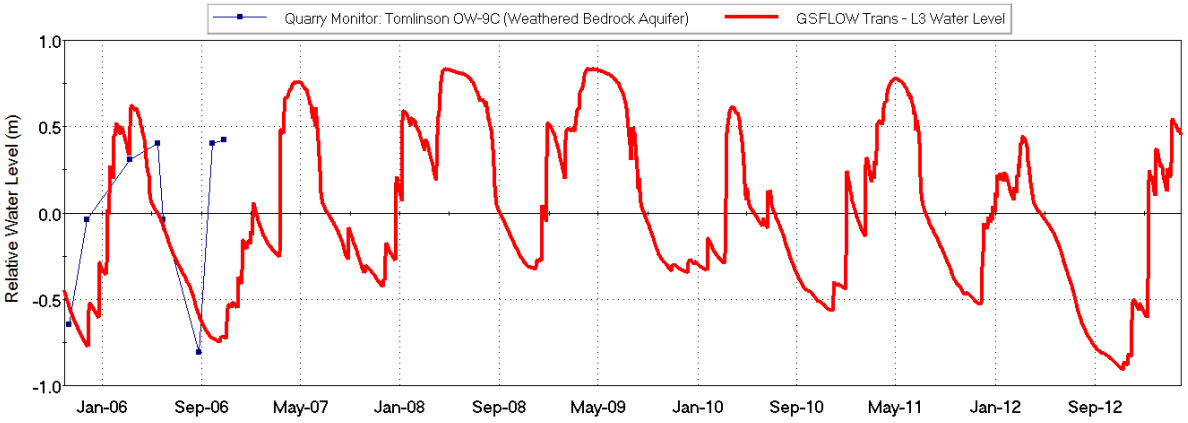

Figure 11.12: Simulated and observed heads in Layer 3 at Tomlinson Quarry Well OW-9C.

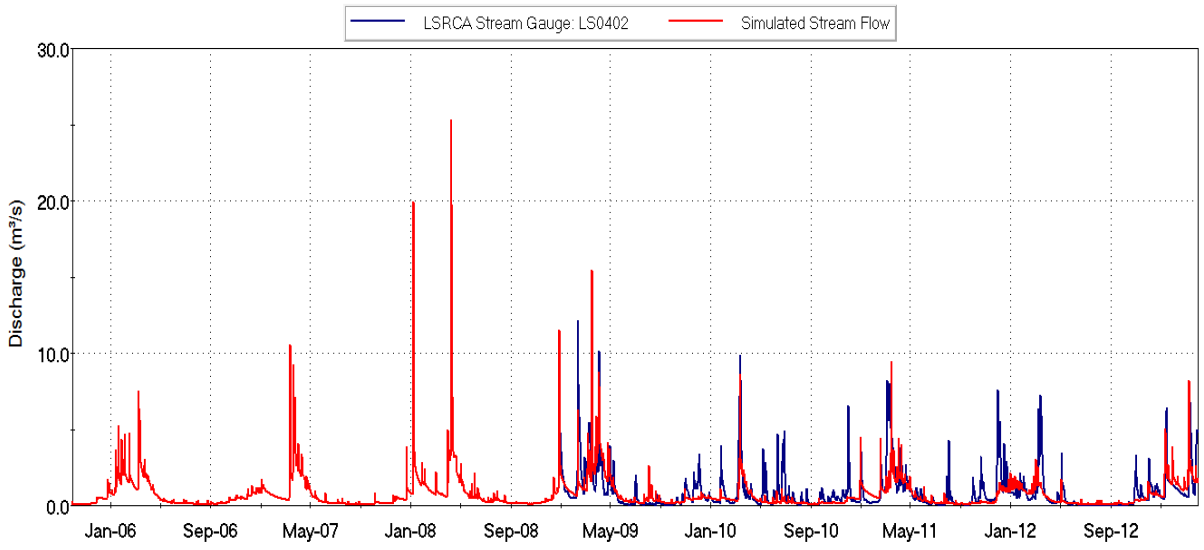

Figure 11.13: Simulated streamflow versus observed mean daily streamflow at Whites Creek at Regional Road 23 (LSRCA ID: LS0402).

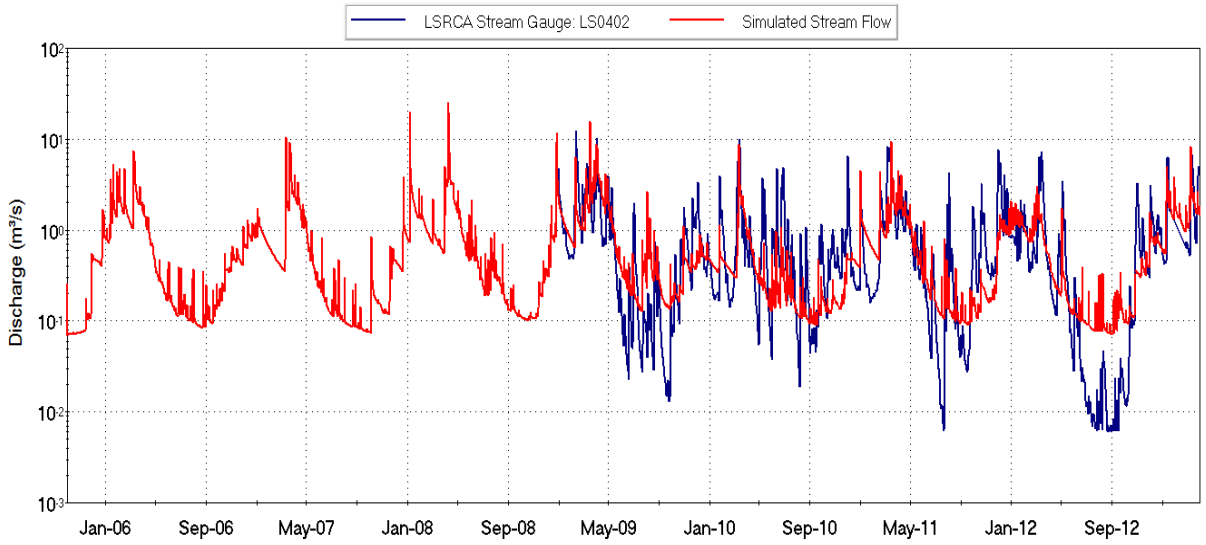

Figure 11.14: Log of simulated streamflow versus log of the observed mean daily streamflow at Whites Creek at Regional Road 23 (LSRCA ID: LS0402).

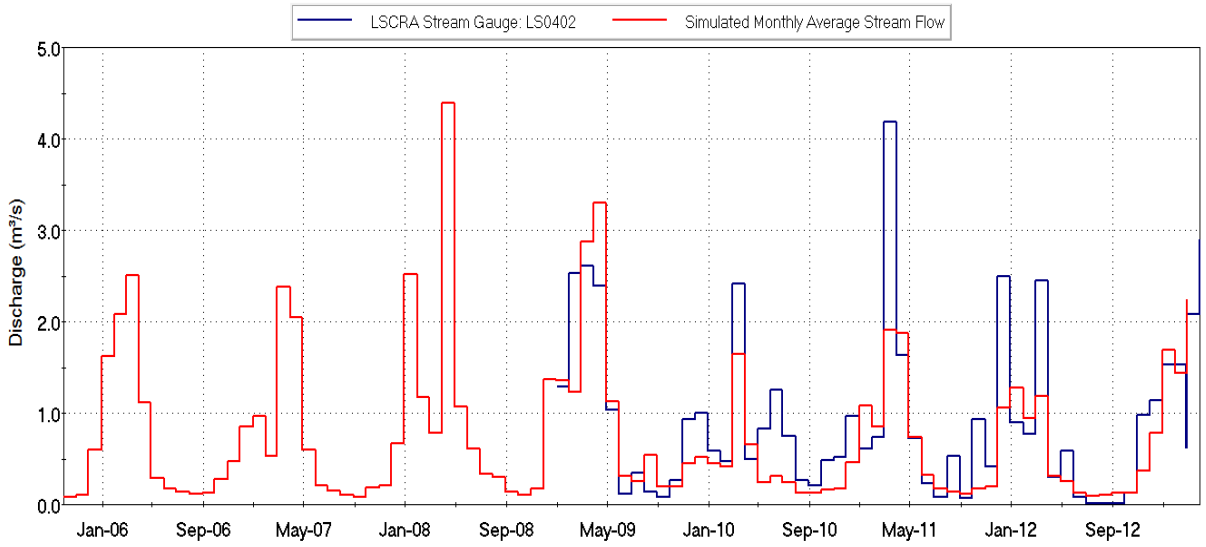

Figure 11.15: Monthly simulated streamflow versus observed streamflow at Whites Creek at Regional Rd. 23 (LSRCA ID: LS0402).

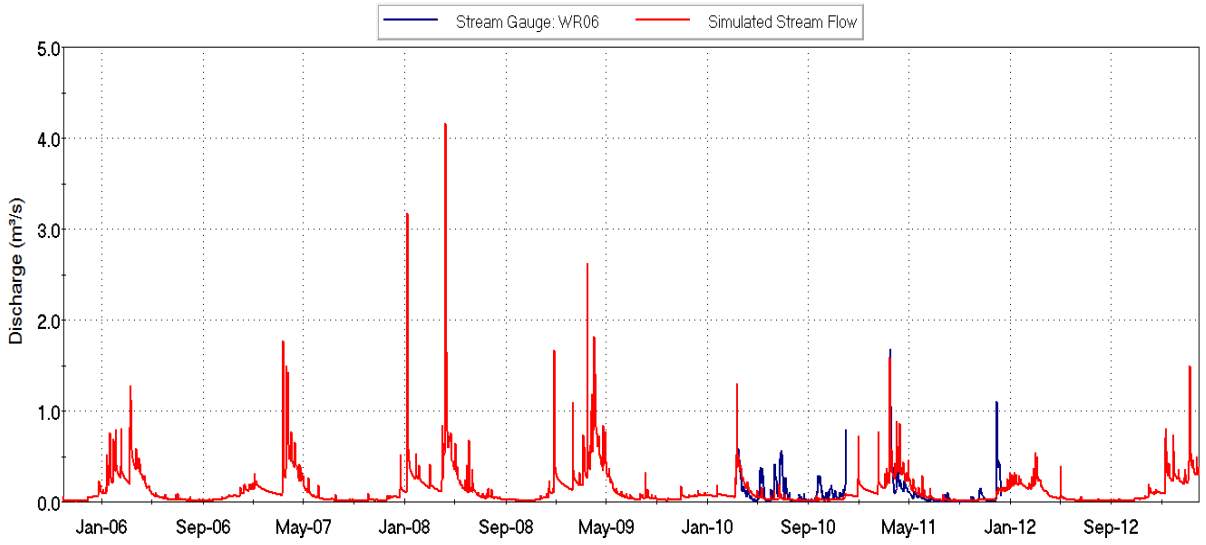

Figure 11.16: Simulated streamflow versus observed daily streamflow at Whites Creek (TrentU-Dillon ID: WR06).

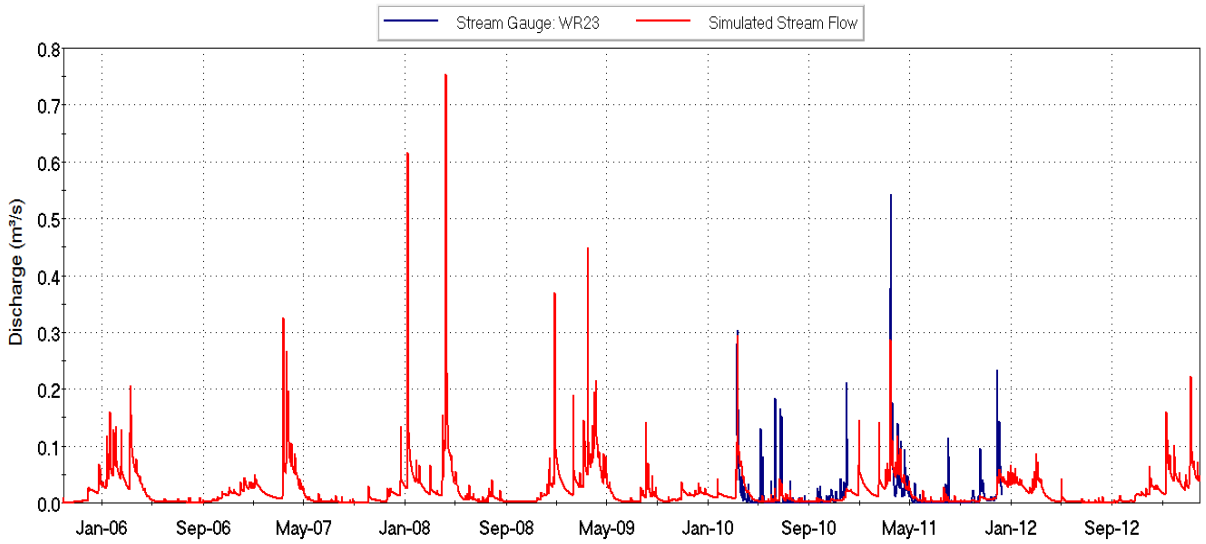

Figure 11.17: Simulated streamflow versus observed daily streamflow at Whites Creek (TrentU-Dillon ID: WR23).

12 Subwatershed Stress Assessment

12.1 Overview

A Tier 2 Water Budget is designed to identify subwatersheds that are potentially stressed from a water quantity perspective. Specifically, the stress assessment evaluates the ratio of the consumptive demand for permitted and non-permitted users to the available water supply (i.e., recharge plus lateral inflow minus water reserve), within each subwatershed and determines whether the ratio, referred to as the percent water demand, exceeds threshold values shown in Table 12.1.

Tier 1 Stress Assessments were conducted for the Ramara Creeks, Whites Creek, and Talbot River subwatersheds using (LSRCA, 2009) and found the subwatersheds were not stressed. The Tier 1 assessment was a high-level screening assessment using simplified water budget accounting to provide an understanding of the available groundwater and surface water resources by subwatershed on an annual and monthly scale. This Tier 2 Water Budget analyzed the available data at the same spatial and temporal scale but with a more complex integrated model.

Estimates of the major components of the water budget have been discussed in the preceding sections of this report, including water demand, water supply (recharge, streamflow, as determined from the model), and water reserve. The Tier 2 stress assessment integrates and compares these estimates to evaluate the overall level of stress within each catchment. Particular care was made to properly represent the interaction between the groundwater and surface water systems in the modelling analyses, as required by the Technical Rules for Assessment Reports. The linkage of the groundwater model to the hydrologic analyses and integrated model calibration helped to ensure a balanced assessment of stress levels.

A Tier 2 analysis requires the evaluation of the following scenarios, based on Table 4.9 in the Water Budget and Water Quantity Risk Assessment Guide (MNR, 2011):

Scenario	Description	Data Restrictions - Demand	Data Restrictions - Supply and Reserve
A	existing system – average	Data related to the study period	Data related to climate and stream flow is the historical data set for climate and streamflow.
B	existing system and future demand	Data related to demand associated with the system within the subwatershed reflects future development in the subwatershed	Data related to climate and stream flow is the historical data set for climate and streamflow. Data related to land cover reflects future development in the subwatershed.
D	existing system and 2-year drought	Data related to the study period	Data related to climate and stream flow reflects the 2-year drought period.
E	existing system and future 2-year drought	Data related to demand associated with an existing system within the subwatershed reflects future development in the subwatershed.	Data related to climate and stream flow reflects the 2-year drought period. Data related to land cover reflects future development in the subwatershed
G	existing system and 10-year drought	Data related to the study period	Data related to climate and stream flow reflects the 10-year drought period.
H	existing system and future 10-year drought	Data related to demand associated with an existing system within the subwatershed reflects future development in the subwatershed.	Data related to climate and stream flow reflects the 10-year drought period. Data related to land cover reflects the future development in the subwatershed.

Scenarios C and F have been eliminated in the table presented here as there are no new "planned" water supply systems in the study area.

12.2 Water Demand Calculation Methodology

The Technical Rules for Assessment Reports provides the following equation for calculating the percent water demand for groundwater:

$$\textit{Percent Water Demand} = \frac{Q_{DEMAND}}{Q_{SUPPLY} - Q_{RESERVE}} \times 100$$

The terms of the equation as follows:

Term	Definition	Calculation
Q_{DEMAND}	Groundwater Consumptive Demand	Groundwater demand is calculated as the estimated average annual and monthly rate of groundwater takings in a subwatershed.
Q_{SUPPLY}	Groundwater Supply	Groundwater supply is calculated as the estimated annual recharge rate plus the estimated groundwater inflow into a subwatershed.
$Q_{RESERVE}$	Groundwater Reserve	Groundwater Reserve is the component of baseflow discharge reserved for ecological needs or other users, defined as 10% of the groundwater discharge to streams in a subwatershed.

Q_{DEMAND} was calculated for study area subwatersheds in the manner prescribed above, as presented in Section 6. Q_{SUPPLY} was calculated in accordance with:

$$Q_{SUPPLY} = Q_{RECHARGE} + Q_{IN}$$

12.3 Tier 2 Stress Assessment Results

12.3.1 Groundwater Stress Assessment: Current Conditions

Output from the numerical model was used to produce tables summarizing the water balance under current and future conditions. The components of the water budget for each subwatershed are shown in Table 12.4 for current conditions.

Using the stress assessment equations presented above, the percent water demand for current conditions are shown in Table 12.5. Under current conditions, all of the watersheds were found to be at a low stress level. The monthly stress assessment under current conditions is presented in Table 12.6.

For comparison, in the previous Tier 1 study (LSRCA, 2009), current conditions percent water demand was found to be 0.2 % (Whites Creek), 1% (Ramara Creeks), and 4% (Talbot River), respectively. Small differences exist between the consumptive demand values derived in the Tier 1 and the values provided in Table 12.5. The Tier 1 study was completed before the introduction of the WTRS and some of the municipal takings were estimated using their maximum permitted rates.

Differences in the methods of estimating recharge, discharge to streams, and cross-watershed flows result in additional variances in the values used in the water demand computations between the two studies.

The monthly stress assessment results for the current conditions show that the percent groundwater demand is at its highest during the summer months of July and August for all three of the study subwatersheds. Percent demands in the Ramara Creeks (2.9%), Talbot River (2.2%) and Whites Creek (0.5%) subwatersheds are below 10% throughout the year, indicating a low stress level.

12.3.2 Groundwater Stress Assessment: Future Conditions

The detailed components of the water budget for each subwatershed are shown in Table 12.7 for future demand conditions. Using the stress assessment equations presented earlier, the percent water demand for future conditions are shown in Table 12.8. The monthly stress assessment under future conditions is presented in Table 12.9. Under future conditions, all of the watersheds remain at the low stress level. These values are consistent with the values derived in the previous Tier 1 study (LSRCA, 2009). On a monthly basis, the maximum percent demands in the Ramara Creeks (3.5%), Talbot River (6.6%) and Whites Creek (0.5%) subwatersheds remain below 10% throughout the year, indicating a low stress level under future conditions.

12.4 Tables and Figures

Table 12.1: Tier 2 groundwater stress thresholds.

Groundwater Quantity Stress Assignment	Average Annual	Monthly Maximum
Significant	> 25%	> 50%
Moderate	> 10%	> 25%
Low	0 – 10%	0 – 25%

Table 12.2: Current groundwater consumption summary.

Current Groundwater Consumption (m^3/yr)						
Watershed Name	**Municipal**	**Unserviced**	**PTTW**	**Quarry Dewatering**	**Agricultural**	**Total Consumption**
Ramara Creeks	109,758	82,095	4,127	0	14,358	210,338
Talbot River	26,481	29,224	6,136	1,018,280	31,960	1,112,081
Whites Creek	0	6,725	0	0	18,607	25,332
Current Groundwater Consumption (m^3/d)						
Watershed Name	**Municipal**	**Unserviced**	**PTTW**	**Quarry Dewatering**	**Agricultural**	**Total Consumption**
Ramara Creeks	301	225	11	0	39	576
Talbot River	73	80	17	2,788	88	3045
Whites Creek	0	18	0	0	51	69

*values subject to round off

Table 12.3: Future groundwater consumption summary.

Future Groundwater Consumption (m^3/yr)						
Watershed Name	**Municipal**	**Unserviced**	**PTTW**	**Quarry Dewatering**	**Agricultural**	**Total Consumption**
Ramara Creeks	150,118	82,095	4,127	0	14,358	250,698
Talbot River	29,147	29,224	6,136	3,341,344	31,960	3,437,811
Whites Creek	0	6,725	0	0	18,607	25,332
Future Groundwater Consumption (m^3/d)						
Watershed Name	**Municipal**	**Unserviced**	**PTTW**	**Quarry Dewatering**	**Agricultural**	**Total Consumption**
Ramara Creeks	411	225	11	0	39	686
Talbot River	80	80	17	9,148	88	9412
Whites Creek	0	18	0	0	51	69

*values subject to round off

Table 12.4: Model water budget details - Current Conditions

Inflows and Outflows (all values in m^3/d)	Ramara Creeks	Talbot River	Whites Creek
Inflow Components			
Recharge in	20,671	142,990	24,250
Stream leakage in	244	2,722	121
Lake leakage in	0	252	0
Lateral inflow	7,782	12,729	9,039
Total Groundwater Inflow:	**28,697**	**158,693**	**33,410**
Outflow Components			
Lateral outflow	10,662	14,204	11,365
Net groundwater discharge to surface features	14,439	132,369	18,150
Net outflow in at constant head cells	3,285	0	3,894
Wells	312	89	0
Total Groundwater Outflow:	**28,698**	**146,662**	**33,409**

*values subject to round off

Table 12.5: Percent Water Demand stress assessment – Current Conditions

Component		Ramara Creeks	Talbot River	Whites Creek
Groundwater Supply	Recharge In	20,671	142,990	24,250
	Stream Seepage	244	2722	121
	Lake Seepage	0	252	0
	Lateral Inflow	7,782	12,729	9,039
	Total:	28,697	158,693	33,410
Groundwater Reserve		1,444	13,237	1,815
Consumptive Demand		575	3045	69
Percent Water Demand		**2.1%**	**2.1%**	**0.2%**

*values subject to round off

Table 12.6: Monthly percent water demand stress assessment – Current Conditions.

Sub-watershed	Area (km^2)	Month	Days	Total Recharge		Lateral Groundwater Flows		Baseflow		Reserve (10% Baseflow)		Groundwater Demand			% Water Demand
				mm/mo	m^3/d	mm/mo	m^3/d	mm/mo	m^3/d	mm/mo	m^3/d	m^3/mo	mm/mo	m^3/d	%
Ramara	139	January	31	4.7	20,915	1.7	7,782	3.2	14,439	0.32	1,444	14,949	0.11	482.2	1.8%
		February	28	4.3	20,915	1.6	7,782	2.9	14,439	0.29	1,444	13,266	0.10	469.6	1.7%
		March	31	4.7	20,915	1.7	7,782	3.2	14,439	0.32	1,444	14,208	0.10	458.3	1.7%
		April	30	4.5	20,915	1.7	7,782	3.1	14,439	0.31	1,444	14,432	0.10	481.1	1.8%
		May	31	4.7	20,915	1.7	7,782	3.2	14,439	0.32	1,444	17,271	0.12	557.1	2.0%
		June	30	4.5	20,915	1.7	7,782	3.1	14,439	0.31	1,444	22,004	0.16	733.5	2.7%
		July	31	4.7	20,915	1.7	7,782	3.2	14,439	0.32	1,444	24,581	0.18	792.9	2.9%
		August	31	4.7	20,915	1.7	7,782	3.2	14,439	0.32	1,444	24,442	0.18	788.5	2.9%
		September	30	4.5	20,915	1.7	7,782	3.1	14,439	0.31	1,444	20,718	0.15	690.6	2.5%
		October	31	4.7	20,915	1.7	7,782	3.2	14,439	0.32	1,444	15,194	0.11	490.1	1.8%
		November	30	4.5	20,915	1.7	7,782	3.1	14,439	0.31	1,444	14,063	0.10	468.8	1.7%
		December	31	4.7	20,915	1.7	7,782	3.2	14,439	0.32	1,444	14,838	0.11	478.6	1.8%
		Totals	**Days**	**mm/a**	**m^3/d**	**mm/a**	**m^3/d**	**mm/a**	**m^3/d**	**mm/a**	**m^3/d**	**m^3/a**	**mm/a**	**m^3/d**	**%**
			365	***55.1***	***20,915***	***20.5***	***7,782***	***38.1***	***14,439***	***3.8***	***1,444***	***209,964***	***1.52***	***575***	***2.1%***
Talbot	365	January	31	1.8	145,964	1.1	12,729	11.2	132,369	1.12	13,237	91,265	0.25	2944	2.0%
		February	28	1.6	145,964	1.0	12,729	10.2	132,369	1.02	13,237	82,995	0.23	2938	2.0%
		March	31	1.8	145,964	1.1	12,729	11.2	132,369	1.12	13,237	91,379	0.25	2948	2.0%
		April	30	1.7	145,964	1.0	12,729	10.9	132,369	1.09	13,237	88,595	0.24	2953	2.0%
		May	31	1.8	145,964	1.1	12,729	11.2	132,369	1.12	13,237	91,897	0.25	2964	2.0%
		June	30	1.7	145,964	1.0	12,729	10.9	132,369	1.09	13,237	97,121	0.27	3237	2.2%
		July	31	1.8	145,964	1.1	12,729	11.2	132,369	1.12	13,237	100,699	0.28	3248	2.2%
		August	31	1.8	145,964	1.1	12,729	11.2	132,369	1.12	13,237	100,273	0.27	3235	2.2%
		September	30	1.7	145,964	1.0	12,729	10.9	132,369	1.09	13,237	96,818	0.27	3227	2.2%
		October	31	1.8	145,964	1.1	12,729	11.2	132,369	1.12	13,237	91,451	0.25	2950	2.0%
		November	30	1.7	145,964	1.0	12,729	10.9	132,369	1.09	13,237	88,441	0.24	2948	2.0%
		December	31	1.8	145,964	1.1	12,729	11.2	132,369	1.12	13,237	91,351	0.25	2947	2.0%
		Totals	**Days**	**mm/a**	**m^3/d**	**mm/a**	**m^3/d**	**mm/a**	**m^3/d**	**mm/a**	**m^3/d**	**m^3/mo**	**mm/a**	**m^3/d**	**%**
			365	***20.9***	***145,964***	***12.7***	***12,729***	***132.4***	***132,369***	***13.2***	***13,237***	***1,112,284***	***3.04***	***3045***	***2.1%***
Whites	104	January	31	6.2	24,371	2.7	9,039	5.4	18,150	0.54	1,815	571	0.01	18	0.1%
		February	28	5.7	24,371	2.5	9,039	4.9	18,150	0.49	1,815	520	0.01	18	0.1%
		March	31	6.2	24,371	2.7	9,039	5.4	18,150	0.54	1,815	571	0.01	18	0.1%
		April	30	6.0	24,371	2.6	9,039	5.2	18,150	0.52	1,815	552	0.01	18	0.1%
		May	31	6.2	24,371	2.7	9,039	5.4	18,150	0.54	1,815	571	0.01	18	0.1%
		June	30	6.0	24,371	2.6	9,039	5.2	18,150	0.52	1,815	5,128	0.05	171	0.5%
		July	31	6.2	24,371	2.7	9,039	5.4	18,150	0.54	1,815	5,299	0.05	171	0.5%
		August	31	6.2	24,371	2.7	9,039	5.4	18,150	0.54	1,815	5,299	0.05	171	0.5%
		September	30	6.0	24,371	2.6	9,039	5.2	18,150	0.52	1,815	5,128	0.05	171	0.5%
		October	31	6.2	24,371	2.7	9,039	5.4	18,150	0.54	1,815	571	0.01	18	0.1%
		November	30	6.0	24,371	2.6	9,039	5.2	18,150	0.52	1,815	552	0.01	18	0.1%
		December	31	6.2	24,371	2.7	9,039	5.4	18,150	0.54	1,815	571	0.01	18	0.1%
		Totals	**Days**	**mm/a**	**m^3/d**	**mm/a**	**m^3/d**	**mm/a**	**m^3/d**	**mm/a**	**m^3/d**	**m^3/mo**	**mm/a**	**m^3/d**	**%**
			365	***73.5***	***24,371***	***31.8***	***9,039***	***63.8***	***18,150***	***6.4***	***1,815***	***25,332***	***0.24***	***69***	***0.2%***

Table 12.7: Model water budget details - Future Conditions

Inflows and Outflows (all values in m^3/d)	Ramara Creeks	Talbot River	Whites Creek
Inflow Components			
Recharge in	20,807	143,315	24,250
Stream leakage in	229	2,902	120
Lake leakage in	0	307	0
Lateral inflow	7,748	12,672	9,051
Total Groundwater Inflow:	**28,784**	**159,196**	**33,421**
Outflow Components			
Lateral outflow	10,484	14,043	11,381
Net groundwater discharge to surface features	14,606	133,291	18,148
Net outflow in at constant head cells	3,272	0	3,892
Wells	422	97	0
Total Groundwater Outflow:	**28,784**	**147,430**	**33,421**

*values subject to round off

Table 12.8: Future groundwater demand.

Component		Ramara Creeks	Talbot River	Whites Creek
Groundwater Supply	Recharge In	20,807	143,315	24,250
	Stream Seepage	229	2,902	120
	Lake Seepage	0	307	0
	Lateral Inflow	7,748	12,672	9,051
	Total:	28,784	159,196	33,421
Groundwater Reserve		1,461	13,329	1,815
Consumptive Demand		686	9412	69
Percent Water Demand		**2.5%**	**6.5%**	**0.2%**

*values subject to round off

Table 12.9: Monthly percent water demand stress assessment – Future Conditions.

Sub-watershed	Area (km^2)	Month	Days	Total Recharge		Lateral Groundwater Inputs		Baseflow		Reserve (10% Baseflow)		Groundwater Demand			% Water Demand
				mm/mo	m^3/d	mm/mo	m^3/d	mm/mo	m^3/d	mm/mo	m^3/d	m^3/mo	mm/mo	m^3/d	%
Ramara	139	January	31	4.7	21,036	1.7	7,748	3.3	14,606	0.33	1,461	17,882	0.13	577	2.1%
		February	28	4.3	21,036	1.6	7,748	3.0	14,606	0.30	1,461	15,807	0.11	560	2.0%
		March	31	4.7	21,036	1.7	7,748	3.3	14,606	0.33	1,461	16,870	0.12	544	2.0%
		April	30	4.6	21,036	1.7	7,748	3.2	14,606	0.32	1,461	17,250	0.12	575	2.1%
		May	31	4.7	21,036	1.7	7,748	3.3	14,606	0.33	1,461	20,764	0.15	670	2.5%
		June	30	4.6	21,036	1.7	7,748	3.2	14,606	0.32	1,461	26,033	0.19	868	3.2%
		July	31	4.7	21,036	1.7	7,748	3.3	14,606	0.33	1,461	29,386	0.21	948	3.5%
		August	31	4.7	21,036	1.7	7,748	3.3	14,606	0.33	1,461	29,198	0.21	942	3.4%
		September	30	4.6	21,036	1.7	7,748	3.2	14,606	0.32	1,461	24,289	0.18	810	3.0%
		October	31	4.7	21,036	1.7	7,748	3.3	14,606	0.33	1,461	18,218	0.13	588	2.2%
		November	30	4.6	21,036	1.7	7,748	3.2	14,606	0.32	1,461	16,753	0.12	558	2.0%
		December	31	4.7	21,036	1.7	7,748	3.3	14,606	0.33	1,461	17,731	0.13	572	2.1%
		Totals	**Days**	**mm/a**	**m^3/d**	**mm/a**	**m^3/d**	**mm/a**	**m^3/d**	**mm/a**	**m^3/d**	**m^3/a**	**mm/a**	**m^3/d**	**%**
			365	***55.5***	***21,036***	***20.4***	***7,748***	***38.5***	***14,606***	***3.9***	***1,461***	***250,180***	***1.81***	***685***	***2.5%***
Talbot	365	January	31	1.8	146,524	1.1	12,672	11.3	133,291	1.13	13,329	288,627	0.79	9311	6.4%
		February	28	1.6	146,524	1.0	12,672	10.3	133,291	1.03	13,329	262,832	0.72	9304	6.4%
		March	31	1.8	146,524	1.1	12,672	11.3	133,291	1.13	13,329	288,754	0.79	9315	6.4%
		April	30	1.7	146,524	1.0	12,672	10.9	133,291	1.09	13,329	279,615	0.77	9320	6.4%
		May	31	1.8	146,524	1.1	12,672	11.3	133,291	1.13	13,329	289,307	0.79	9332	6.4%
		June	30	1.7	146,524	1.0	12,672	10.9	133,291	1.09	13,329	288,182	0.79	9606	6.6%
		July	31	1.8	146,524	1.1	12,672	11.3	133,291	1.13	13,329	298,159	0.82	9618	6.6%
		August	31	1.8	146,524	1.1	12,672	11.3	133,291	1.13	13,329	297,694	0.81	9603	6.6%
		September	30	1.7	146,524	1.0	12,672	10.9	133,291	1.09	13,329	287,855	0.79	9595	6.6%
		October	31	1.8	146,524	1.1	12,672	11.3	133,291	1.13	13,329	288,822	0.79	9317	6.4%
		November	30	1.7	146,524	1.0	12,672	10.9	133,291	1.09	13,329	279,449	0.77	9315	6.4%
		December	31	1.8	146,524	1.1	12,672	11.3	133,291	1.13	13,329	288,721	0.79	9314	6.4%
		Totals	**Days**	**mm/a**	**m^3/d**	**mm/a**	**m^3/d**	**mm/a**	**m^3/d**	**mm/a**	**m^3/d**	**m^3/mo**	**mm/a**	**m^3/d**	**%**
			365	***21.0***	***146,524***	***12.7***	***12,672***	***133.3***	***133,291***	***13.3***	***13,329***	***3,438,016***	***9.41***	***9413***	***6.5%***
Whites	104	January	31	6.3	24,370	2.7	9,039	5.4	18,148	0.54	1,815	571	0.01	18	0.1%
		February	28	5.7	24,370	2.5	9,039	4.9	18,148	0.49	1,815	520	0.01	18	0.1%
		March	31	6.3	24,370	2.7	9,039	5.4	18,148	0.54	1,815	571	0.01	18	0.1%
		April	30	6.1	24,370	2.6	9,039	5.2	18,148	0.52	1,815	552	0.01	18	0.1%
		May	31	6.3	24,370	2.7	9,039	5.4	18,148	0.54	1,815	571	0.01	18	0.1%
		June	30	6.1	24,370	2.6	9,039	5.2	18,148	0.52	1,815	5,128	0.05	171	0.5%
		July	31	6.3	24,370	2.7	9,039	5.4	18,148	0.54	1,815	5,299	0.05	171	0.5%
		August	31	6.3	24,370	2.7	9,039	5.4	18,148	0.54	1,815	5,299	0.05	171	0.5%
		September	30	6.1	24,370	2.6	9,039	5.2	18,148	0.52	1,815	5,128	0.05	171	0.5%
		October	31	6.3	24,370	2.7	9,039	5.4	18,148	0.54	1,815	571	0.01	18	0.1%
		November	30	6.1	24,370	2.6	9,039	5.2	18,148	0.52	1,815	552	0.01	18	0.1%
		December	31	6.3	24,370	2.7	9,039	5.4	18,148	0.54	1,815	571	0.01	18	0.1%
		Totals	**Days**	**mm/a**	**m^3/d**	**mm/a**	**m^3/d**	**mm/a**	**m^3/d**	**mm/a**	**m^3/d**	**m^3/mo**	**mm/a**	**m^3/d**	**%**
			365	***73.9***	***24,370***	***31.8***	***9,039***	***63.8***	***18,148***	***6.4***	***1,815***	***25,332***	***0.24***	***69***	***0.2%***

13 Drought Scenarios

The Tier 2 Water Budget analysis also evaluated the effects of sustained drought on the water budget of each of the study subwatersheds. The drought analysis assessed the response of groundwater levels, groundwater discharge to streams, total streamflow and stage in the wetlands. This is different from the Source Water Protection studies, which focus principally on predicting the effects of drought conditions on municipal wells.

Two drought analyses were conducted, involving a total of four scenario simulations. The first analysis represented an extreme condition assuming no recharge occurs to the groundwater system for a two-year period, under both existing conditions and future land use and water-taking conditions. The second analysis examined how the subwatersheds would respond to conditions similar to a historic 10-year period of low rainfall. The simulation of the extended drought period, corresponding to 1957 through 1967, provided an opportunity to evaluate the influence of groundwater and wetland storage on drought response. Results of the two drought analyses are discussed below.

13.1 2-year Drought Simulation

A 2-year drought assessment was completed by setting recharge rates to zero across the study area and running the model for a two-year period. Under these extreme conditions, the water table is seen to decline across the model and groundwater discharge to streams is also significant reduced. For the current conditions scenario, the simulated groundwater heads in Layer 3 (weathered bedrock) at the end of the two-year drought simulation and the change in water level from the start of the simulation (with average annual recharge) are presented in Figure 13.1 and Figure 13.2, respectively. Figure 13.3 and Figure 13.4 present the simulated heads in Layer 3 and the change in simulated levels at the end of the two-year drought for the future conditions scenario.

The response to the drought is very similar for both scenarios; the largest declines in simulated heads occur in the topographic high points in the model, which generally represent areas of groundwater recharge. Changes in head were generally between 0.5 and 2.5 metres, although changes as high as 15 m were noted in a few locations in the model. Despite the reduced heads, none of the municipal pumping wells went dry during the two-year drought under current or future conditions.

Groundwater discharge to streams at the start and end of the two-year drought (under current conditions) are presented in Figure 13.5 and Figure 13.6, respectively. The percent change in the surface discharge due to the drought is presented in Figure 13.7 for the current conditions scenario. Figure 13.8 and Figure 13.9 present the groundwater discharge to streams at the start and end of the two-year drought under future conditions, and Figure 13.10 presents the percent change. The largest impacts due to drought are seen in the headwater tributaries across the model, which are sustained mainly by groundwater discharge that occurs where the streambed intersects the water table. These tributaries are therefore sensitive to small changes in groundwater levels. Table 13.1 summarizes the change in groundwater discharge to surface features on a subwatershed basis for the current and future conditions scenarios.

13.2 10-year Drought Simulation

The 10-year drought scenario was analyzed using the transient GSFLOW model. The model run spanned from October 1953 to October 1967 and used MNR in-filled hourly precipitation data for stations near the study area. Annual and monthly precipitation for the period is shown in Figure 13.11 and Figure 13.12, respectively. The model run encompassed the drought period (October 1956 to September 1967) with an additional three years for model start-up. The simulations were run using future land use conditions.

All components of the water budget are affected by the decrease in precipitation over the drought period. For example, Figure 13.15 shows annual actual evapotranspiration (AET) averaged over the study area. The AET varies considerably because, with less precipitation, there is less water available for ET in areas of well-drained soils (such as the alvar plain). Figure 13.15 shows that monthly potential evapotranspiration (PET) averaged over the study area does not vary greatly from year to year but that monthly AET varies considerably. Monthly average soil moisture (Figure 13.16), in turn, fluctuates because of differences in precipitation and AET. Groundwater recharge varies from year to year as shown in Figure 13.17. Monthly average groundwater recharge, shown in Figure 13.18, also varies considerably between the wetter and drier months with many consecutive months having little or no recharge.

Figure 13.19 presents the simulated heads in Layer 3 (weathered bedrock aquifer) at the beginning of the 10-year drought period. For this study, simulated monthly average conditions (i.e., aquifer heads and streamflow) in July 1956 were close to the annual average values for 1955 and 1956 and represent average conditions prior to the start of the drought period. The month in which the lowest head occurred varied across the study area with March 1959 most frequent in the uplands (as shown in the hydrograph in Figure 13.20) and November 1964 in the lowlands (as shown in the hydrograph in Figure 13.21). The differences in simulated heads between these two dates were generally small and the patterns in drought response were similar. For this study, monthly average conditions for November 1964 were taken to represent the most severe drought conditions. Simulated average monthly heads for November 1964 are shown in Figure 13.22. Decrease in the simulated heads (drawdowns) between July 1956 and November 1964 is shown in Figure 13.23.

The areas most affected by the drought are similar to those in the two-year drought simulation. As might be expected, the drawdowns are not as severe as those predicted by the 2-year drought scenario, with drawdowns generally less than 1.5 m rather than the less than 2.5 m as predicted in the 2-year simulation. Some areas, particularly in the southeast show a large decrease (over 10 m) but these areas are mostly outside the study watersheds. No municipal pumping wells went dry during the 10-year drought assessment.

Total streamflow at the start of the drought (i.e., July 1956) and at the most severe period of the drought (i.e., November 1964) are presented in Figure 13.24 and Figure 13.25, respectively. Total streamflow, as output from the GSFLOW model, includes contributions from overland runoff and channel precipitation as well as from groundwater inflow. The decrease in total streamflow was determined by comparing the July 1956 and November 1964 simulated flows and is shown in Figure 13.26. Figure 13.27 presents the percent change in total streamflow between the two periods. Decreases occur in the headwater tributaries, which accumulate downstream and are added to the losses experienced in the downstream reaches. Model results indicate that the largest relative impact on streamflow occurs in the headwater streams with many showing nearly 100% decrease in flow. The main tributaries are generally affected to a lesser degree.

Simulated groundwater discharge to streams at the start of the drought and at the most severe period of the drought are presented in Figure 13.28 and Figure 13.29, respectively. Simulated groundwater discharge to streams, as shown in these figures, represents the accumulated leakage

into the streams across the stream bed (also referred to as “hyporheic flow”). Interflow and groundwater discharge to land surface in the stream valleys also contributes to “baseflow” but, in GSFLOW, these flows are included in overland runoff to streams. The percent decrease in groundwater discharge to streams was determined by comparing the July 1956 and November 1964 simulated flows and is shown in Figure 13.26. Model results indicate that the large relative impact on groundwater discharge to streams occurs mainly in the alvar plain area, with many tributaries showing nearly 100% decrease in flow. The main tributaries of Rohallion Creek and Upper Talbot Creek are affected to a lesser degree. This is most likely due to the combination of higher hydraulic conductivity and low storage properties in the shallow bedrock of the alvar plain while the lower hydraulic conductivity and higher storage properties keep the water levels higher. This differs from the two-year drought impacts (shown in Figure 13.10) which had a more severe effect across the study watersheds. Table 13.2 summarizes the change in total streamflow and groundwater discharge to the major streams in each subwatershed.

The net monthly average groundwater discharge to all stream channels in each of the study watersheds is shown in Figure 13.31. Groundwater seepage to streams is at its minimum in late-summer/early fall and reaches a maximum in the late spring. The Talbot subwatershed, due to its larger size and the presence of the high recharge areas associated with the alvar plain, has the highest net groundwater discharge of the study catchments. Ramara Creeks and Whites Creek have very similar rates of groundwater discharge and show similar response to drought conditions. The response in these two watersheds to dry periods in April 1959 and September/October 1960 is more extreme than in the Talbot River subwatershed. The rates of groundwater discharge are less affected by drought after 1960 in Ramara Creeks and Whites Creek while the Talbot River subwatershed groundwater discharge rates decrease slightly during that period, reaching a minimum in October/November 1964.

Seepage to stream channels can also be measured on a reach-by-reach basis. Groundwater seepage to the reach immediately upstream of the LSRCA gauge on Whites Creek is shown on Figure 13.33. Discharge out of the groundwater system to the stream channel is considered a loss by GSFLOW and is negative on this plot. Seepage varies significantly on a daily basis (shown in blue) and monthly average values are used for long term comparisons. Large spikes can be observed on the daily hydrograph which correspond to surface runoff or snowmelt events. When stage in the channel increases during these flows, the gradient across the streambed decreases as well, reducing the volume of groundwater seeping into the stream. During large events, the gradient can reverse, forcing surface water into the aquifer. Water leaks back out over time after the stage has receded and groundwater heads rise. Several events of this nature can be observed on Figure 13.33. It also follows that groundwater discharge to streams intersecting the water table will typically be maximized during periods of low flow or stage in the early spring before the water table enters its summer recession. Figure 13.34 further illustrates this relationship between stream stage and aquifer head. When the stage in the creek exceeds the head in the groundwater system, seepage is reversed. A slight decreasing trend can be seen in the positive groundwater seepage over the drought period.

To better illustrate the connections between the groundwater system and specific surface features, groundwater seepage was plotted along the stream channels shown in Figure 13.35. Groundwater seepage along the entire main channel of Wainman’s Creek in the Ramara Creeks subwatershed in July 1956 and November 1964 is plotted on Figure 13.36. Chainage starts at Lake Simcoe and ends at a first-order stream in the Mara County Forest Wetland. Similar plots are presented for the Upper Talbot River (Figure 13.37) and for Whites Creek (Figure 13.38). The leakage values have all been normalized by the length of stream channel per cell.

High rates of seepage are generally noted at the downstream ends of the streams especially where the till layers are relatively thinner. Groundwater discharge is noted in all the wetland areas. Discharge rates are decreased significantly in November 1964 at the height of the 10-year drought.

The alvar plain provides high recharge to portions of the study area subwatersheds but the feature has low storage capacity. As such, the watersheds fed directly by the alvar are less buffered from the effects of long term drought due to the relatively small storage capacity in the bedrock aquifers. As will be discussed in the recharge area assessment (Section 14), many of the streams are recharged locally and the presence of deep flow paths tied to significant recharge areas was limited.

13.3 Tables and Figures

Table 13.1: Two-year drought impact on groundwater discharge to surface features.

Component	Ramara Creeks	Talbot River	Whites Creek
Current Conditions			
Average groundwater discharge (m^3/d)	10,112	118,166	13,647
Groundwater discharge at end of 2-year drought (m^3/d)	3,931	32,488	3,567
Percent Reduction	**61%**	**73%**	**74%**
Future Conditions			
Average groundwater discharge (m^3/d)	9,398	113,466	13,644
Groundwater discharge at end of 2-year drought (m^3/d)	3,736	30,558	3,566
Percent Reduction	**60%**	**73%**	**74%**

Table 13.2: Ten year drought impact on total streamflow and groundwater discharge to stream channels.

Component (m^3/s)	Wainman's Creek	Butternut Creek	Rohallion Creek	Upper Talbot River	Whites Creek
Monthly average total streamflow – July 1956	0.191	0.062	0.222	0.411	0.222
Monthly average total streamflow – November 1964	0.057	0.019	0.092	0.173	0.097
Percent Reduction	**70%**	**69%**	**59%**	**58%**	**56%**
Monthly groundwater discharge to streams - July 1956	0.056	0.021	0.100	0.158	0.104
Monthly groundwater discharge to streams - Nov. 1964	0.035	0.011	0.056	0.094	0.071
Percent Reduction	**38%**	**46%**	**44%**	**41%**	**32%**
*Note: Change in flow in the Lower Talbot River is not shown because it is affected by the change in assumed monthly inflows from Balsam Lake to Mitchell Lake between July and November.					

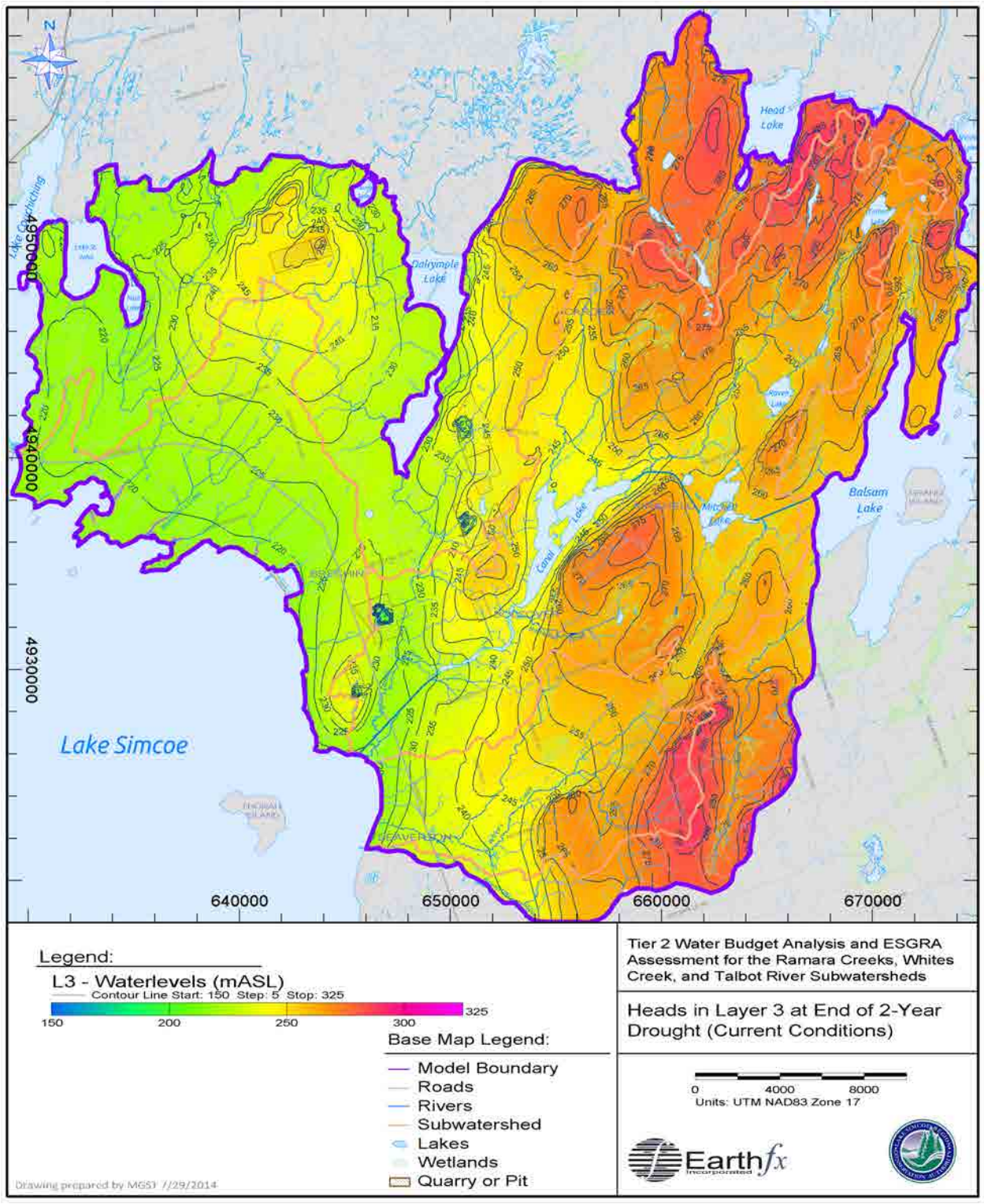

Figure 13.1: Simulated heads in Layer 3 (weathered bedrock) at the end of the two-year drought (current conditions).

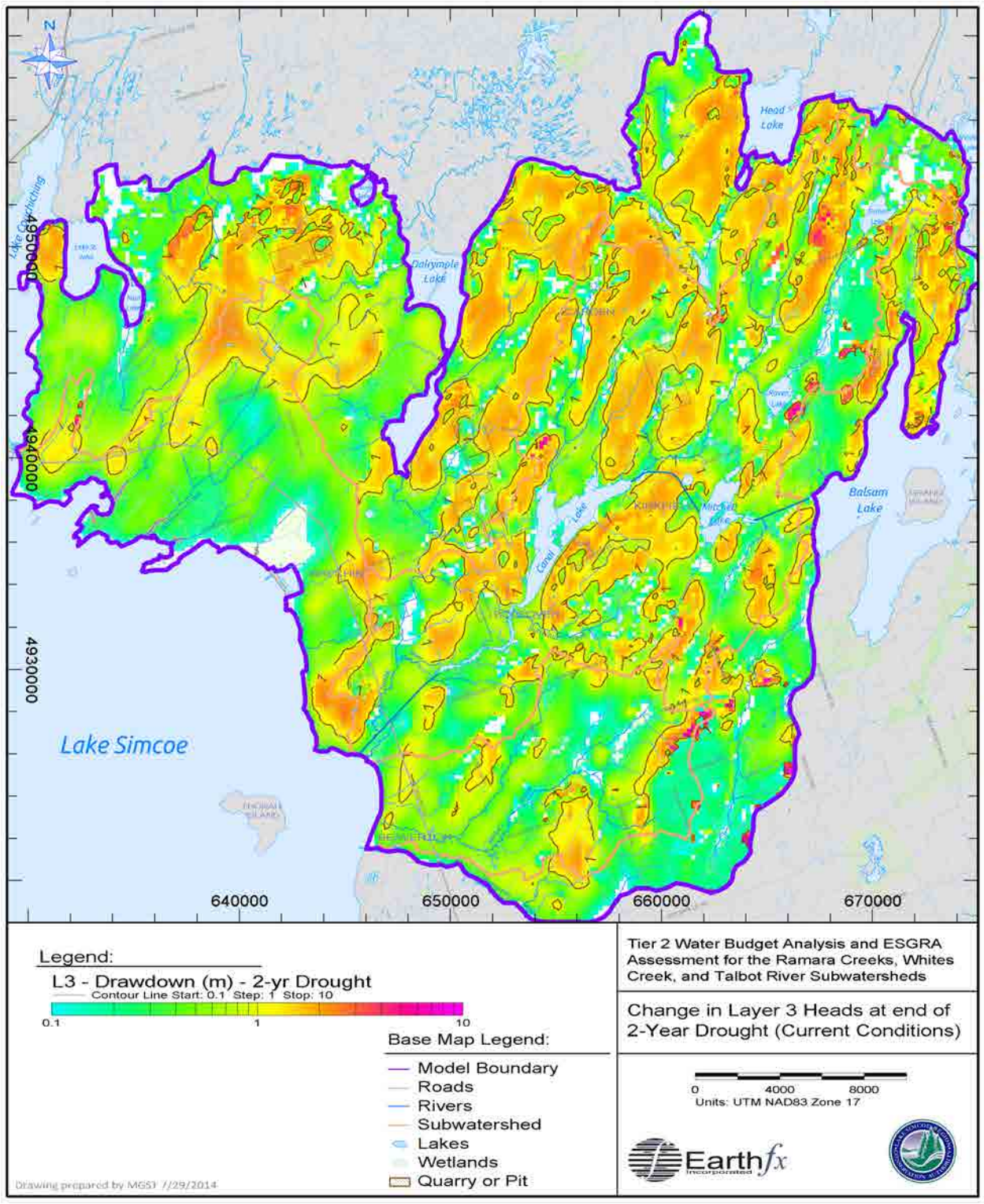

Figure 13.2: Change in Layer 3 heads after a two-year drought with no groundwater recharge (current conditions).

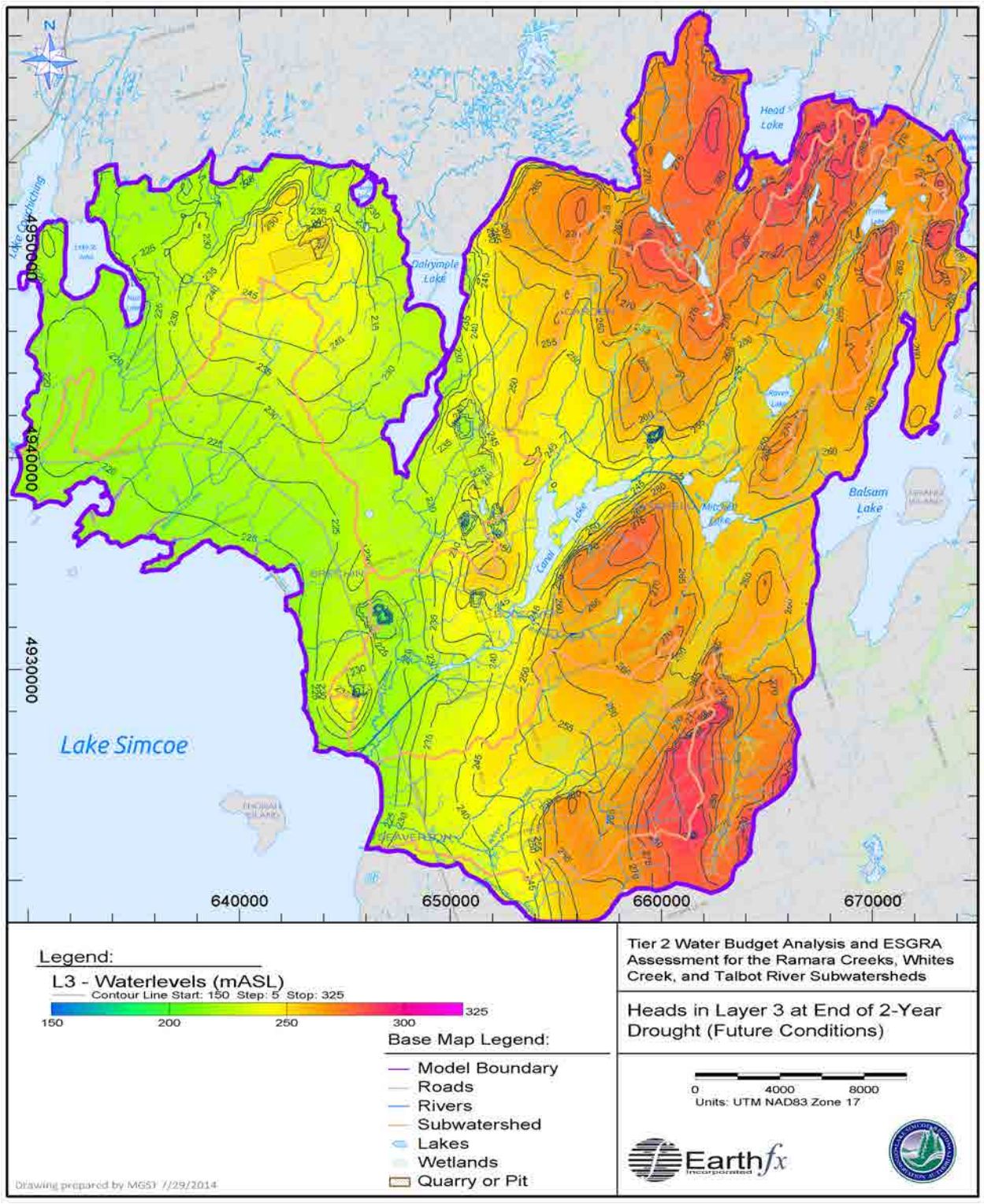

Figure 13.3: Simulated heads in Layer 3 (weathered bedrock) at end of two-year drought under future conditions.

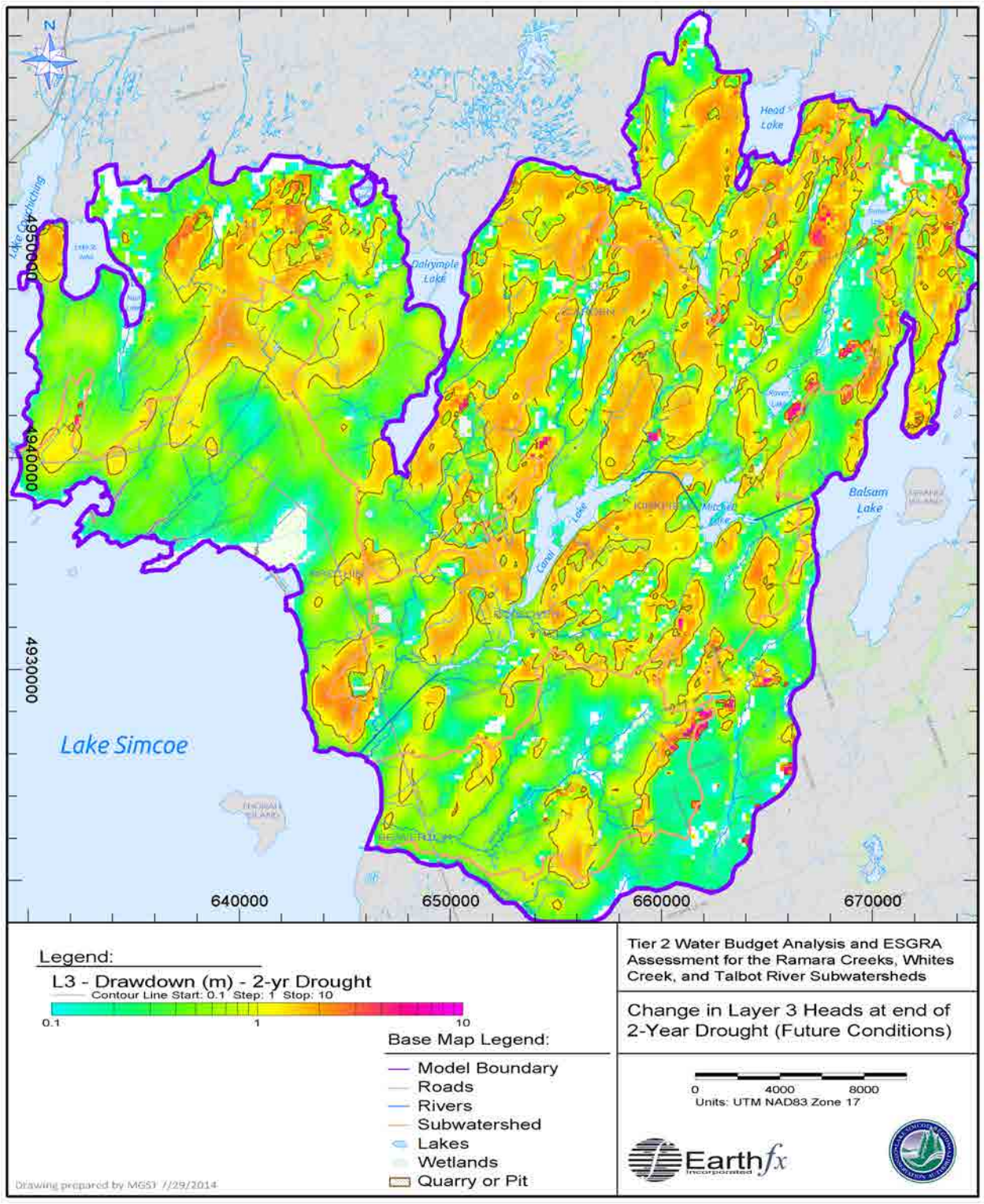

Figure 13.4: Change in Layer 3 (weathered bedrock contact aquifer) after two-year drought (future conditions).

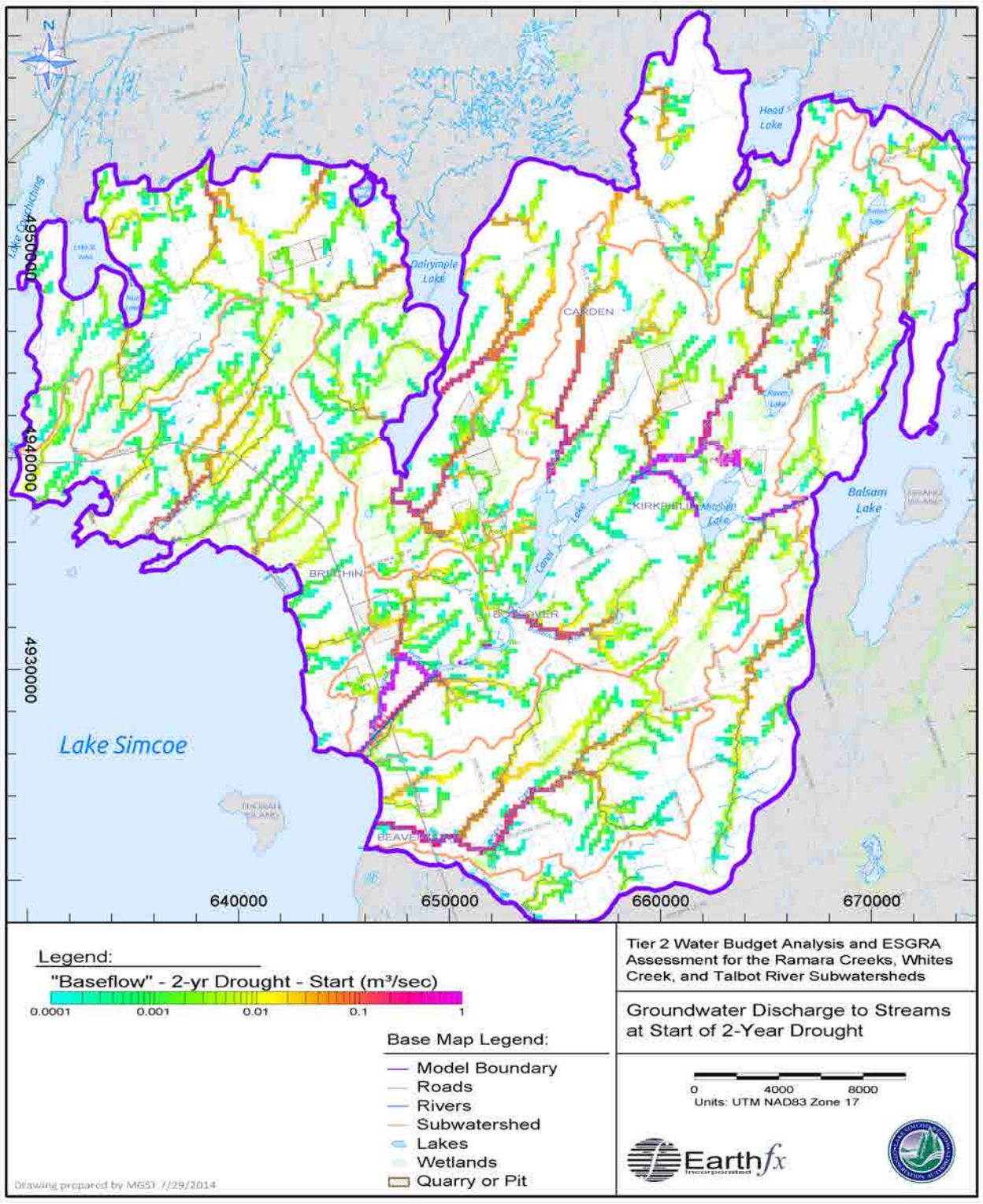

Figure 13.5: Simulated groundwater discharge to streams (baseflow) at start of two-year drought (current conditions).

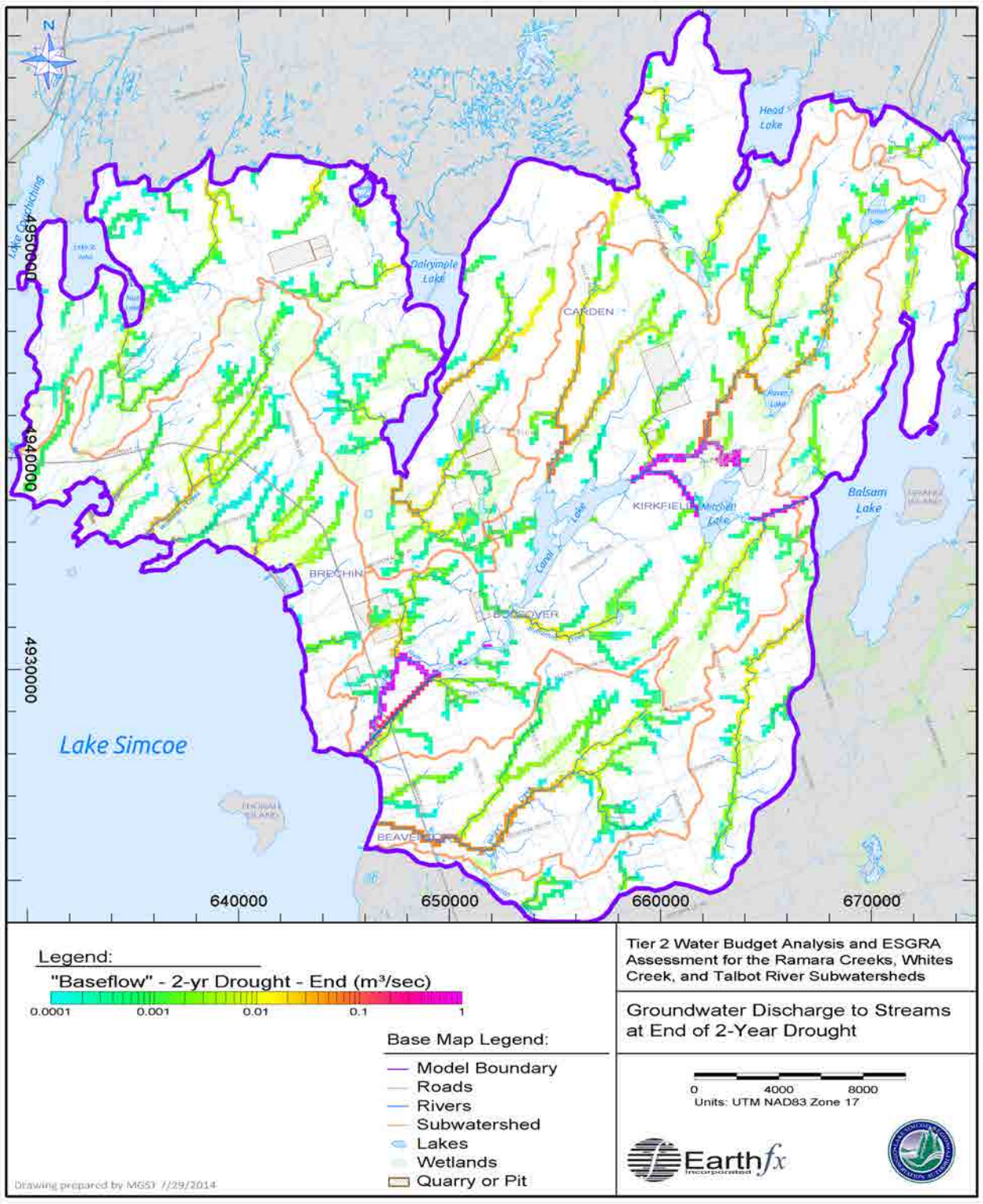

Figure 13.6: Simulated groundwater discharge to streams (baseflow) at end of two-year drought (current conditions).

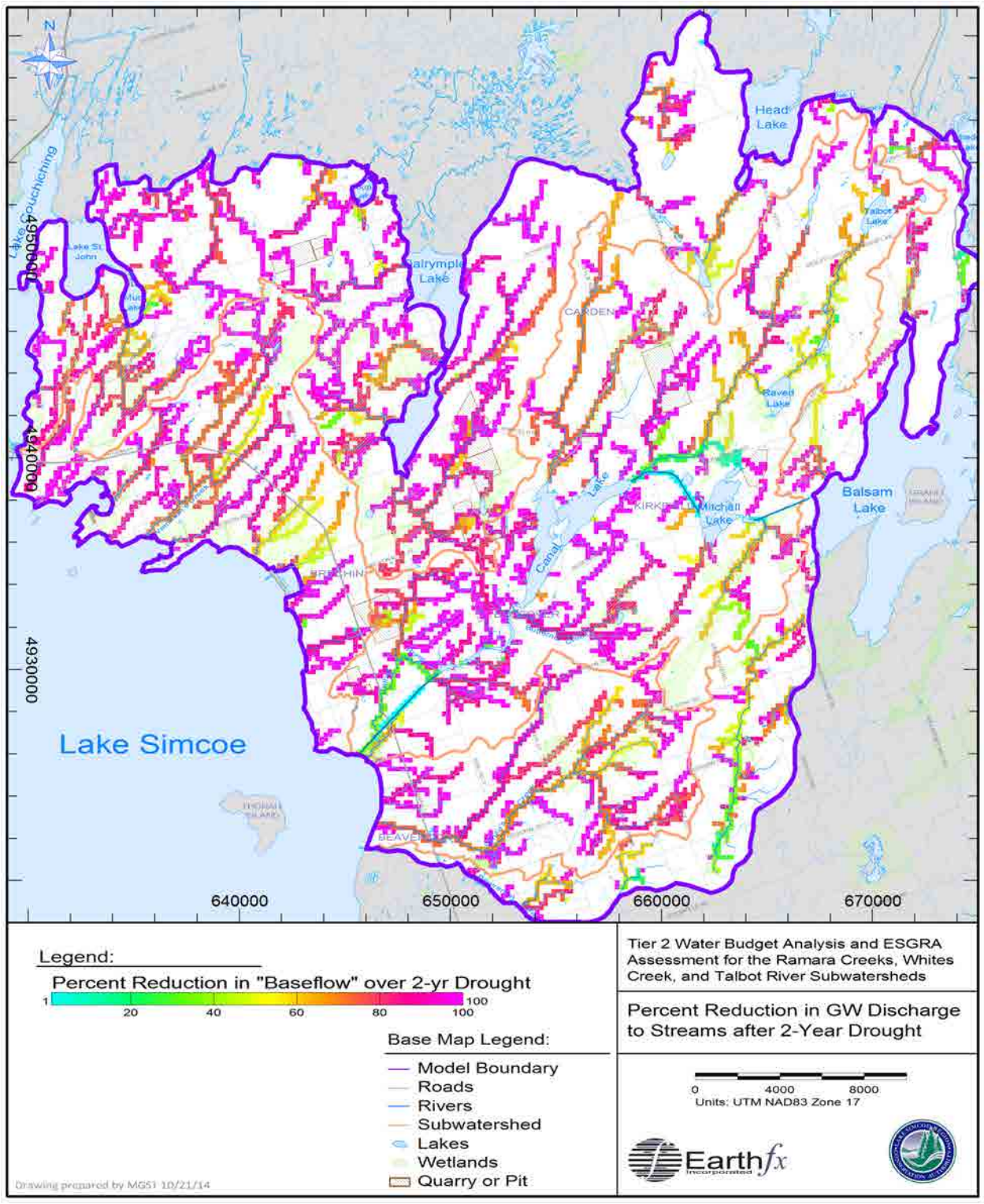

Figure 13.7: Percent reduction in baseflow at the end of the two-year drought (current conditions).

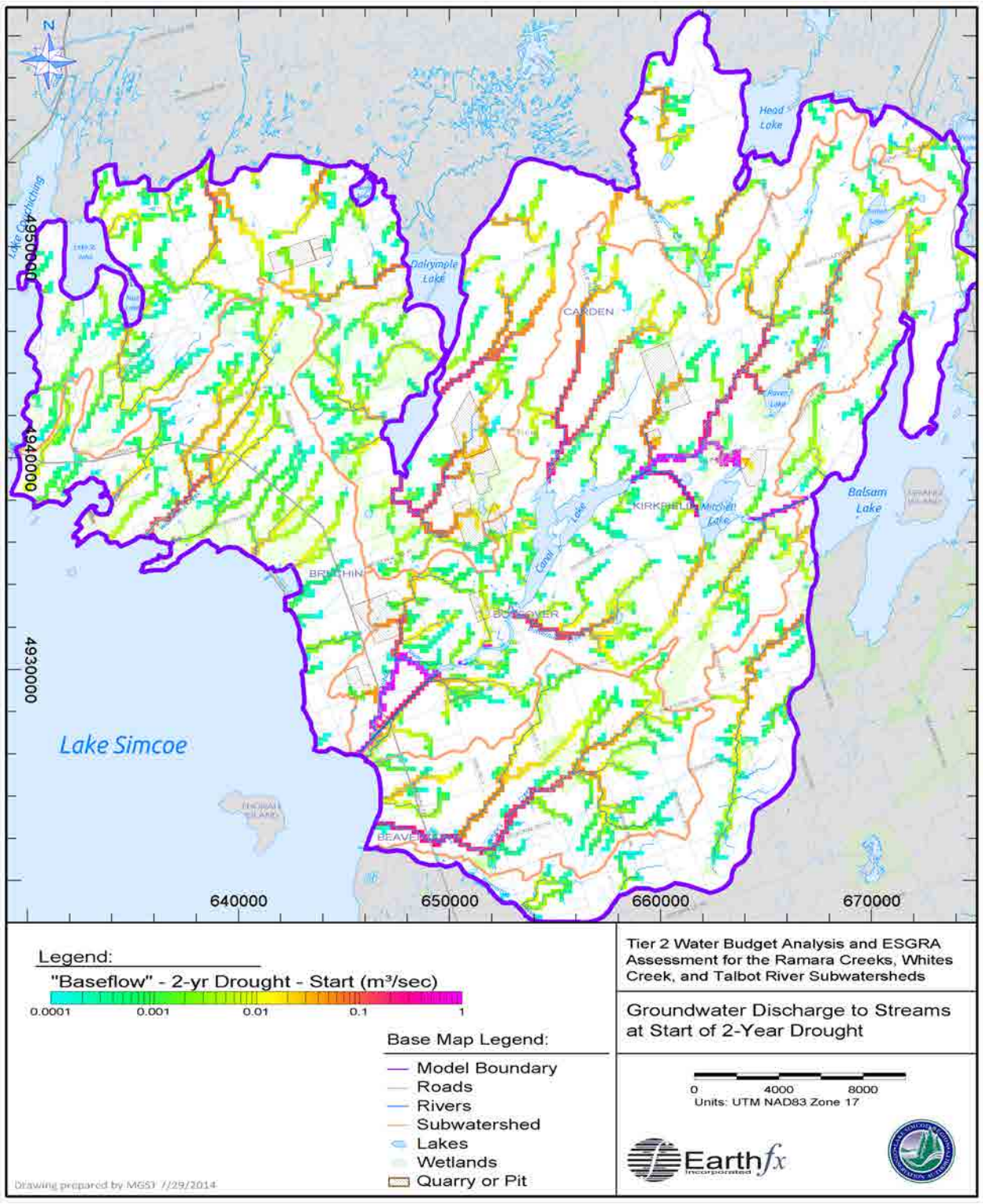

Figure 13.8: Simulated groundwater discharge to streams (baseflow) at the start of the two-year drought (future conditions).

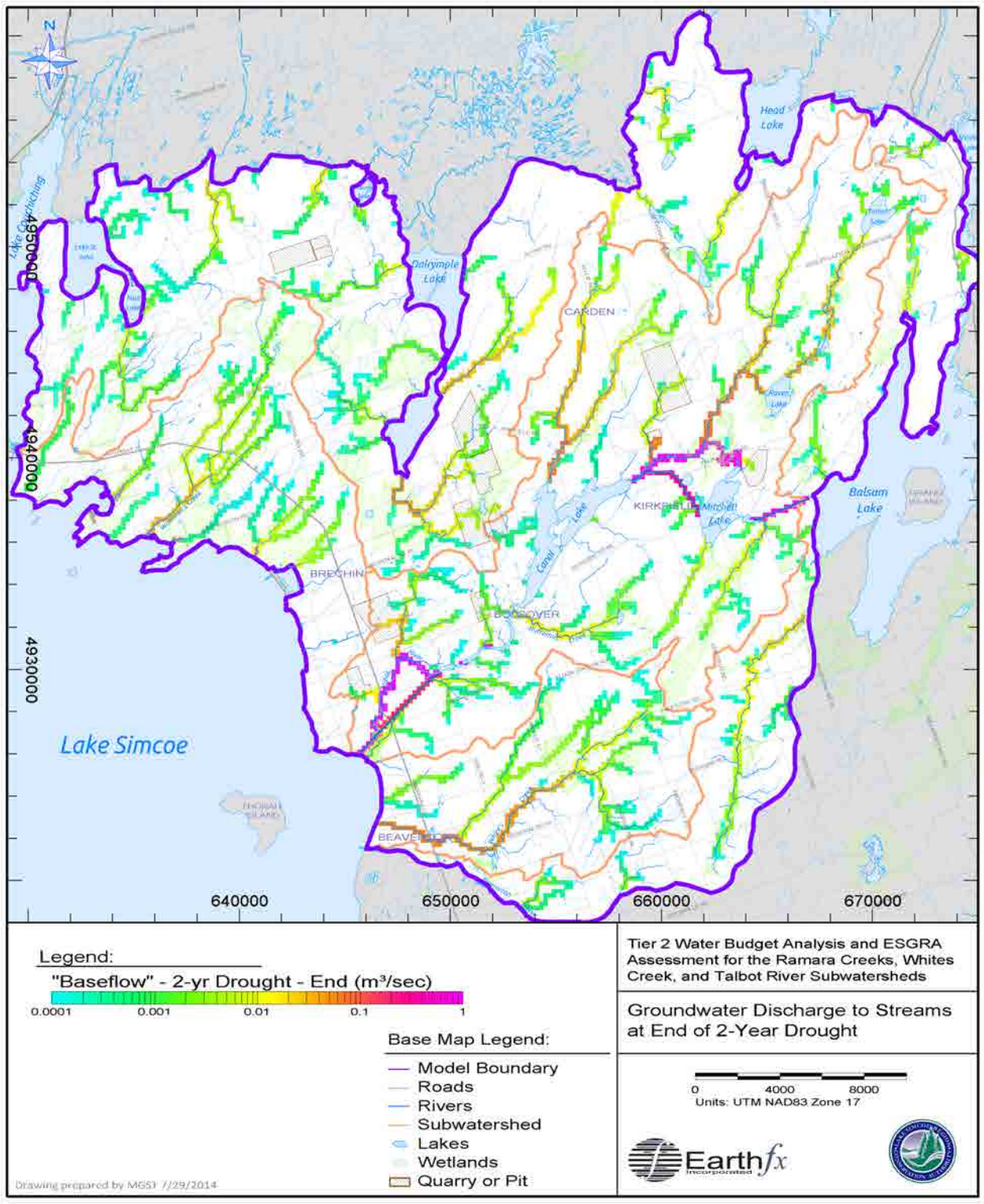

Figure 13.9: Simulated groundwater discharge to streams (baseflow) at the end of the two-year drought (future conditions).

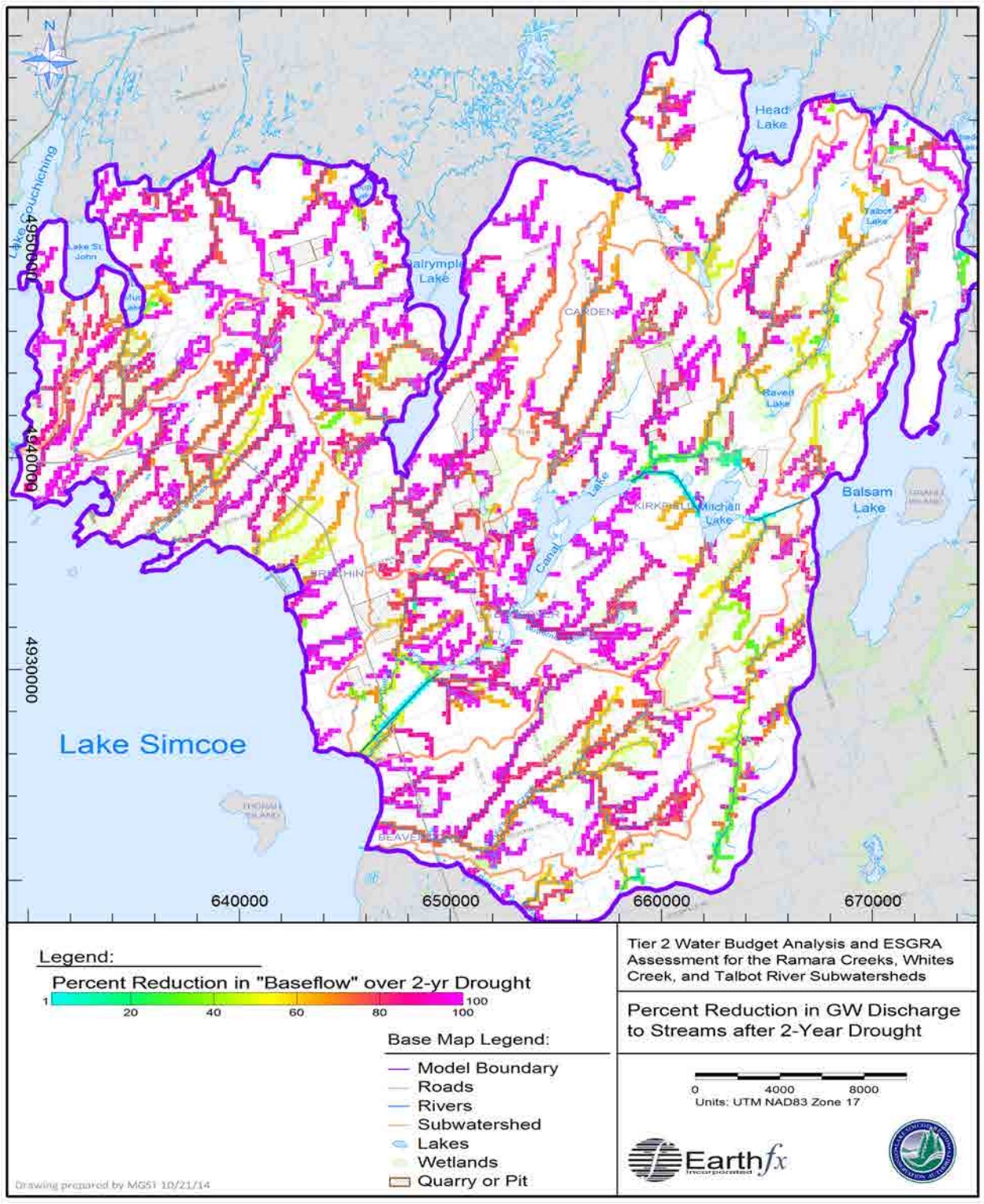

Figure 13.10: Percent reduction in baseflow at the end of the two-year drought (future conditions).

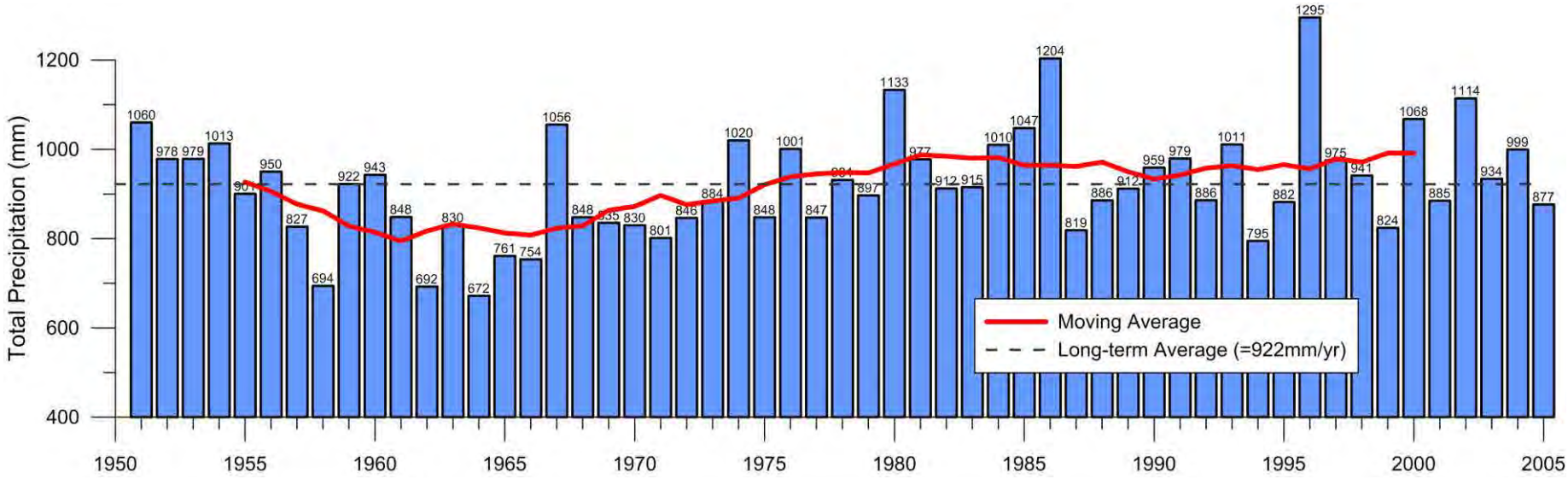

Figure 13.11: Annual average rainfall by water year within the study area (Drought starts in 1957 and ends in 1966).

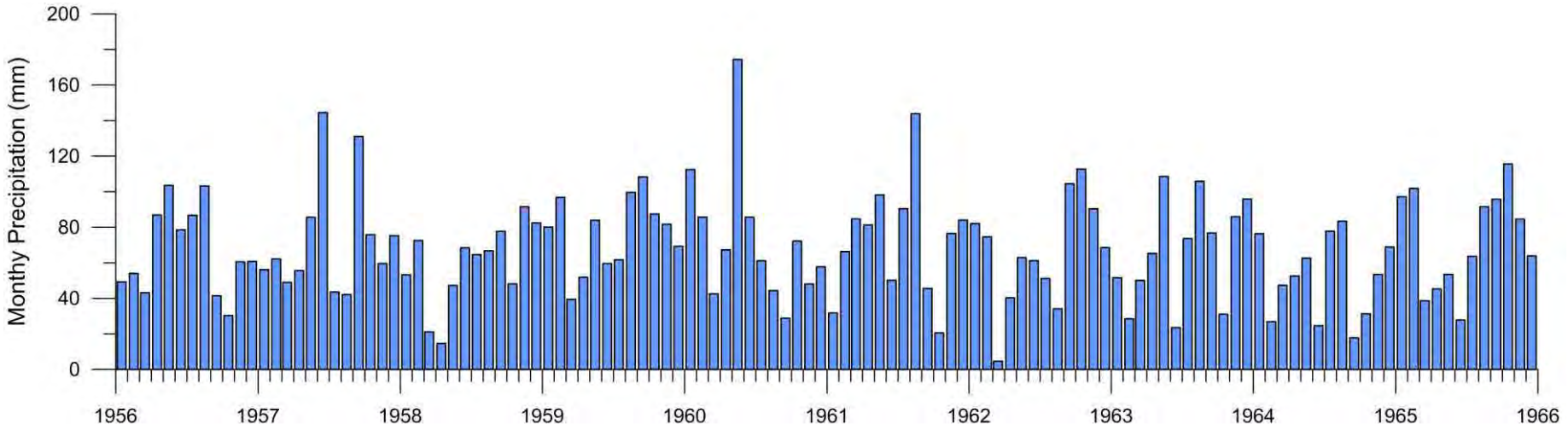

Figure 13.12: Monthly rainfall averaged across the study area during the 10-year drought.

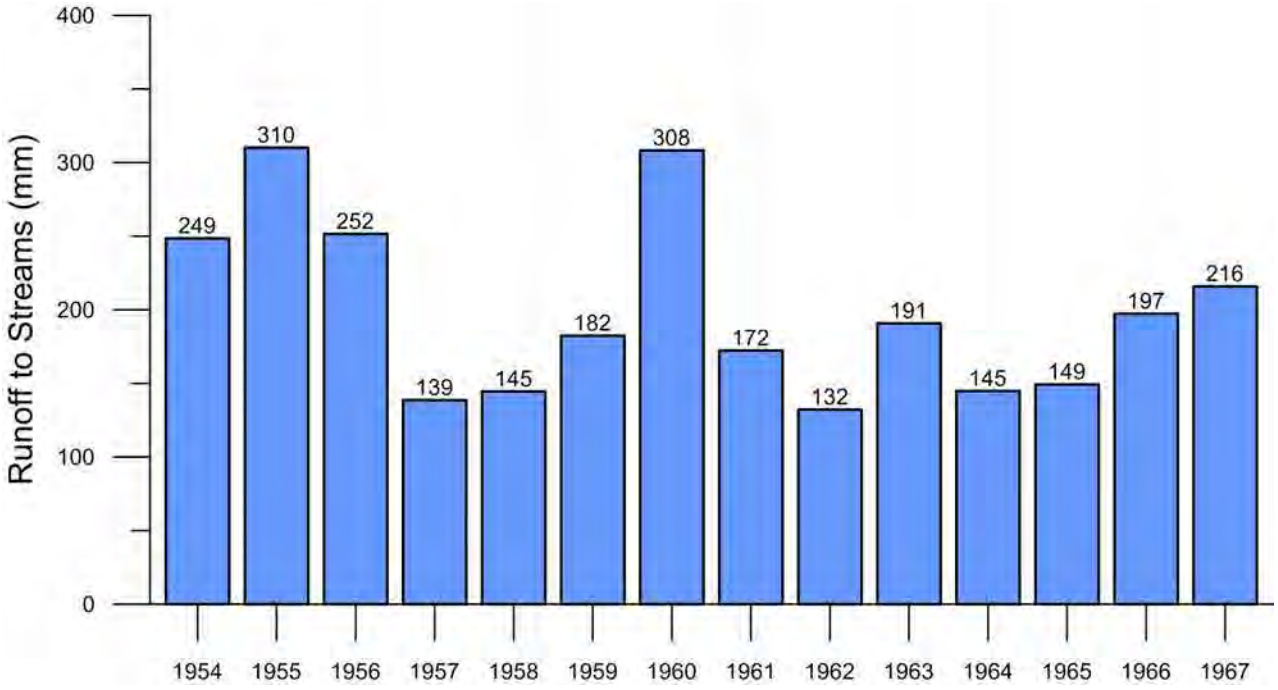

Figure 13.13: Annual overland runoff to streams, by water year, averaged over the study area.

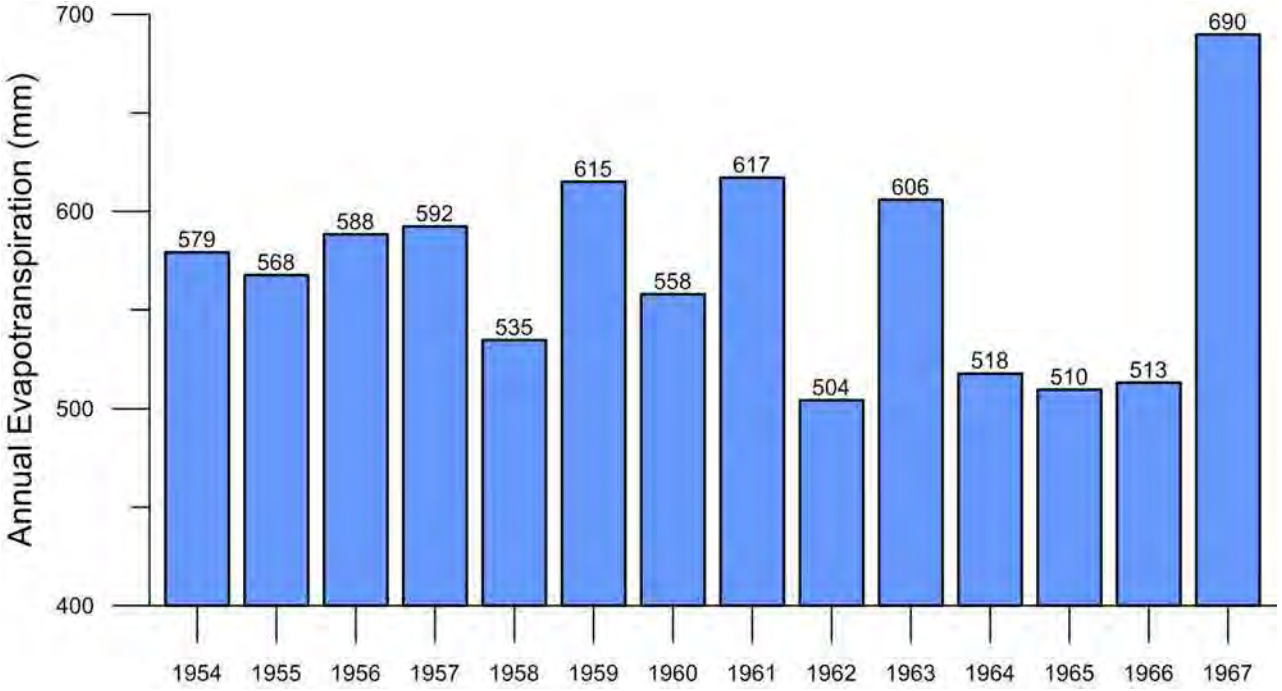

Figure 13.14: Actual evapotranspiration, by water year, averaged over the study area.

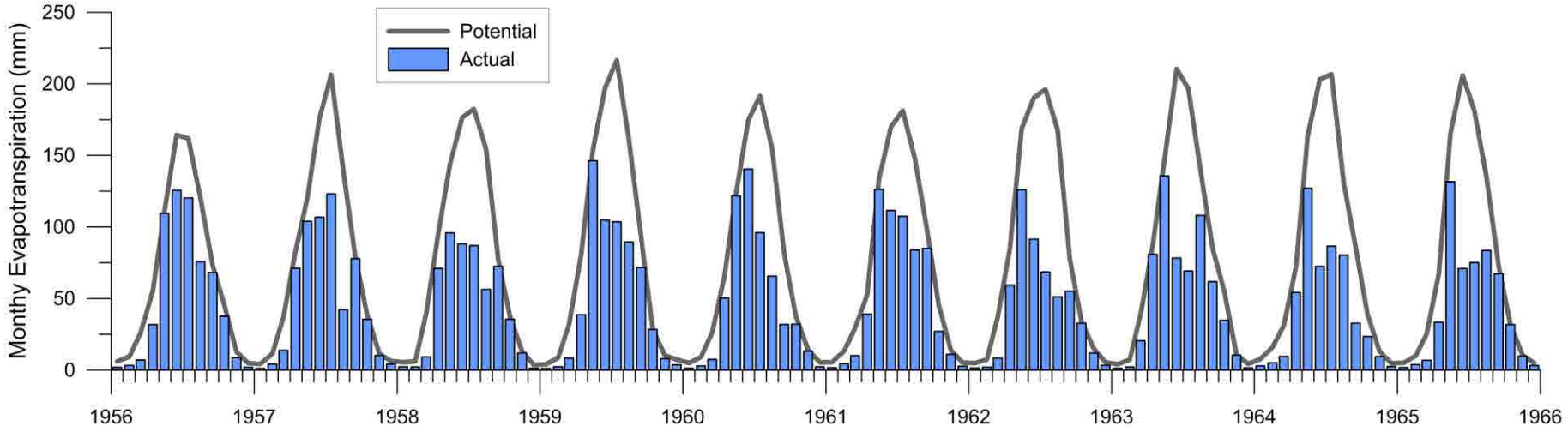

Figure 13.15: Monthly PET and AET averaged over the study area during the 10-year drought.

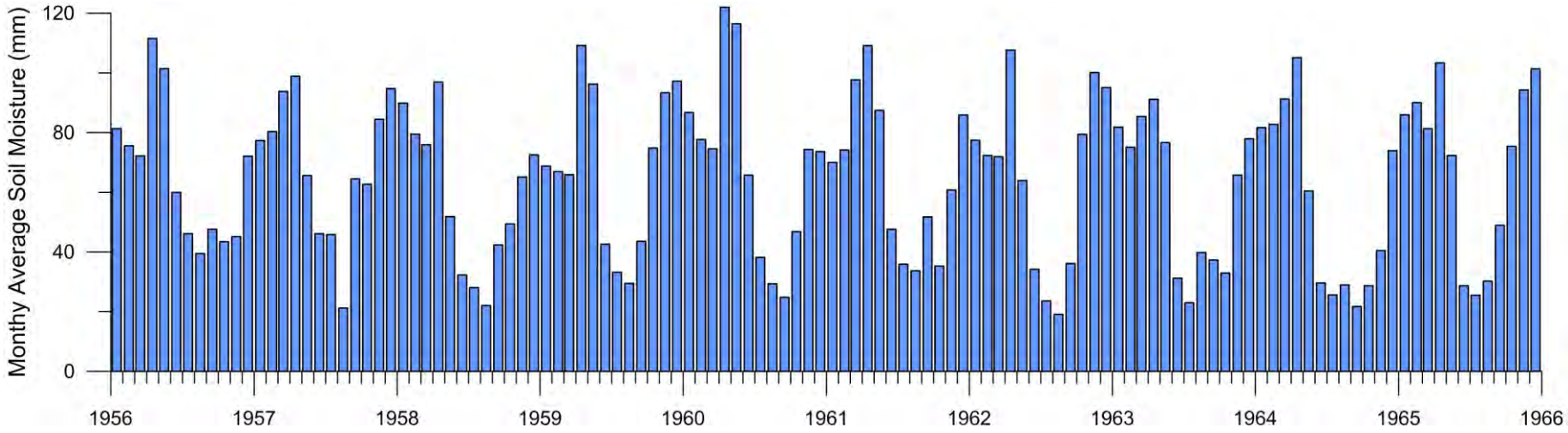

Figure 13.16: Monthly soil moisture averaged over the study area during the 10-year drought.

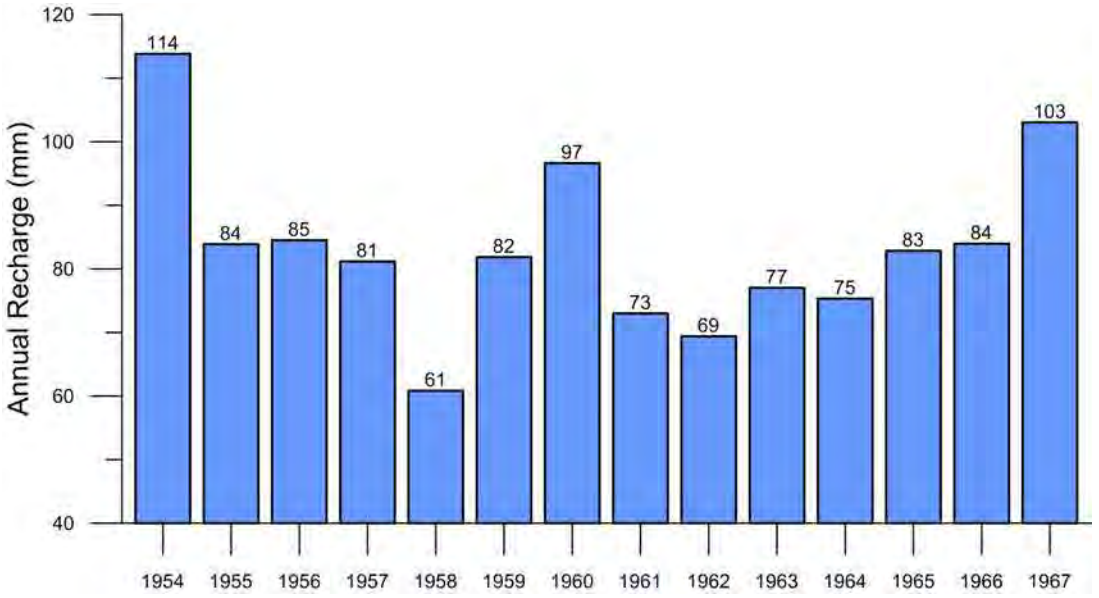

Figure 13.17: Annual groundwater recharge by water year averaged over the study area.

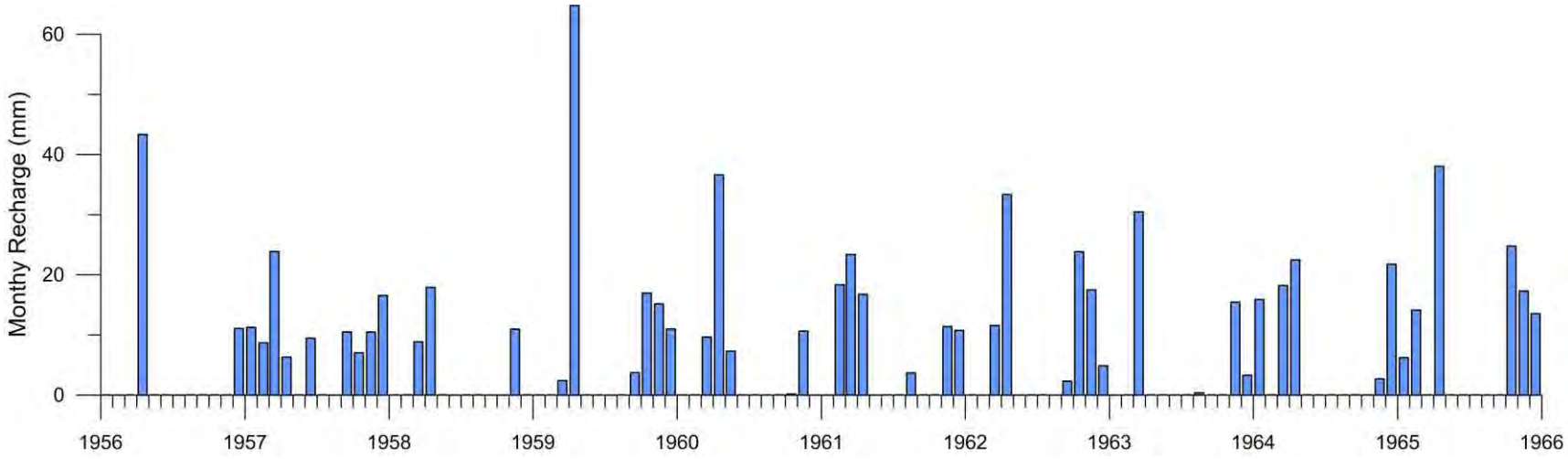

Figure 13.18: Monthly variation in groundwater recharge during the 10-year drought.

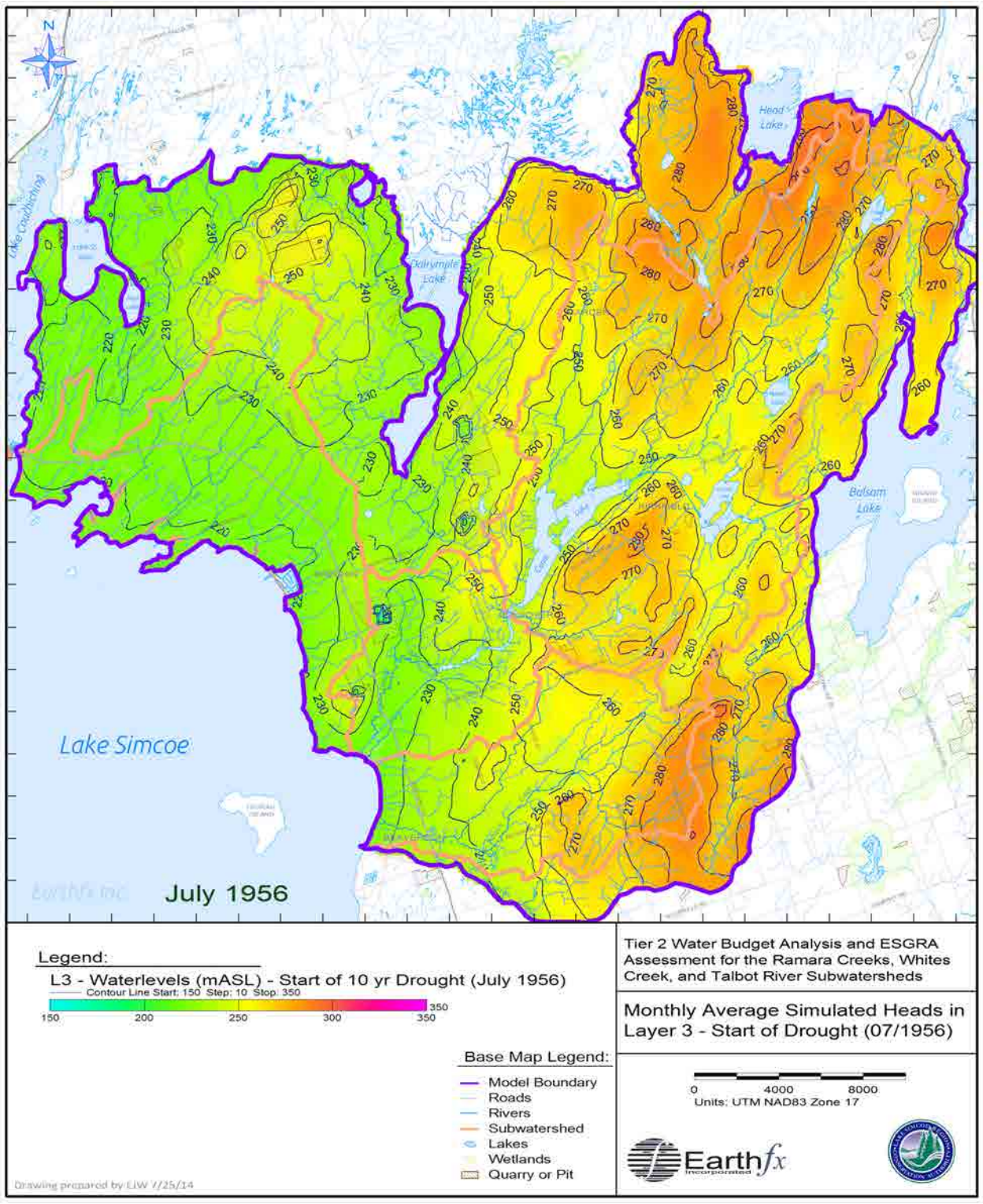

Figure 13.19: Simulated monthly average heads in Layer 3 (weathered bedrock) at start of drought (November 1956).

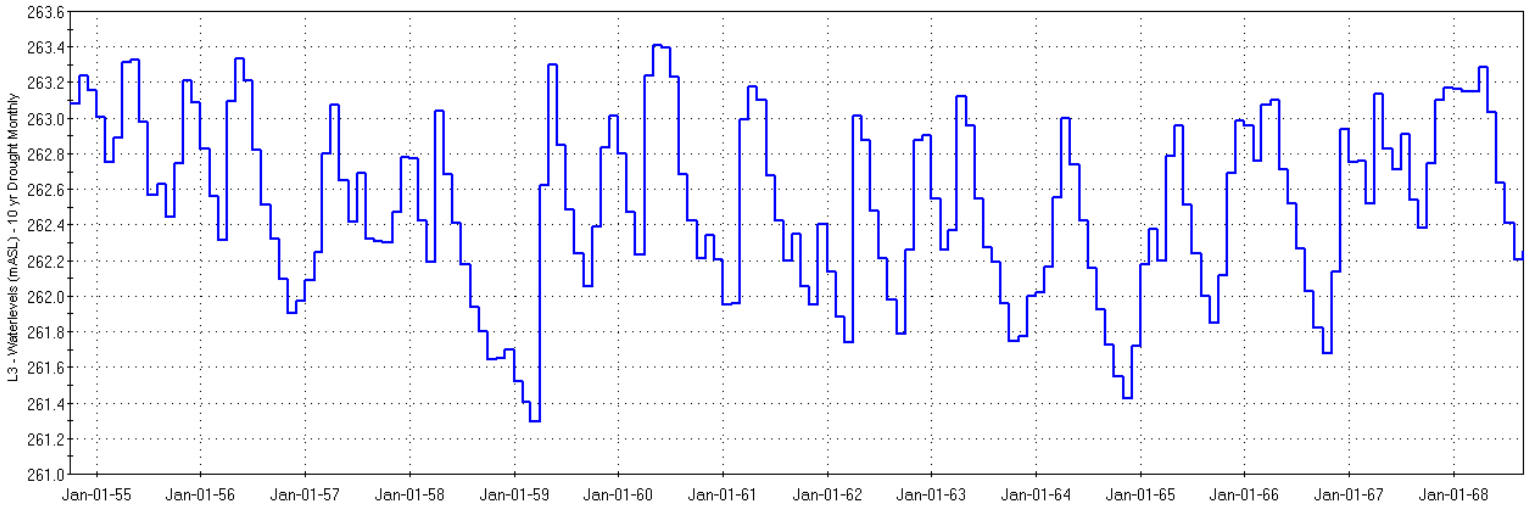

Figure 13.20: Simulated monthly average heads in Layer 3 during the 10-yr drought in an upland area at Kirkfield Rd. and Wylie Rd.

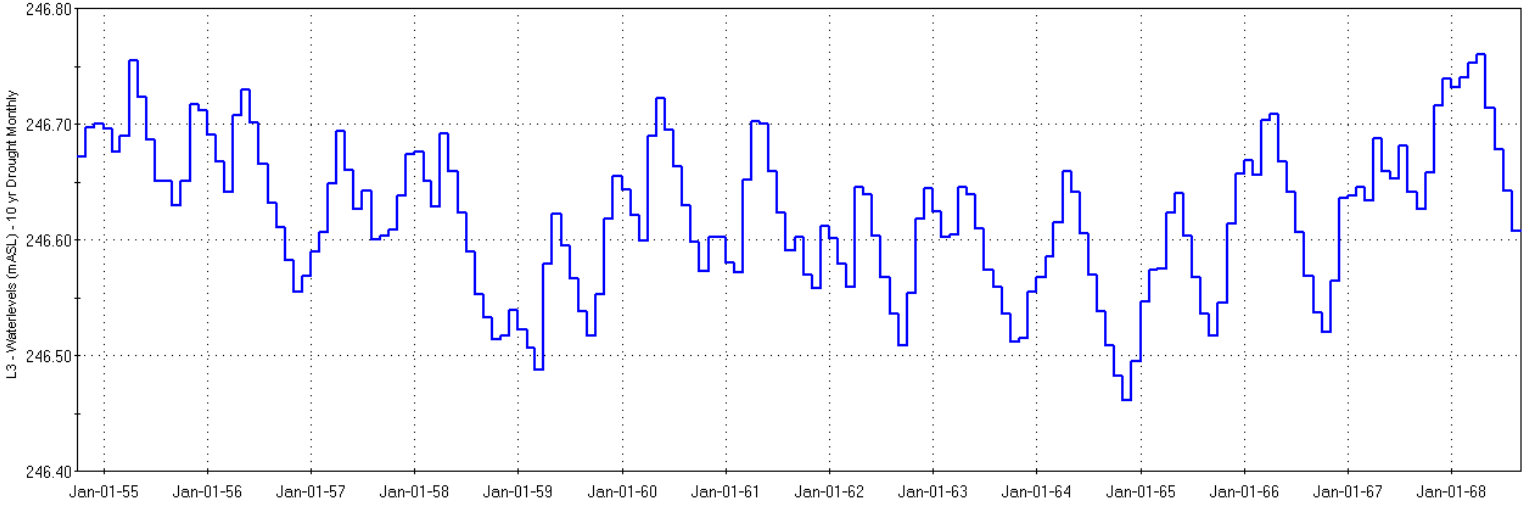

Figure 13.21: Simulated monthly average heads in Layer 3 during the 10-yr drought in a lowland area at Kirkfield Rd. and Fitzgerald Lane.

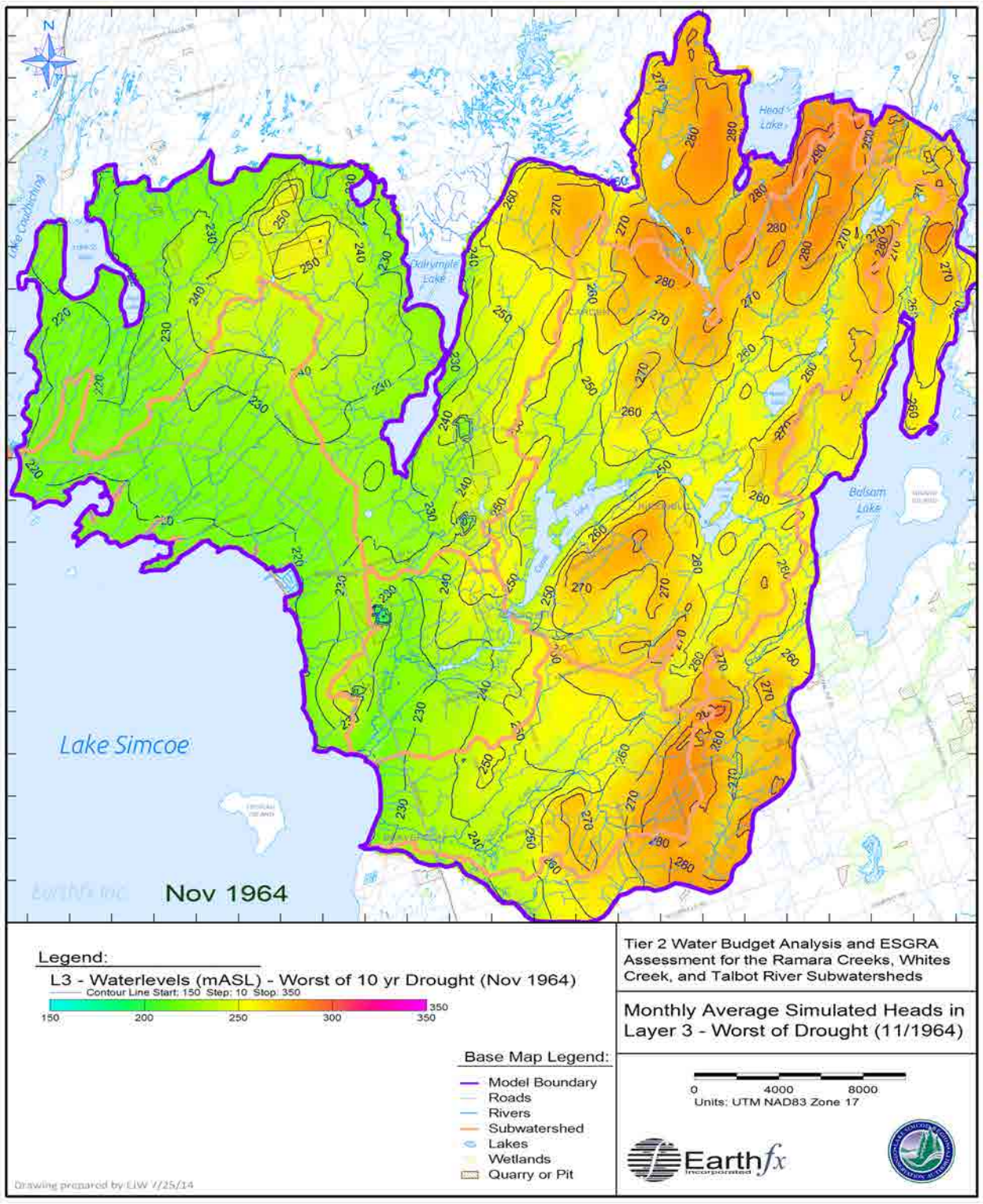

Figure 13.22: Simulated monthly average heads in Layer 3 (weathered bedrock) at worst of drought (November 1964).

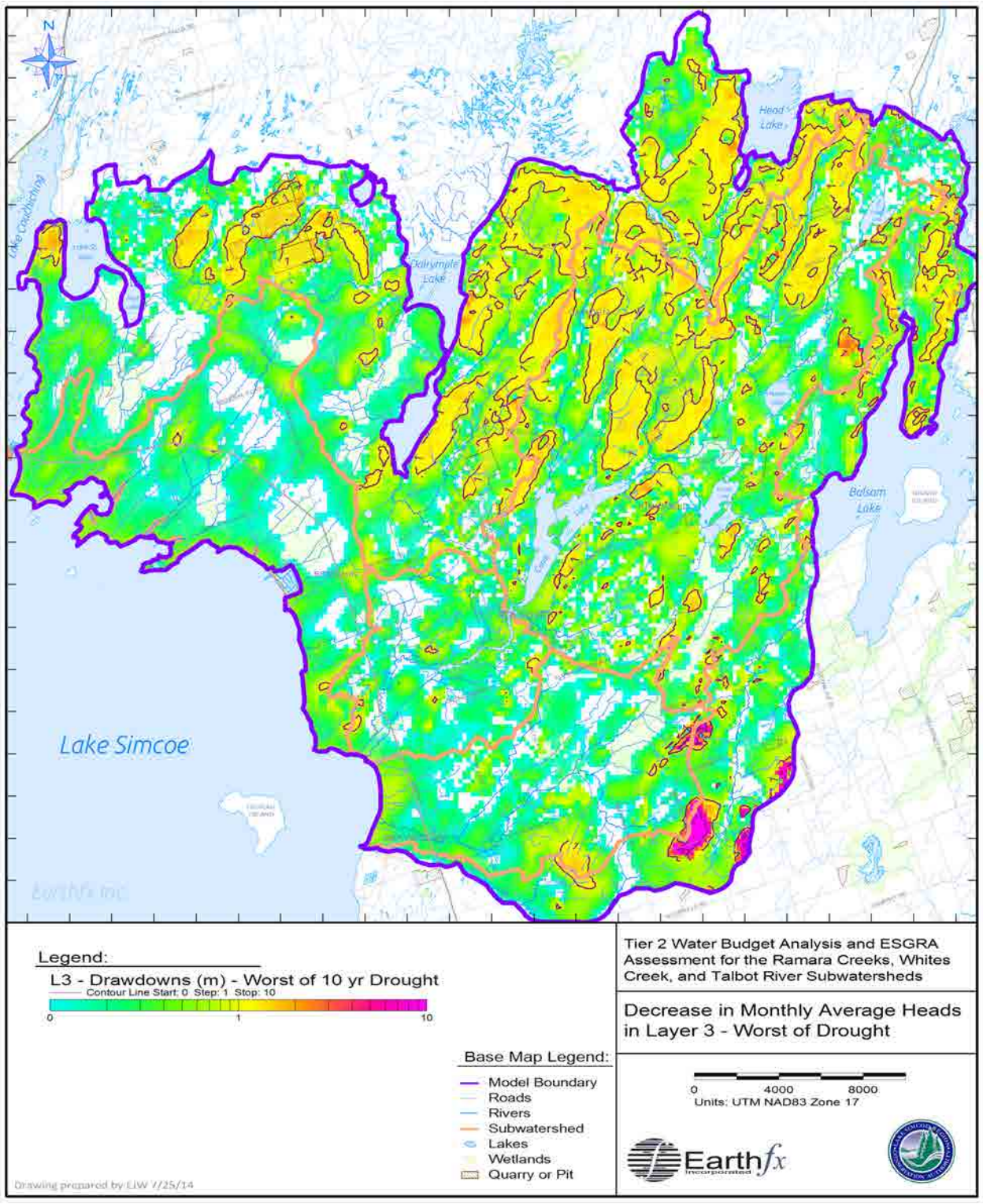

Figure 13.23: Decrease in simulated monthly average heads in Layer 3 at worst of drought (November 1964).

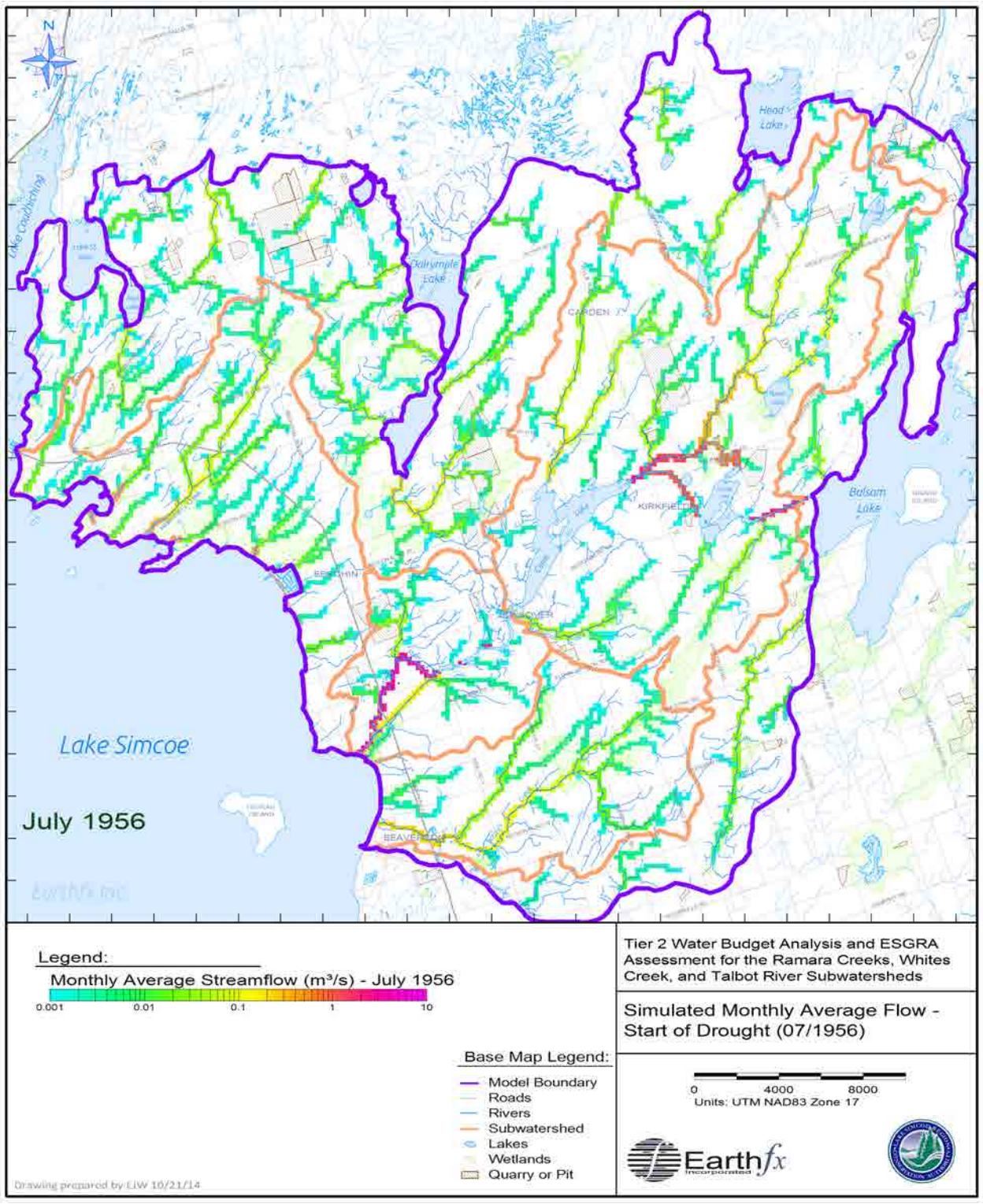

Figure 13.24: Simulated streamflow (in m^3/s) at the start of the 10-year drought.

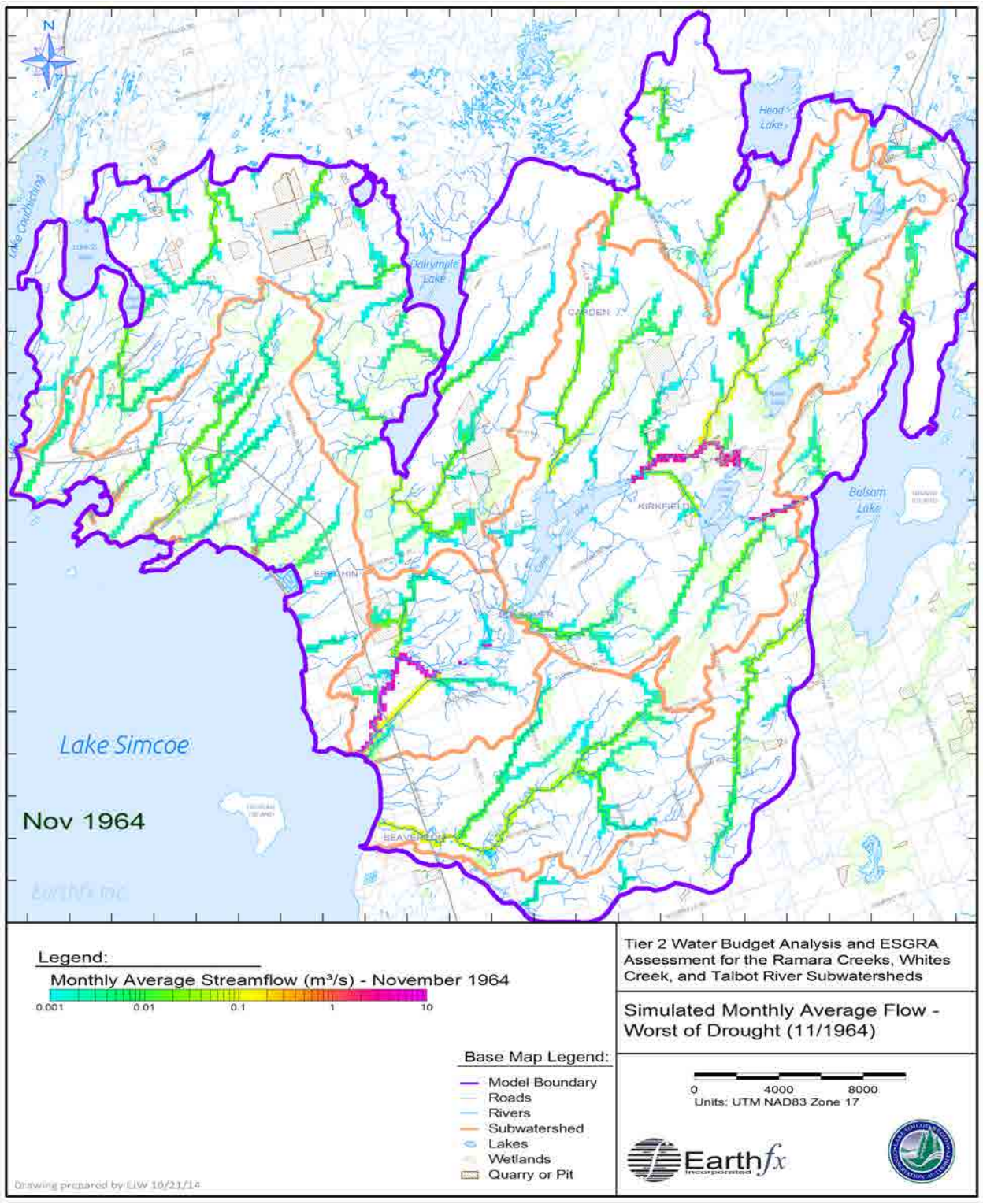

Figure 13.25: Simulated streamflow (in m^3/s) at the worst of the 10-year drought.

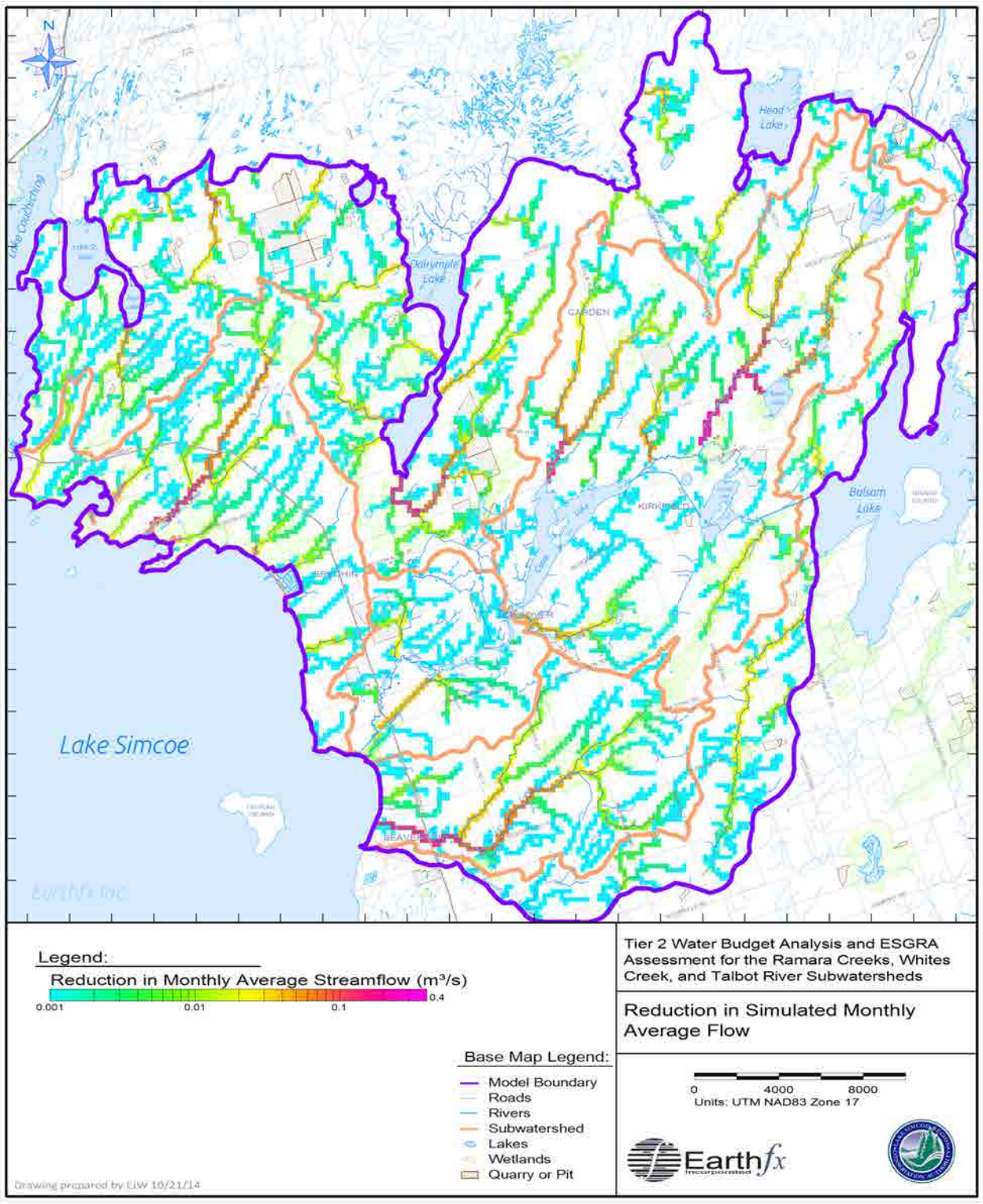

Figure 13.26: Reduction in simulated monthly average flow (July 1976 versus November 1964).

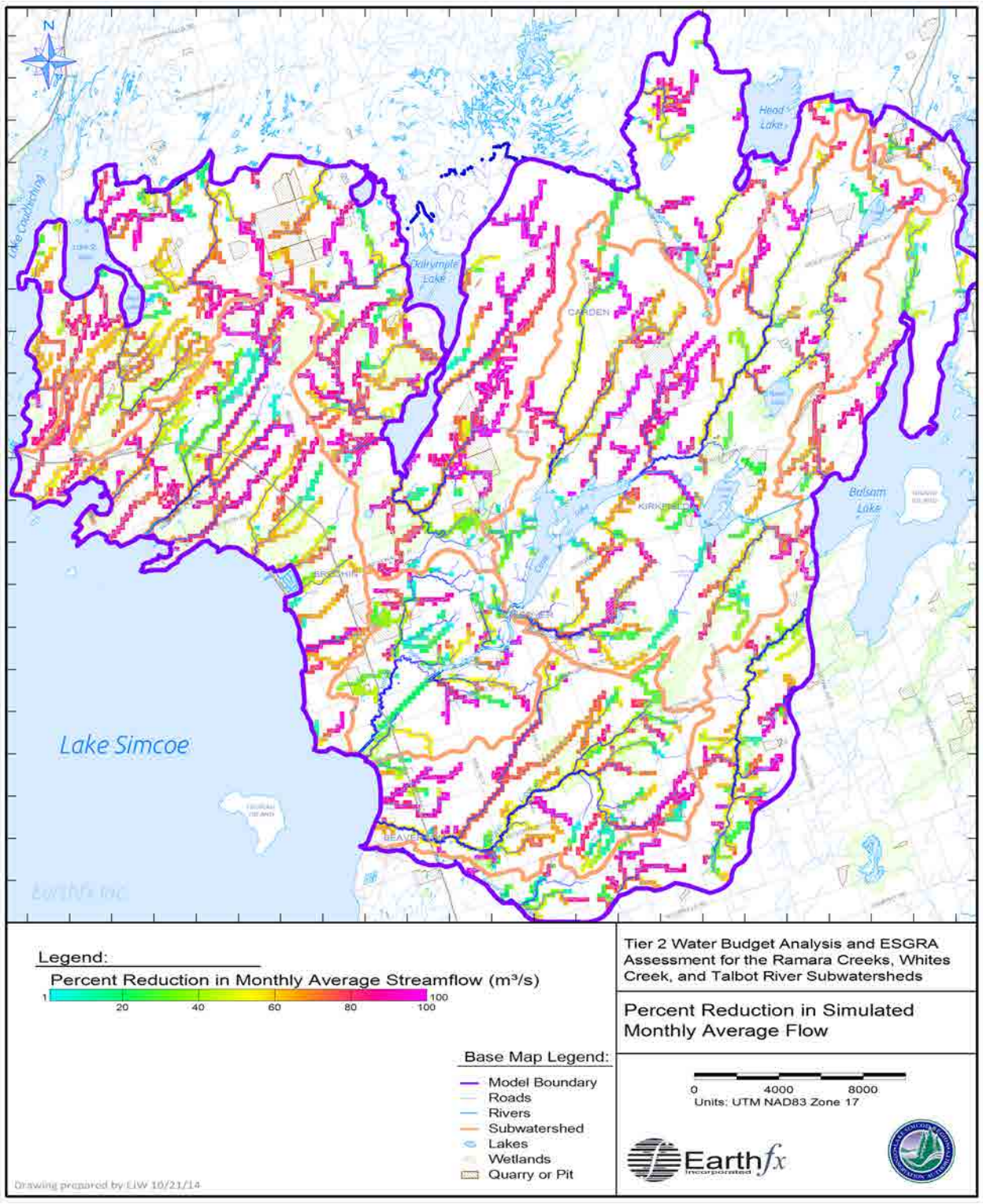

Figure 13.27: Percent reduction in simulated monthly average flow (July 1976 versus November 1964).

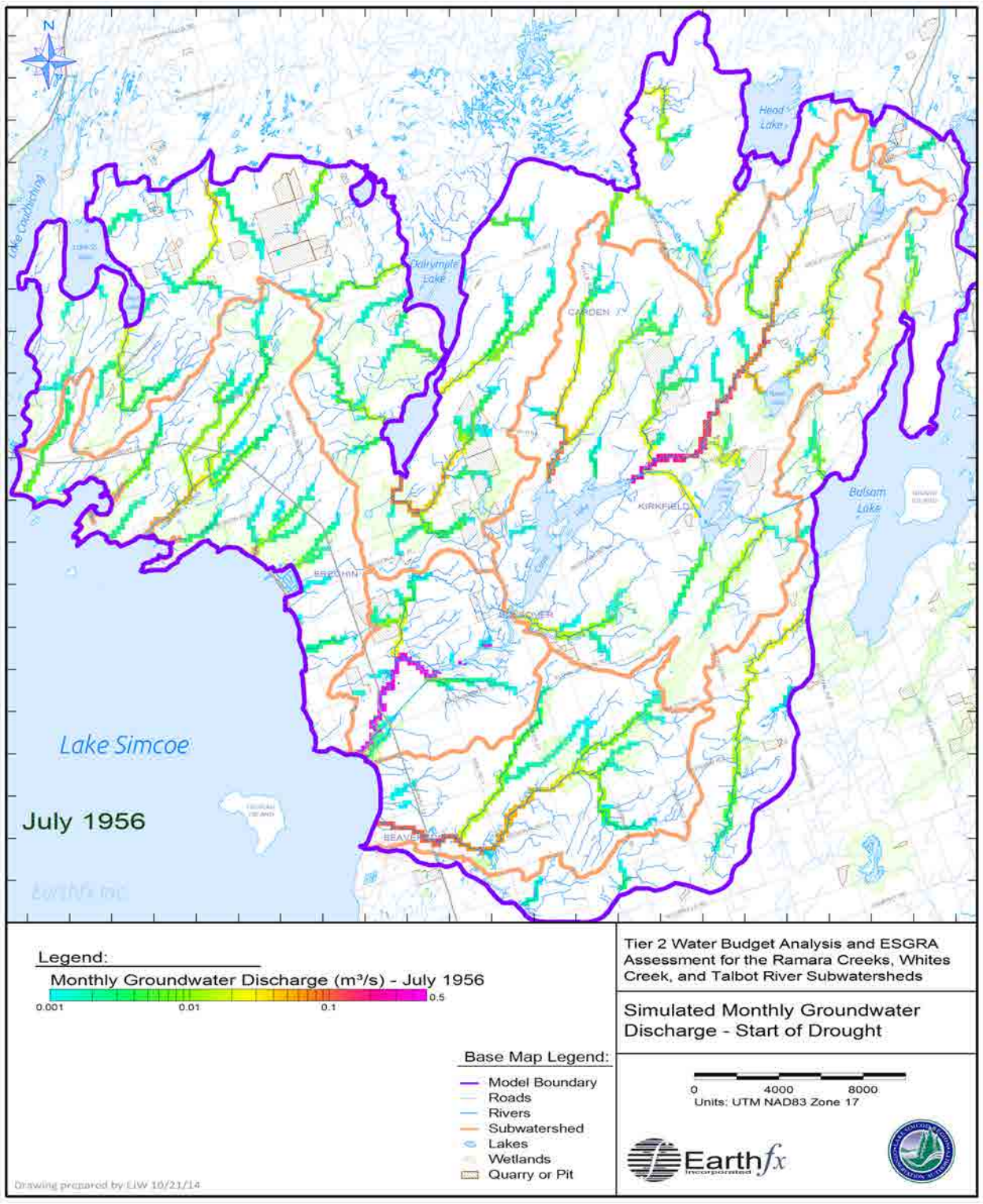

Figure 13.28: Simulated groundwater discharge to streams in July 1956 at the start of the 10-yr drought.

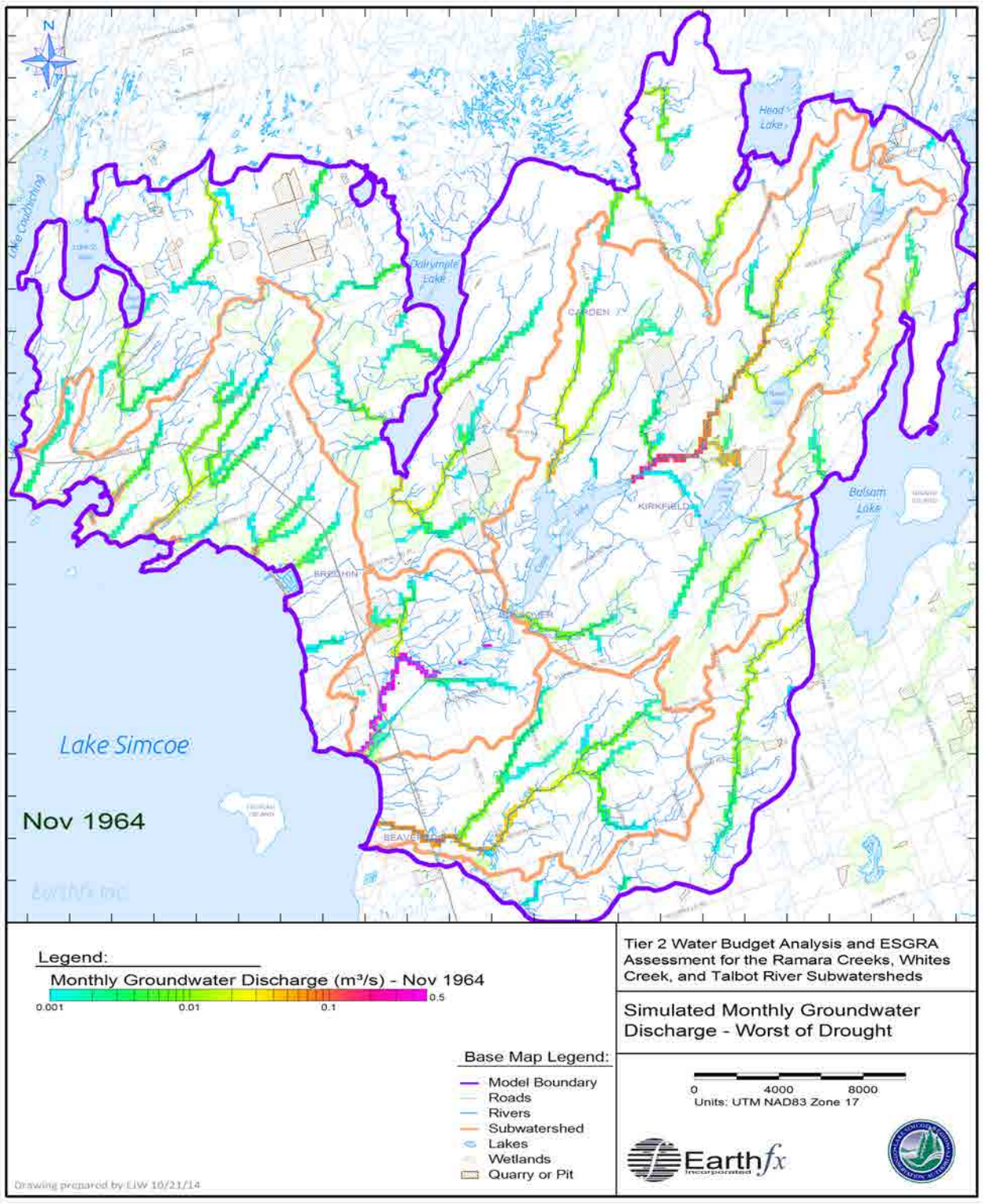

Figure 13.29: Simulated groundwater discharge to streams in November 1964 at the worst of the 10-yr drought.

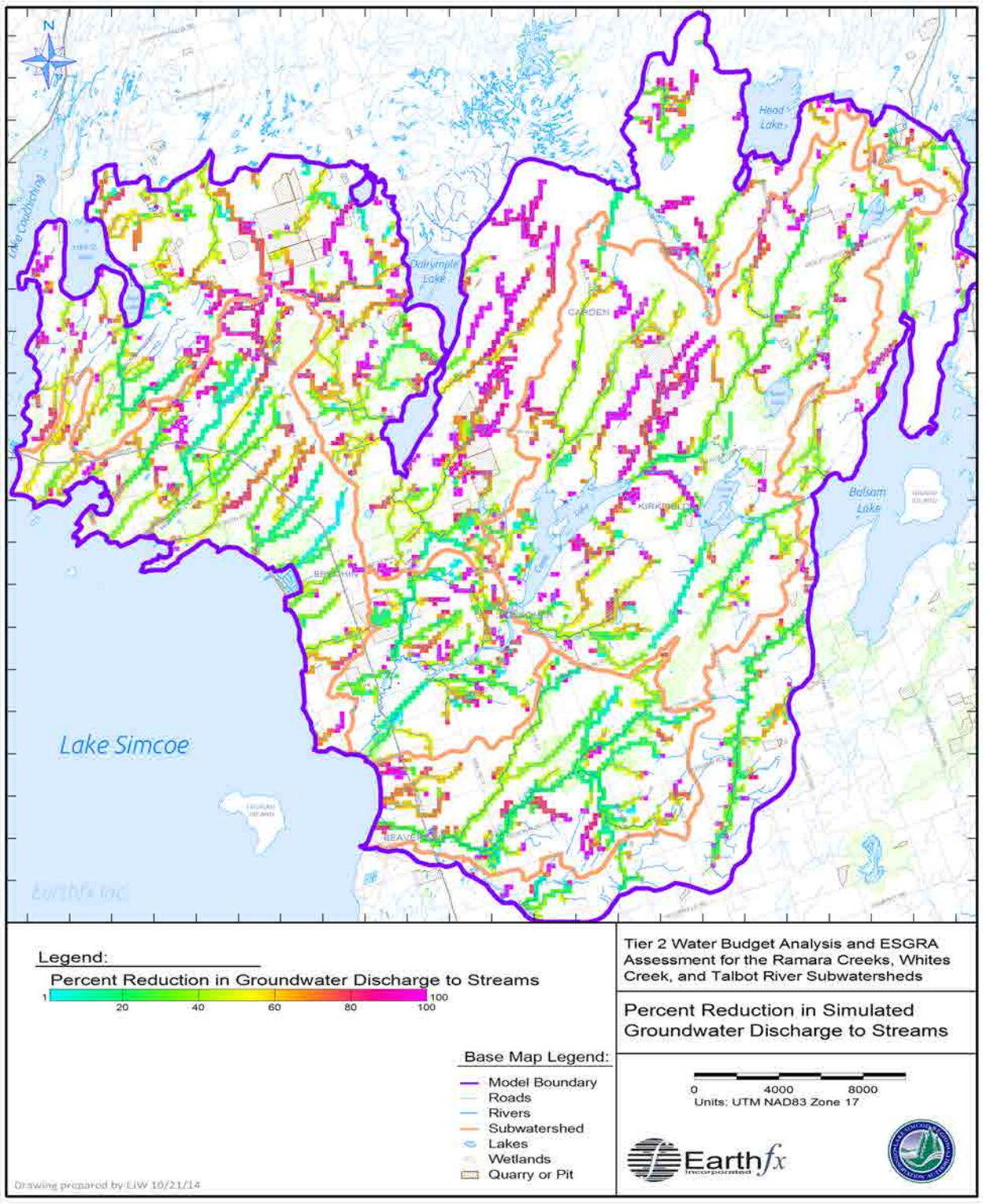

Figure 13.30: Percent reduction in simulated groundwater discharge to streams (July 1976 versus November 1964).

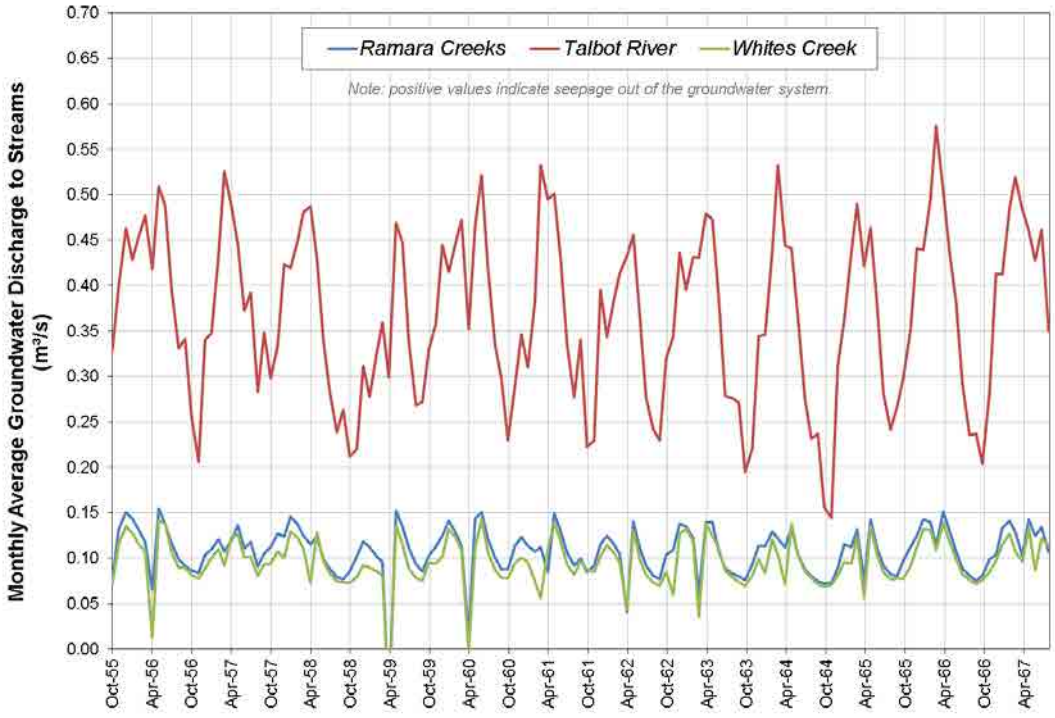

Figure 13.31: Simulated monthly average groundwater discharge to stream channels (m^3/s) in the study catchments.

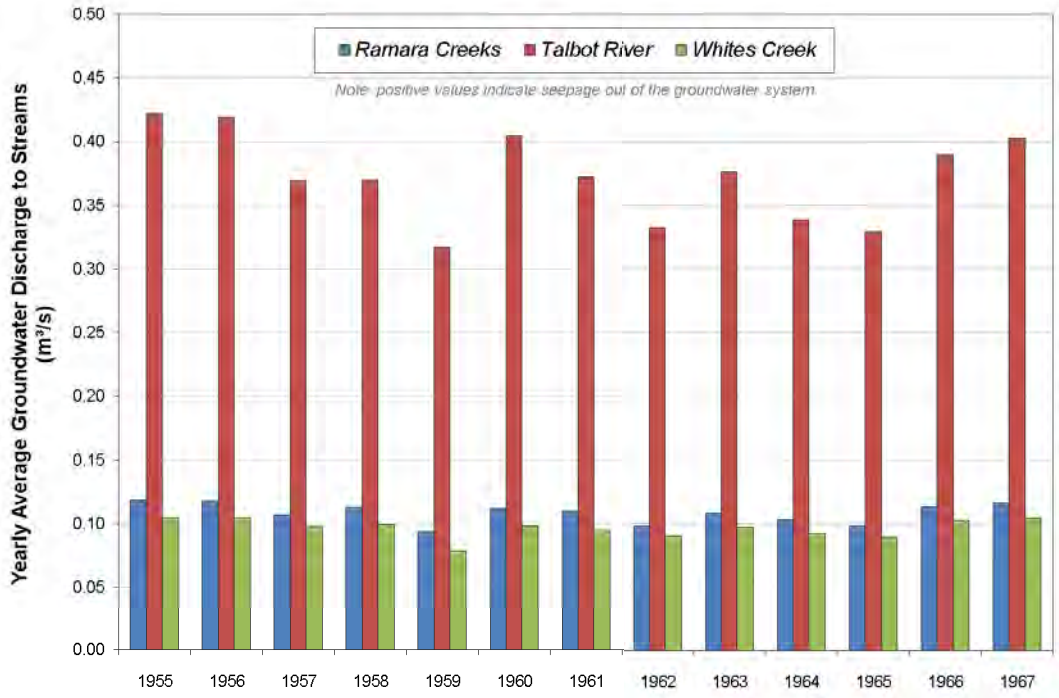

Figure 13.32: Simulated annual average groundwater discharge to stream channels (m^3/s) in the study catchments.

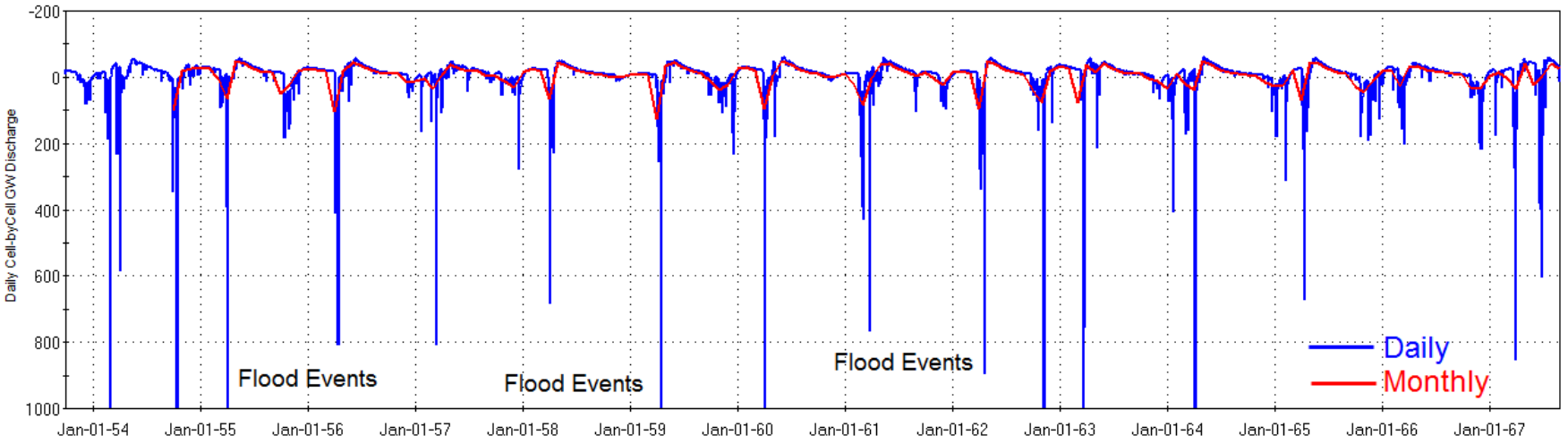

Figure 13.33: Simulated groundwater seepage to Whites Creek from the model cell immediately adjacent to the LSRCA gauge.

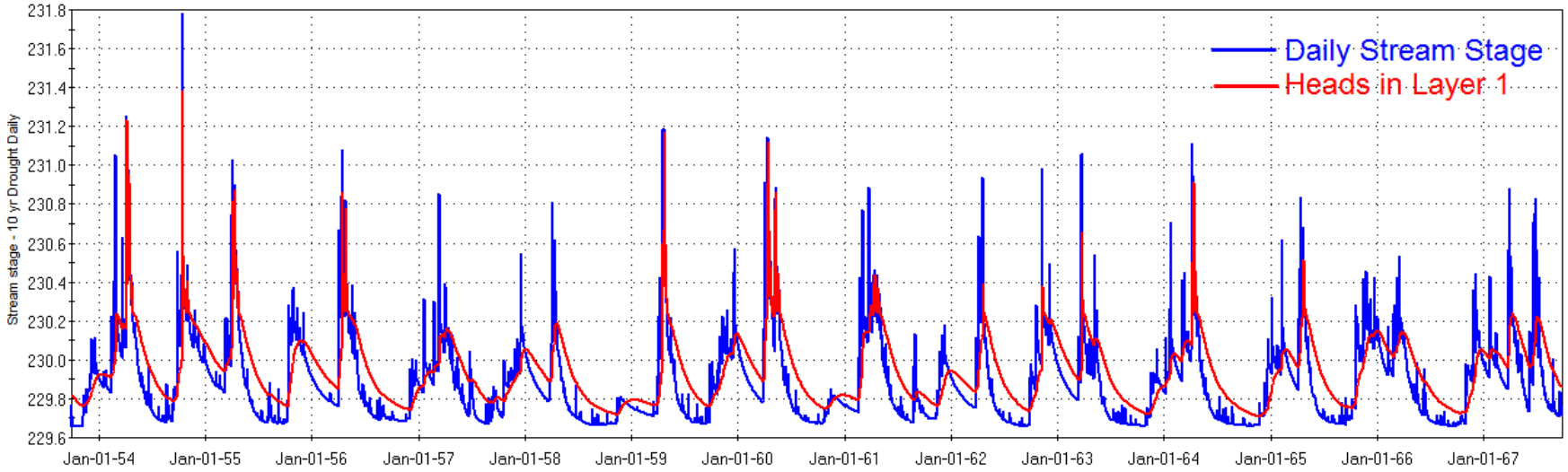

Figure 13.34: Simulated stream stage and head in Layer 1 in the model cell adjacent to the LSRCA gauge on Whites Creek.

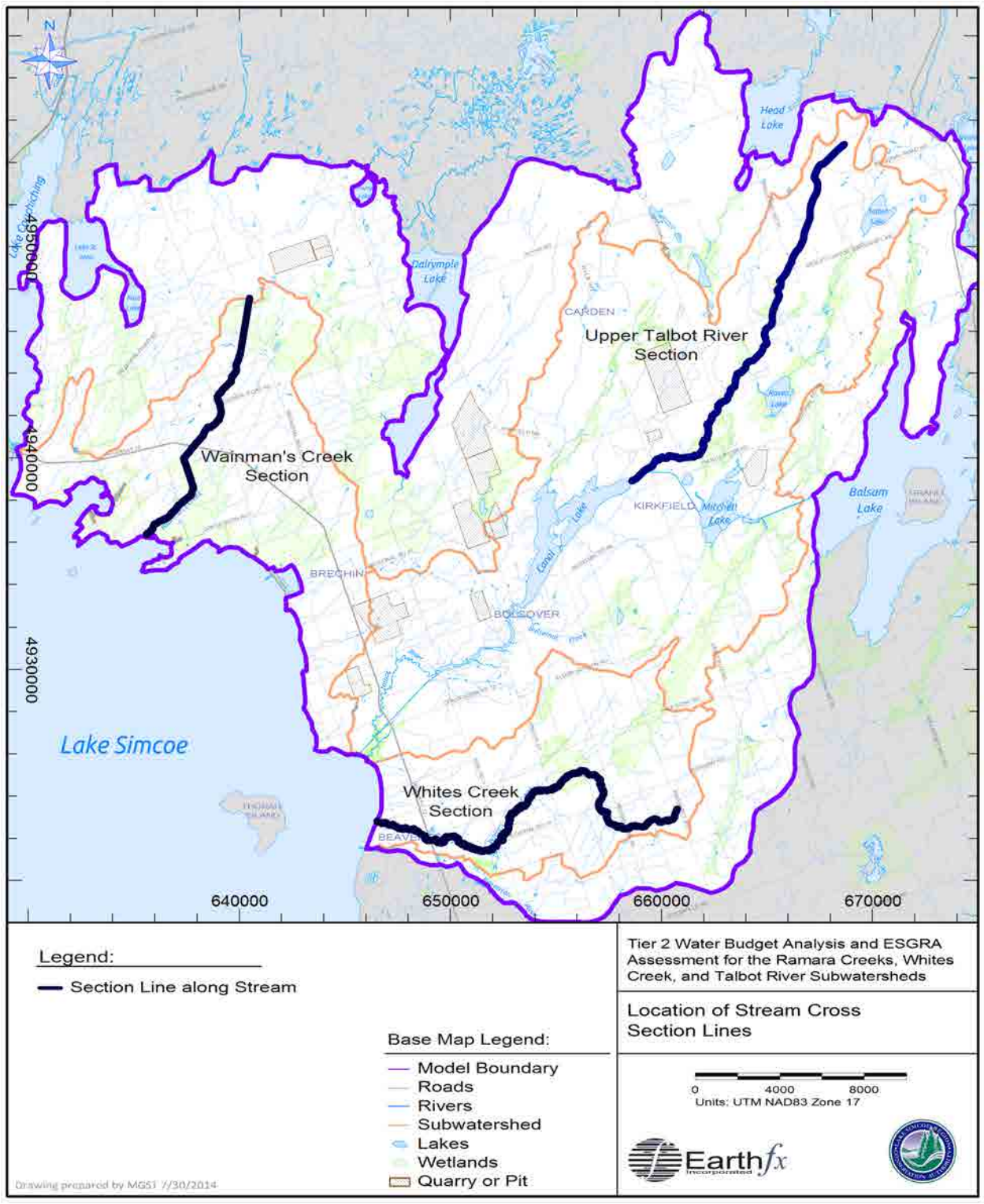

Figure 13.35: Location of lines for stream cross sections.

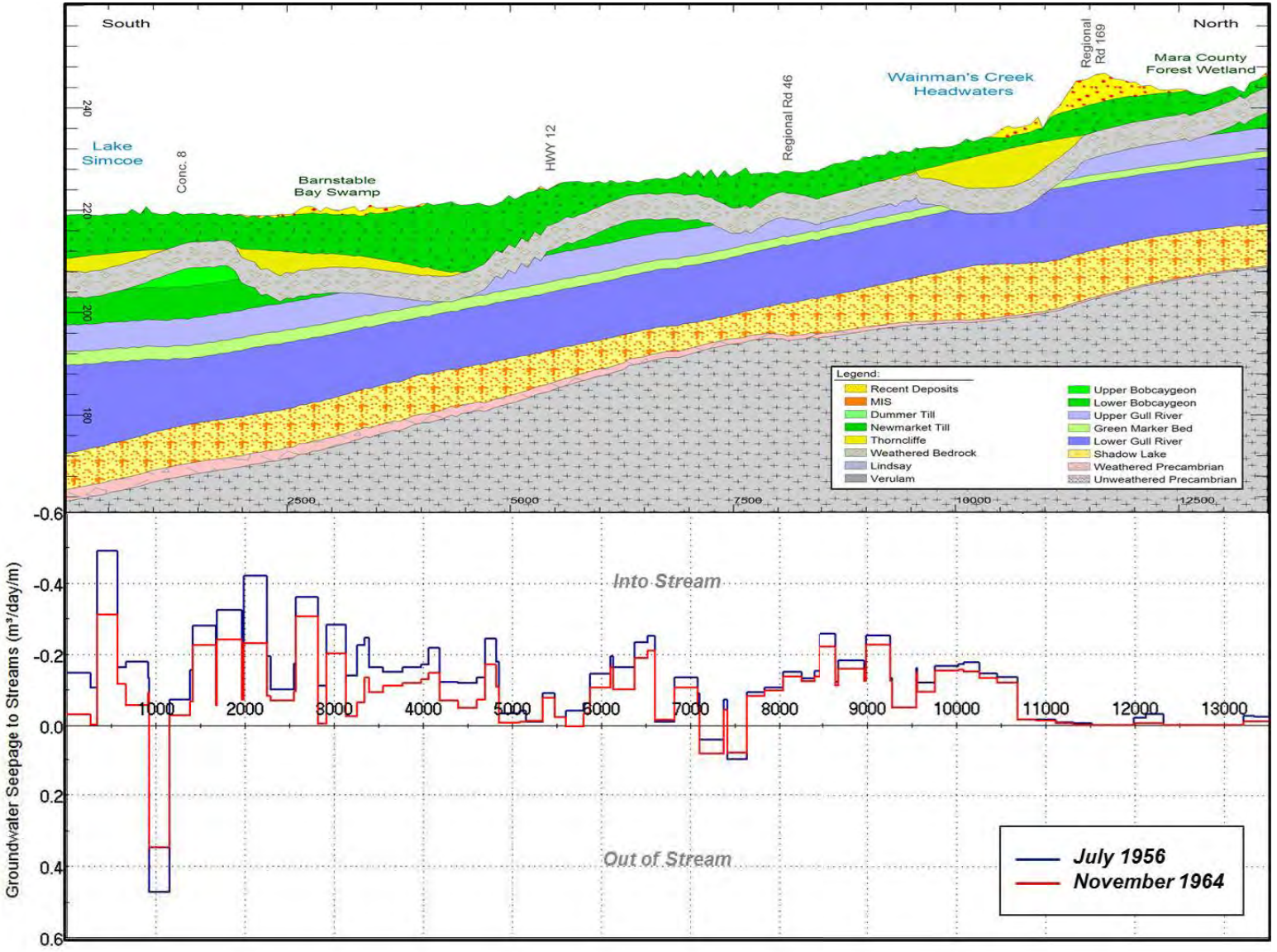

Figure 13.36: Cross section along Wainman's Creek (Ramara Creeks subwatershed) showing simulated groundwater discharge to streams in July 1956 and November 1964.

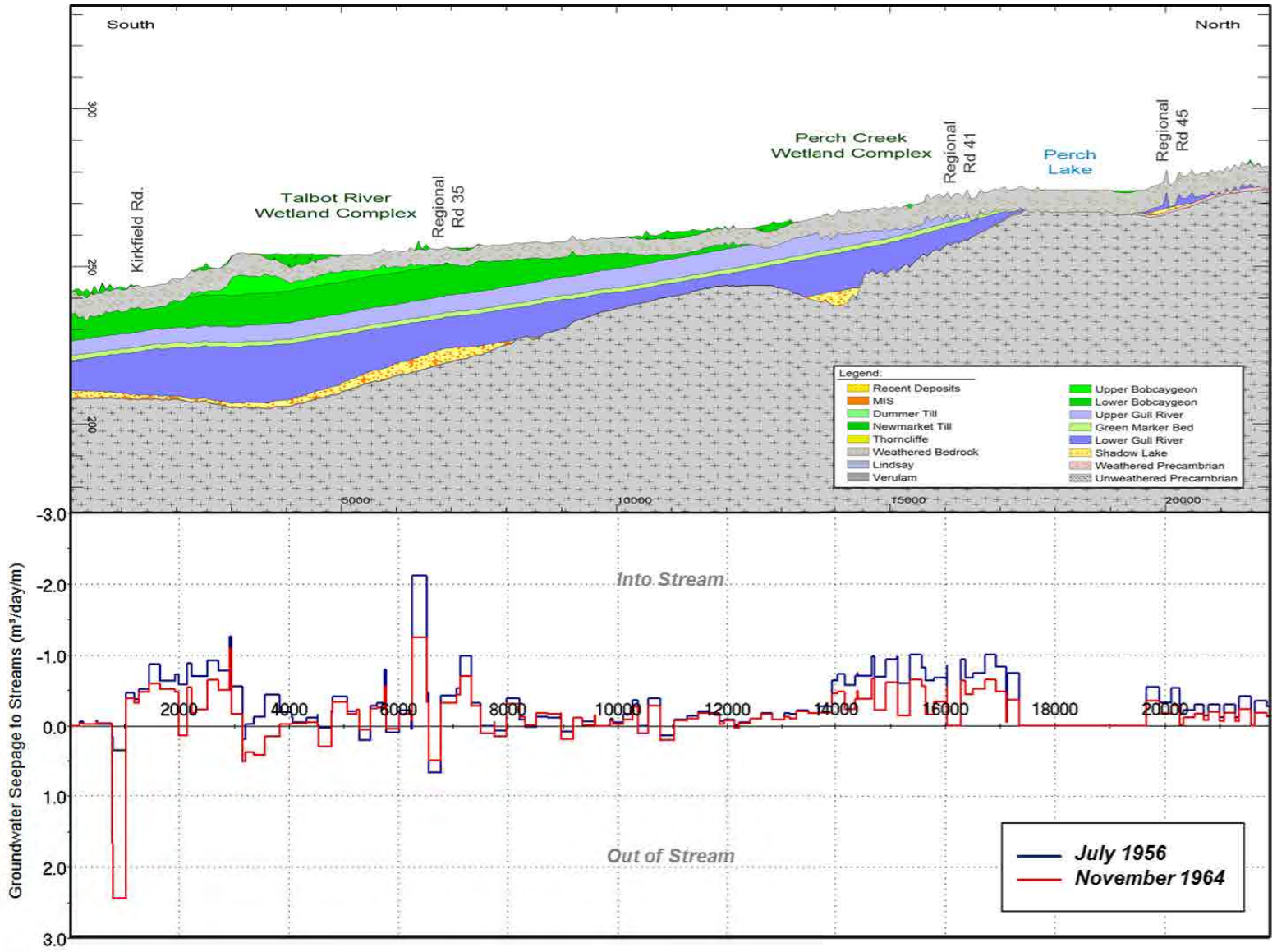

Figure 13.37: Cross section along the Upper Talbot River showing simulated groundwater discharge to streams in July 1956 and November 1964.

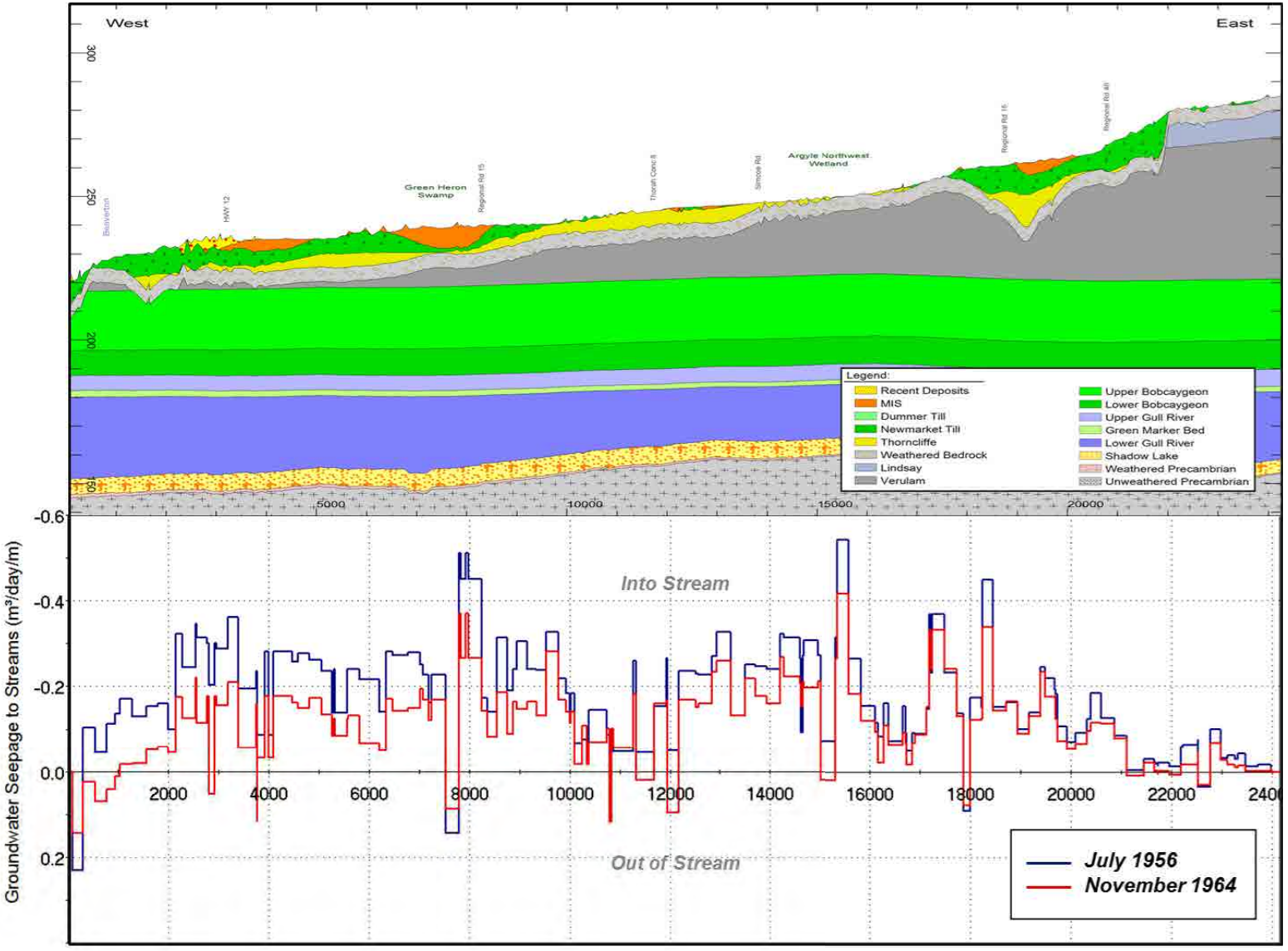

Figure 13.38: Cross section along Whites Creek showing simulated groundwater discharge to streams in July 1956 and November 1964.

14 ESGRA Assessment

14.1 Overview

Policy 6.36-DP and 6.37-SA of the Lake Simcoe Protection Plan discusses the need to define and identify "significant groundwater recharge areas" (SGRA) and "ecologically significant groundwater recharge areas" (ESGRA). SGRAs are defined as areas of above average recharge (1.15 times the average recharge rate) and were delineated for the entire Lake Simcoe basin in an earlier study (Earth*fx*, 2010). ESGRAs are identified as areas of land that are responsible for supporting groundwater systems that sustain sensitive features like cold water streams and wetlands. To establish the ecological significance of the recharge area, a linkage must be present between the recharge areas and the ecologically significant feature (e.g., a reach of a cold water stream, a wetland, or an area of natural or scientific interest). The identification of an ESGRA is not related to the volume of recharge that may be occurring, rather they represent pathways in which recharge, if it occurred, would reach that feature. While delineating ESGRAs is an important task in establishing the linkage between a recharge area and an ecologically sensitive feature it is not a certainty that ESGRAs will coincide with SGRAs, as they may not support high volumes of recharge. While ESGRAs and SGRAs are not mutually exclusive, the areas where they do coincide support high volumes of recharge and support ecologically sensitive features.

This section documents (1) the application of the integrated model to analyze groundwater pathlines and thereby establish these linkages and (2) the application of cluster analysis to delineate the extent of the ESGRAs.

14.2 ESGRA Delineation Methodology

Earth*fx* developed a general methodology for delineating ESGRAs as part of a recent ESGRA delineation study for the Barrie, Lovers and Hewitt Creek watersheds (Earth*fx*, 2012), and applied it successfully in a subsequent study of the Oro North, Oro South, and Hawkestone Creeks subwatersheds (Earth*fx*, 2013). A brief summary of the approach is provided below.

14.2.1 Particle Tracking

Particle tracking is an accepted methodology for visualizing and understanding groundwater flow paths. It is particularly useful in areas with complex, three-dimensional groundwater flow. As discussed in previous chapters, an integrated groundwater/surface water flow model was developed for the subwatersheds of the Ramara Creeks, Whites Creek, and Talbot River based on the USGS GSFLOW code (Markstrom et al, 2008). The MODFLOW-NWT submodel was applied to determine groundwater heads in each cell in a three-dimensional mesh used to represent the aquifers and aquitards in the study area as well as to determine the flows across each face of the cell.

The heads and cell-by-cell fluxes were saved for post-processing by the USGS MODPATH v6.0 code (Pollock, 2012). The MODPATH code uses output from MODFLOW-NWT along with estimates of aquifer porosity to determine local groundwater velocities within each cell. Virtual particles can then be released at any point within a cell and forward tracked from one cell to the next until it reaches a model boundary or an internal discharge point (e.g., a stream or well). Particles can also be tracked backwards from any discharge point in the model to their points of origin. Pathlines can be displayed by connecting the points along the flow path (see Figure 14.1). Particle endpoints (i.e., the location at which the flow path intersect land surface – representing the exit points when forward

tracking or the entry points when backward tracking) can also be displayed or recorded in a database for further analysis.

For forward tracking in the direction of flow, particles are usually introduced in a uniform distribution across the model area. Forward tracking can be applied to help define and visualize the regional flow system. With forward tracking it is often necessary to release an extremely large number of particles to clearly delineate the flow paths that support ecologically significant features.

With backward tracking, particles are introduced in a dense distribution at a point of interest (e.g., an ecological feature supported by groundwater discharge) and traced back to the point of recharge. A benefit of reverse tracking is that attention can be focused on a limited set of specific ecological features.

Practical limits to the number of particles that can be applied uniformly across the model area and limits in the number of particles that can be packed into a discharge area may cause some small variations in model results. Differences can occur when simulating flow in complex flow fields. For example, if groundwater is moving through "windows" in a regional aquitard, it may be difficult to identify all the possible particle paths through the windows if only a limited number of particles are released. Figure 14.2 is a schematic showing a particle release density that fails to capture flow through a window in a regional aquitard.

The key advantage of backward tracking is that clusters of particle endpoints can help identify recharge areas that are important to a specific ecological feature. The density of particle endpoints can be used as an indicator of the significance of the recharge area. This is the basis for the delineation of ESGRAs in this study.

14.2.2 Bivariate Kernel Density Cluster Analysis

Once the backward particle-tracking endpoints originating from ecological features have been identified, clusters of endpoints are examined to determine ESGRA boundaries. The method used to analyze endpoint clusters was adopted from published, peer-reviewed cluster analysis methodologies. Earth*fx* tested and refined the technique so that it could be applied to other subwatersheds and ensure that delineation of ESGRAs across Southern Ontario could be conducted in a consistent manner. Details of the method developed to objectively evaluate endpoint clusters and delineate ESGRAs are presented in Earth*fx* (2012).

Typically, particle tracking endpoints cluster in areas of focused higher recharge; while areas of diffuse recharge may end up with distributed, individual or small groups of particles. Manually or visually distinguishing between endpoints belonging to a cluster and isolated particles (outliers) can be rather subjective. For the purpose of this paper, “clusters” are defined as areas with a relatively high density of particle track endpoints. Endpoints that lie outside of the clusters are considered of lower significance and are excluded on the basis that they do not represent an ecologically significant volume of recharge. The delineated clusters are deemed to represent ESGRAs based on the assumption that the density of particle track endpoints correlate to recharge areas that are significant to sustaining groundwater discharge within these ecological features.

A consistent and repeatable method of identifying clusters was developed based on multivariate kernel density function, (^ as defined by Wand and Jones (1993). In its two-dimensional (bivariate) form, it is given as:

^ -∑ -(–) [1]

where:

= the total number of endpoints;
= the smoothing (or bandwidth) parameter; and
= the distance between endpoint and the point in space being evaluated.

The choice of the Gaussian kernel function is somewhat arbitrary as a uniform, triangular or inverse-squared distance kernel (amongst others) could also be used to define the distribution of particles within a cluster. The Gaussian distribution is consistent, however, with the dispersive processes typically encountered in groundwater flow due to heterogeneity and variations in hydraulic conductivity. It is also our findings that the cluster evaluation is more sensitive to the bandwidth parameter (i.e., the smoothing parameter) than the choice of kernel. The kernel provides a weighting function; giving stronger weights to endpoints in close proximity to the point in space that is being evaluated.

A second phase of cluster processing is needed to normalize the density field and eliminate areas of relatively small density. This helps to eliminate ESGRAs of very small areal extent and to infill any "doughnut-holes" present in an ESGRA. Removing areas of small density is accomplished by first defining a delineation cut-off threshold (ε) and eliminating all areas where the calculated density is less than a ε^{th} of the maximum evaluated ^ie)., eliminating all areas where ^) ——

Earth*fx* (2012) discussed the results of varying ε and on the extent of the ESGRAs. The analysis showed that a delineation cut-off threshold on the order of produced better results and ensured that any area where the evaluated ^is less than 1% of the maximum (^)was removed **from** the final ESGRA coverage.

In Earth*fx* (2012), the minimum allowable ESGRA extent was set to 0.045 km², which corresponded to the average model element area. Similarly, doughnut-holes less than 0.045 km² were filled in to produce continuous ESGRA delineations. The Normalized Bivariate Kernel Density Estimation (NBKDE) procedure with the application of the delineation thresholds and the removal of outliers and holes defined the final ESGRAs. The advantage of the NKBDE method is that it is unbiased compared to grid-based counting methods which are dependent on grid size, origin, and orientation.

14.3 ESGRA Delineation Results

14.3.1 Particle Tracking Results

For the purpose of this study, all stream reaches, wetlands, and lakes internal to the three study sub-watersheds (see Figure 4.16) were assumed to be significant. Accordingly, all of these features were represented explicitly in the numerical model. There are a number of criteria that could be used to identify ecological significant features, each with a required threshold and an associated level of uncertainty. For example, thermal regime (e.g., cold water vs. warm water stream reaches), minimum average discharge (environmental flows), or biological indicators (e.g., benthic invertebrate indices) could be used. Data to support the selection of feature based on these criteria would

require a watershed scale field program, this level of study has not been undertaken to date. To provide a conservative estimate of significant recharge areas, all features were selected for study. Figure 14.3 presents the model release locations for the backward tracking analysis from significant features in the Ramara Creeks, Whites Creek and Talbot River sub-watersheds.

Particles were released at the top of model Layer 1 in a manner consistent with the methodologies outlined by Earth*fx* (2012). Released particles were tracked backwards from the surface water feature, through the groundwater system, and to their originating model cell. Pathlines may cross through multiple cells and model layers; particle paths within each cell are determined by the simulated groundwater flows across each cell face. The hydraulic conductivity, porosity, and thickness of each model cell are considered when calculating the groundwater velocities.

For model cells containing a stream segment, particles were released on a 10 x 10 m spacing to ensure that enough particles were included to delineate the interactions between the groundwater, stream channel and the riparian areas adjacent to the stream. None of the paved canal reaches were included in the ESGRA analysis, as these were not identified as being ecologically sensitive features. A total of 400 particles were released in each 200 by 200 m model cell.

Particles were also tracked back from wetland features identified in the ELC mapping provided by LSRCA, along with seven lakes (Canal Lake, Kirkfield Lake, Mitchell Lake, Raven Lake, Talbot Lake, Johnston Lake, and Perch Lake) located within the Talbot River sub-watershed. Particles were also tracked backward from the portion of the Trent-Severn waterway located downstream of Canal Lake, which is represented as a lake in the GSFLOW model (none of the paved canal reaches were included in the ESGRA analysis). Consistent with other significant features, particles were released in these model cells on a 10 by 10 m spacing.

A total of 2,489,200 particles were released into model cells with significant features for the backward tracking analysis (Figure 14.3). It should be noted that the mapped wetlands contain areas that may have saturated soils and/or standing water for only parts of the year. The GSFLOW model accounts for the time-dependent variation in soil saturation and water-table position in these areas. For this analysis, however, the full extents of the mapped wetlands were considered as ecologically significant features, not just the permanently saturated or inundated areas. A density of 10 m x 10 m was found to be more than adequate to identify all the relevant recharge pathlines in this model, and is greater than the 20 m x 20 m particle release density used in the pilot study (Earth*fx*, 2012).

The endpoints of the backward tracked particles released from streams, wetlands and lakes, respectively, are shown on Figure 14.4. Of the particles released, 1,306,800 (52%) were released into discharging cells. These were used for endpoint analysis and ESGRA delineation. The remaining particles were released into cells that were found to be locally recharging the groundwater system (e.g., a losing stream reach or a part of a wetland contributing groundwater recharge). These particles did not leave the starting cell and were therefore excluded from the endpoint analysis. Of the valid endpoints, 1,267,165 (96.7%) remained within the study area subwatersheds, while the rest tracked backward into neighbouring subwatersheds.

Figure 14.5 illustrates the pathlines from the significant features within the study subwatersheds. For illustrative purposes, particles were released at a sparser density of only four particles per model cell (100 by 100 m particle spacing). This was because the density of the pathlines is so high at the finer 10 m by 10 m spacing that individual pathlines cannot be presented on the figure. As can be seen, a small number of pathlines cross subwatershed boundaries and track back to recharge areas outside of the study subwatersheds. As noted, approximately 3% of the pathlines leave the study subwatershed boundaries. The number of pathlines leaving the study subwatersheds is not large, and the pathlines generally do not extend far beyond the subwatershed boundaries. Nevertheless, it

does indicate that some surface water features, in particular some of the headwaters of the Ramara Creeks and Talbot River, are likely receiving significant quantities of lateral groundwater inflow from recharge zone within the Carden Plains alvar, outside their subwatershed boundaries.

The pathlines also help to illustrate the connections between the groundwater system and specific surface features. For example, long pathlines from both wetlands and streams in the Ramara Creeks subwatershed can be seen extending northward toward the topographic high located between Dalrymple Lake and Lake St. John. As noted previously in Chapter 5, this area is also associated with a regional high point in the groundwater levels and is interpreted to act as a significant recharge zone. Within the Talbot River and Whites Creek subwatersheds, many of the pathlines for the streams, wetlands and lakes track backward to areas outside of the interpreted extents of the bedrock tunnel valley features in which many of the surface water features are located (Figure 14.6). This pattern is particularly apparent in the southwest trending wetland complex (and associated pathlines) originating just south of Mitchell Lake.

14.3.2 ESGRA Delineation

ESGRAs were delineated by analyzing the particle endpoint locations using the bivariate kernel density estimation technique for cluster analysis discussed above. The sensitivity of cluster analysis results were assessed by varying the NBKDE smoothing parameter (h) and the delineation threshold (ε). The smoothing parameter was varied in steps from 10 to 500 m and the delineation threshold was varied in steps from 10 to 1000. Table 14.1 presents the percent of endpoints within the delineated ESGRAs with respect to the number of particles released (excluding particles that did not leave their starting cell). Table 14.2 presents the corresponding total area delineated as potential ESGRAs for various values of the NBKDE parameters (h, ε). Area as a percentage of the study subwatersheds is provided on Table 14.3. Table 14.4 presents the ESGRA cluster density (i.e., the number of endpoints that are contained within a potential ESGRA divided by the total combined ESGRA coverage area).

Based on the results shown in Table 14.1 through Table 14.4, the optimal kernel smoothing parameter h was set to 25 m, which is equal to half the grid cell spacing for the kernel analysis (performed on a 50 m by 50 m grid). A delineation threshold, $\varepsilon = 200$ (or $1/\varepsilon = 0.005$), was chosen because it proved to consistently identify particle clusters while meeting the following criteria:

- rejection of endpoints that clearly did not belong to any cluster;
- delineation of clusters with a relatively high density of particle endpoints; while
- not incorporating areas where endpoint density is low or zero.

The final combined ESGRA mapping using these parameter values is provided in Figure 14.7, which shows ESGRA delineation for all ecological features including streams, riparian zones, ponds, and wetlands. To visually illustrate the clustering, Figure 14.8 overlays all reverse particle tracking endpoints (black dots) on top of the final ESGRA zones. Of the released particles, 98% are included in ESGRA zones. ESGRAs having an area less than 0.045 km² were excluded, consistent with the approach of Earthfx (2012).

Table 14.5 provides a breakdown of the ESGRA coverage within each of the three study subwatersheds. The coverage varies between catchments, with 36% coverage within the Talbot River subwatershed versus 26% and 27% within the Ramara Creeks and Whites Creek subwatersheds, respectively. The smaller percent ESGRA coverage in the Ramara Creeks subwatershed reflects that key upland recharge features are responsible for sustaining many of the surface water features within the post-glacial silts and sands of the proto-Lake Simcoe shoreline

sediments. In the Whites Creek subwatershed, many of the backtracking particle pathlines terminate beyond the northern edge of the catchment, indicated that surface water features in this subwatershed are supported by ESGRAs within the Talbot River subcatchment, contributing to the relatively small percent ESGRA coverage in the Whites Creek subwatershed. Furthermore, the present of silt dominated Newmarket Till in both the Ramara Creeks and Whites Creek subwatersheds likely results in reduced groundwater recharge within much of their respective watershed areas.

The delineation of ESGRAs in the Talbot River subwatershed generally correspond to the tops of the incised bedrock valleys, a trend noted through inspection of backward-tracked particle pathlines compared to inferred valley locations, shown in Figure 14.6. These bedrock valleys dominate the up-catchment landscape of the Talbot River subwatershed, with wetlands and rivers occupying the bottom of the valleys being sustained by groundwater seepage supplied from atop the valley slopes; the result is an increased coverage of discrete ESGRAs within this catchment.

14.3.3 Forward Tracking Verification

Forward particle tracking was used verify the reverse particle tracking analysis and demonstrate that:

- the particle release density used in the backward tracking was sufficient; and,
- other significant recharge areas contributing to the streams and wetlands were not missed.

Forward tracking also provided a tool to assess linkages between recharge areas within the study area and ecologically significant features in adjacent subwatersheds.

Particles were released on a 10 by 10 m spacing across the upper faces of all cells in the three study area subwatersheds. A small buffer area around Lake Simcoe (which is represented with constant head boundaries) was excluded. A total of 6,047,600 particles were released. Of these, about 4.3 million particles moved to a point outside of the release cell, while the remaining particles were placed in cells that proved to be discharge points in the model.

Figure 14.9 illustrates the resulting forward-tracking particle endpoints from the three study subwatersheds. Particle endpoints from the Ramara Creeks subwatershed generally fall within the topographic boundary of this catchment, which suggests that cross-boundary flow to surface features in other catchments is minimal. By contrast, the presence of particle tracking endpoints from the Talbot River and Whites Creek subwatersheds in one another's catchment areas indicates that surface water features along the shared catchment boundary of the Talbot and Whites subwatersheds are supported by groundwater recharge from both subwatersheds. Other evidence of cross-boundary flow is the location of a number of forward tracking endpoints from the Talbot and Whites subwatersheds along the model boundary, particularly to the south and to the east.

As a verification exercise, forward tracking was conducted from the delineated ESGRAs shown in Figure 14.7. Particles were released on a 10 x 10 m spacing grid over the ESGRAs and forward tracked to a final destination. Results are shown in Figure 14.10. It can be observed that the majority of the particle tracks end either in, or adjacent to, the stream and wetland features. Because of the cross-watershed boundary flows, some particles released from the ESGRAs exit the study area and may help support ecological features in other catchments, specifically the wetland complex immediately south of Dalrymple Lake.

It can be seen that, in general, forward tracking of particles distributed across the study watersheds results in endpoints located along the headwater streams and wetlands of each of the catchments. Several of the wetlands in the Ramara Creeks subwatershed and a number of stream reaches along

the shore of Lake Simcoe are seen to have sparse particle endpoint coverage. These wetlands and streams are situated in the low-lying till and glaciolacustrine sediments and are likely supplied primarily by runoff which collects and recharges the water table.

Comparing the endpoints of the forward tracked particles released across entire study area (Figure 14.10) to the endpoints of forward-tracked particles released only at ESGRAs provides a qualitative assessment of the adequacy of the ESGRA delineation. (Forward tracking from the study area could show pathlines that were unaccounted for in the backward-tracking exercise.) By comparing the two figures, it can be seen that there are no additional pathlines intersecting ecologically significant areas. This confirms that the number of backward tracked pathlines (or the resolution of released particles) was sufficient to delineate ESGRAs with the groundwater model.

14.3.4 ESGRA Delineation from Cold Water Features

For discussion proposes, ESGRAs were also delineated by tracking back from cold water features. For this analysis, all groundwater-fed wetland and lakes were assumed to be cold water features. Cold water stream reaches were identified from watercourse mapping provided by LSRCA staff (Figure 14.11). Identified cold water streams are limited to the Whites Creek subwatershed, with no cold water streams identified within the Talbot River or Ramara Creeks subwatersheds. As a result, the number of particles released has been reduced by 56%.

The distance (h) and cut-off (ε) parameters for the cluster analysis were based on the previous optimization analysis with all streams to allow comparison between two ESGRA mapping efforts. As all the wetland and lake endpoints (which have not changed) and the remaining stream endpoints are used for this analysis, the optimal cluster values remain similar. Figure 14.12 presents the ESGRA delineation when considering only the identified cold water features.

A comparison with the complete ESGRA delineation is provided in Figure Figure 14.13. The ESGRAs identified in the Whites Creek subwatershed are largely unchanged; however, a number of areas previously identified (when considering all streams) in the Talbot River and Ramara Creeks subwatersheds have been eliminated. Considering only cold water features within the study subwatersheds results in an ESGRA delineation that covers 16% of the study area, less than half the size of the previous delineation which included warm water streams (Table 14.6). Additionally, the percentage of the Ramara Creeks subwatershed delineated as an ESGRA is reduced from 26% to 9%. While the Ramara Creeks streams have been mapped as warm water reaches, there are undoubtedly local recharge features that support these streams to some extent. Excluding all the warm water reaches from the analysis prevents local or riparian recharge zones from being mapped as ESGRAs.

14.4 Comparison of ESGRA and SGRA Results

Significant groundwater recharge areas were delineated by Earth*fx* (2010) for the Lake Simcoe watershed utilizing a PRMS-based hydrologic model. SGRAs were delineated as per Technical Rule 44(2)(1) as: "*areas where the rate of recharge is greater than a factor 1.15 of the average recharge across the area"* (MOE, 2009). The SGRAs identified in the study area are shown in Figure 14.14. It should be noted that these SGRAs were defined based on the average recharge across all watersheds contributing to Lake Simcoe.

As noted earlier, it is not a certainty that these areas of higher than average recharge coincide with ESGRAs. Figure 14.15 compares the ESGRAs delineated in this study with the SGRAs identified in Earth*fx* (2010). Annual average recharge over the study area was estimated to be 141 mm/yr in the

Earth*fx* (2010) SGRA delineation, while the average recharge (presented in Figure 9.14) reflects an updated recharge estimate of 135 mm/yr across the study area. As shown in Figure 14.15, SGRAs comprise a larger area than the ESGRAs, particularly within the Talbot subwatershed and along the lower portions of the Whites Creek subwatershed, near Lake Simcoe (as indicated by the green shaded area). Much of the differences between the mapped extents of the SGRAs and ESGRAs is likely a result of delineating the SGRAs using only a surface water model while the ESGRAs are delineated using an integrated model.

Although comprising less area compared to the SGRAs, many of the ESGRA delineated zones overlap those classified as SGRA in the previous Earth*fx* (2010) study (orange shaded areas in Figure 14.15). The model provides the linkages between the recharge and discharge areas and helps identify the portions of the SGRAs that provide significant recharge to the target areas. The model captures the interaction between the surface and groundwater processes that affect the distribution of recharge and groundwater flow patterns. As an example, SGRAs identified along the lower portion of the Talbot and Whites Creek catchments are associated with areas mapped as surficial sands; however, the presence of an underlying low permeability till sequence restricts recharge and model results indicate that the water table is near surface throughout much of this area leading to higher Dunnian runoff and lower recharge rates.

In summary, while the SGRAs represent high volume recharge areas, ESGRAs better represent recharge areas that contribute to features of ecological significance within the study subwatersheds. Areas where ESGRAs and SGRAs overlap, for example, along the tops of the incised bedrock valleys in the Talbot River and Whites Creek subwatersheds, provide significant volumes of recharge to ecologically sensitive features in the study area subwatersheds. The SGRAs may also provide flow to areas outside of the study area subwatersheds. ESGRAs which don't coincide with SGRA, such as those in the central portion of the Ramara Creek subwatershed, tend to represent lower volume, localized flow systems which provide flows needed to maintain the ecologically significant features (in this case, the large wetland complex to the north of Lagoon City, along the shore of Lake Simcoe).

14.5 Tables and Figures

Table 14.1: Percent of endpoints covered by every ESGRA with varying smoothing parameter and delineation threshold .

1/ε	h = 10	h = 25	h = 50	h = 100	h = 150	h = 250	h = 500
0.1	15.3%	25.1%	27.1%	44.5%	63.3%	85.0%	92.4%
0.05	30.7%	49.6%	56.2%	76.3%	88.0%	97.0%	99.0%
0.01	76.0%	92.2%	95.4%	98.7%	99.6%	100%	100%
0.005	90.2%	**98.0%**	98.8%	99.8%	99.9%	100%	100%
0.001	98.3%	100%	100%	100%	100%	100%	100%

Table 14.2: Total area (km^2) of potential ESGRAs with varying smoothing parameter and delineation threshold .

1/ε	h = 10	h = 25	h = 50	h = 100	h = 150	h = 250	h = 500
0.1	3.4	7.7	11.3	39.2	95.7	250.1	416.6
0.05	11.4	28.1	44.1	121.0	219.8	409.8	560.8
0.01	85.2	148.1	208.5	342.5	455.6	582.7	684.8
0.005	136.6	**206.0**	272.3	409.0	509.9	612.2	714.7
0.001	192.8	283.7	369.4	497.8	573.9	653.3	768.9

Table 14.3: Percent area covered by potential ESGRAs with varying smoothing parameter and delineation threshold .

1/ε	h = 10	h = 25	h = 50	h = 100	h = 150	h = 250	h = 500
0.1	0.6%	1.3%	1.9%	6.4%	15.7%	41.1%	68.5%
0.05	1.9%	4.6%	7.2%	19.9%	36.2%	67.4%	92.3%
0.01	14.0%	24.4%	34.3%	56.3%	75.0%	95.9%	112.7%
0.005	22.5%	**33.9%**	44.8%	67.3%	83.9%	100.7%	117.6%
0.001	31.7%	46.7%	60.8%	81.9%	94.4%	107.5%	126.5%

Table 14.4: Potential ESGRA point density (end points per km^2) with varying smoothing parameter and delineation threshold .

1/ε	*h* = 10	*h* = 25	*h* = 50	*h* = 100	*h* = 150	*h* = 250	*h* = 500
0.1	59,303	42,605	31,277	14,858	8,641	4,444	2,897
0.05	35,226	23,074	16,674	8,238	5,232	3,092	2,308
0.01	11,651	8,138	5,976	3,766	2,858	2,242	1,908
0.005	8,629	**6,221**	4,742	3,187	2,562	2,134	1,828
0.001	6,663	4,604	3,537	2,625	2,277	2,000	1,700

Table 14.5: Percentage of subwatershed covered by potential ESGRAs (h = 25).

Subwatershed	1/ε = 0.005
Ramara Creeks	26%
Talbot River	36%
Whites Creek	27%
Total	33%
Area outside of study area	5.8 km^2

Table 14.6: Percentage of subwatershed covered by potential wetland and cold water stream ESGRAs (h = 25).

Subwatershed	1/ε = 0.005
Ramara Creeks	9%
Talbot River	16%
Whites Creek	22%
Total	16%
Area outside of study area	1.9 km^2

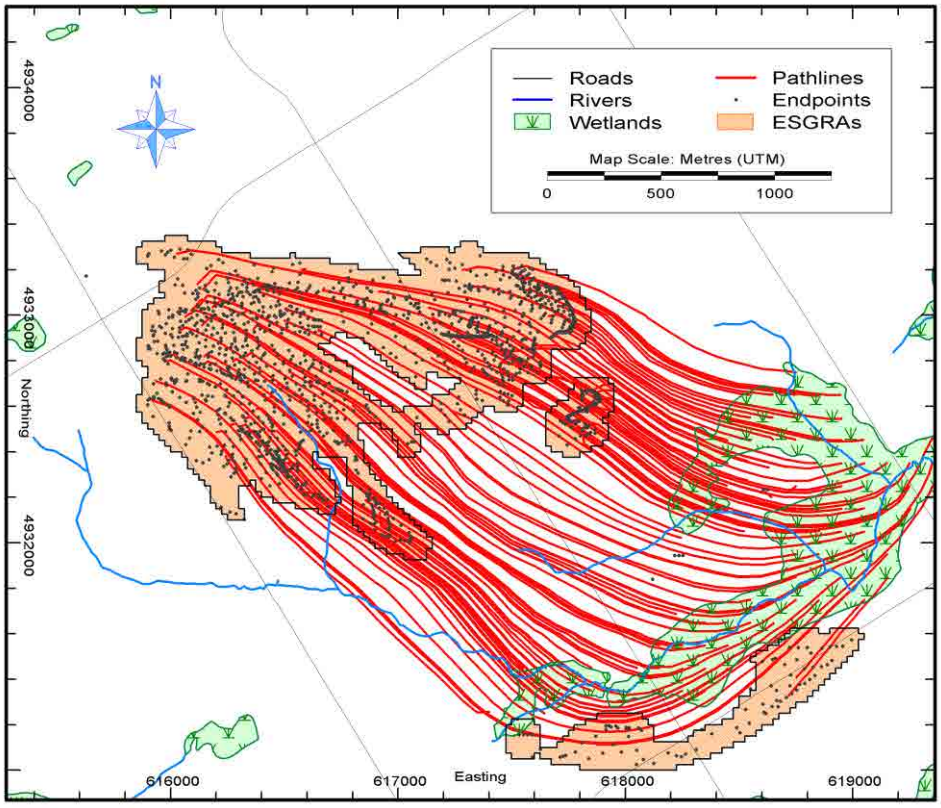

Figure 14.1: Example of backward particle-tracking from a significant feature to areas of ecologically significant recharge.

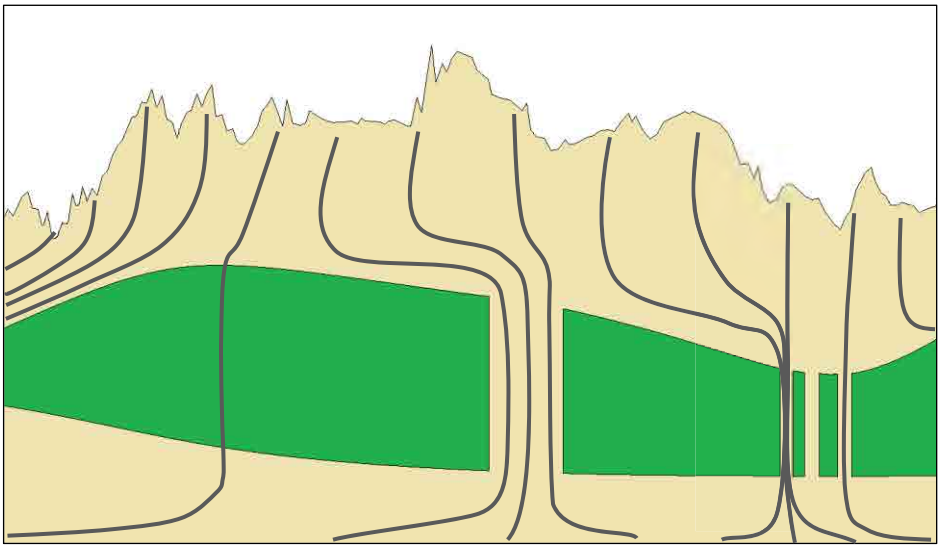

Figure 14.2: Pathline tracks through windows in a regional aquitard (green).

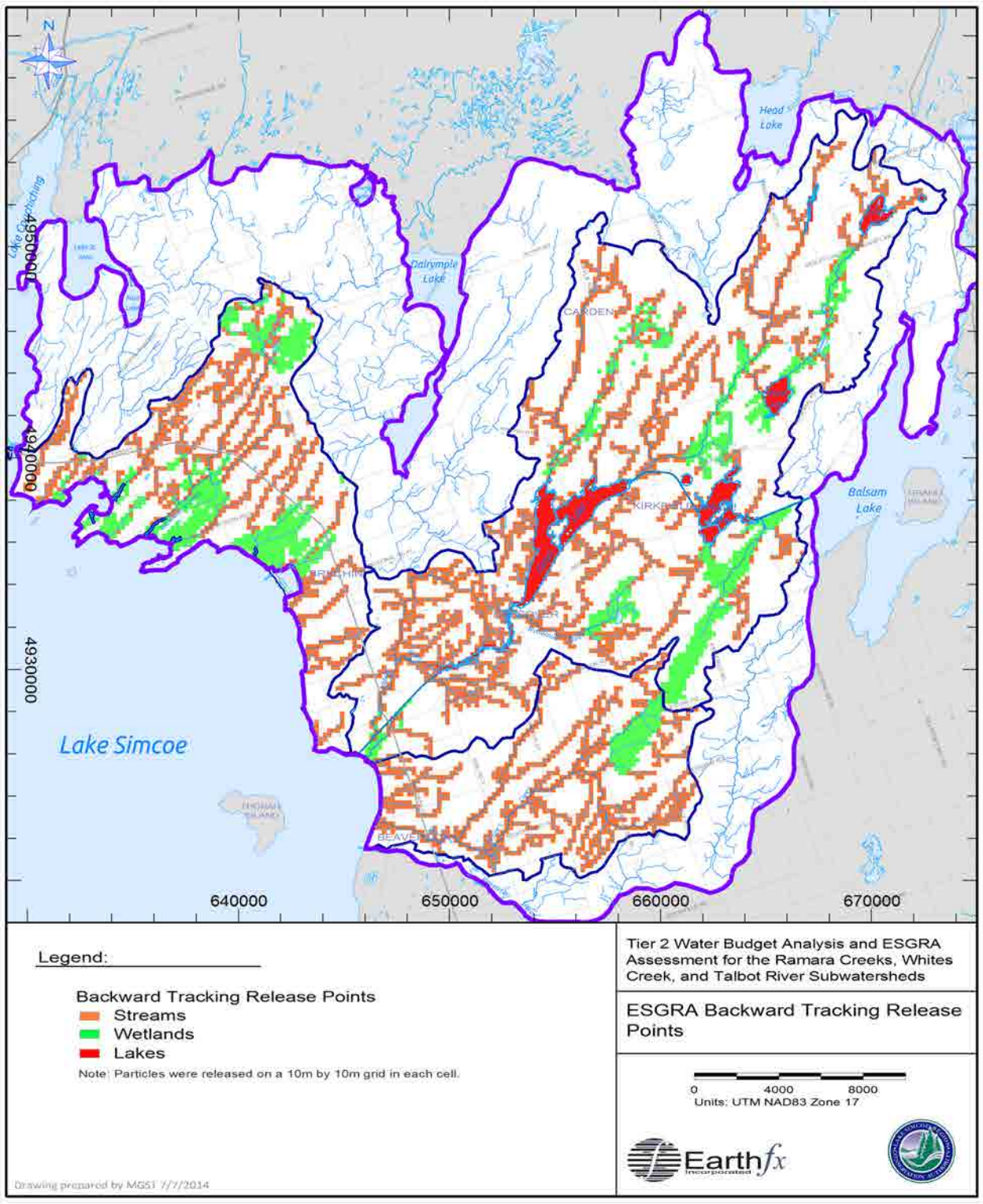

Figure 14.3: ESGRA backward tracking release points.

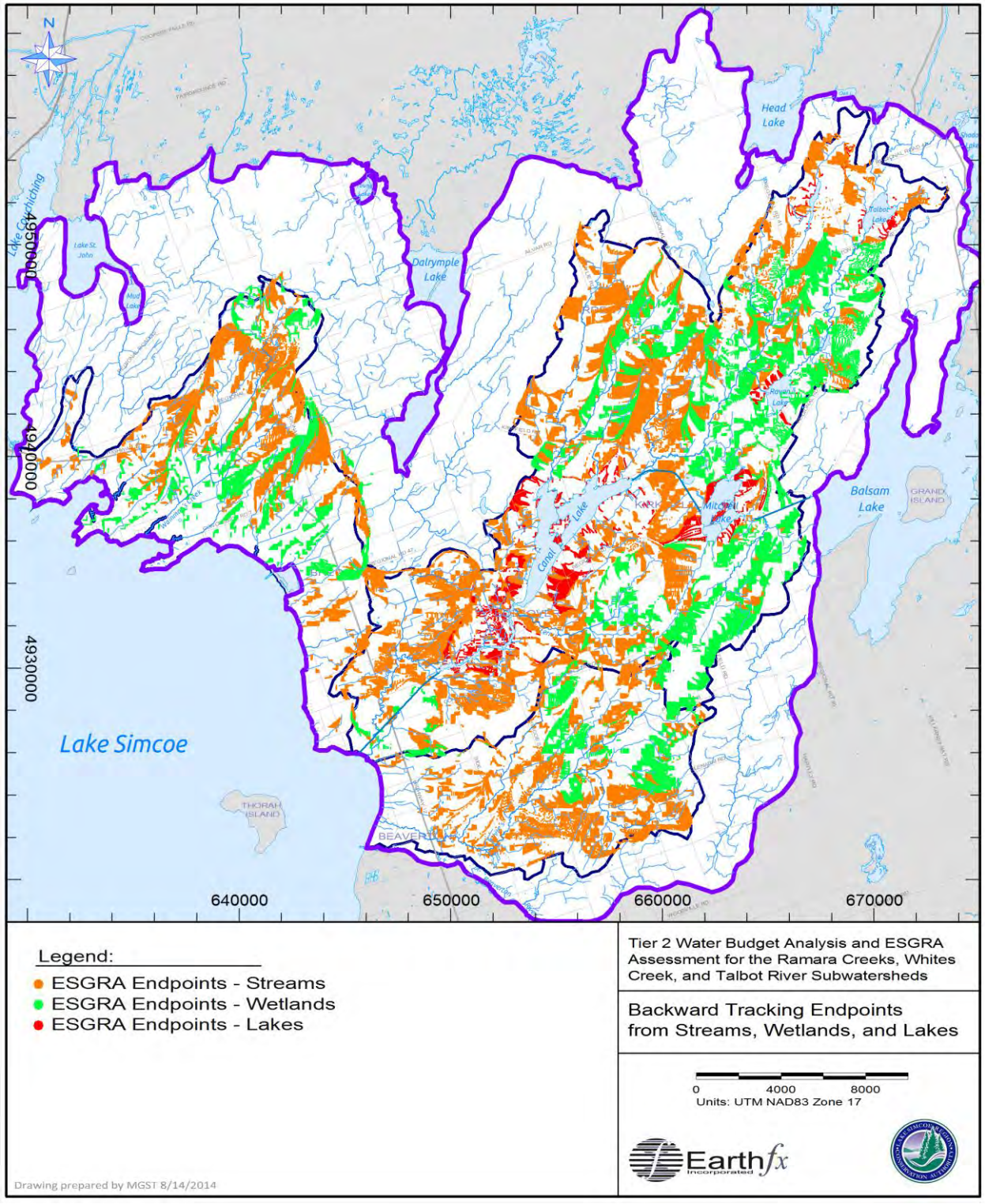

Figure 14.4: ESGRA endpoints for backward tracking from streams, wetlands and lakes.

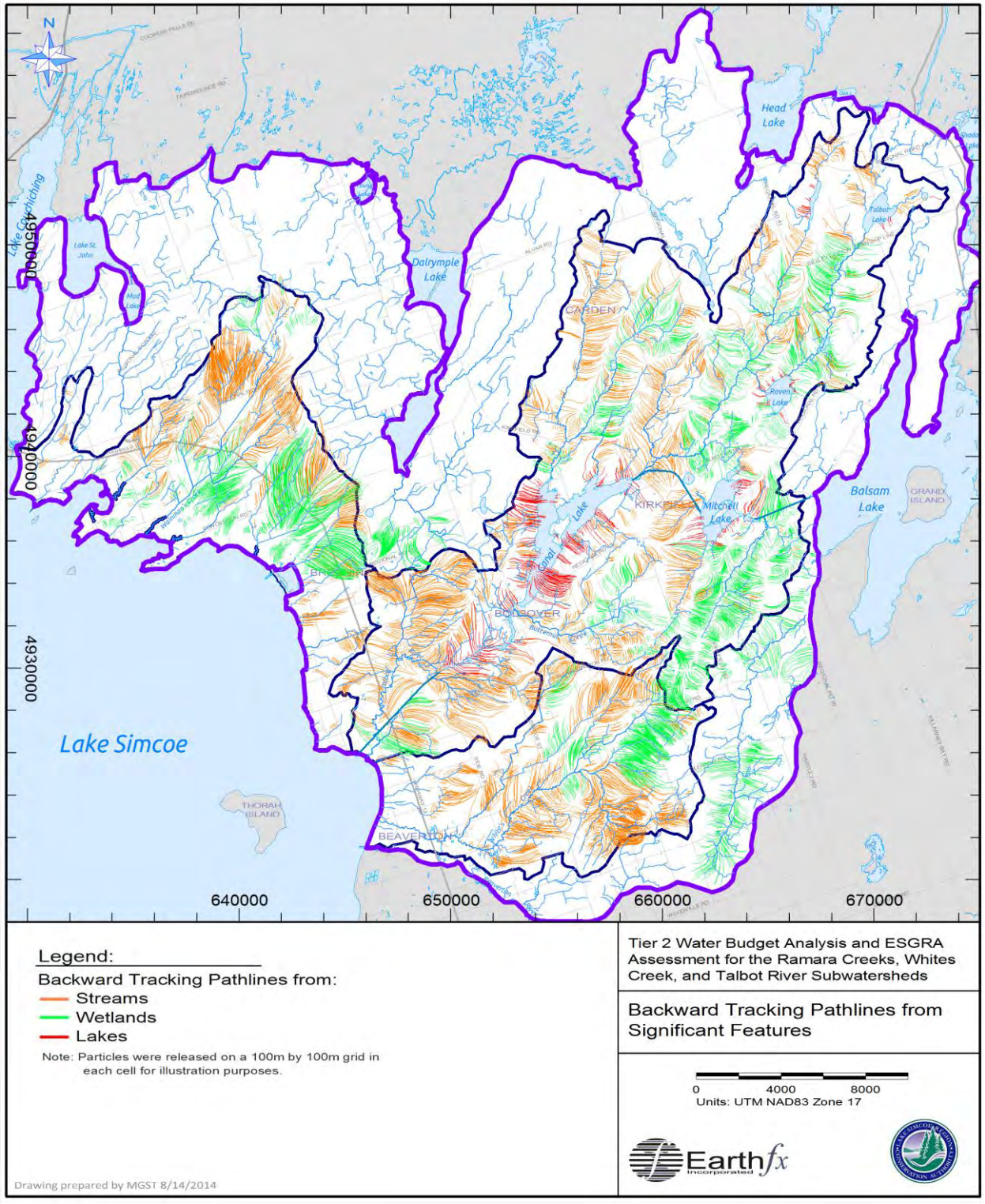

Figure 14.5: Backward tracking pathlines from significant features.

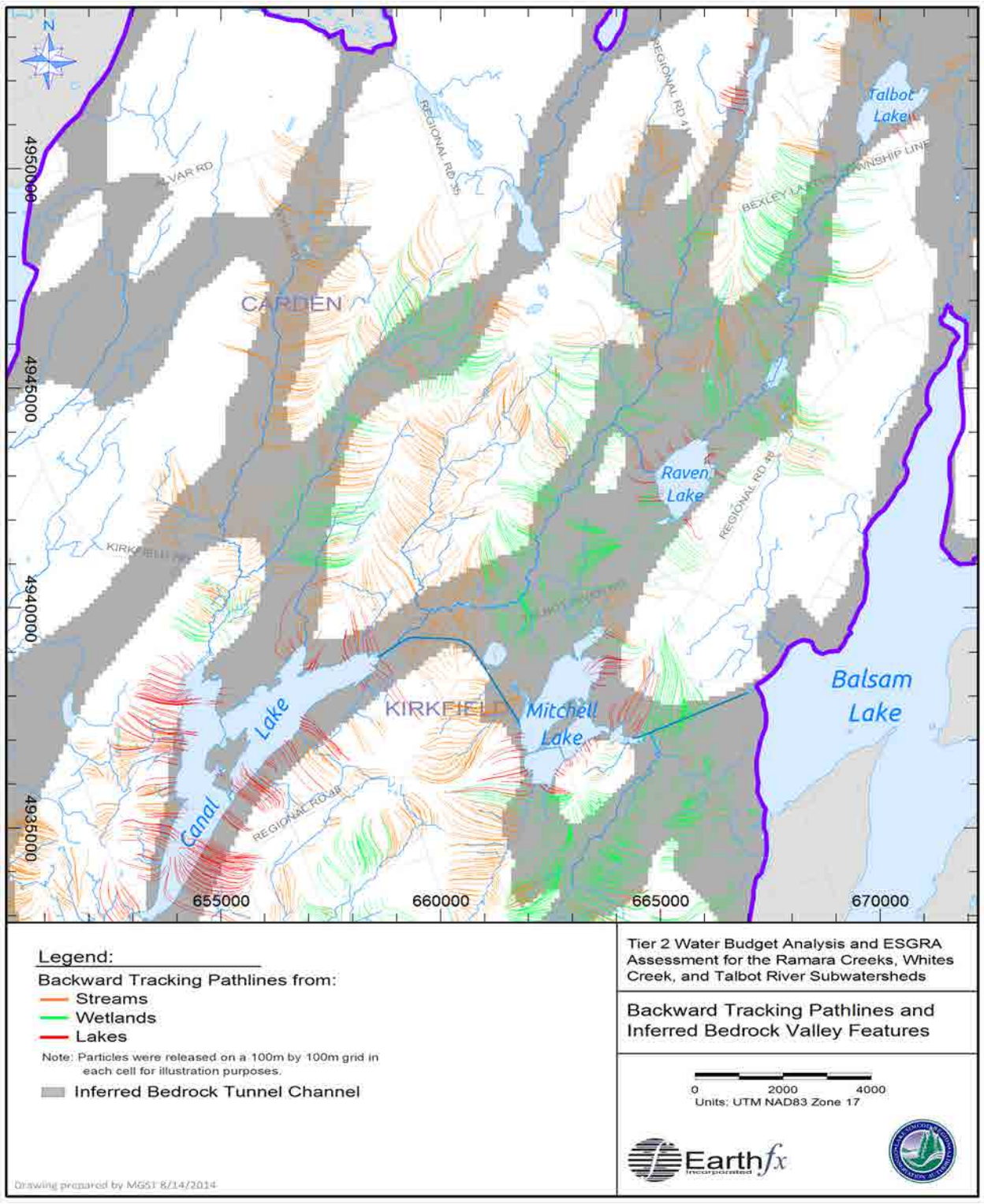

Figure 14.6: Backward tracking pathlines and inferred bedrock tunnel channels.

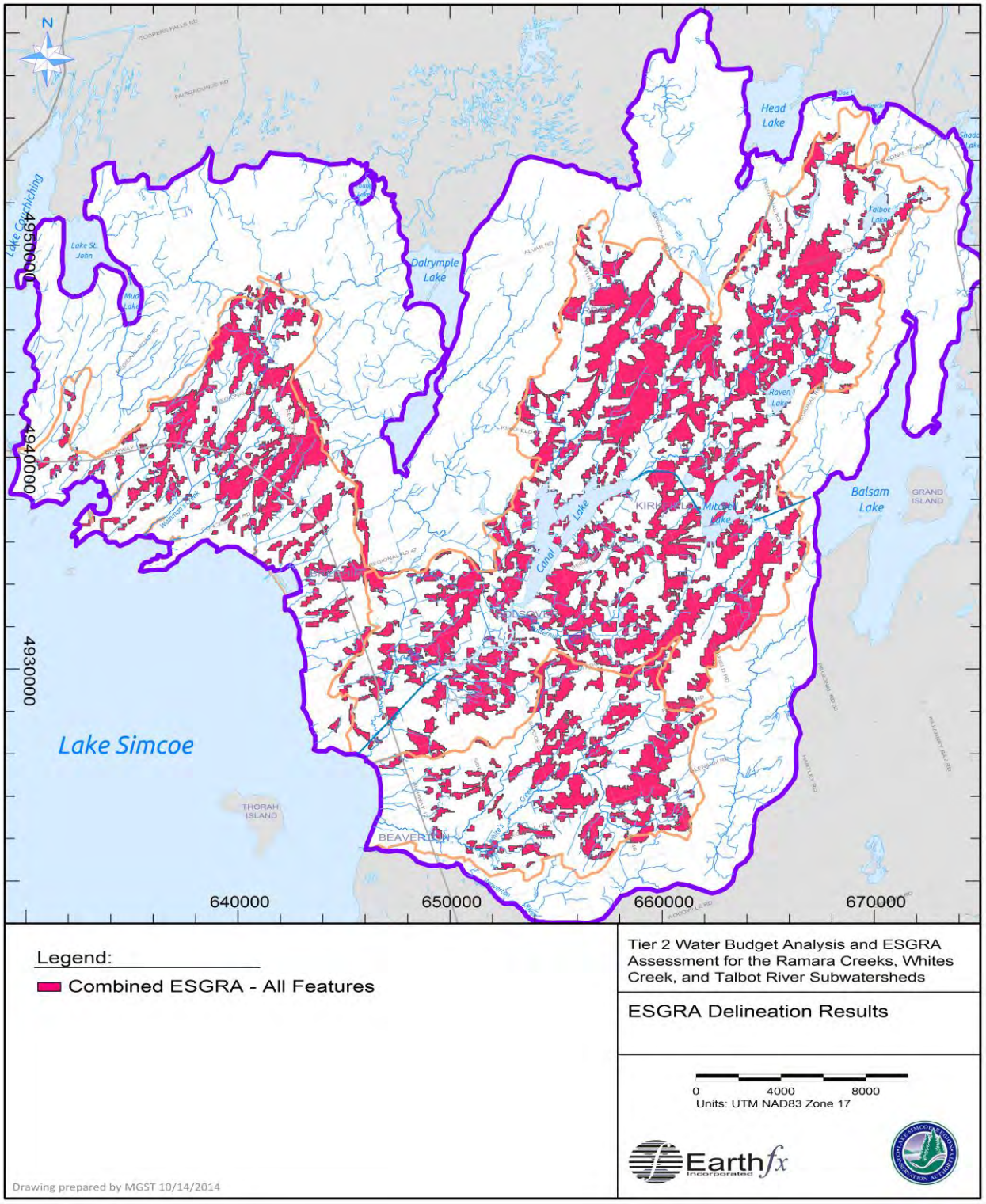

Figure 14.7: Combined ESGRA delineation by backtracking from all features (h=25, ε=200).

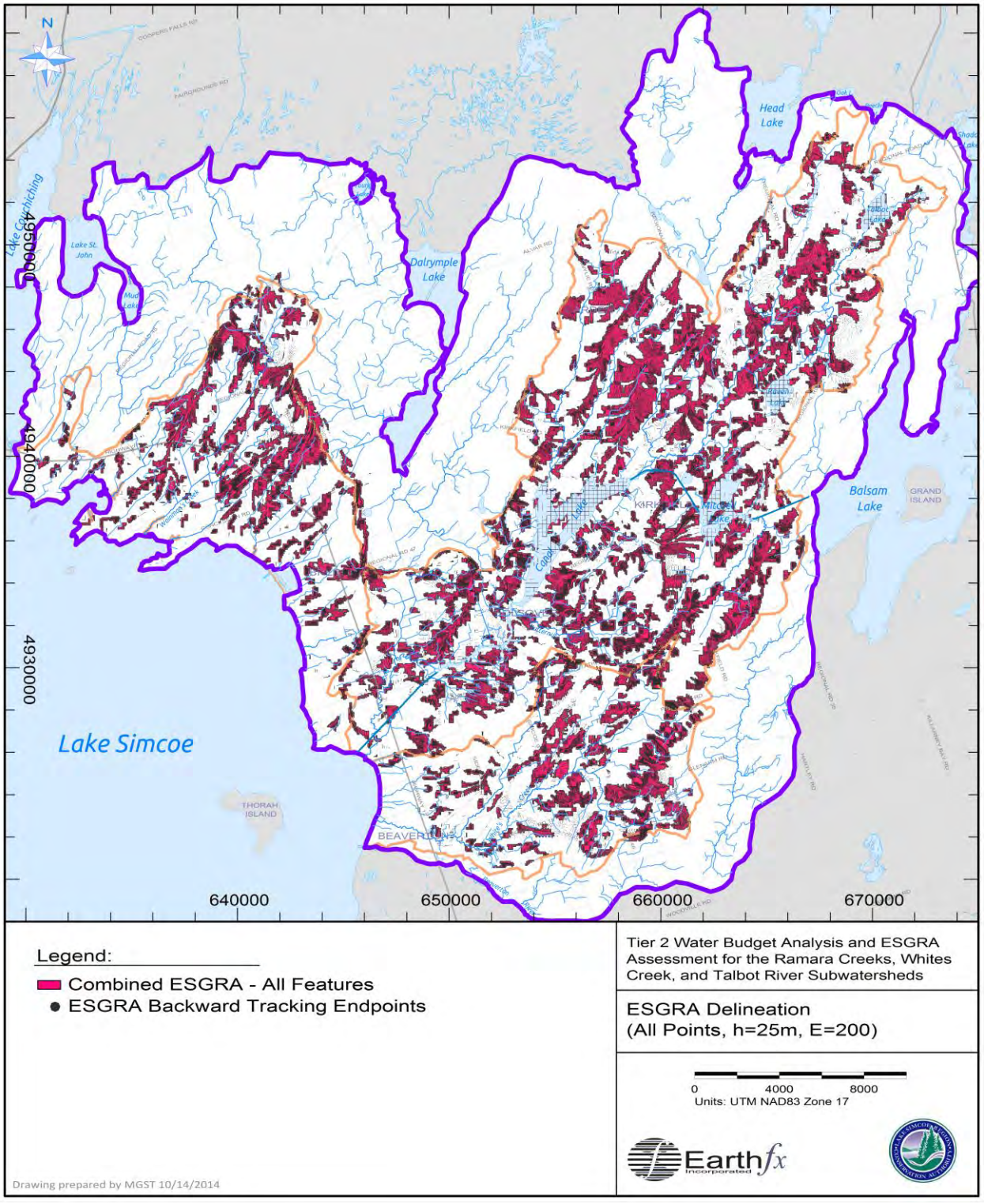

Figure 14.8: ESGRA delineation and overlay of all endpoints (h=25, ε=200).

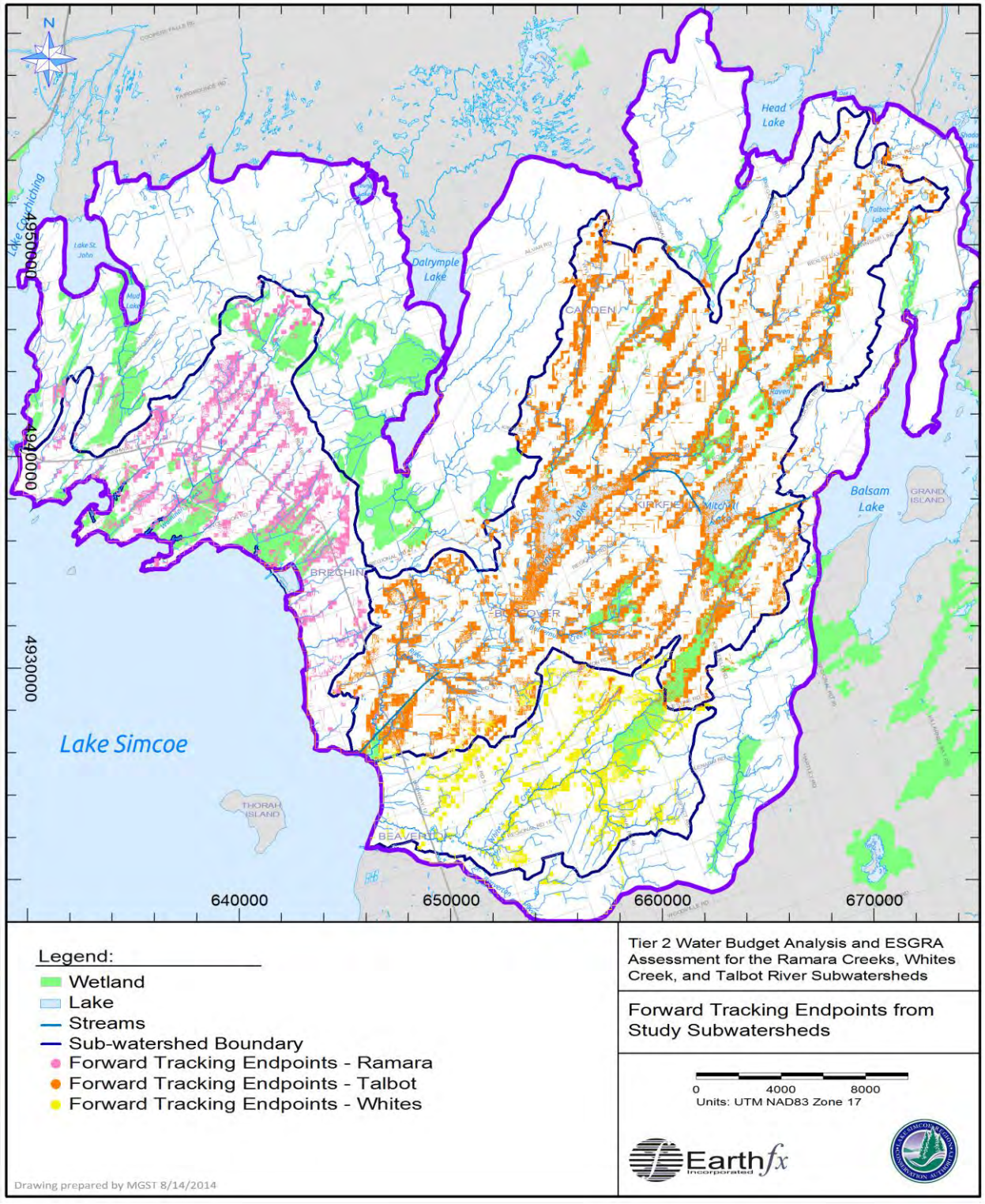

Figure 14.9: Endpoints from forward tracking particles released in study sub-watersheds.

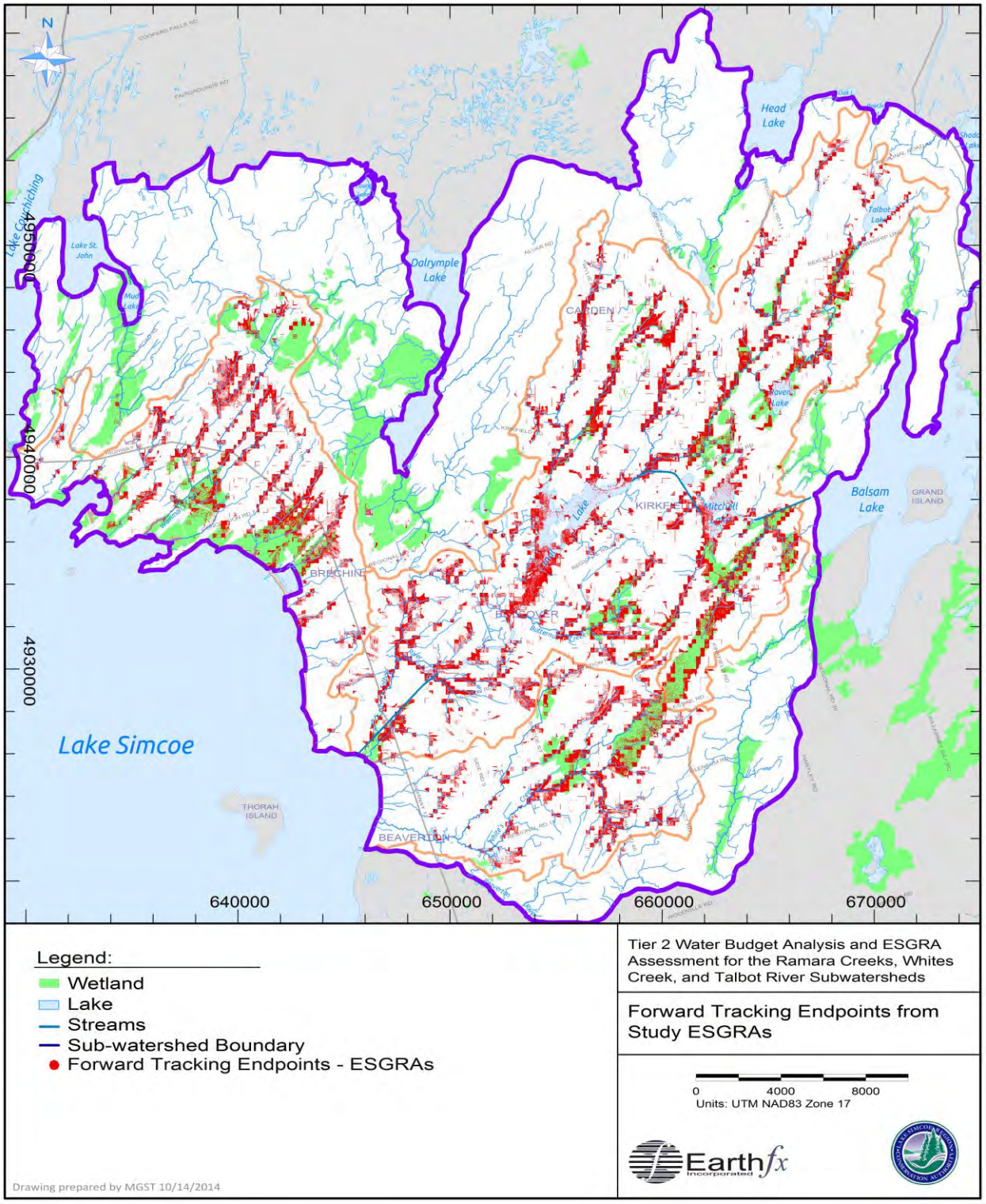

Figure 14.10: Endpoints from forward tracking particles released in delineated ESGRAs.

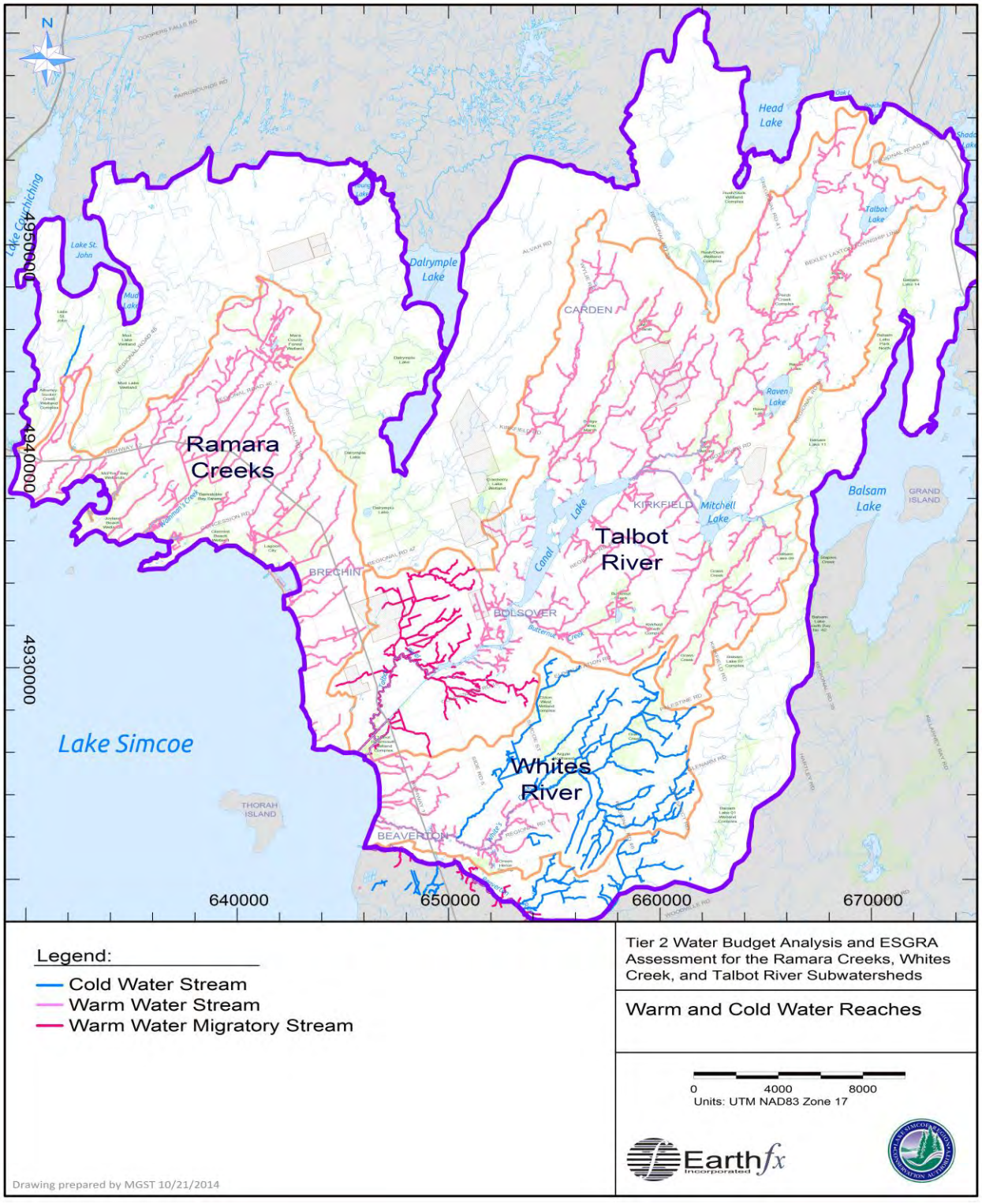

Figure 14.11: Thermal classification of study area streams.

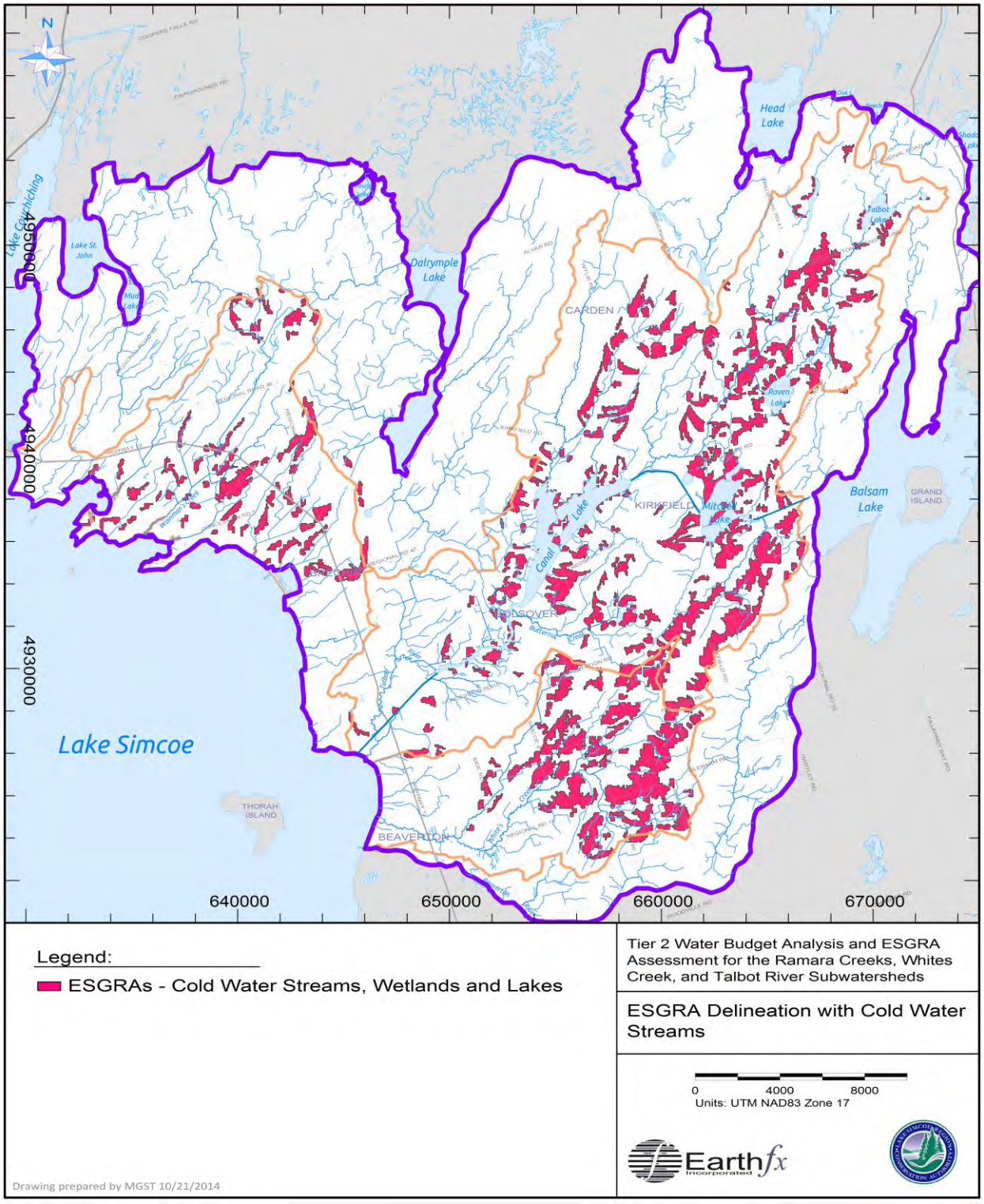

Figure 14.12: ESGRA delineation by backtracking from wetlands and cold water streams only (h=25, ε=200).

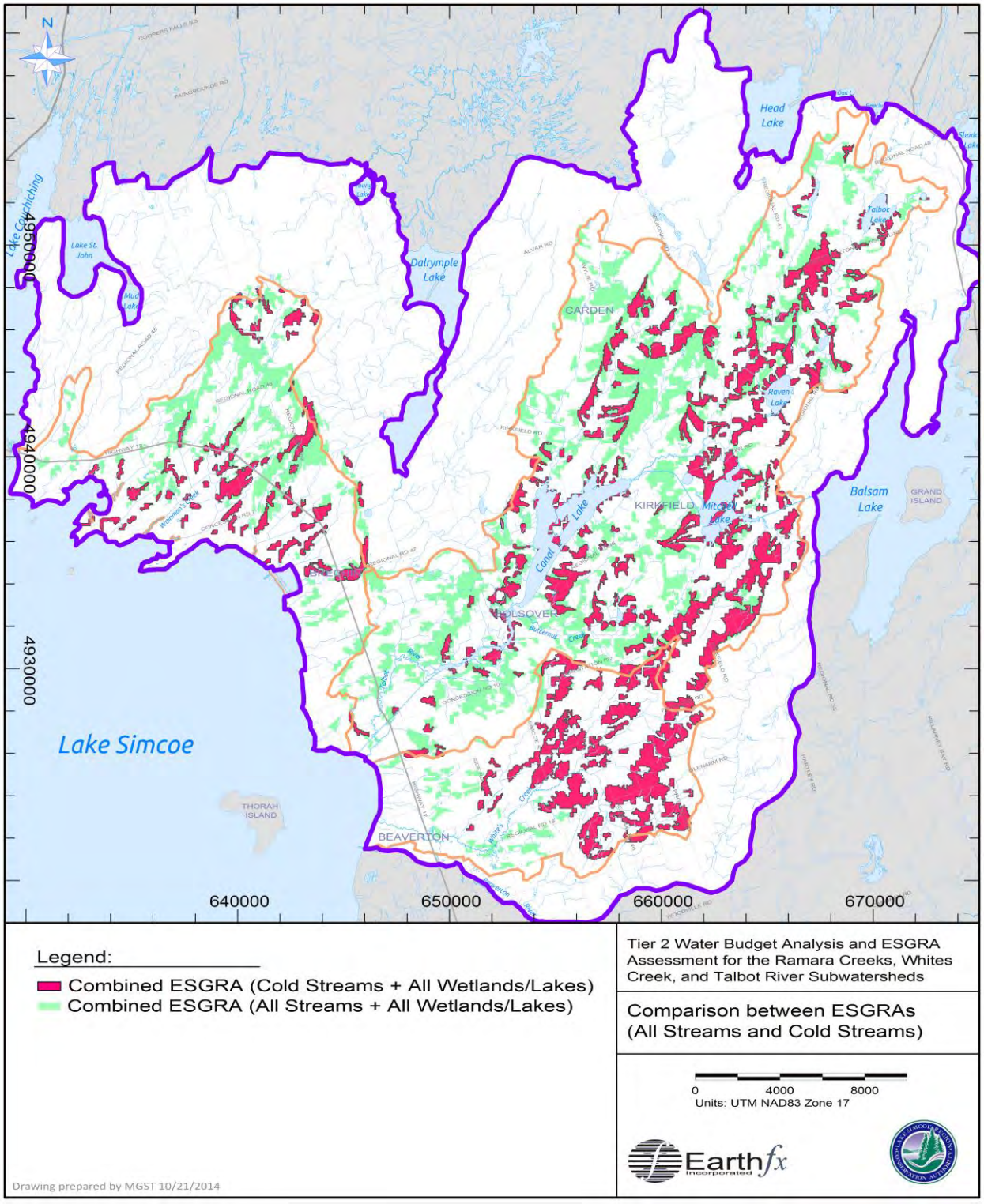

Figure 14.13: Final ESGRA mapping (all streams and wetlands) compared to ESGRAs which support wetlands and cold water stream reaches.

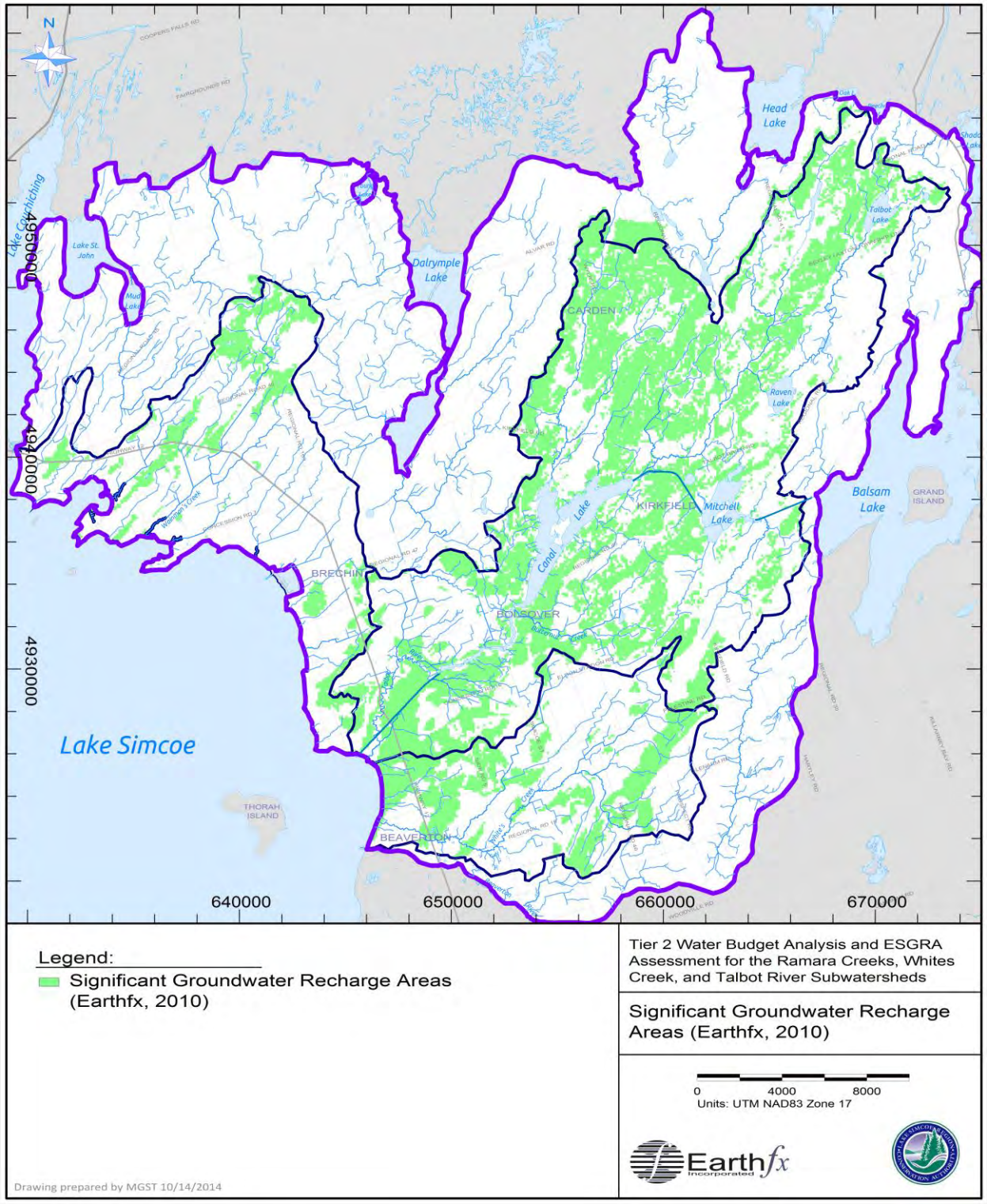

Figure 14.14: Significant Groundwater Recharge Areas (Earth*fx*, 2010).

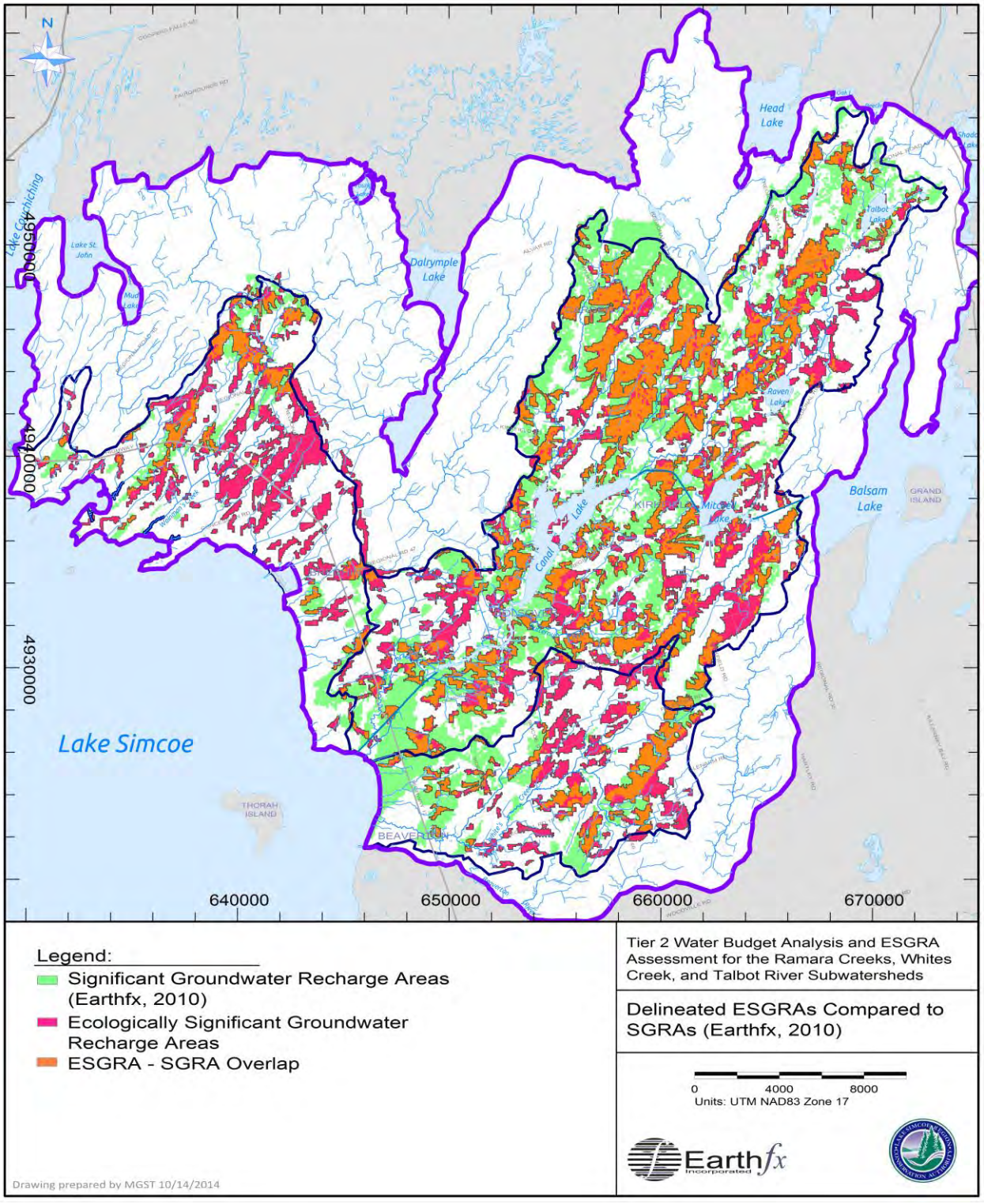

Figure 14.15: Delineated ESGRAs compared to previously identified SGRAs.

15 Climate Change Assessment

An assessment of the effects of global climate change on the surface water and groundwater resources in the Ramara Creeks, Talbot River, and Whites Creek subwatersheds was conducted as part of this study. Climate change scenario analysis followed recommendations in the Guide for Assessment of Hydrologic Effects of Climate Change in Ontario (EBNFLO and AquaResource, 2010). A brief introduction on climate change as it relates to water resources in Ontario, based on discussions and sources cited in EBNFLO and AquaResource (2010), is provided below.

15.1 Global Climate Change and Climate Change in Ontario

The Fourth Assessment Report (AR4) of the Intergovernmental Panel on Climate Change (IPCC) concluded that "warming of the climate system is unequivocal, as is now evident from observations of increases in global average air and ocean temperatures, widespread melting of snow and ice and rising global average sea level" (IPCC, 2007b). Global average annual surface temperature increased 0.74°C between 1906 and 2005 (IPCC, 2007c). Also, temperatures over land areas have warmed at a faster rate than over oceans (IPCC, 2007b). Precipitation increased 0.5-1% per decade in the 20th century over most land areas in the Northern Hemisphere. Some observed global changes in climate relevant to water resources are summarized in Table 15.1.

Table 15.1: Observed changes in global climate relevant to water resources (from Bates *et al*., 2008, IPCC, 2001b, and Solomon *et al*., 2007).

Observed Changes in Global Climate	
Increase in the number, frequency and intensity of heavy precipitation events, even in areas where total precipitation has decreased.	Decrease in snow cover in most areas of the cryosphere, especially during the spring and summer months
Reductions (approximately two weeks) in the annual duration of lake and river ice cover in the mid and high latitudes of the Northern Hemisphere.	Increase in actual ET from 1950 to 2000 over most dry regions (greater availability of water on or near land surface from increased precipitation and larger atmospheric capacity for water vapour due to higher temperature).
Increase in annual runoff in high latitudes	Altered river flow in regions where winter precipitation falls as snow; more winter precipitation falling as rain.
Higher water temperatures in lakes.	Earlier snowmelt, due to warmer temperatures.
Fewer numbers of frost days, cold days, cold nights and more frequent hot days and hot nights.	Decrease in diurnal temperature range (0.07° C per decade) between 1950 and 2004 but little change from 1979 to 2004 as maximum and minimum temperatures increase at same rate

Local climate change in Ontario has also been observed and includes some of the effects summarized in Table 15.2. Predictions of projected changes in Ontario climate are based on global circulation model (GCM) simulations. Over 30 different GCM-scenario combinations indicate that total annual precipitation could increase by 2 to 6%, while temperatures could increase by 2 to 4°C by the 2050s over the Great Lakes Basin (Bruce *et al.*, 2003). Changes in extreme warm temperatures are expected to be greater than changes in the annual mean temperature (Kharin and

Zwiers, 2005). The number of days exceeding 30°C is projected to more than double by the 2050s in Southern Ontario (Hengeveld and Whitewood, 2005). Heat waves and drought may become more frequent and longer lasting.

Table 15.2: Observed changes in Ontario Climate.

Observed Changes in Ontario Climate	
Annual average air temperatures across the province increased from 0 to 1.4° C; the greatest warming occurred in the spring for the period 1948 to 2006, (Lemmen *et al*., 2008).	The number of warm days and night-time winter temperatures increased between 1951 and 2003 (Bruce *et al*., 2006a).
Total annual precipitation increased 5-35% since 1900, (Zhang *et al*., 2000) and the number of days with precipitation (rain and snow) increased (Vincent and Mekis, 2006).	Water vapour in the Great Lakes Basin and Southern Ontario has increased more than 3% from 1973 to 1995, contributing to higher intensity rainfall events (Ross and Elliott, 2001).
Increased night-time temperatures in the summer has been linked to more intense convective activity and rainfall contributing to greater annual precipitation (Dessens, 1995).	The number of strong cyclones increased significantly across the Great Lakes over the period 1900 to 1990 (Angel and Isard, 1998).
Heavier, more frequent and intense rainfall events have been detected in the Great Lakes Basin since the 1970s.	The maximum intensity for 1-day, 60-minute and 30-minute duration rainfall events increased on average by 3-5% per decade from 1970 to 1998 (Adamowski et al., 2003).
The frequency of intense daily rain events increased from 0.9% (1910 to 1970) to 7.2% (1970 to 1999) for very heavy events and from 1.5% to 14.1% for extreme events (Soil and Water Conservation Society, 2003).	Precipitation as snow in the spring and fall has decreased significantly in the Great Lakes-St. Lawrence basin between 1895 and 1995, although total annual precipitation has increased, (Mekis and Hogg, 1999).
An increase in lake-effect snow has been recorded since 1915 (Burnett et al., 2003).	

Most climate modelling results suggest that annual precipitation totals will likely increase across Ontario; however, summer and fall precipitation amounts may decrease up to 10% in southern portions of the Province. Winter precipitation may increase as much as 10% in the south (Lemmen *et al*., 2008). More winter precipitation is very likely to fall as rain. Lake effect snow will likely increase until the end of the 21st century, then snowfall may be replaced by lake-effect rainfall events (Kunkel *et al*., 2002 and Burnett *et al*., 2003). Extreme rainfall events in Ontario are expected to increase by 5% per decade while severe winter storms may increase in intensity. Thirty minute and daily extreme rainfall may increase by 5% and 3% per decade, respectively (Bruce *et al*., 2006b).

To better cope with climate change and to evaluate strategies for protecting Lake Simcoe watersheds in the near future, tools can be developed and applied to evaluate the effects of climate change on the groundwater and surface water system on a watershed and subwatershed scale. Issues that could be addressed include the degree to which less frequent but more intense rainfall events increase runoff and decrease groundwater recharge in the watersheds. Other factors, such as increased ET (due to higher temperature and increased solar radiation) or the increased drought frequency and severity could also be evaluated in terms of the net change to groundwater recharge and streamflow. Decreased groundwater recharge may lead to a decrease in the water available for domestic and public supply as well as decrease baseflow needed to support aquatic habitat in wetlands and streams. Increased runoff could lead to increased stream bank erosion and sediment transport. The effectiveness of mitigation measures, such as water conservation, alternate water

supplies, regulation of water use, increased water storage for flow augmentation, and others could be evaluated using these same tools. This study demonstrates the use of a watershed-scale integrated groundwater/surface water model used in conjunction with transient GCM datasets to evaluate the effects of climate change on the regional hydrologic and hydrogeologic systems.

15.2 Climate Change Studies Completed in the Lake Simcoe Watershed

Several climate change studies have been undertaken in the Lake Simcoe basins; a brief summary of relevant projects is provided below. MacRitchie and Stainsby (2011) applied climate change projections from 10 climate models to a simple water balance model to estimate the future effects of climate change on water quality and quantity. The study predicted increased surface water runoff in the winter months and decreased water availability in the summer. Additionally, the authors anticipate an increase in the frequency of low water levels and drought events during the summer along with an increased risk of flooding in winter.

Chu (2011) assessed the vulnerability of wetlands, streams and rivers within the Lake Simcoe watershed to climate change. Future changes to physical habitats were assessed by pairing biological indicators (e.g., fish habitat) to GCM scenario parameters (e.g., temperature and precipitation). Results indicated that 89%of the wetlands within the watershed will be vulnerable to drying and shrinkage resulting from increases in air temperatures and decreases in precipitation.

The effects of changing land use and climate on the hydrology and carbon budget of the Lake Simcoe Watershed was studied by Oni et al. (2012). GCM data was applied to a subbasin-scale hydrologic model (HBV) to predict dissolved organic carbon fluxes to Lake Simcoe under future conditions. The hydrologic model suggested increased variability in the predicted runoff in spring and winter seasons relative to the historical baseline condition. Further use of the linked hydrologic-carbon model (HBV-INCA) was made by Crossman et al. (2013) to analysis the Black River watershed in greater detail. The model predicted higher winter flows, reduced summer flows and an earlier snowmelt in the watershed. Based on the predicted changes to the hydrologic regime, and increased overall temperatures, the study concluded that total phosphorus loading to Lake Simcoe is likely to increase throughout the 21st century which will have a negative effect on the Lake's ecological and trophic status.

To mitigate future stresses on the Lake Simcoe Watershed, the Ontario Ministry of the Environment has drafted the Lake Simcoe Climate Change Adaptation Strategy (2013). The document notes many possible impacts to water quantity in the watershed, including: a reduction in groundwater recharge; depletion of soil moisture in summer months; variation in stream-flow regimes and lake levels that may affect fish and wildlife habitats and sediment transport processes; and changes to ice cover that may affect evaporation, infiltration, shoreline erosion, precipitation, seasonality and lake-effect snow. The adaptation plan identifies a number of strategic actions that can be undertaken to strengthen the Lake Simcoe watersheds reliance to future change. It provides an adaptive management framework to monitor, evaluate, and react to future climate impacts. A detailed discussion of the development of proposed adaptation strategy can be found in Lemieux et al. (2014).

15.3 Global Circulation Models and Downscaling

Climate predictions are done with Global Circulation Models (GCMs) that simulate atmospheric and ocean circulation across the world and the interaction with the land masses and sea ice. The models are built on a large grid with cells ranging from 250 to 400 km on a side and can therefore

not resolve storm events at the local scale. Results of long-term GCM simulations are presented in terms of annual, seasonal, and monthly change in climate variables such as temperature, precipitation, solar radiation, and wind speed.

There are 21 GCM models, developed by different government and/or academic research groups in different countries. For example, the Canadian Centre for Climate Modelling and Analysis (CCCMA) a division of the Climate Research Branch of Environment Canada, has developed CGCM4/CanCM4, a fourth generation atmospheric GCM. The models differ in their grid scales and in assumptions regarding clouds, interaction mechanisms, and sub-grid scale processes. An inter-model comparison showed that the models simulate the seasonal cycle and large-scale geographical variations in surface temperature very well. Correlation between observed and modelled temperature is 95% or better (U.S. Climate Change Science Program (USCCSP), 2008 and Covey *et al.*, 2003). Simulated precipitation, however, showed only a 50 to 60% correlation for seasonal mean precipitation at the scale of a few hundreds of kilometres (USCCSP, 2008 and Covey *et al.*, 2003). When precipitation is sorted into light, moderate and heavy categories, models reproduced the observed extent of moderate precipitation (10 to 20 mm/day) but underestimated the extent of heavy precipitation and overestimated the extent of light precipitation (Dai, 2006).

Each model has different sets of predictions based on different greenhouse gas (GHG) emission scenarios. The scenarios are based on different assumptions regarding factors such as future demographic, socioeconomic, cultural, and technological change. In the IPCC Fourth Assessment Report, a subset of three scenarios was selected for projecting climate change in the 21st century. This subset (labelled B1, A1B and A2) represents 'low', 'medium' and 'high' emission scenarios assuming no mitigation (Meehl *et al.*, 2007).

While the model assumptions, construction details, and emission scenarios differ, the IPCC considers each model prediction to be equally valid. It is recommended that climate change impact assessment studies use as many scenarios of climate change as possible to cover a wide range of potential outcomes. The objective of this approach is to conduct an unbiased assessment of future climate change, account for uncertainties in the predictions, and develop adaptation strategies that would be resilient to a wide range of possible future outcomes.

As noted above, the GCMs cannot predict local-scale behaviour at a scale smaller than the grid size. As well, the GCMs cannot account for spatial variability at a fine scale (e.g., local land use, topography, and surface water features, and are instead more representative of large-scale, average climate characteristics and potential changes. Different methods are available for downscaling GCM outputs for use in local-scale models. EBNFLO and AquaResource (2010) discuss several methods including the "change-field' method, synthetic and analogue data sets, statistical downscaling, weather generators, and regional climate models. The change-field method was selected for this analysis and is described briefly below.

15.4 Change Field Method

The change field method involves calculating mean monthly changes in future climate based on output from the GCM models. As a first step, gridded output from the GCMs is summarized as monthly averages for each selected climate parameter. The period spanning 1961-1990 was used to represent baseline climate conditions and the 2050s (2040-2069 or 2041-2070) were used as future conditions for this study. Shifts in the mean values and scale factors (e.g., a +2.5°C increase in average daily temperature and a +10% increase in total precipitation for January) were determined and used to modify the baseline climate data set and derive a range of future climate data sets. Change field data sets have been preprocessed and are available at the Canadian Climate Change Scenarios Network (CCCSN) for many GCM runs. The modified climate data sets

are used as input to local-scale models, such as the integrated surface water/groundwater model developed in this study, so that the simulated future response (e.g., future streamflow and groundwater levels) can be compared to the baseline response.

The change field method has been widely adopted due to its ease of use. The primary advantage is the ability to generate change fields for a wide variety of GCM/emission scenario combinations and thereby investigate a wide-range of predicted responses and develop an improved understanding of uncertainty associated with local-scale responses to future climate change. One of the key limitations of the change field method for hydrologic impact assessment, however, is that potential impacts of climate change on inter-annual or day-to-day variability of climate parameters are not represented. The change field method alters the time series averages but the variability inherent in the dataset remains the same. Specifically, changes in sequences of wet and dry days are not altered by this method nor are patterns of intense precipitation events. This can lead to an underestimation of future floods, droughts, groundwater recharge and snow-melt timing (Bates *et al*., 2008). These limitations should be kept in mind when reviewing the findings of this study.

15.5 Selection of GCMs and Emissions Scenarios

Two methods are discussed in EBNFLO and Aquaresources (2010) for selecting a subset out of the 57 GCM/emissions scenarios to use in a hydrologic assessment:

- the scatter plot method to bound the uncertainty using four scenarios that reflect the extreme range of changes projected for temperature and precipitation conditions; and
- the percentile method using a maximum of 10 scenarios.

In the percentile method, which was used in this study, the GCM results, as sampled at Ontario climate stations, were ranked in ascending order, first based on their mean annual temperature change field and then based on the mean annual precipitation change field. A percentile was assigned to each climate scenario, and the 5^{th}, 25^{th}, 50^{th}, 75^{th}, and 95^{th} percentiles were selected for temperature and for precipitation change. Because one of the scenarios (MRICGCM2.3.2a – SRB1) was included in both the temperature and precipitation change selection for the Orillia Brain climate station, there are nine (rather than 10) unique GCM/emission scenarios considered in the percentile method (yellow circles in Figure 15.1).

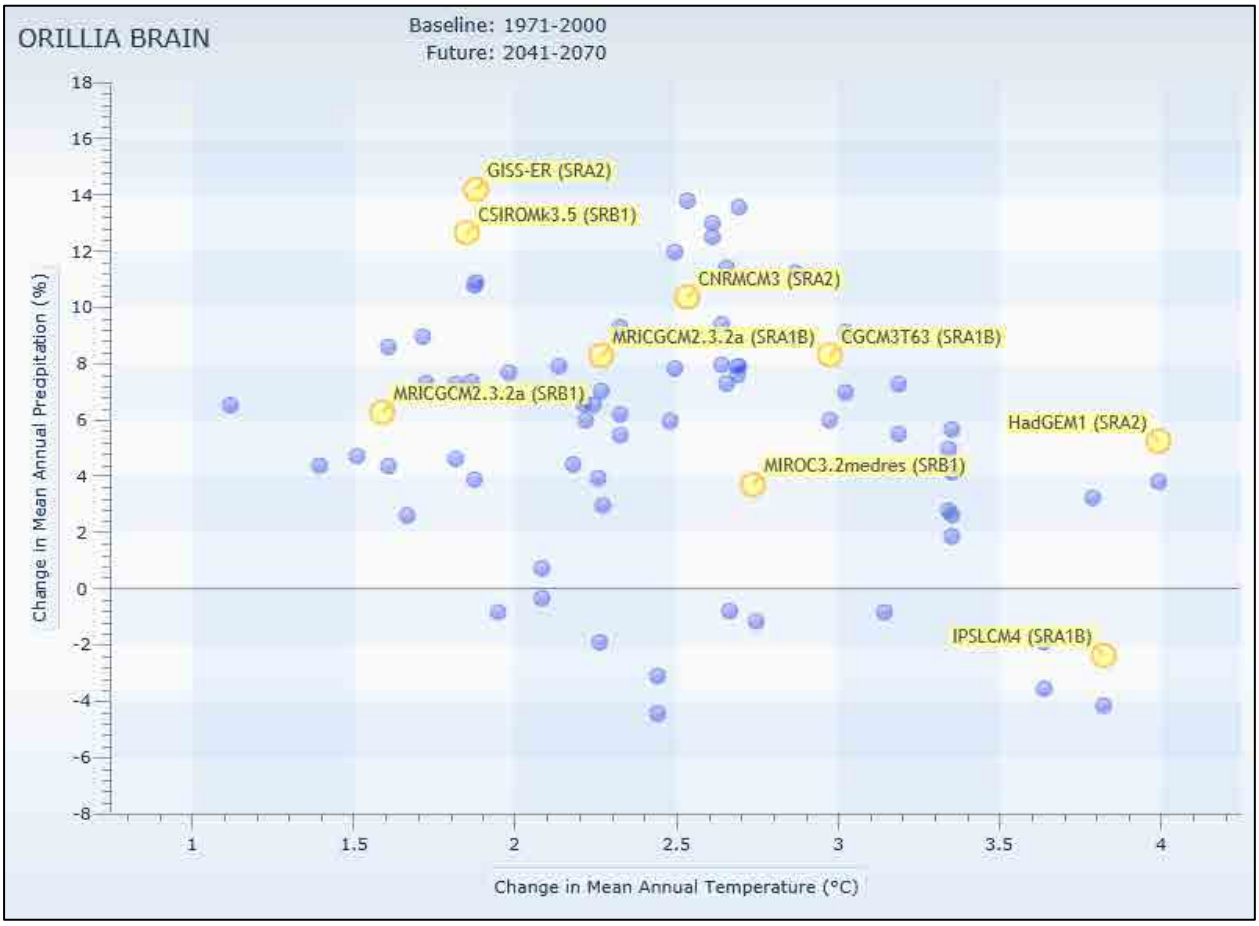

Figure 15.1: Scatterplot of climate scenarios, as sampled at the Orillia Brain climate station, based on their mean annual temperature and mean annual precipitation change fields (yellow circles show scenarios selected for use in the percentile method).

15.6 Climate Data Inputs

To analyze the impacts of future climate change on the Ramara Creeks, Talbot River, and Whites Creek subwatersheds, a series of long-term (29-year) climate change scenarios were simulated with the GSFLOW model. The percentile method was used to select the GCM/Emissions scenarios for this study.

To facilitate climate change studies, MNR has established a website where climate data sets needed for the different scenarios can be downloaded (http://climate.aquamapper.com/). Climate data sets with the applied change fields were obtained for the Orillia Brain AES climate station (AES: 6115811) which is the closest to the study area, as shown in Figure 15.1. Climate data sets could have been prepared by spatially interpolating data from Orillia-Brain, Fenelon Falls, and Woodville over the study area, however, the percentile method results in different subsets of scenarios for each station. As well, the day-to-day variability in the observations would have made the effects of the climate change variation harder to isolate and interpret.

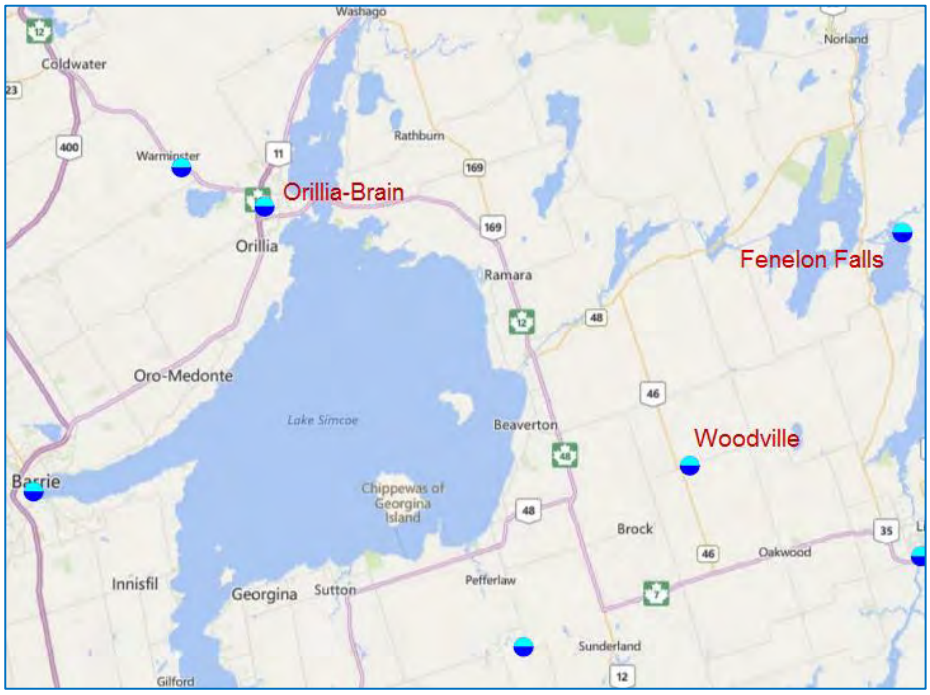

Figure 15.1: Climate stations with GCM/emissions scenario data processed by MNR showing stations close to the study area (red labels).

To use the MNR site, a baseline time period and a future time period were selected. After discussion with the LSRCA, it was decided that a baseline period of 1971-2000 and a future period representing 2041-2070 would be utilized. Next, a subset of GCM/emission scenarios was selected from the scenarios available. The baseline climate data set was adjusted based on the change fields for each of the nine selected GCMs and their respective climate change/emissions scenario listed in Table 15.3. The change fields are calculated as the difference or ratio between annual averages for the baseline (1961-1990) and the 2050s (2041-2070).

Table 15.3: Climate change scenarios selected for the percentile method.

No.	GCM	Scenario	Percentile
1	CGCM3T63	SRA1B	Temp-75
2	CNRMCM3	SRA2	Temp-50
3	CSIROMk3.5	SRB1	Precip-95
4	GISS-ER	SRA2	Temp-25
5	HadGEM1	SRA2	Temp-95
6	IPSLCM4	SRA1B	Precip-5
7	MIROC3.2medres	SRB1	Precip-25
8	MRICGCM2.3.2a	SRA1B	Precip-75
9	MRICGCM2.3.2a	SRB1	Temp-5/Pre-50

Figure 15.2 shows the average annual precipitation for the baseline period. The average for the entire simulation period is equal to 1029 mm/yr. Figure 15.3 shows monthly precipitation for a portion of the baseline period to illustrate natural variability, ranging from 0 mm in July 1989 to 200 mm in August 1986.

Figure 15.4 shows the range in monthly change fields used to scale the precipitation data for the nine climate change scenarios presented as box-whisker plots. The zero line represents the baseline scenario. As can be seen, monthly precipitation increases in the majority of scenarios except for June and July resulting in generally wetter falls, winters, and springs and drier summers. Figure 15.5 shows the statistics for monthly precipitation values after the change field scaling was applied to each climate scenario. Finally, Figure 15.6 shows the variation in annual average precipitation for each of the climate change scenario (grey lines) with respect to the baseline conditions (thick blue line). The individual climate change scenarios are not identified on this figure in keeping with the idea that each scenario is considered to be equally probable.

Figure 15.7 shows the range in monthly change fields used to shift the temperature data for the nine climate change scenarios. All the scenarios show an increase in temperature of at least 1°C in all months. The median temperature shift ranges from 1.8 to 3.2°C, with winter (January and February) and late summer/fall (August and September) having the highest increase. Figure 15.8 and Figure 15.9 show the statistics for monthly minimum and maximum temperature, respectively, after the change field shift was applied to each climate scenario. It should be noted that the minimum and maximum temperatures are shifted by the same amounts.

15.7 Predicted Hydrologic Impacts

The GSFLOW model was run 10 times to simulate baseline conditions and each of the nine climate change scenarios. Daily outputs from the PRMS and MODFLOW sub-models were stored for each model cell on a daily basis for the 29-year simulation. These data were post-processed to create monthly, annual, and study-period averages for all critical model outputs. Ensemble averages were obtained, wherein the results for the nine climate scenarios were aggregated and averaged.

Summaries of flows in all stream reaches and subcatchment-based water balances were also produced. Water budget components include precipitation, canopy interception, potential ET, actual ET, lake evaporation, Dunnian (saturation excess) overland runoff, Hortonian (infiltration excess) overland runoff, interflow, infiltration, and groundwater recharge as well as state variables such as soil moisture and snow pack depth. Streamflow, depth of flow, lake stage and depth, as well as simulated heads, groundwater discharge to streams, lakes, and to the soil zone, as well as state variables for the groundwater system such as change in aquifer storage are also saved on a daily basis. Select model results are presented as hydrographs and maps in this section of the report.

All components of the water budget are affected by changes in precipitation and temperature under the future climate scenarios. The results discussed in this section are presented in terms of monthly and annual average values aggregated over the study area. Spatial variation under baseline conditions is presented as maps showing cell-based averages of model results averaged over the 29-year baseline simulation period. For simplification, the climate change results are presented as cell-based averages for the 29-year simulation period averaged over all climate change scenarios.

Average annual baseline precipitation is 1029 mm/year, as noted earlier. The average of annual average precipitation for all climate runs is 1129 mm/year representing a 9.1% increase over baseline conditions. There is no spatial variability in the precipitation used in the simulation because all input data came from a single station. Figure 15.10 shows the simulated annual average throughfall (precipitation minus interception losses) in mm/year, under baseline conditions and Figure 15.11 shows annual average throughfall averaged over all climate runs. A general increase is noted across the study area due to the increase in average precipitation. The percent increase in throughfall is shown in Figure 15.12. Although the range in the percent change is tightly centred on 9%, there are localized differences due to the spatial variability in the vegetative cover type and

holding capacity, and the rates of evaporation which are dependent on temperature and slope aspect.

Figure 15.13 shows the variation in simulated annual average maximum snow depth for each of the climate change scenarios with respect to the simulated baseline conditions. Annual average maximum snow depth decreases in most years in most of the scenarios primarily due to the increase in winter temperatures. Figure 15.14 shows the range in average monthly snow depth (in mm) over the simulation period. Median snow depths decrease significantly in all scenarios.

Figure 15.15 shows the variation in simulated annual average potential ET for each of the climate change scenarios with respect to the simulated baseline conditions. Figure 15.16 shows the range in average monthly potential ET values over the simulation period. Both the monthly and annual values show an increase in potential ET. This is expected as the Jensen-Haise method selected to estimate potential ET in the PRMS sub-model is strongly dependent on temperature. Figure 15.17 shows the simulated annual average potential ET, in mm/year, under baseline conditions and Figure 15.18 shows average potential ET averaged over all climate runs. PET shows some slight spatial variability over the study area in all scenarios due to changes in slope aspect. Potential ET is sensitive to temperature and therefore increases under climate change. Although the magnitude of the increase varied across the study area, the percent increase (not shown) was nearly uniform at around 8.6%.

Actual ET varies in a complex manner as a function of PET, vegetative cover type and density, and available soil moisture. The soil moisture, in turn, varies as a function of many processes including infiltration, ET losses, gravity drainage, and interflow. Figure 15.19 shows the variation in simulated annual average potential ET for each of the climate change scenarios with respect to the simulated baseline conditions. AET increases in all years in almost all the scenarios. Figure 15.20 shows the range in average monthly potential ET values over the simulation period. Median monthly AET rates increase in all months except in the summer months where the lack of available moisture may limit ET in some scenarios. Figure 15.21 shows the spatial distribution of simulated annual average actual ET, in mm/year, under baseline conditions and Figure 15.22 shows average actual ET averaged over all climate runs. Actual ET rates increase for 4 to 12 % over the study area with the higher increases seen in the alvar area.

Figure 15.24 shows the variation in simulated annual average daily soil moisture content (in mm) for each of the climate change scenarios with respect to the simulated baseline conditions. Soil moisture content increases in all years for most scenarios due to increased precipitation. Smaller average increases in precipitation in conjunction with higher potential ET rates likely reduces average soil moisture in the other scenarios. Figure 15.25 shows the range in daily soil moisture content averaged on a monthly basis over the simulation period. The results here are typical of many of the model outputs and reflect the warmer and wetter winter conditions and hotter and drier summer condition. Median monthly moisture content increases in the late fall and winter months but decreases in the other months. Figure 15.26 shows the spatial variation in percent change in average annual daily soil moisture content (after ET losses). The decrease in soil moisture in the alvar is a result of the higher actual ET rates in an area that has low soil moisture storage capacity. Increases in soil moisture are evident in the till-covered areas despite the increase in ET due to the increase in infiltration (caused by higher precipitation).

Finally, groundwater recharge is affected by all the runoff and soil water balance processes. Figure 15.27 shows the variation in simulated annual average groundwater recharge (in mm/yr) for each of the climate change scenarios with respect to the simulated baseline conditions. Groundwater recharge does not appear to vary significantly when averaged over the study area. Figure 15.28 shows the range in monthly average groundwater recharge over the simulation period. The results show the typically high recharge during the spring freshet and fall with little or no recharge during the

summer months. Median monthly groundwater recharge under climate change increases significantly in the late fall and winter months and decreases during March and April but is little changed in the other months. Figure 15.29 shows the spatial distribution in percent change in annual average net groundwater recharge, in mm/year, as seen by the MODFLOW submodel. Percent increases ranging from 20 to 50% (40 to 60 mm/yr) occur over the alvar. Little to no increase occurs over the till covered areas. The increases are balanced by larger localized decreases in net groundwater recharge which occur in the stream valleys which function as groundwater discharge areas.

15.8 Predicted Hydrogeologic Impacts

To illustrate the behaviour of the groundwater system under future climate change scenarios, the transient results were compared at six inspection points across the study subwatersheds. The locations of the inspection points are presented in Figure C.1 and statistics pertaining to the simulated groundwater levels at these inspection points are provided in Appendix C. Inspection points were selected to highlight local groundwater responses in significant hydrogeologic features, including upland recharge areas, lowland discharge areas, the Shadow Lake aquifer in the vicinity of the Western Trent and Palmina wellfield, and the Carden Plain alvar.

Across the study area, groundwater heads under the climate change scenarios experienced an earlier and more prolonged response to the spring freshet, combined with less dramatic decreases in water level over the winter months of January to March, compared to the baseline climate scenario. This can be attributed to the wetter winters predicted by the GCMs, with a larger portion of the winter precipitation expected to fall as rain rather than snow. In addition, warmer temperatures during the winter is expected to cause a reduction in the average snowpack and ice coverage, which would otherwise serve to impede the movement of precipitation and runoff into the subsurface. The result of these climate change factors is an overall increase in groundwater recharge, maintaining higher groundwater heads throughout the winter months compared to the baseline scenario. In addition, the increased proportion of rain (compared to snow) during the winter months shifted the spring freshet to earlier in the season, in return, producing a broader crest in the spring groundwater levels that generally occurs a month earlier than in the baseline simulation.

Appendix C.3 presents the climate change response of the deep Shadow Lake aquifer near the Western Trent-Palmina wellfield, where the aquifer is well confined by the overlying bedrock aquitards. The impacts of climate change are generally muted and despite some deviation between climate change scenarios, mean monthly groundwater values generally all fall within the interquartile range of the baseline scenario. Annual daily maximum and minimum values are also fairly consistent, falling within +/- 0.1 m of the baseline values at the Bolsover Wellfield groundwater inspection point (Appendix C.3). Nevertheless, the impact of increased recharge during the winter is visible in the monthly average groundwater levels for the months of January through May.

Apart from the trend of increased groundwater levels during the winter and early spring, differences between the baseline and climate change scenarios are generally small for the remaining months of the year. This is evidenced by average simulated monthly groundwater levels from the climate change scenarios that fall within the interquartile range of the baseline scenario for nearly all of the groundwater inspection points presented in Appendix C.

Figure 15.30 and Figure 15.31 present climate change statistics for the average monthly groundwater discharge to streams and lakes within the study area, respectively. The seasonal pattern of groundwater discharge to surface water features echoes the previously discussed winter time response to climate change: since groundwater levels are anticipated to be higher during the winter months, it follows the discharge into surface water features will also increase during these

months due to the larger hydraulic gradient. The predicted impacts on the hydraulics of the study sub-watersheds are discussed in further detail in the following section.

For all of the climate change scenarios, municipal and private permitted groundwater takings (presented in Section 6) were simulated. Based on a review of all 10 scenarios, none of the groundwater wells with permitted takings went dry at any time during the 29 year climate change simulations.

Uncertainty among the different climate change scenarios regarding groundwater response can be assessed by the box and whisker plots for the average monthly water levels presented in Appendix C. Higher certainty is associated with a smaller interquartile range (box) for the monthly averages among the climate change scenarios. In general, agreement between climate change models is highest during the late spring and early summer months, ranging from May to August, with more deviation observable from September through to April. Nevertheless, climate change scenarios consistently indicate the aforementioned increase in groundwater levels during the winter and early spring.

15.9 Predicted Streamflow Impacts

Simulated streamflow was interrogated at several locations within the model domain. A number of streamflow parameters were analyzed to characterize the impact of predicted climate change on the simulate baseline reference regime. Annual average, maximum, and 7-day minimum streamflow are presented for the climate change scenarios and compared with the baseline condition. A statistical analysis of monthly average streamflow along with flow duration curves for each simulation is also presented. Typical daily and monthly hydrographs are included for comparison of event timing, magnitude, and recession characteristics. For clarity, the figures associated with this analysis have been grouped by observation location in Appendix D; a summary of the predicted changes in streamflow under future conditions is provided below.

Significant changes in runoff timing are predicted during the winter and spring months. Warmer winter conditions with higher average precipitation are predicted in the climate change scenarios and this in turn leads to higher winter streamflows. Most scenarios predict an increase in median streamflow for December through March in all study area streams (e.g., as shown on Figure D.10 for Whites Creek). Precipitation that would be stored in the snowpack consequently runs off as streamflow during mid-winter melt and rain-on-snow runoff events. The hydrographs which present daily stream flow between water year 1986 and 1988 (e.g., Figure D.4 for Whites Creek) show a marked increase in mid-winter runoff events.

While the freshet peak timing is similar between the baseline and the climate change scenarios, the magnitude of the peaks vary. At some of the observation locations, there was no consistent trend in peak streamflow (i.e., in the Upper Talbot River as shown on Figure D.36). Rohillion Creek, however, shows an increase in maximum annual streamflow (Figure D.50), this is likely due to this catchments flashy, karstic nature.

Low flow conditions were investigated by calculating the annual 7-day low flow at each observation site for the various scenarios. There were decreasing trends observed at all locations except for the Lower Talbot River (Figure D.27) where the assumed diversion from the Trent watershed supports the system under low flow conditions. With the shift in timing of the freshet, more water is moved off the study catchments earlier; this resulted in a shift in the timing of spring recharge. This shift in recharge from April to March produces a corresponding shift in the onset of low water periods. With a longer summer low flow period occurring earlier, the duration and severity of low flow increases. Increasing temperatures combined with a shift in spring recharge timing will increase the stress

placed on study area streams during the summer months. Upper Talbot River (Figure D.37) and Rohallion Creek (Figure D.51) appear to be the most severely affected, again, due to the alvar which provides little storage to support streamflow during the even warmer summer months.

Accumulated groundwater discharge to streams represents the cumulative net flux of water between the groundwater system and all the contributing reaches to the observation points. While strictly representing the exchange of water through the bed of the stream, this parameter is analogous to hyporheic exchange. The average accumulated groundwater discharge for the Upper Talbot River (Figure D.42) and Rohallion Creek (Figure D.56) show that during the warmer summer months of July through September, the predicted groundwater discharge is decreased under the climate change scenarios, while the same figure for Whites Creek (Figure D.14) indicates little to no decrease in accumulated groundwater discharge for the climate change scenarios. This pattern supports the identified trend in low flow conditions caused by differences in groundwater/stream bank storage between the till and post-glacial sediments of the Whites Creek catchment and the alvar dominated Rohallion Creek and the Upper Talbot River catchments.

The net effect of these changes in timing, magnitude, and extreme flows results in a predicted shift in the hydrologic regime of the study area streams. This change is summarized in the flow duration curves at each observation location. The typical response, presented on Figure D.6 for Whites Creek, is an increase in higher flows with a corresponding decrease in lower flows centered on the 50^{th} percentile. These catchments are relatively rural, freshet dominated catchments. With a warmer, wetter winter predicted under future conditions, freshet flows are increased. Correspondingly, by shifting the timing of spring recharge, the severity and duration of the low flow period is increased.

These trends are more succinctly summarized on the box and whisker plots of average monthly streamflow. For Whites Creek (Figure D.11) there is a predicted increase in the median monthly streamflow for December through March with decreases predicted in all other months. This pattern of change is predicted in streams across the watershed, with median winter stream flow increasing by as much as 50%. While the decrease in average summer flows does not approach this scale, the severity of drought and extreme low flow periods is predicted to increase. These predicted changes to the hydrologic regime will undoubtedly have impacts on stream ecology and geomorphology. Further study into the specific impacts of these predicted changes should be incorporated into future watershed assessments.

15.10 Figures

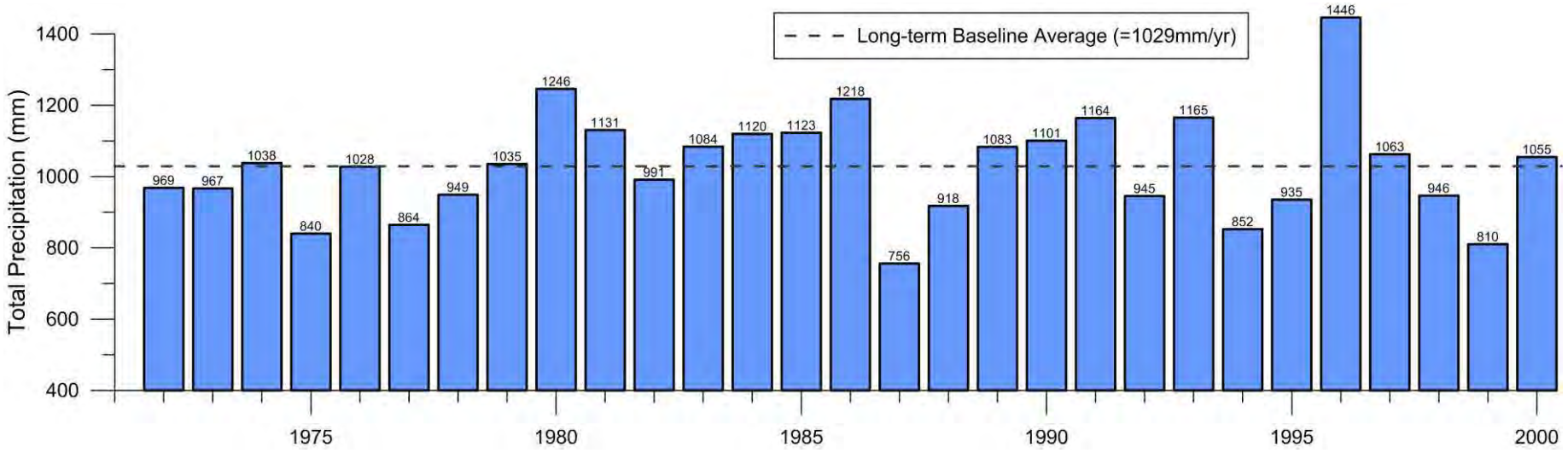

Figure 15.2: Annual average precipitation by water year under baseline conditions.

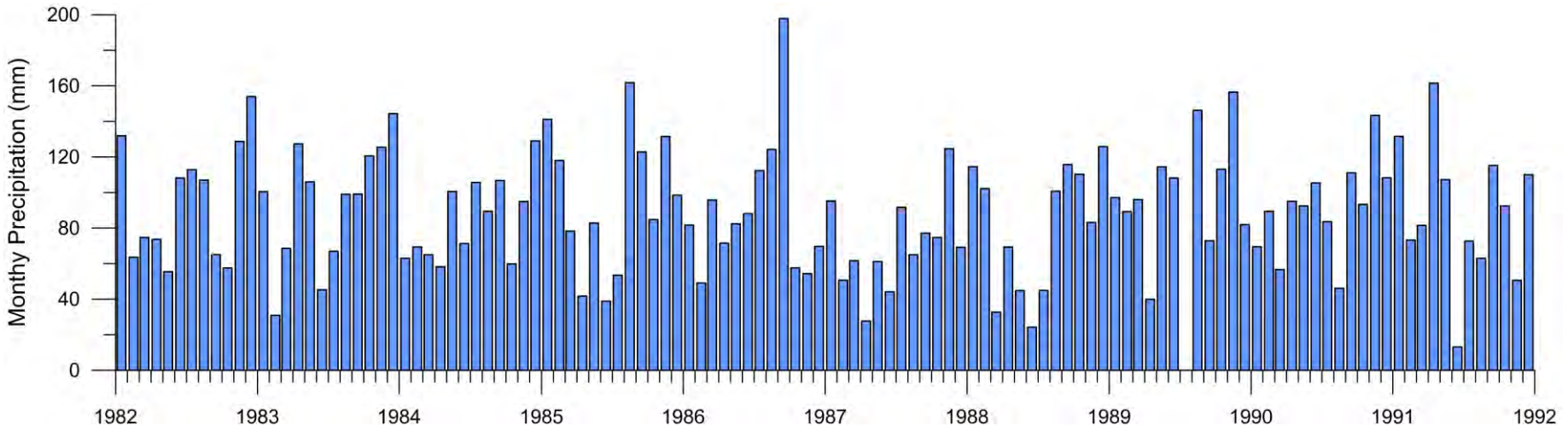

Figure 15.3: Monthly baseline precipitation, January 1982 through December 1992.

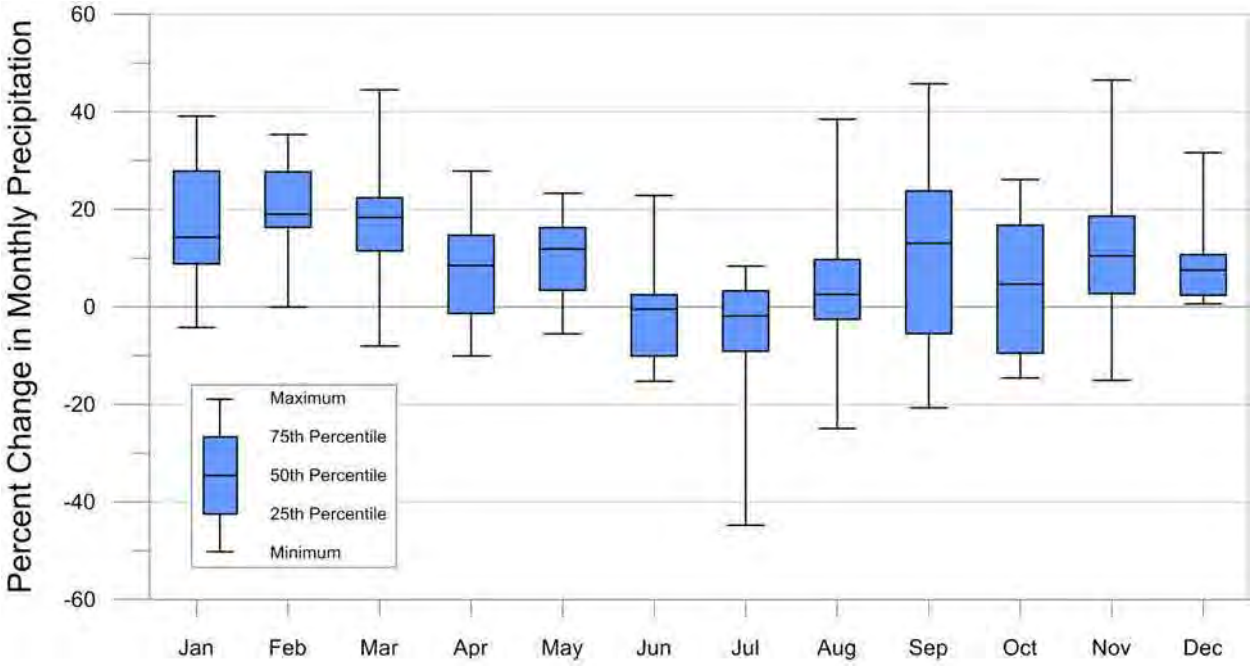

Figure 15.4: Monthly precipitation change field statistics for the climate scenarios selected for this studies.

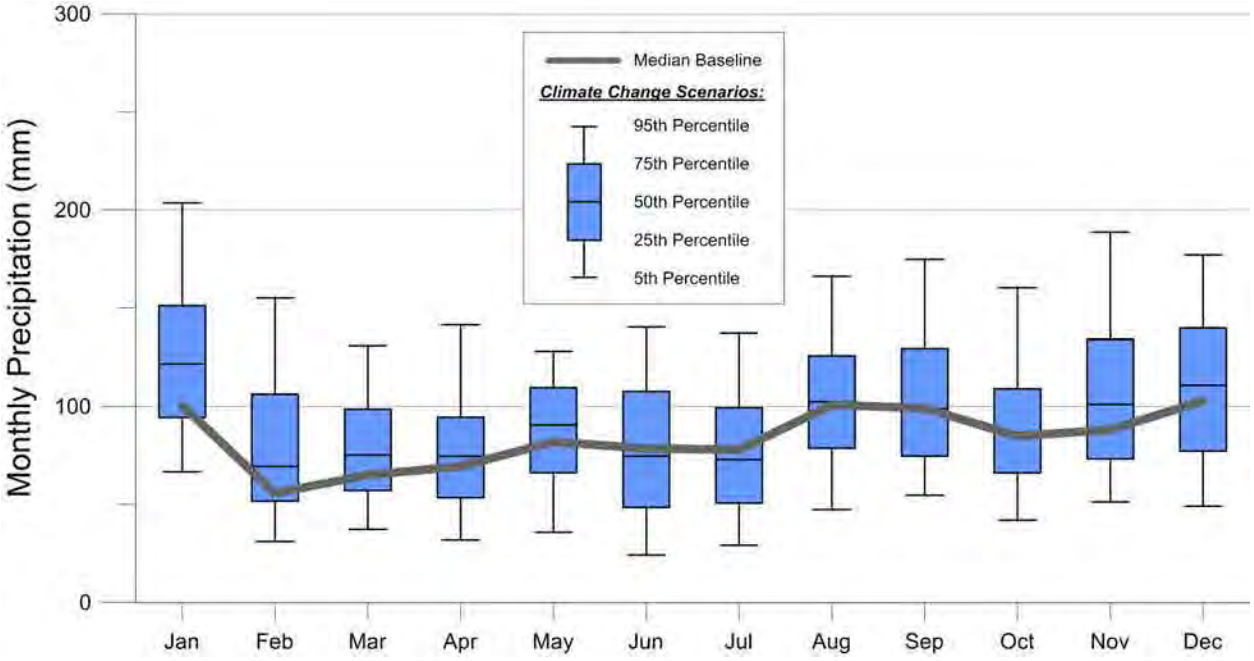

Figure 15.5: Monthly precipitation statistics for the simulation period (water year 1972 through 2000).

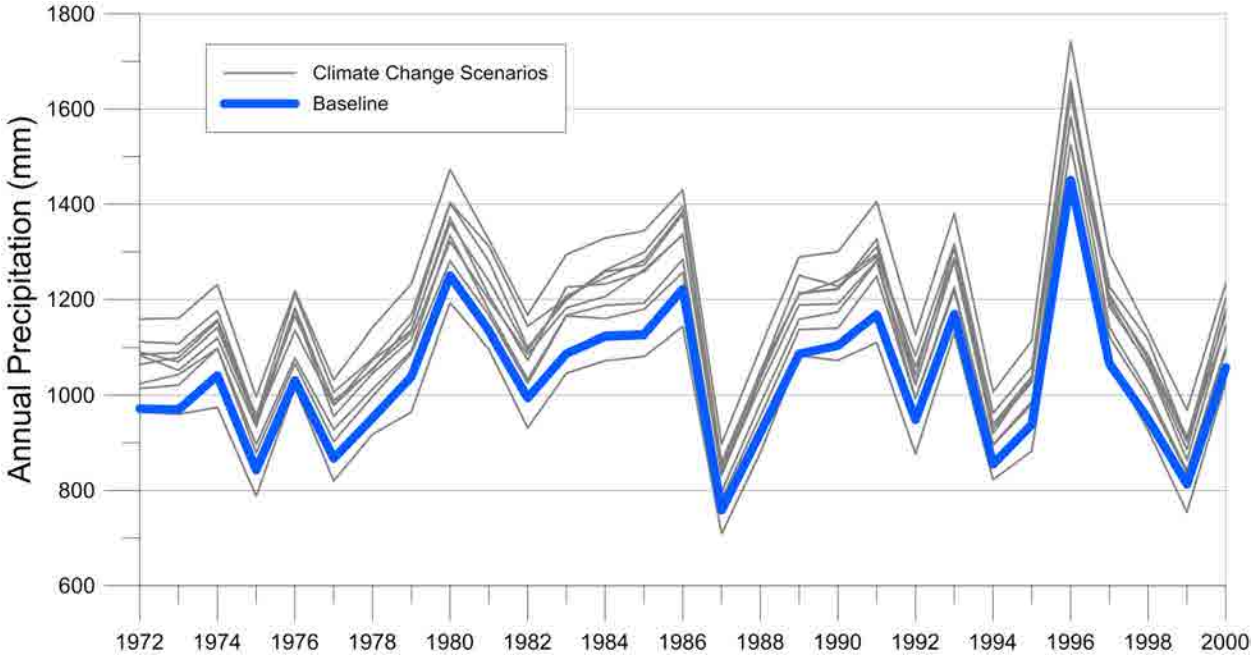

Figure 15.6: Annual precipitation applied over the study area, by water year, for the climate change scenarios.

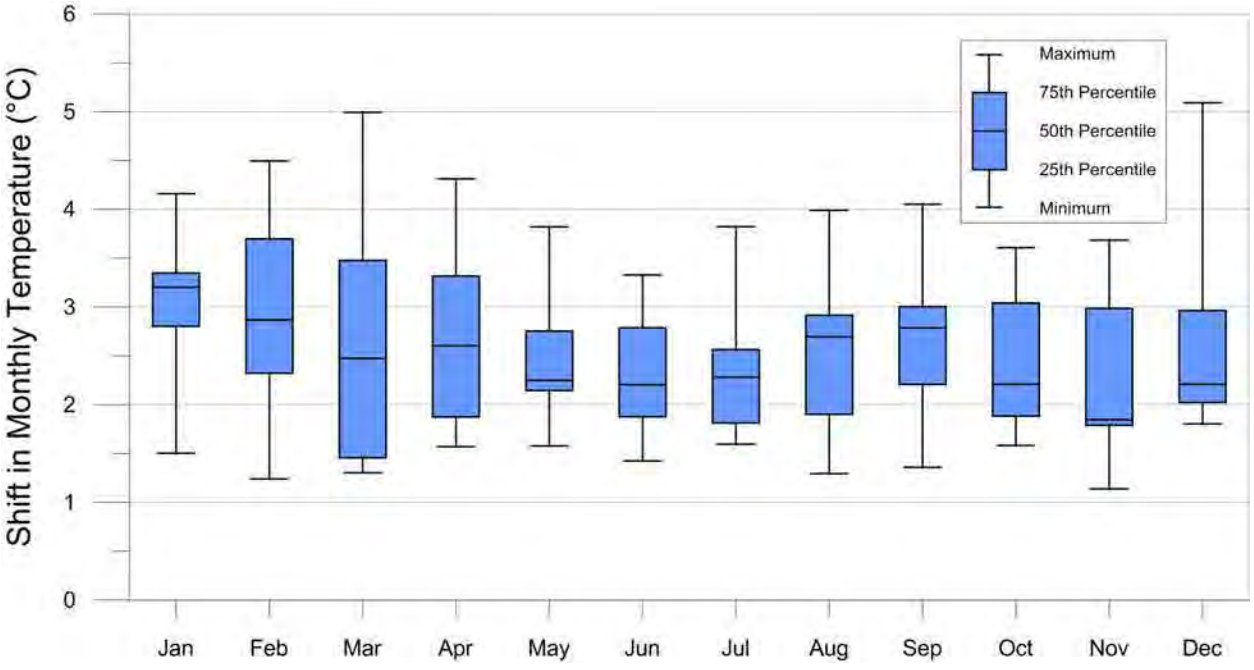

Figure 15.7: Monthly temperature change field statistics.

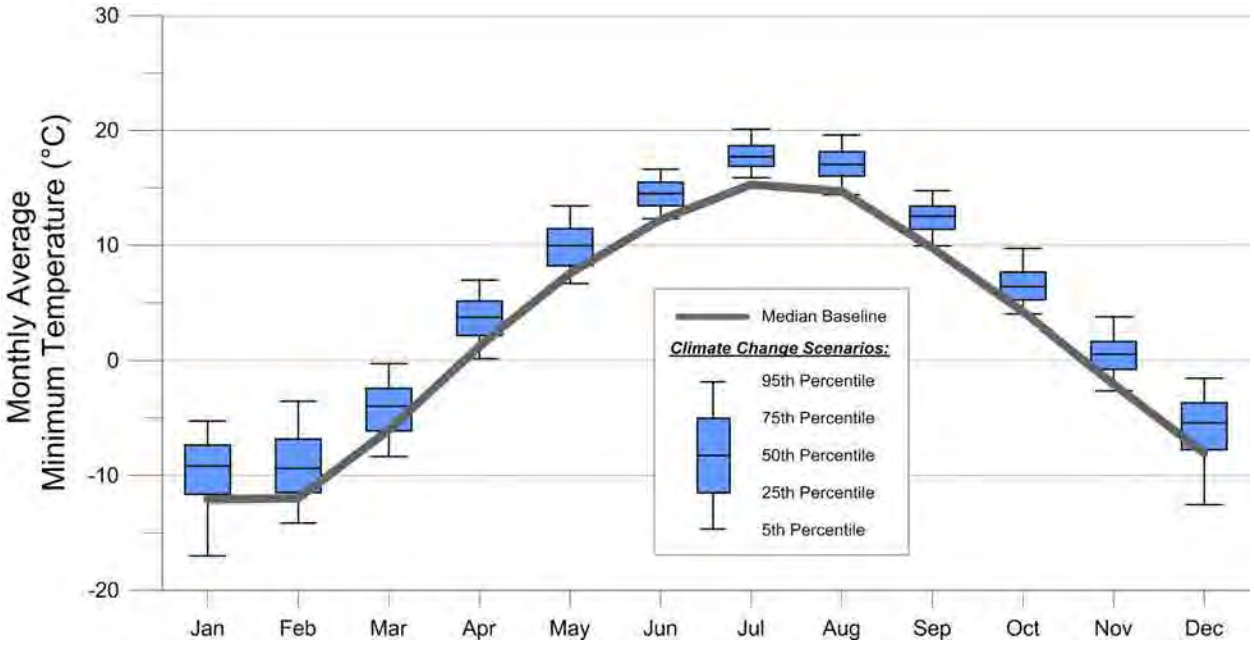

Figure 15.8: Monthly minimum temperature statistics for the simulation period (water year 1972 through 2000).

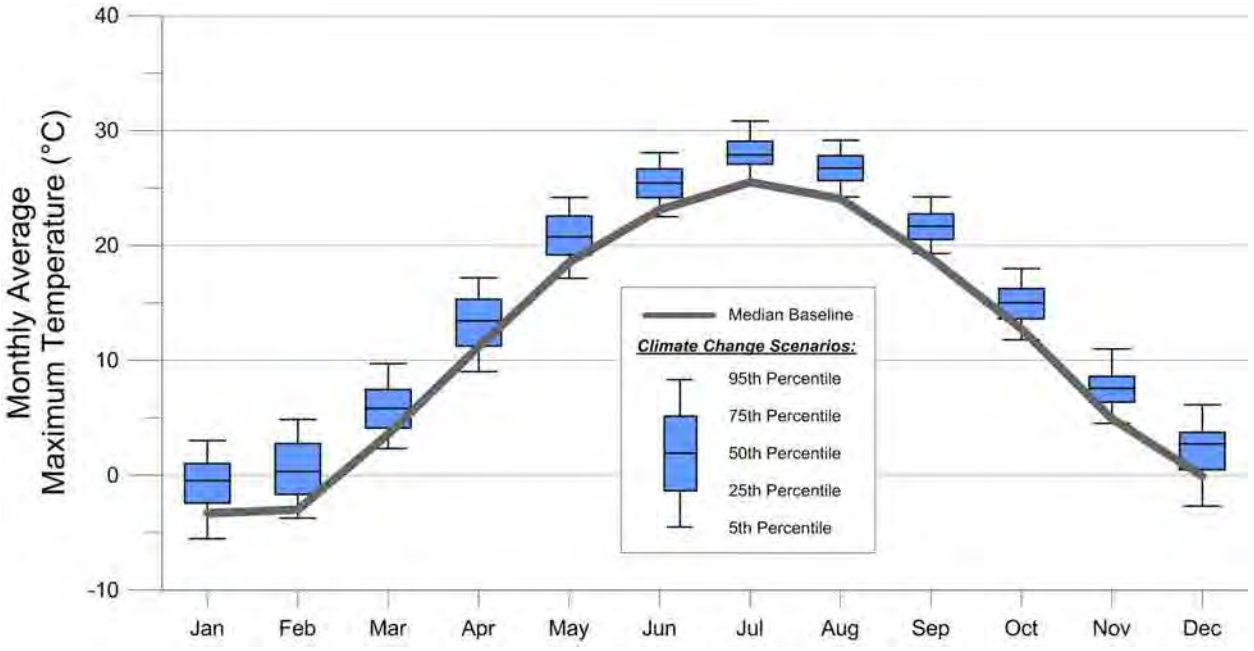

Figure 15.9: Monthly maximum temperature statistics for the simulation period (water year 1972 through 2000).

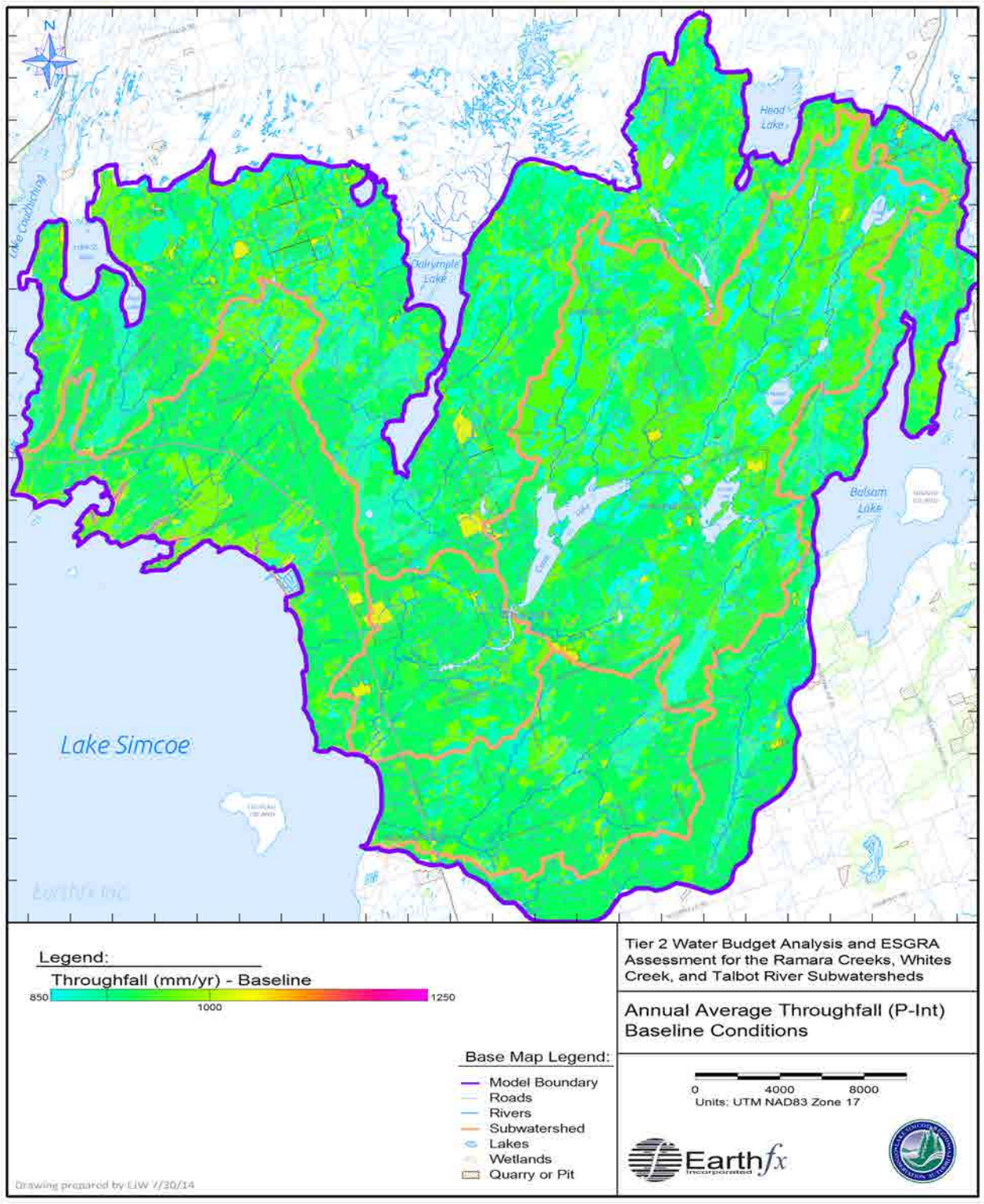

Figure 15.10: Annual average throughfall (precipitation minus interception) over the 29-year simulation period for baseline conditions.

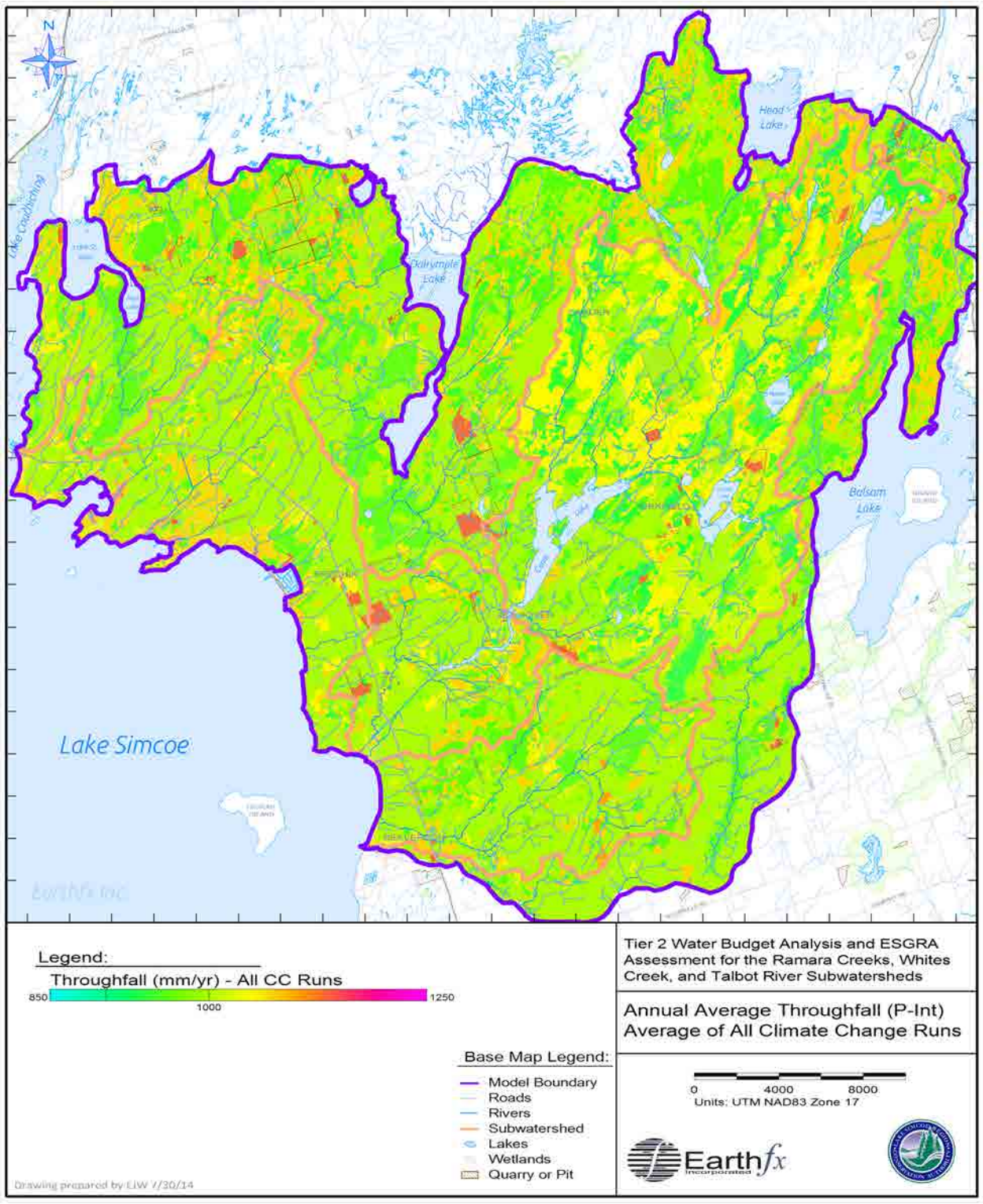

Figure 15.11: Annual average throughfall (precipitation minus interception) over the 29-year simulation period averaged over all the climate change scenarios.

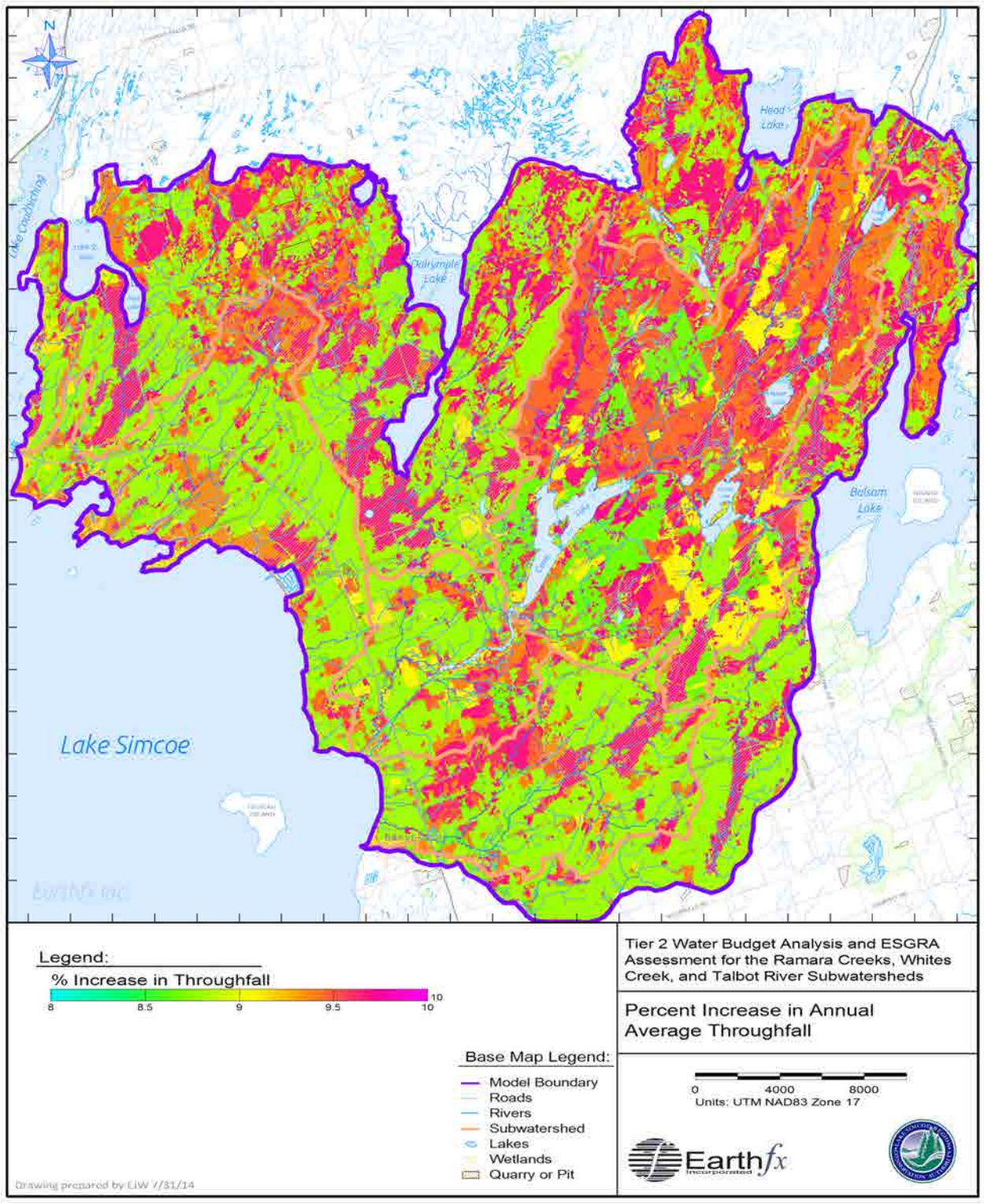

Figure 15.12: Percent increase in annual average throughfall.

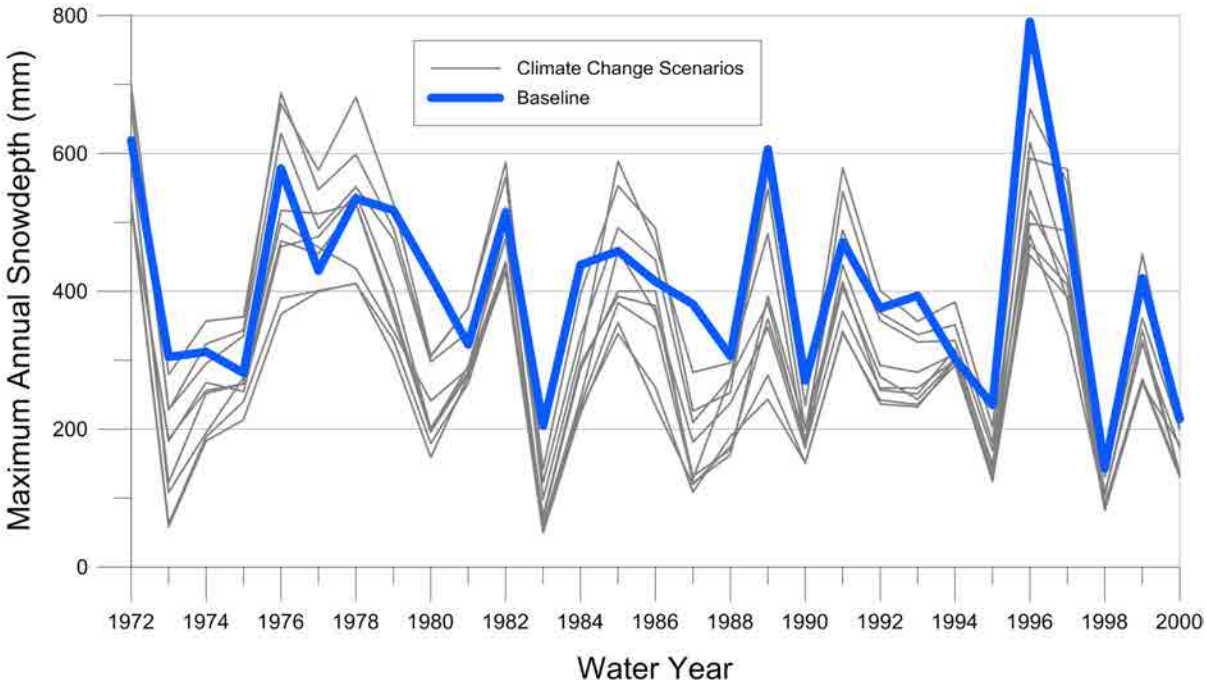

Figure 15.13: Average annual maximum snow depth over the study area by water year.

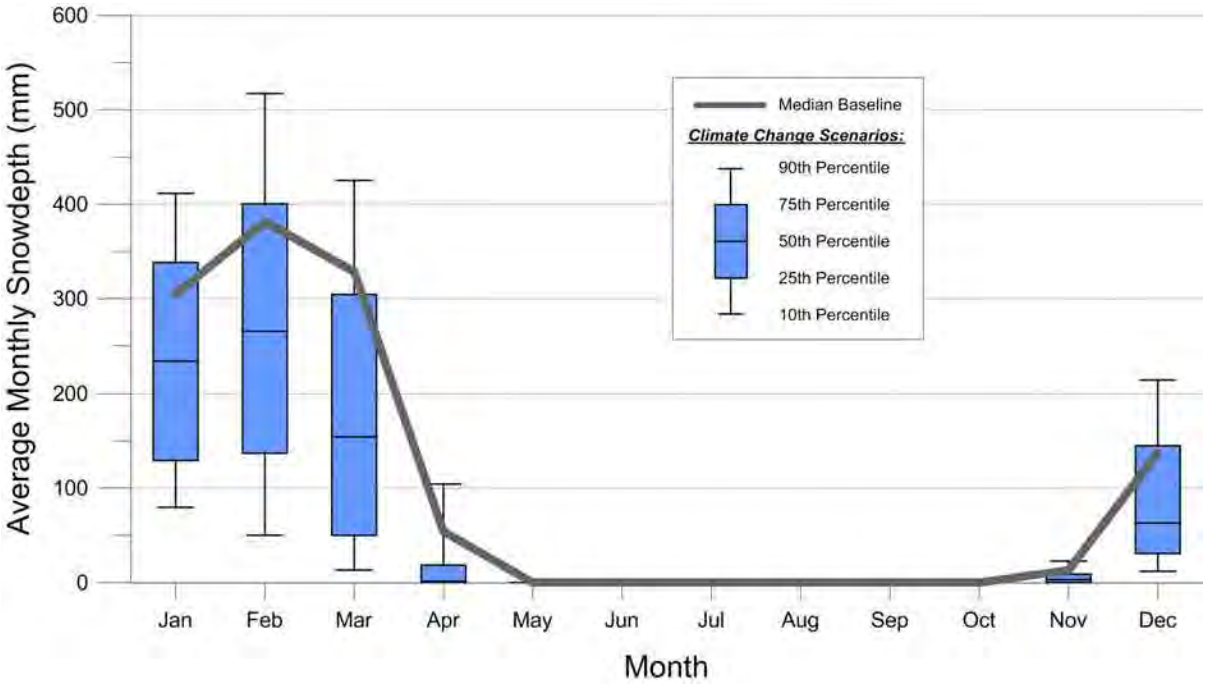

Figure 15.14: Monthly average snow depth statistics over the study area.

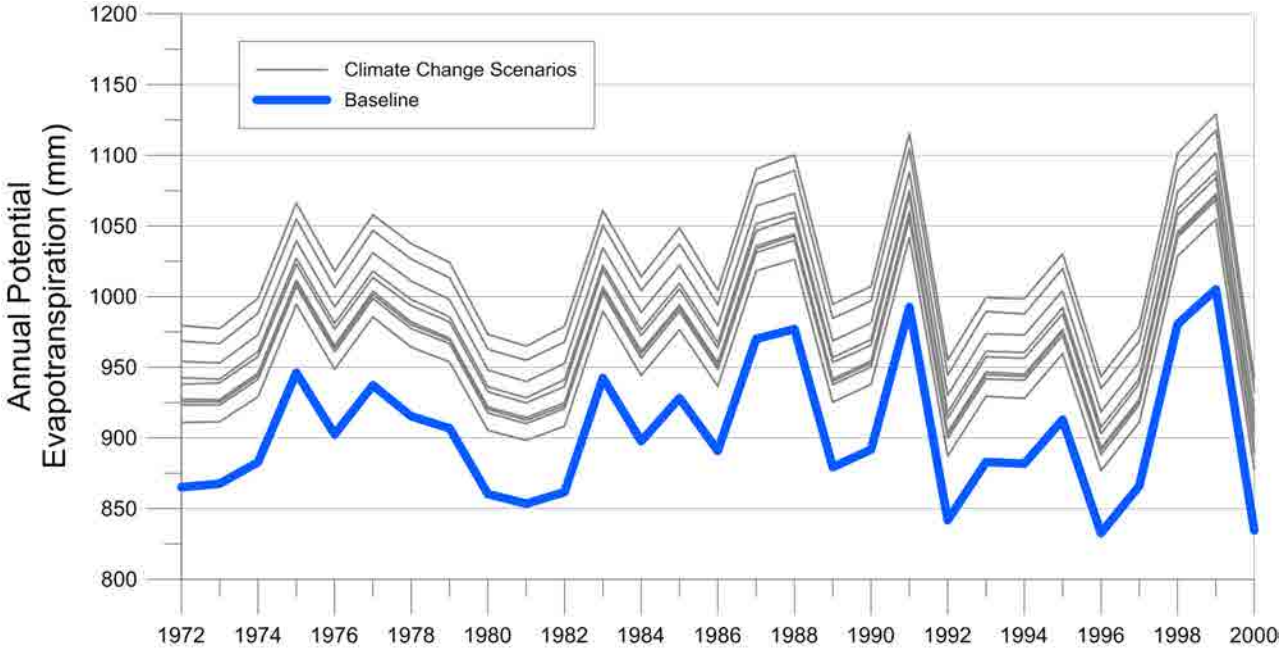

Figure 15.15: Annual average potential ET in the study area by water year.

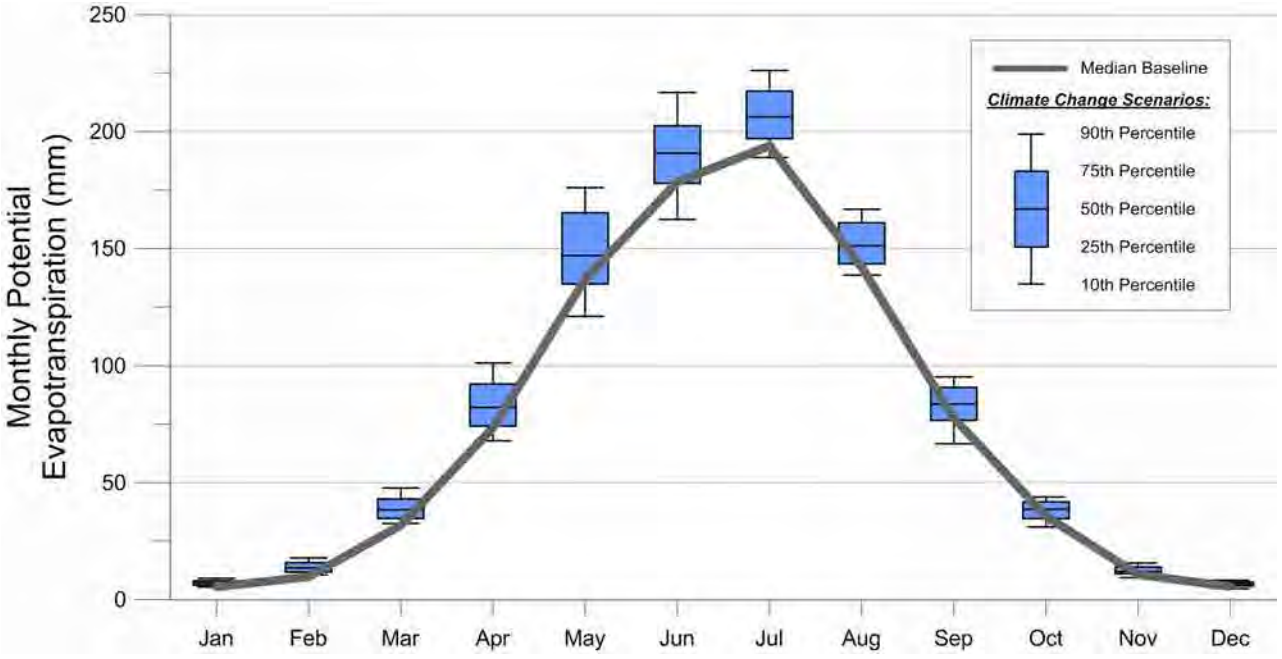

Figure 15.16: Monthly potential ET statistics for the study area.

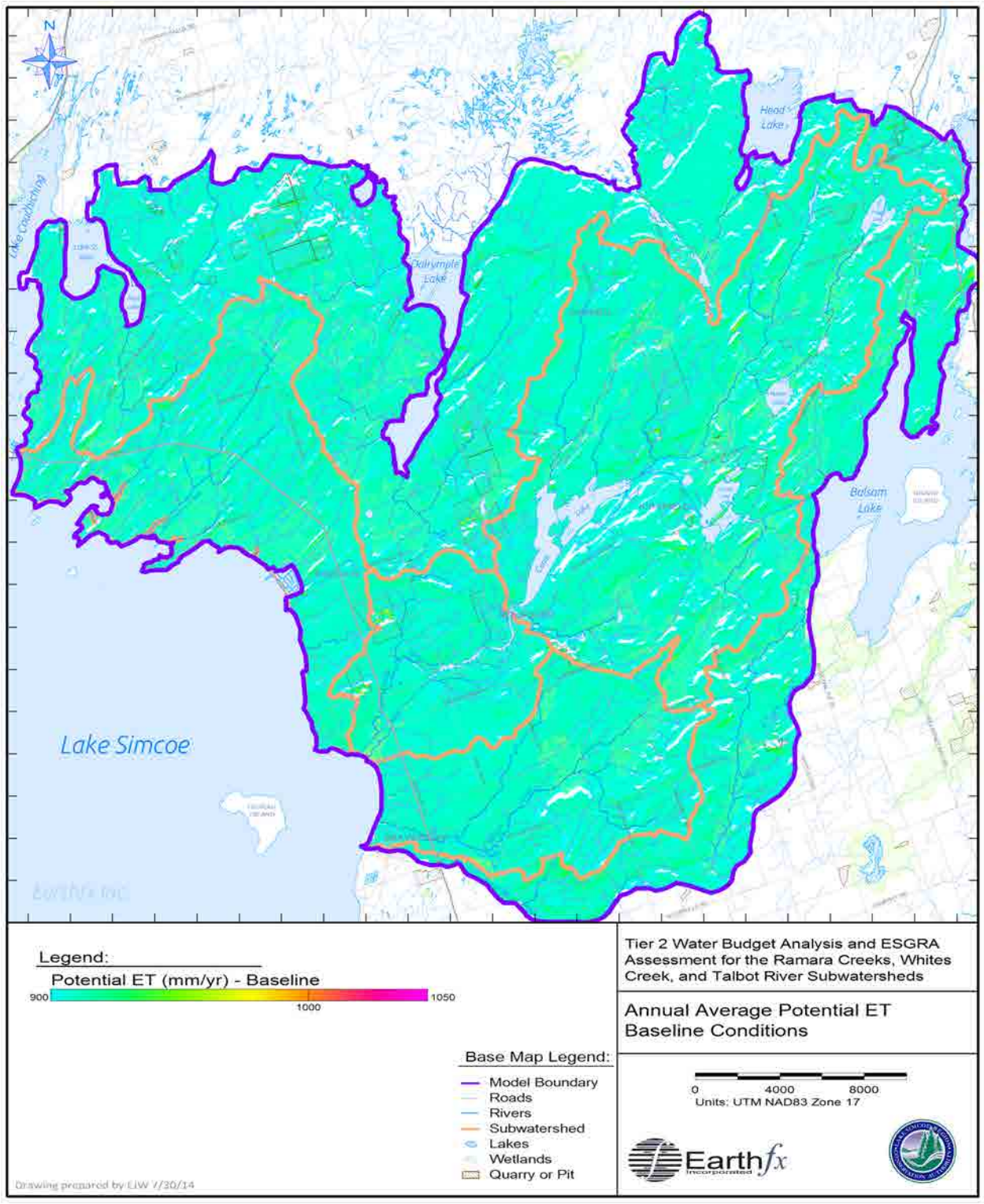

Figure 15.17: Annual average potential ET over the simulation period for baseline conditions.

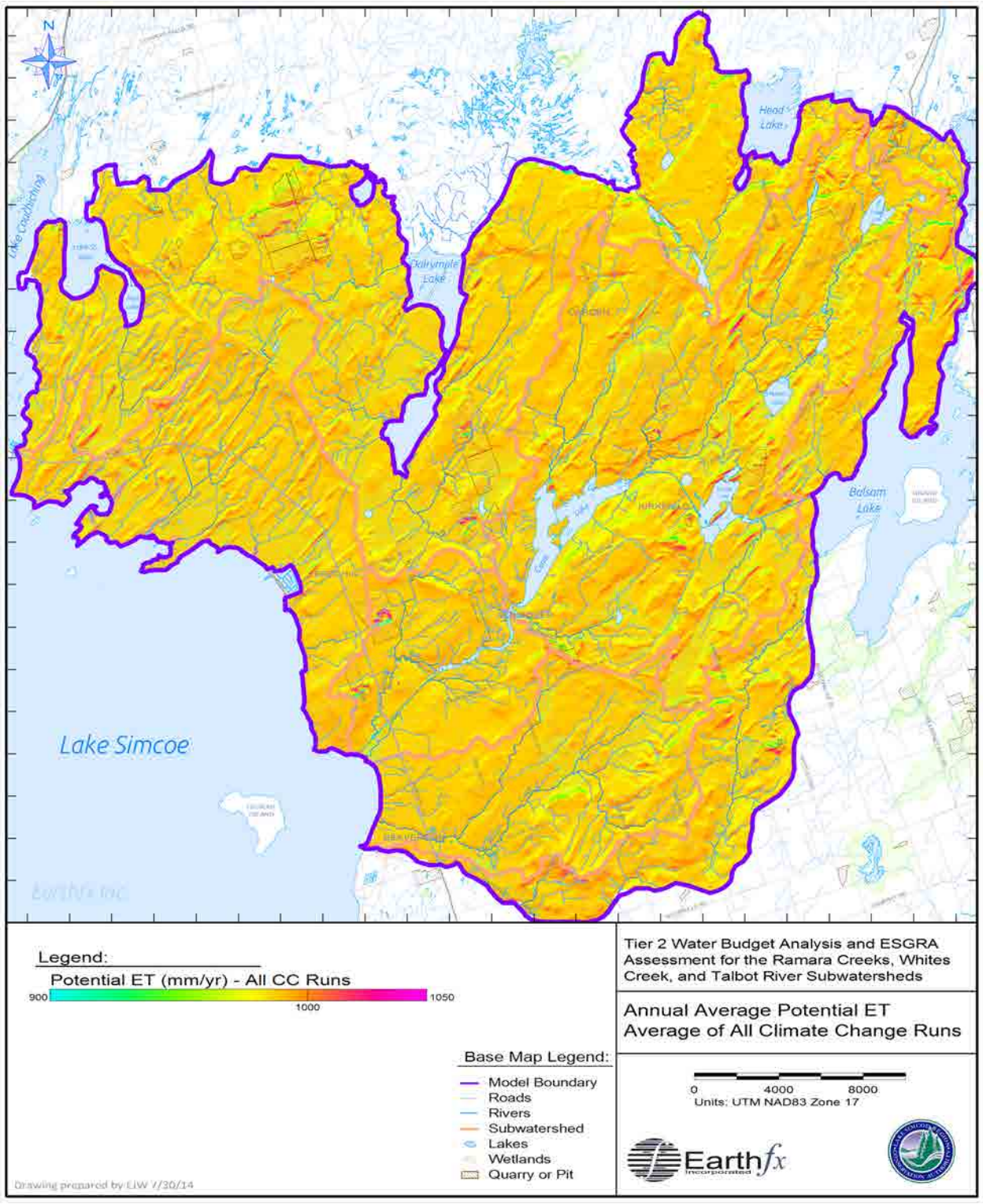

Figure 15.18: Annual average potential ET over the simulation period averaged over all the climate change scenarios.

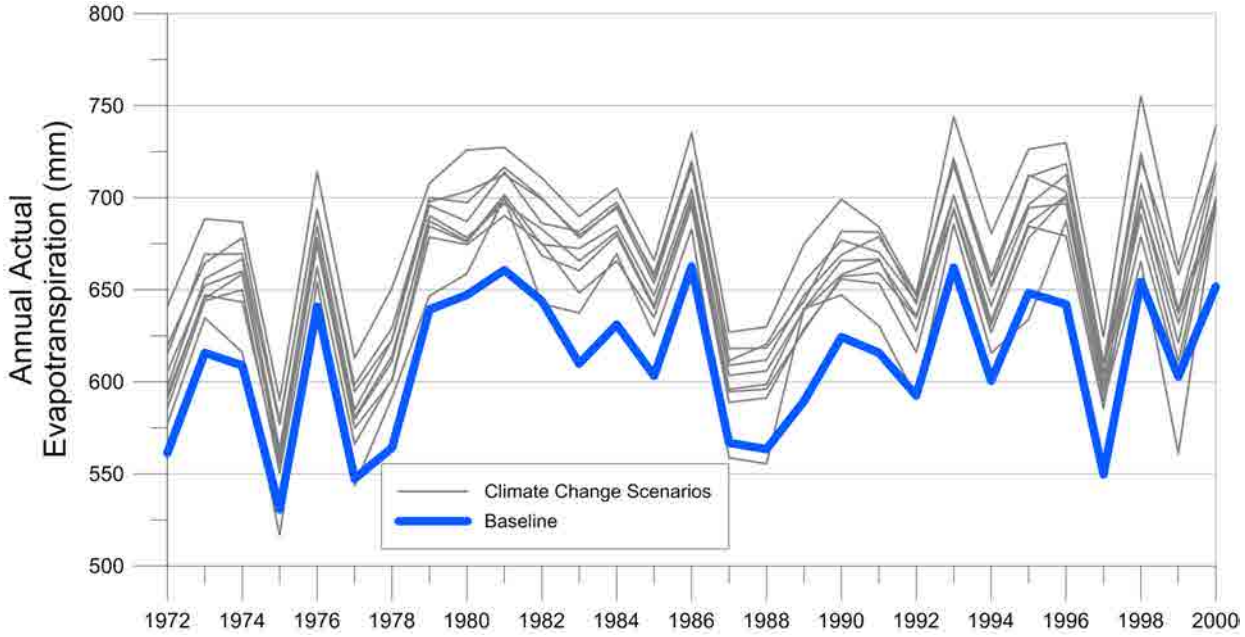

Figure 15.19: Annual average actual ET in the study area by water year.

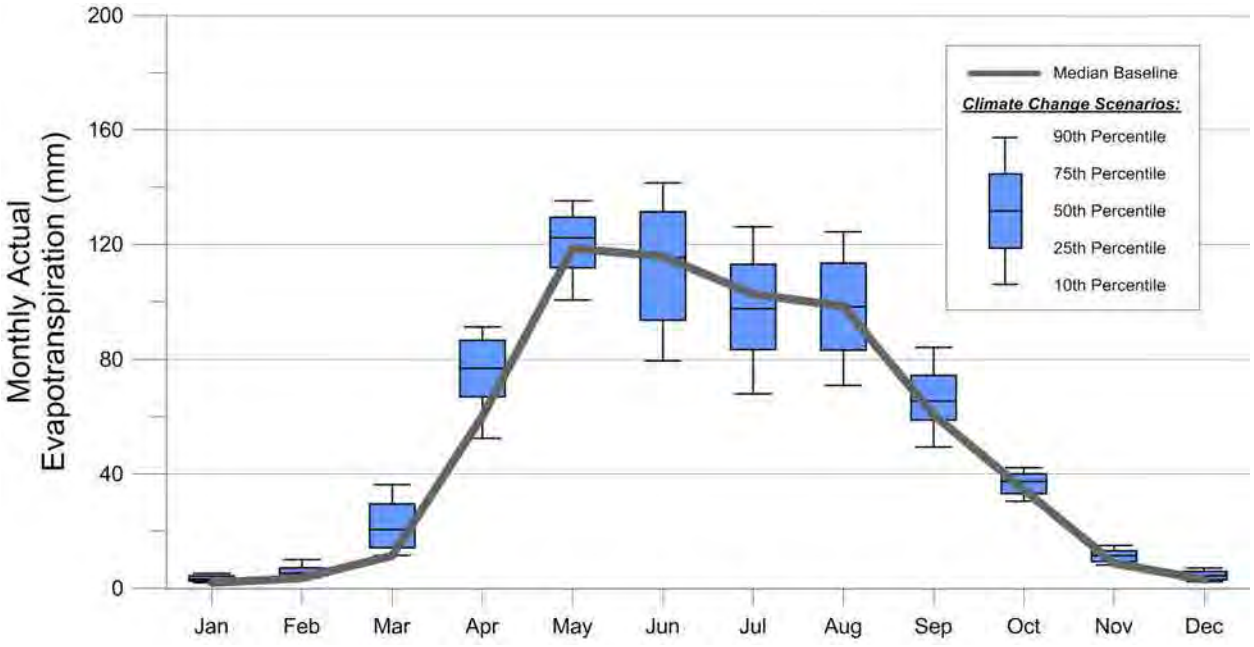

Figure 15.20: Monthly average actual ET statistics for the study area.

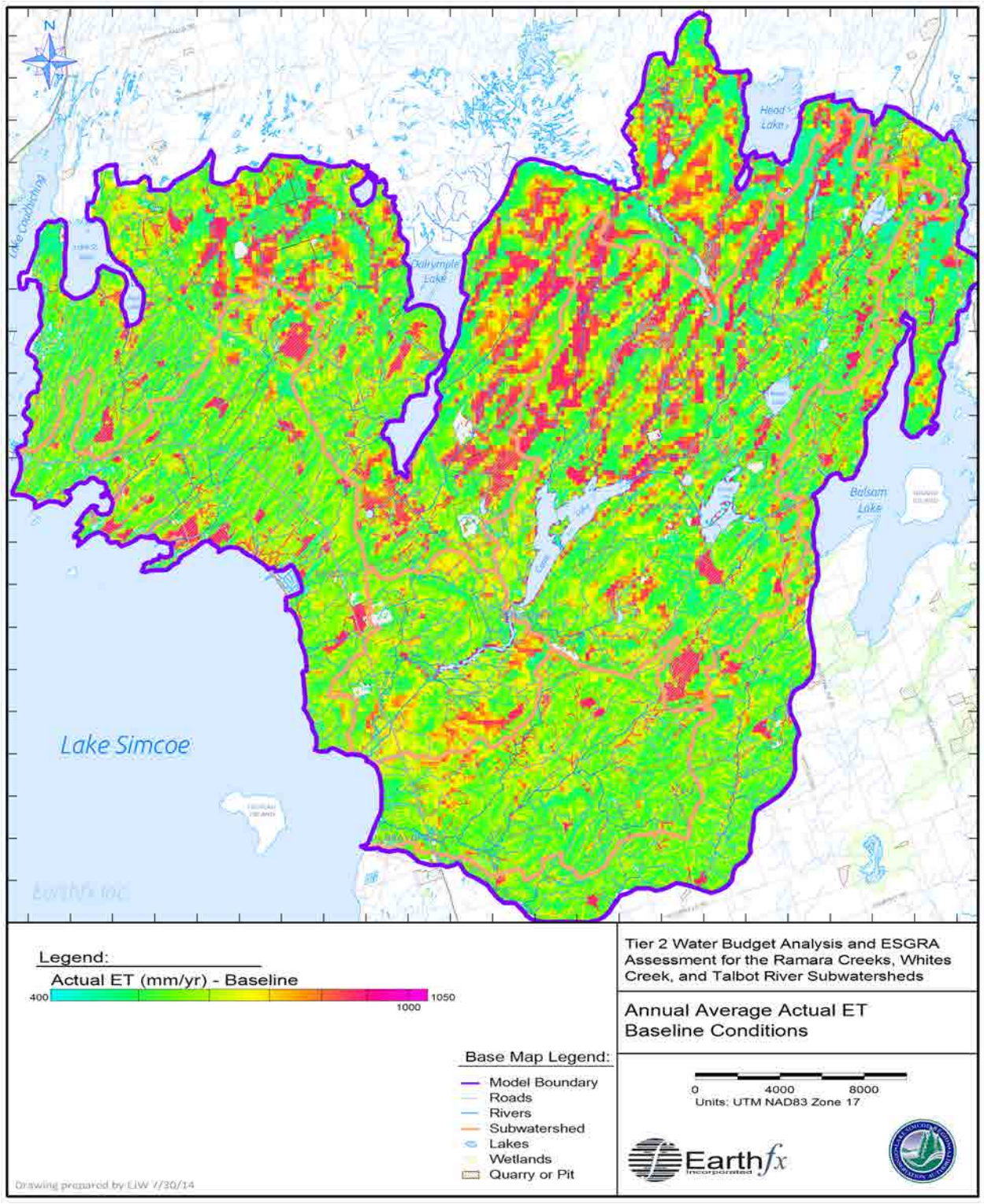

Figure 15.21: Annual average actual ET over the simulation period for baseline conditions.

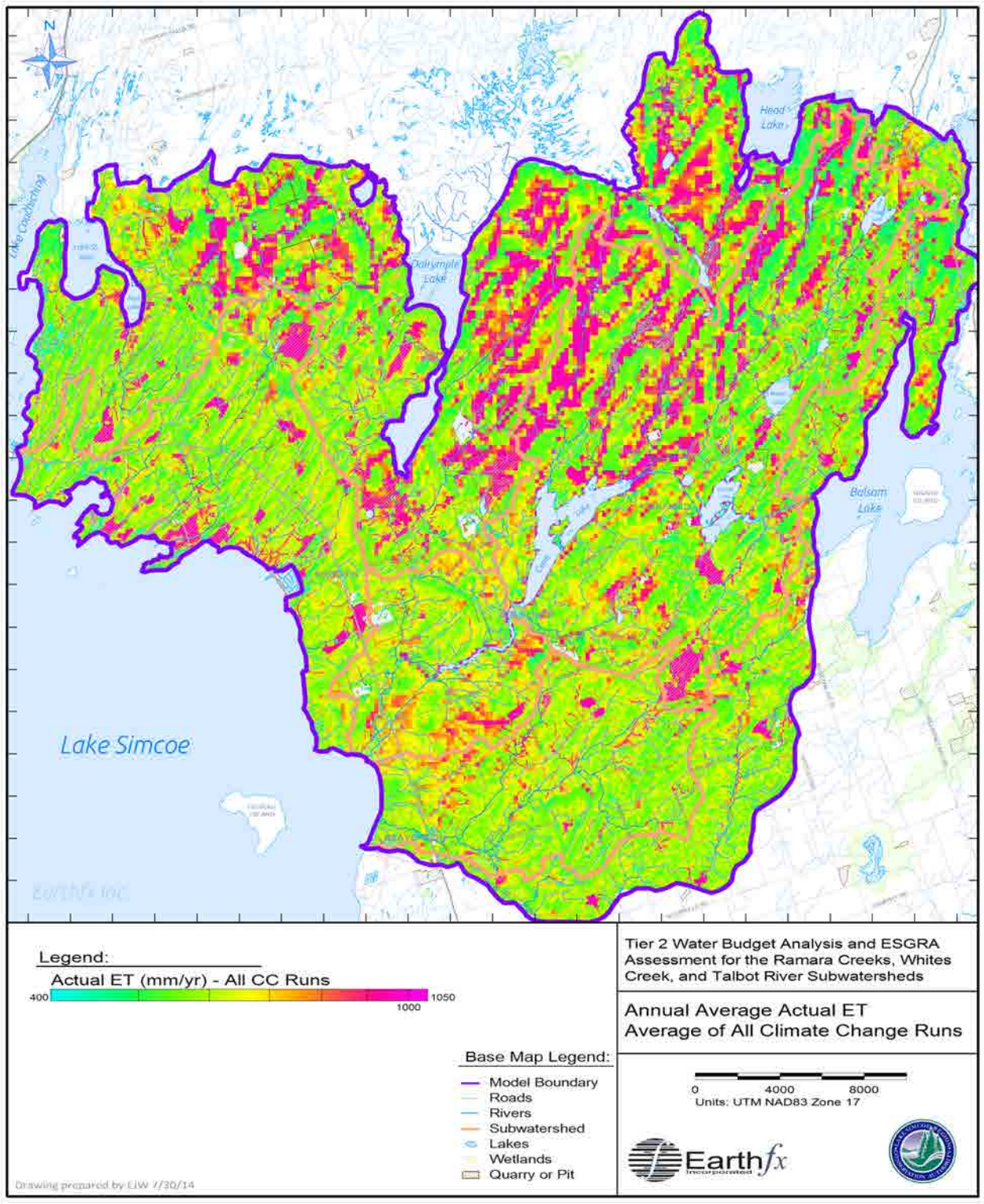

Figure 15.22: Annual average actual ET over the simulation period averaged over all the climate change scenarios

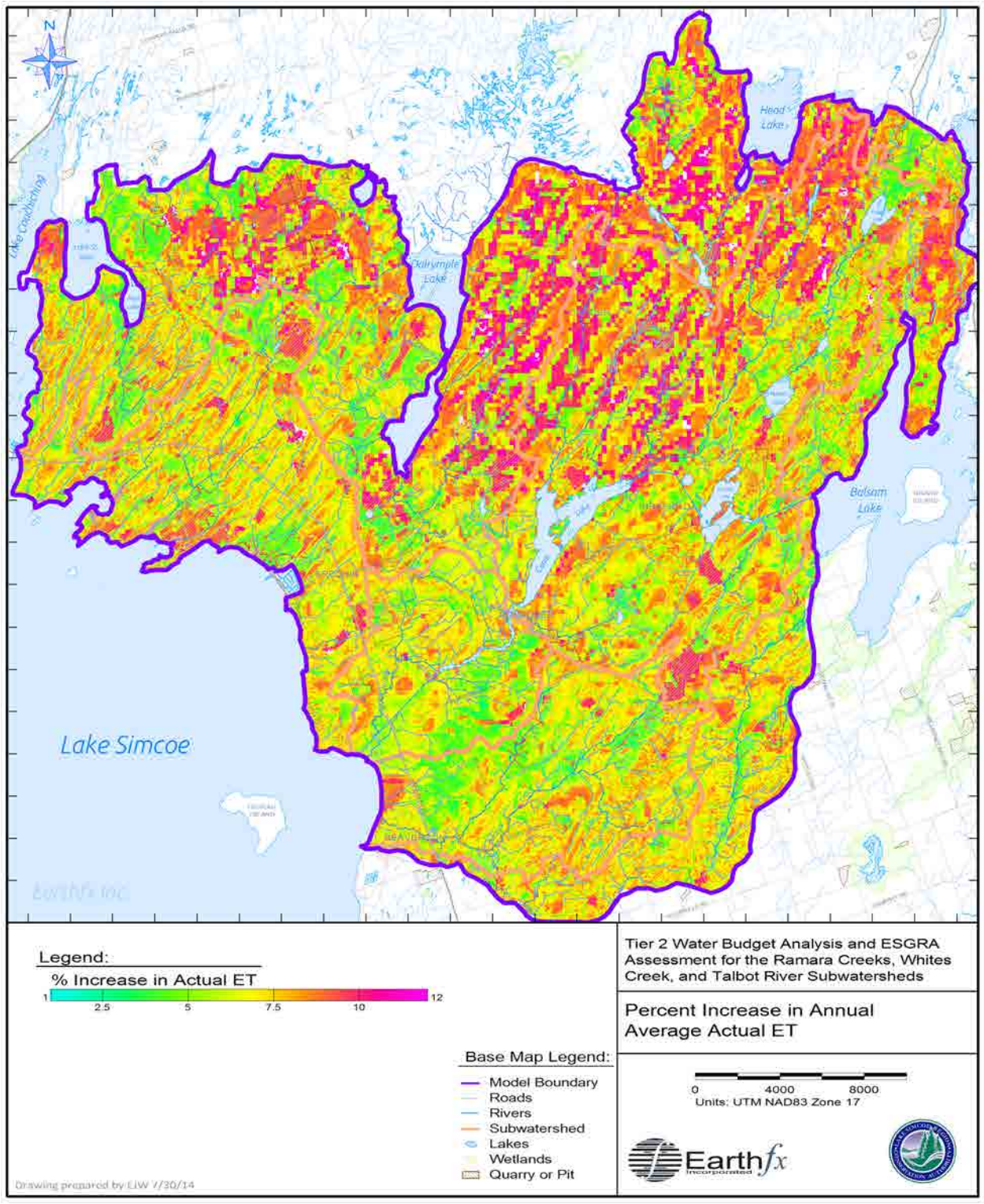

Figure 15.23: Percent increase in annual average actual ET.

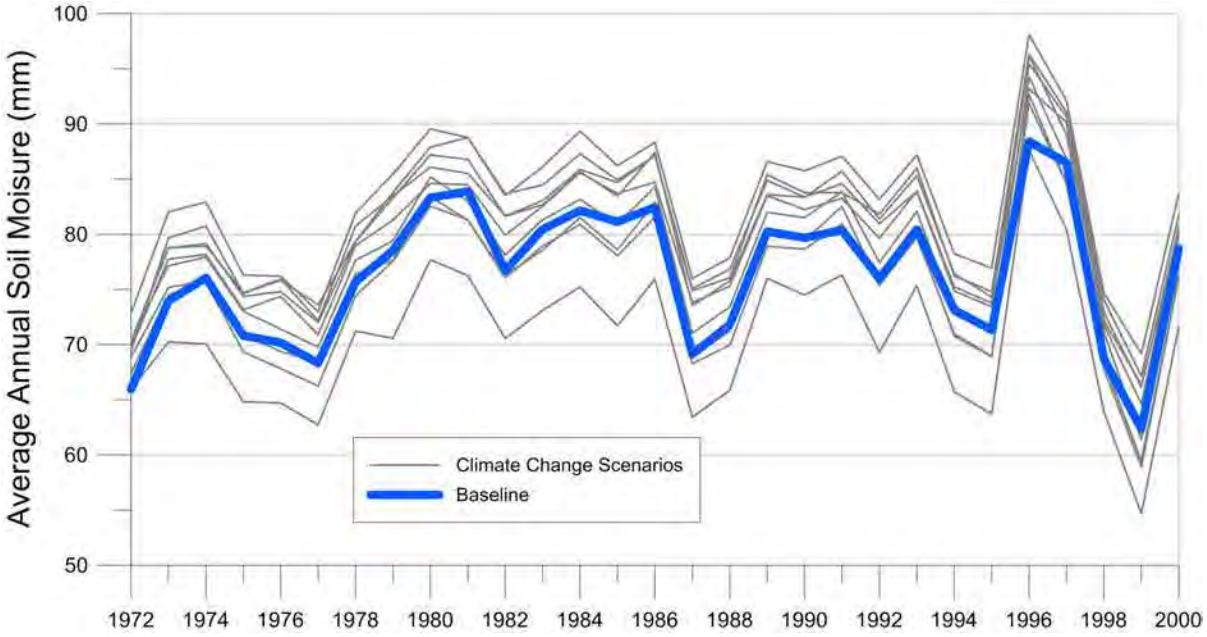

Figure 15.24: Annual average daily soil moisture content over the study area by water year.

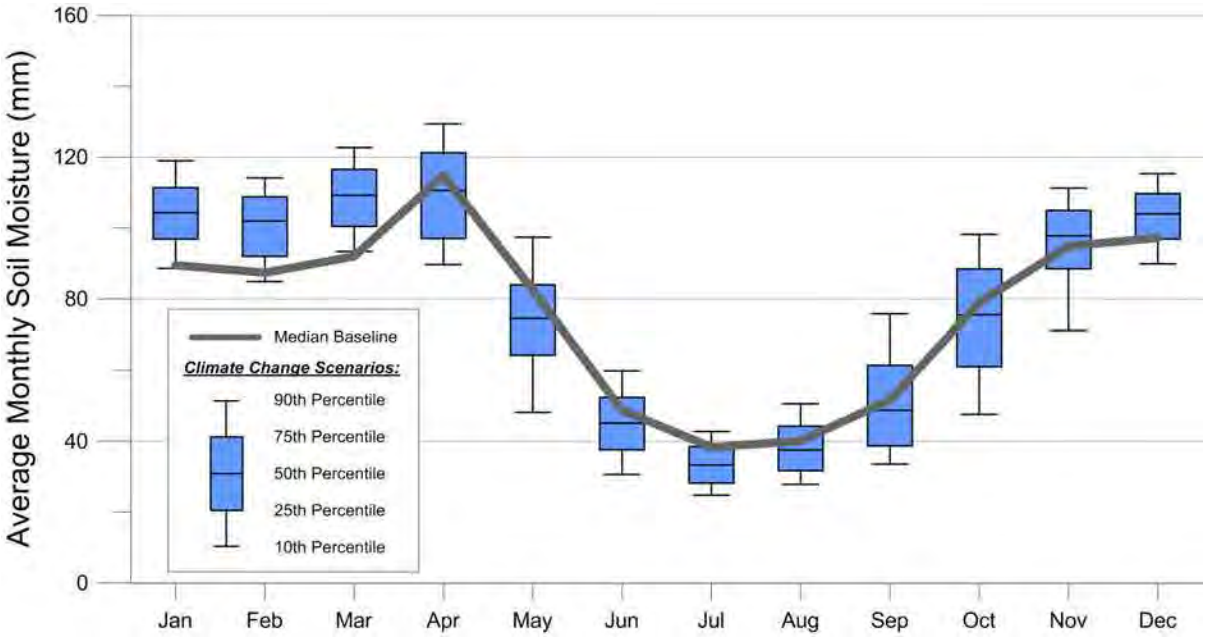

Figure 15.25: Monthly average daily soil moisture content statistics for the study area.

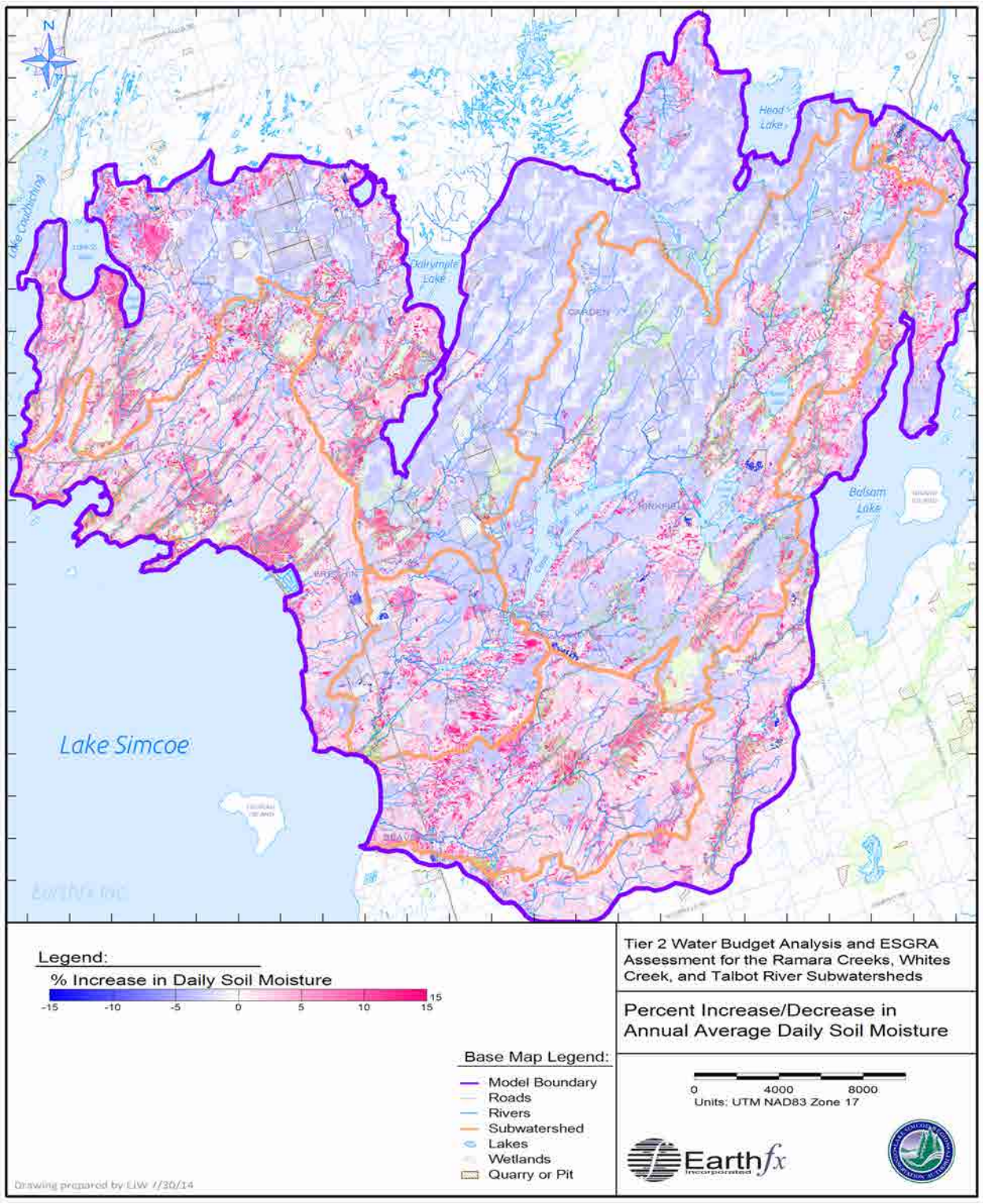

Figure 15.26: Percent change in annual average daily soil moisture content.

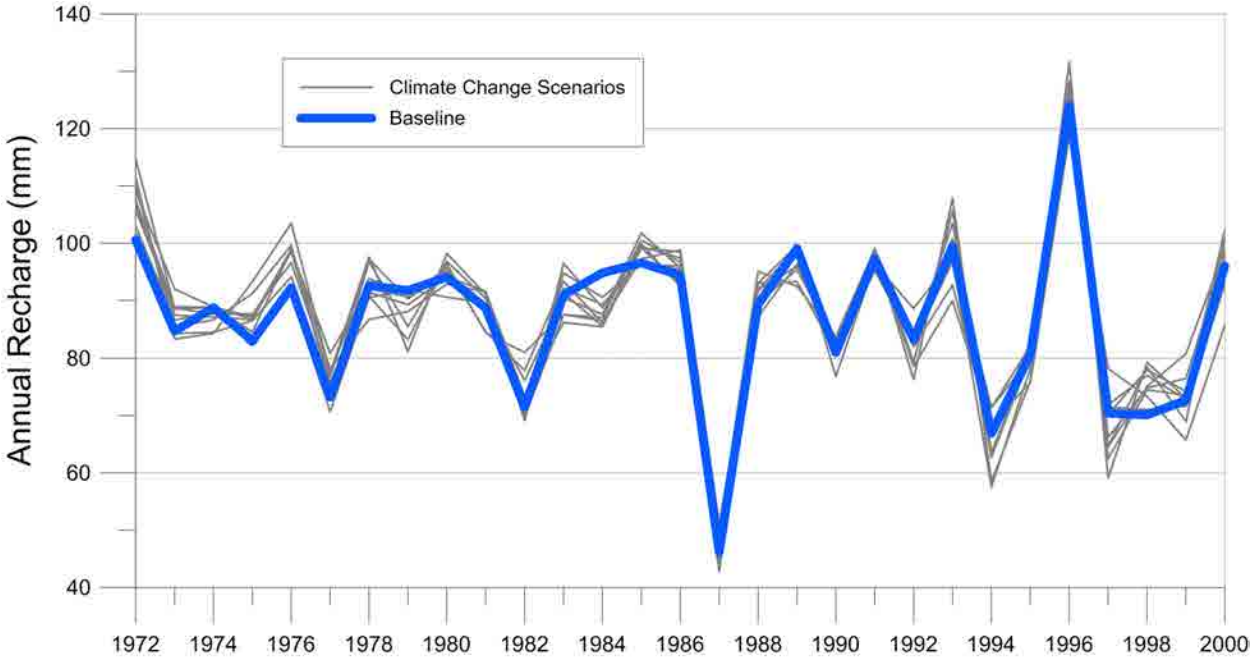

Figure 15.27: Annual average groundwater recharge in the study area by water year.

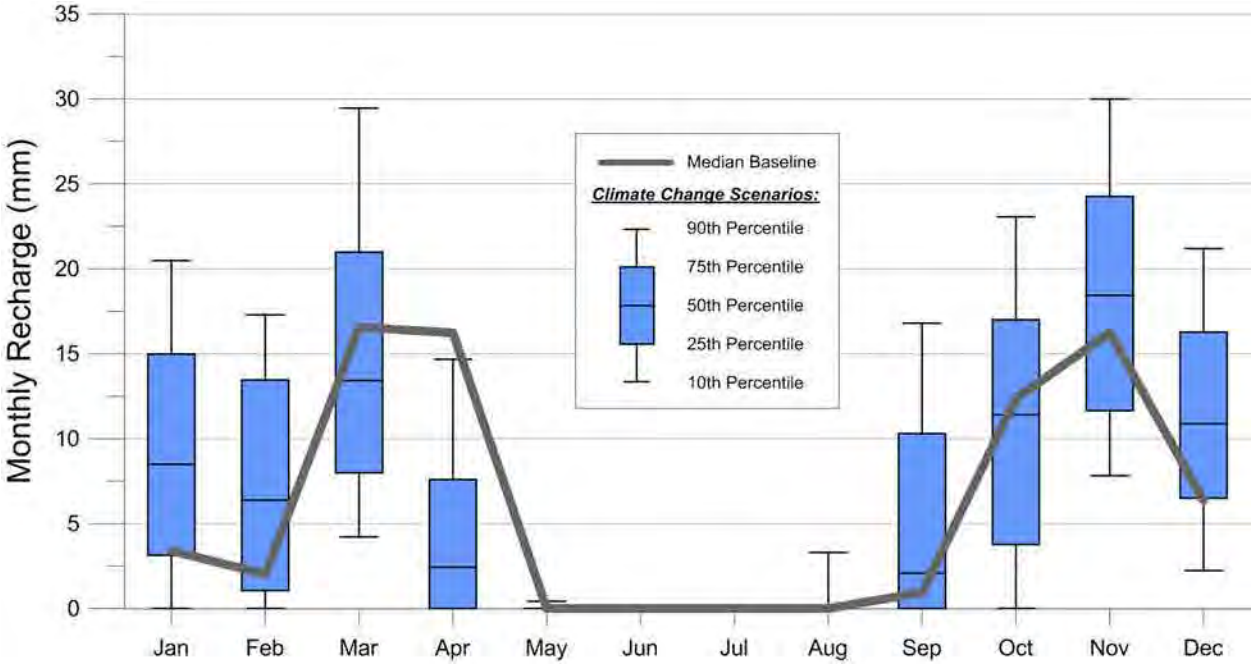

Figure 15.28: Monthly average groundwater recharge statistics for the study area.

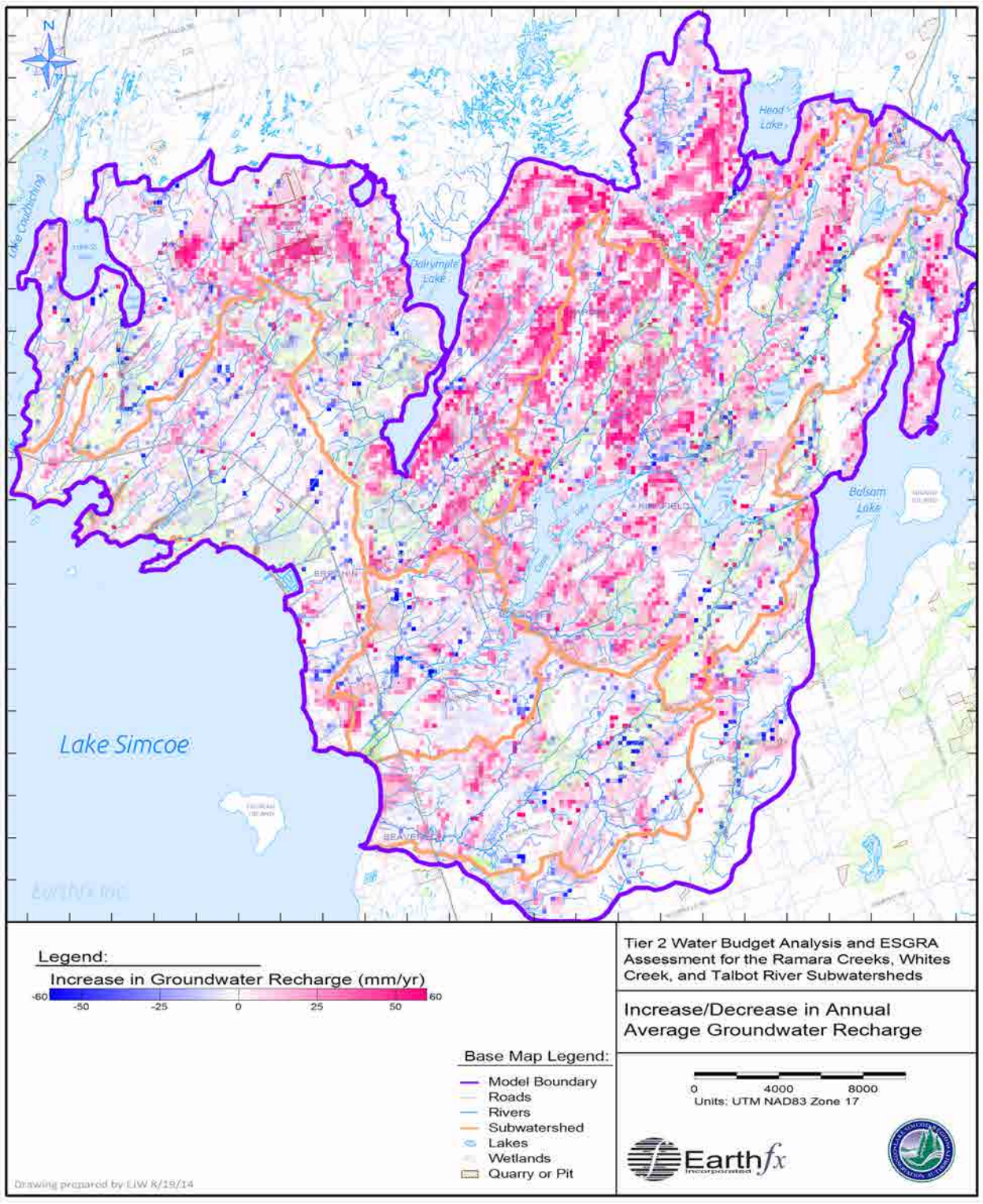

Figure 15.29: Change in annual average net groundwater recharge.

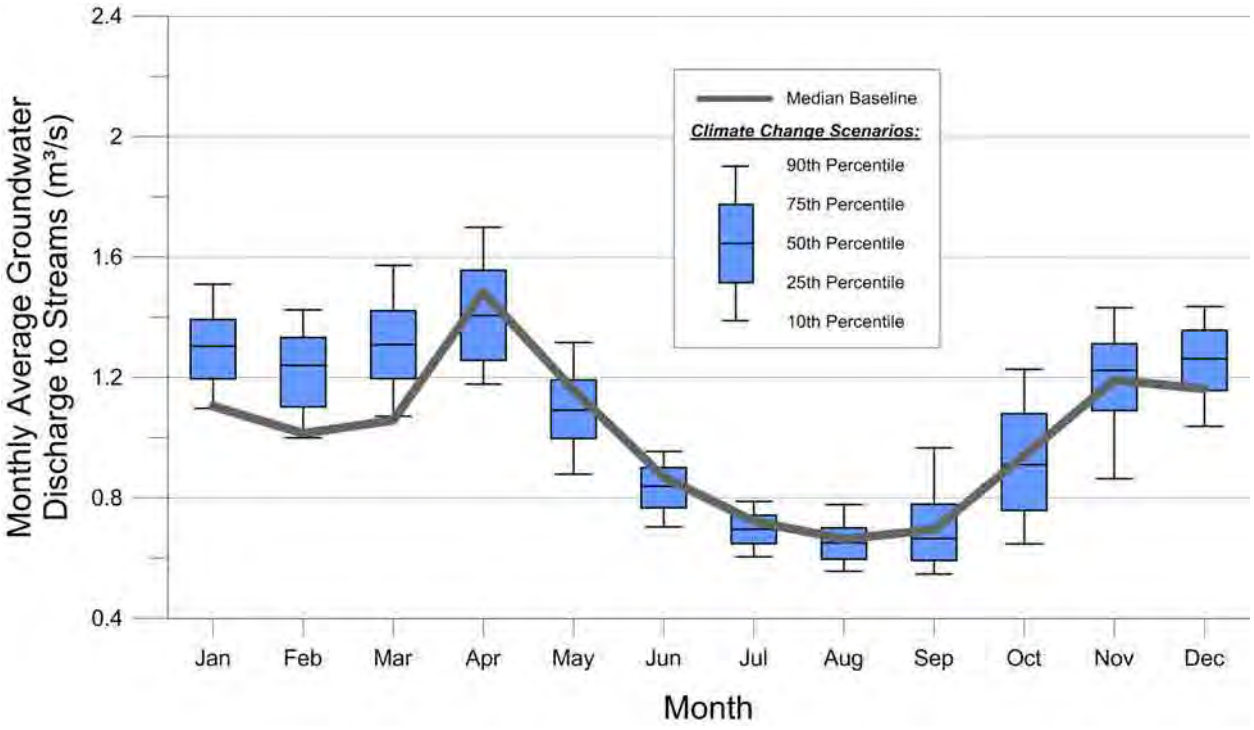

Figure 15.30: Monthly simulated groundwater discharge to study area streams.

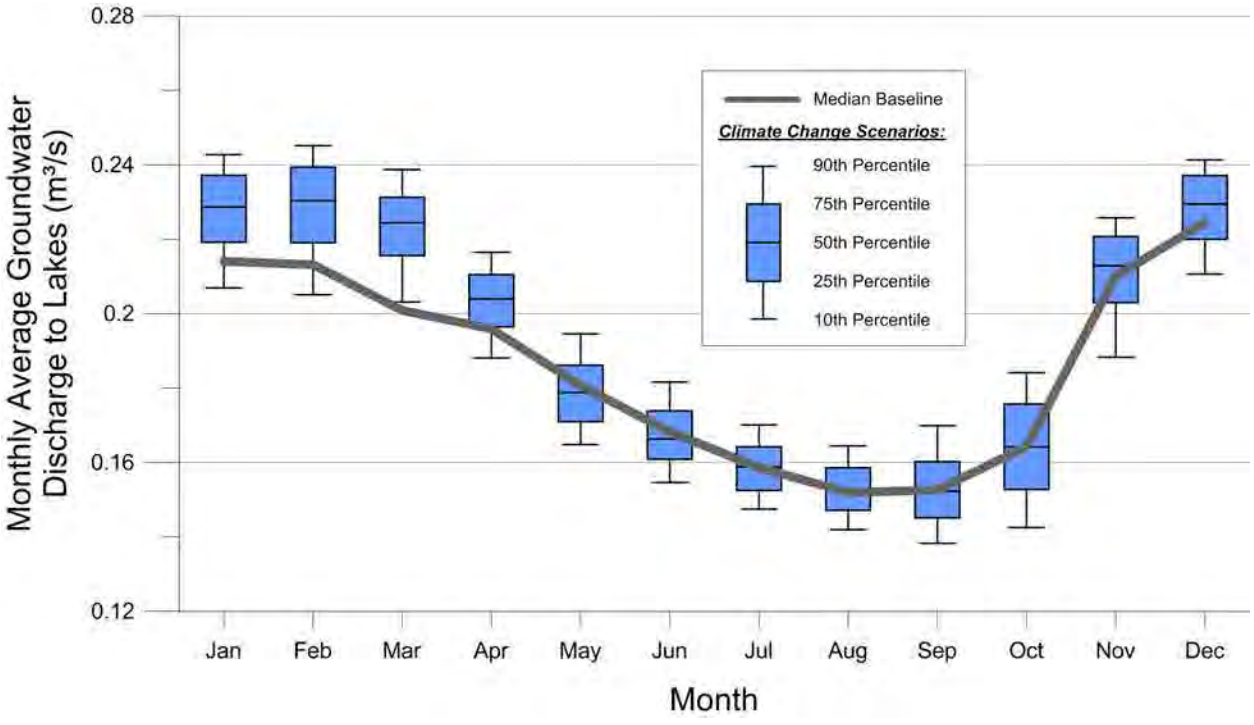

Figure 15.31: Monthly simulated groundwater discharge to study area lakes.

16 Summary and Recommendations

The Tier 2 Water Budget and ESGRA Analysis was conducted primarily to describe the water budget elements of and evaluate potential stress levels within the Ramara Creeks, Whites Creek and Talbot River subwatersheds. A second objective of this study was to identify and analyze ecologically significant groundwater recharge areas (ESGRAs) within the study subwatersheds. The third objective of this study was to assess how the study subwatersheds will respond to potential future stresses, including drought and climate change.

This report presents the completion of the data compilation, conceptualization, model construction and calibration, and steady-state analyses (including water budgets, stress assessments, and ESGRA delineation), and transient analyses of drought and climate change scenarios.

16.1 Model Development

The study included development of conceptual stratigraphic and hydrostratigraphic models for the study area. A three-dimensional representation of the conceptual stratigraphic models was created by mapping the tops of each geologic unit and then overlaying them. A similar three dimensional model was created for the hydrostratigraphic model. The hydrostratigraphic model surfaces, with some modifications to preserve minimum thicknesses, were transformed into the layer tops and bottoms needed for the MODFLOW-NWT groundwater flow sub-model.

Initial estimates of hydraulic properties for the groundwater model were obtained from a review of reported aquifer testing and previous modelling studies. Static water level data were interpolated to provide insight into groundwater flow patterns in the study area and to provide calibration targets. Long-term water level data from PGMN and quarry wells were also analyzed and, although sparse, they provided calibration targets for the transient model.

An assessment of the hydrologic setting was presented including an analysis of climate and streamflow data. Streamflow data are extremely limited in the study area, both in the number of gauged locations and the period of record. Special consideration was given to the operations of the Trent-Severn Waterway which affects both the surface water flow and groundwater flow in the Talbot River subwatershed. Despite requests, no information was provided by Parks Canada other than what was available on their website.

The study analyzed current consumptive groundwater use and projected future water use. Future quarry takings were represented explicitly within the integrated model by representing the future (20-year) build out and the groundwater surface water flows to the quarries.

Climate, soil property, land-use, and topographic data were assembled and used to construct a PRMS sub-model for the study area. The model computes a separate soil water balance for each cell on a 50-m grid and routes overland runoff to streams and lakes using a cascading flow algorithm. The PRMS pre-calibration to the limited observed streamflow data was done to determine reasonable values for model parameters as well as to obtain an initial estimate for average groundwater recharge used in the groundwater sub-model pre-calibration.

Based on a detailed understanding of the site, reflected in the developed hydrologic, geologic and hydrostratigraphic conceptual models, a steady-state groundwater flow sub-model was constructed for the study area, ensuring that key features of the site hydrogeology were carried forward into the numerical representation. The study area was subdivided vertically into seven numerical model

layers, where each layer was occupied by one or more of the fourteen hydrostratigraphic units, extending down from the surficial sediments and alvar weathered bedrock to the Precambrian basement. Assignment of hydraulic parameters to models layers proceeded through selection of representative values, informed by field measurements from previous studies, along with automated calibration techniques (e.g., Monte Carlo analyses). Calibration targets included 2,533 static water level measurements from the MOE Well Record Database, quarry monitoring reports and consultant studies, as well as streamflow measurements for Whites Creek and quarry discharges.

Following this approach, a calibrated groundwater flow sub-model was completed for the study area, including representation of all streams, lakes, wetlands, as well as permitted groundwater takings from commercial and domestic wells, and operational dewatering for the 11 quarries represented in the model. Model calibration statistics indicated an excellent fit with the available groundwater dataset, providing validation the subsequent application of the model for updated Tier 2 water budget and ESGRA analyses.

The GSFLOW model represents an integration of the surface water and groundwater sub-models in which each system can provide feedback to the other. The GSFLOW model provides a better representation of the complex flow processes that occur in natural systems particularly those with a highly responsive shallow water table. The long-term transient analyses conducted with the GSFLOW code provide much insight when assessing seasonal and annual variations (e.g., dry years and wet years), change in water use, drought and future climate change.

16.2 Tier 2 Stress and Drought Assessment

The updated Tier 2 stress assessments conducted under steady state conditions showed that none of the study subwatersheds are currently in a stressed condition. For future conditions, pumping rates at the municipal wells were increased to reflect anticipated population growth, these scenarios also included a representation of future quarry build-out (based on 20-year projections). These simulations predicted that the study subwatersheds will not be stressed over the 20-year horizon. Two-year (extreme) and 10-year (historic) drought conditions were also analyzed. The largest impacts due to drought are seen in the headwater tributaries across the study area, which are sustained mainly by groundwater discharge that occurs where the streambed intersects the water table. As might be expected, more drastic drawdowns of approximately 0.5 to 2.5 m were predicted in the extreme 2-year drought, while less severe drawdowns generally less than 1.5 m were predicted by the 10-year drought. The alvar plain was found to provide high recharge to portions of the study area subwatersheds but the feature has low storage capacity. As such, the watersheds fed directly by the alvar are less buffered from the effects of long term drought due to the relatively small storage capacity in the bedrock aquifers. No municipal pumping wells were found to go dry during either the 2-year or 10-year drought simulations.

16.3 ESGRA Delineation

An Ecologically Significant Groundwater Recharge Area (ESGRA) assessment was completed for the Ramara Creeks, Whites Creek, and Talbot River subwatersheds using the calibrated Ramara-Whites-Talbot Tier 2 GSFLOW model. Reverse particle tracking and cluster analysis techniques were used to define ESGRAs. The ESGRA methodology was applied to establish linkages between specific recharge areas and ecologically significant surface water features. For this study, all streams and all wetlands in the three study area subwatersheds were considered to be significant. Cluster analysis was used to convert the particle endpoint distribution into a uniform gridded parameter that was evaluated for significance and compared across watersheds and features.

Application of the normalized bivariate kernel density estimation technique provided a quantitative and repeatable method for cluster endpoint density analysis ESGRA delineation. Further screening of the delineated ESGRA, based on optimized h and ε values, eliminated isolated ESGRAs having an area less than 0.045 km² and in-filled small holes, consistent with the approach of (Earth*fx*, 2012).

Forward tracking across the study area and from the delineated ESGRAs was used to confirm the analyses and ensure that no critical flow paths were overlooked. During forward tracking from each of the three study subwatersheds, several surface water features in the Talbot River and Whites Creek subwatersheds were found to be supplied (at least in part) by recharge from the across their common catchment boundary. This demonstrated the need for a regional-scale approach to assessing ecologically significant recharge areas that extends beyond topography-based catchment boundaries, to which groundwater flow regimes do not necessarily conform.

The ESGRA analysis was particularly useful for delineating areas of groundwater recharge that play an important role in local-scale hydrologic systems by sustaining nearby surface water features, that were not captured in the broader SGRA analysis. One such example is the recharge area identified within the post-glacial lacustrine sands and silts along the central portion of the Ramara Creeks subwatershed that supports the wetland complex directly to the south, along the shores of Lake Simcoe.

The final ESGRA delineation comprised 33% of the combined area of the three study subwatersheds. Comparisons with previously defined SGRAs showed that only parts of the SGRAs (about half the area) contributed to ecologically significant features, with the greatest consistency found along the tops of incised bedrock valleys in the Talbot River and Whites Creek subwatersheds, which act as local recharge zones for the surface water features in the valleys below.

16.4 Climate Change Assessment

An assessment of the predicted effects of global climate change on the surface water and groundwater resources in the Ramara Creeks, Talbot River, and Whites Creek subwatersheds was conducted as part of this study. This was accomplished through the use of the watershed-scale integrated groundwater-surface water model in conjunction with transient GCM datasets to evaluate the effects of climate change on the regional hydrologic and hydrogeologic systems. A total of 9 GCM datasets were identified for this study using the percentile method, which is a statistically based method for ensuring that selected climate scenarios represent both the central tendencies of the GCMs, as wells as the more extreme projections. Because of the limitation of GCMs to predict local scale behavior beyond their 250 to 400 km model cells, the “change-field” method was selected to generate a series of climate change datasets for local area from baseline data that were used as inputs for the integrated surface water/groundwater model developed in this study.

Analysis of the hydrologic predictions of the climate change scenarios showed that monthly precipitation is anticipated to increase in the majority of scenarios except during the months of June and July, resulting in a generally wetter fall, winter and spring with a drier warm season. All the scenarios showed an increase in temperature of at least 1°C in all months. The median temperature shift ranged from 1.8 to 3.2°C, with winter (January and February) and late summer/fall (August and September) having the highest increase. The average of annual average precipitation for all climate runs was 1,129 mm/year representing a 9.1% increase over baseline conditions (1,029 mm/year). .

Groundwater recharge is predicted to increase with climate change. Warmer and wetter fall and winter seasons allow more water to enter the groundwater system. Furthermore, the timing of the spring recharge is predicted to shift, with more recharge occurring earlier in the spring. The warmer

winters predicted by the climate change models result in less accumulated snow, and with less water stored in the snowpack into mid-spring, groundwater recharge in April and May is expected to decrease.

Groundwater heads under the climate change scenarios experienced an earlier and more prolonged response to the spring freshet, combined with less dramatic decreases in water levels over the winter months of January to March. This was attributed to the wetter, warmer winters predicted by the GCMs, with a larger portion of the winter precipitation expected to fall as rain rather than snow. The seasonal pattern of groundwater discharge to surface water features echoes the water level response to climate change, with discharge into surface water features experiencing an increase during the winter months due to the larger hydraulic gradient towards the surface water features.

There was a predicted increase in the median monthly streamflow December through March, with decreases predicted in all other months. This pattern of change is predicted in streams across the watershed, with median winter streamflow increasing by as much as 50%. While the decrease in average summer flows does not approach this magnitude, the severity of drought and extreme low flow periods is predicted to increase. These predicted changes to the hydrologic regime will undoubtedly have impacts on stream ecology and geomorphology. Further study into the specific impacts of these predicted changes should be incorporated into future watershed assessments.

16.5 Recommendations

Earth*fx* recommends that LSRCA continue to maintain and expand the environmental monitoring network in the three study subwatersheds. Meteorological data are sparse in the study area, and this area is hydro-climatically distinct from the southern and western portions of the Lake Simcoe watershed. Of greatest importance to future studies would be the installation of a synoptic weather station centrally located within the study area.

The PGMN network in the study subwatersheds should ideally be expanded. Wells should be added that are not affected by quarry operations and are not close to pumping wells or regulated lakes and canals. Of particular importance is monitoring the alvar areas which are sensitive to drought conditions and climate change. Stream gauging in the alvar areas, on the Upper Talbot River and/or Rohallion Creek) should also be considered to enhance the understanding of the movement of water through this environmentally sensitive area.

Given the difficulties obtaining information from Parks Canada, stage and flows should be independently monitored along the Trent-Severn Waterway unless an effective data sharing agreement can be obtained. There is evidence to suggest that the Trent watershed is contributing a significant amount of flow into the Talbot River subwatershed via Balsam Lake. The canal between Mitchell and Balsam Lake is an ideal location for the installation of an acoustic doppler profiler to characterize the movement of water across the watershed boundary.

As part of their respective permits to take water and certificate of approval for aggregate extraction, the quarrying operations in the study area are required to collect and report environmental data from groundwater and surface water monitoring installations around their sites. Although only a small portion of this data was made available for this study, it proved a valuable addition to the otherwise sparse transient groundwater datasets. It is recommended that quarry owners and operators be approached about providing their environmental datasets, in particular continuous logger data, for use in future studies to better understand the hydrology and hydrogeology of the subwatersheds.

17 Limitations

Services performed by Earth*fx* Incorporated were conducted in a manner consistent with a level of care and skill ordinarily exercised by members of the environmental engineering and consulting profession. This report presents the results of data compilation and computer simulations of a complex hydrogeologic setting. Data errors and data gaps are likely present in the information supplied to Earth*fx*, and it was beyond the scope of this project to review each data measurement and infill all gaps. Models constructed from these data are limited by the quality and completeness of the information available at the time the work was performed. Computer models represent a simplification of the actual hydrologic and hydrogeologic conditions. The applicability of the simplifying assumptions may or may not be suitable to a variety of end uses.

This report does not exhaustively cover an investigation of all possible environmental conditions or circumstances that may exist in the study area. If a service is not expressly indicated, it should not be assumed that it was provided. It should be recognized that the passage of time affects the information provided in this report. Environmental conditions and the amount of data available can change. Any discussion relating to the conditions are based upon information that existed at the time the conclusions were formulated.

This report was prepared by Earth*fx* Incorporated for the sole benefit of Lake Simcoe Region Conservation Authority. Any use which a third party makes of this report, any reliance thereon, or decisions made based on it, are the responsibility of such third parties. Earth*fx* Incorporated accepts no responsibility for damages, if any, suffered by any third party as a result of decisions made or actions taken based on this report.

Report prepared by:

Dirk Kassenaar, M.Sc., P.Eng.
President, Senior Hydrogeologist

E.J. Wexler, M.Sc., M.S.E., P.Eng.
Vice President, Senior Hydrogeologist

Mike Takeda, M.A.Sc.
Hydrogeologist

Peter John Thompson, M.A.Sc.
Hydrologist

Asoka Kodippili, P.Geol.
Hydrogeologist, Data Analyst

John Ford, B.A.
Senior Geologist

18 References

Adamowski, K., J. Bougadis, and G. Pessy., 2003. Influence of trend on short duration design storms, pp. 15. Department of Civil Engineering, University of Ottawa.

Allen, W. A., 2002. Wa-nant-gi-tche-ang: canoe route to Lake Huron through southern Algonquia. Ontario Archaeology, 73, 38-68.

American Society for Testing and Materials, 2000. Standard Guide for Subsurface Flow and Transport Modeling (ASTM) D5880-95.

Anderson, E.A., 1968. Development and testing of snow pack energy balance equations. Water Resource Research, v. 4, no. 1, p. 19-37.

Anderson, M.P. and Woessner W.W., 1992, Applied Ground Water Modelling -- Simulation of flow and advective transport. Academic Press, USA.

Angel, J. R., and S. A. Isard. 1998. The frequency and intensity of Great Lakes cyclones. J. of Climate, 11:61-71.

Angus, J.T., 1988. A Respectable Ditch: A History of the Trent Severn Waterway, 1833-1920. McGill-Queen's University Press, 472 p.

AquaResource Inc. and EBNFLO Environmental, 2011. Future Climate Datasets Guide (version 1.2) for The Ontario Ministry of Natural Resources. 23 p.

AquaResource Inc., 2008. MNR Climate Data Gap Filling Project – Data Review. A Technical Memorandum to the Ontario Ministry of Natural Resources. August, 2008, 12 p.

Armstrong, D.K. and Dodge, J.E.P., 2007. Paleozoic geology of southern Ontario - Ontario Geological Survey, Miscellaneous Release--Data 219, attributed digital compilation map with outcrop photos.

Armstrong, D.K. and Carter, T.R. 2010. The subsurface Paleozoic stratigraphy of southern Ontario; Ontario Geological Survey, Special Volume 7, 301 p.

Armstrong, D.K. and Anatas, A.S. 1993, Paleozoic Geology of the Orillia Area, Southern Ontario: Ontario Geological Survey, Open File Map 222, scale 1:50,000.

Azimuth Environmental Consulting Inc., 2009, Additional 72-hour pumping test results McCarthy Quarry, prepared for Ministry of the Environment, 35 p.

Barnett, P.J., 1992, Quaternary geology of Ontario; in Geology of Ontario, Ontario Geological Survey, Special Volume 4, p.1011-1088.

Barth, C., 2005, Hydrologic Modelling of a Groundwater Dominated Watershed using a Loosely Coupled Modelling Approach. Friedrich-Schiller-Universitat Jena.

Bates, B., Z. Kundzewicz, S. Wu, and J. Palutikof. 2008. Climate Change and Water, Technical Paper of the Intergovernmental Panel on Climate Change, IPCC Secretariat, pp. 210. Intergovernmental Panel on Climate Change, Geneva, Switzerland.

Batu, V., 1998, Aquifer Hydraulics: A Comprehensive Guide to Hydrogeologic Data Analysis. Toronto: John Wiley & Sons, Inc.

Bear, J., 1979, Hydraulics of Groundwater: McGraw Hill, NY, 567 p.

Bedient, P.B., W.C. Huber, 2002, Hydrology and Floodplain Analysis, 3rd ed. Prentice Hall. NJ, 763 p.

Bergström, S., 1976, Development and application of a conceptual runoff model for Scandinavian catchments, SMHI RHO 7, Norrköping, 134 p.

Bergström, S., 1995, The HBV Model in: Computer Models of Watershed Hydrology, ed. V.P. Singh, p. 443-476.

Beven, K.J. and Binley, A., 1992, The Future of Distributed Models: Model Calibration and Uncertainty Prediction, Hydrological Processes 6, p. 279-298.

Brett, C.E., Tepper, D.H., Goodman, W.M., LoDuca, S.T., and Eckert, B.Y., 1995, Revised stratigraphy and correlations of the Niagaran Provincial Series (Medina, Clinton, and Lockport groups) in the type area of Western New York: U.S. Geological Survey Bulletin 2086, 66 p.

Bruce, J., H. Martin, P. Colucci, G. McBean, J. McDougall, D. Shrubsole, J. Whalley, R. Halliday, M. Alden, L. Mortsch, and B. Mills. 2003. Climate Change Impacts on Boundary and Transboundary Water Management, Climate Change Action Fund Project Natural Resources Canada Project A458/402, pp. 161, Ottawa, Ontario.

Bruce, J., W. Dickinson, and D. Lean. 2006a. Planning for Extremes: Adapting to Impacts on Soil and Water from Higher Intensity Rains with Climate Change in the Great Lakes Basin, pp. 69. Ontario Chapter of the Soil & Water Conservation Society.

Bruce, J., M. Egener, and D. Noble. 2006b. Adapting to Climate Change: A Risk-based Guide for Ontario Municipalities, pp. 39.

Burnett, A., M. Kirby, H. Mullins, and W. Patterson. 2003. Increasing Great Lake–effect snowfall during the twentieth century: a regional response to global warming? Journal of Climate, 16:3535-3542.

Chapman, L.J. and Putnam, D.F., 1984, The physiography of southern Ontario: Ontario Geological Survey, Special Volume 2, 270 p.

Chapman, L.J. and Putnam, D.F., 2007, The physiography of southern Ontario; Ontario Geological Survey, Miscellaneous Release – Data 228, digital version of physiography maps.

Cole Engineering, 2012, Hydrologic Modelling for Orillia Creeks and Talbot River Watersheds -- Final Report: prepared for the Lake Simcoe Region Conservation Authority, July 2012.

Coulibaly, P. and Evora, N. D., 2007, Comparison of neural network methods for infilling missing daily weather records, Journal of Hydrology, v. 341, p. 27-41.

Chow, V.T. (ed.), 1964, Handbook of Applied Hydrology: A Compendium of Water-Resources Technology, McGraw-Hill Book Company, New York, 1418 p,

Chu, C., 2011. Vulnerability indicators for Lake Simcoe and the wetlands, streams and rivers within the Lake Simcoe watershed. Prepared for the Nature Conservancy of Canada.

Covey, C., K. AchutaRao, U. Cubasch, P. Jones, S. Lambert, M. Mann, T. Phillips, and K. Taylor. 2003. An overview of results from the Coupled Model Intercomparison Project. Global and Planetary Change, 37:103-133.

Cramer, B.D., Bergström, S.M., Kleffner, M., Schmitz, B., and Bradley, D., 2011, Revision of the position of the Ordovician–Silurian boundary in southern Ontario: regional chronostratigraphic implications of δ13C chemostratigraphy of the Manitoulin Formation and associated strata; Canadian Journal of Earth Sciences, v. 48, no. 11, p. 1447-1470.

Crossman, J., Futter, M., Oni, S., Whitehead, P., Jin, L., Butterfield, D., Baulch, H., and Dillon, P., 2013, Impacts of climate change on hydrology and water quality: Future proofing management strategies in the Lake Simcoe watershed, Canada: Journal of Great Lakes Research, v. 39, no. 1, p. 19-32.

Dai, A. 2006. Precipitation characteristics in eighteen coupled climate models. Journal of Climate, 19:4605-4630.

Dessens, J. 1995. Severe convective weather in the context of a nighttime global warming. Geophysical Research Letters, 22:1241-1244.

DeWalle, D.R., and Rango, A., 2008, Principles of snow hydrology: Cambridge University Press, Cambridge, U.K., 410 p.

Dickinson, W.T., Whiteley, H.Q., 1970, Watershed areas contributing to runoff: International Association of Hydrologic Sciences Publicati.

Dixon Hydrogeology Limited, 2002, Revised permit to take water, Lot 1, Concession 1, Geographic Township of Mara, Township of Ramara, County of Simcoe – McCarthy Property: Dixon Hydrogeology Limited, April 11, 2002.

Duan, Q.Y., V.K. Gupta, and S. Sorooshian, 1993, Shuffled Complex Evolution Approach for Effective and Efficient Global Minimization, Journal of Optimization Theory and Applications 76(3), p.501-521.

Earth*fx* Incorporated, 2008, Simulation of groundwater flow in the vicinity of the proposed McCarthy Quarry, Brechin, Ontario: prepared for Azimuth Environmental Consulting Incorporated, March 28, 2008.

Earth*fx* Incorporated, 2010, Water Balance Analysis of the Lake Simcoe Basin using the Precipitation-Runoff Modelling System (PRMS): prepared for the South Georgian Bay - Lake Simcoe Source Protection Region, October 2010. 106 p.

Earth*fx* Incorporated, 2012, Barrie, Lovers, and Hewitt Creeks – Ecologically Significant Groundwater Recharge Area Assessment and Sensitivity Analysis: Report prepared for Lake Simcoe Region Conservation Authority.

Earth*fx* Incorporated, 2013, Tier 2 Water Budget Analysis and Water Quantity Stress Assessment for the Oro North and South and Hawkestone Creeks Subwatersheds, prepared for Lake Simcoe Region Conservation Authority, May 2013, 201 p.

EBNFLO Environmental and AquaResource Incorporated, 2010, Guide for Assessment of Hydrologic Effects of Climate Change in Ontario: prepared for the Ontario Ministry of Natural Resources and Ministry of the Environment in partnership with Credit Valley Conservation, June 2010.

Ely, D.M., 2006, Analysis of sensitivity of simulated recharge to selected parameters for seven watersheds modeled using the precipitation-run-off modeling system. USGS Scientific Investigations Report 2006-5041, 21 p.

Fetter, C.W., 1980, Applied Hydrogeology. Charles E. Merrill Publishing Co, 488 p.

Finamore, P.F. and Bajc, A.F., 1984, Quaternary geology of the Orillia area, Southern Ontario: Ontario Geological Survey, Map Geological Series Preliminary Map P2697, scale 1:50,000.

Fleming, R.B., 1991, The Railway King of Canada: Sir William Mackenzie, 1849-1923. University of British Columbia Press, 316 p.

Freeze, R.A. and J.A. Cherry, 1979, Groundwater; Prentice-Hall Inc., 604 p.

Fulton, R.A., J.P. Breidenbach, D.-J. Seo, D.A. Miller, 1998, The WSR-88D Rainfall Algorithm. Weather and Forecasting 13(2), p. 377-395.

Gartner Lee Ltd., 1995, Hydrogeological Study for Permit to Take Water Carden Quarry, prepared for Miller Paving Ltd., 106 p.

Golder Associates Limited, 2004, Hydrogeologic review in support of an application to renew permit to take water 74-P-3069, LaFarge Brechin Quarry: Golder Associates Limited, March 12, 2004.

Golder Associates Limited, 2005, North Simcoe groundwater study - Township of Ramara (Appendix H), January 2005.

Golder Associates Limited, 2007, Hydrogeological and hydrological assessments in support of a Category 2, Class “A” quarry below water – R.W. Tomlinson Limited proposed Brechin Quarry, former Township of Carden, City of Kawartha Lakes, Ontario: Golder Associates Limited, December, 2006.

Golder Associates Limited, 2012, Cumulative impacts assessment for groundwater takings in the Carden Plain area: submitted to the Ontario Stone, Sand and Gravel Association, September 2012.

Harbaugh, A.W., 2005, MODFLOW-2005, The U.S. Geological Survey modular ground-water model—the Ground-Water Flow Process: U.S. Geological Survey Techniques and Methods 6-A16.

Harden Environmental Incorporated, 2004, Permit to take water application, James Dick Construction Limited, Gamebridge Quarry Lots 11 and 12 Concession A, Ramara Township, Simcoe County: Harden Environmental Incorporated, March 8, 2004.

Hartzell, C.L., A.B. Super, 2000, Development of a WSR-88D Based Snow Accumulation Algorithm for Quantitative Precipitation Estimates Over Southwestern Oregon in: 16th International Conference on Interactive Information and Processing Systems for Meteorology, Oceanography, and Hydrology, 80th American Meteorological Society Annual Meeting, 9-14 January 2000, Long Beach, CA, p. 373-376.

Hengeveld, H., and B. Whitewood. 2005. Understanding Climate Change - 2005, pp. 57. Environment Canada, Meteorological Service of Canada.

Holroyd, E.W. III, 1999, Snow Accumulation Algorithm for the WSR-88D Radar: Supplemental Report. U.S. Department of The Interior, Bureau of Reclamation. Denver, Colorado. 39p.

Hunt, R., Walker, J., Selbig, W., Westenbroek, S., and Regan, R., 2013, Simulation of climate-change effects on streamflow, lake water budgets, and stream temperature using GSFLOW and SNTEMP, Trout Lake Watershed, Wisconsin: US Geological Survey Scientific Investigations Report 5159. U.S. Dept. of the Interior, U.S. Geological Survey. Reston, Va.

Huntington, J.L., and R.G. Niswonger, 2012. Role of surface-water and groundwater interactions on projected summertime streamflow in snow dominated regions: An integrated modeling approach. Water Resources Research 48(11): doi: 10.1029/2012WR012319.

Intergovernmental Panel on Climate Change (IPCC), 2001b. Climate Change 2001: Synthesis Report. Contribution of Working Groups I, II, and III to the Third Assessment Report of the Intergovernmental Panel on Climate Change. Cambridge University Press, Cambridge, United Kingdom, and New York, New York, Geneva, Switzerland.

IPCC. 2007a. Climate Change 2007: Impacts, Adaptation and Vulnerability. Contribution of Working Group II to the Fourth Assessment Report of the Intergovernmental Panel on Climate Change. Cambridge University Press, Cambridge, United Kingdom and New York, New York.

IPCC. 2007b. Climate Change 2007: Synthesis Report. Contribution of Working Groups I, II, and III to the Fourth Assessment Report of the Intergovernmental Panel on Climate Change. Cambridge University Press, Cambridge, United Kingdom and New York, New York, Geneva, Switzerland.

IPCC. 2007c. Summary for Policymakers. In S. Solomon, D. Qin, M. Manning, Z. Chen, M. Marquis, K. Averyt, M. Tignor and H. Miller (eds.), Climate Change 2007: The Physical Science Basis. Contribution of Working Group I to the Fourth Assessment Report of the Intergovernmental Panel on Climate Change, pp. 18. Cambridge University Press, Cambridge, United Kingdom and New York, New York.

Jagger Hims Limited, 1991, Detailed geological and hydrogeological evaluation – Marden Quarry Property, Township of Mara: Jagger Hims Limited, June 21, 1991.

Jensen, M.E., and H.R. Haise, 1963. Estimating Evapotranspiration from Solar Radiation. Journal of the Irrigation and drainage division proceedings of the American Society of Civil Engineers. p. 15-41.

Johnson, M.D., Armstrong, D.K., Sanford, B.V., Telford, P.G., and Rutka, M.A., 1992, Paleozoic and Mesozoic Geology of Ontario: in Geology of Ontario, Ontario Geological Survey, Special Volume 4, Part 2, p.907-1008.

Julian, P.Y., 2002, River Mechanics, Cambridge University Press, 434 p.

Karrow, P.F., 2009, Update of Revisions to the Early Silurian stratigraphy of the Niagara Escarpment: integration of sequence stratigraphy, sedimentology and hydrogeology to delineate hydrogeologic units; in Summary of Field Work and Other Activities 2009, Ontario Geological Survey, Open File Report 6240, p. 25-1 to 25-20.

Karrow, P.F., A. Dreimanis, P.J. Barnett, 2000. A proposed diachronic revision of Late Quaternary time-stratigraphic classification in the eastern and northern Great Lakes area; Quaternary Research, V. 54, no. 1, p. 1-12.

Kassenaar, D., 2013. VIEWLOG (version 4). Microsoft Windows. Toronto, ON: VIEWLOG Systems Inc.

Kassenaar, J.D.C. and Wexler, E.J., 2006, Groundwater modelling of the Oak Ridges Moraine area: YPDT-CAMC Technical Report #01-06: Available at http://www.ypdt-camc.ca.

Kharin, V., and F. Zwiers, 2005. Estimating extremes in transient climate change simulations. Journal of Climate, 18:1156-1173.

Klemeš, V., 1986, Operation testing of hydrological simulation models, Hydrological Sciences Journal, 31(3), p. 13-24.

Kornelsen, K.C. and P. Coulibaly, 2013, McMaster Mesonet soil moisture dataset: description and spatio-temporal variability analysis. Hydrology and Earth System Sciences 17, p. 1–18.

Kunkel, K. E., N. E. Westcott, and D. A. R. Kristovich. 2002. Assessment of Potential Effects of Climate Change on Heavy Lake-Effect Snowstorms Near Lake Erie. J. Great Lakes Res., 28:521-536.

Lake Simcoe Region Conservation Authority, 2009, Tier 1 water budget and water quantity assessment for the Lake Simcoe Watershed.

Leavesley, G.H., Litchty, R.W., Troutman, B.M. and Saindon, L.G., 1986, Precipitation-Runoff Modeling System: User's Manual. Water Resources Investigations Report 83-4283. USGS. Denver Colorado.

Lemieux, C. J., Gray, P. A., Douglas, A. G., Nielsen, G., & Pearson, D., 2014. From science to policy: The making of a watershed-scale climate change adaptation strategy. Environmental Science & Policy, 42, 123-137.

Lemmen, D., F. Warren, J. Lacroix, and E. Bush. 2008. From Impacts to Adaptation: Canada in a Changing Climate 2007, pp. 448. Government of Canada, Ottawa, Ontario.

Linsley, R.K., Kohler, M.A., and Paulhus, J.L.H., 1975, Hydrology for Engineers. 2nd ed. McGraw-Hill Company, 482 p.

Long Associates consulting Ltd., 1993, Gormley Aggregates Division Essroc Canada Inc. Permit to Take Water Application, 52 p.

Looper, J.P., B.E. Vieux, 2013, Distributed Hydrologic Forecast Reliability Using Next-Generation Radar, Journal of Hydrologic Engineering, v. 18, p.260-268.

MacRitchie S. and E. Stainsby, 2011. Lake Simcoe Watershed climate change vulnerability assessment: Water quality and quantity. Prepared by Environmental Monitoring and Reporting Branch, Ministry of the Environment as part of the Lake Simcoe Climate Change Adaptive Capacity Assessment project.

Markstrom, S.L., Niswonger, R.G., Regan, R.S., Prudic, D.E., and Barlow, P.M., 2008, GSFLOW: Coupled ground-water and surface-water flow model based on the integration of the Precipitation-Runoff Modeling System (PRMS) and the Modular Ground-Water Flow Model (MODFLOW-2005): U.S. Geological Survey Techniques and Methods 6-D1, 240 p.

Marshall, J., W.M. Palmer, 1948, The distribution of raindrops with size, Journal of Atmospheric Science 5(4), p. 165–166.

Meehl, G., T. Stocker, W. Collins, P. Friedlingstein, A. Gaye, J. Gregory, A. Kitoh, R. Knutti, J. Murphy, A. Noda, S. Raper, I. Watterson, A. Weaver, and Z.-C. Zhao. 2007. Global Climate Projections. In S. Solomon, D. Qin, M. Manning, Z. Chen, M. Marquis, K. Averyt, M. Tignor and H. Miller (eds.), Climate Change 2007: The Physical Science Basis. Contribution of Working Group I to the Fourth Assessment Report of the Intergovernmental Panel on Climate Change, pp. 747-846. Cambridge University Press, Cambridge, United Kingdom and New York, NY.

Mekis, E., and W. Hogg. 1999. Rehabilitation and analysis of Canadian daily precipitation time series. Atmosphere Ocean, 37:53-85.

Merritt, M.L., and Konikow, L.F., 2000, Documentation of a computer program to simulate lake-aquifer interaction using the MODFLOW groundwater flow model and the MOC3D solute-transport model: U.S. Geological Survey Water-Resources Investigations Report 00-4167, 146 p.

MMM Group, 2008, Draft Hydrologic Modelling Report - Pefferlaw River, Uxbridge Brook, Beaver River, White's Creek and Beaverton Creeks: prepared for the Lake Simcoe Region Conservation Authority, September 2008.

Monenco Consultants Ltd., 1991, Summary of Hydrogeological and Hydrological Report - Carden Quarry, prepared for Gormley Aggregates Division, 14 p.

Moore, I.D., Grayson, R.B. and Ladson, A.R., 1991, Digital Terrain Modelling: A Review Of Hydrological, Geomorphological, and Biological Applications, in: Terrain Analysis And Distributed Modelling In Hydrology Edited By K.J. Beven And I.D. Moore. John Wiley & Sons.

Nash, J.E. and J.V. Sutcliffe, 1970, River flow forecasting through conceptual models, Part I - A discussion of principles. Journal of Hydrology 10, p. 282-290.

National Topographic System, 1999a, Beaverton Ontario, Map: Produced by the Centre for Topographic Information, Natural Resources Canada, (Scale: 1:50,000).

National Topographic System, 1999b, Fenelon Falls Ontario, Map: Produced by the Centre for Topographic Information, Natural Resources Canada, (Scale: 1:50,000).

National Topographic System, 1999c, Lindsay Ontario, Map: Produced by the Centre for Topographic Information, Natural Resources Canada, (Scale: 1:50,000).

National Topographic System, 1999d, Orillia Ontario, Map: Produced by the Centre for Topographic Information, Natural Resources Canada, (Scale: 1:50,000).

Niswonger, R.G., Panday, S., and Ibaraki, M., 2011, MODFLOW-NWT, A Newton formulation for MODFLOW-2005: U.S. Geological Survey Techniques and Methods 6–A37, 44 p.

Niswonger, R.G. and D.E. Prudic, 2005, Documentation of the Streamflow-Routing (SFR2) package to include Unsaturated Flow beneath Streams- a modification to SFR1; U.S. Geological Survey Techniques and Methods 6-A13, 50 p.

Niswonger, R.G., Prudic, D.E., and Regan, R.S., 2006, Documentation of the Unsaturated-Zone Flow (UZF1) Package for modeling unsaturated flow between the land surface and the water table with MODFLOW-2005: U.S. Geological Survey Techniques and Methods, Book 6, Chapter A19, 62 p.

Niswonger, R.G., K.K. Allander, and A.E. Jeton, 2014. Collaborative modelling and integrated decision support system analysis of a developed terminal lake basin. Journal of Hydrology: doi: 10.1016/j.jhydrol.2014.05.043.

Obled, C. and B. Rosse, 1977, Mathematical Models of a Melting Snowpack at an Index Plot. Journal of Hydrology 32, p. 139-163.

Oni, S., Futter, M., Molot, L., and Dillon, P., 2012, Modelling the long term impact of climate change on the carbon budget of Lake Simcoe, Ontario using INCA-C: Science of the total environment, v. 414, p. 387-403.

Ontario Geological Survey, 2003, Surficial geology of southern Ontario: Ontario Geological Survey Miscellaneous Release – Data, MRD-128, digital compilation of southern Ontario surficial geological mapping.

Ontario Geological Survey, 2010, Surficial geology of southern Ontario; Ontario Geological Survey, Miscellaneous Release—Data 128–Revised, attributed digital compilation map.

Ontario Ministry of Environment, 2009, Technical Rules: Assessment Report, Clean Water Act (original release 2006).

Ontario Ministry of the Environment, 2009. Lake Simcoe Protection Plan. Toronto, ON: Queen's Printer for Ontario.

Ontario Ministry of Environment, 2011, Technical Rules: Assessment Report, Clean Water Act (original release 2006).

Ontario Ministry of the Environment, 2013. DRAFT: Lake Simcoe Climate Change Adaptation Strategy. Available online from the Ontario Environmental Registry (http://www.ebr.gov.on.ca).

Ontario Ministry of Natural Resources [MNR], 2005, Provincial Digital Elevation Model, Version 2.0.0 [Computer File]. Peterborough, ON (Accessed August 2006).

Ontario Ministry of Natural Resources [MNR], 2007, Southern Ontario Land Resource Information System (SOLRIS) Version 1.2 [Computer File]. Peterborough, ON (Accessed October 2010).

Ontario Ministry of Natural Resources [MNR], 2008. Southern Ontario Land Resource Information System (SOLRIS). Phase 2 – Data Specification Version 1.2, April, 2008. 17 p.

Ontario Ministry of Natural Resources [MNR], 2010, OHN Watercourse Coverage [Computer File]. Peterborough, ON (Accessed September 2010).

Ontario Ministry of Natural Resources, 2011, Water budget and water quantity risk assessment guide, Drinking Water Source Protection Program: prepared by AquaResource Inc. for the Ontario Ministry of Natural Resources and the Ontario Ministry of the Environment.

Piggot, A.R., Moin, S. and Southam, C., 2005, A revised approach to the UKIH method for the calculation of baseflow: Hydrological Sciences, 50(5). p. 911-920

Rees, G.W., 2006, Remote sensing of snow and ice: CRC Press - Taylor and Francis Group, Boca Raton, FL, 285 p.

Rendon, S.H., B.E. Vieux, C.S. Pathak, 2013, Continuous Forecasting and Evaluation of Derived Z-R Relationships in a Sparse Rain Gauge Network Using NEXRAD, Journal of Hydrologic Engineering 18(2), p. 175-182.

Rosenfeld, D., D.B. Wolff, and D. Atlas, 1993, General probability-matched relations between radar reflectivity and rain rate. J. Appl. Meteor., v. 32, p. 50-72.

Ross, R., and W. Elliott. 2001. Radiosonde-based northern hemisphere tropospheric water vapor trends. Journal of Climate, 14:1602-1612.

Schroeter and Associates, 2008, Meteorological Data Missing-Value Fill-in Study for Ontario (Draft 2). A technical memorandum addressed to Lorrie Minshall, P.Eng., Grand River Conservation Authority, Cambridge, Ontario, Wednesday June 13, 2007, 37 p.

Schroeter, H.O., D.K. Boyd and H.R. Whiteley, 2000, Filling Gaps In Meteorological Data Sets Used For Long-Term Watershed Modelling, presented at the Ontario Water Conference 2000 in Richmond Hill, April 2000, 16 p.

Seibert, J. and B.L. McGlynn, 2007, A new triangular multiple flow direction algorithm for computing upslope areas from gridded digital elevation models, Water Resources Research, v. 43, 8 p.

Seibert, J. and Vis, M., 2012, Teaching hydrological modeling with a user-friendly catchment-runoff-model software package, Hydrology and Earth System Sciences, v. 16, p. 3315–3325.

Seidel, K., and Martinec, J., 2004, Remote sensing in snow hydrology runoff modelling, and effect of climate change: Springer - Praxis Publishing, Chichester, U.K., 150 p.

Sieck, L.C., S.J. Burges, M. Steiner, 2007. Challenges in obtaining reliable measurements of point rainfall. Water Resources Research 43(1), W01420 10.1029/2005WR004519

Soil and Water Conservation Society. 2003. Conservation Implications of Climate Change: Soil Erosion and Runoff from Cropland, pp. 24. Soil and Water Conservation Society, Ankeny, Iowa.

Solomon, S., D. Qin, M. Manning, Z. Chen, M. Marquis, K. Averyt, M. Tignor, and H. Miller. 2007. Climate Change 2007: The Physical Science Basis. Contribution of Working Group I to the Fourth Assessment Report of the Intergovernmental Panel on Climate Change, pp. 996. Cambridge University Press, Cambridge, United Kingdom and New York, New York.

Spitz, K. and Moreno, J., 1996, A Practical Guide to Groundwater and Solute Transport Modeling, John Wiley & Sons Inc: New York.

Tanvir Hassan, S.M., M.W. Lubczynski, R.G. Niswonger, and Z. Su, 2014. Surface-groundwater interactions in hard rocks in Sardon catchment of western Spain: an integrated modeling approach. Journal of Hydrology: doi: 10.1016/j.jhydrol.2014.05.026.

Todd, D.K., 1980, Groundwater Hydrology, John Wiley and Sons: New York, 535 p.

USCCSP. 2008. Weather and climate extremes in a changing climate. Regions of focus: North America, Hawaii, Caribbean, and U.S. Pacific Islands. In G. A. M. T.R. Karl, C.D. Miller, S. J. Hassol, A.M. Waple and W.L. Murray (ed.), A report by the U.S.Climate Change Science Program and the Sub-committee on Global Change Research, pp. 164. Dept. of Commerce, NOAA's National Climatic Data Center, Washington, D.C.

Vincent, L., and E. Mekis. 2006. Changes in daily and extreme temperature and precipitation indices for Canada over the twentieth century. Atmosphere Ocean, 44:177-193.

Waterloo Hydrogeologic Incorporated, 2002, Groundwater modelling of the proposed McCarthy Quarry: Waterloo Hydrogeologic Incorporated, April 2002.

Woolfenden, L.R., & T. Nishikawa. 2014. Simulation of groundwater and surface-water resources of the Santa Rosa Plain watershed, Sonoma County, California. U.S. Geological Survey Scientific Investigations Report 2014-5052. U.S. Dept. of the Interior, U.S. Geological Survey. Reston, Va.

Ward, A.D. and S.W. Trimble, 2003, Environmental Hydrology, 2nd ed. Lewis Publishers, New York. 475 p.

Yeung, C.W., 2005, Rainfall-runoff and water balance models for management of the Fena Valley Reservoir, Guam. USGS Scientific Investigations Report 2004-5287, 52 p.

Appendix A Analysis and Bias Correction of NEXRAD Digital Precipitation Array

NEXRAD Doppler radar tower

A.1 NEXRAD

The Next-Generation Radar (NEXRAD) is a freely-available climate dataset distributed by the National Weather Service (NWS), an agency of the National Oceanic and Atmospheric Administration (NOAA) of the United States Department of Commerce. The data utilized in this study, is in the form of the NEXRAD Digital Precipitation Array (DPA): estimated one hour precipitation accumulations reported every 6-10 minutes. The NEXRAD network consists of 159 high-resolution Doppler weather stations operated by the NWS. The NEXRAD station KBUF (Buffalo, NY) was chosen for its location with respect to the study area. The KBUF dataset is given in 9087 distributed 18.5 km² (4.3 x 4.3 km) cells which span a radius of 232 km. The study site and the stations used for NEXRAD bias correction are located roughly 175 km from the KBUF radar station.

At the centroid of every NEXRAD cell, a UTM NAD83 location was determined and defined as a Virtual Climate Station (VCS). Every VCS was associated with an independent temporal precipitation dataset and common interpolation techniques were used to infill areas between them. Spatial infilling between the VCSs, which were spaced roughly 4.3 km apart, was based on an inverse-distance-squared interpolation method performed while only considering VCSs within a 12 km radius (for reasons to be discussed below). The interpolation was performed against a raster field with a uniform cell resolution of 500 m. Of the 9087 VCSs that exist in the KBUF dataset, only 329 were considered for Ramara, Whites, Talbot model area.

The period of record of the collected NEXRAD-KBUF dataset was from February 23, 1996 to April 20, 2013. The compressed daily data files (in the form of *.tar.Z files) were downloaded from the

NWS website (radar.weather.gov). As the NEXRAD data are downloadable in daily packages, a quick screening of the data quality can be assessed, Figure A.2 plots the cumulative missing data-days. Only 85 days out of a record length of 6267 day, or 1.4%, were missing.

The number of NEXRAD-KBUF DPA precipitation intensity measurements ranged from 0 to 20 recordings per hour. The current network of WSR-88D weather radars are controlled by a series of preprogrammed Volume Coverage Patterns (VCP) which vary the instrument rotation speed, elevation angle, and transmitter pulse frequency and width. The VCP is selected by the radar operator based on the type of weather occurring. For example, during clear weather the instrument scan time is 10 minutes compared to the 5 or 6 minute scan time of a storm-mode VCP. The slower rotation during clear weather allows for increased sensitivity when the signal-to-noise ratio of the instrument is lower. The frequency of recordings per hour shows a bi-modal distribution, with 6 and 10 recordings per hour being the most frequent (Figure A.3).

The large dataset was then screened such that only the DPA measurements at, or close to, the top of the hour (TOTH) was selected to ensure that consistent rainfall measurements in near-exact hourly increments were obtained. This step is required since, as discussed above, the number of measurements per hour can vary, and there is no guarantee a measurement will exactly correspond to the hourly interval. The TOTH algorithm used here has been described in Earth*fx* (2013) and was able to extract hourly estimates of which 96% reported between 23/02/1996 15:56 and 20/04/2013 22:59 had their recording taken ±5 min from the TOTH. Figure A.4 illustrates the distribution of hourly measurements and their proximity to the TOTH. Where no TOTH measurement were available, an attempt was made to interpolate a pair or measurements that occurred before and after the TOTH, provided that they were themselves less than an hour apart. If no NEXRAD measurements were available for interpolation, data from the rain gauge network was used to infill the missing periods in order to obtain a complete record set.

The NEXRAD-KBUF DPA dataset has a data availability (number of reported hours per total possible hours) of 96.1% for the period of February 23, 1996, 16:00 to April 20, 2013, 23:00 Coordinated Universal Time (UTC). In Figure A.5 data availability as a percentage of total hours per year are displayed. The total number of reported hours per year are displayed above each vertical bar (note that 1996 and 2013 are incomplete years).

Of the point-scale rain gauge stations introduced in Section 4.1, a total of 12 precipitation stations were available for bias correction for the period of February 23, 1996, 16:00 to April 20, 2013, 23:00 UTC. These stations are shown in Figure A.1 along with the distribution of NEXRAD VCSs. At most, 8 of these 12 precipitation stations reported data on a single day (Figure A.6) and on average there tends to be 5-6 stations of simultaneous data over the NEXRAD-KBUF period of record at any given time (Figure A.7).

A.2 NEXRAD as a Model Input

The Ramara, Whites, Talbot GSFLOW model covers an area of roughly 1,100 km². Climate data is spare in the study area (see), and the data quality and the period of record of each individual station varies; at times, a point in the model domain can exceed 10 km from the nearest station with usable data. With distributed models such as GSFLOW, methods are required to interpolate *point-scale* rain gauge data into a 2-dimensional *field* of spatially-distributed rainfall. While the limitations of spatial interpolation methods have long been recognised (Coulibaly and Evora, 2007), all interpolation methods also suffer from their dependence on the accuracy of the nearest gauge informing the interpolation method. Additionally, given the potential difficulties in obtaining good quality data at point-scale gauges (Sieck et.al., 2007), an interpolation technique will inevitably propagate any point-scale errors in space, which depending on the distance to the next-nearest gauge, can extend across large swaths of the model area.

An alternative to spatial interpolation techniques is to utilize radar-derived precipitation intensity estimates to inform the spatial distribution of point-scale volumetric precipitation measurements. Rather than building a precipitation field based on the interpolation of point-scale measurements, the field is provided by the radar data and the *mean-field* volume of precipitation is corrected according to the point rain gauge measurements. Volumetric correction is achieved by assessing the bias between the radar data and the point-scale data then applying a bias correction factor to the radar data, in an attempt to remove systematic error (Bedient and Huber, 2002). The systematic error between radar and point-scale-interpolated precipitation fields is herein referred to as Mean-Field Bias (MFB). The MFB defined here differs slightly from that of (Bedient and Huber, 2002; Looper, J.P., B.E. Vieux, 2013; and Rendon et.al., 2013) in that these authors only considered the bias between the rain gauge and the specific radar pixel in which the point gauge is located. (Mean-field bias used in this sense is a misnomer; could have been more aptly termed mean-*point* bias.) Either way, when determining MFB, the correction factors are computed using an even weighting of all stations with available data at a given time step, reducing the potential for gauge errors to propagate in space.

Another advantage in using radar fields over interpolated fields is that orographic effects would be captured. For example, the study area is closely situated to the Niagara Escarpment and roughly a third of the gauges lie below the escarpment at an elevation of roughly 75 masl versus roughly 250 masl above the escarpment. The escarpment's steep elevation change can alter the character of prevailing storms, possibly creating locally-distinct weather patterns.

A.3 NEXRAD-KBUF DPA Dataset

The digital precipitation array provides approximate rainfall hourly accumulations on a 6-10 minute basis from measured rainfall intensities. The intensities are determined by combining two relationships, one relating Reflectivity (Z) to drop size distribution, the other relating drop size distribution to rainfall rate (R) (Bedient and Huber, 2002). When combined, Z-R relationship offers a convenient way to relate radar reflectance to rainfall intensity. The Z-R relationships generally follow the power-law form , where and are fitting coefficients.

Marshall and Palmer (1948) appear to have offered the first empirical approximation for the fitting coefficients setting and . However, the Marshall-Palmer was limited to only stratiform events and two more-widely forms have used in practice (Rendon et.al., 2013): and for tropical events (Rosenfeld et.al., 1993); and and for convective events (Fulton et.al., 1998). With the exception of some tropical regions, the Fulton relationship is used to produce rainfall intensity estimates from the Weather Surveillance Radar-1988 Doppler (WSR-88D) radars employed by the NWS-NEXRAD program (Fulton et.al., 1998), and was thus employed in developing their DPA product. Other attempts have been made to adjust the Z-R relationship fitting parameters to capture snowfall (Holroyd, 1999; Hartzell and Super, 2000) that had coefficient ranging from 50 to 200 and from 0 to 2.0.

A.4 Bias Correction

The removal of systematic error in the NEXRAD DPA dataset was performed on a daily basis such that more point-scale rain gauges can be used for comparison. The DPA dataset was first converted into hourly timesteps by selecting all DPA measurements occurring closest to the top-of-the-hour, and the time was converted from UTC to Eastern Standard Time (EST). All sub-daily data from NEXRAD and point gauges were summed to synoptic daily (8am-8am) precipitation totals consistent with the EC dataset. Daylight savings were not accounted for the bias correction was applied on a daily basis and a one-hour shift would only consist of a 4% error in daily volumes and by assuming that high-intensity storms at 8am are extremely rare. Once the bias correction procedure was

completed, the daily correction factors were applied back to hourly DPA data, and inputted directly into the GSFLOW model. The following describes in detail the bias correction procedure.

The first step was to determine the spatial correlation of the NEXRAD VCS network. This was accomplished using common geostatistical techniques where the error between VSC pairs, at times where one VCS of the pairings reported a measureable event, was compared to their respective distance, similar to that of Julian (2002). By selecting an arbitrary threshold correlation coefficient of 0.5, which would correspond to the axiom that the variance in one VCS can be explained by the variance in the paired VCS only 50% of the time, it can be shown that VSCs with a distance greater than 20 km apart tend not to be well correlated (Figure A.8). From , a distance of 12 km was shown to be the maximum distance from which a reliable interpolation from a point gauge could be obtained; however, with a VCS spatial separation of 4.3 km, a 12 km maximum interpolation distance would end up incorporating up to 21 individual VSCs. Incorporating such a large number of VCSs may cause for a spurious interpolated field as any point in space could have an interpolated value even though the closest surrounding VCSs may have no measured precipitation. Therefore, the NEXRAD field interpolation was accomplished using only the nearest 5 VCSs, corresponding to an interpolation radius of 6 km.

Next, climate gauge daily totals were interpolated across the study area using Thiessen Polygons to a maximum distance of 12 km, keeping consistent with the knowledge gained from the geostatistical analysis. Radar daily totals were interpolated using an inverse-distance-squared algorithm using VSCs within the 12 km limit. Interpolations were conducted on a 500 m uniform grid, 100 rows by 120 columns, incorporating 329 VCS. From these interpolations, the Gauge (G) and Radar (R) mean-field rainfall was determined and the daily MFB was calculated using (Bedient and Huber, 2002):

$$\sum$$

where is the number of field cells (

A genetic optimization routine (Duan et.al., 1993) was then applied in order to reduce the root-mean-square error (RMSE) among the 12,000 field cells in an attempt to reduce the overall MFB. This was accomplished by first selecting all field cells that exhibited greater than or equal to 1 mm/day of precipitation calculated at *both* NEXRAD and gauge fields. Next, the NEXRAD field was decomposed back to reflectance (Z), and new and coefficients to the Z-R relationship was determined such that the RMSE between the fields was minimized. The range of acceptable Z-R coefficients were kept to within documented values: and .

The optimization routine proved to be quite successful in reducing the MFB. As illustrated in Figure A.9, the MBF, as indicated by the scatter around the 1:1 line, is greatly reduced when an optimized Z-R relationship is found. The coefficient of determination is increased from 0.44 to 0.97 and the residual sum of squares is reduced from from 9,230 to 449 mm².

Using the updated Z-R relationship, the NEXRAD rainfall totals were corrected and applied to the model, resulting in a precipitation field that honours both the volumes measured at ground rainfall gauges and the radar-recorded spatiotemporal rainfall distribution.

A.5 References

Bedient, P.B., W.C. Huber, 2002. Hydrology and Floodplain Analysis, 3rd ed. Prentice Hall. NJ. 763 pp.

Coulibaly, P., and Evora, N. D. 2007. Comparison of neural network methods for infilling missing daily weather records. *Journal of Hydrology*, *341*(1), 27-41.

Duan, Q.Y., V.K. Gupta, and S. Sorooshian, 1993. Shuffled Complex Evolution Approach for Effective and Efficient Global Minimization. Journal of Optimization Theory and Applications 76(3) pp.501-521.

Fulton, R.A., J.P. Breidenbach, D.-J. Seo, D.A. Miller, 1998. The WSR-88D Rainfall Algorithm. Weather and Forecasting 13(2), p. 377-395.

Hartzell, C.L., A.B. Super, 2000. Development of a WSR-88D Based Snow Accumulation Algorithm for Quantitative Precipitation Estimates Over Southwestern Oregon in: *16th International Conference on Interactive Information and Processing Systems for Meteorology, Oceanography, and Hydrology, 80th American Meteorological Society Annual Meeting, 9-14 January 2000, Long Beach, CA*, p. 373-376.

Holroyd, E.W. III, 1999. Snow Accumulation Algorithm for the WSR-88D Radar: Supplemental Report. U.S. Department of The Interior, Bureau of Reclamation. Denver, Colorado. 39pp.

Kornelsen, K.C. and P. Coulibaly, 2013. McMaster Mesonet soil moisture dataset: description and spatio-temporal variability analysis. Hydrology and Earth System Sciences 17. pp. 1–18.

Looper, J.P., B.E. Vieux, 2013. Distributed Hydrologic Forecast Reliability Using Next-Generation Radar. Journal of Hydrologic Engineering 18:260-268.

Marshall, J., W.M. Palmer, 1948. The distribution of raindrops with size. Journal of Atmospheric Science 5(4), p. 165–166.

Rendon, S.H., B.E. Vieux, C.S. Pathak, 2013. Continuous Forecasting and Evaluation of Derived Z-R Relationships in a Sparse Rain Gauge Network Using NEXRAD. Journal of Hydrologic Engineering 18(2), p. 175-182.

Rosenfeld, D., D.B. Wolff, and D. Atlas, 1993: General probability-matched relations between radar reflectivity and rain rate. J. Appl. Meteor., 32, 50-72.

Sieck, L.C., S.J. Burges, M. Steiner, 2007. Challenges in obtaining reliable measurements of point rainfall. Water Resources Research 43(1), W01420 10.1029/2005WR004519

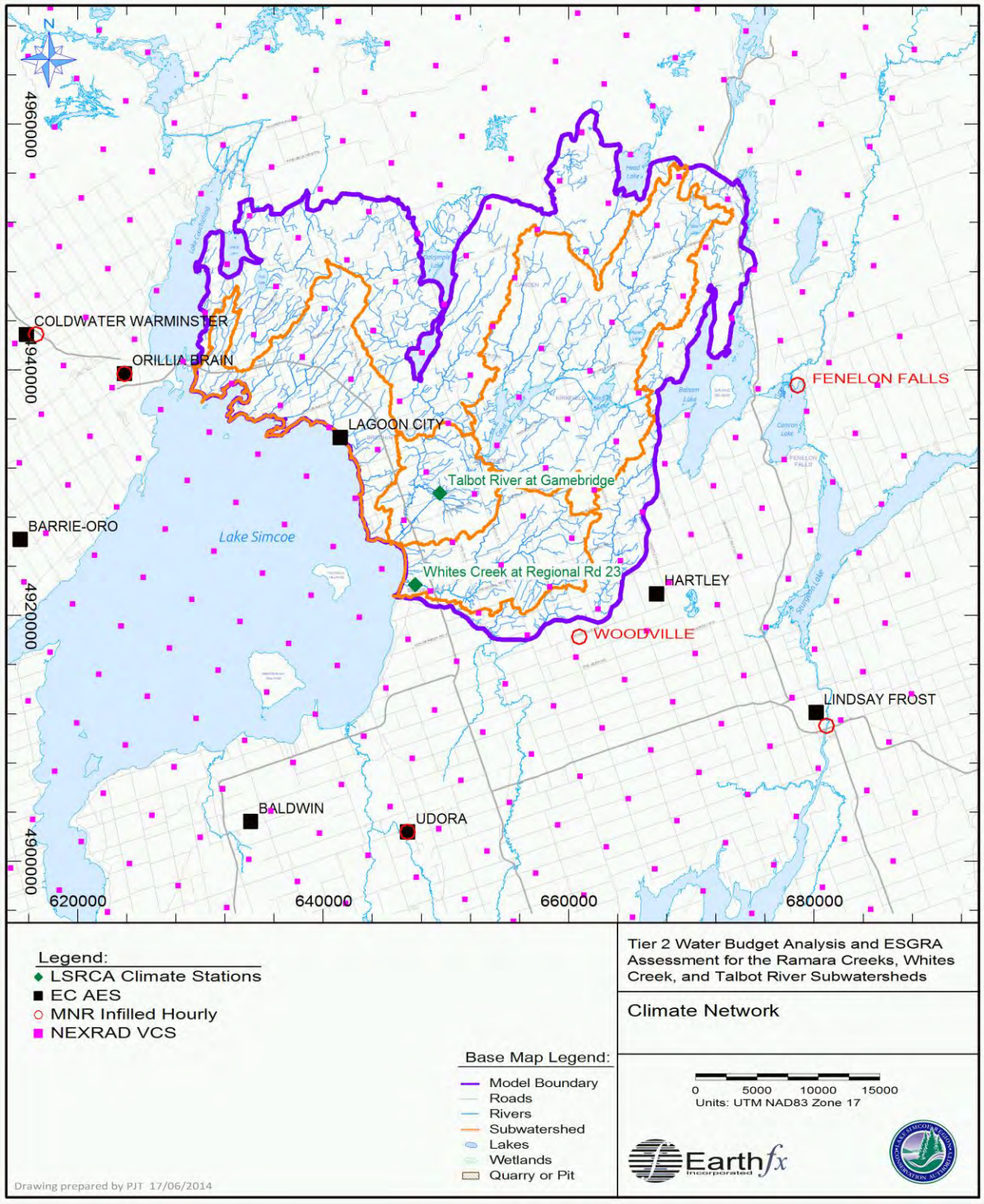

Figure A.1: Distribution of local climate stations available for NEXRAD bias correction in close proximity to the study area (note superimposed NEXRAD cell centroids (i.e., Virtual Climate Stations – VCS)

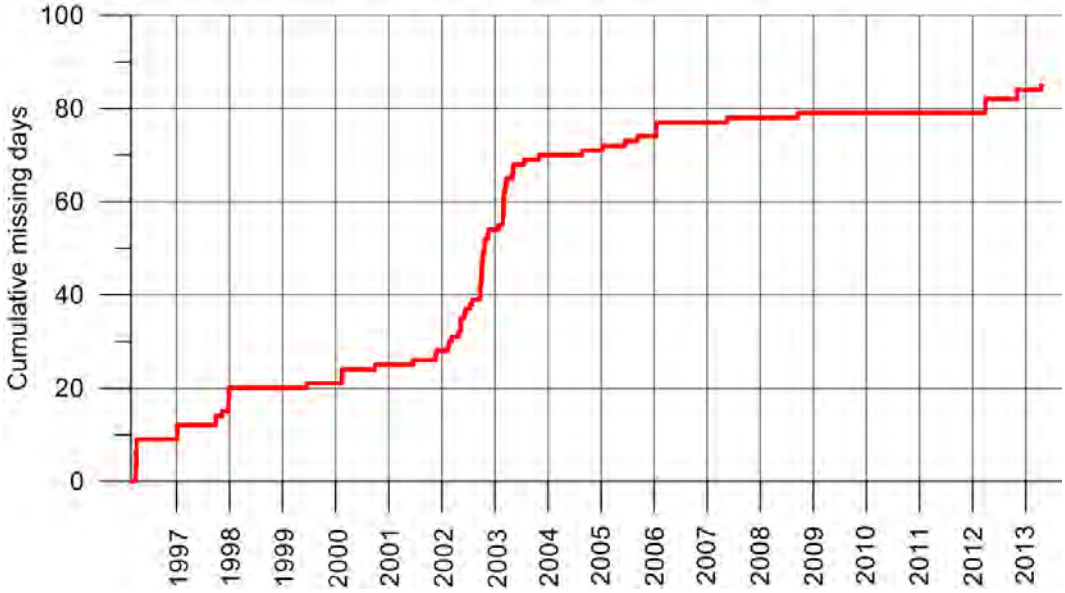

Figure A.2: Cumulative distribution of missing days in the NEXRAD-KBUF dataset from a total of 6,267.

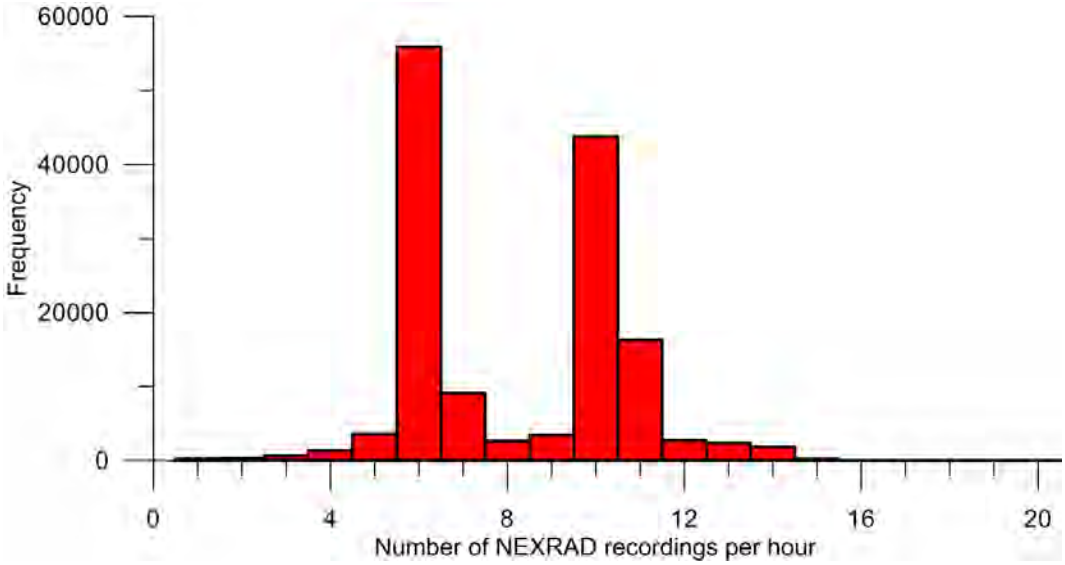

Figure A.3: Distribution of NEXRAD Digital Precipitation Array recording frequency at KBUF.

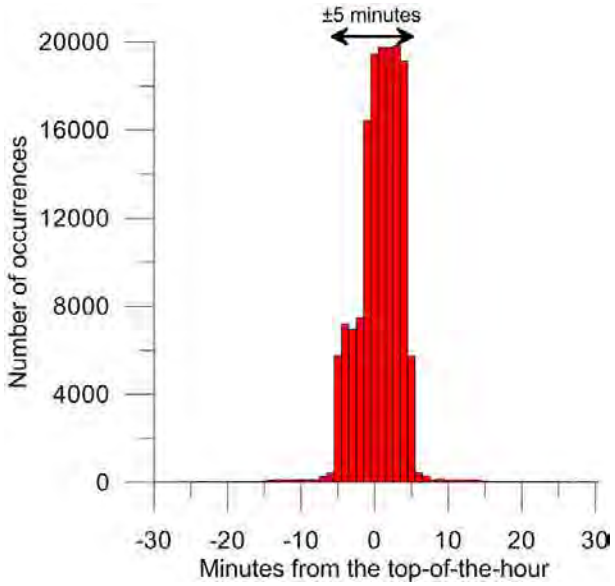

Figure A.4: Histogram of hourly DPA recordings used as opposed to their relative time difference from the top of the hour.

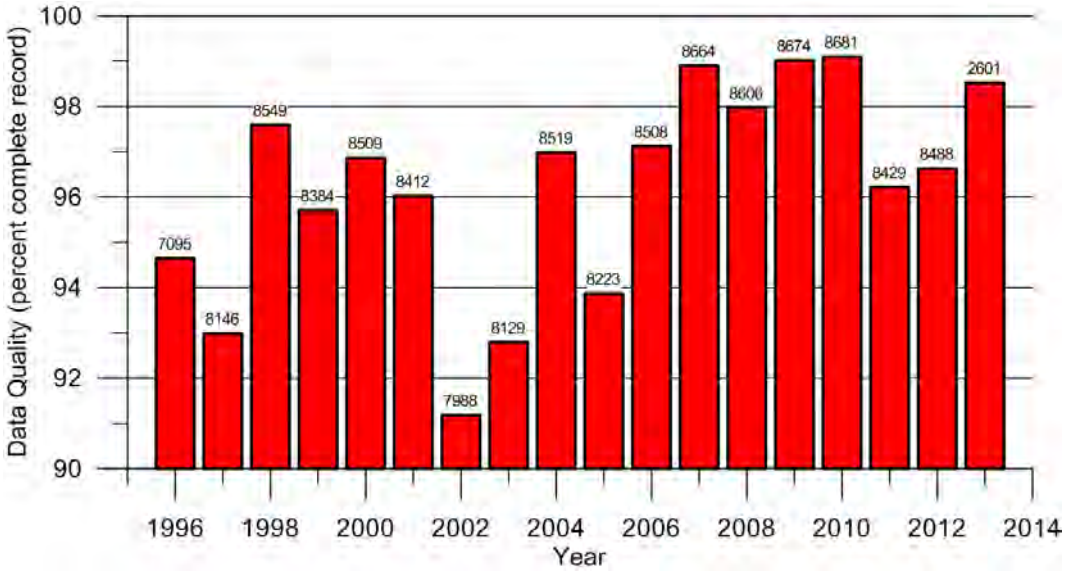

Figure A.5: Annual NEXRAD Digital Precipitation Array data availability at KBUF. Note: there are 8760 hours per (non-leap) year.

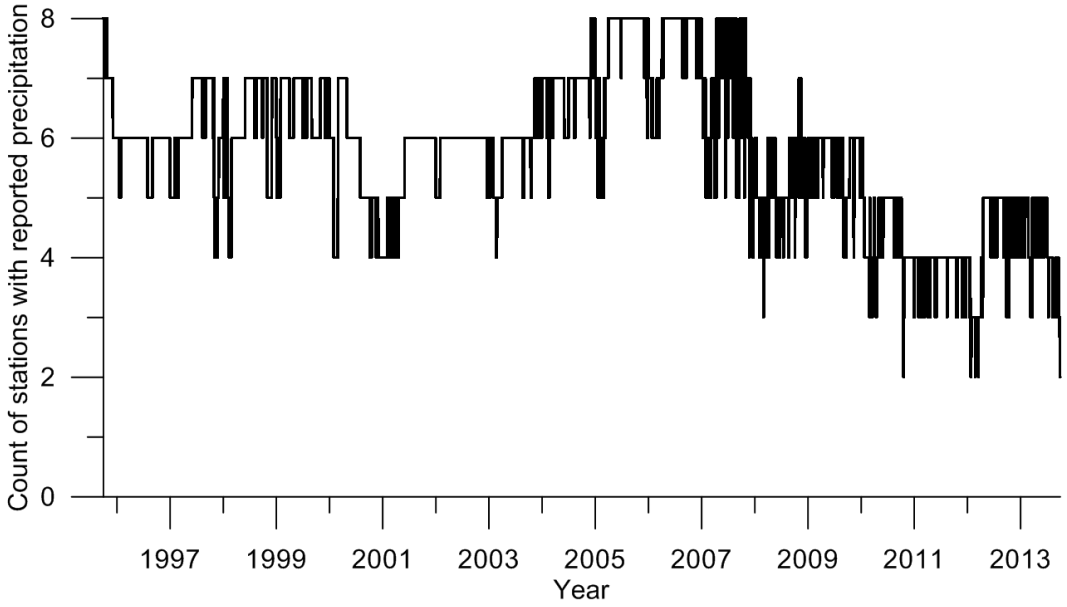

Figure A.6: Time series of the number of stations available for NEXRAD bias correction.

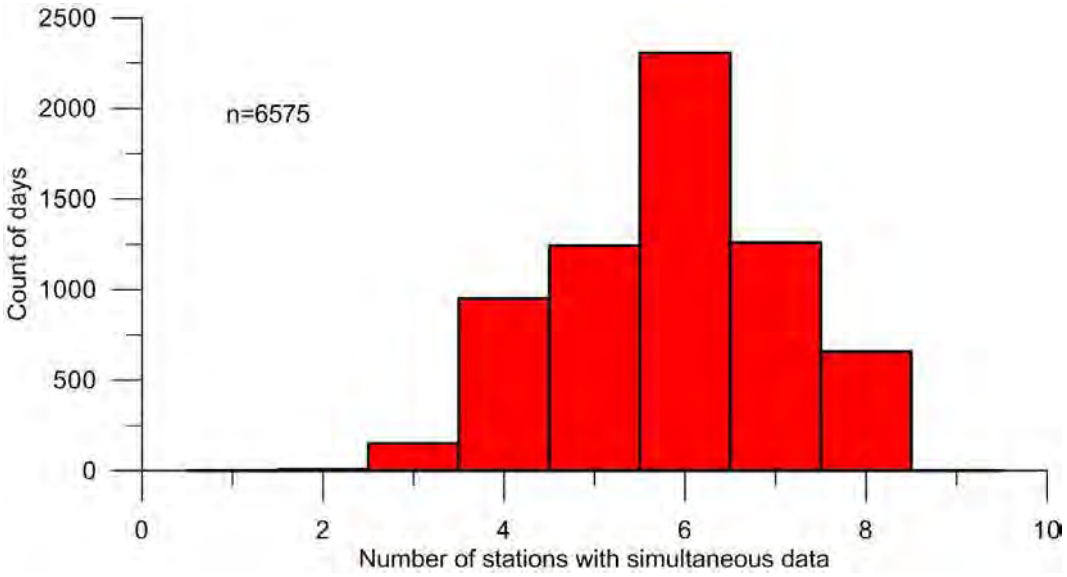

Figure A.7: Histogram of available stations for NEXRAD bias correction for the period of February 23, 1996 to April 20, 2013.

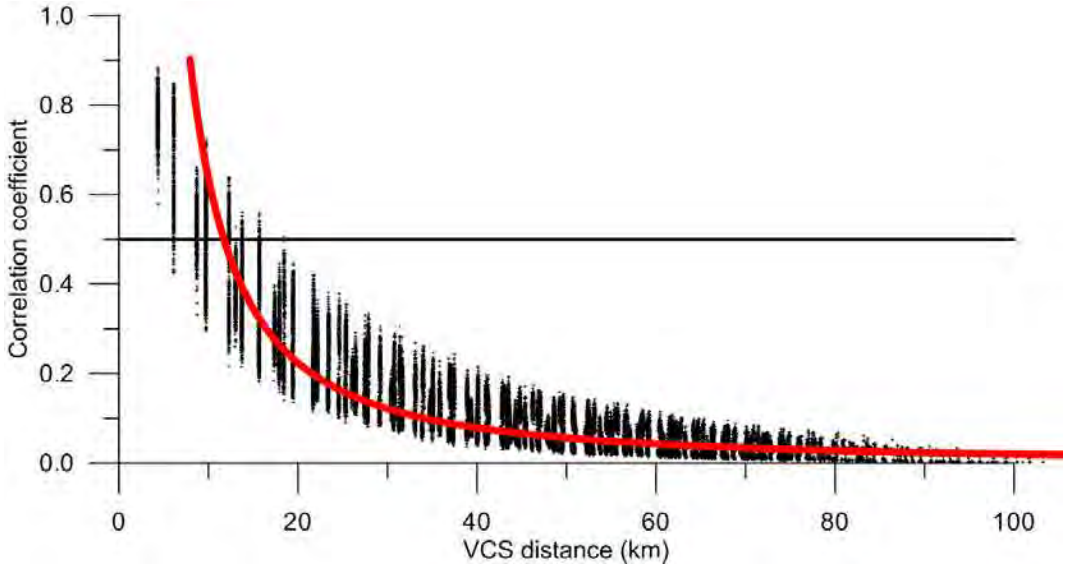

Figure A.8: NEXRAD KBUF DPA VCS inter-correlation with respect to separation distance.

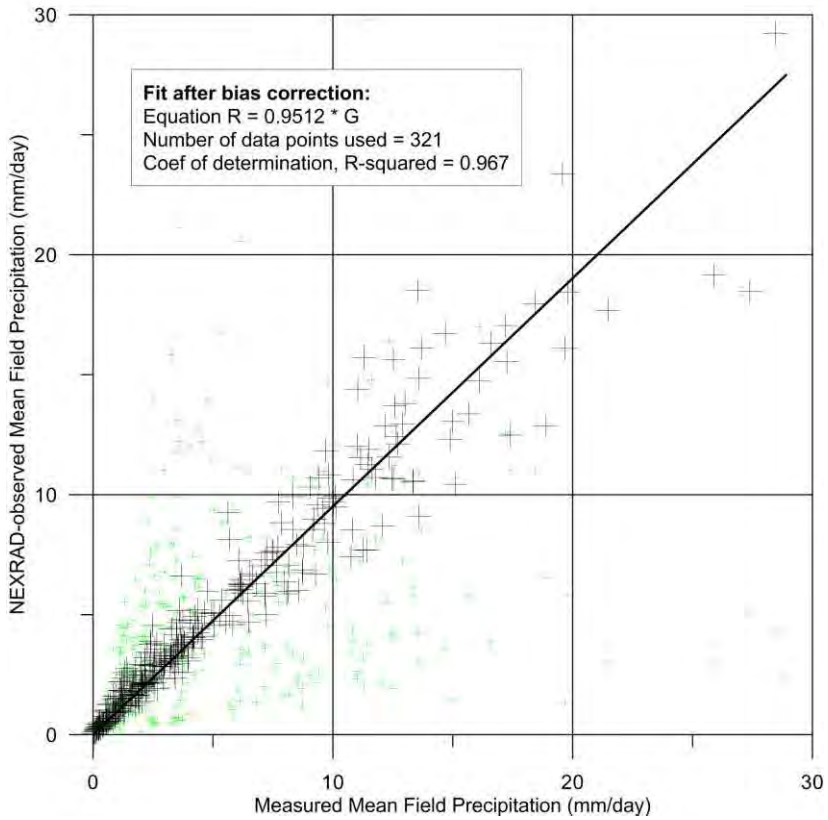

Figure A.9: Results of the NEXRAD MFB optimization routine. Mean field precipitation prior to optimization is in green, after optimization in black.

Appendix B Predicted Future Sub-basin Recharge

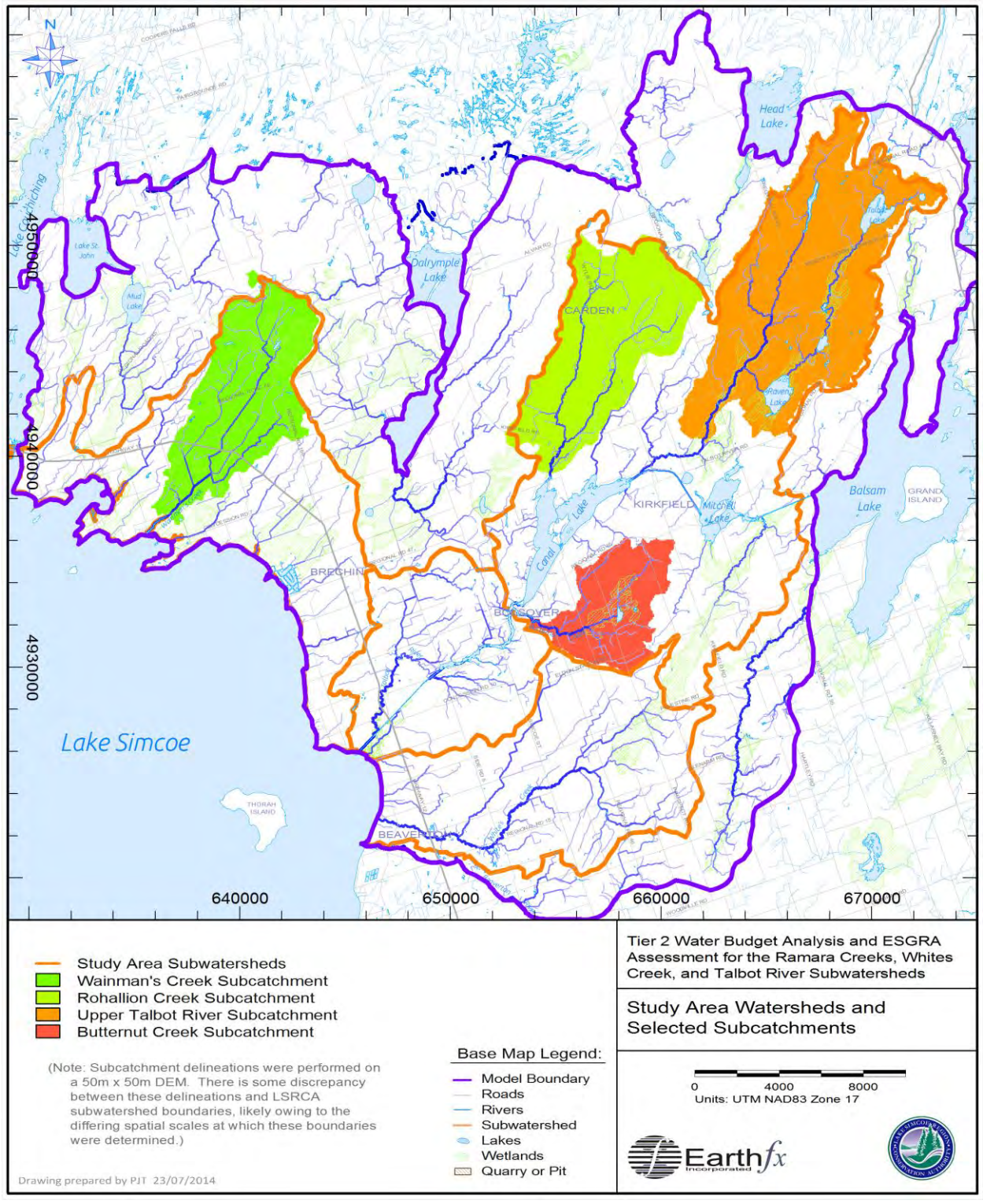

Figure B.1: Study subwatersheds and selected subcatchments.

B.1 Whites Creek Subwatershed

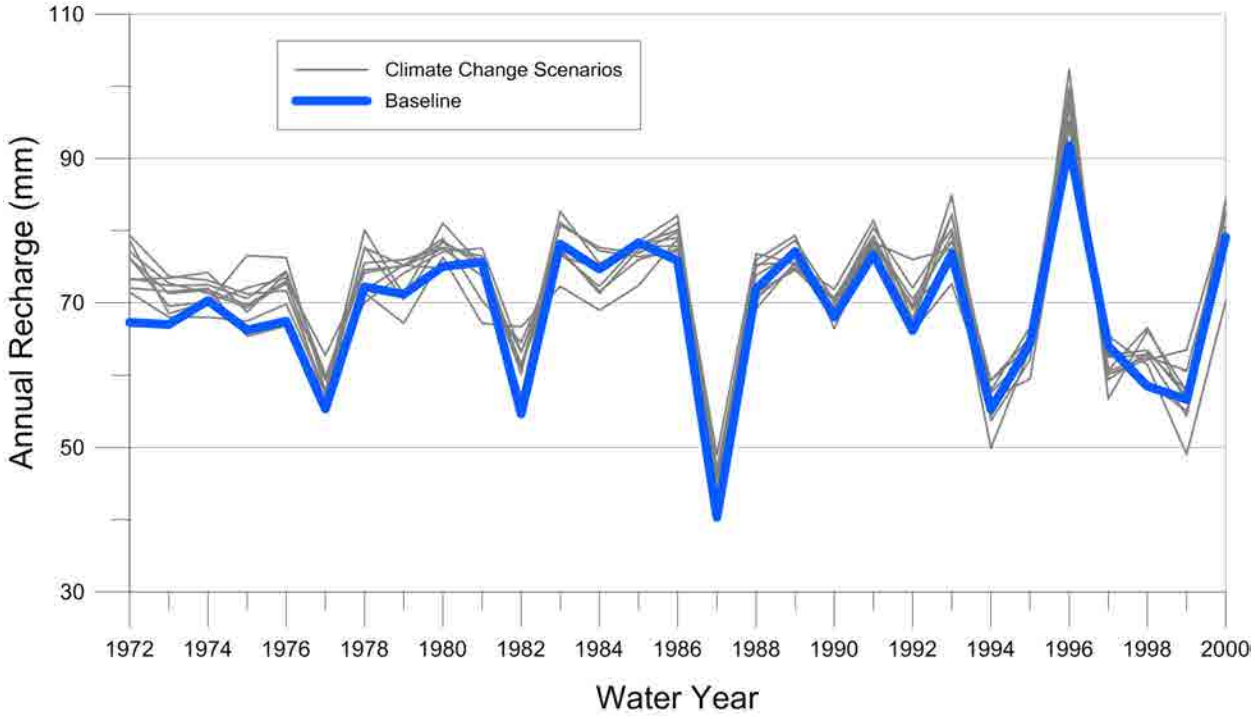

Figure B.2: Average annual simulated basin recharge by water year in the Whites Creek subwatershed.

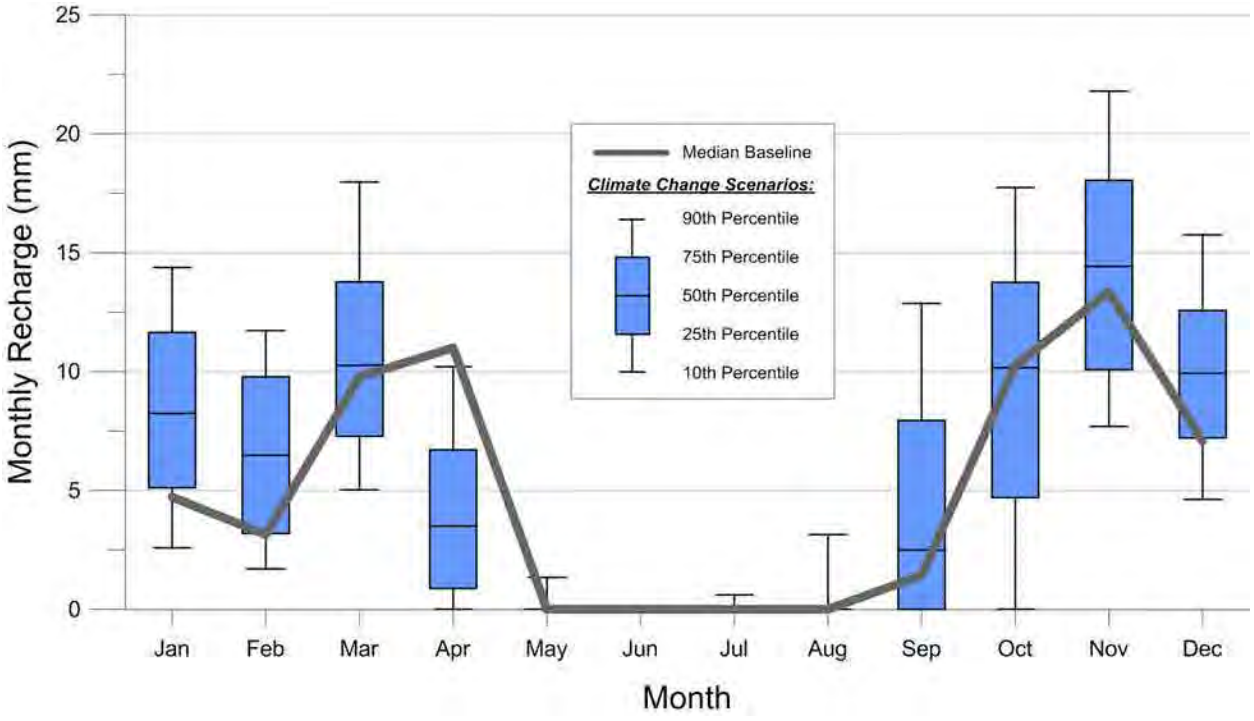

Figure B.3: Monthly simulated basin recharge statistics for the Whites Creek subwatershed.

B.2 Talbot River Subwatershed

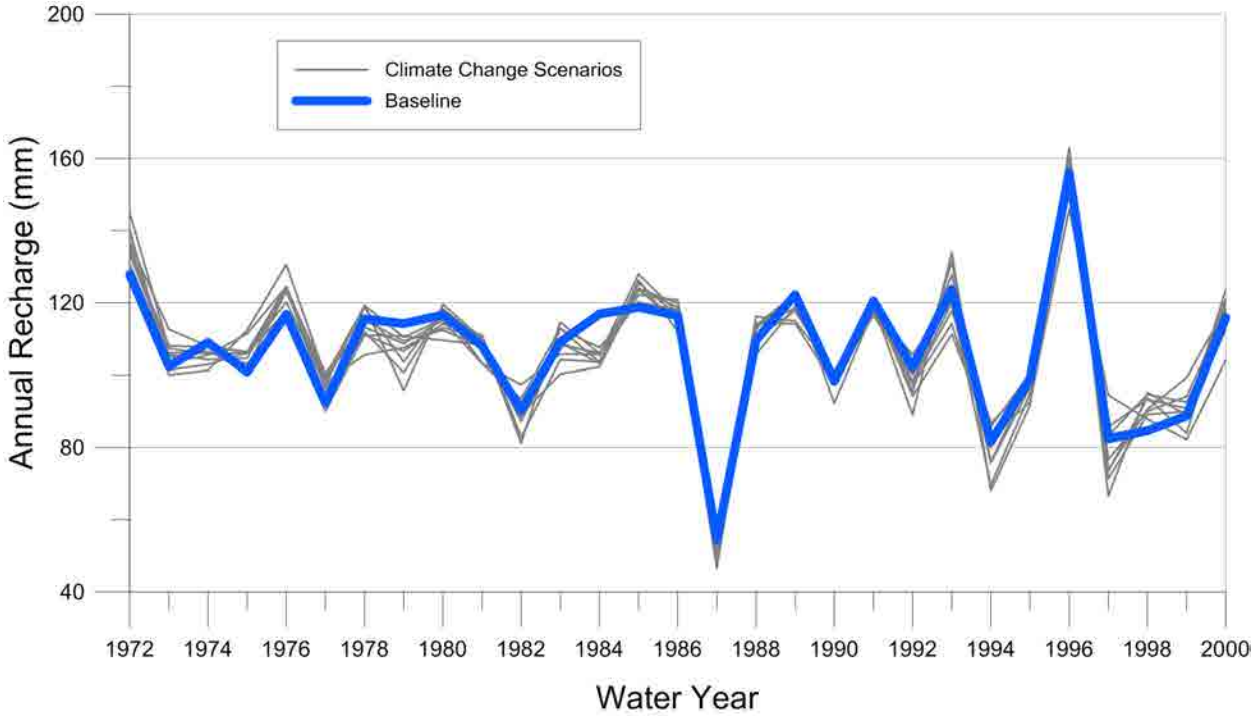

Figure B.4: Average annual simulated basin recharge by water year in the Talbot River subwatershed.

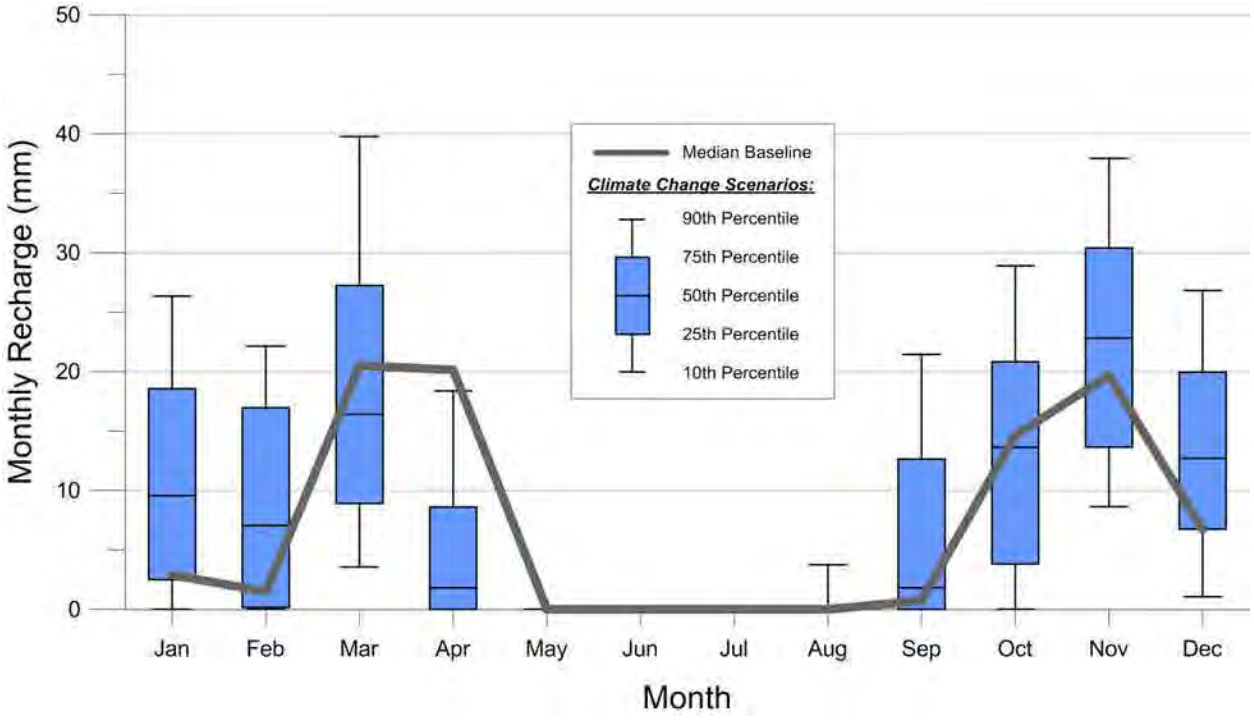

Figure B.5: Monthly simulated basin recharge statistics for the Talbot River subwatershed.

B.3 Ramara Creeks Subwatershed

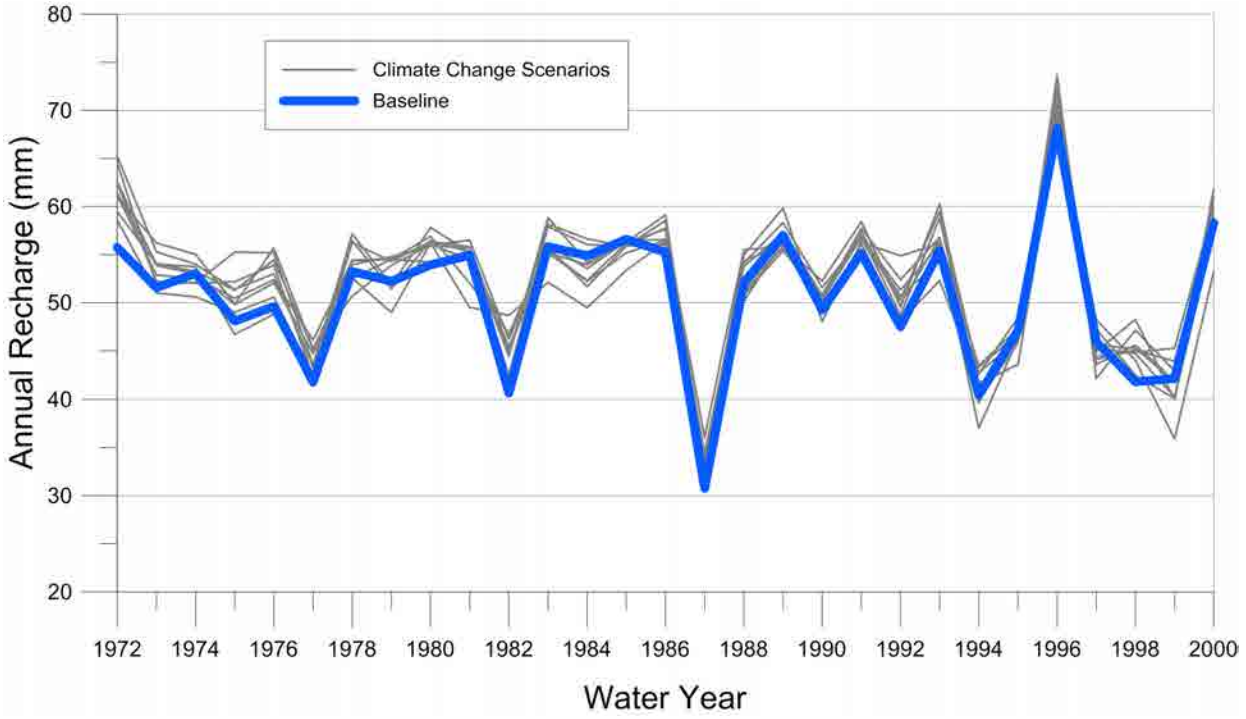

Figure B.6: Average annual simulated basin recharge by water year in the Ramara Creeks subwatershed.

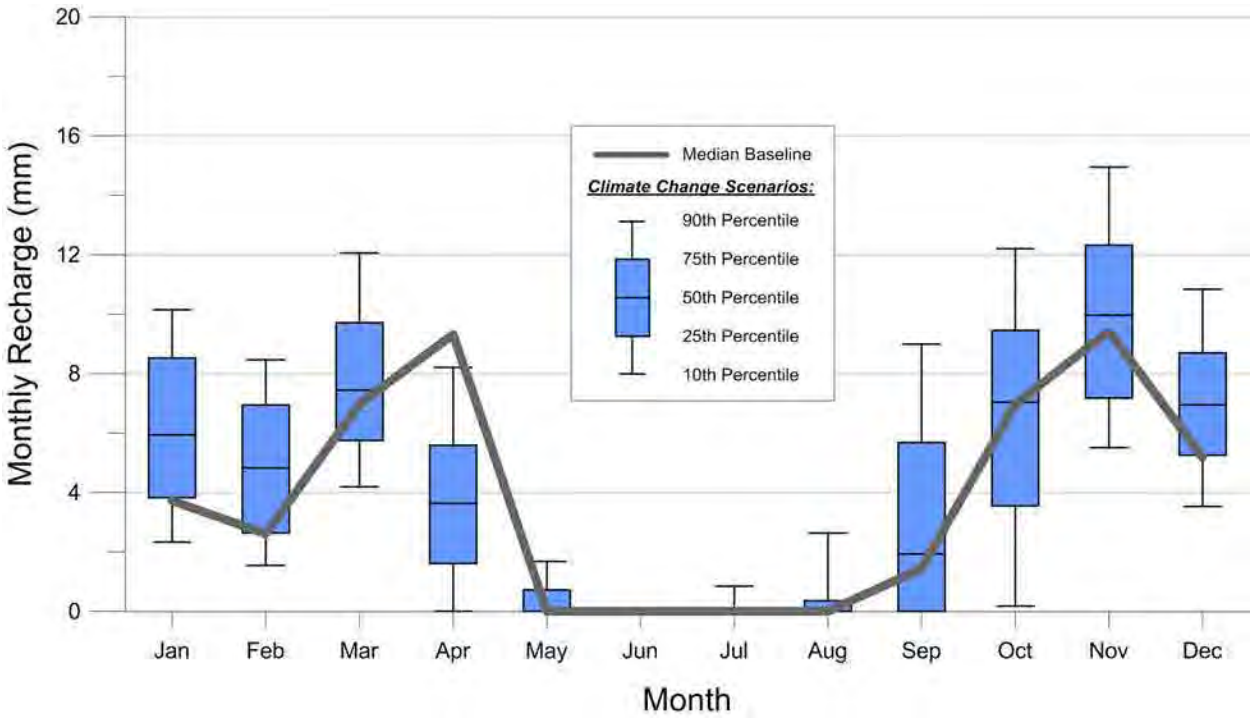

Figure B.7: Monthly simulated basin recharge statistics for the Ramara Creeks subwatershed.

B.4 Rohallion Creek Subcatchment

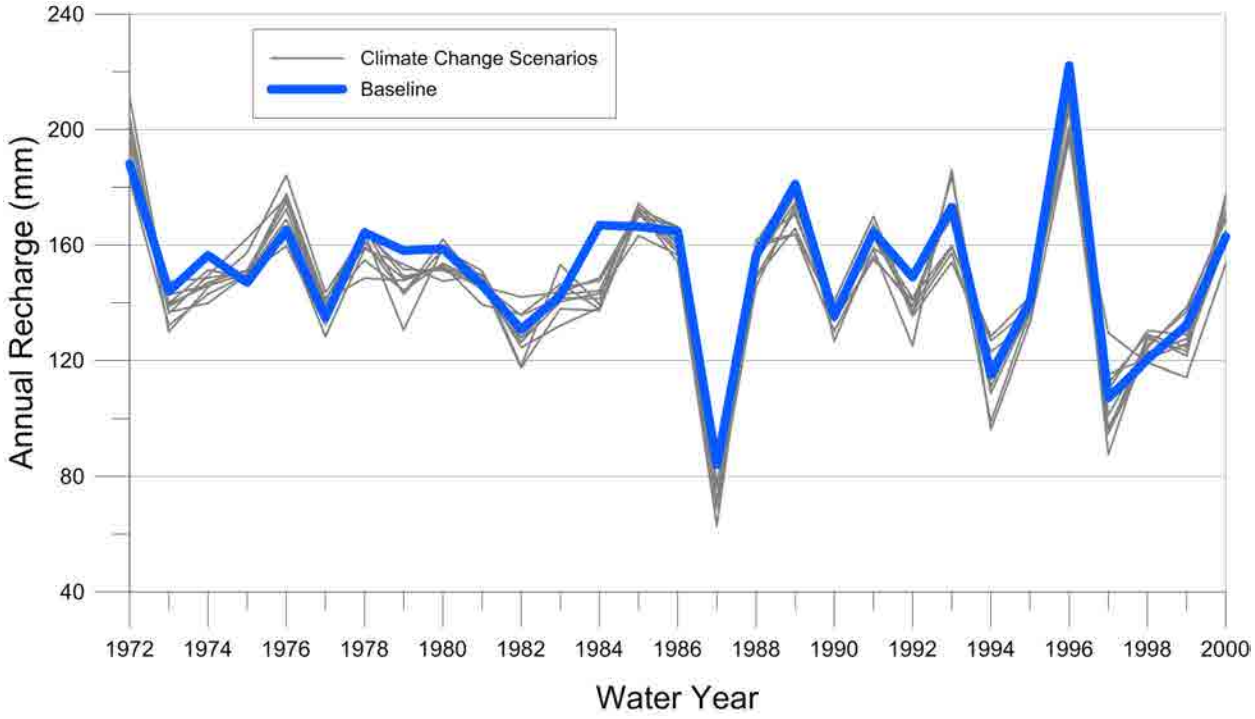

Figure B.8: Average annual simulated basin recharge by water year in the Rohallion Creek subcatchment.

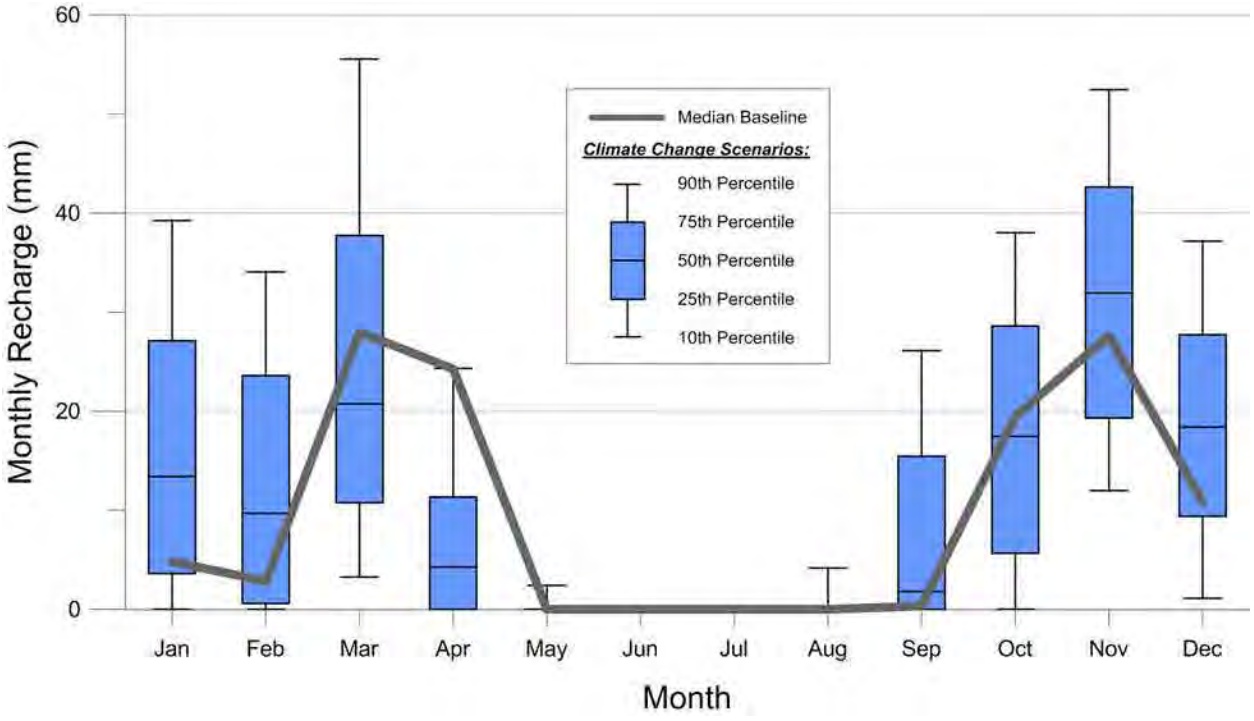

Figure B.9: Monthly simulated basin recharge statistics for the Rohallion Creek subcatchment.

B.5 Upper Talbot River Subcatchment

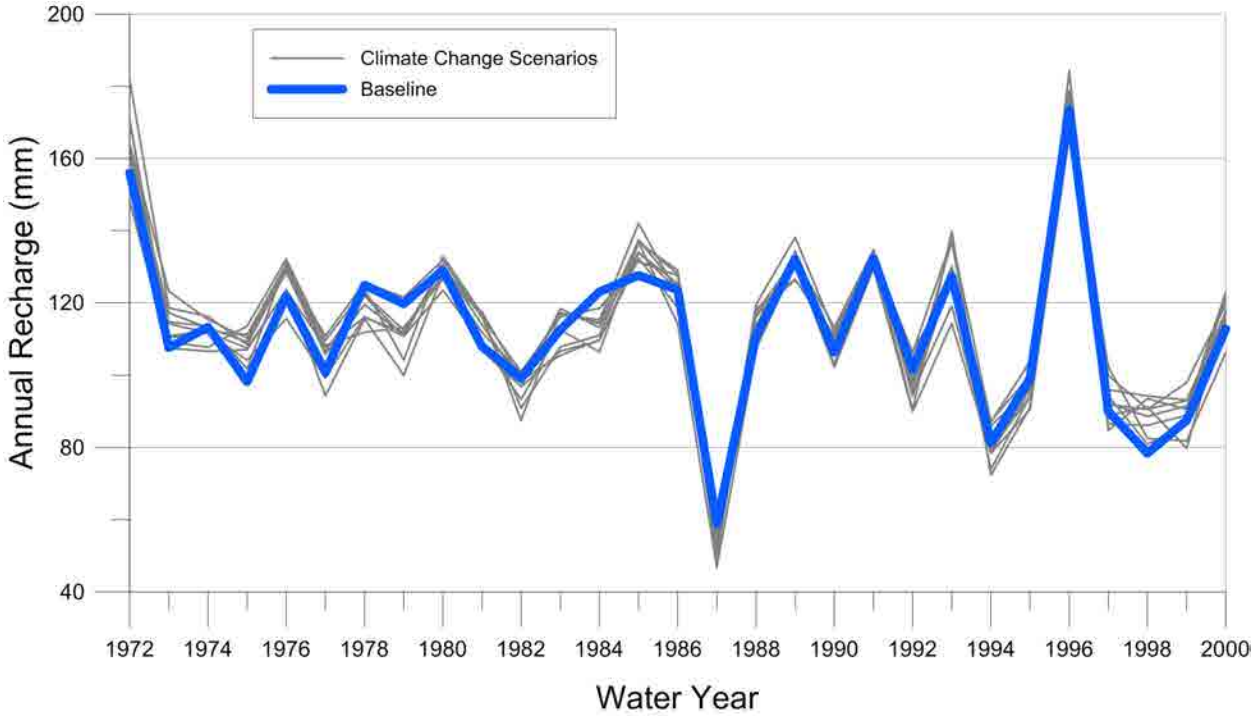

Figure B.10: Average annual simulated basin recharge by water year in the Upper Talbot River subcatchment.

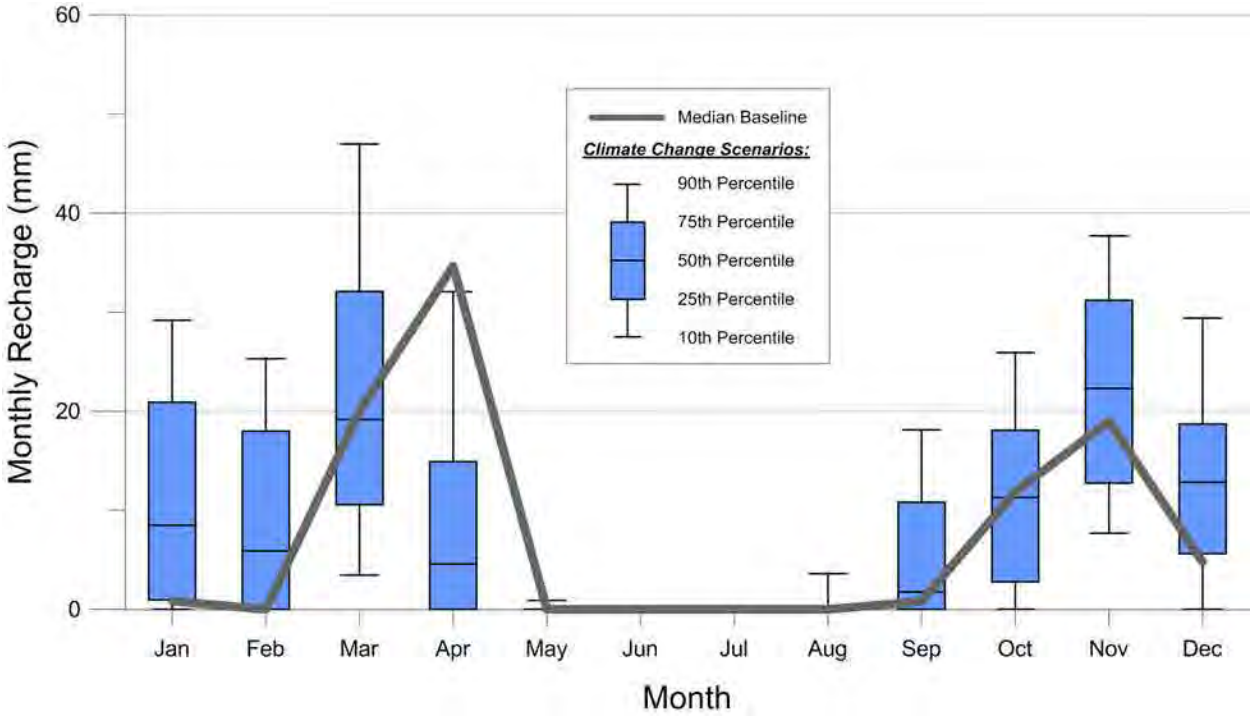

Figure B.11: Monthly simulated basin recharge statistics for the Upper Talbot River subcatchment.

B.6 Butternut Creek Subcatchment

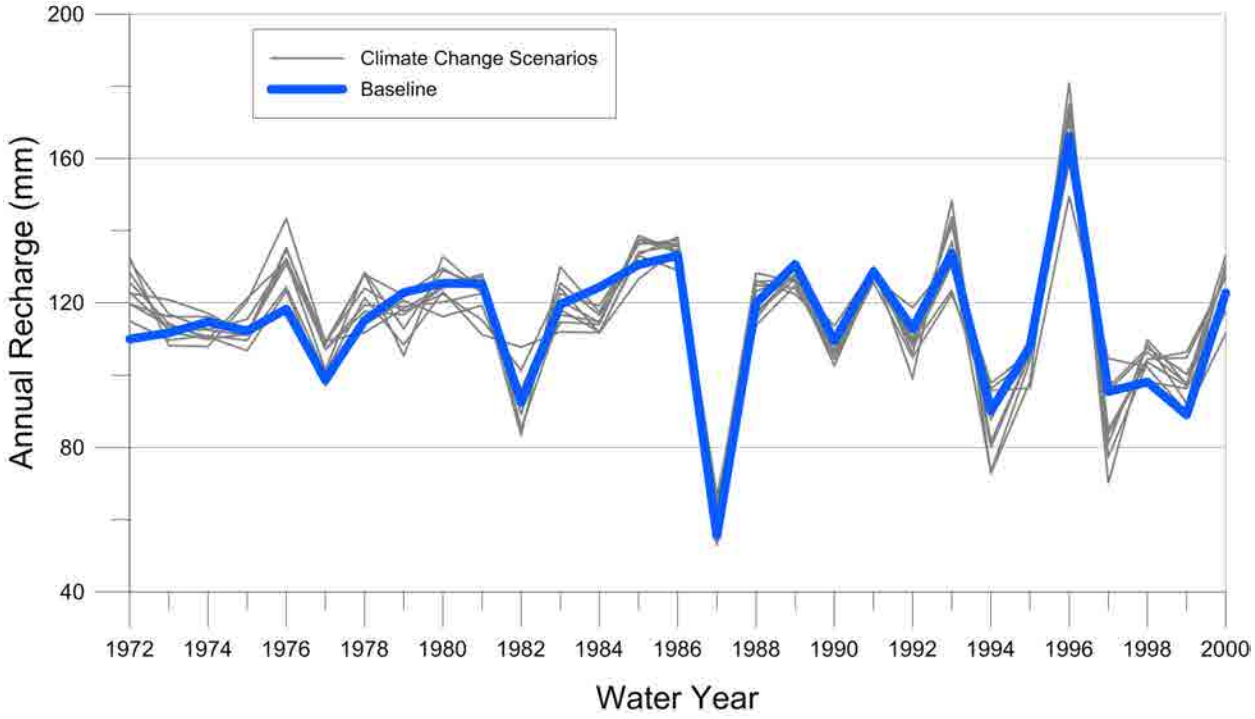

Figure B.12: Average annual simulated basin recharge by water year in the Butternut Creek subcatchment.

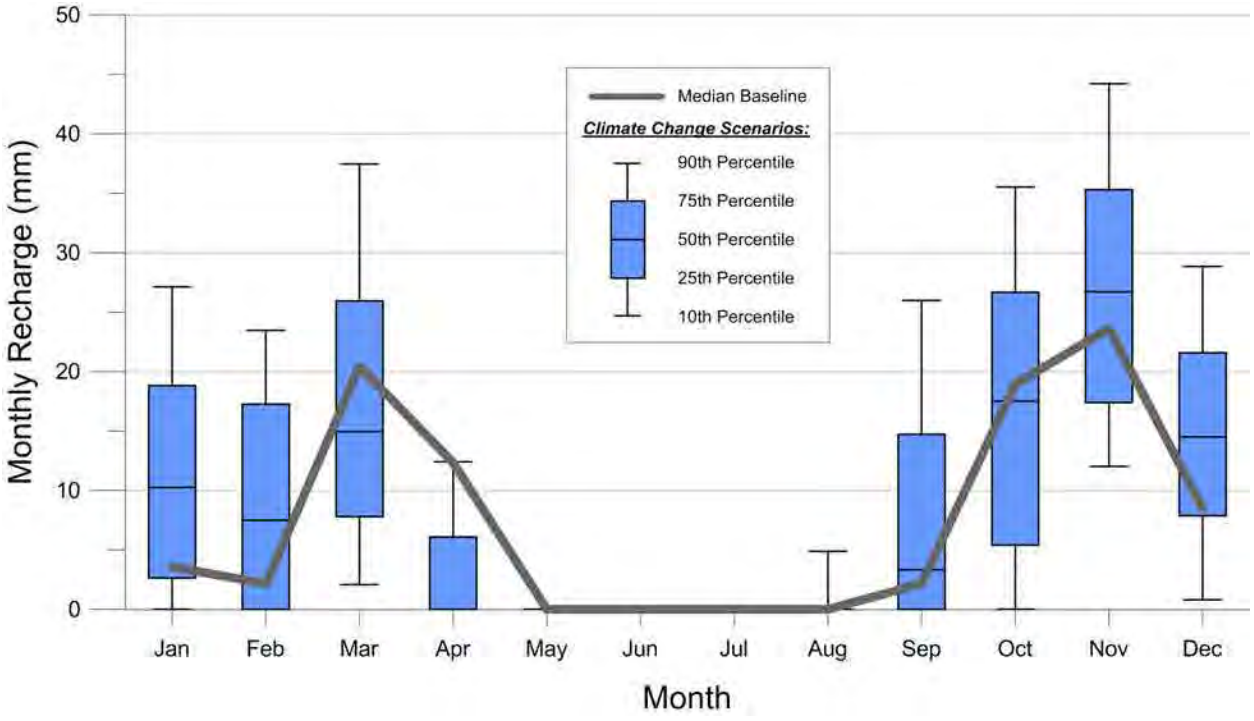

Figure B.13: Monthly simulated basin recharge statistics for the Butternut Creek subcatchment.

B.7 Wainman's Creek Subcatchment

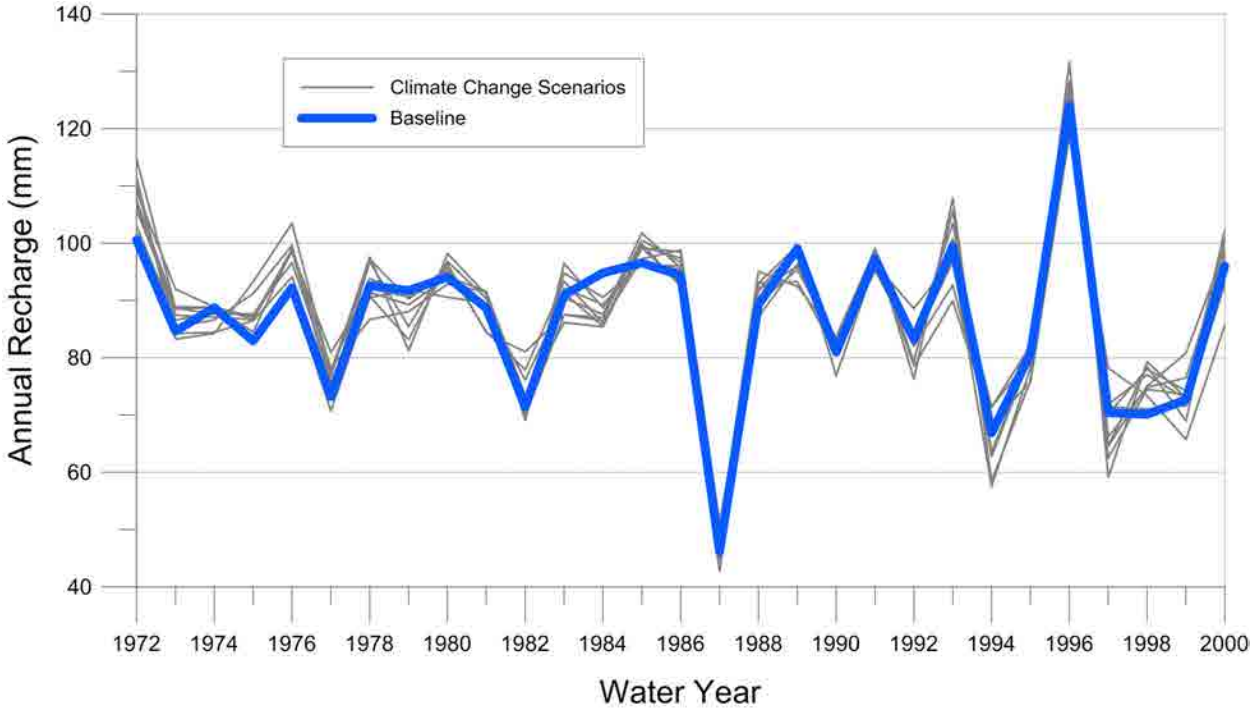

Figure B.14: Average annual simulated basin recharge by water year in the Wainman's Creek subcatchment.

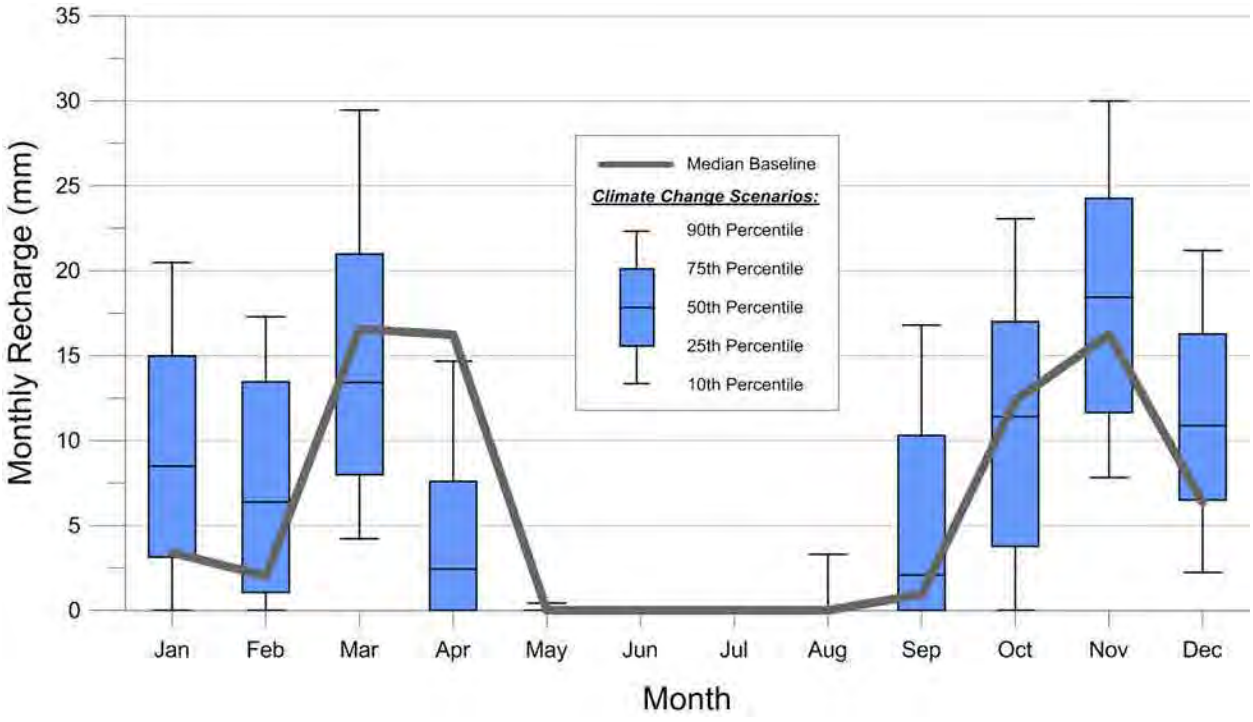

Figure B.15: Monthly simulated basin recharge statistics for the Wainman's Creek subcatchment.

Appendix C Predicted Future Groundwater Levels

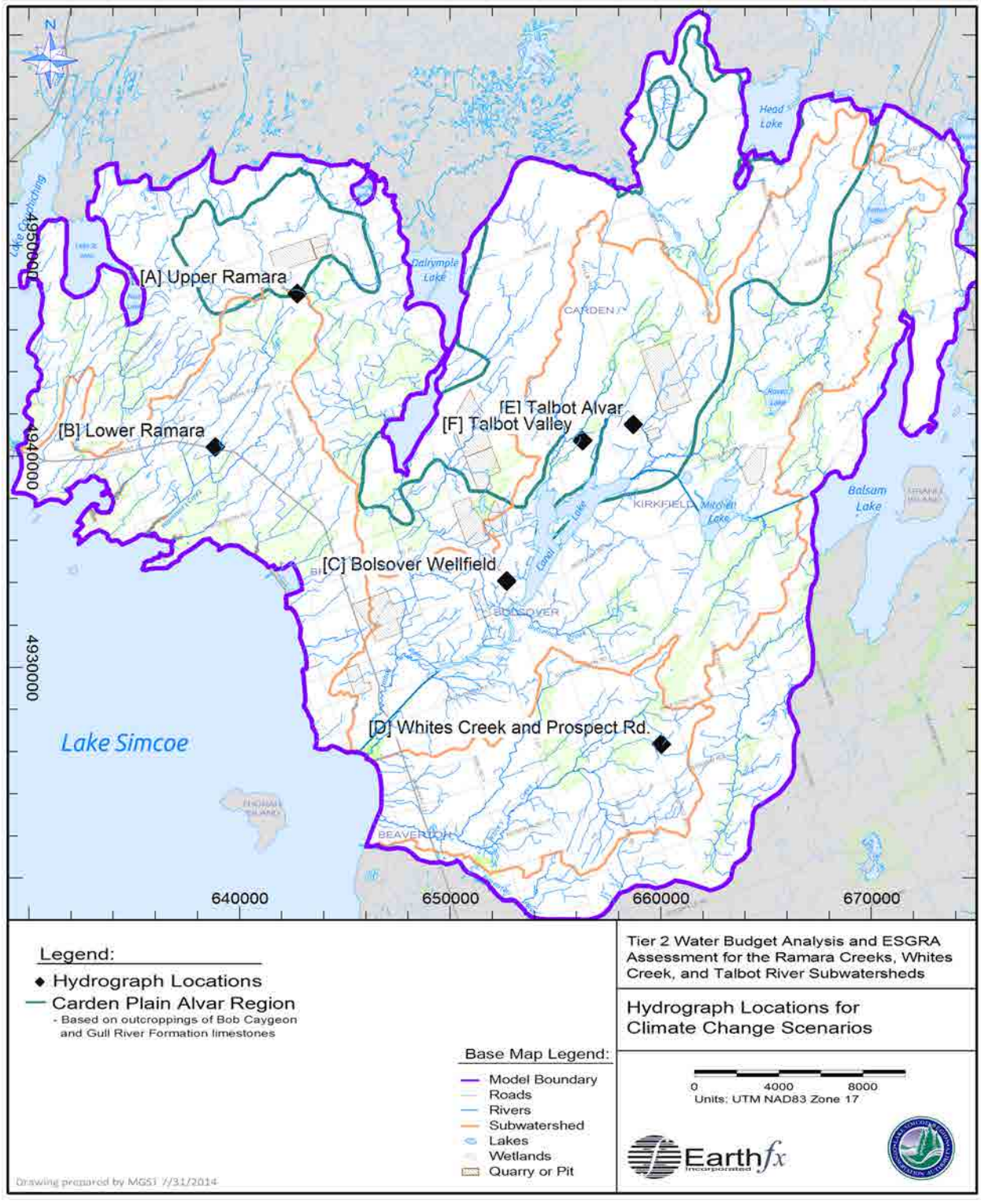

Figure C.1: Simulated groundwater level inspection points.

C.1 Location A – Upper Ramara

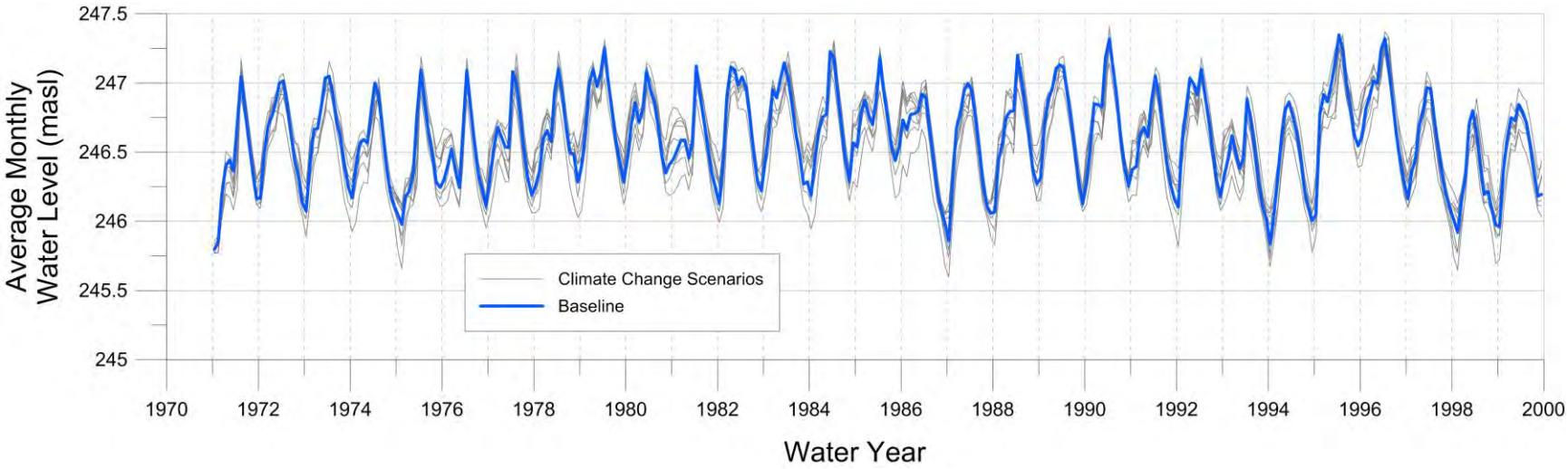

Figure C.2: Simulated monthly average groundwater level by water year at Location A (layer 3).

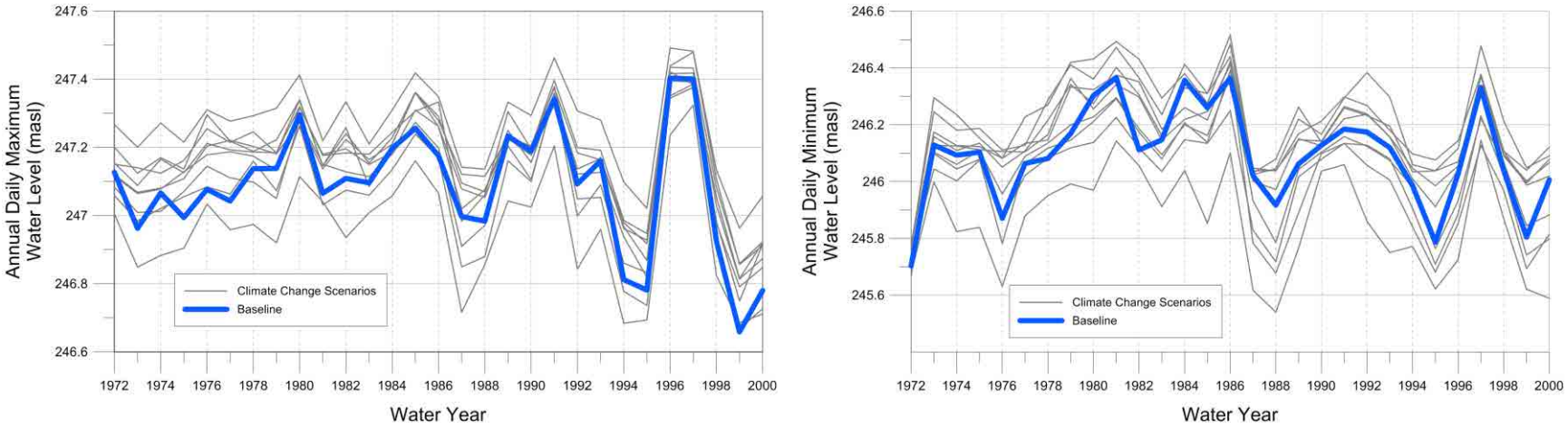

Figure C.3: Simulated maximum (left) and minimum (right) annual groundwater levels at Location A (layer 3).

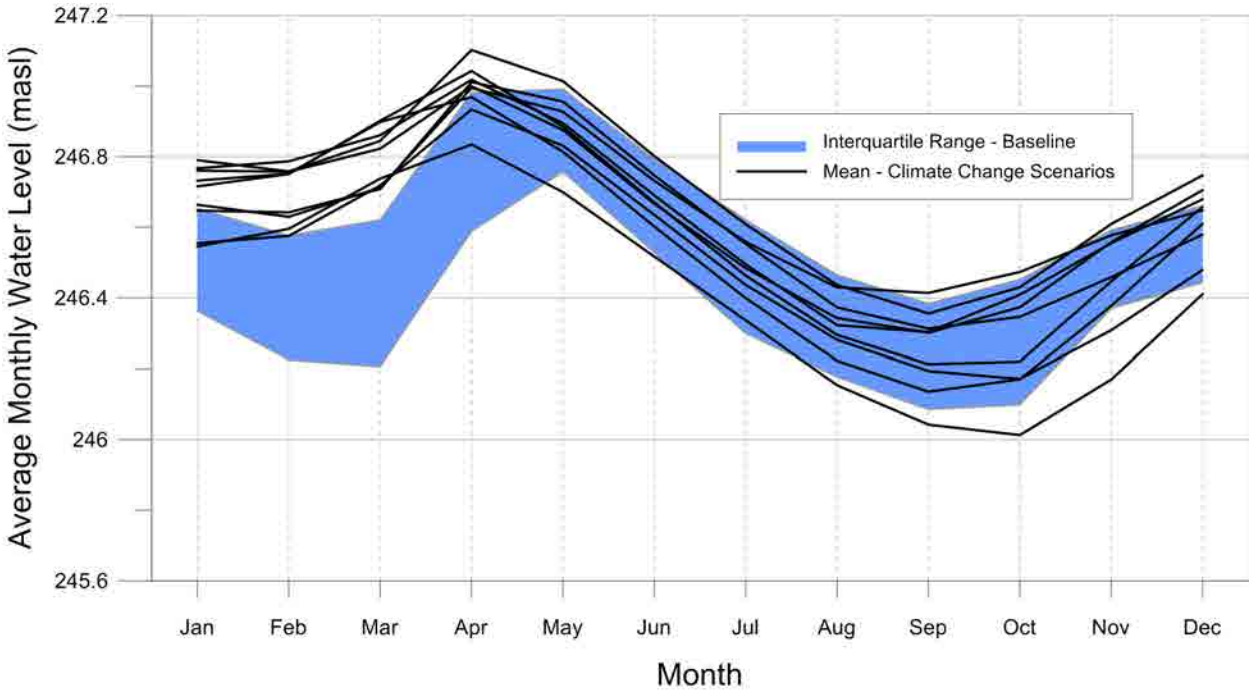

Figure C.4: Average simulated monthly groundwater levels at Location A (layer 3).

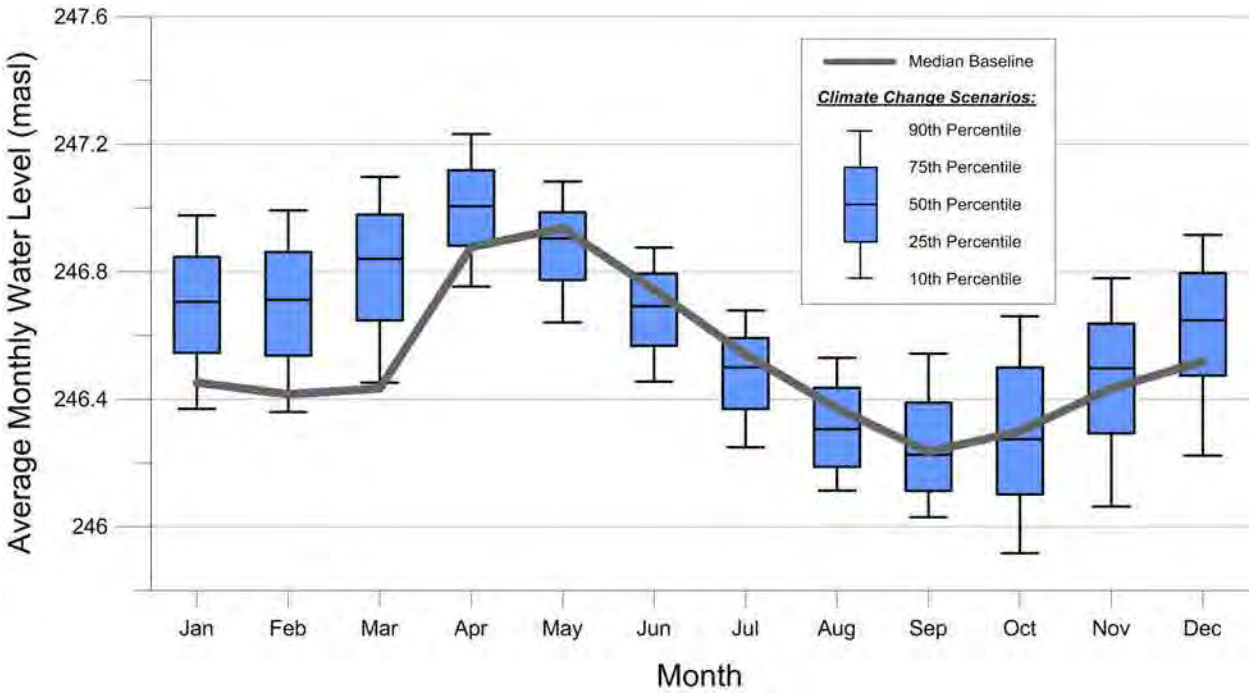

Figure C.5: Monthly simulated groundwater level statistics for Location A (layer 3).

C.2 Location B – Lower Ramara

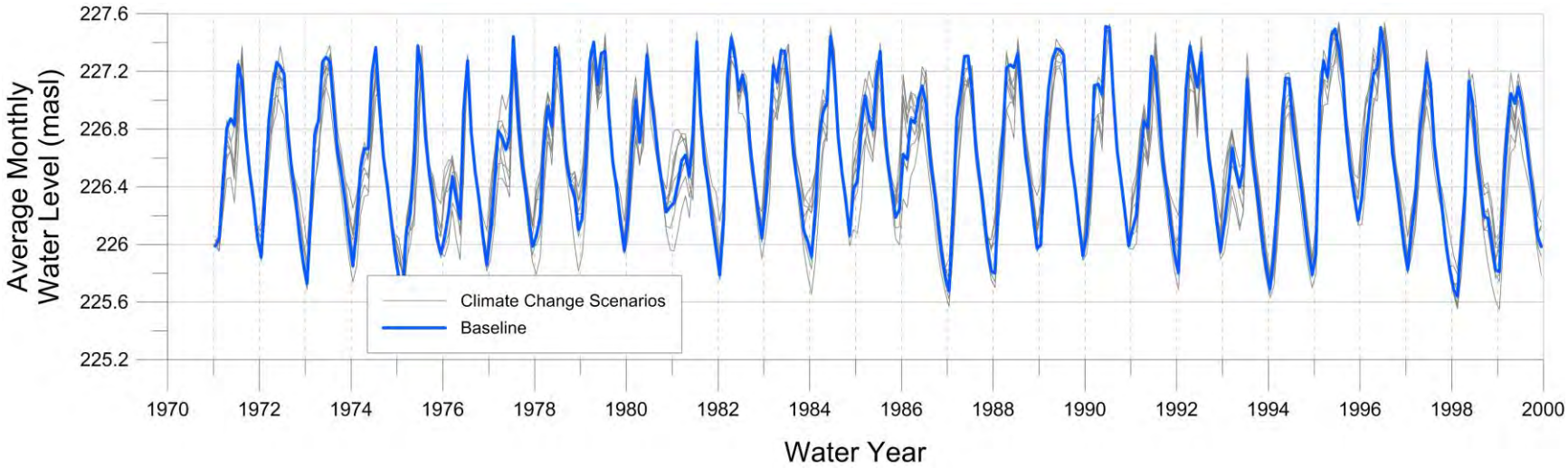

Figure C.6: Simulated monthly average groundwater level by water year at Location B (layer 3).

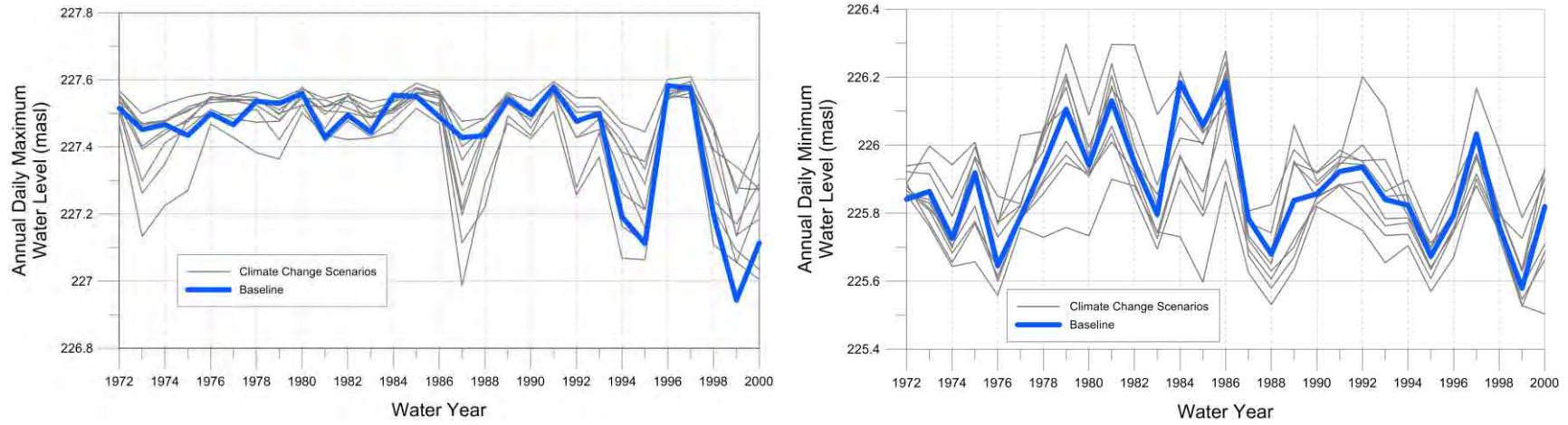

Figure C.7: Simulated maximum (left) and minimum (right) annual groundwater levels at Location B (layer 3).

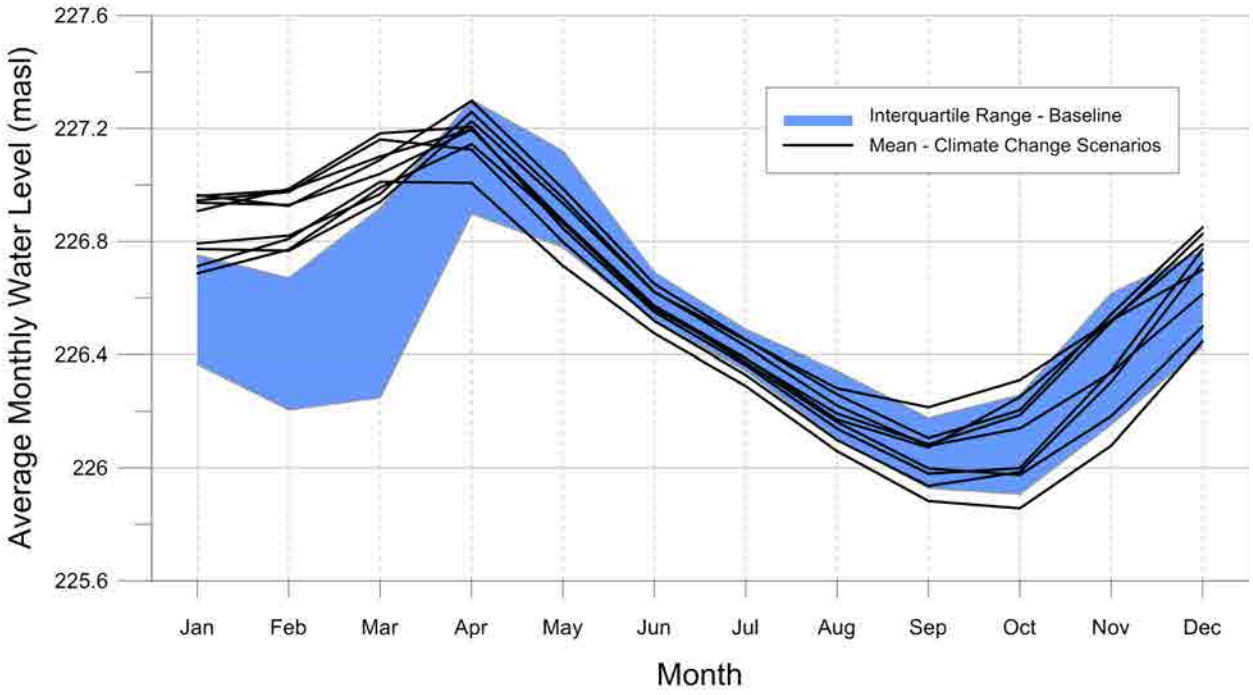

Figure C.8: Average simulated monthly groundwater levels at Location B (layer 3).

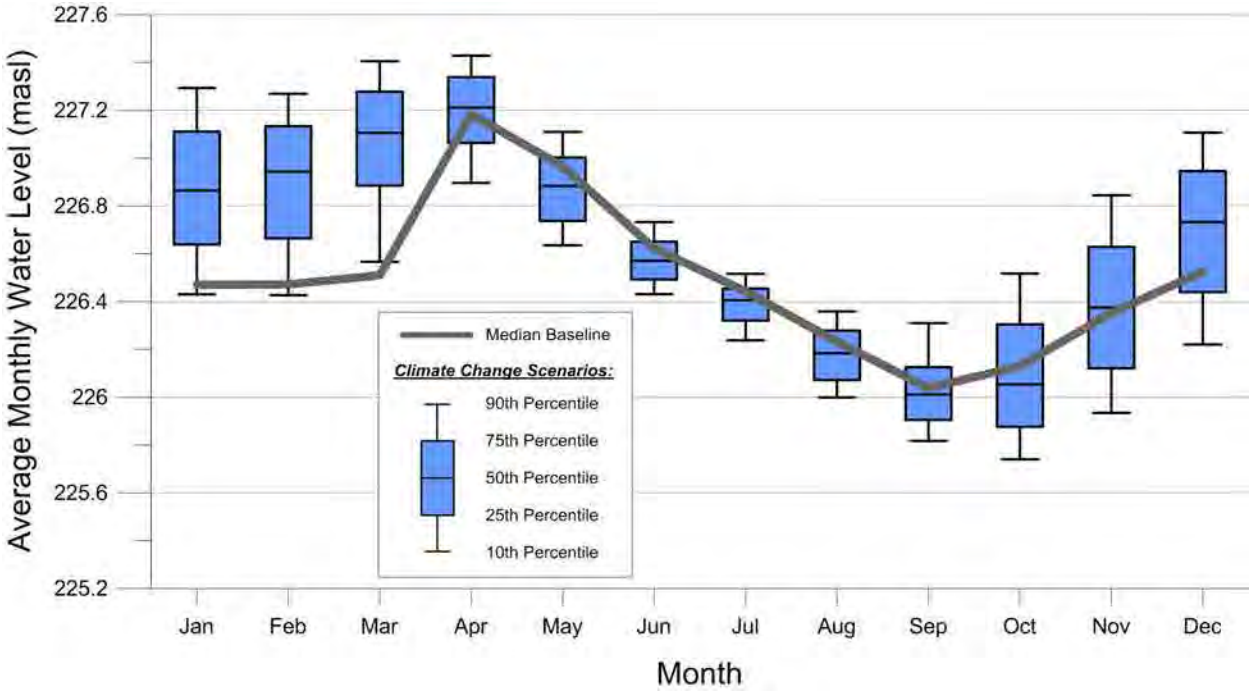

Figure C.9: Monthly simulated groundwater level statistics for Location B (layer 3).

C.3 Location C – Bolsover Wellfield

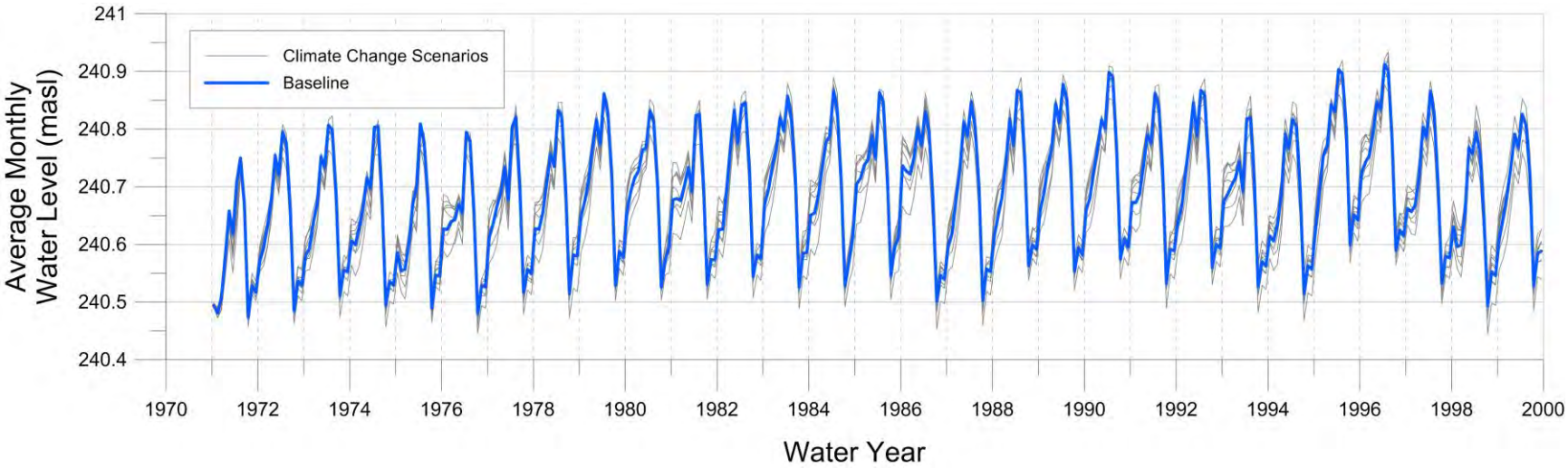

Figure C.10: Simulated monthly average groundwater level by water year at Location C (layer 7).

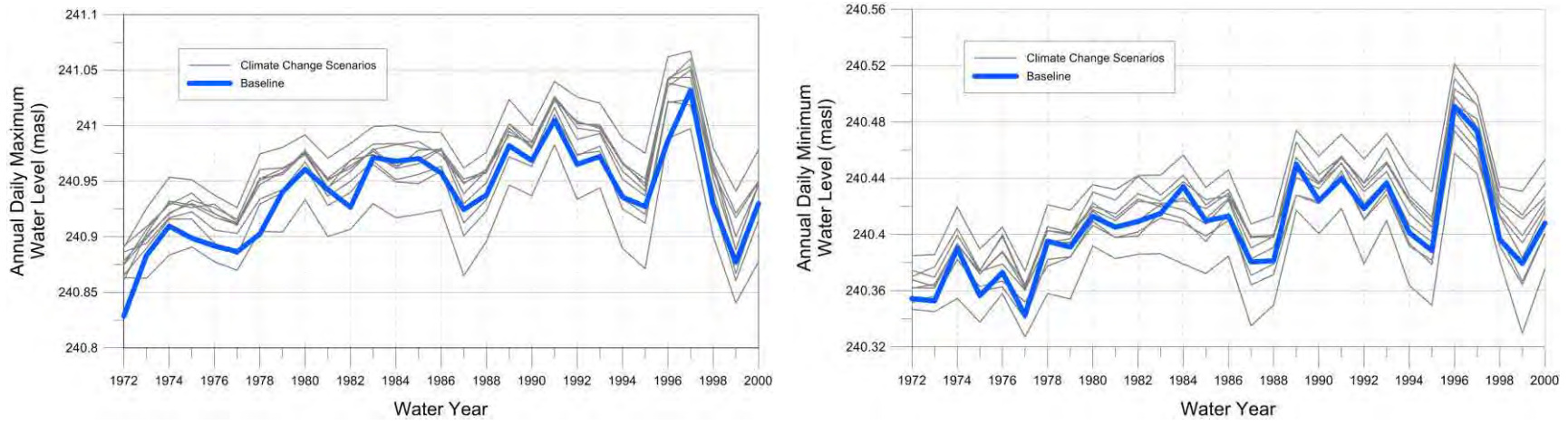

Figure C.11: Simulated maximum (left) and minimum (right) annual groundwater levels at Location C (layer 7).

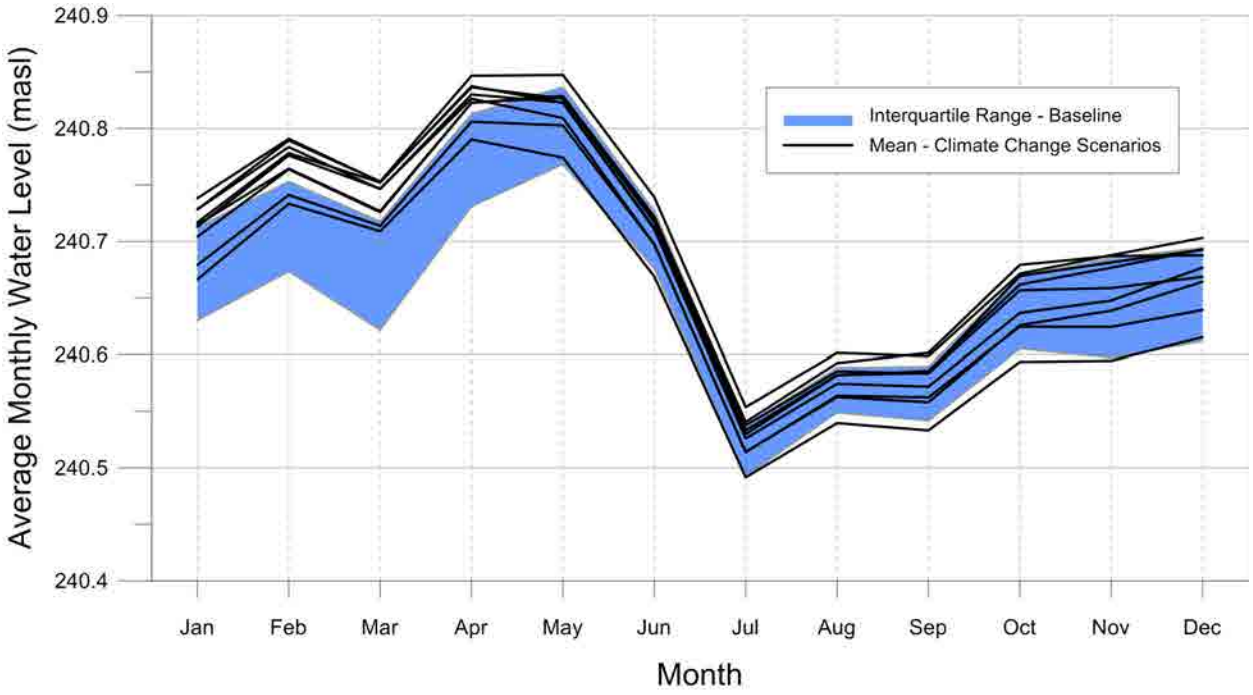

Figure C.12: Average simulated monthly groundwater levels at Location C (layer 7).

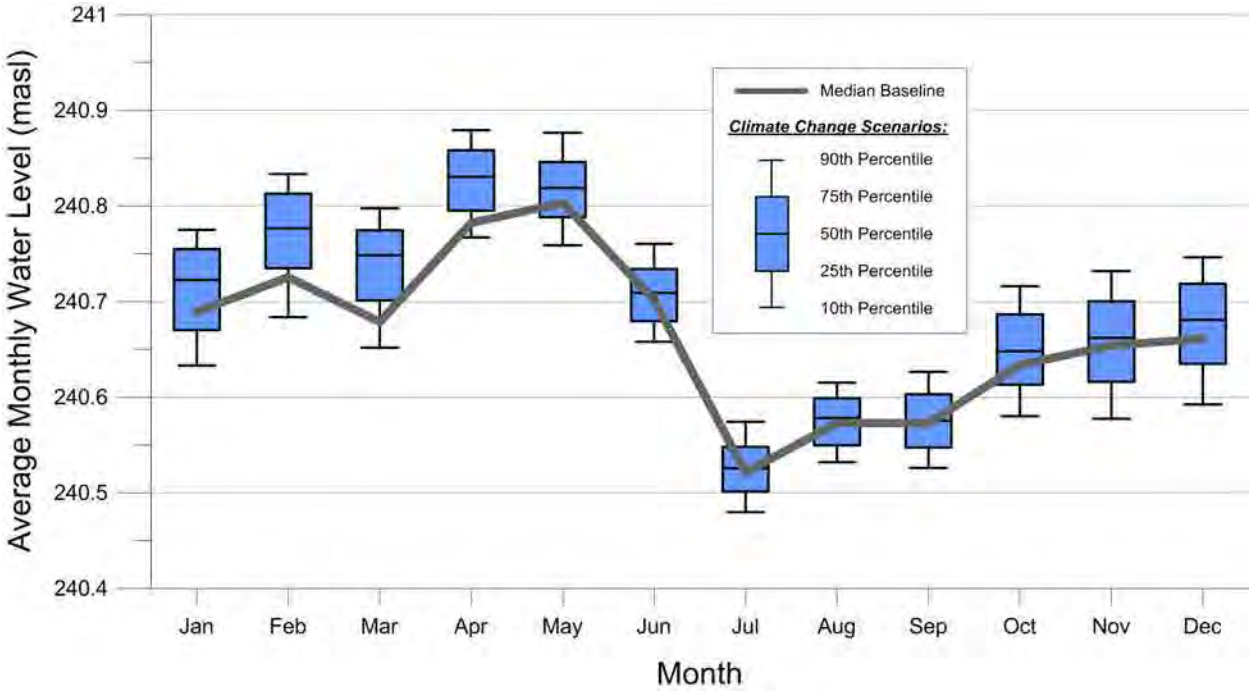

Figure C.13: Monthly simulated groundwater level statistics for Location C (layer 7).

C.4 Location D – Whites Creek and Prospect Rd.

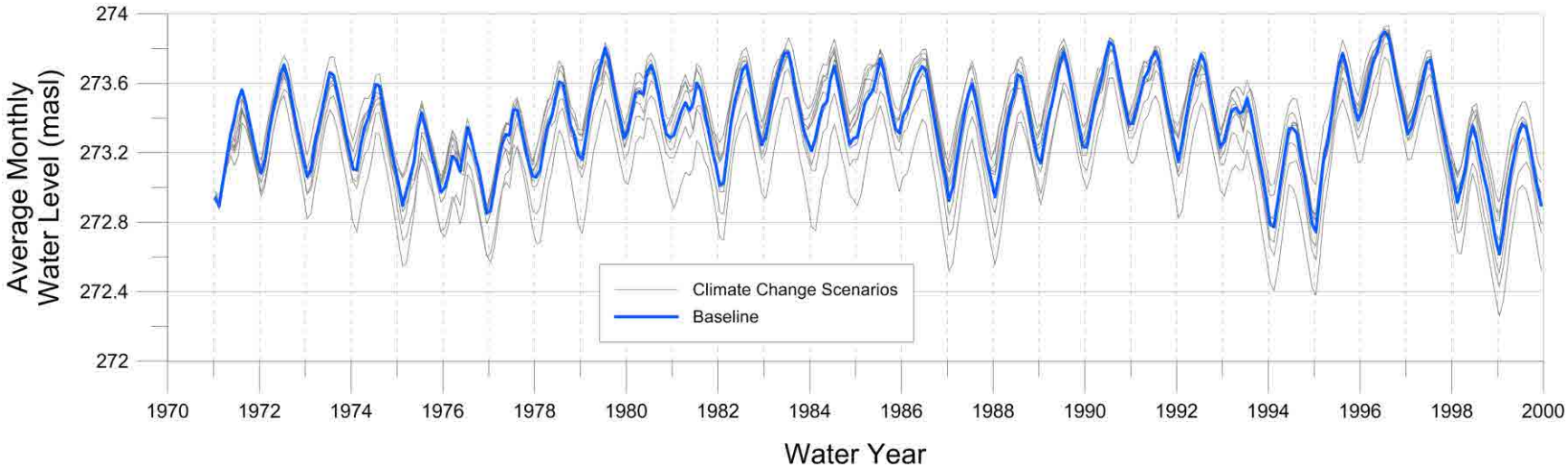

Figure C.14: Simulated monthly average groundwater level by water year at Location D (layer 3).

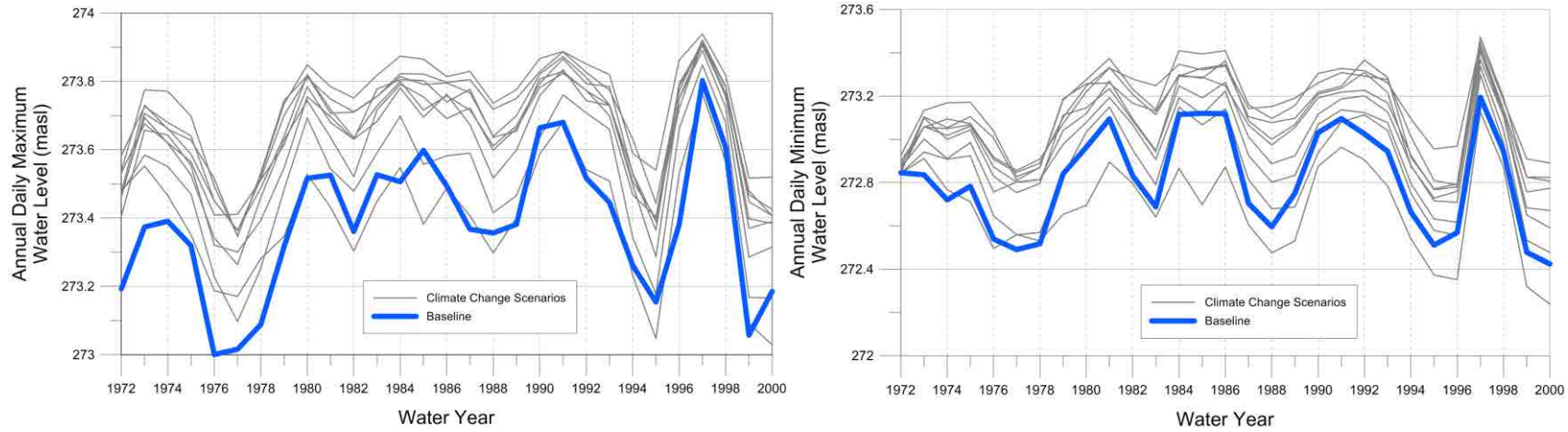

Figure C.15: Simulated maximum (left) and minimum (right) annual groundwater levels at Location D (layer 3).

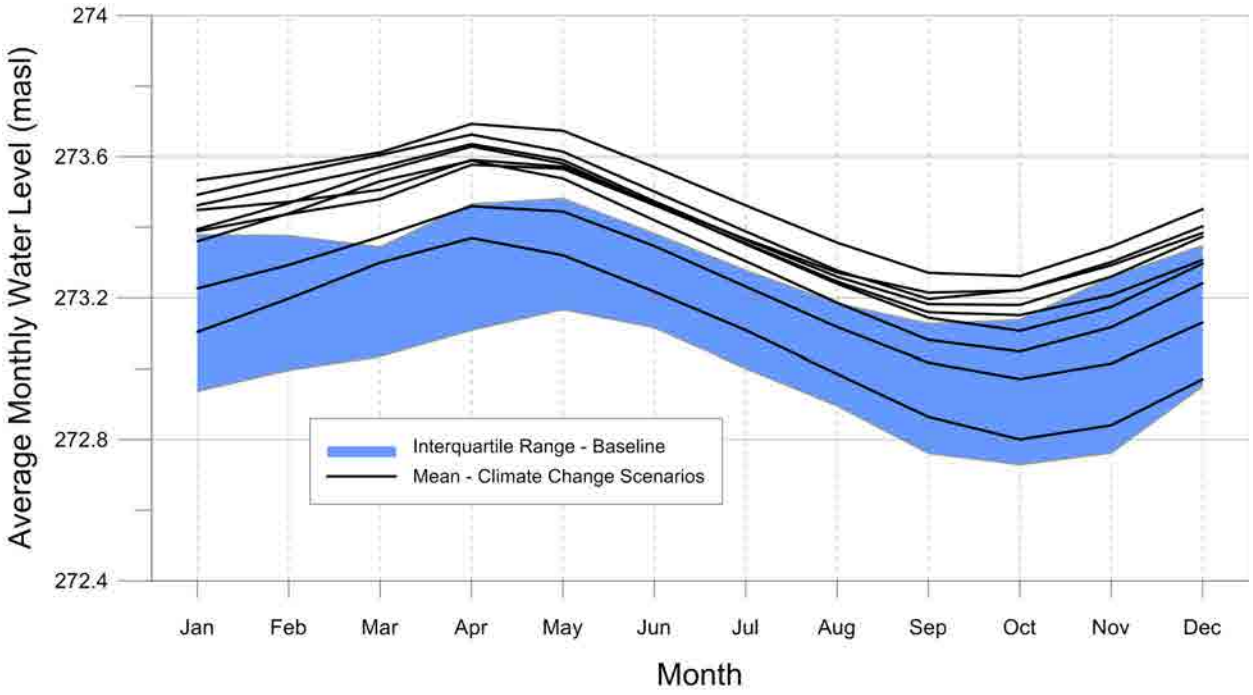

Figure C.16: Average simulated monthly groundwater levels at Location D (layer 3).

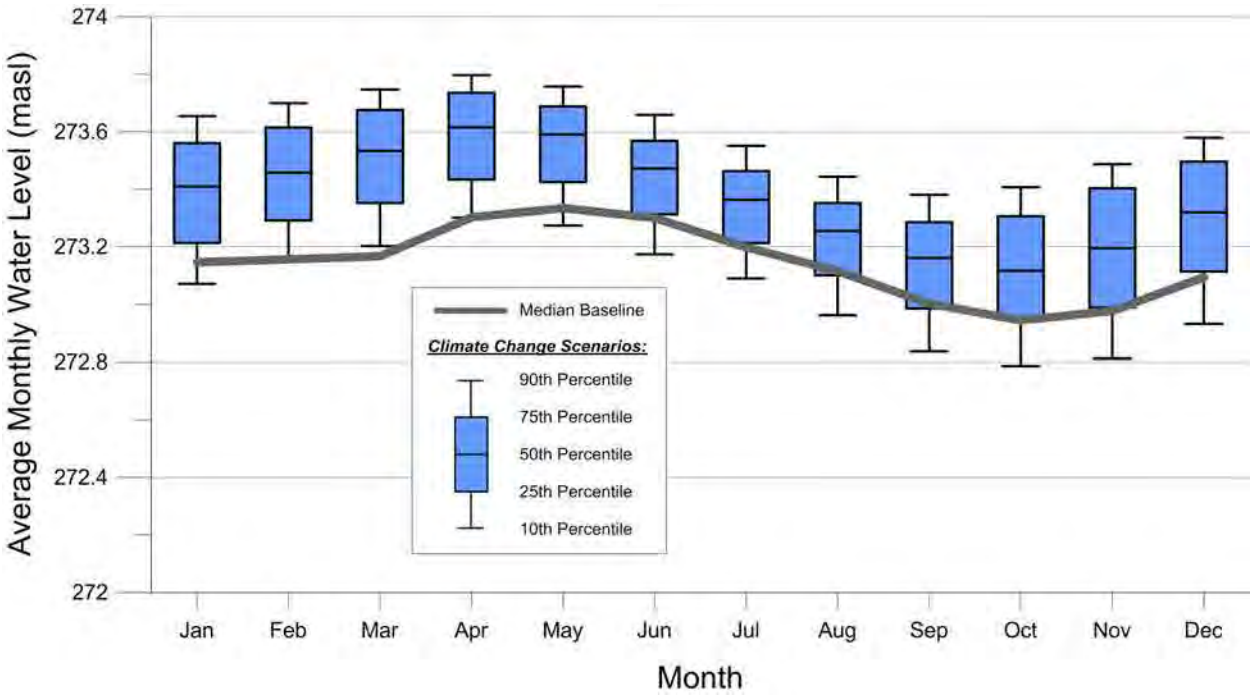

Figure C.17: Monthly simulated groundwater level statistics for Location D (layer 3).

C.5 Location E – Talbot Alvar

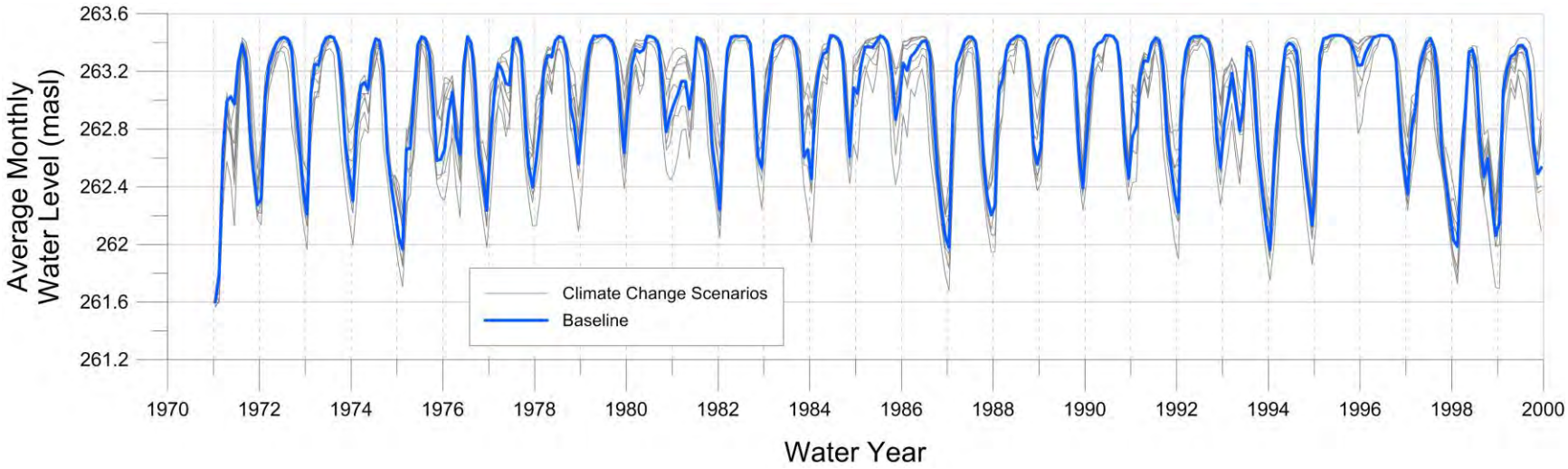

Figure C.18: Simulated monthly average groundwater level by water year at Location E (layer 3).

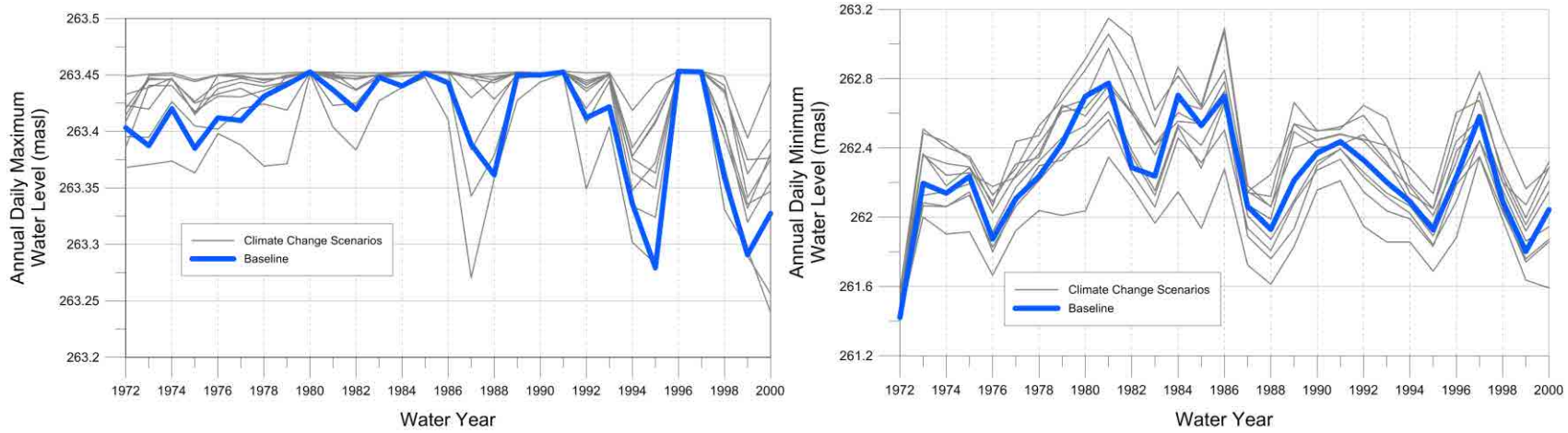

Figure C.19: Simulated maximum (left) and minimum (right) annual groundwater levels at Location E (layer 3).

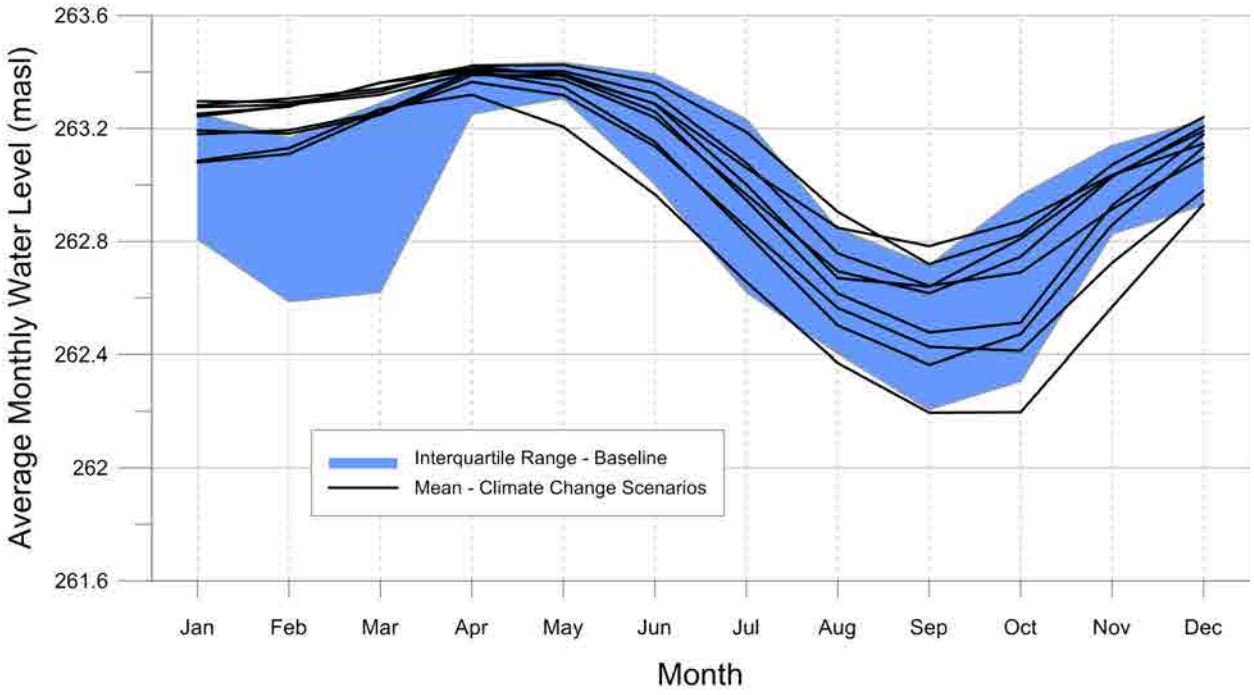

Figure C.20: Average simulated monthly groundwater levels at Location E (layer 3).

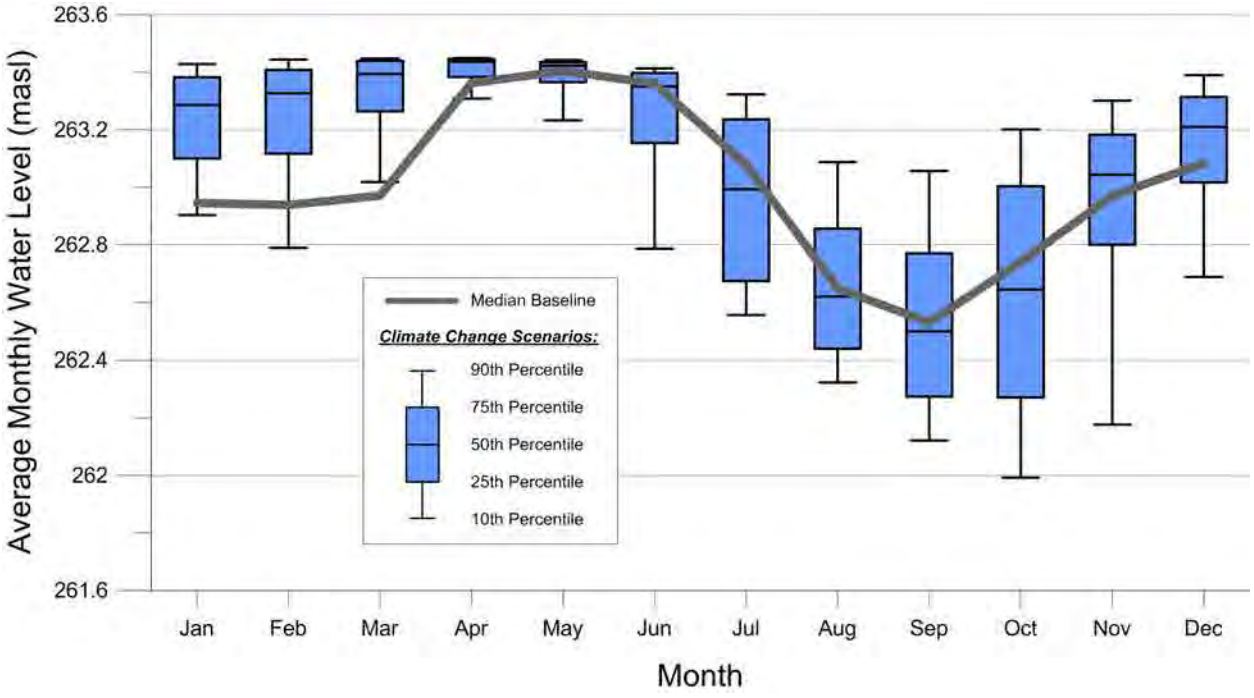

Figure C.21: Monthly simulated groundwater level statistics for Location E (layer 3).

C.6 Location F – Talbot Valley

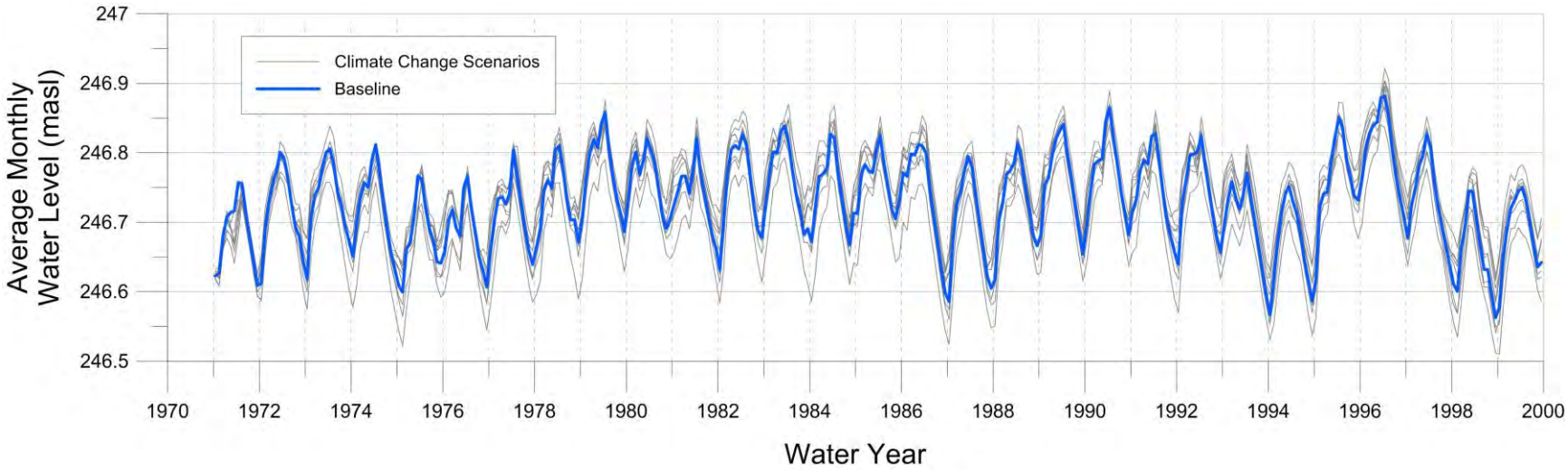

Figure C.22: Simulated monthly average groundwater level by water year at Location F (layer 3).

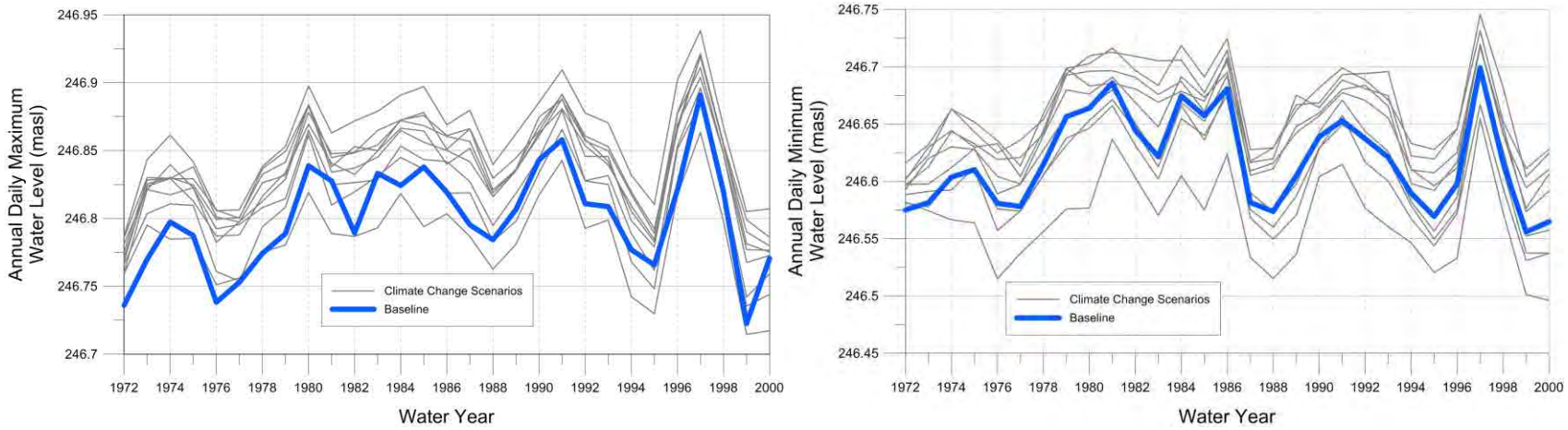

Figure C.23: Simulated maximum (left) and minimum (right) annual groundwater levels at Location F (layer 3).

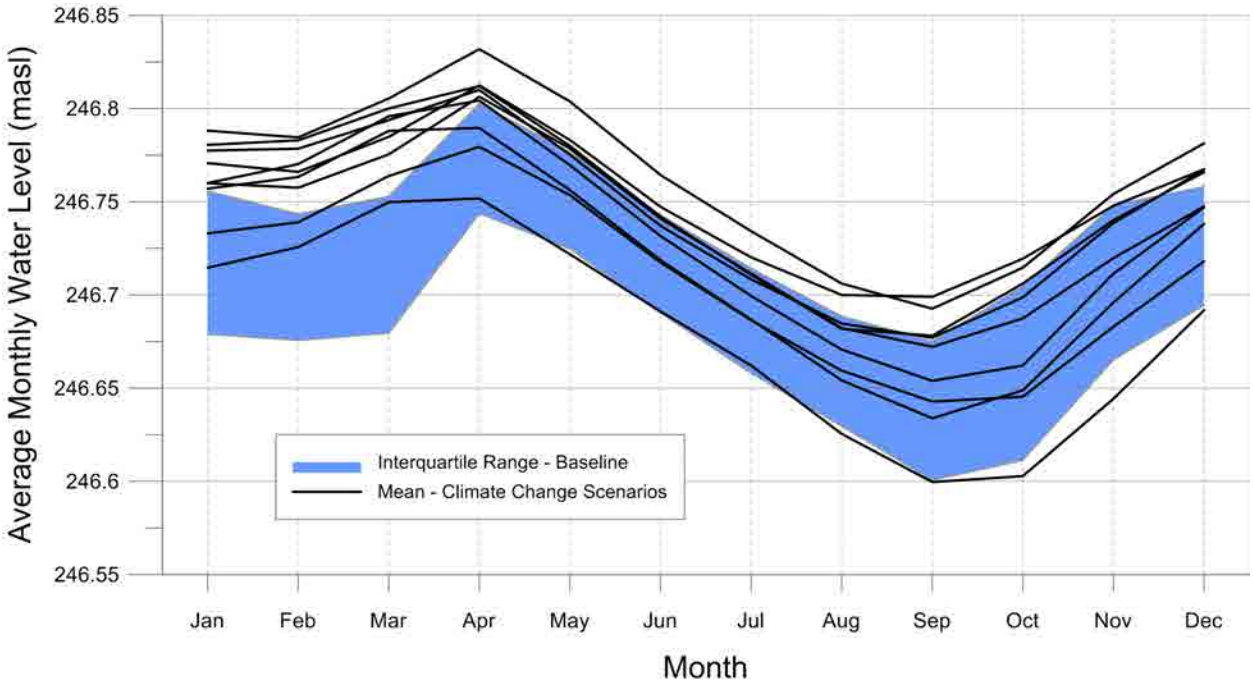

Figure C.24: Average simulated monthly groundwater levels at Location F (layer 3).

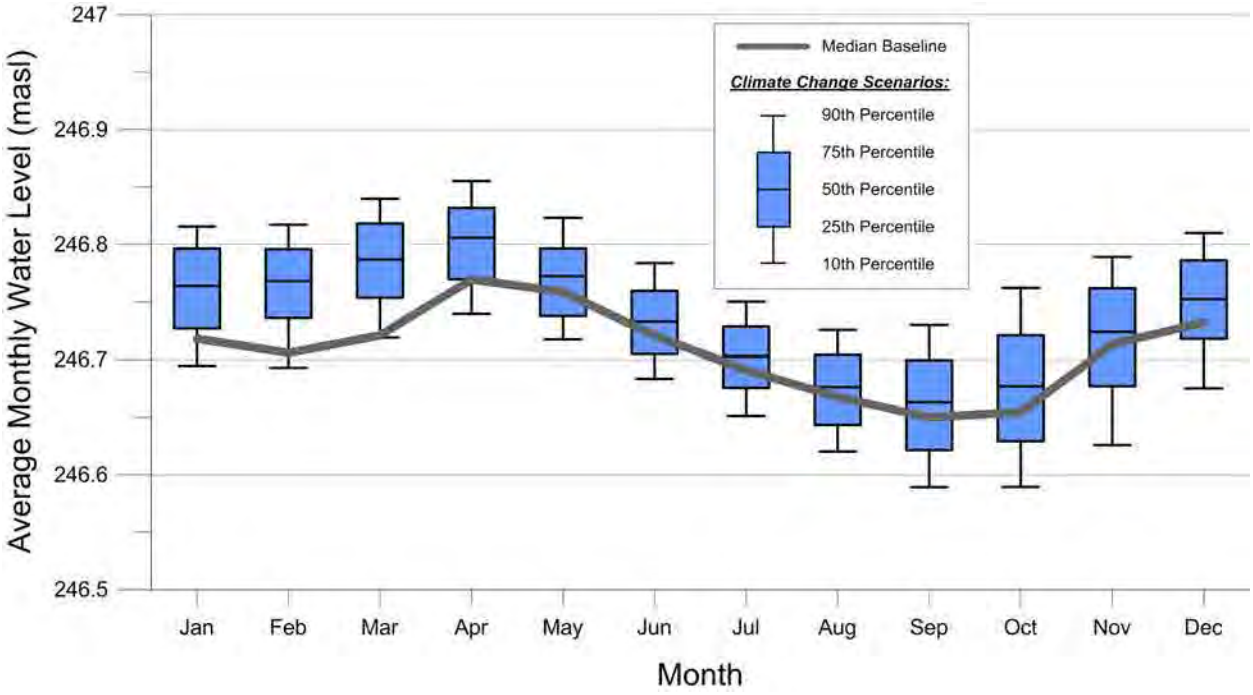

Figure C.25: Monthly simulated groundwater level statistics for Location F (layer 3).

Appendix D Predicted Future Streamflow

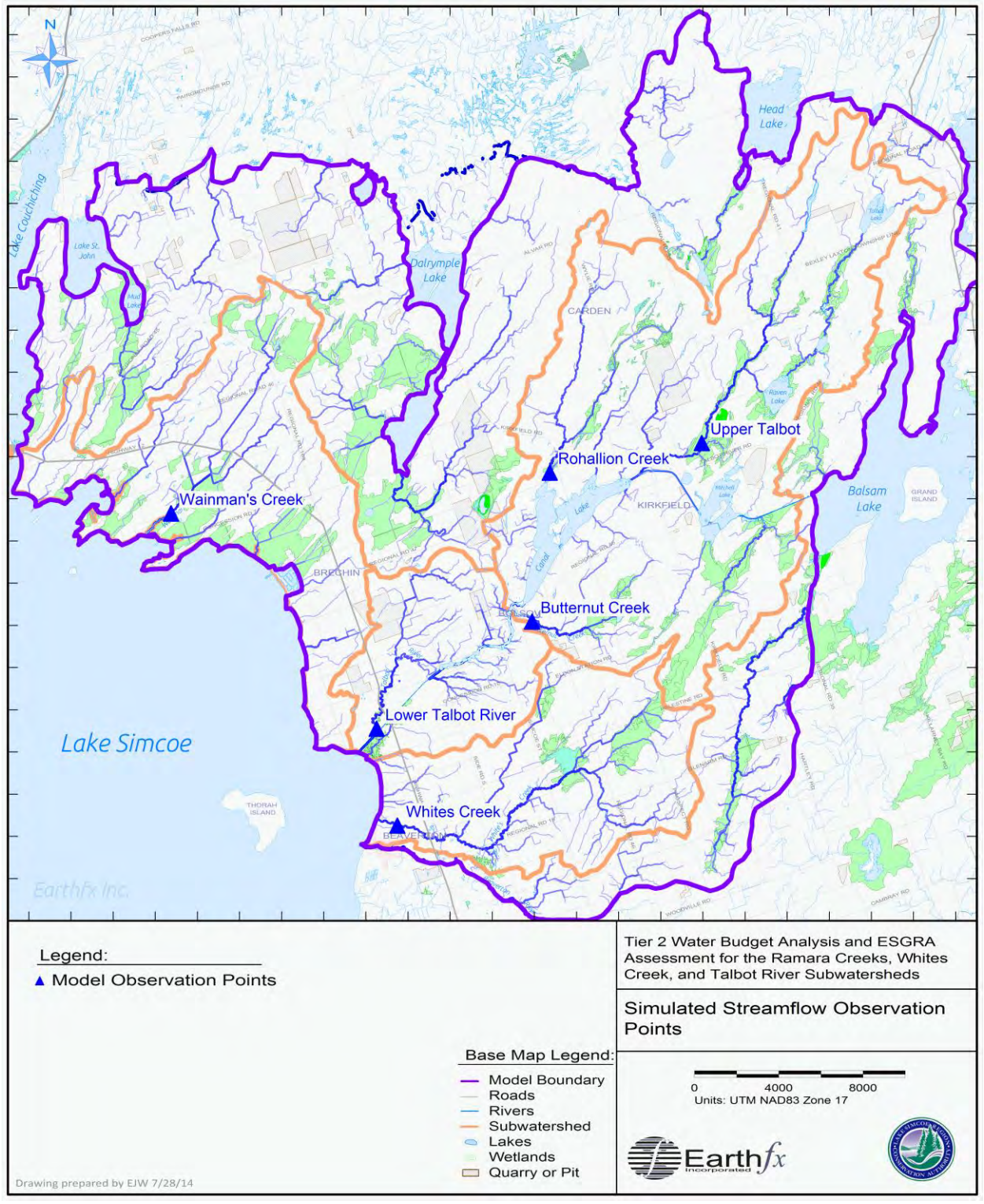

Figure D.1: Streamflow observation locations.

D.1 Whites Creek

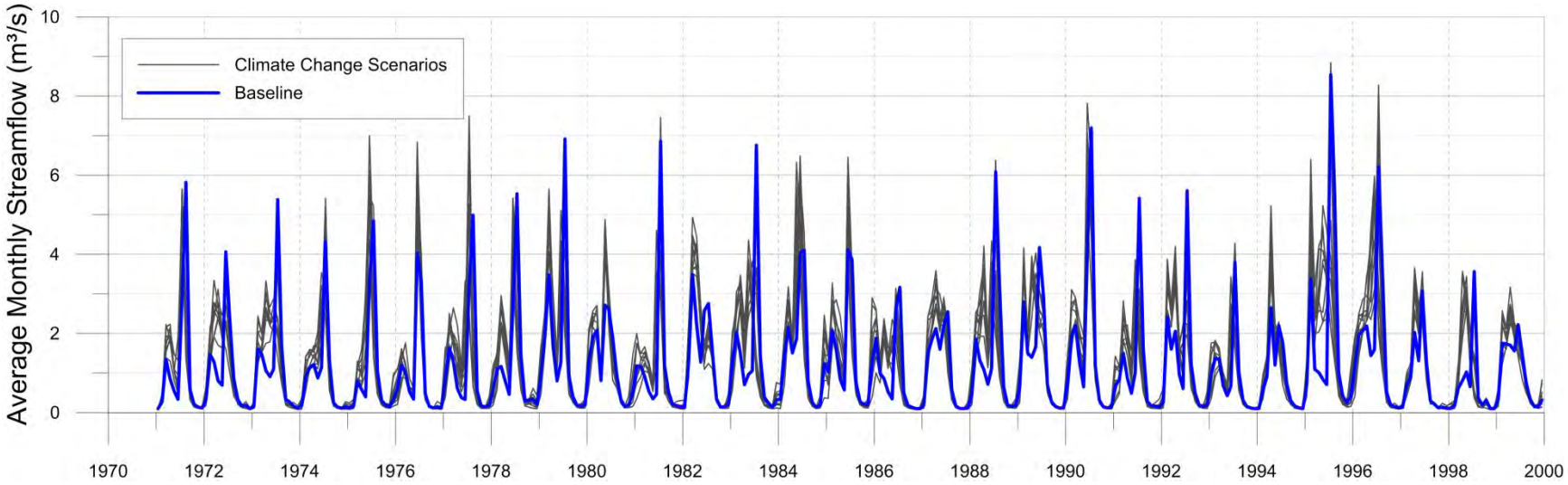

Figure D.2: Simulated monthly average streamflow by water year in Whites Creek.

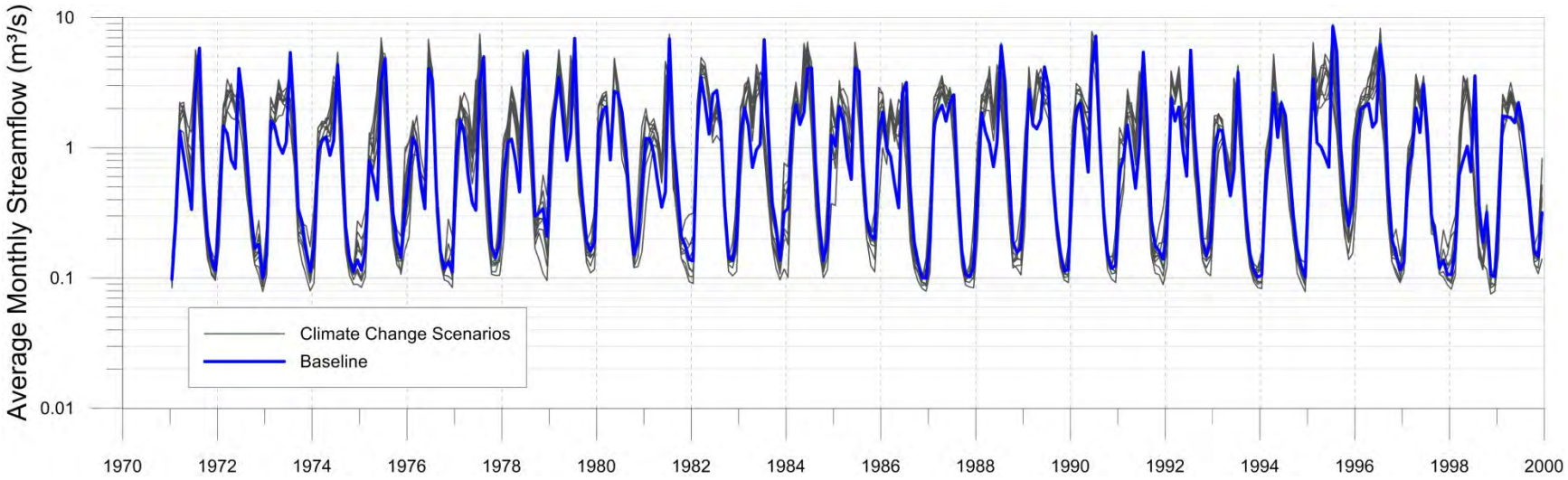

Figure D.3: Log simulated monthly average streamflow by water year in Whites Creek.

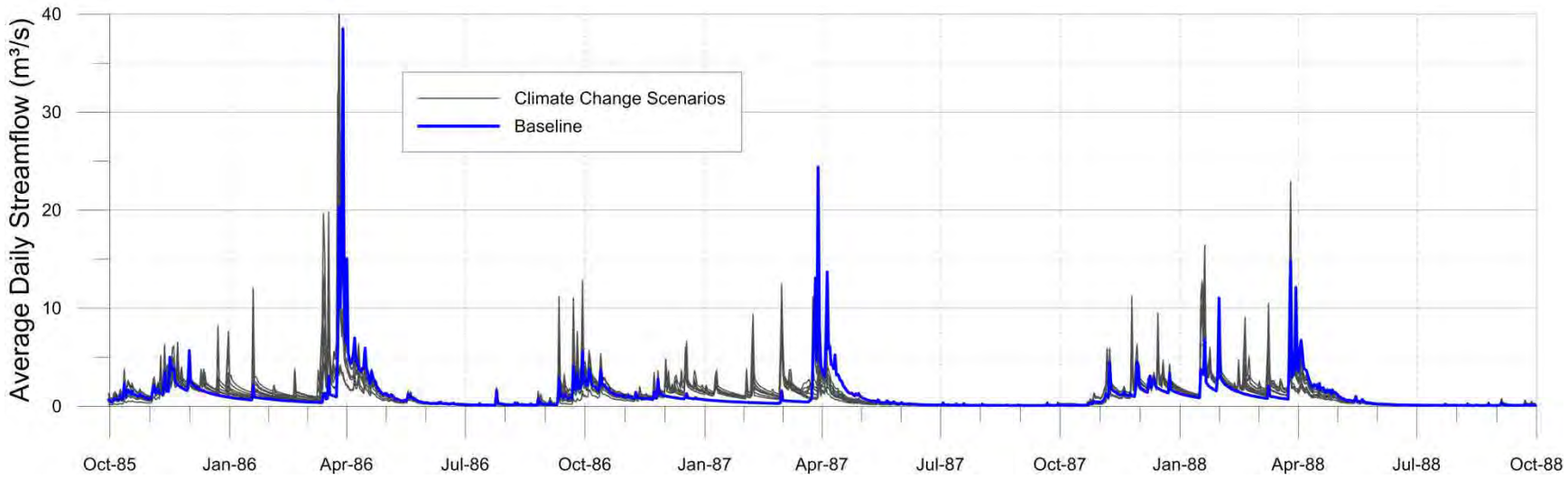

Figure D.4: Simulated daily streamflow in Whites Creek, water year 1986 through 1988.

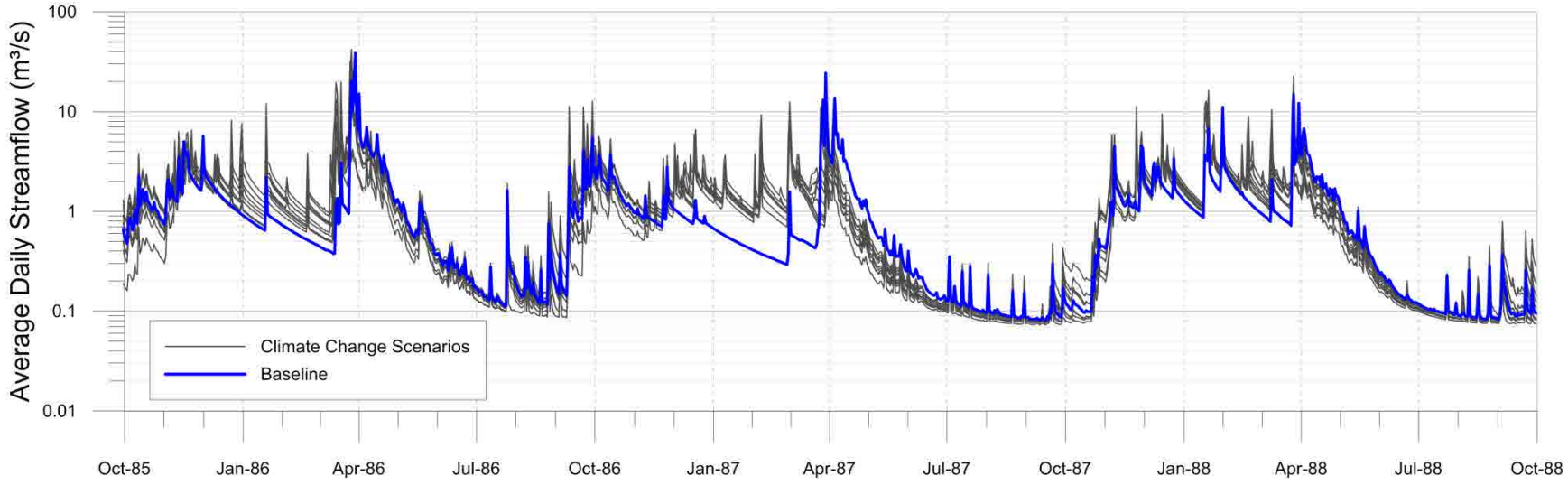

Figure D.5: Log simulated daily streamflow in Whites Creek, water year 1986 through 1988.

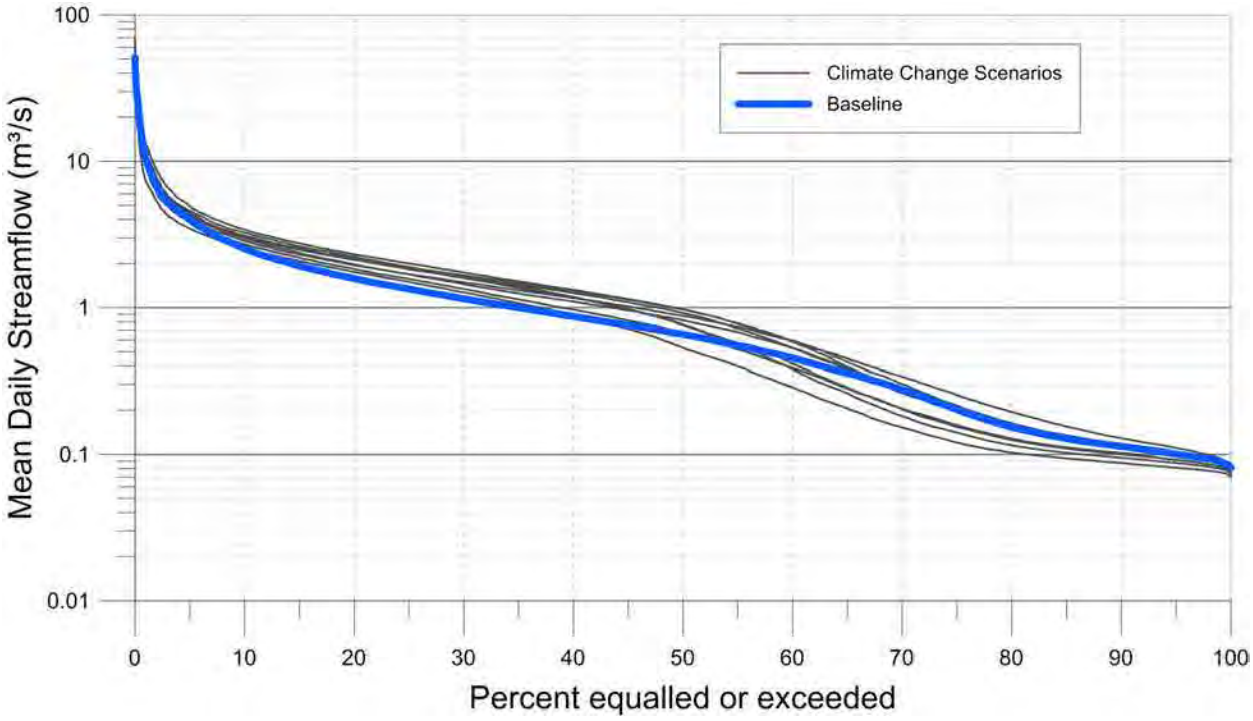

Figure D.6: Whites Creek streamflow duration curve, water year 1973 through 2000.

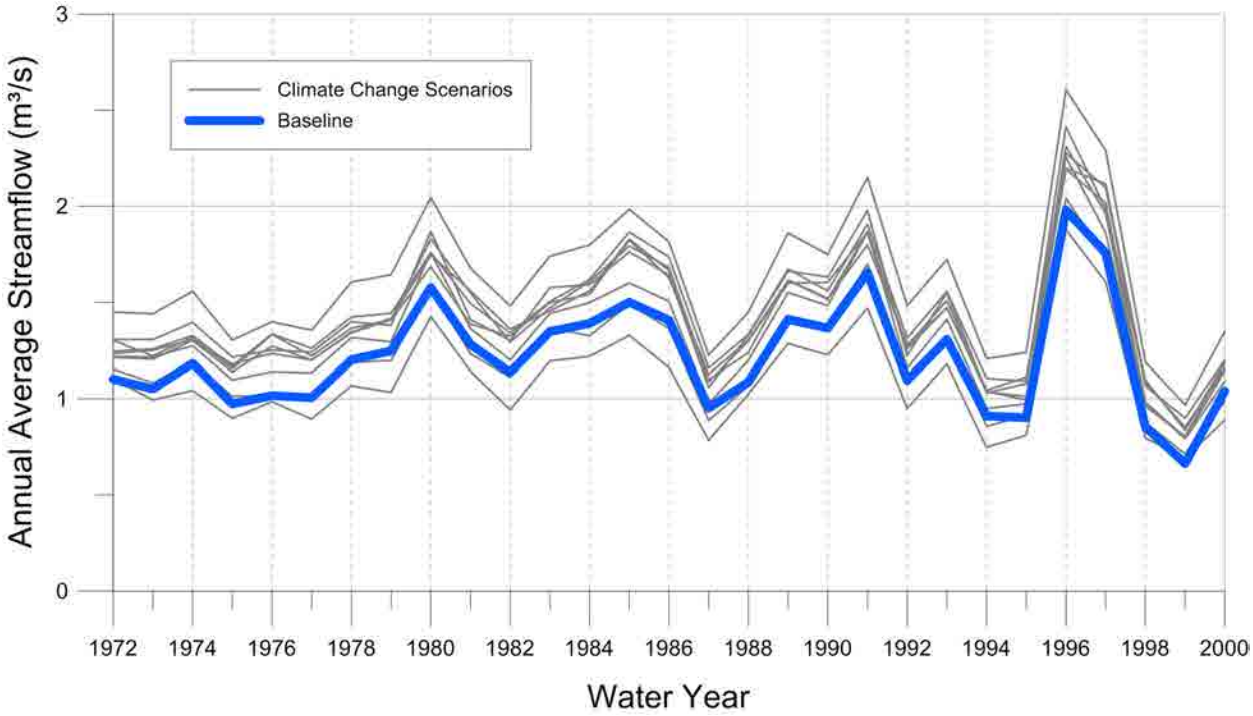

Figure D.7: Average annual simulated streamflow by water year in Whites Creek.

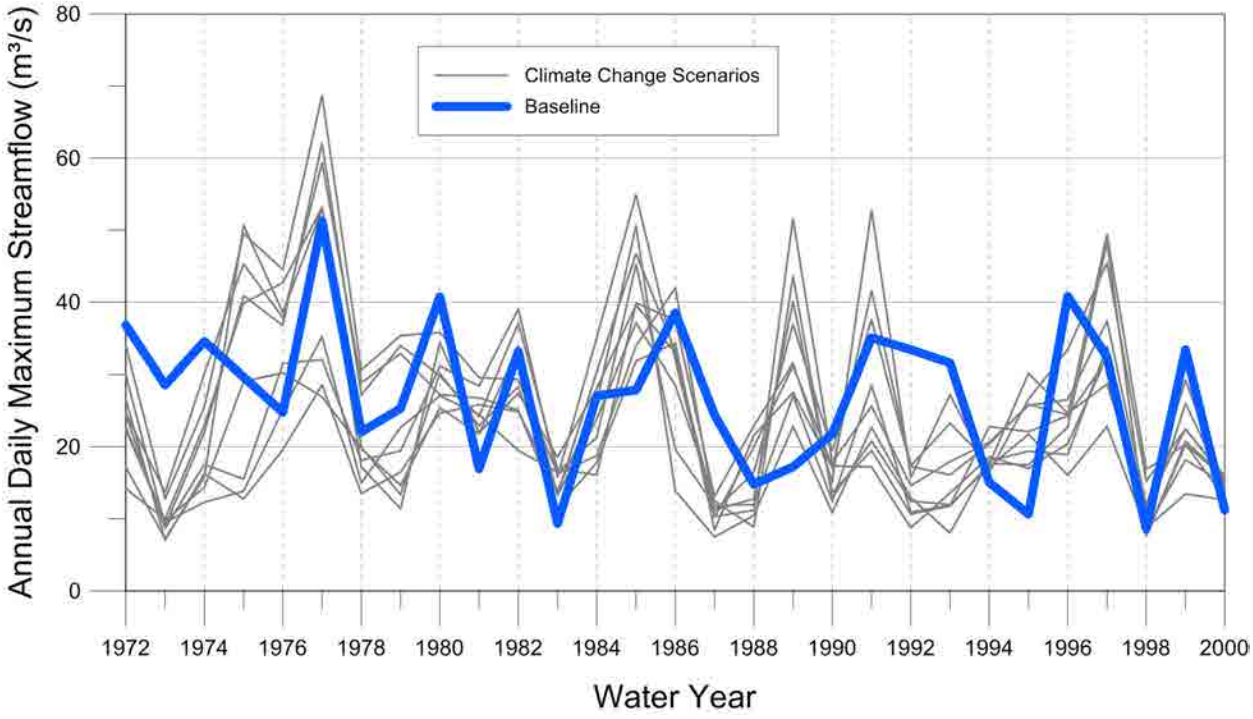

Figure D.8: Annual maximum simulated daily streamflow by water year in Whites Creek.

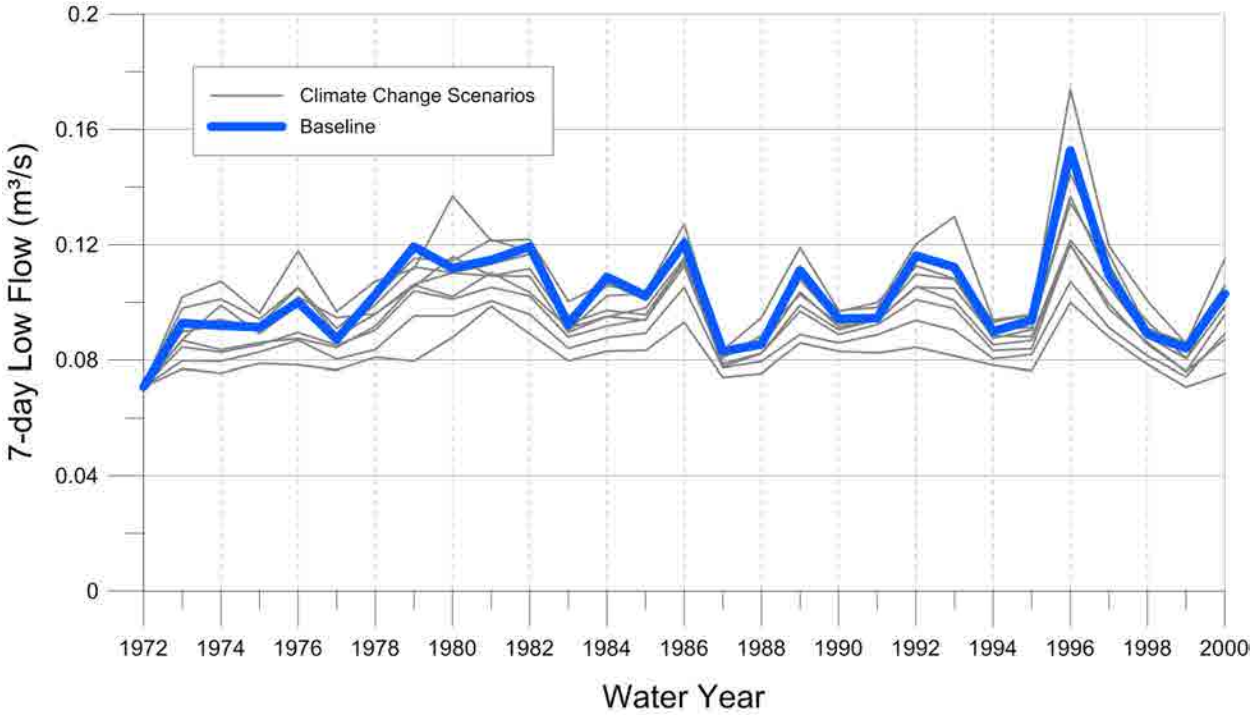

Figure D.9: Annual simulated 7-day low flow by water year in Whites Creek.

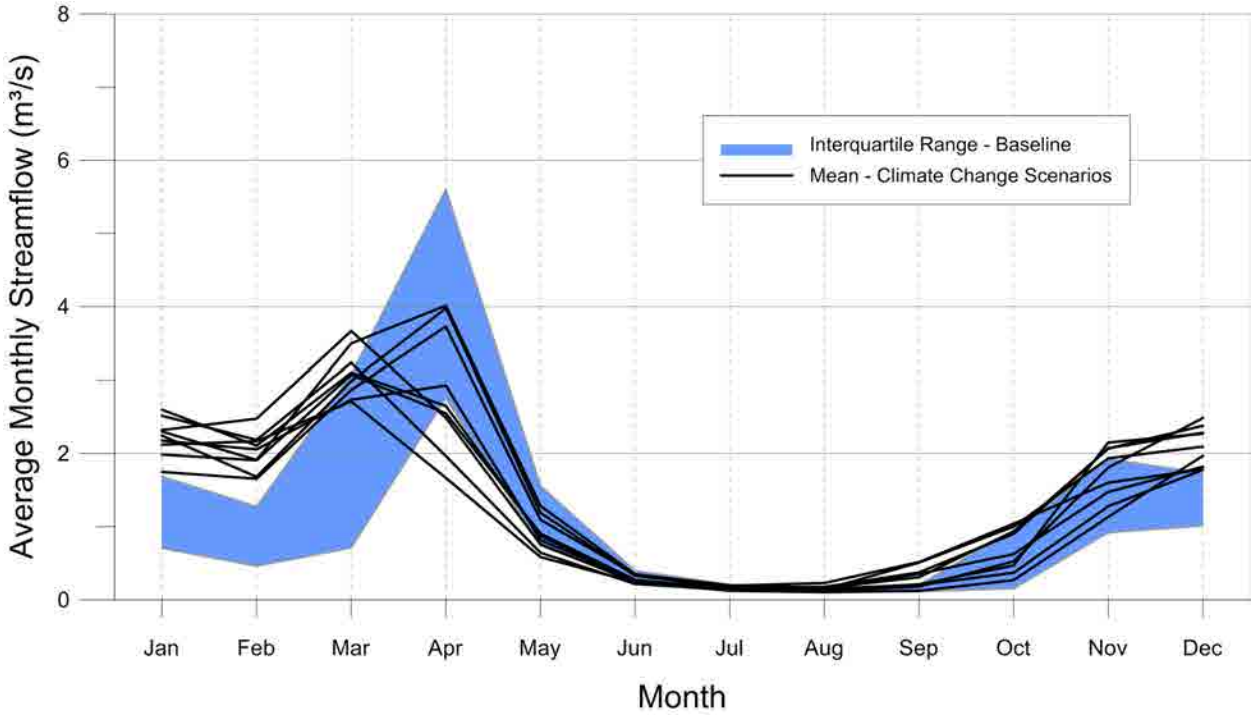

Figure D.10: Average simulated monthly streamflow in Whites Creek.

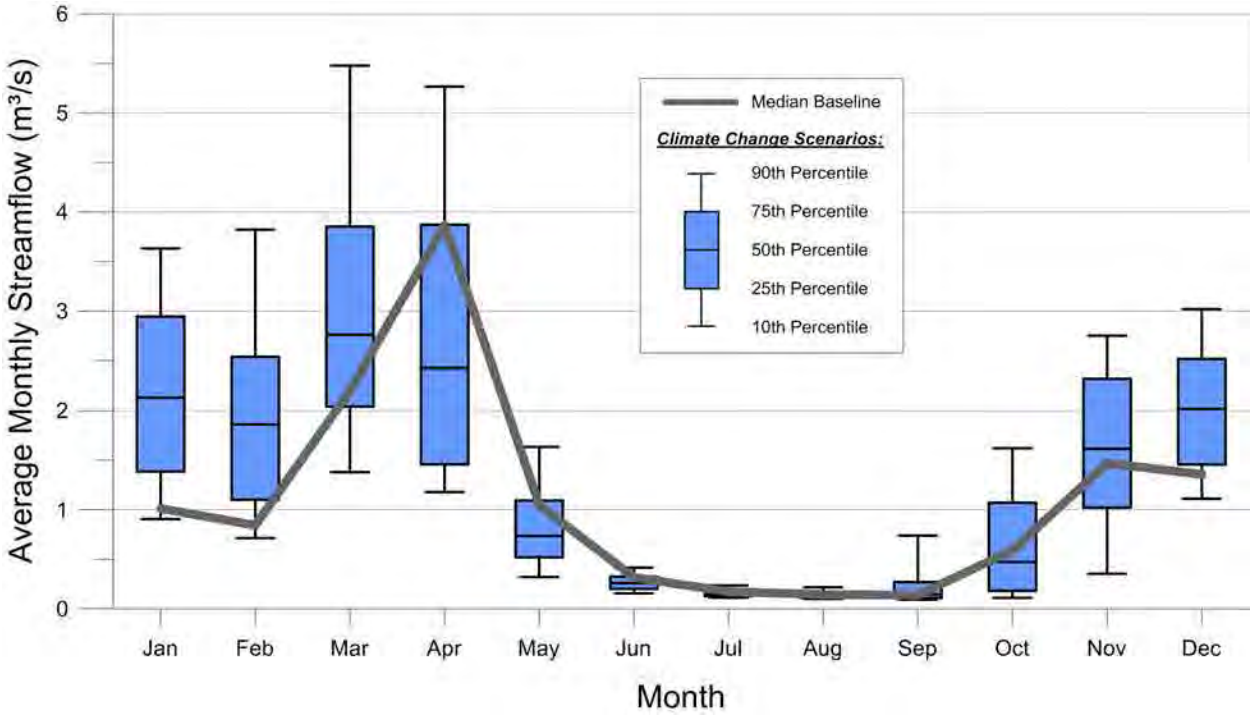

Figure D.11: Monthly simulated streamflow statistics for Whites Creek.

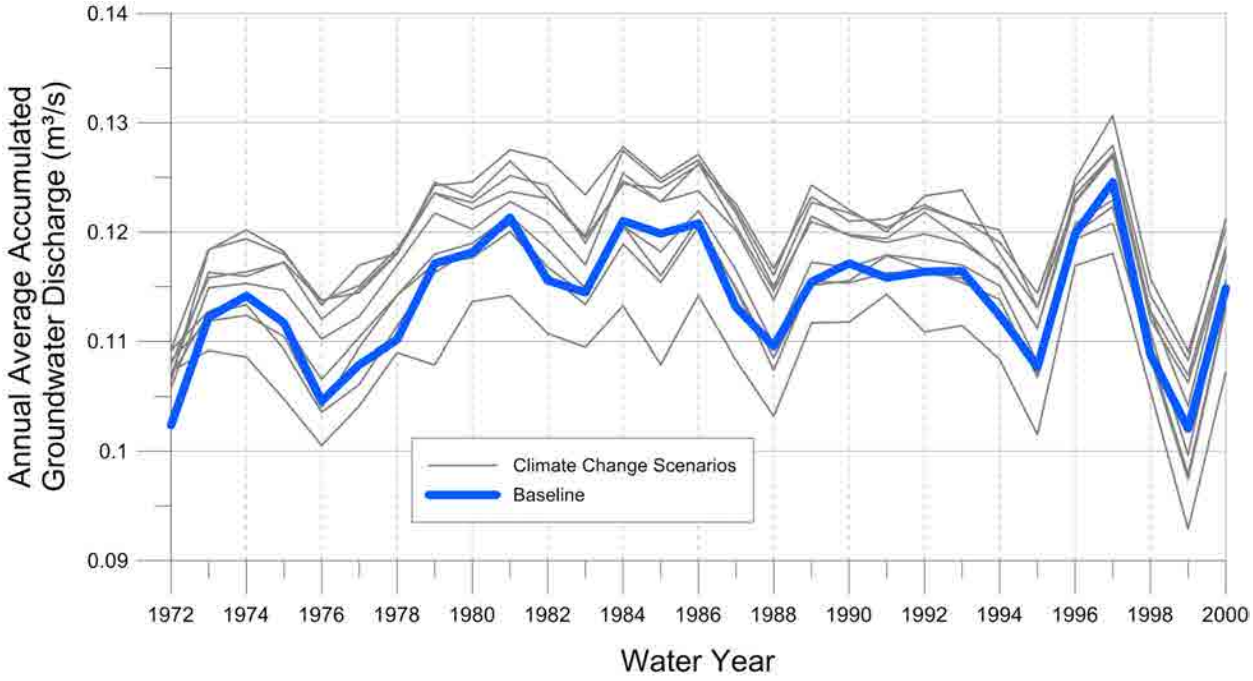

Figure D.12: Annual simulated average accumulated groundwater discharge by water year in Whites Creek.

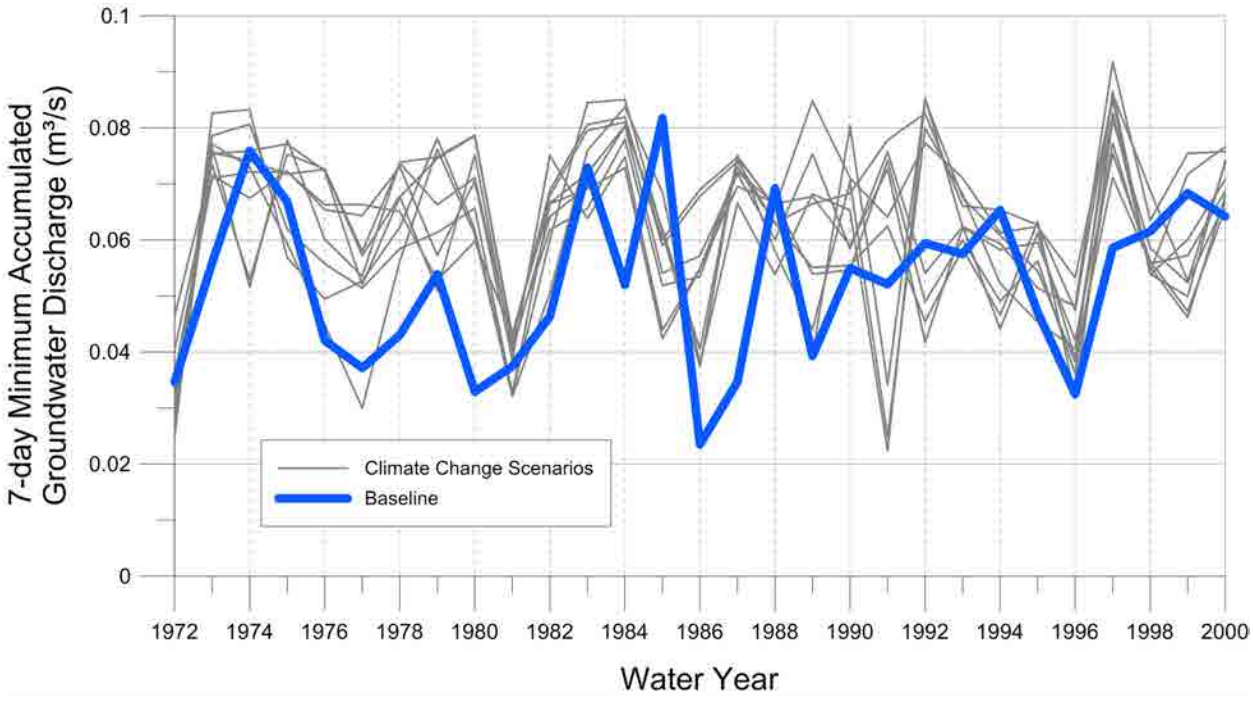

Figure D.13: Annual simulated 7-day low in accumulated groundwater discharge by water year in Whites Creek.

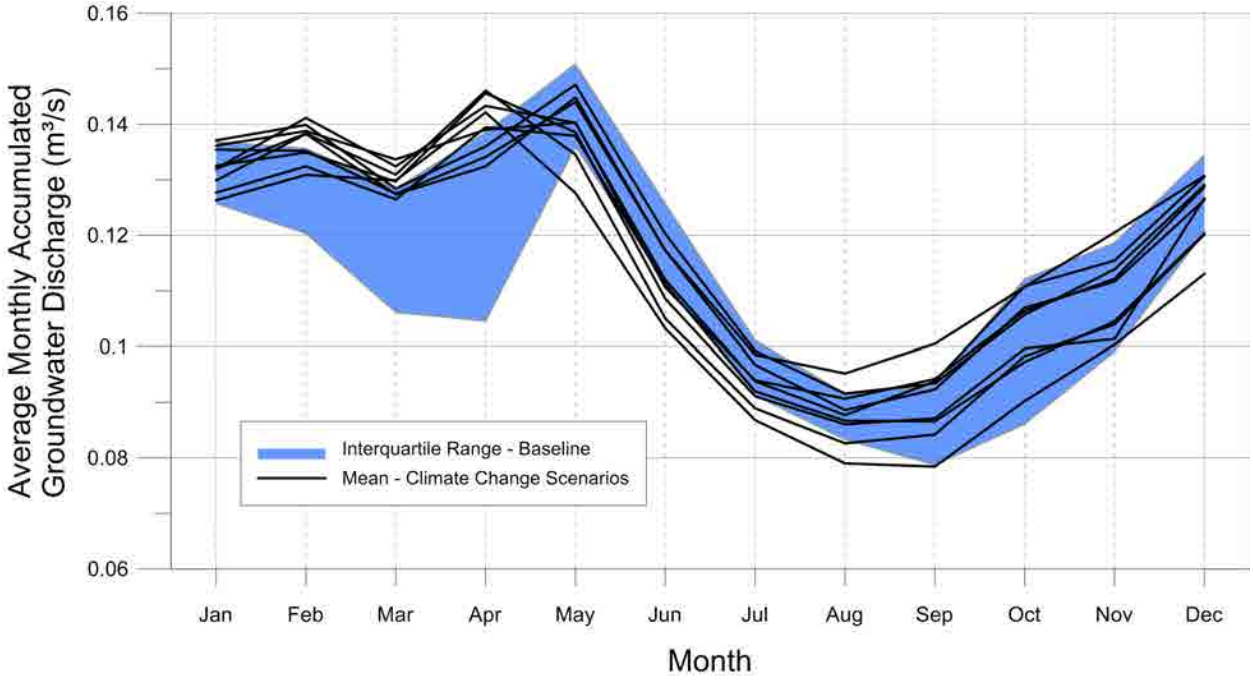

Figure D.14: Average monthly simulated accumulated groundwater discharge in Whites Creek.

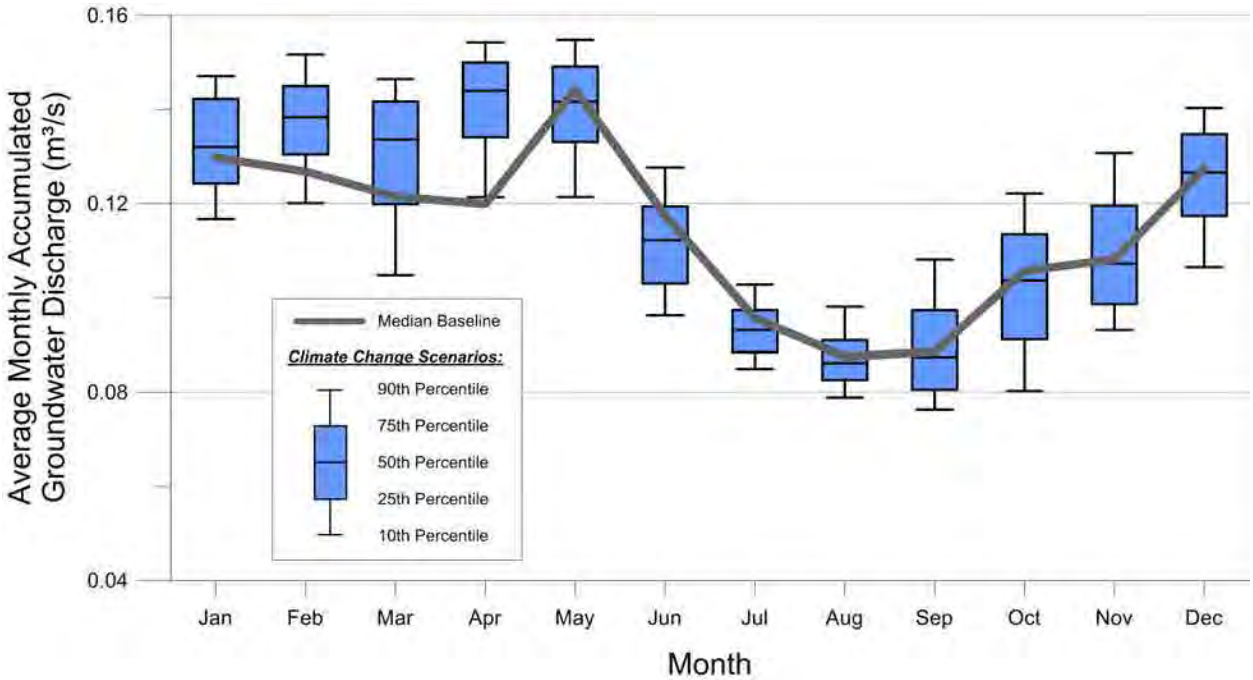

Figure D.15: Monthly simulated accumulated groundwater discharge statistics for Whites Creek.

D.2 Lower Talbot River

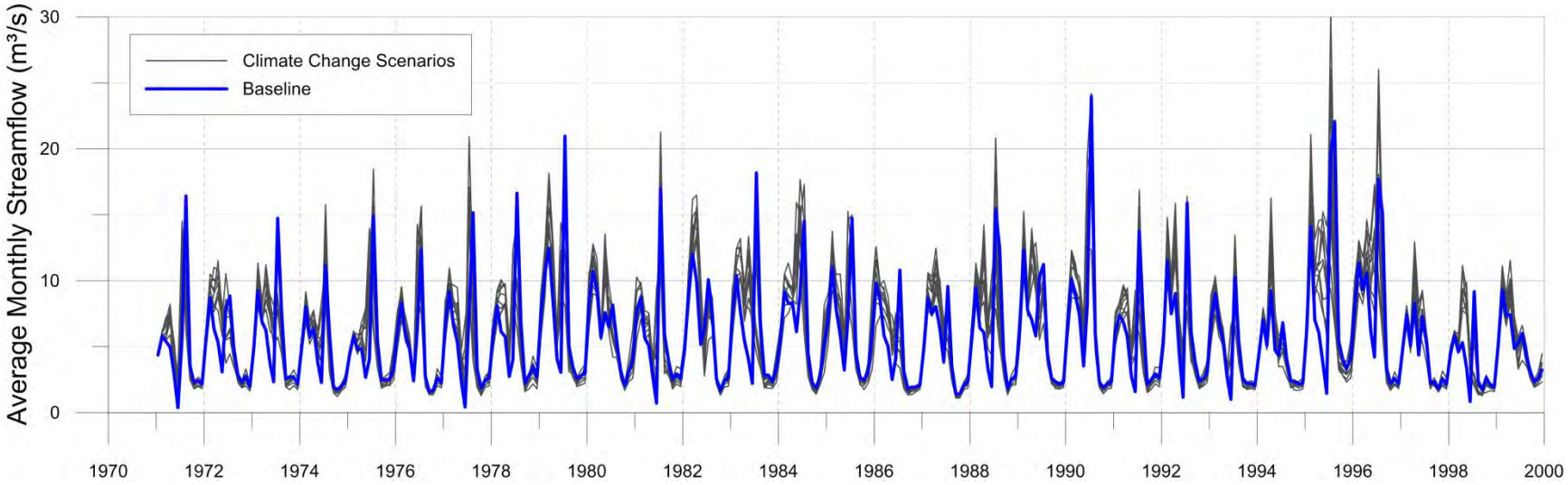

Figure D.16: Simulated monthly average streamflow by water year in the Lower Talbot River.

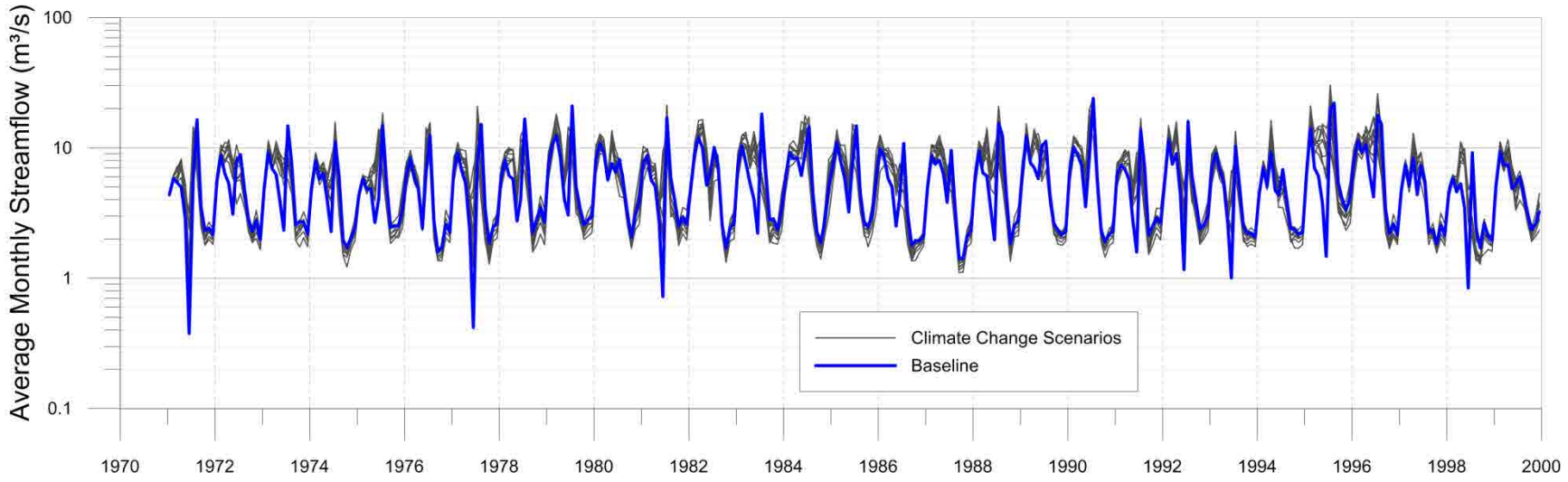

Figure D.17: Log simulated monthly average streamflow by water year in the Lower Talbot River.

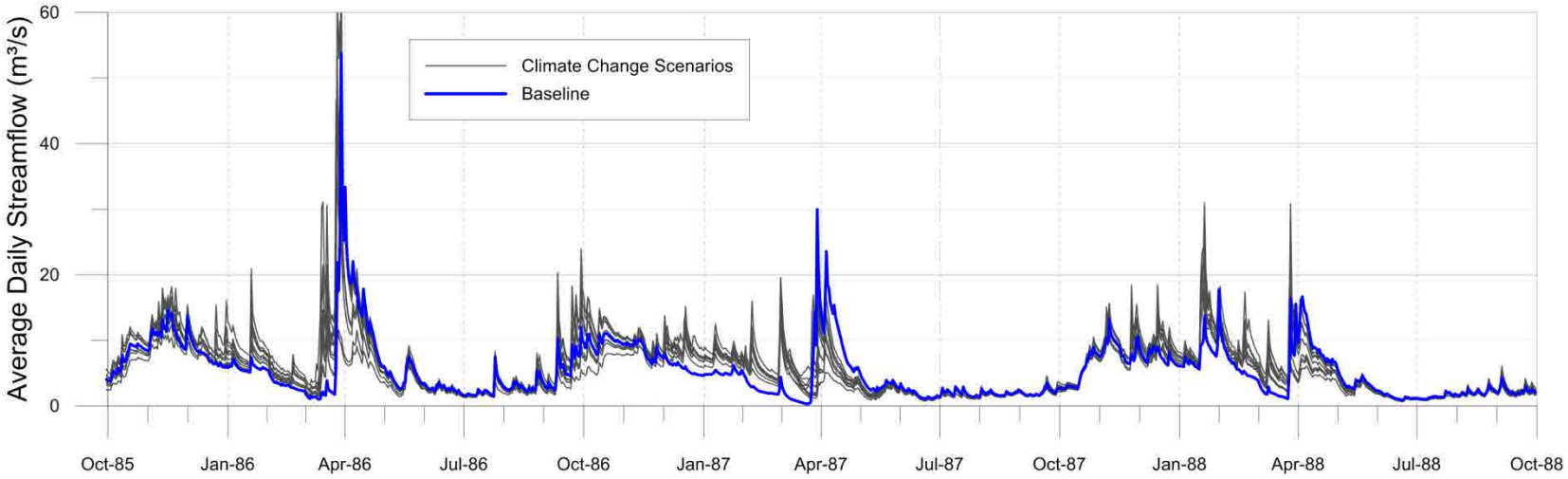

Figure D.18: Simulated daily streamflow in the Lower Talbot River, water year 1986 through 1988.

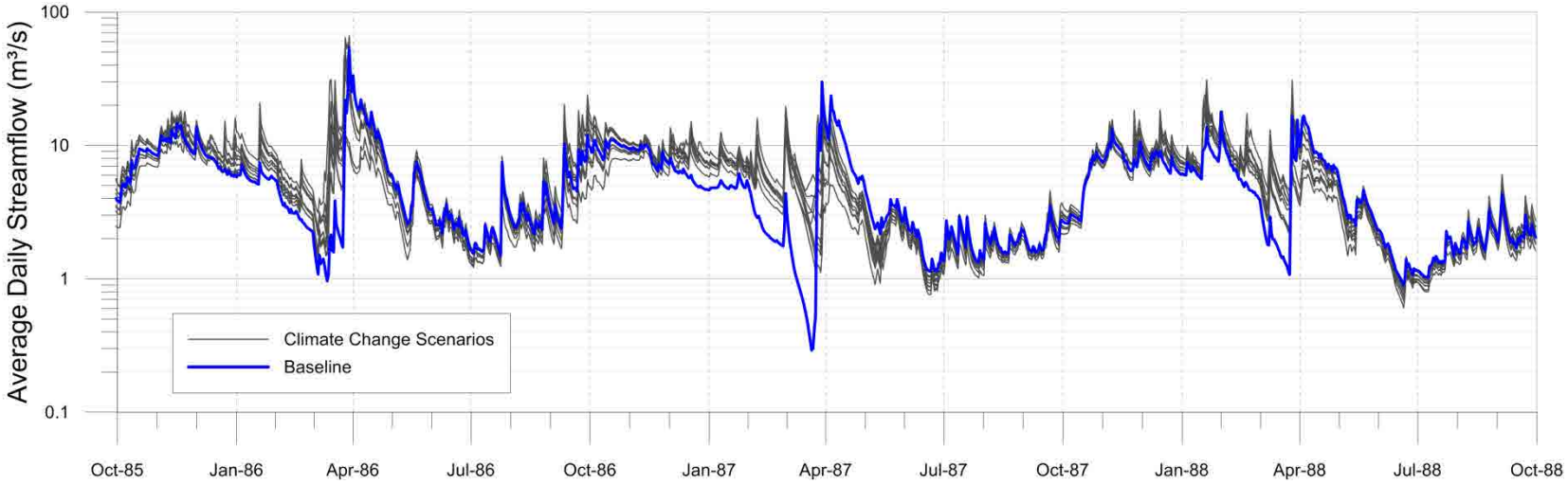

Figure D.19: Log simulated daily streamflow in the Lower Talbot River, water year 1986 through 1988.

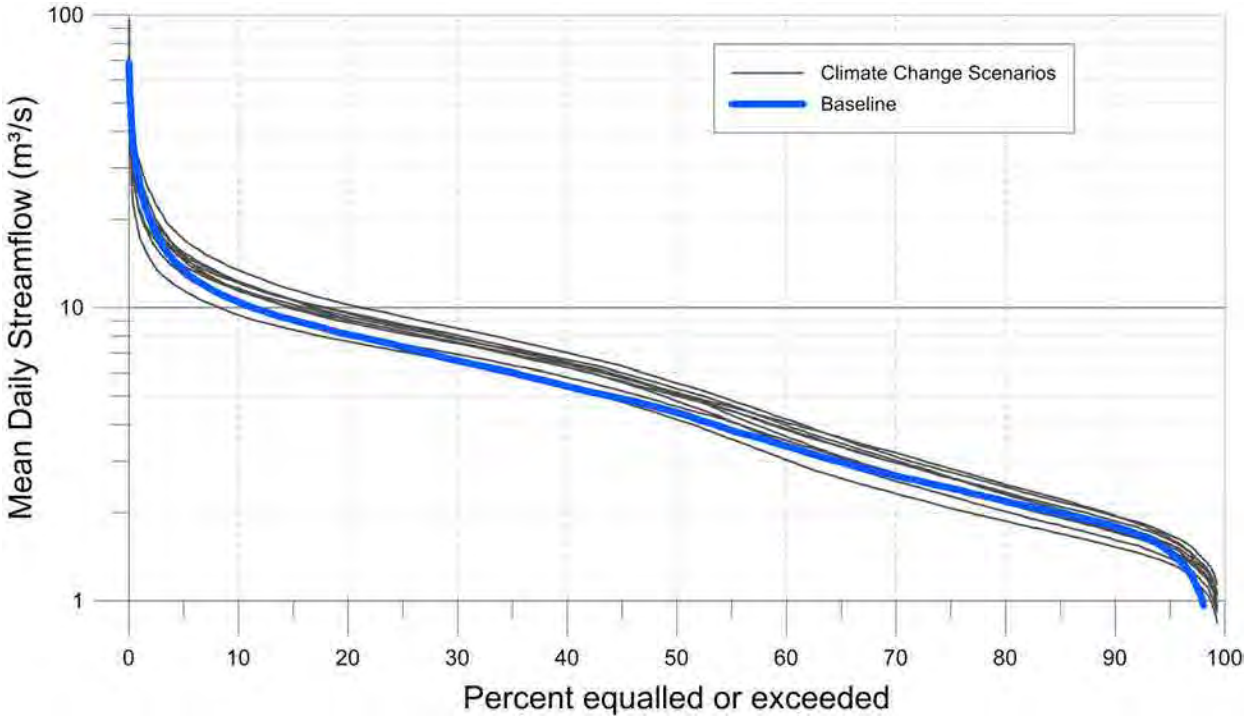

Figure D.20: Lower Talbot River streamflow duration curve, water year 1973 through 2000.

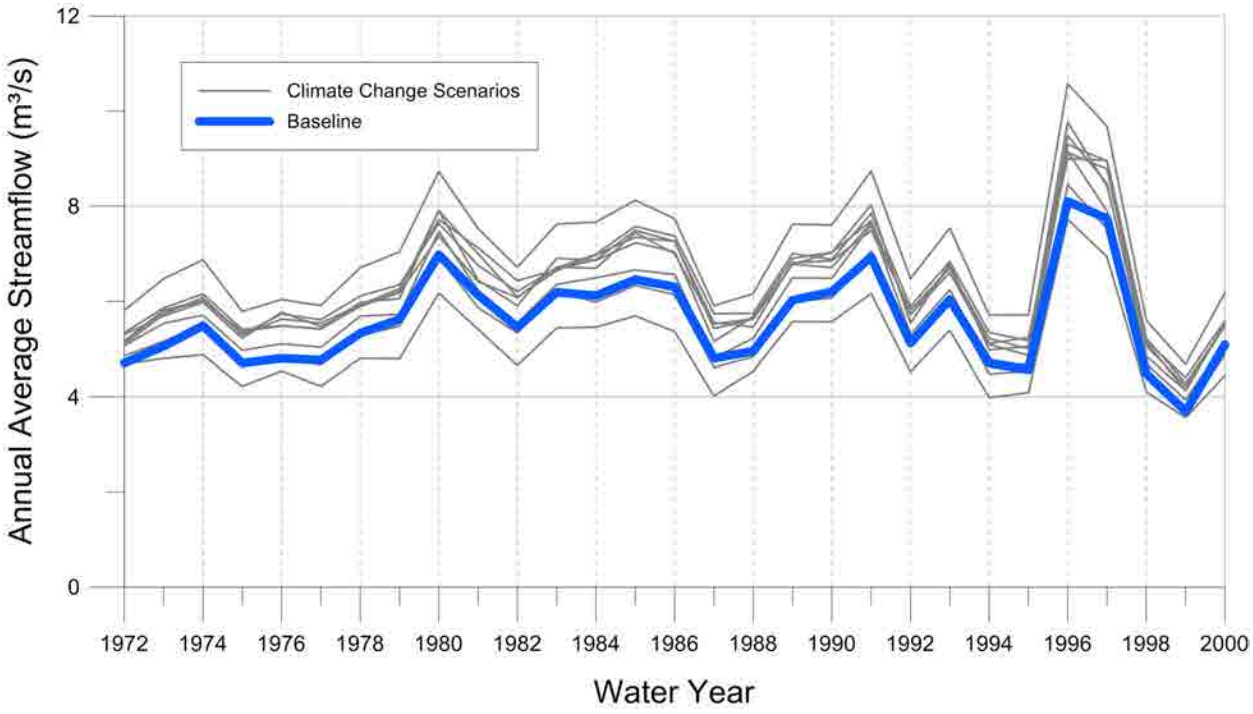

Figure D.21: Average annual simulated streamflow by water year in the Lower Talbot River.

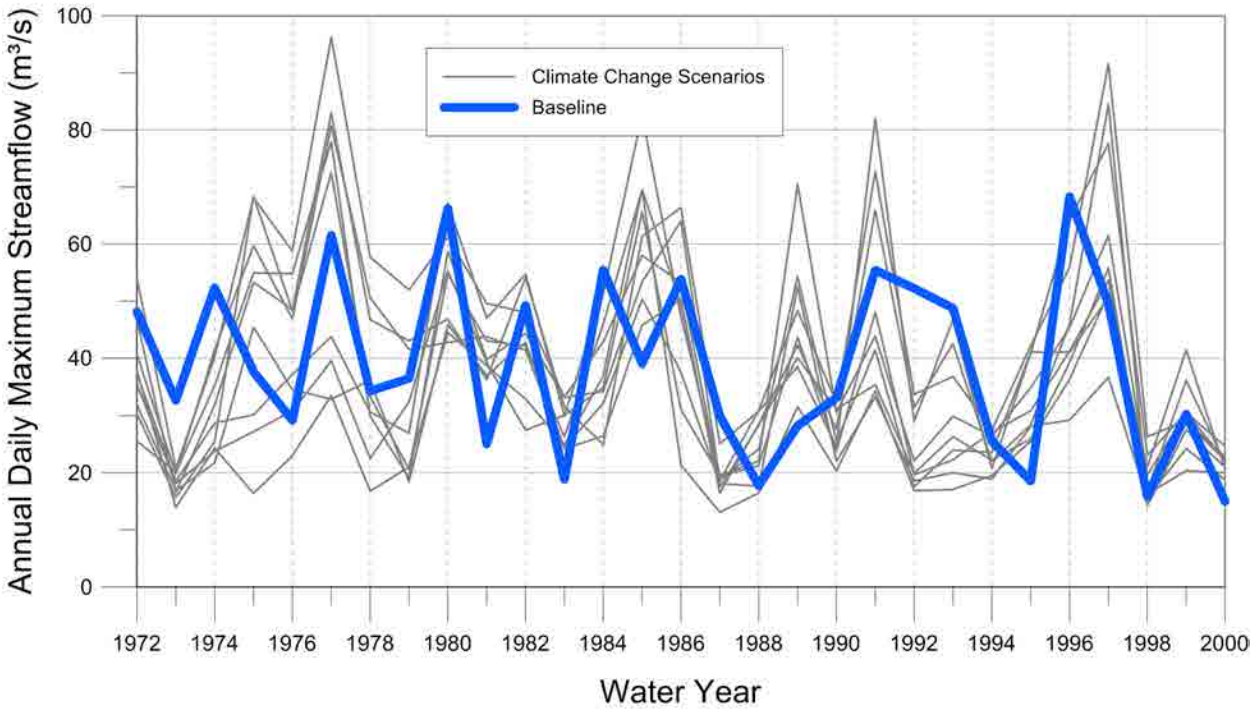

Figure D.22: Annual maximum simulated daily streamflow by water year in the Lower Talbot River.

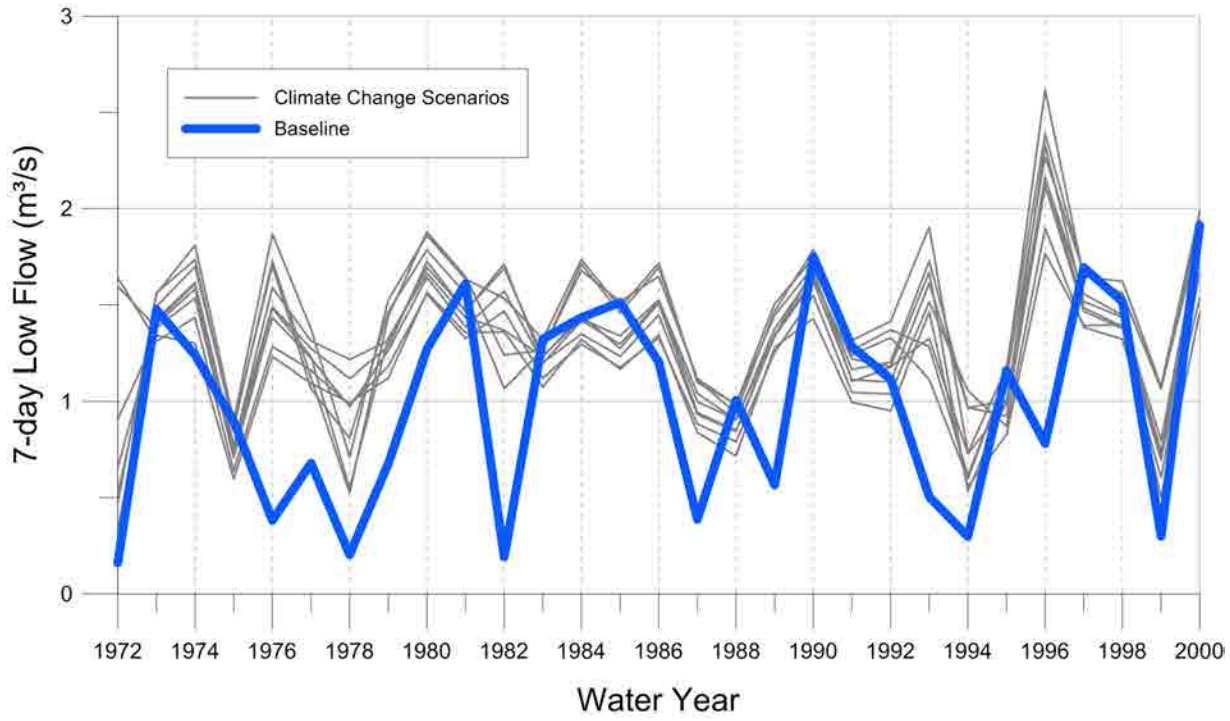

Figure D.23: Annual simulated 7-day low flow by water year in the Lower Talbot River.

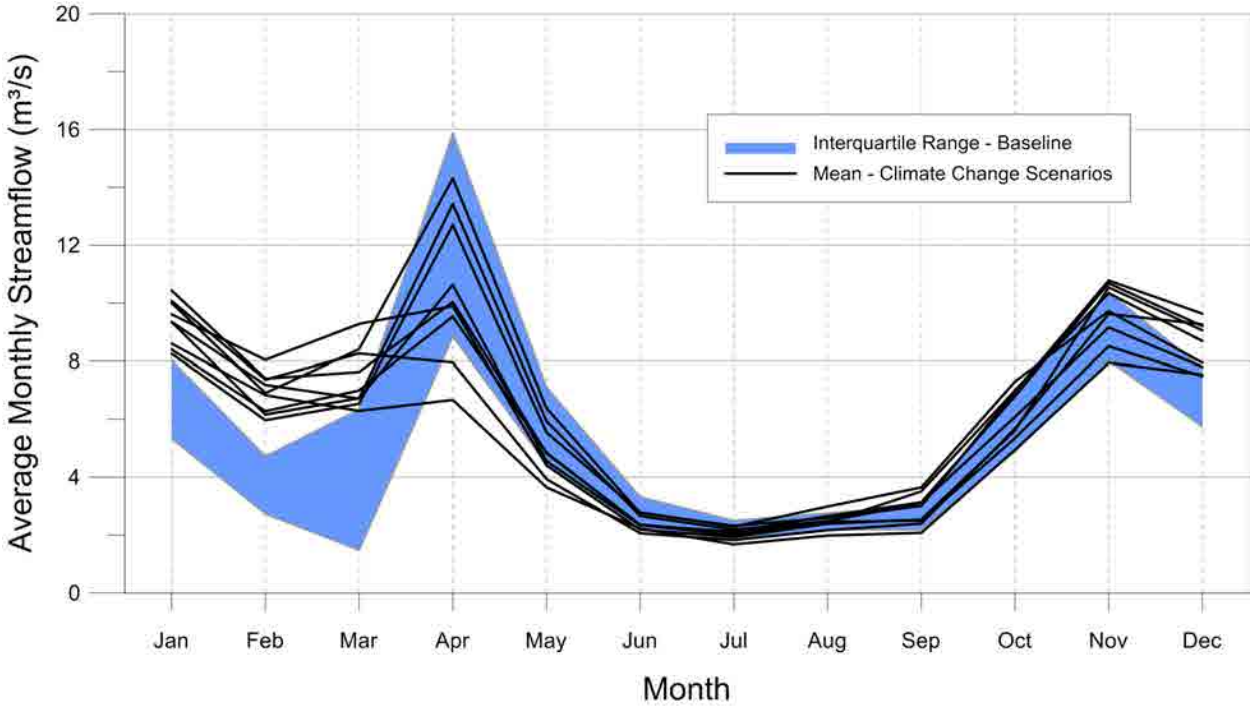

Figure D.24: Average simulated monthly streamflow in the Lower Talbot River.

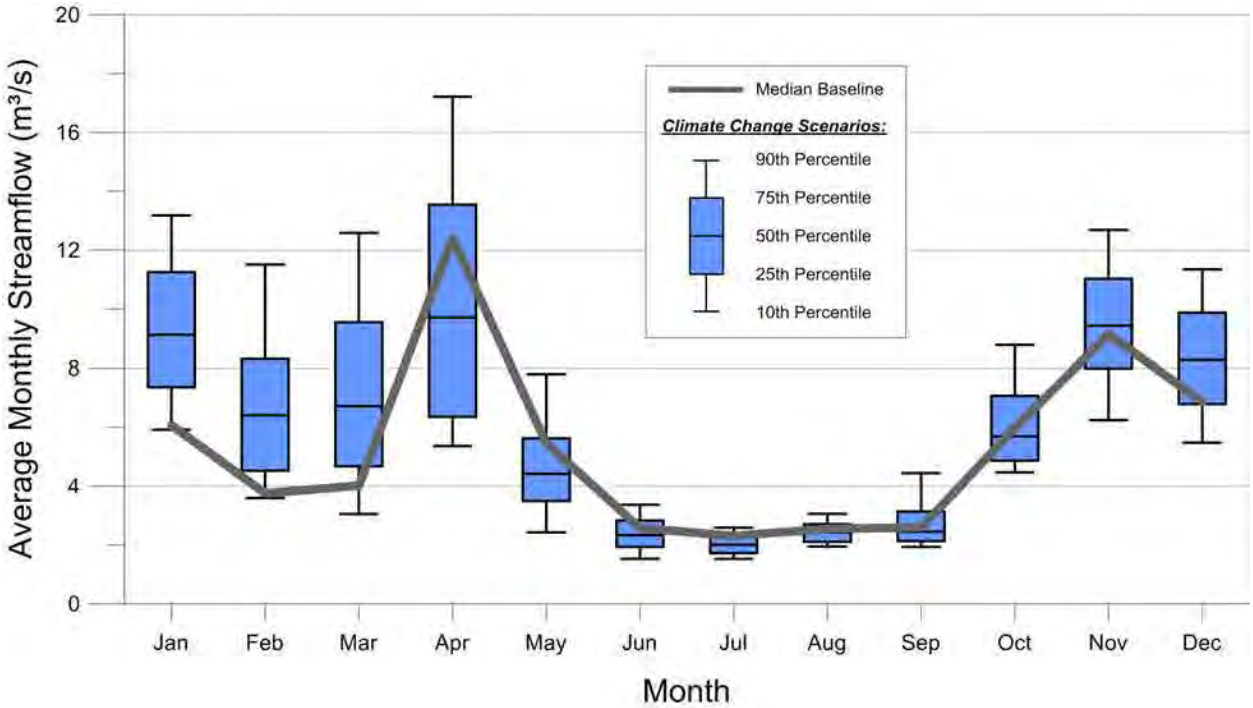

Figure D.25: Monthly simulated streamflow statistics for the Lower Talbot River.

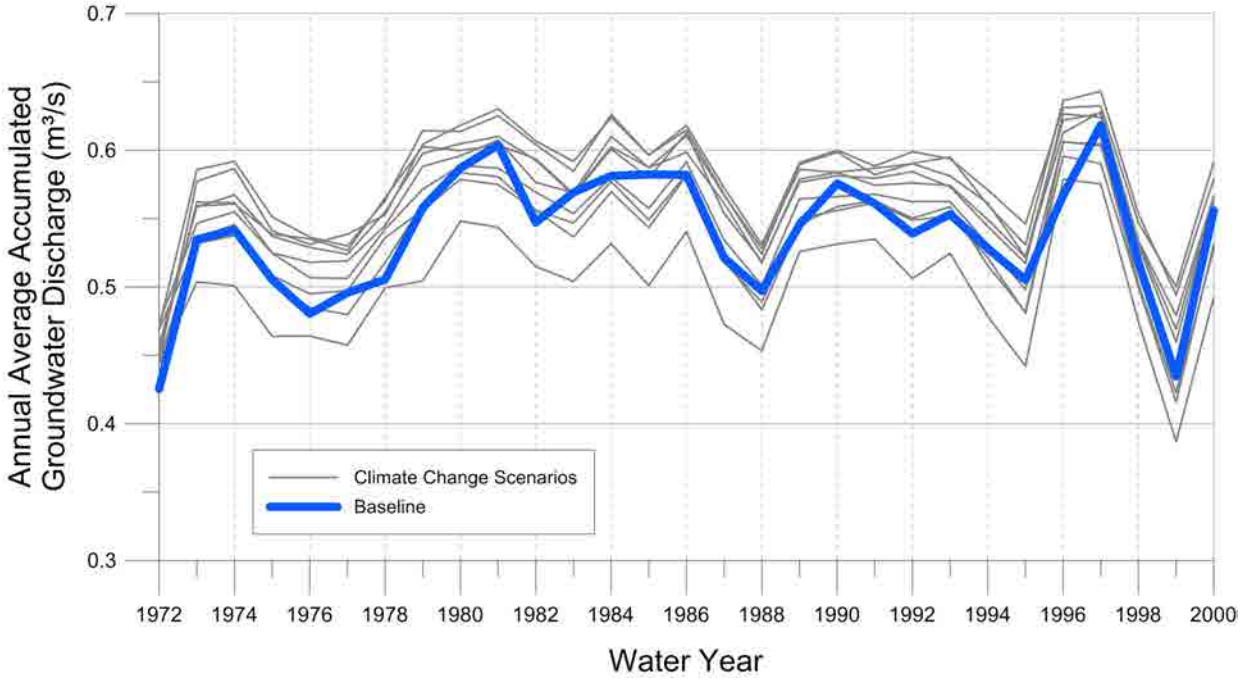

Figure D.26: Annual simulated average accumulated groundwater discharge by water year in the Lower Talbot River.

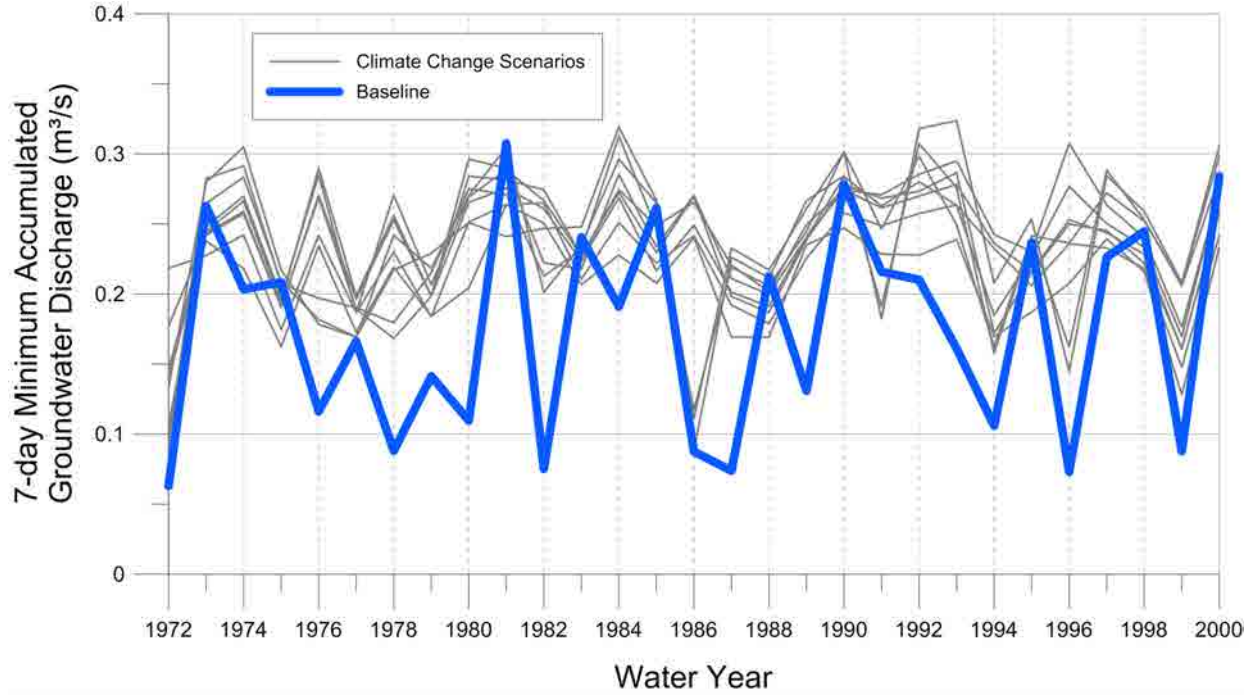

Figure D.27: Annual simulated 7-day low in accumulated groundwater discharge by water year in the Lower Talbot River.

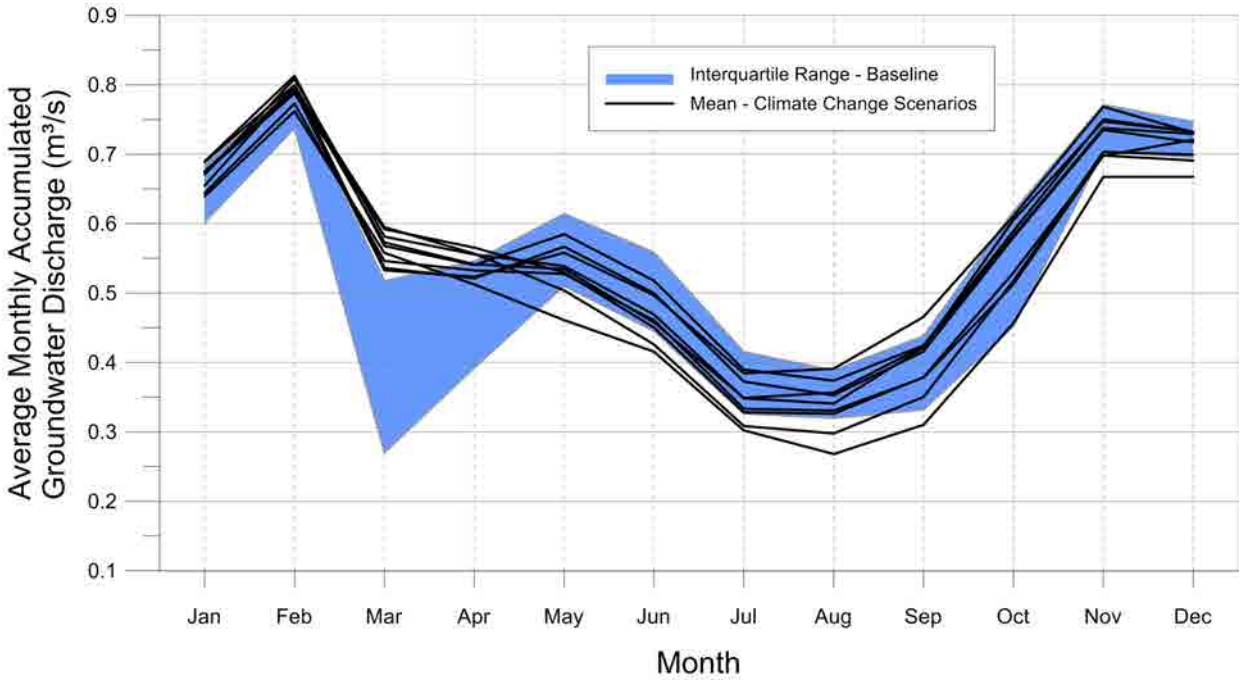

Figure D.28: Average monthly simulated accumulated groundwater discharge in the Lower Talbot River.

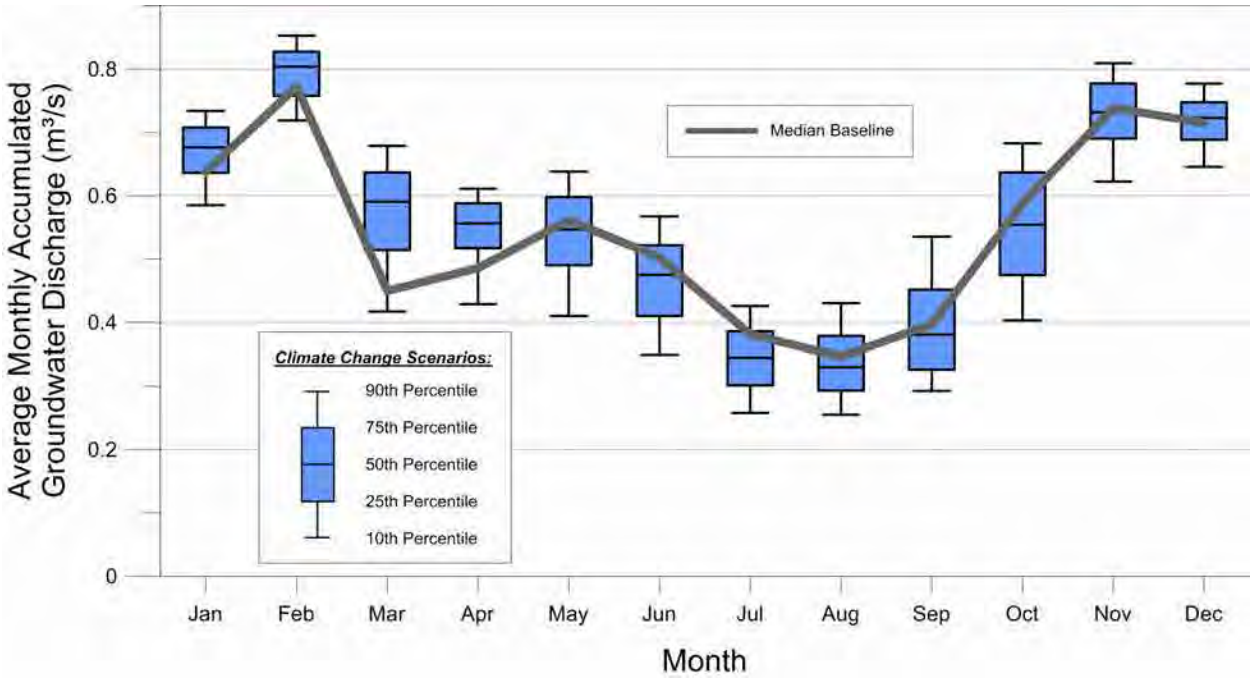

Figure D.29: Monthly simulated accumulated groundwater discharge statistics for the Lower Talbot River.

D.3 Upper Talbot River

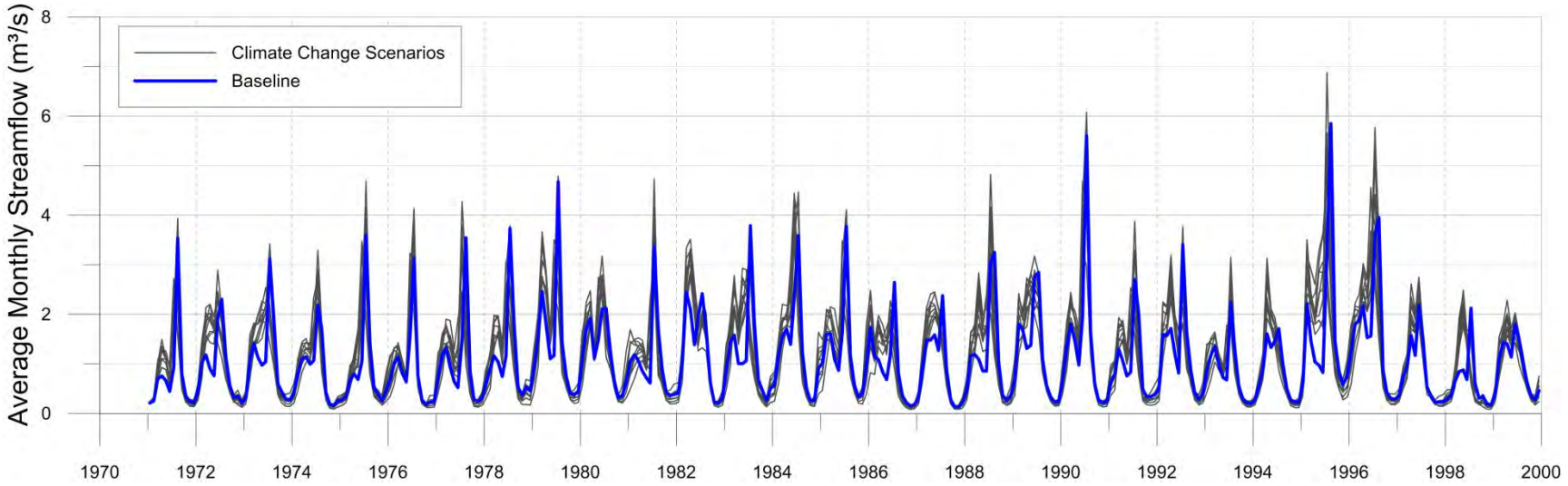

Figure D.30: Simulated monthly average streamflow by water year in the Upper Talbot River.

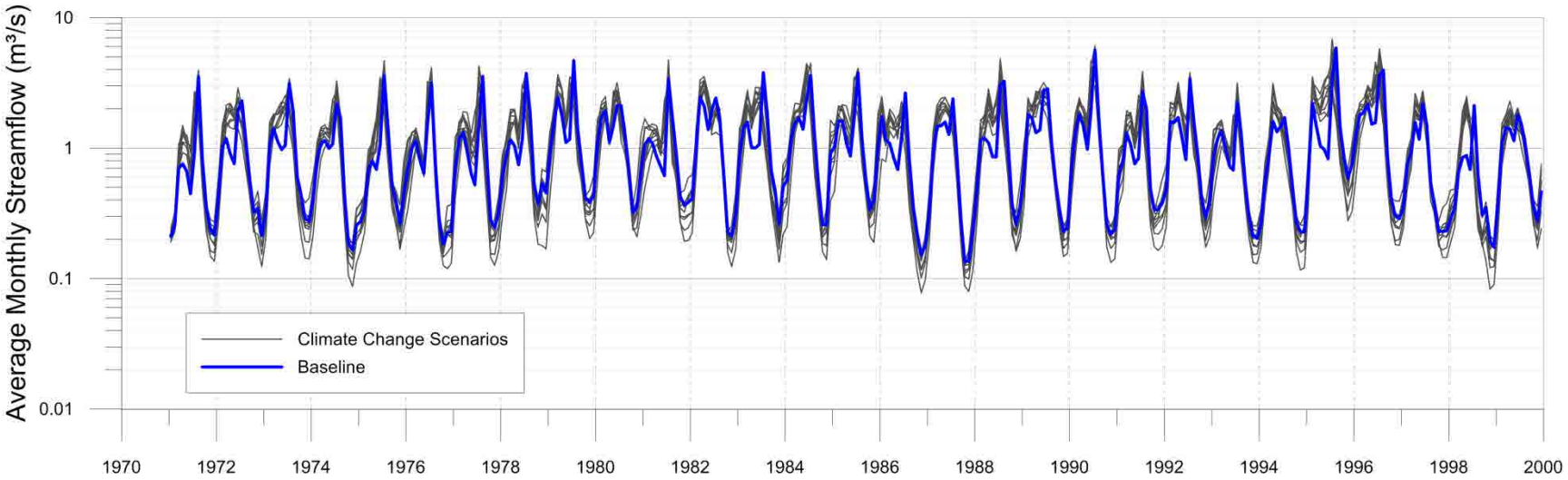

Figure D.31: Log simulated monthly average streamflow by water year in the Upper Talbot River.

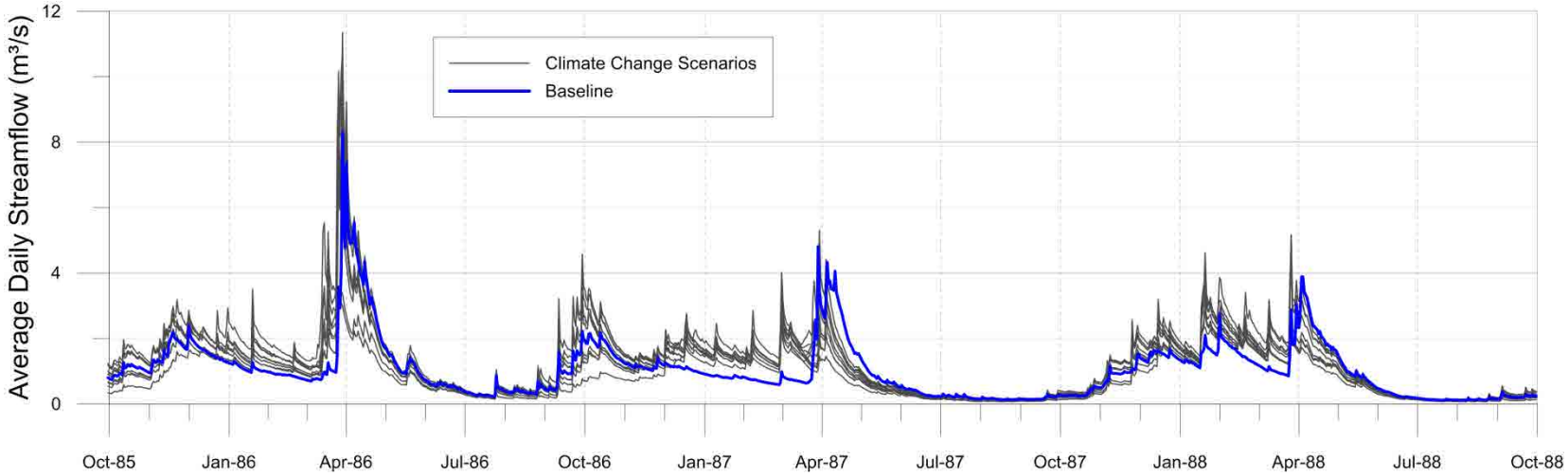

Figure D.32: Simulated daily streamflow in the Upper Talbot River, water year 1986 through 1988.

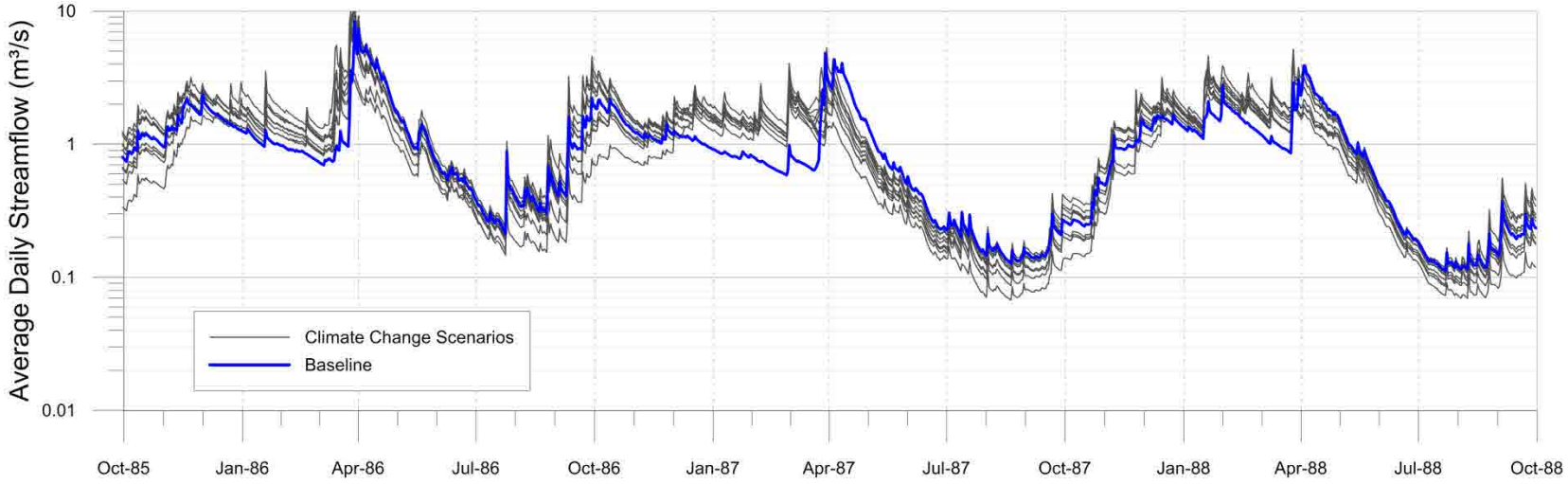

Figure D.33: Log simulated daily streamflow in the Upper Talbot River, water year 1986 through 1988.

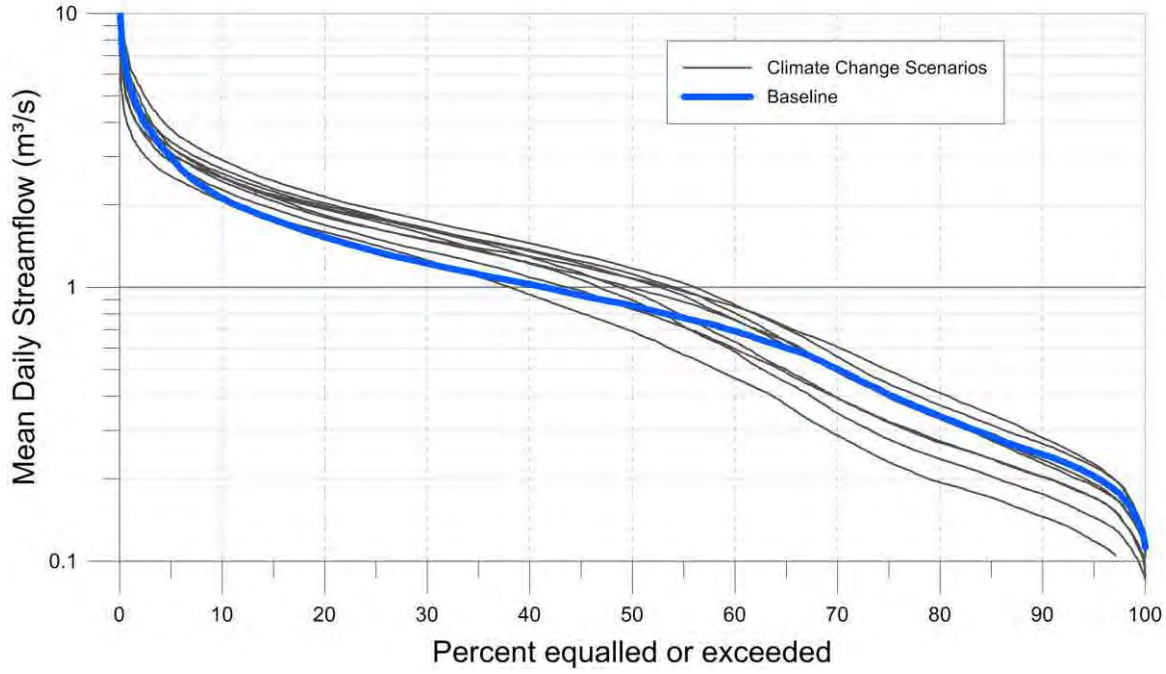

Figure D.34: Upper Talbot River streamflow duration curve, water year 1973 through 2000.

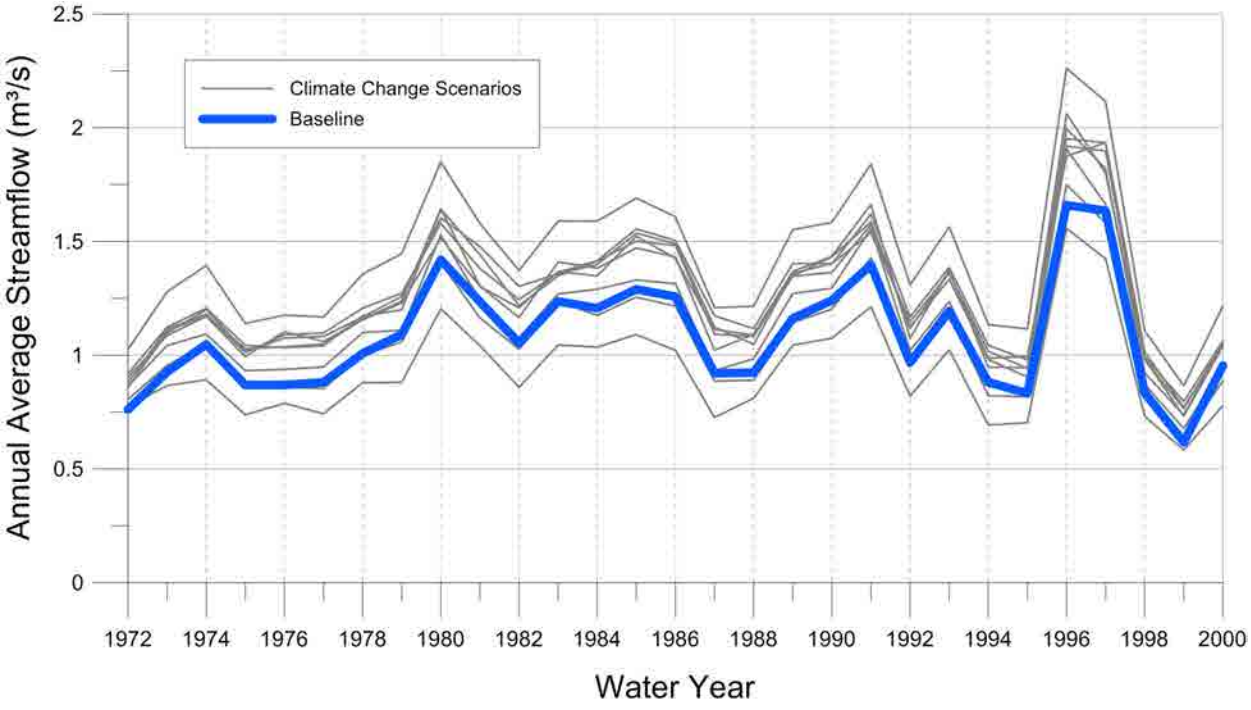

Figure D.35: Average annual simulated streamflow by water year in the Upper Talbot River.

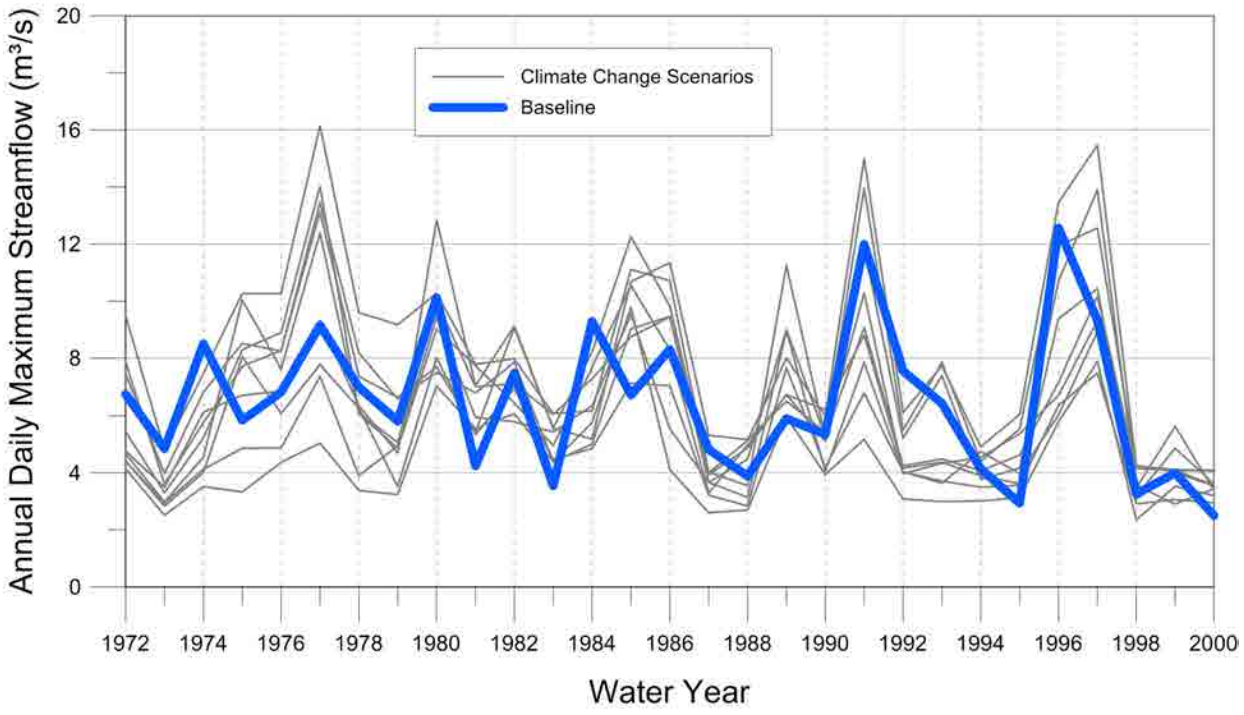

Figure D.36: Annual maximum simulated daily streamflow by water year in the Upper Talbot River.

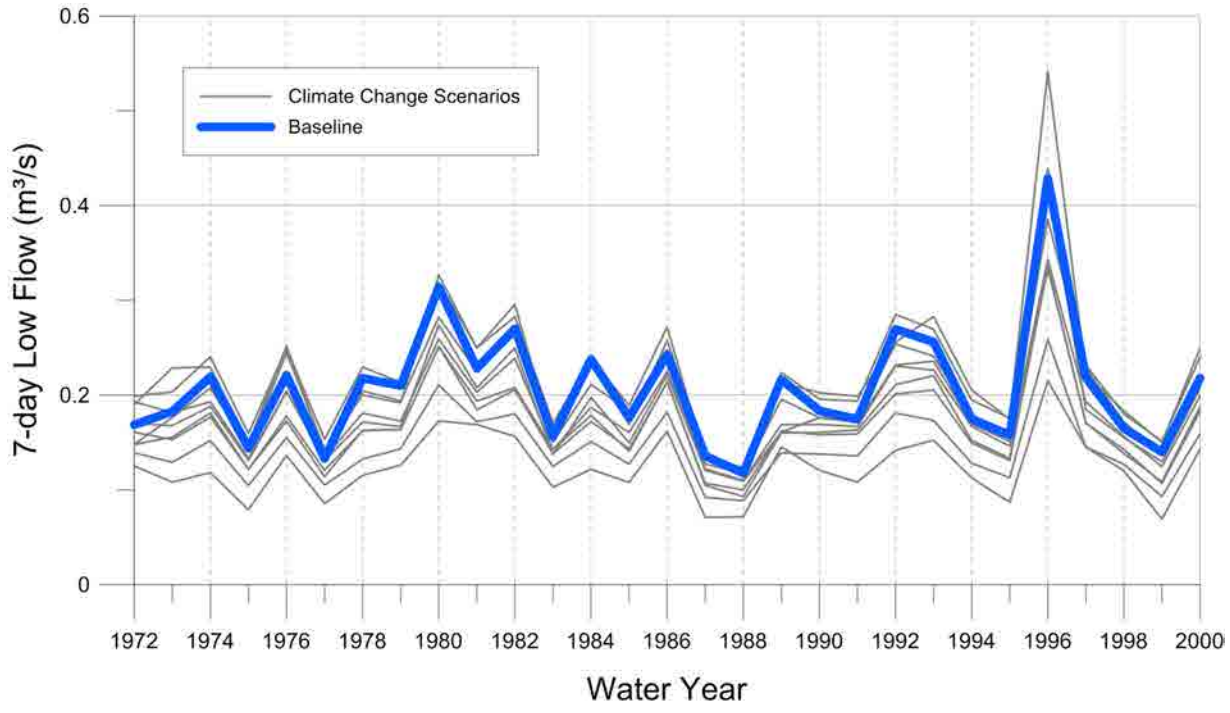

Figure D.37: Annual simulated 7-day low flow by water year in the Upper Talbot River.

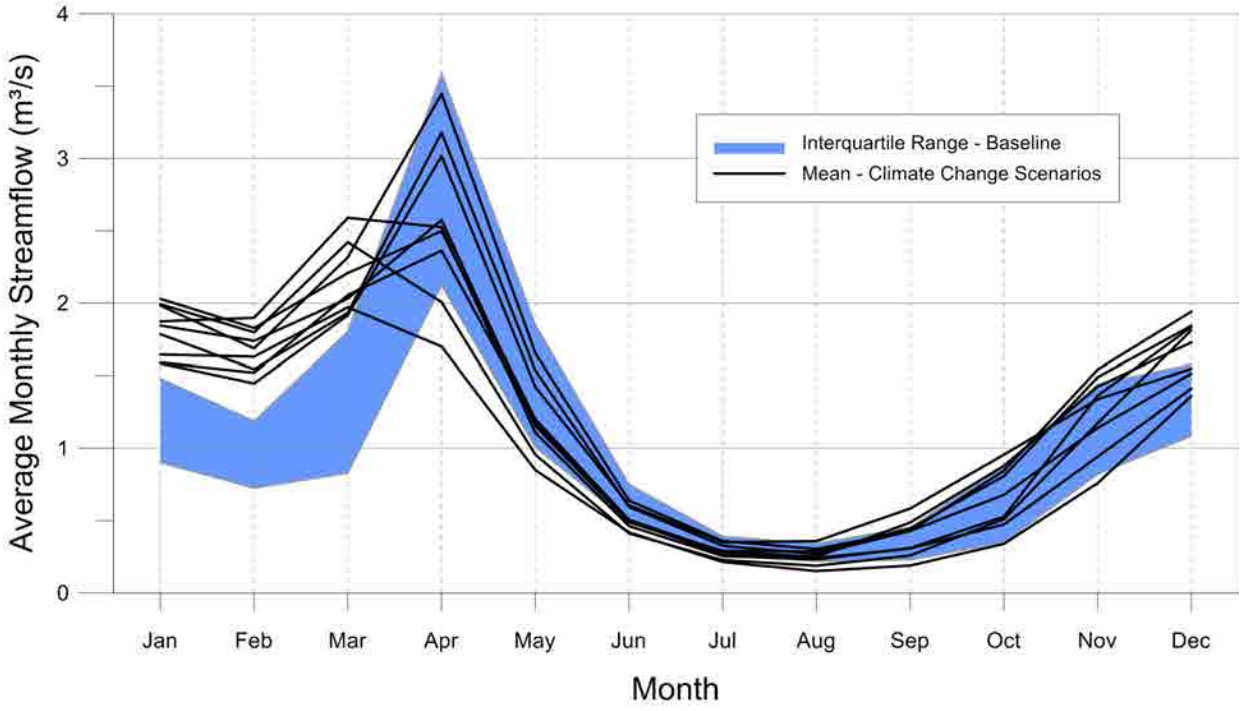

Figure D.38: Average simulated monthly streamflow in the Upper Talbot River.

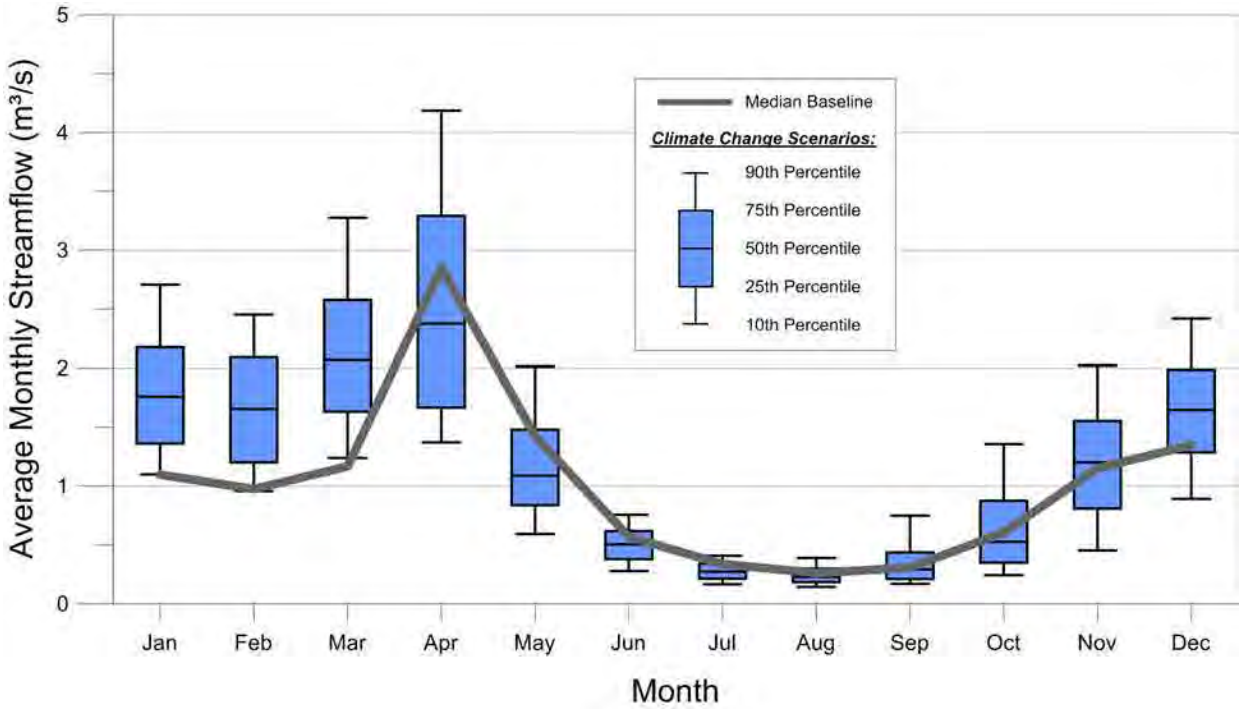

Figure D.39: Monthly simulated streamflow statistics for the Upper Talbot River.

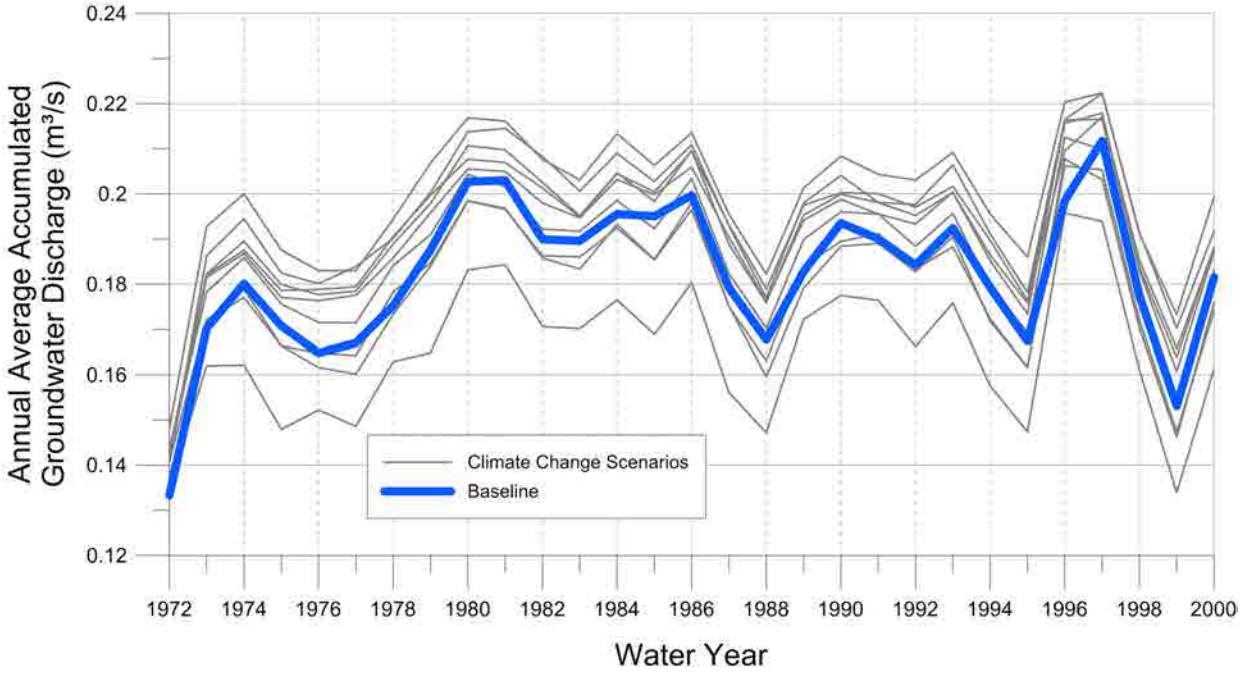

Figure D.40: Annual simulated average accumulated groundwater discharge by water year in the Upper Talbot River.

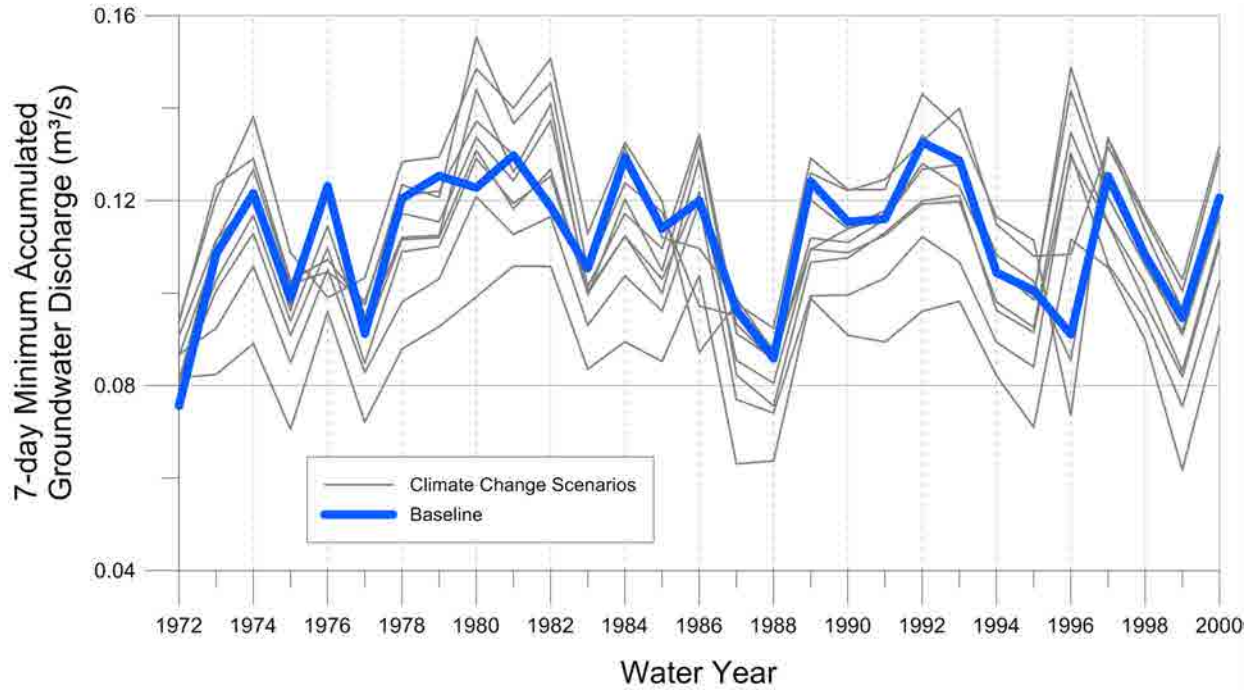

Figure D.41: Annual simulated 7-day low in accumulated groundwater discharge by water year in the Upper Talbot River.

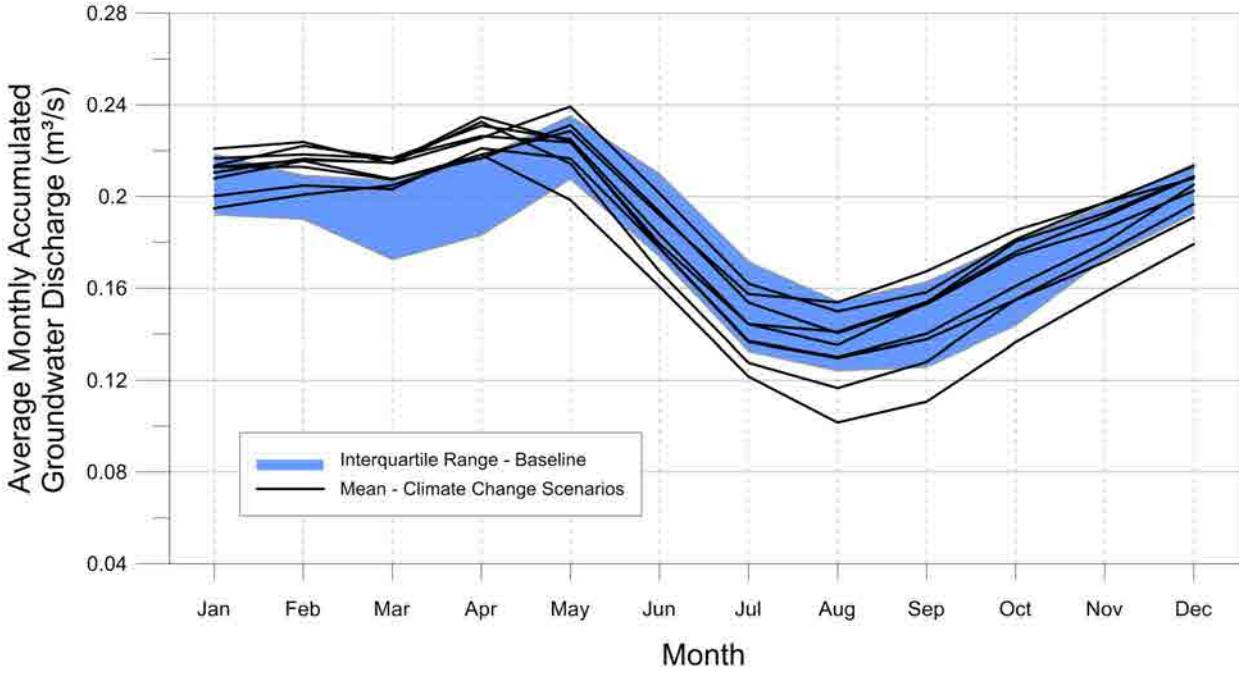

Figure D.42: Average monthly simulated accumulated groundwater discharge in the Upper Talbot River.

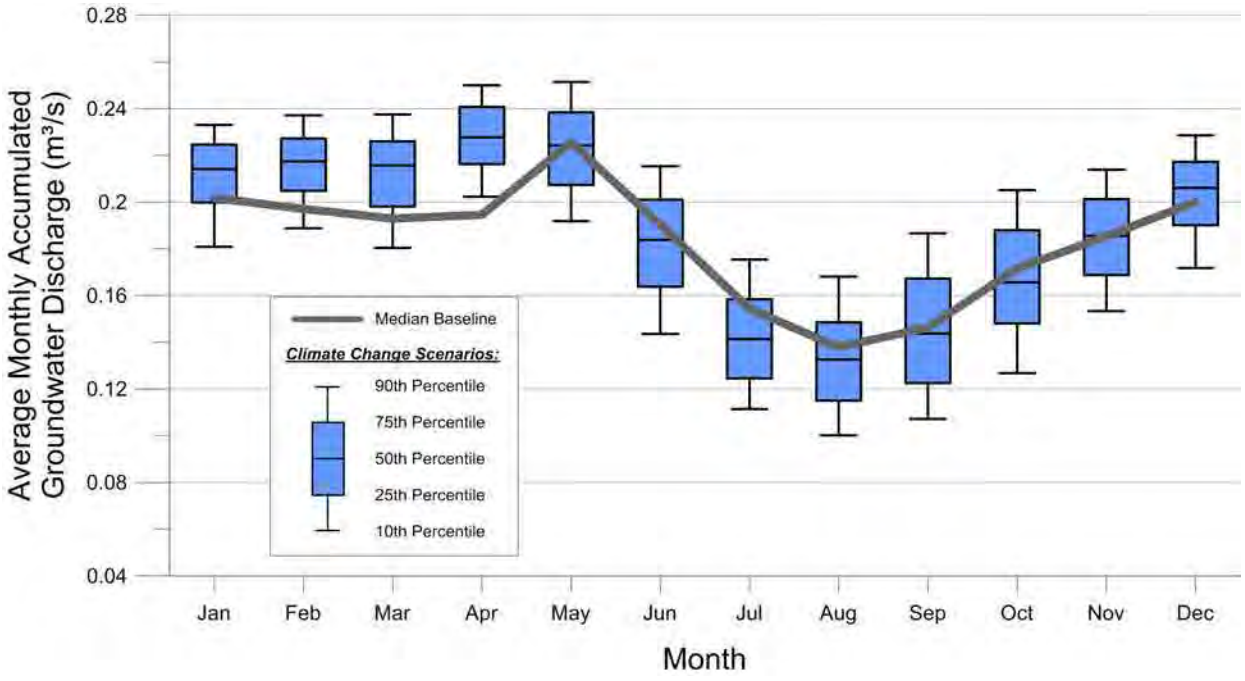

Figure D.43: Monthly simulated accumulated groundwater discharge statistics for the Upper Talbot River.

D.4 Rohallion Creek

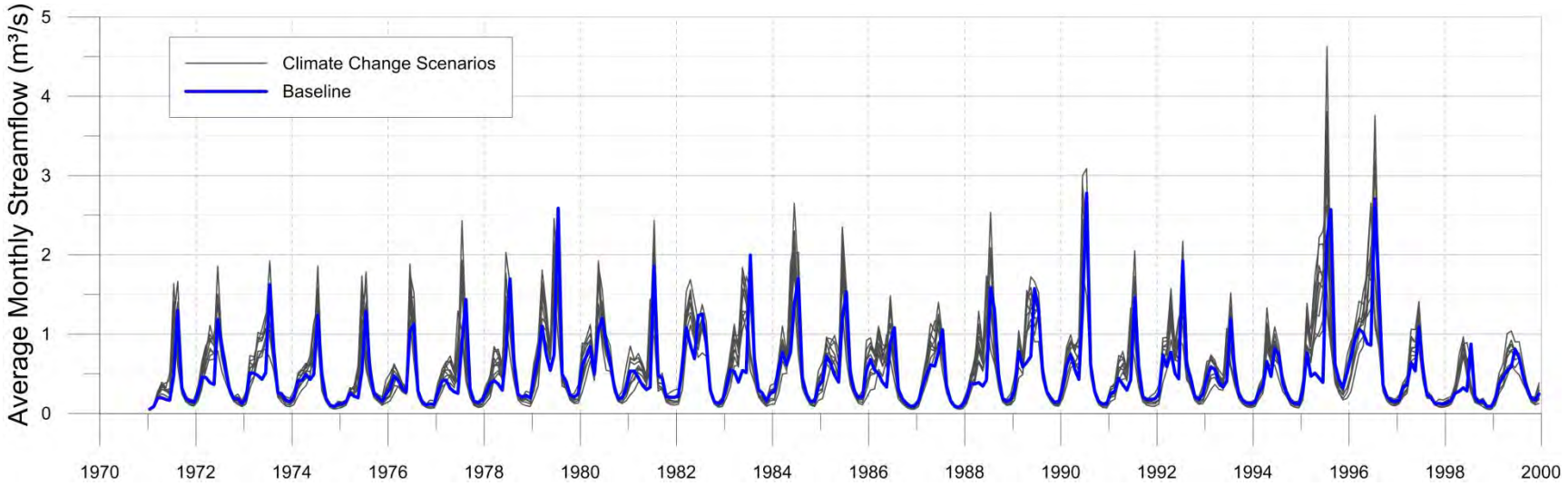

Figure D.44: Simulated monthly average streamflow by water year in Rohallion Creek.

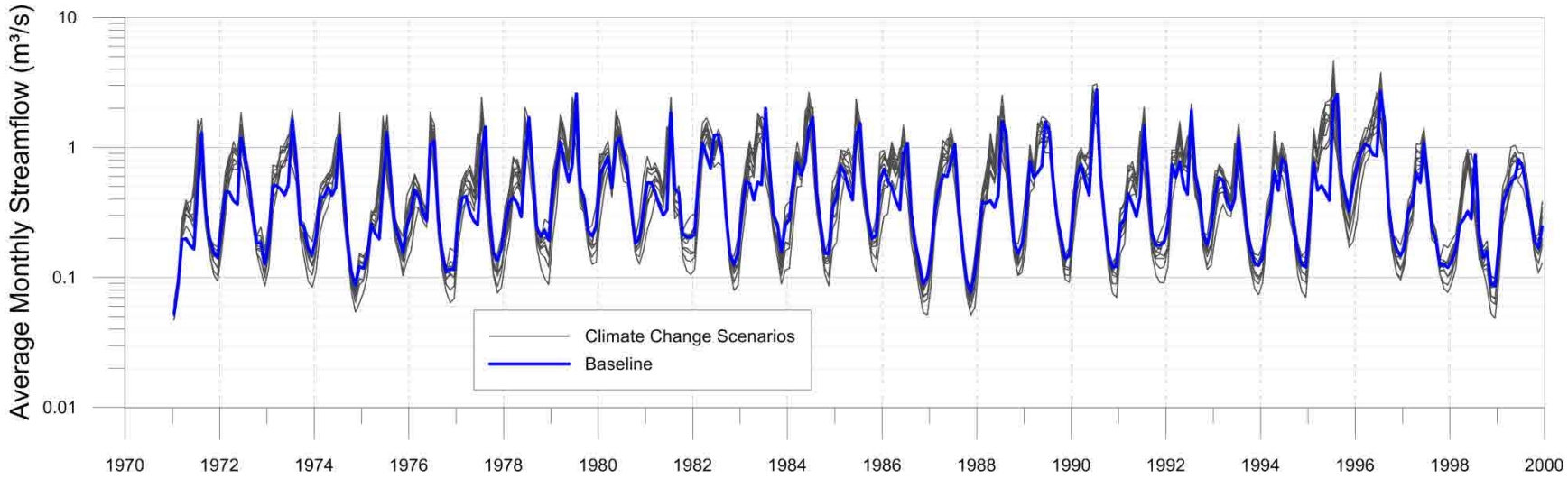

Figure D.45: Log simulated monthly average streamflow by water year in Rohallion Creek.

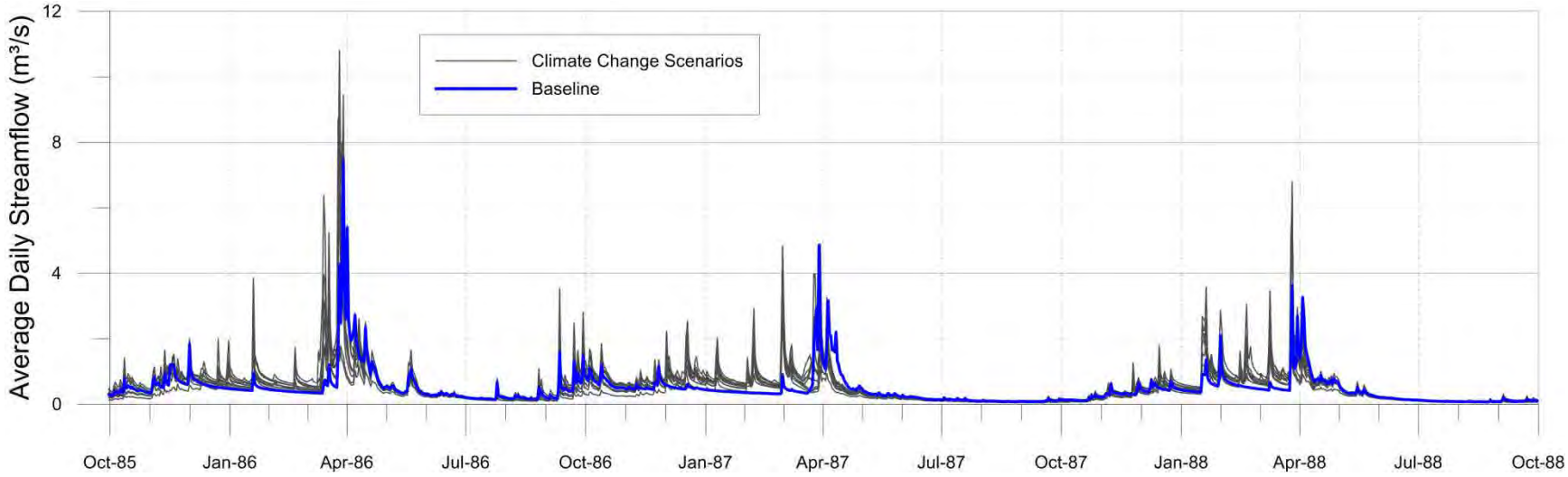

Figure D.46: Simulated daily streamflow in Rohallion Creek, water year 1986 through 1988.

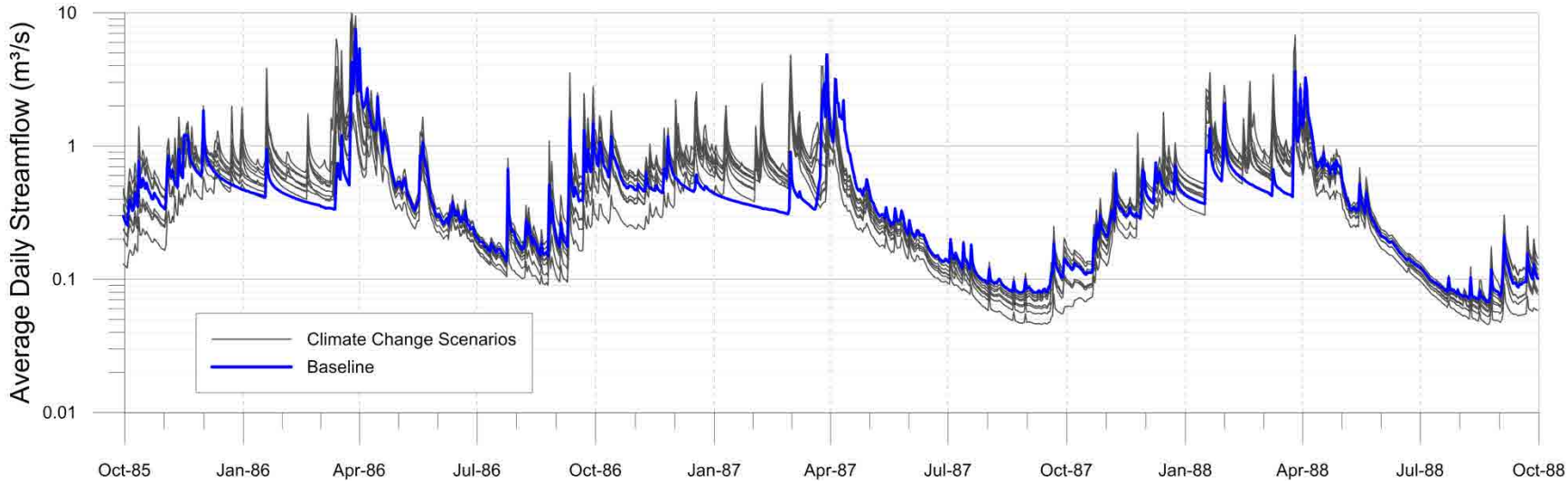

Figure D.47: Log simulated daily streamflow in Rohallion Creek, water year 1986 through 1988.

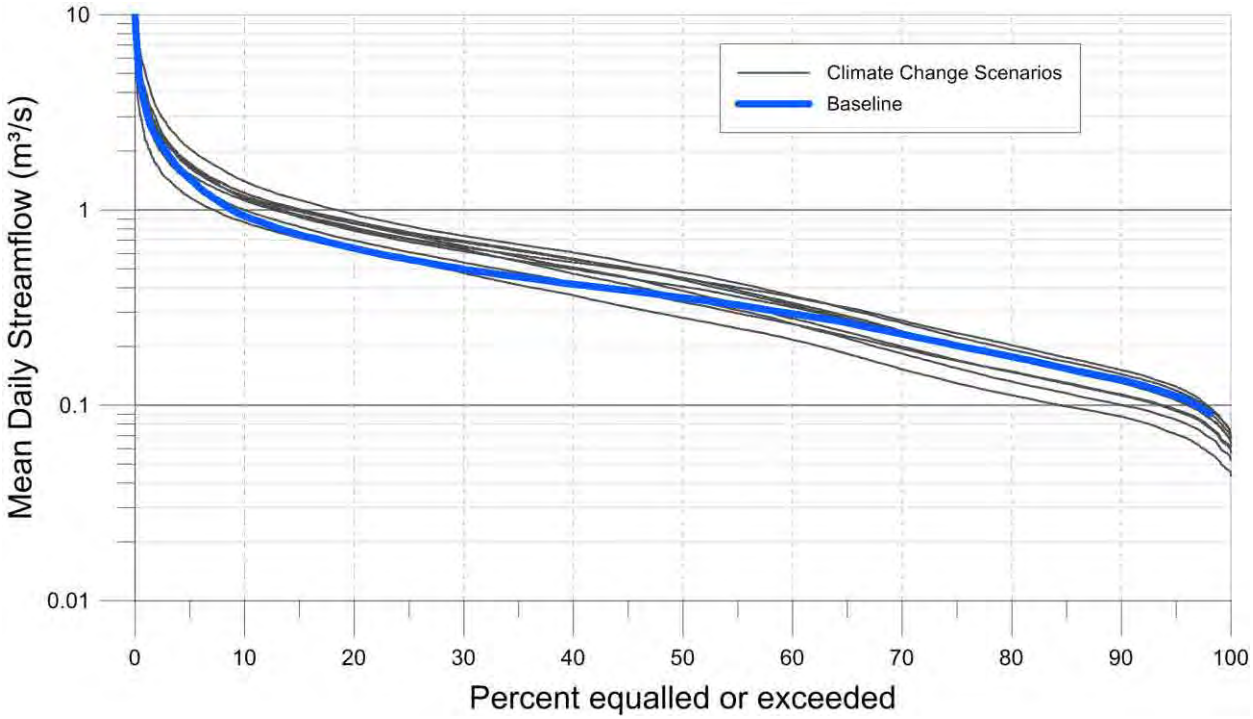

Figure D.48: Rohallion Creek streamflow duration curve, water year 1973 through 2000.

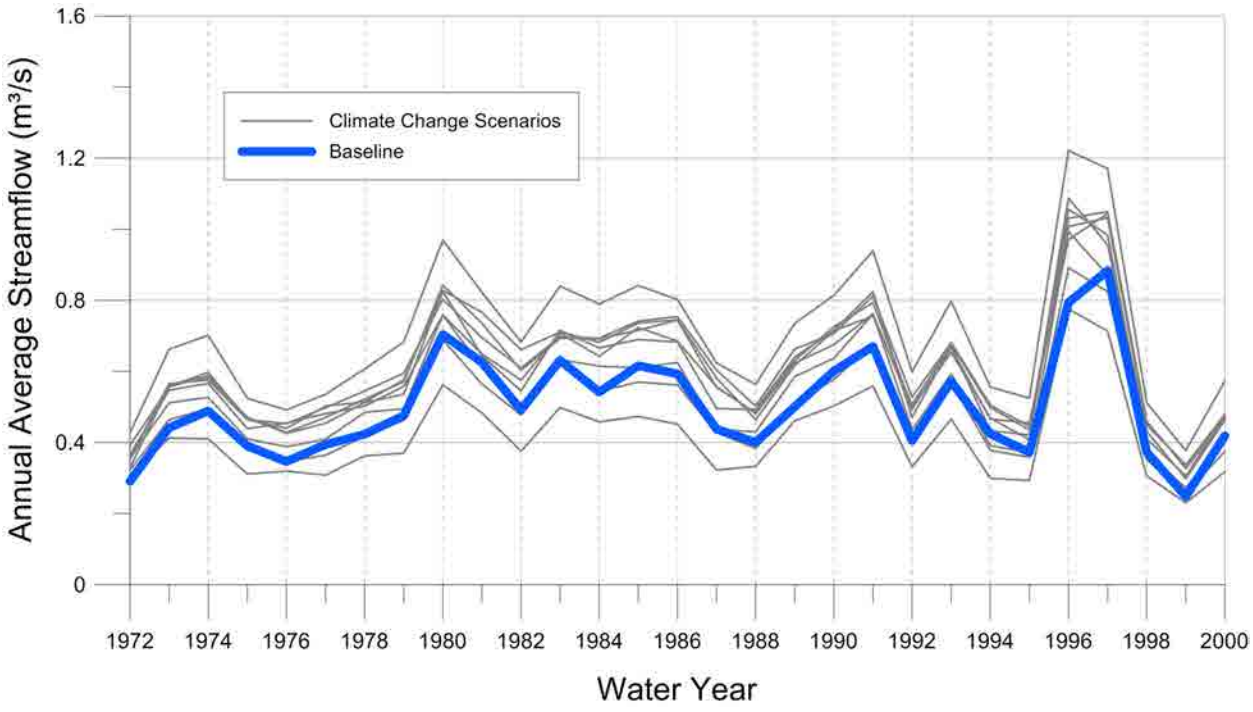

Figure D.49: Average annual simulated streamflow by water year in Rohallion Creek.

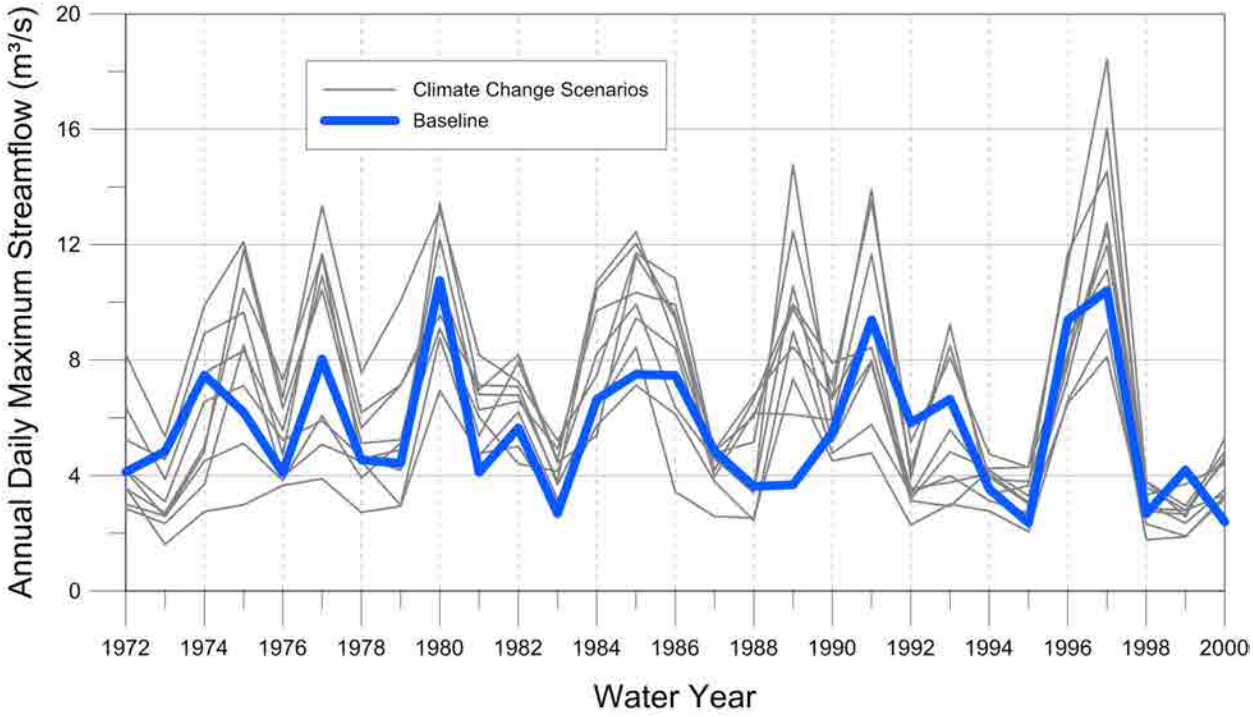

Figure D.50: Annual maximum simulated daily streamflow by water year in Rohallion Creek.

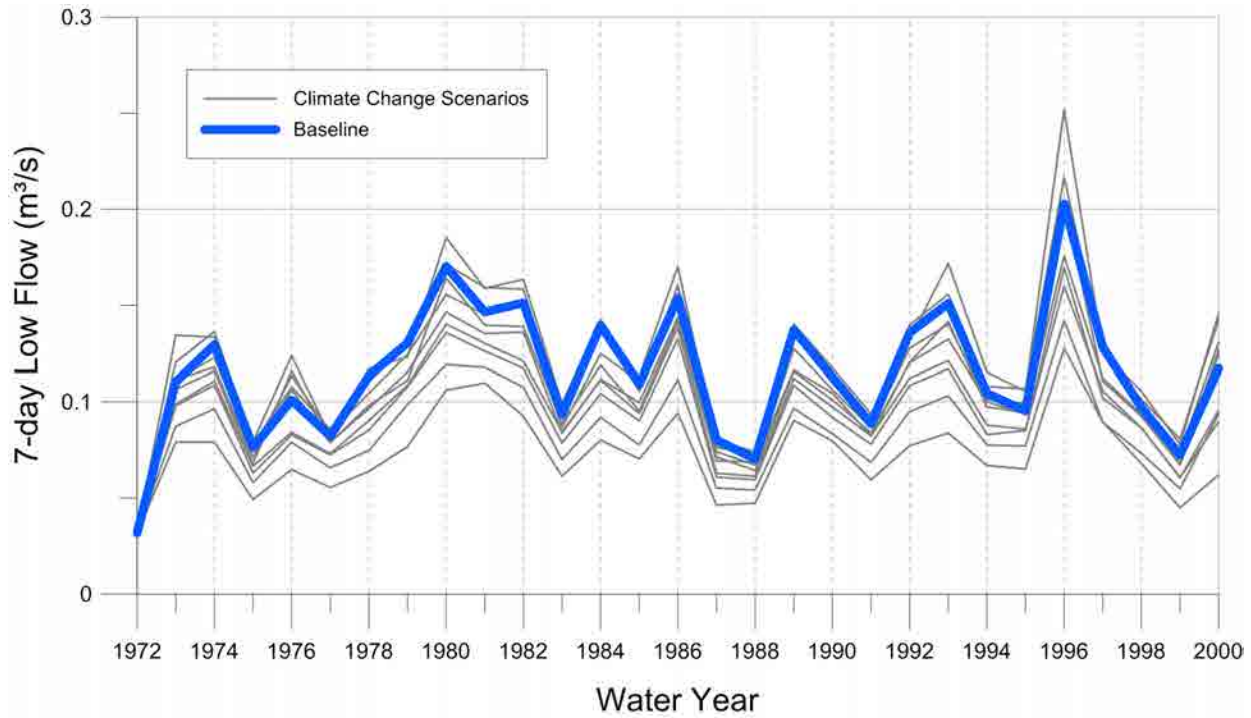

Figure D.51: Annual simulated 7-day low flow by water year in Rohallion Creek.

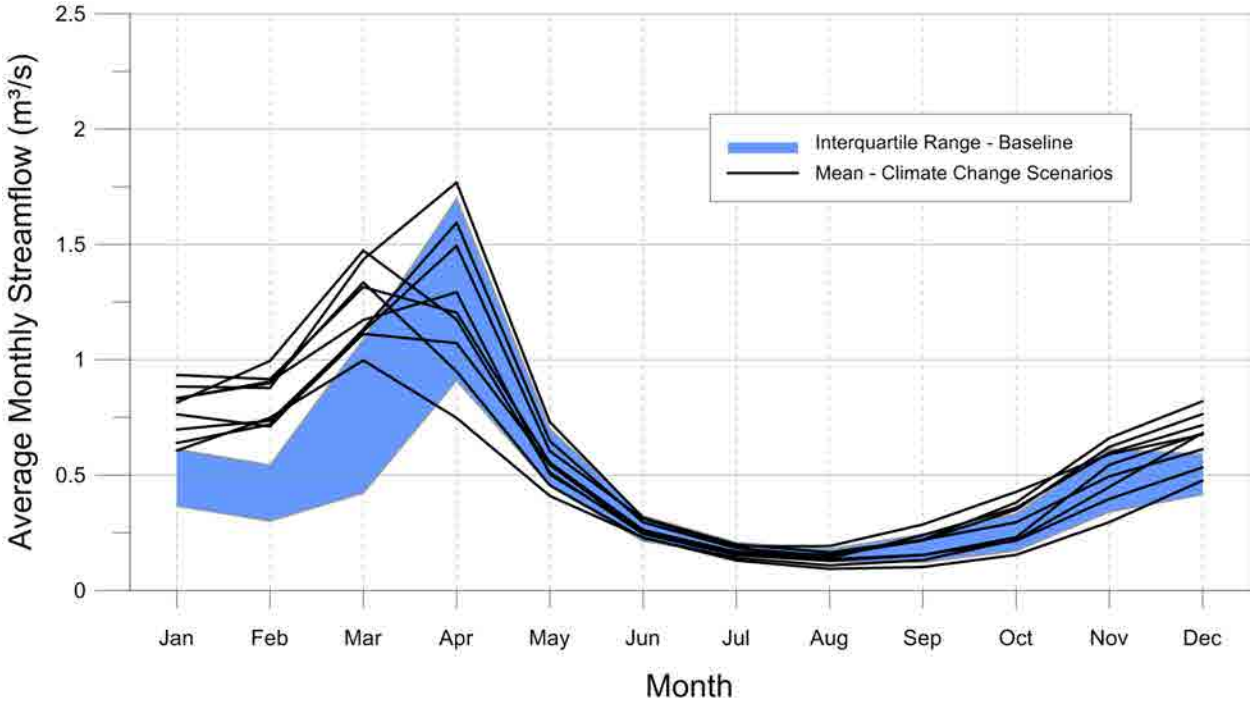

Figure D.52: Average simulated monthly streamflow in Rohallion Creek.

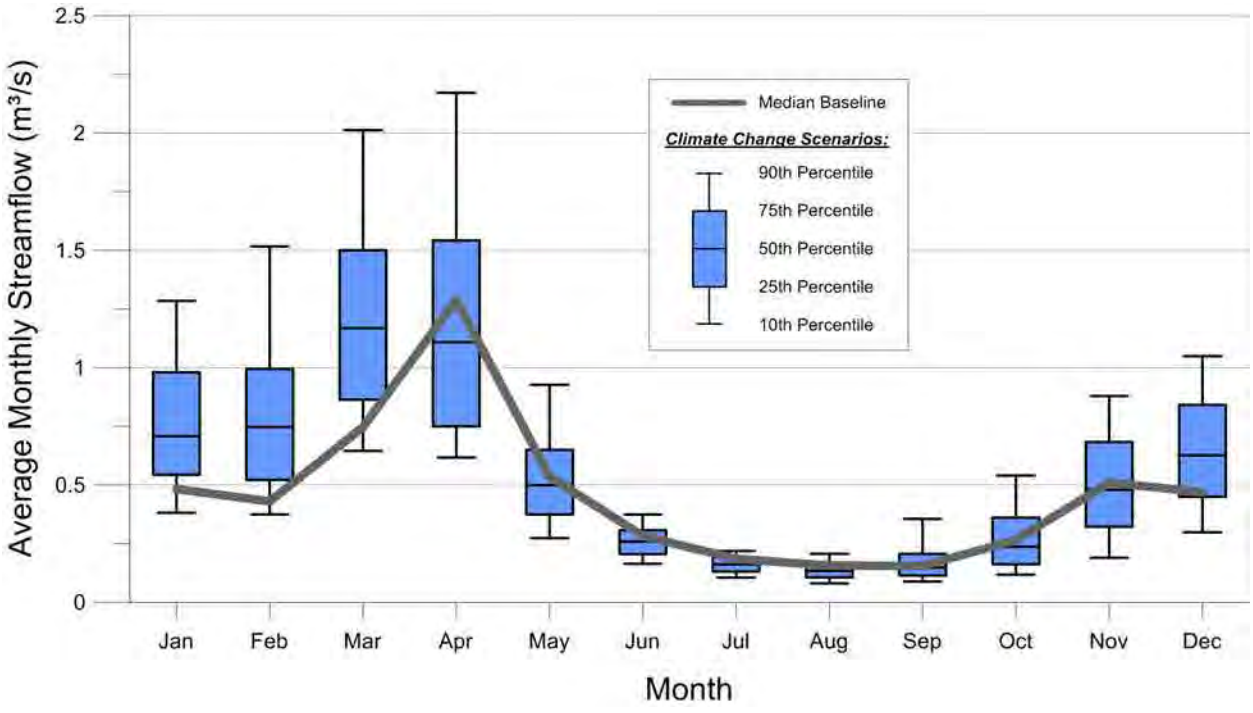

Figure D.53: Monthly simulated streamflow statistics for Rohallion Creek.

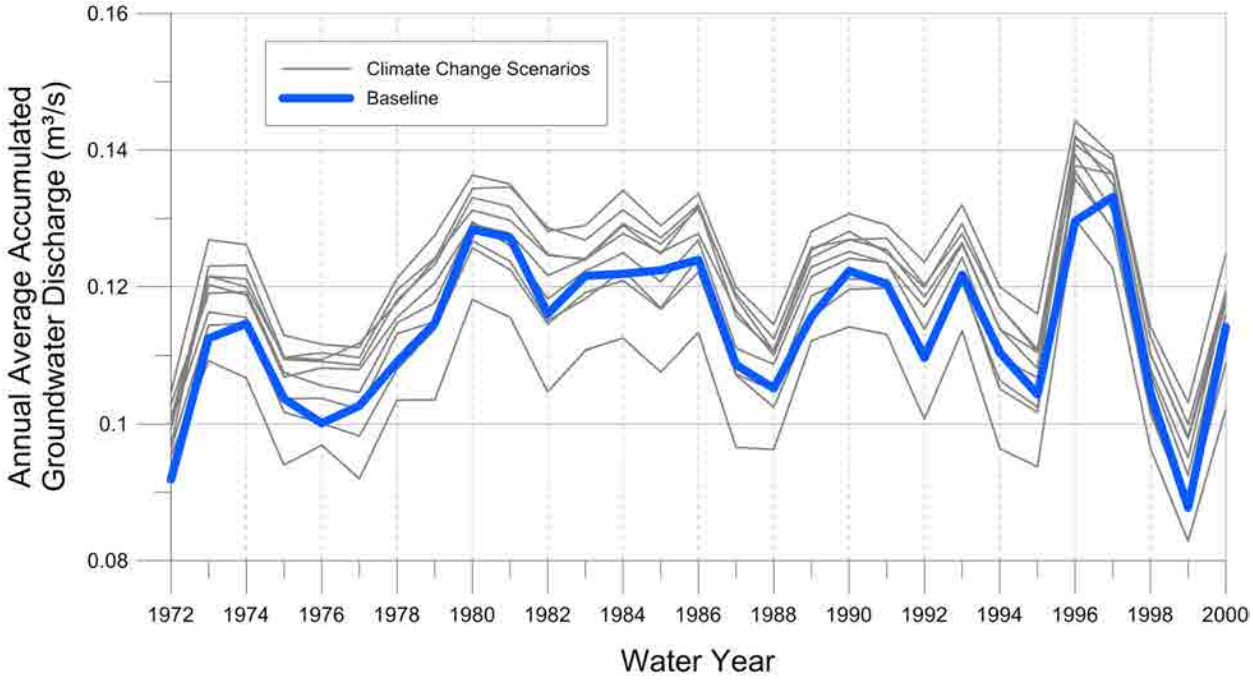

Figure D.54: Annual simulated average accumulated groundwater discharge by water year in Rohallion Creek.

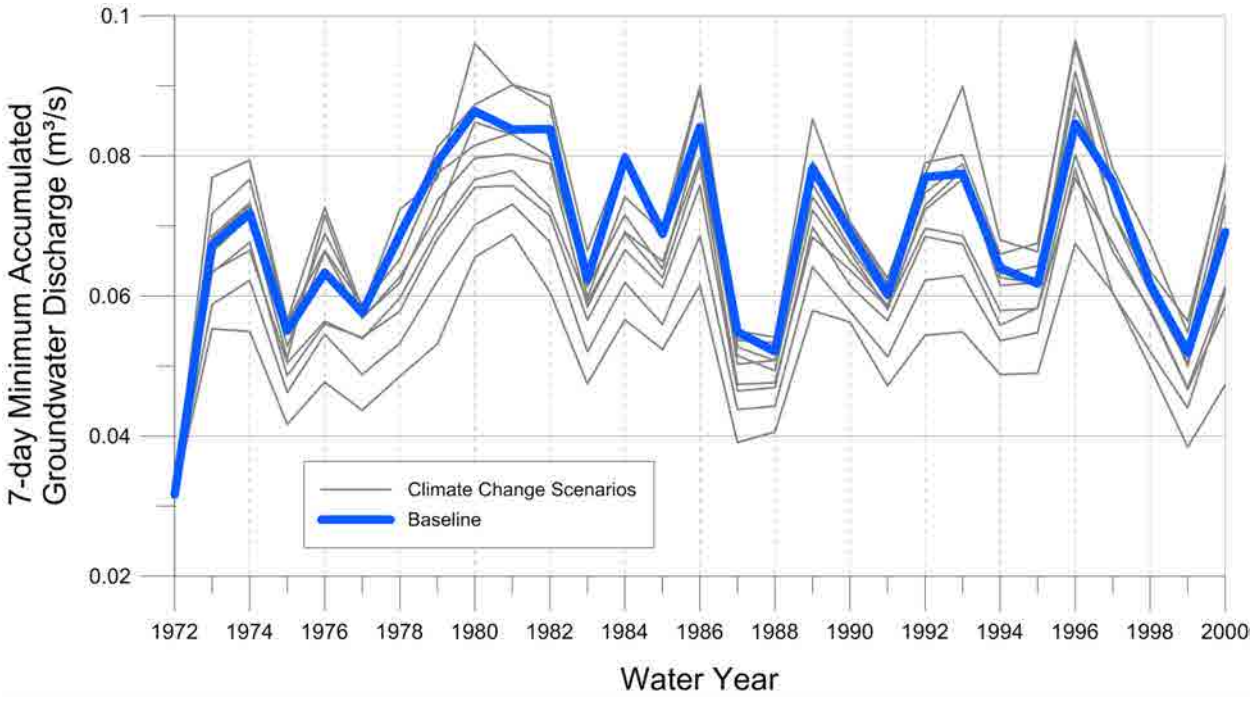

Figure D.55: Annual simulated 7-day low in accumulated groundwater discharge by water year in Rohallion Creek.

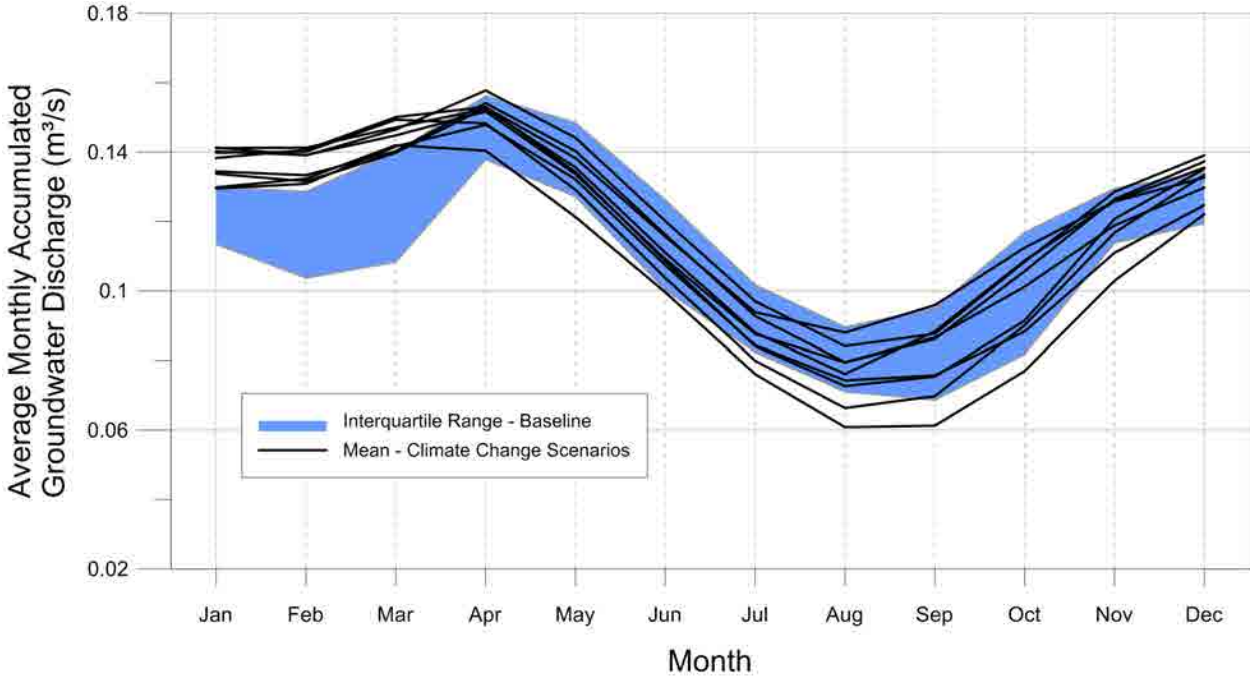

Figure D.56: Average monthly simulated accumulated groundwater discharge in Rohallion Creek.

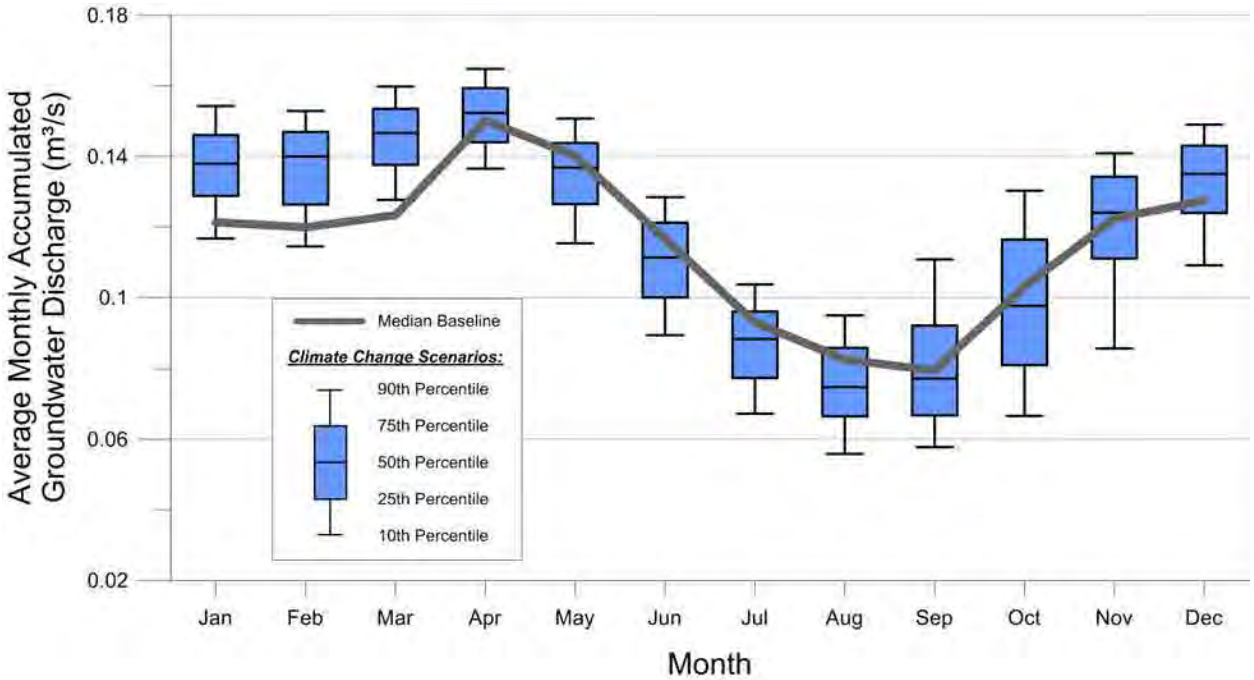

Figure D.57: Monthly simulated accumulated groundwater discharge statistics for Rohallion Creek.

D.5 Butternut Creek

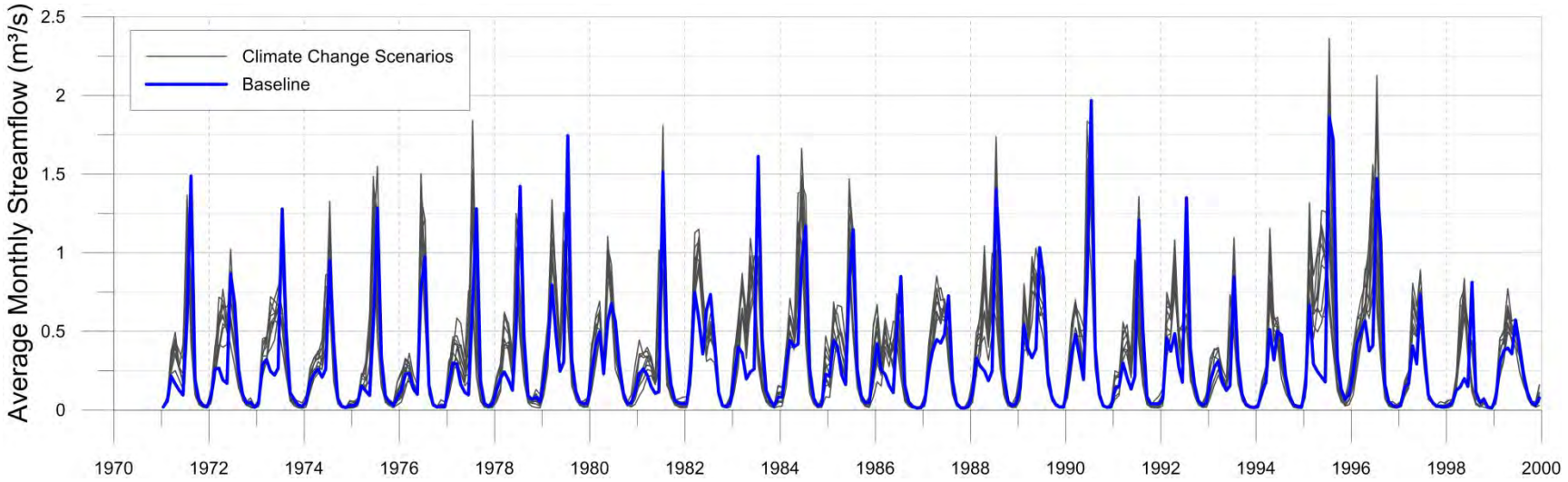

Figure D.58: Simulated monthly average streamflow by water year in Butternut Creek.

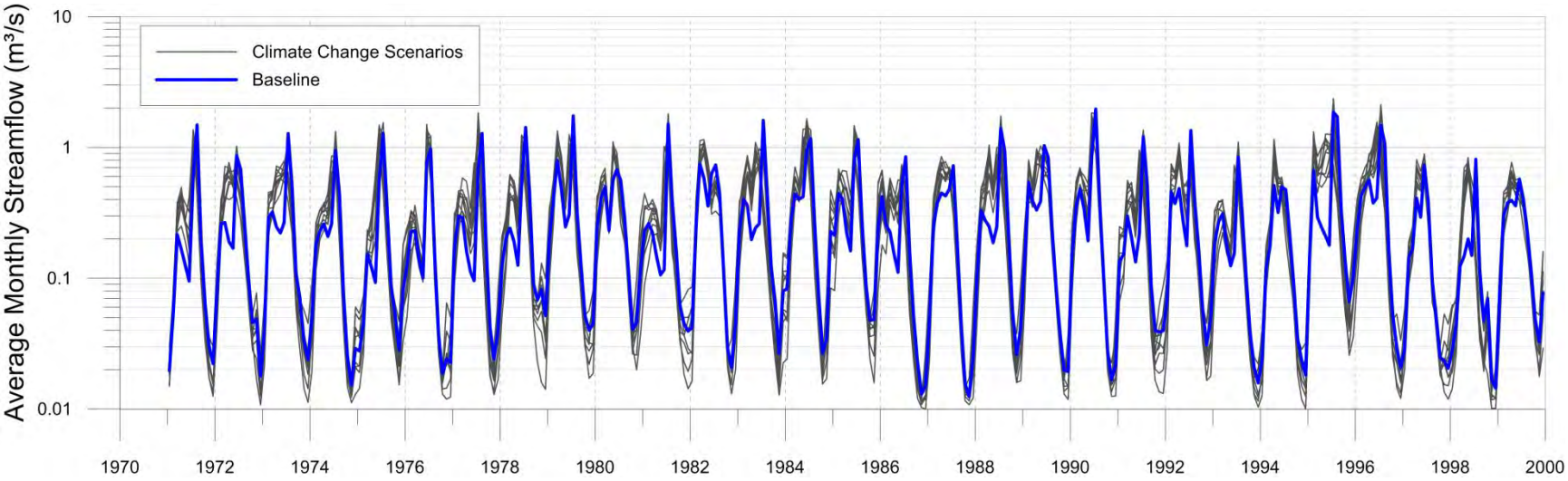

Figure D.59: Log simulated monthly average streamflow by water year in Butternut Creek.

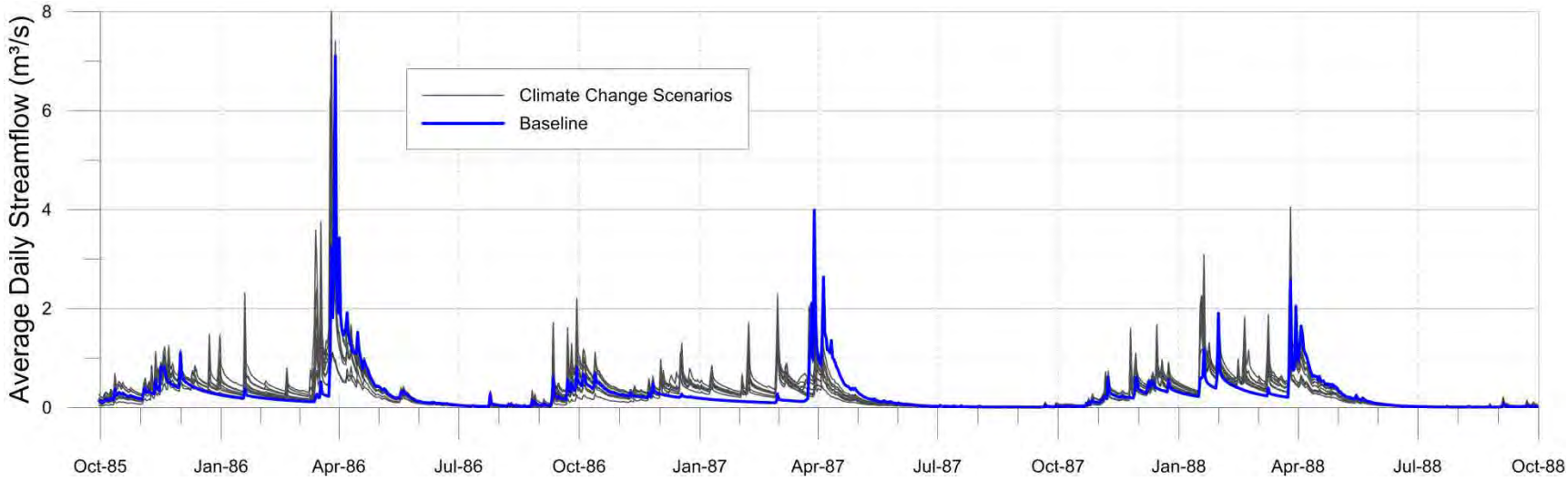

Figure D.60: Simulated daily streamflow in Butternut Creek, water year 1986 through 1988.

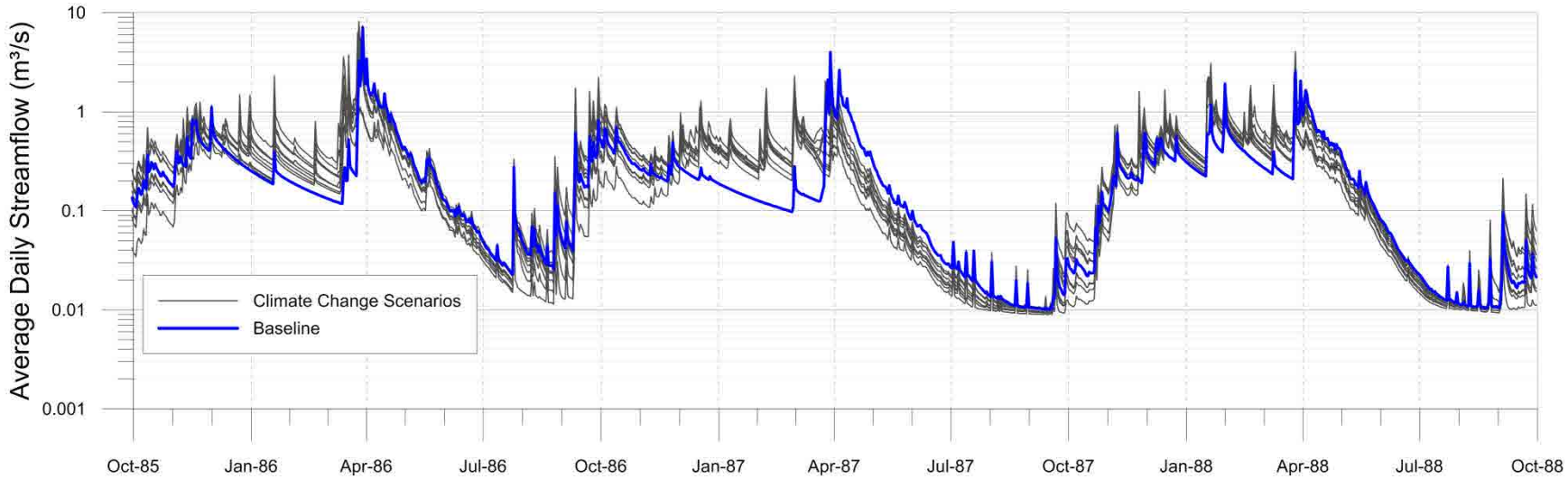

Figure D.61: Log simulated daily streamflow in Butternut Creek, water year 1986 through 1988.

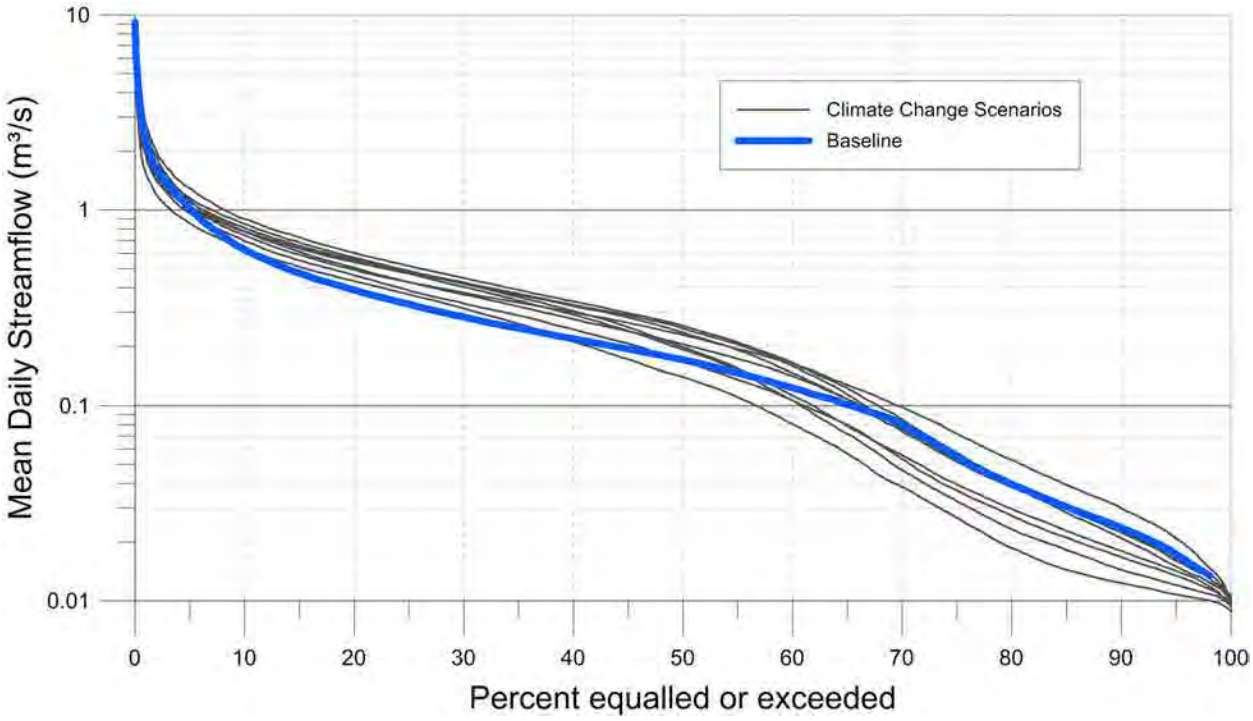

Figure D.62: Butternut Creek streamflow duration curve, water year 1973 through 2000.

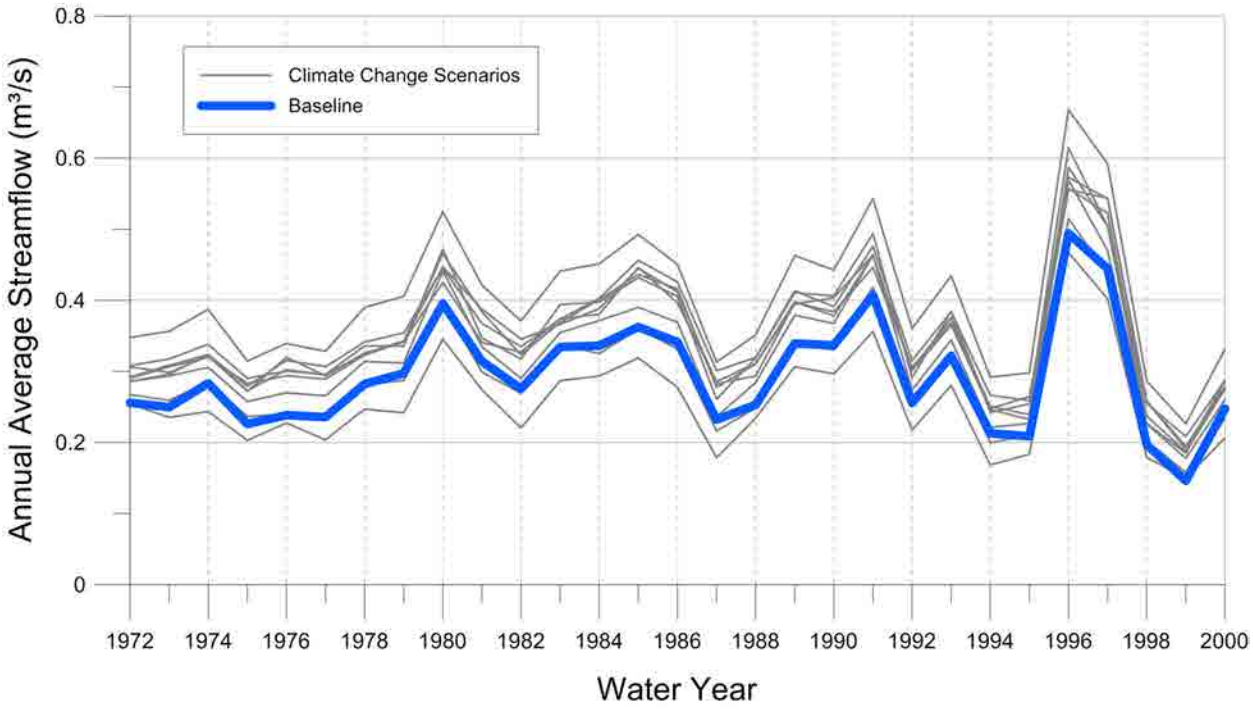

Figure D.63: Average annual simulated streamflow by water year in Butternut Creek.

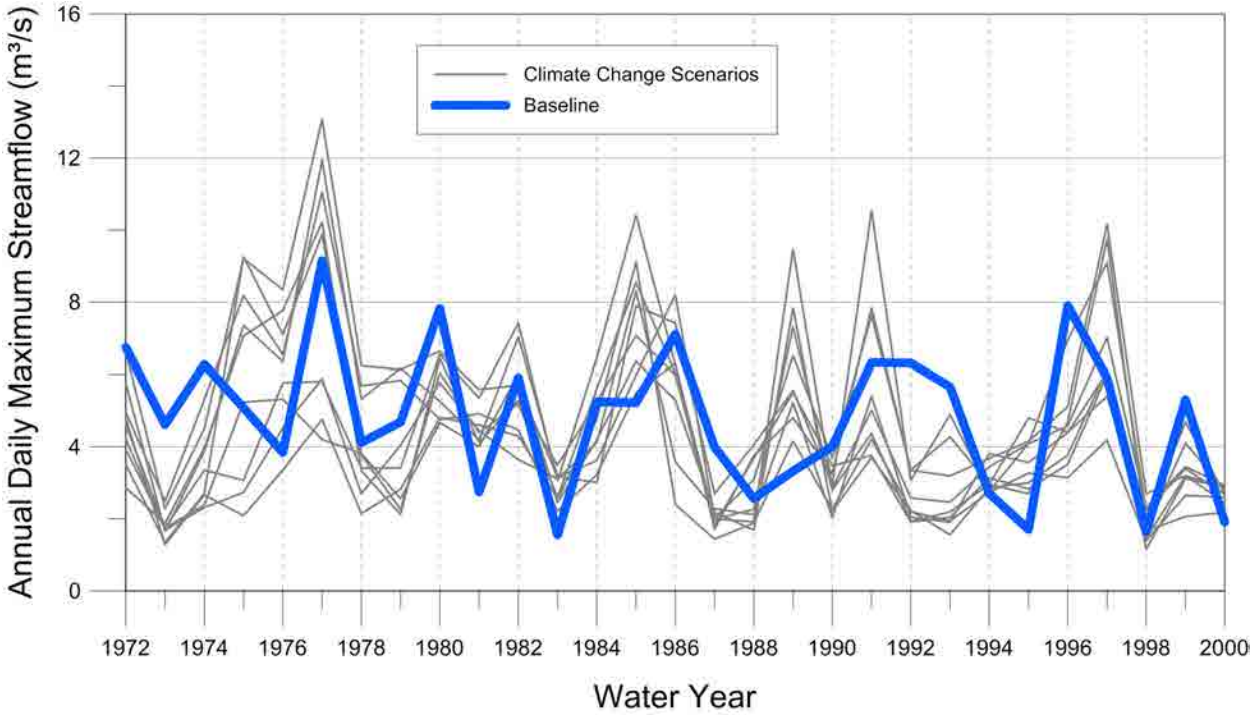

Figure D.64: Annual maximum simulated daily streamflow by water year in Butternut Creek.

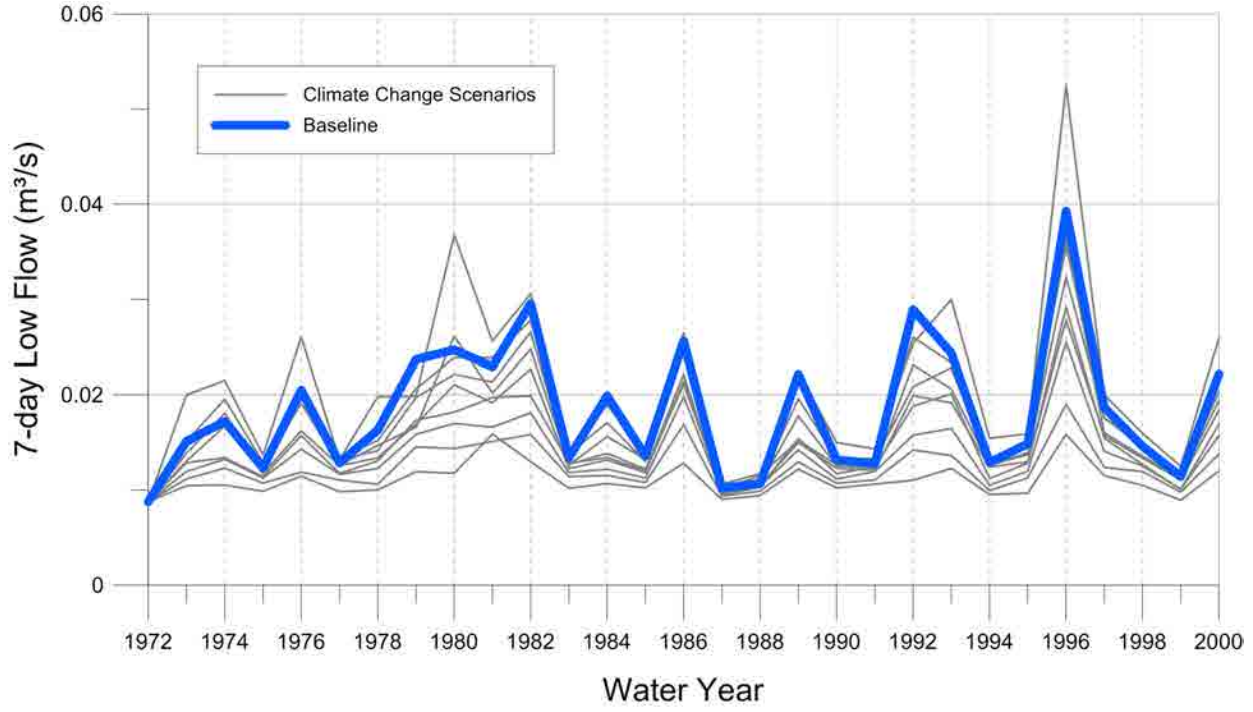

Figure D.65: Annual simulated 7-day low flow by water year in Butternut Creek.

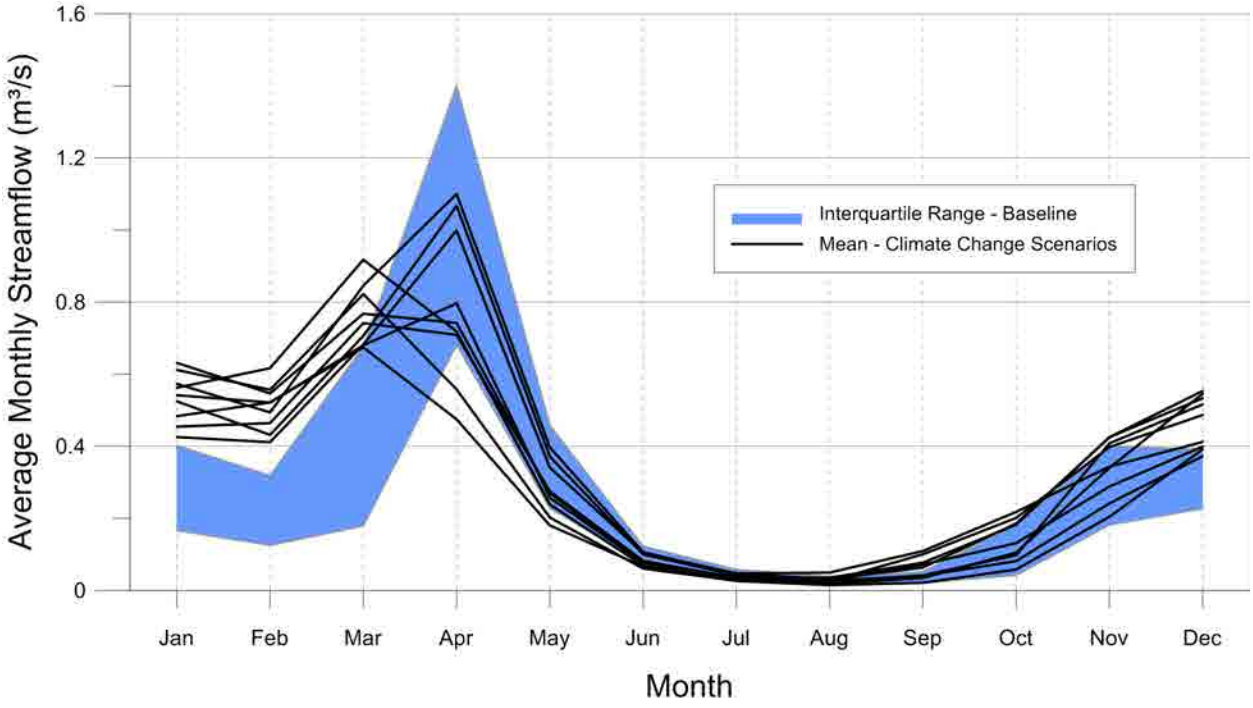

Figure D.66: Average simulated monthly streamflow in Butternut Creek.

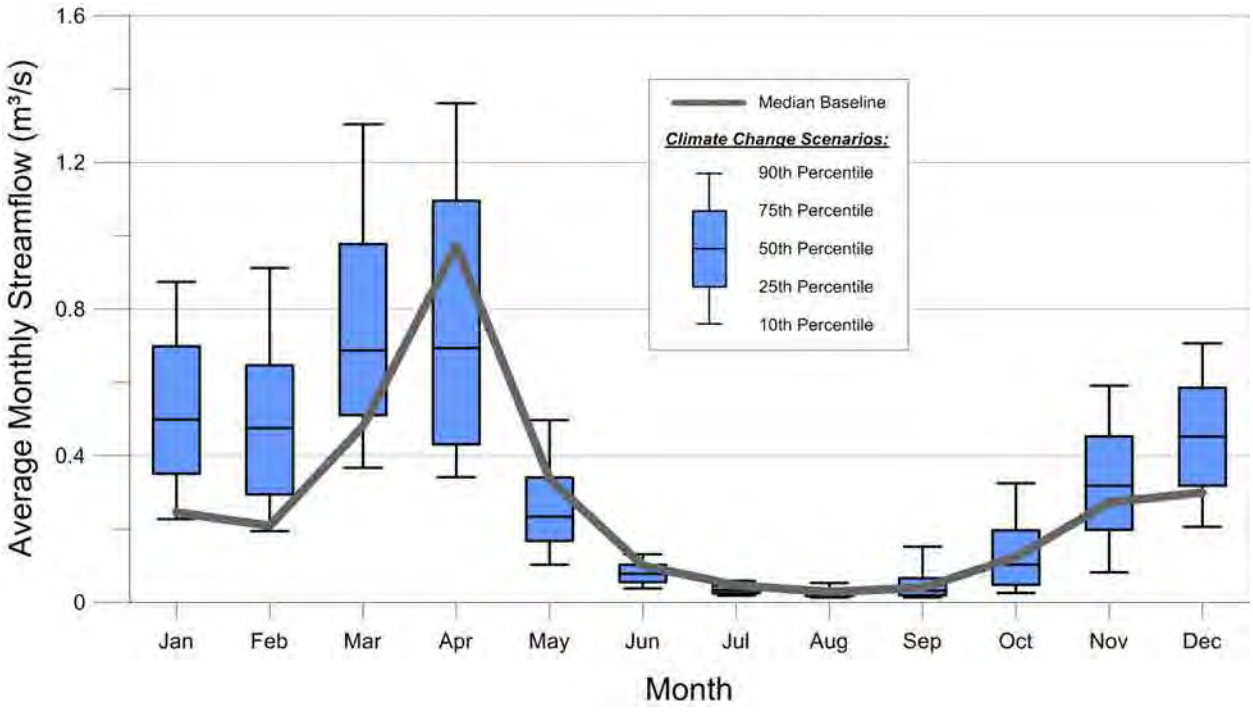

Figure D.67: Monthly simulated streamflow statistics for Butternut Creek.

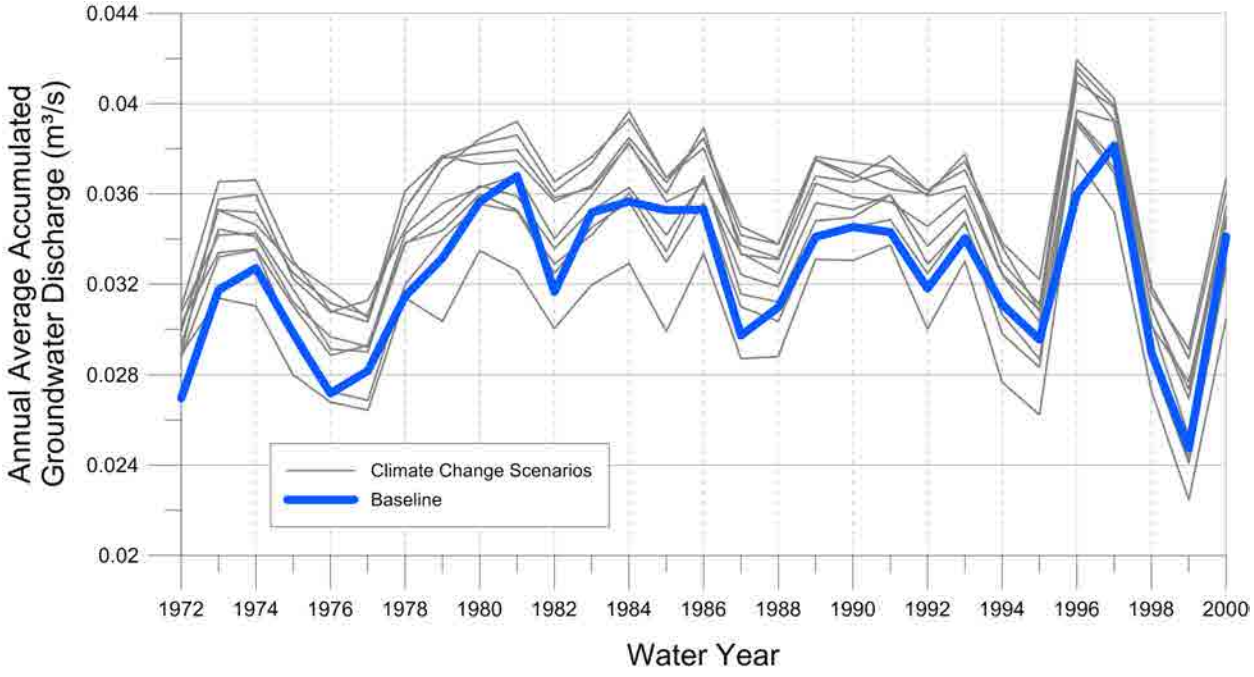

Figure D.68: Annual simulated average accumulated groundwater discharge by water year in Butternut Creek.

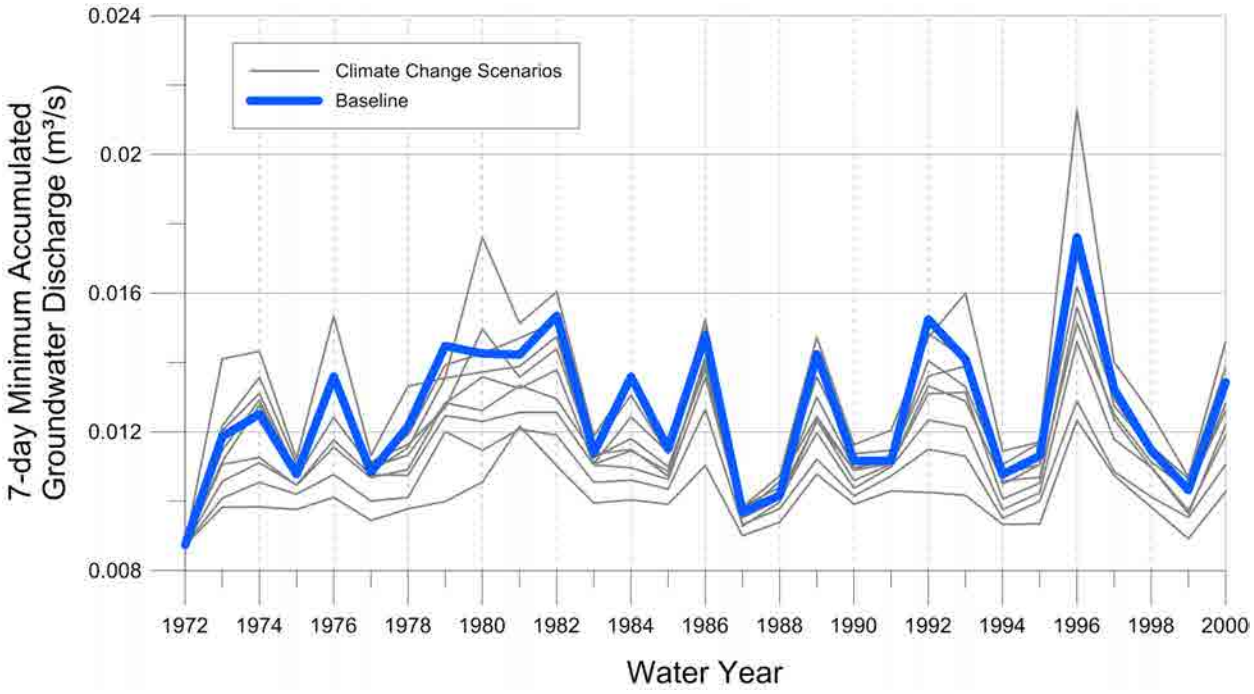

Figure D.69: Annual simulated 7-day low in accumulated groundwater discharge by water year in Butternut Creek.

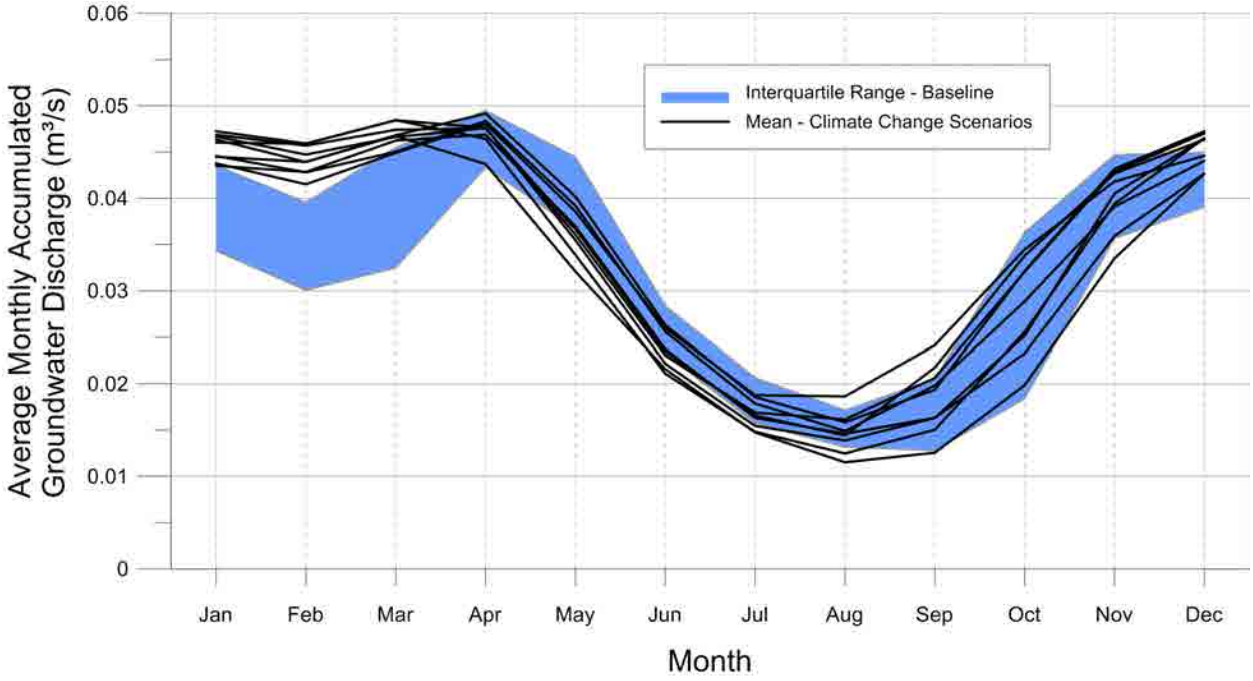

Figure D.70: Average monthly simulated accumulated groundwater discharge in Butternut Creek.

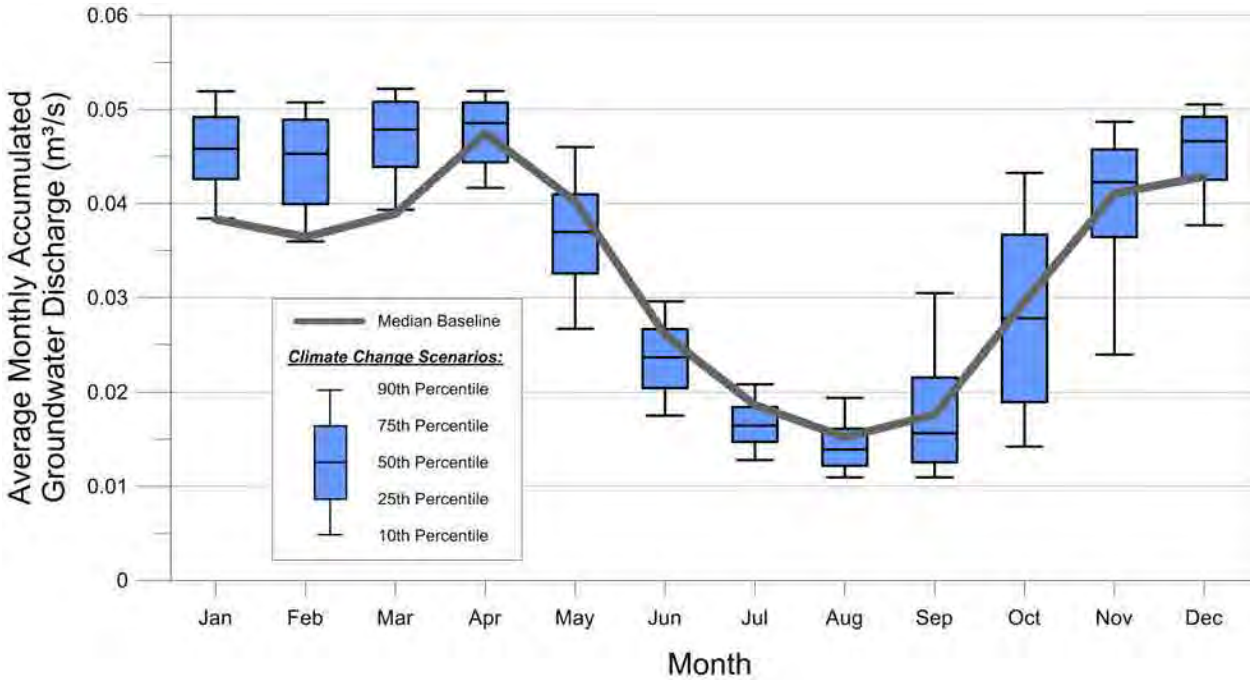

Figure D.71: Monthly simulated accumulated groundwater discharge statistics for Butternut Creek.

D.6 Wainman's Creek

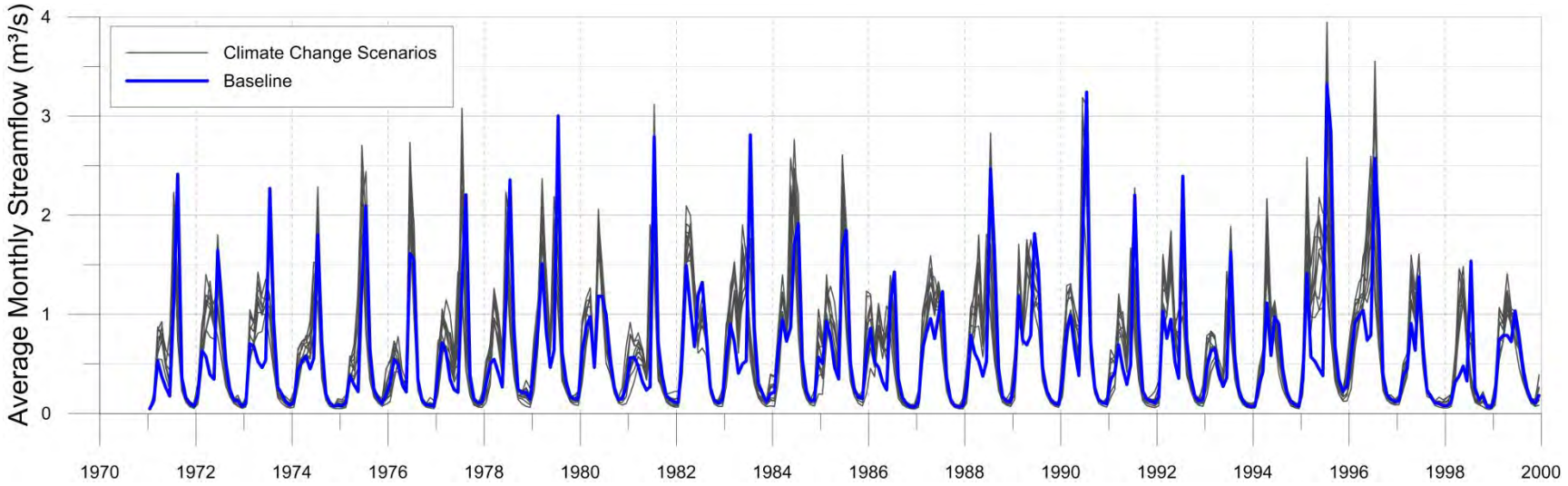

Figure D.72: Simulated monthly average streamflow by water year in Wainman's Creek.

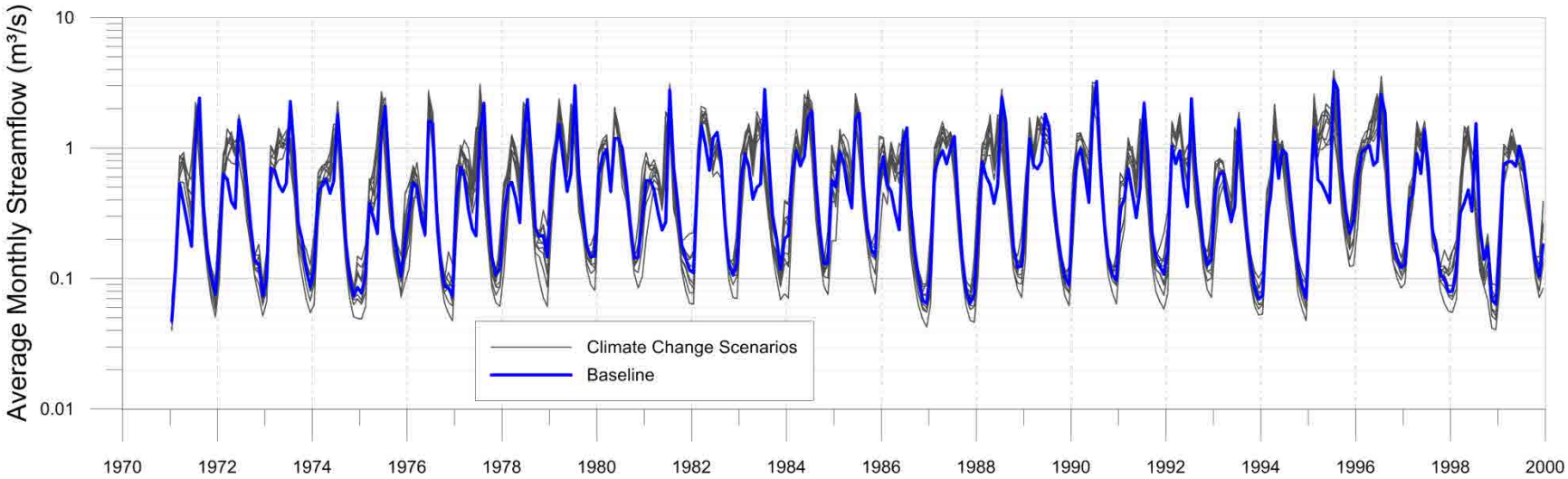

Figure D.73: Log simulated monthly average streamflow by water year in Wainman's Creek.

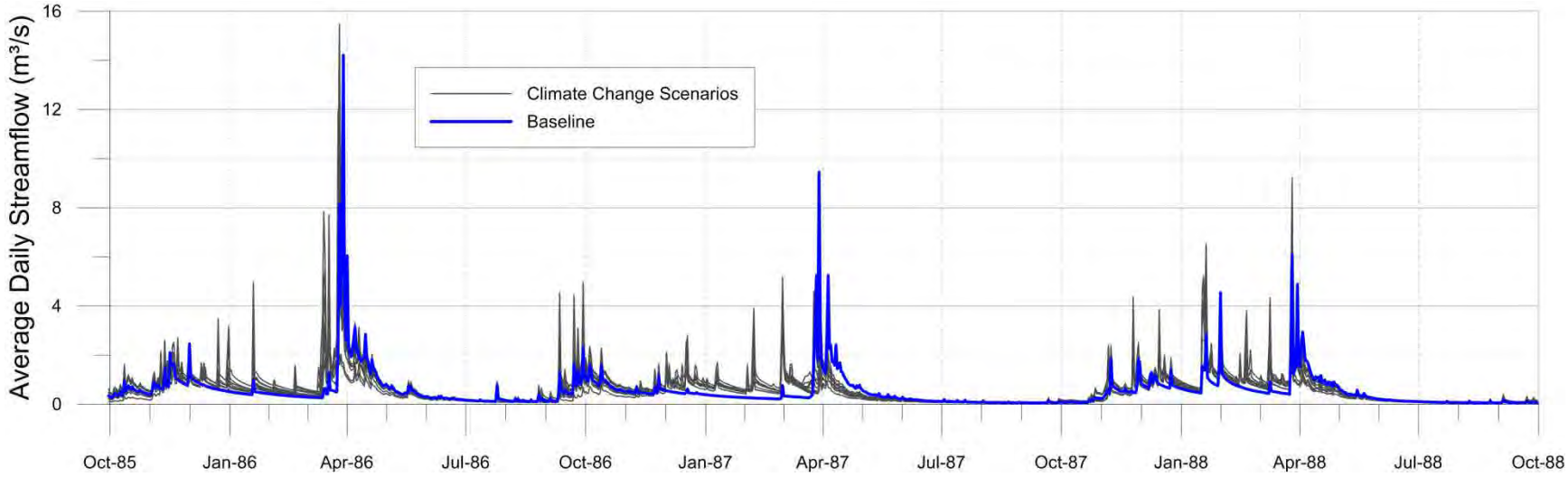

Figure D.74: Simulated daily streamflow in Wainman's Creek, water year 1986 through 1988.

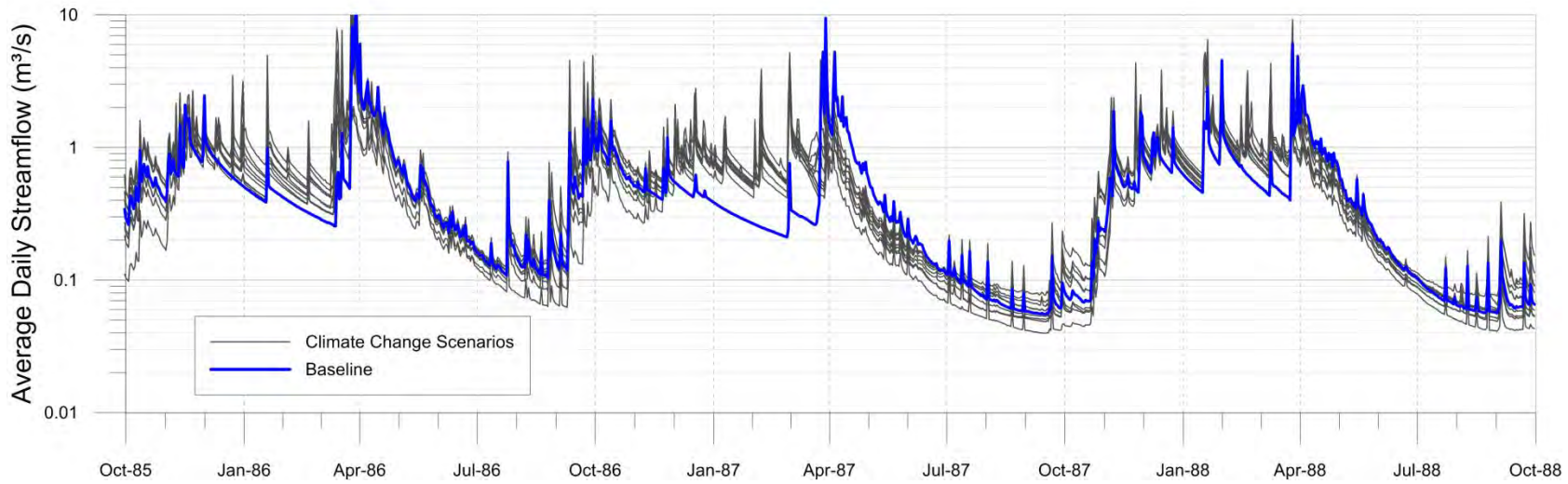

Figure D.75: Log simulated daily streamflow in Wainman's Creek, water year 1986 through 1988.

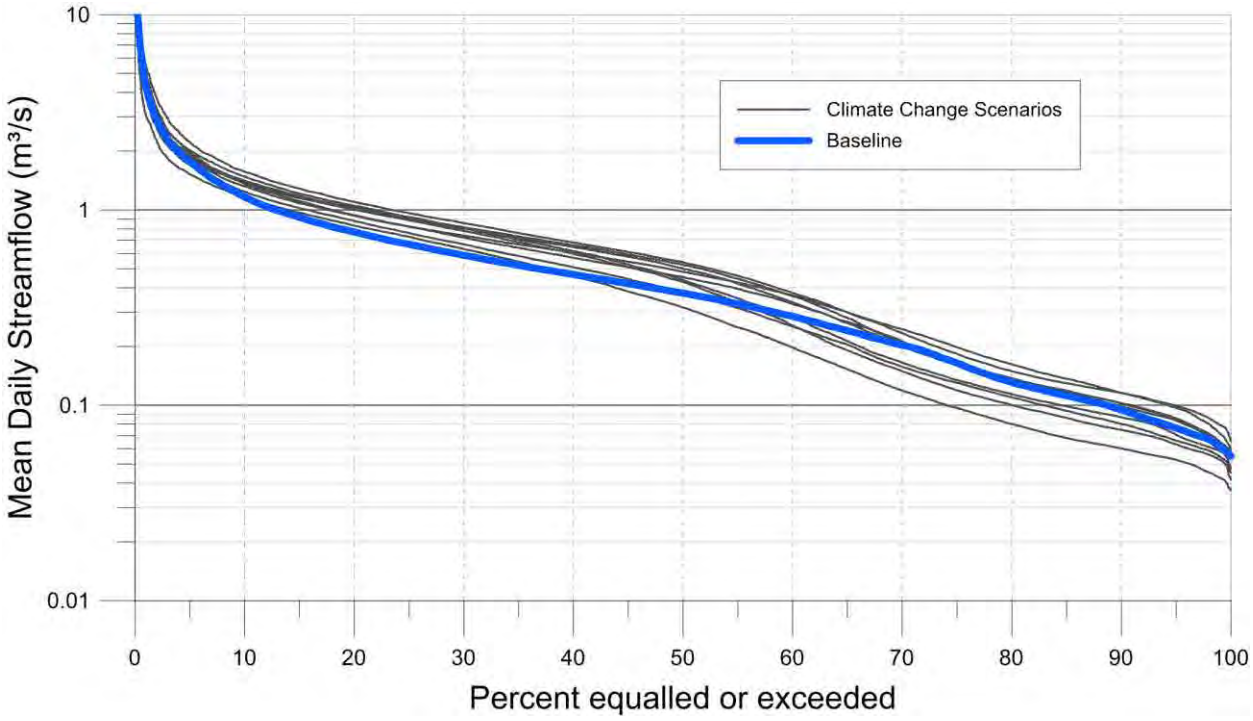

Figure D.76: Wainman's Creek streamflow duration curve, water year 1973 through 2000.

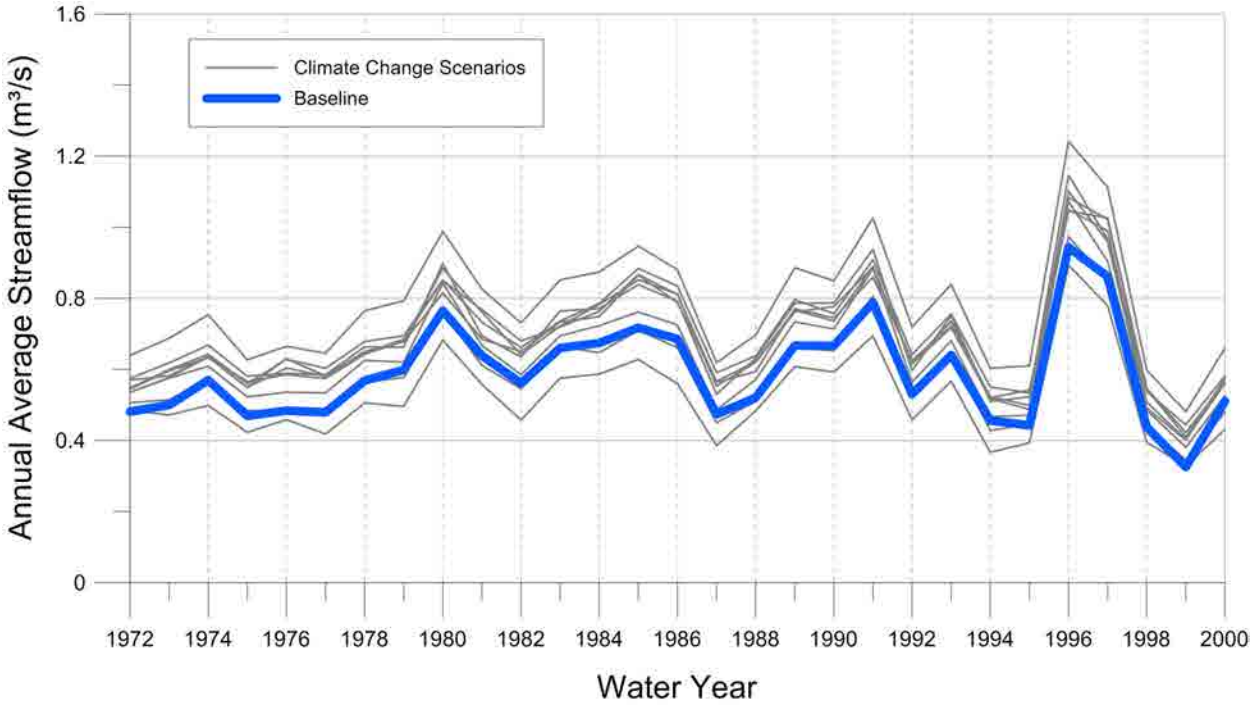

Figure D.77: Average annual simulated streamflow by water year in Wainman's Creek.

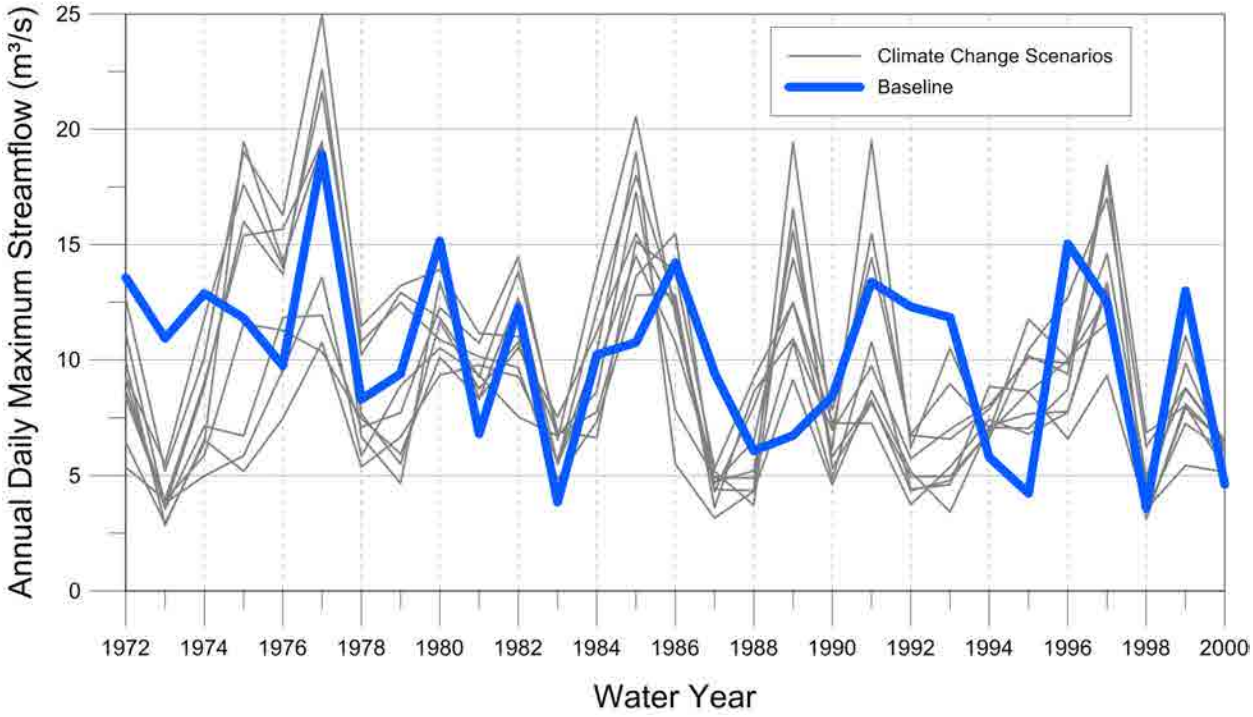

Figure D.78: Annual maximum simulated daily streamflow by water year in Wainman's Creek.

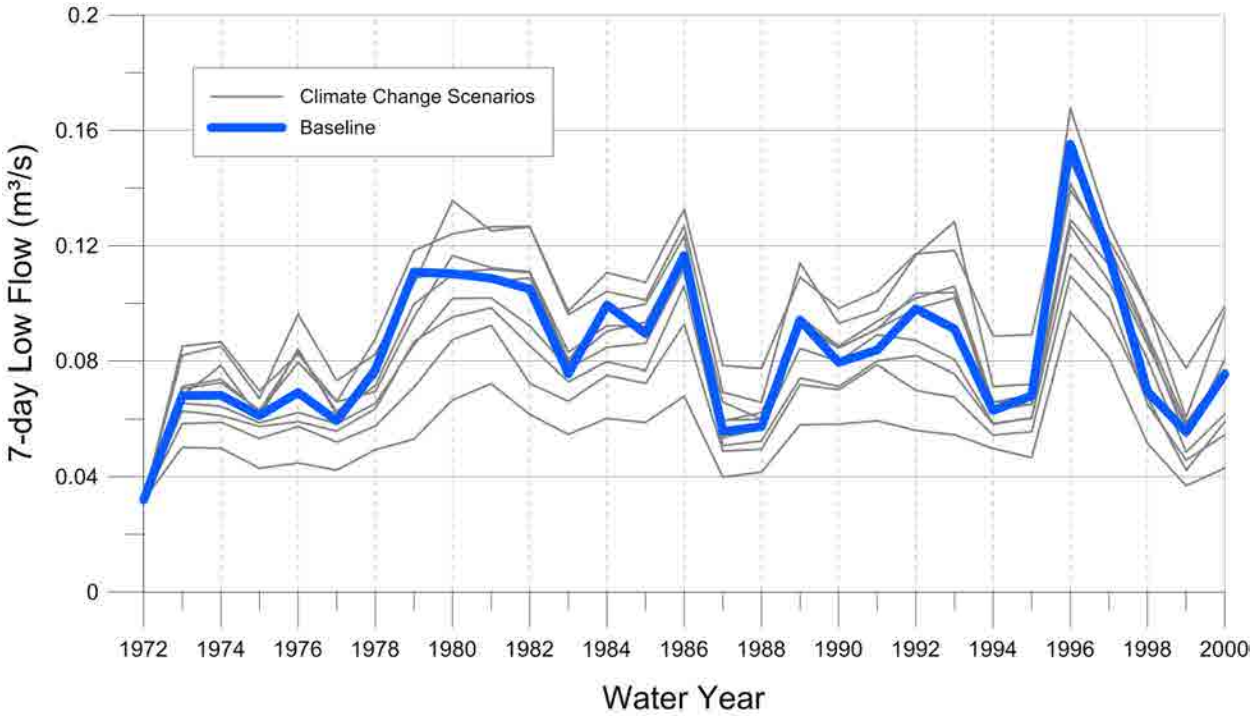

Figure D.79: Annual simulated 7-day low flow by water year in Wainman's Creek.

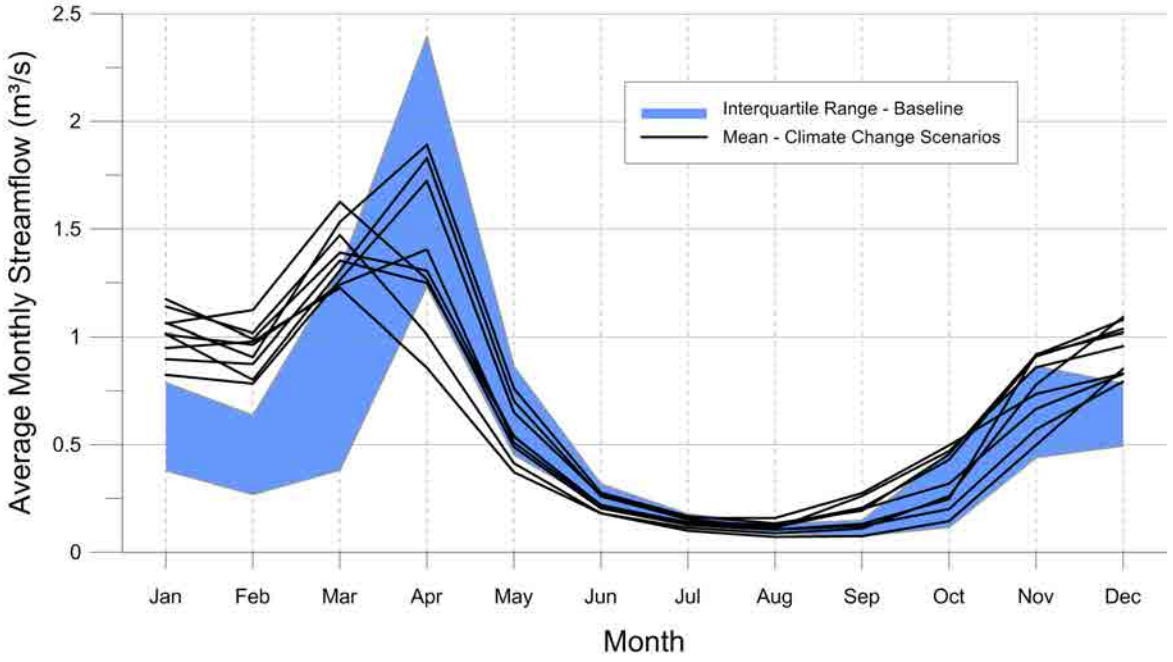

Figure D.80: Average simulated monthly streamflow in Wainman's Creek.

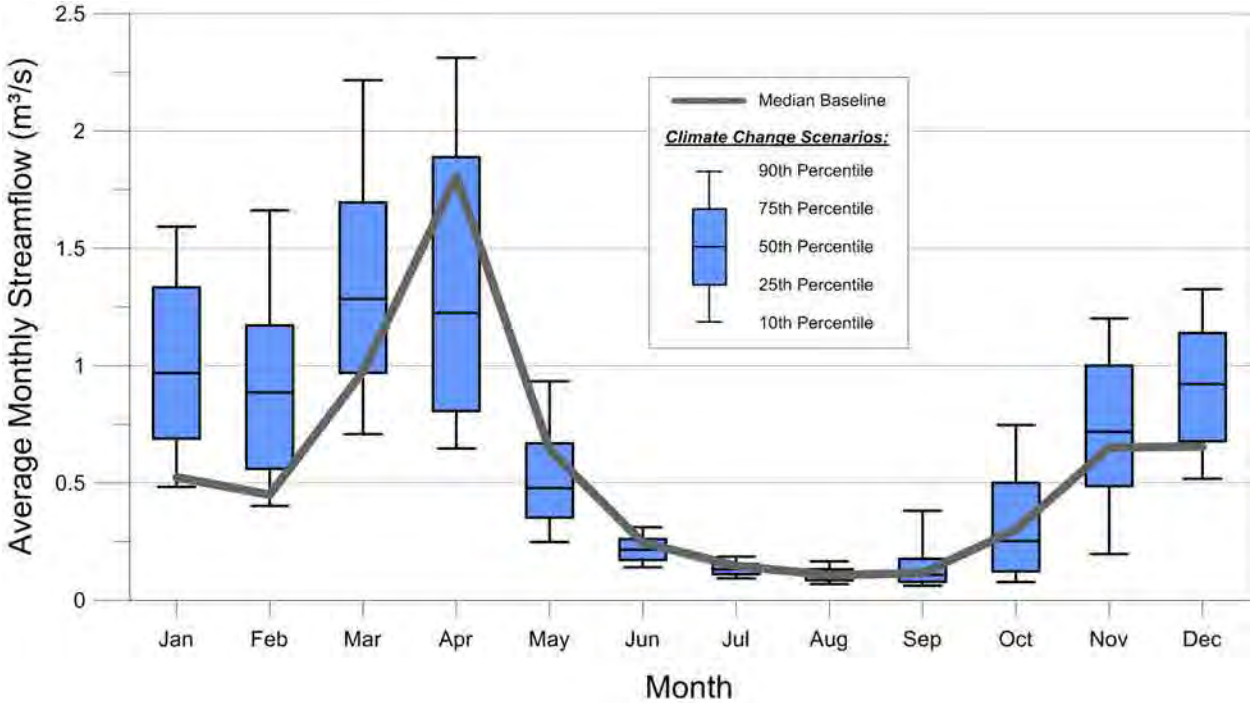

Figure D.81: Monthly simulated streamflow statistics for Wainman's Creek.

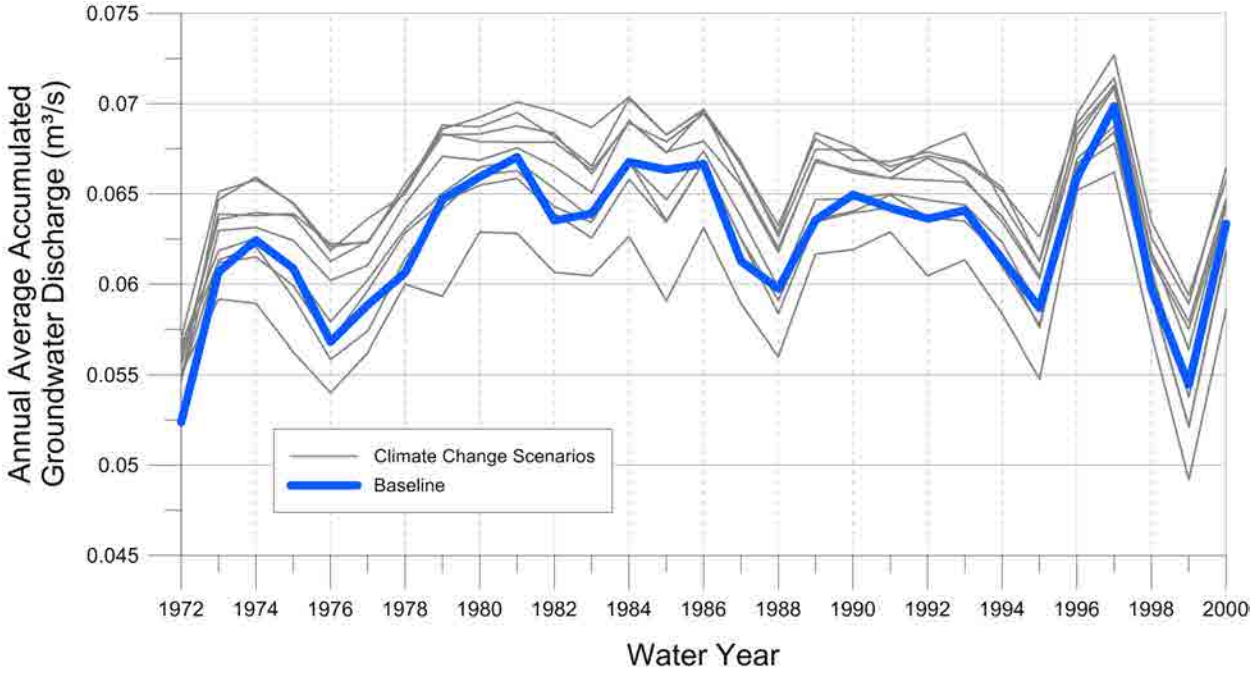

Figure D.82: Annual simulated average accumulated groundwater discharge by water year in Wainman's Creek.

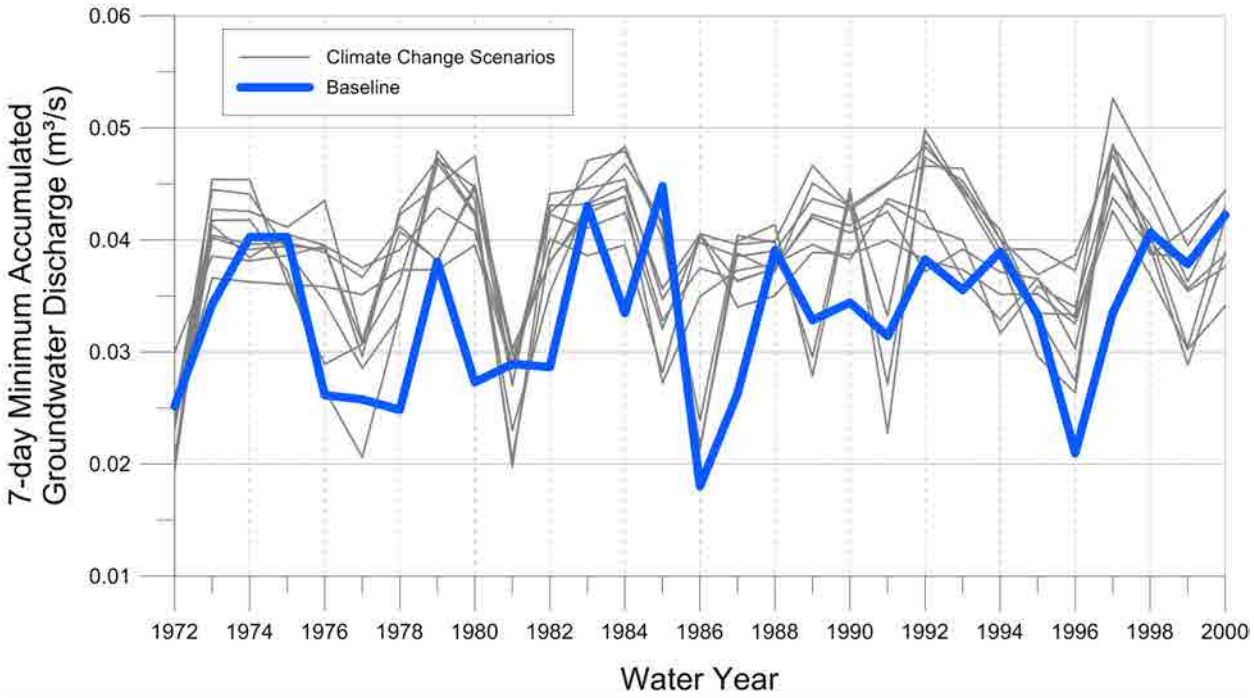

Figure D.83: Annual simulated 7-day low in accumulated groundwater discharge by water year in Wainman's Creek.

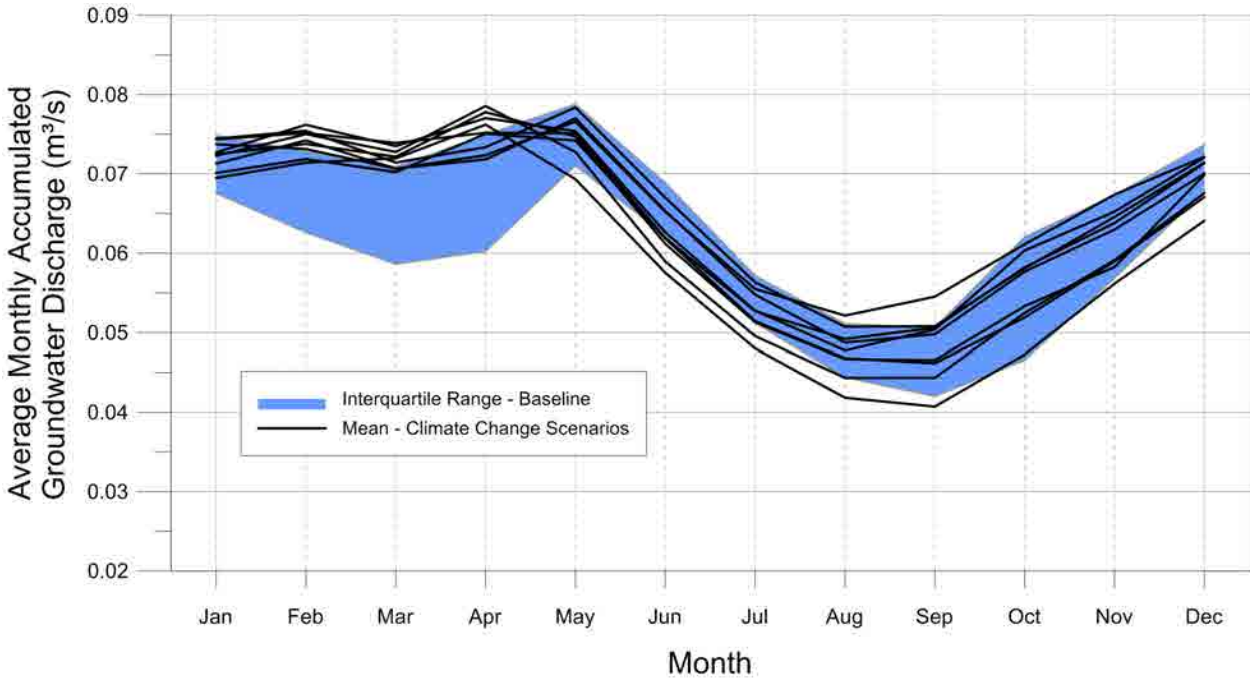

Figure D.84: Average monthly simulated accumulated groundwater discharge in Wainman's Creek.

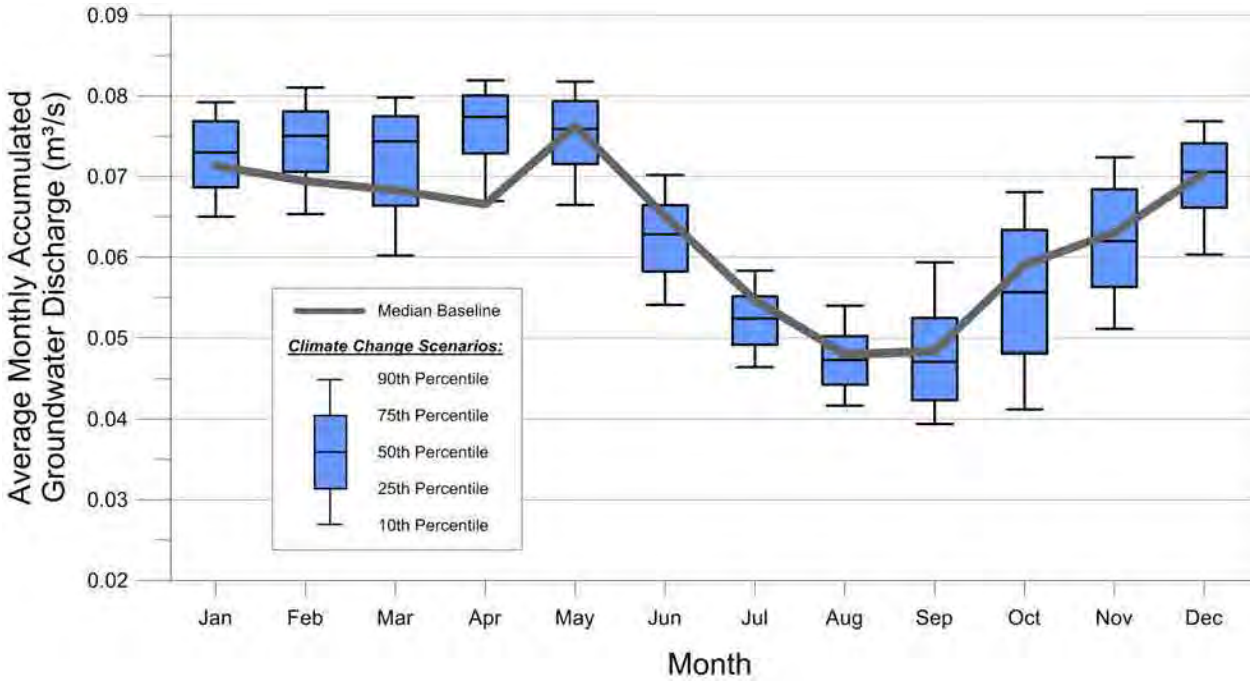

Figure D.85: Monthly simulated accumulated groundwater discharge statistics for Wainman's Creek.